MITIGATION OF DIFFERENTIAL MOVEMENTS AT RAILROAD BRIDGE TRANSITION ZONES

BY

STEPHEN T. WILK

DISSERTATION

Submitted in partial fulfillment of the requirements
for the degree of Doctor of Philosophy in Civil Engineering
in the Graduate College of the
University of Illinois at Urbana-Champaign, 2017

Urbana, Illinois

Doctoral Committee:

Professor Timothy D. Stark, Chair
Professor Gholamreza Mesri
Professor Emeritus James H. Long
Professor John S. Popovics
J. Riley Edwards
Professor Roman Makhnenko

ABSTRACT

Railroad transitions are track locations that experience a rapid change in track structure, such as a bridge or crossing. These locations are prone to differential movement and require frequent resurfacing to maintain an acceptable track geometry for both passing freight and high-speed passenger trains. In an effort to reduce the frequency of track resurfacing, an instrumentation and numerical modeling study was undertaken to (1) identify the root causes of the differential movement at transition zones, (2) develop and improve existing measurement techniques to evaluate track performance, and (3) recommend potential design, remedial, and resurfacing techniques to reduce and/or mitigate the differential movement. The two objectives of the field instrumentation program are: (a) develop a general overview of the loading environment and track movement and (b) develop a mobile system that focuses on tie behavior by measuring rail and crosstie displacements. Three-dimensional dynamic numerical modeling of bridge transition zones was also performed to investigate how changes in ballast settlement affect the transition zone loading environment.

Based on field measurements and numerical modeling, three “root causes” were identified for differential movement at railway bridge transitions: (1) lack of track displacement on the bridge to balance transition zone track displacement, (2) increased applied loads in the transition zone, and (3) reduced-performance ballast conditions in the transition zone. To prevent the observed permanent vertical displacements, the following recommendations for future transition design are: (1) increase transient and permanent track displacements on the bridge to balance approach settlements, (2) use compacted and durable ballast and a working drainage system in the approach, (3) reduce ballast and subgrade settlement by increasing approach confinement in the approach, and (4) installing a resilient layer between the bottom of the concrete tie and top of the ballast to reduce ballast and tie degradation.

ACKNOWLEDGEMENTS

It is a great honor to thank the people who made this thesis possible. I would first like to express my overwhelming gratitude for my advisor, Professor Timothy D. Stark, and it has been an honor to be his Ph.D. student. I had to opportunity to work on a wide range of projects and he shared his experience and knowledge in the fields of geotechnical and railroad engineering. Without his teaching, advice, and ideas, this thesis would not be possible.

I would like to thank Professors Gholamreza Mesri, James H. Long, John S. Popovics, Roman Makhnenko and J. Riley Edwards for agreeing to serve as members of my committee. I am appreciative of the RAILTEC group at the University of Illinois at Urbana-Champaign for including me in their group meetings, which exposed me to various aspects of railroad research and new perspectives. Special thanks to Professor Jerry R. Rose from the University of Kentucky at Lexington who provided instruction about the practical aspects of railroad engineering and was vital for obtaining track time. A great deal of my work would not be possible without his assistance and support.

With regards to the Amtrak and Norfolk Sourthern instrumentation, I want to thank Professor Erol Tutumluer and Debakanta Mishra at Boise State University for instrumenting the initial sites. This includes the assistance from Mike Tomas, Marty Perkins, and Carl Walker of Amtrak and Brad Kerchoff of Norfolk Southern. Ted Sussmann from Volpe Center was helpful in providing direction and adding new perspectives to the project. I would also like to thank Cam Stuart and Hugh Thompson from the Federal Railroad Administration (FRA) for funding and direction. This entire project would not be possible without their support. I would also like to thank Amtrak, CSX, NS, P&L, and UP for track access.

The students at the University of Illinois at Urbana-Champaign were very helpful and supportive and also made life enjoyable during my stay. I am especially grateful to my first officemate Navid Jafari, who helped me get settled and introduced me to student life at UIUC. Multiple students contributed to the work presented in this thesis, including Tom Dehlin, Lishen He, Congyue Fang, Yang Jiang, Arthur Tseng, and many others. I would also like to acknowledge and thank Thierno Kane, Ozgun Numanoglu, Vashish Taukoor, Alfonso Diaz, Ryan Sisk, Joseph Harmon, Donovan Holder, Sean Hayter, and many others for their support.

Finally, I would like to thank my family for their love and encouragement. The patience and support of my mother, Susan, and father, Leonard, was much appreciated along with their support and that of my brother Gregory.

TABLE OF CONTENTS

CHAPTER 1

INTRODUCTION

1.1 Statement of Problem

Railroad bridge transition zones are track locations that experience a rapid change in stiffness and support as passing trains transition from soft track laying on granular materials to a stiff track placed on a fixed structure. Accelerated track settlement is often observed within the transition region, requiring frequent maintenance from railroad companies to maintain a smooth running surface for passing trains. This represents an increasing cost and safety concern for railroad companies as freight and passenger lines are expected to be incrementally upgraded to accommodate longer, heavier, and faster trains.

The root causes of the accelerated track settlement in the transition zone are generally attributed to the lack of track settlement on the bridge and increased loads in the transition zone. Reduced-performance ballast and subgrade material within the transition zone also likely contribute to the problem. Despite being an issue for over a hundred years, no solution has reliably remediated the problem.

The purpose of this research is to better characterize the progressive deterioration of transition zones and recommend existing or new solutions to help remediate or reduce the differential settlement between the bridge and transition zone. Secondary objectives include the development of a non-invasive instrumentation setup that can be mobilized to characterize the performance of a track location within a single day.

1.2 Research Objectives

The main research objectives are to: (1) identify the root causes of the differential movement at transition zones, (2) develop and improve existing measurement techniques to evaluate track performance, and (3) recommend potential design, remedial, and resurfacing techniques to reduce and/or mitigate the differential movement. To accomplish these objectives, the study involves four major tasks and following objectives:

(1) Determine the depth at which the majority of permanent and transient displacement is occurring (Task I),
(2) Determine the root cause(s) of differential movement at the ten instrumented high-speed and freight lines (Task I),
(3) Develop a non-invasive instrumentation system to evaluate the tie-ballast interaction (Task II),
(4) Use track instrumentation to gain evidence of increase loads in transition zones (Task II),
(5) Compare the performance of various transition designs (Task II)
(6) Develop and calibrate both static and dynamic numerical models to determine the Young's Modulus values within the substructure (Task III),
(7) Use numerical model to identify evidence of increase loads from unsupported ties in the open track and transition zone (Task III),
(8) Simulate the progressive settlement of a railroad bridge transition zone (Task III),
(9) Develop a chain of events and list root causes explaining the deterioration of transition zones (Task IV),
(10) Develop strategies for reducing transition zone settlement (Task IV), and
(11) Recommend transition zone design, remedial, and resurfacing measures (Task IV).

1.3 Scope and Outline

The thesis is divided into seven chapters with Tasks I through IV representing Chapters 3 through 6. Chapter 1 is the introduction.

Chapter 2 introduces railroad track components, ballast behavior, track behavior and maintenance cycle, and transition zone behavior. This section should provide the necessary information to understand the subsequent four primary Tasks.

Chapter 3 presents Task I and analyzes high-speed passenger and freight data from ten instrumented sites. The analysis investigates which locations experience the greatest settlement and the depth at which this settlement is occurring. The transient track behavior, including wheel loads, tie loads, and elastic deformation, is compared with the permanent settlement to develop correlations and identify root causes.

Chapter 4 presents Task II and introduces a non-invasive instrumentation system to evaluate track and transition zone locations. This system is implemented at eight main sites to correlate track geometry with quantitative measurement values and investigate evidence of increased loads at the tie-ballast interface. Chapter 4 also compares the effectiveness of multiple transition zone design techniques and looks into the behavior of multiple existing transition zones.

Chapter 5 presents Task III and introduces a numerical model that is calibrated with field measurements from Task I. The model is used to investigate the impact of unsupported ties on the loading environment and simulate the progressive settlement of a bridge transition zone.

Chapter 6 presents Task IV and provides an explanation for the progressive deterioration of railroad bridge transition zones. A unified theory of how to prevent and remediate transition zones is introduced along with new ideas of how to resurface transition zones.

Chapter 7 presents a summary and conclusions of the research.

CHAPTER 2

BACKGROUND AND LITERATURE REVIEW

Diagnosing the root causes of accelerated settlement at track transitions requires a realistic view of the variation in potential track conditions, limitations of current knowledge and the abilities to accurately measure meaningful variables, and uncertainties in track and material behavior. The purpose of the Background and Literature Review section is to present these factors in a meaningful way using the existing literature and provide the reader necessary background information to understand Tasks I through IV and its contributions. The scope of this section is to only introduce necessary track transition topics; however, more detailed literature reviews may be included within each Task chapter as necessary.

The Chapter begins by introducing the modern railroad track structure and its components (Chapter 2.1) to summarize the purpose, variations, and history of the track structure along with some design specifications. Subsequent subsections describe ballast behavior (Chapter 2.2), track behavior (Chapter 2.3), and finally transition zone behavior (Chapter 2.4). The behavior subsections begins with laboratory ballast behavior in Chapter 2.2 because it is the simplest contributor to long-term transition zone settlement. Next, the interaction between the ballast and remaining track structure is introduced and explained in Chapter 2.3 along with the track maintenance cycle. Lastly, the interaction between the track structure and fixed structures such as a bridge are introduced and explained in Chapter 2.4.

2.1 Track Structure

The Track Structure subsection provides a basic overview of the various modern track structure components along with a brief history of their evolution to its modern form. This is included to give context to the current structure and provide direction for potential improvements.

The modern railroad track structure consists of multiple components that work in conjunction to provide a smooth running surface for trains and disperse the high wheel loads to the subgrade (Kerr, 2003). The track structure is typically divided between the *superstructure*, which generally consists of the rail, crossties, and fastening system, and the *substructure*, which

generally consists of ballast, subballast, and subgrade. Figure 2.1 shows two photographs of the modern crosstie track structure along with a typical cross-sectional diagram. *Special structures* are also considered a part of the track structure and can include bridges, tunnels, culverts, and retaining walls (Kerr, 2003) and are discussed in Chapter 2.4.

(a)

(b)

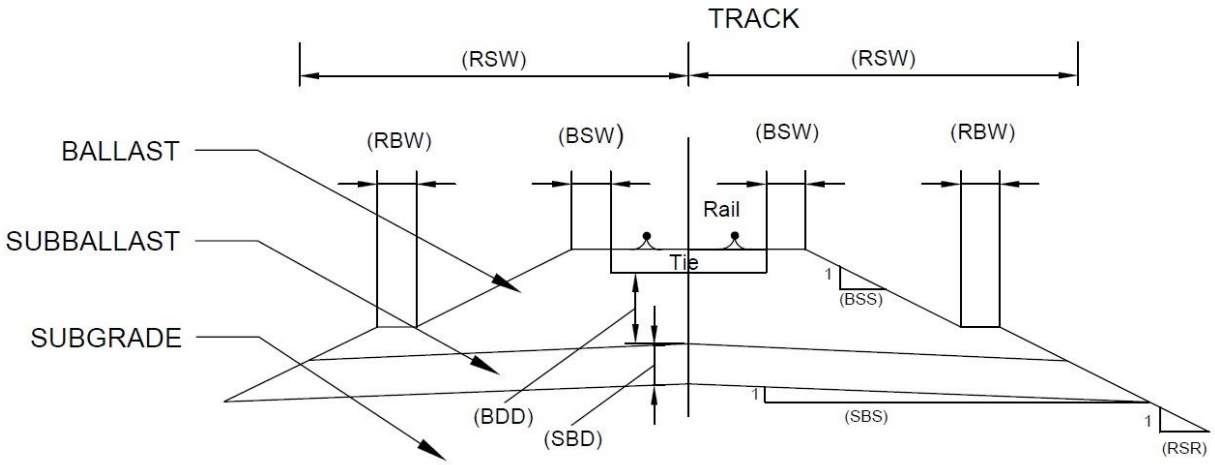

Ballast:
BDD = Depth of Ballast
BSW = Ballast Shoulder Width
BSS = Ballast Side Slope Run

Subballast:
SBD = Subballast Depth
SBS = Subballast Side Slope Run

Roadbed:
RSW = Roadbed Shoulder Width
RSR = Roadbed Side Slope Run
RBW = Roadbed Berm Width

(c)

Figure 2.1: Diagram of typical railroad track structure (modified from AREMA, 2016).

The modern railroad track structure has continuously evolved over the past few hundred years from its roots as guiderails for coal wagons in mines to vast transnational networks transporting freight and passengers. As transport speed, weight, and tonnage increased, innovations to increase track structural capacity and resiliency followed, primarily from trial and error. The period from late 1700's to the late 1800's experienced much experimentation with various rail shapes, fastening systems, and tie configurations. By the end of the 1800s, the Stevens steel rail on crossties emerged as the dominant track structure configuration and remains so to this day (Figure 2.1). Innovations in the past century typically involved improving material strength, i.e. larger rails or concrete crossties, inclusion of addition track components to improve track resiliency, i.e. under-tie pads, and a push towards non-ballast track for high-speed passenger trains.

2.1.1 Superstructure – Rail

The rail is essentially a long steel beam that functions to: (1) disperse high wheel loads to the underlying crossties, (2) provide a smooth running surface, and (3) provide a guideway for passing trains. The currently used Stevens railhead shape was originally designed in the 1830s and became the dominant railhead by the late 1890s because of its lighter rail section, ease at attaching to crossties, and large bending stiffness in both the vertical and horizontal planes (Kerr, 2003). A detailed look into various railhead shapes can be found in Kerr (2003). As trains eventually became faster and heavier, improvements in the rail have generally involved increasing the area and weight of rail sections, using higher-quality steel, and improving casting practices. Typical rail sections in the United States range between 115 to 140 lb/yd.

Since rails must be manufactured and transported at finite lengths (typically 78 feet), two common methods are used to join rail in track. The first is by using a separate steel plate called a joint to connect the two rails. A gap must exist between the rails to allow for expansion and contraction from temperature changes and the joints are often associated with impacts, increased loads, and increased settlements. The second method involves welding together the two rails and is called continuous welded rail (CWR). This method is popular for highly-trafficked track because it reduces, but not eliminates, the negative effects of the joint.

2.1.2 Superstructure – Crossties

In ballasted track, railroad crossties function to: (1) hold track gauge, (2) distribute the high wheel loads from the rail to the underlying ballast, (3) anchor against lateral and longitudinal movements, and (4) allow substructure drainage (Kerr, 2003). The crosstie orientation, i.e. ties oriented perpendicular to the rail and laid at discrete intervals, became dominant by the late 1890's and has remained to this day. Other tie orientations have been experimented with but none have shown to be superior to the crosstie configuration in ballasted track (Kerr, 2003). Popular tie materials are timber and concrete but other materials such as steel and composite ties are often experimented with.

Crosstie dimensions vary by country and were developed from basic stress analyses and trial and error (Kerr, 2003). In North America, timber crossties are typically 7 inches in depth, 9 inches in width, and have a length of 8.5 feet. The crosstie length was selected to reduce rail rotation during loading (Kerr, 2003). Typical tie spacing in North America is 19.5 inches for timber ties and 24 inches for concrete ties. Smaller tie spacing reduce rail bending between ties, reduce tie loads, and increase track stiffness while larger tie spacing reduce costs so the selected spacing typically balance the above factors. Automated tamping represents an additional constraint as 15 inches is typically needed for the tamping clamps to get into the crib. The crib is defined as the space in between the ties.

Timber ties are commonly used in U.S. freight corridors because of their low cost and resiliency. While susceptible to splitting and decay, innovations in chemical treatments have extended timber crosstie lifespans from 8 years to about 25 years, keeping it competitive with concrete crossties (Kerr, 2003). Prestressed concrete crossties have been used since the 1800's but did not fully emerge in the United States until the 1970's. During this time, freight lines experienced a significant increase in wheel loads (27.5 kips to 32.5 kips / 122 kN to 145 kN) and train length from the advent of the diesel locomotive and the implementation of sealed roller bearings. This upgrade in train weight and tonnage resulted in the rapid deterioration of track gauge and components in some regions of the United States. On Amtrak's Northeast Corridor (NEC) passenger lines, the train speed was upgraded to 120 mph and therefore required tighter track geometry restrictions (Kerr, 2003). Concrete ties were believed to be superior at maintaining track gauge and higher capacity and resilience and therefore were introduced in many regions in the United States but often experience more problems than initially expected so

are still only used in select applications (Kerr, 2003). Both timber (Figure 2.1a) and concrete ties (Figure 2.1b) are currently used in the U.S. and installation depends on environmental conditions, tonnage, and railroad company preference. Steel and composite ties are currently tested and improved but have not been widely implemented.

2.1.3 Superstructure – Fastening System

Fastening systems function to connect and restrain movement between the rail and crossties and often acts as an intermediate layer for better load distribution to the tie and damping of vibrations. For timber ties, cut spikes and metal tie plates are commonly used because of cost and resiliency (see Figure 2.1a). For concrete ties and some timber tie locations, spring clip fastening systems are common (see Figure 2.1b) because spikes cannot be driven into concrete ties and spring clip fastening systems offer more damping and maintain better contact between the rail and crosstie.

2.1.4 Substructure – Ballast

The top substructure layer consists of angular rock particles called ballast. The function of the ballast, as set by the United States Federal Track Safety Standards (FTSS, 2014), are: (1) transmit and distribute the load of the track and railroad rolling equipment to the subgrade, (2) restrain the track laterally, longitudinally, and vertically under dynamic loads imposed by railroad rolling equipment and thermals stresses exerted by the rail, (3) provide adequate drainage for the track, and (4) maintain proper track crosslevel, surface, and alinement.

The importance of a strong, well-drained support layer underneath the crosstie was recognized early in railroad history and modifications over the past century have typically emphasized improving ballast characteristics and increasing the ballast depth to reduce particle degradation and subgrade failure in reaction to upgrades to heavier, faster, and longer trains. The ballast section can be observed in Figure 2.1(c), in which the ballast extends below the crosstie and to the sides. AREMA (2016) recommends a *ballast depth (BDD)* of at least 12 inches but this depth can be increased in case of a weak subgrade material. A *ballast shoulder (BSW)* is also used to laterally restrain the crossties and is typically designed at 12 inches. The *ballast side slope run (BSW)* is typically set at a 2:1 ratio. These definitions are displayed in Figure 2.1(c).

A strong ballast material to prevent particle degradation is desired for track with high wheel loads so strong granite or traprock is often recommended for mainline track. Quartzite, Carbonate, and slag rock are less commonly used. Multiple ballast gradations are accepted in AREMA (2016) and are displayed in Table 2.1. Figure 2.2 compares some typical gradations, including: mainline gradation AREMA #4a, yard gradation AREMA #5, and a typical subballast gradation. Standards for sampling and transporting ballast can be referenced in Chapter 1 Part 2 of the AREMA manual. Ballast performance and testing is further elaborated in Chapter 2.2.

Table 2.1: Recommended ballast gradations (AREMA, 2016)

Size No.	Percent Passing									
	3”	**2.5”**	**2”**	**1.5”**	**1”**	**0.75”**	**0.5”**	**0.25”**	**No. 4**	**No. 8**
24	100	90-100		25-60		0-10	0-5	-	-	-
25	100	80-100	60-85	50-70	25-50		5-20	0-10	0-3	-
3	-	100	95-100	35-70	0-15		0-5	-	-	-
4A	-	100	90-100	60-90	10-35	0-10		0-3	-	-
4	-	-	100	90-100	20-55	0-15		0-5	-	-
5	-	-	-	100	90-100	40-75	15-35	0-15	0-5	-
57	-	-	-	100	95-100		25-60		0-10	0-5

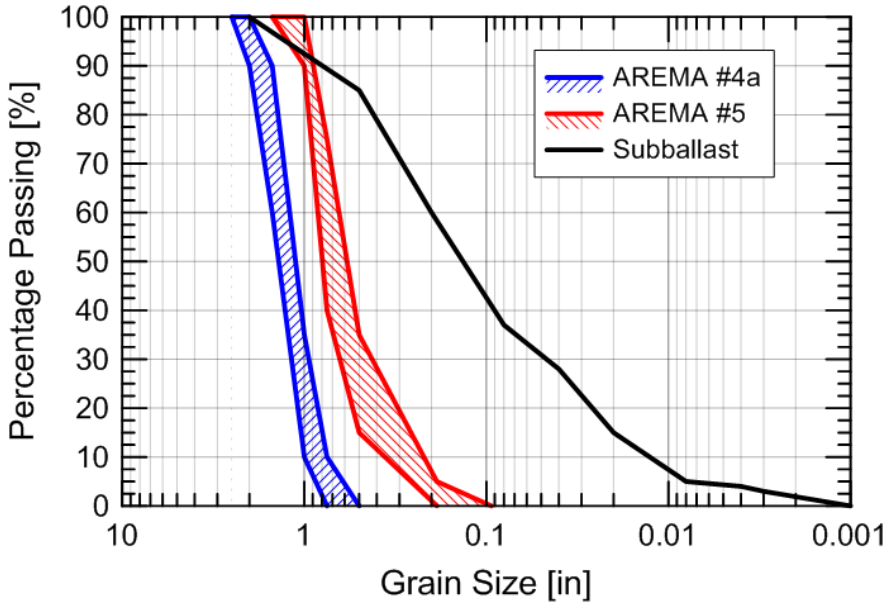

Figure 2.2: Example ballast and subballast gradations.

2.1.5 Substructure – Subballast

The subballast layer serves as an interlayer between the ballast and subgrade and facilitates drainage. The *subballast depth (SBD)* is typically between 6 to 12 inches and is typically sloped (SBS) between a 1:24 to 1:40 ratio to facilitate drainage. A cross-section diagram can be referenced in Figure 2.1(c). If a subballast layer is not designed, it can naturally form from ballast breakdown and mixing of the lower ballast and upper subgrade layers.

The gradation is such to attempt to minimize penetration between the ballast and subgrade layers. Ballast penetrating into the subgrade can produce local depressions that fill with water. Subgrade particles infiltrating into the ballast matrix "fouls" the ballast, leading to a reduction in performance. Fouled and reduced-performance ballast is explained in detail in Chapter 2.2.3.

2.1.6 Substructure – Subgrade

The subgrade is typically the natural soil or a fill soil and often the weakest layer of the track system. The depth of the ballast layer is dictated by preventing plastic deformations in the subgrade layer. Various solutions are used in the case of weak subgrades and can vary from cut-and-fill techniques, strengthening with grout, or avoiding the location all together. Papers on subgrade foundation analysis and design can be found in Li and Selig (1998a,b).

2.2 Laboratory Ballast Behavior

The Laboratory Ballast Behavior subsection reviews observed ballast behavior from laboratory tests. This is important for understanding track settlement in the field because ballast settlement is a major contributor. The subsection introduces: (1) ballast characteristics, (2) behavior of new (clean) ballast, (3) behavior of reduced-performance ballast, and (4) influence of tie-ballast gaps.

2.2.1 Ballast Characteristics

As mentioned in the previous section, railroad ballast consists of angular rock particles that support and restrain the track superstructure. Similar to all granular materials, repeated loadings results in ballast settlement and predictions of the magnitude and rate of settlement is important for maintaining track geometry. To better understand and predict ballast behavior, laboratory

tests have been performed to determine ballast behavior and optimal ballast characteristics. The scope of this section is not to identify ideal ballast characteristics, but list the important factors and reasons certain characteristics are desired.

Indraratna et al. (2012) states that four main factors govern ballast behavior:

(1) characteristics of constituting particles,
(2) bulk properties of the granular assembly,
(3) loading characteristics, and
(4) particle degradation.

A brief summary of each factor is explained below. A more detailed look into each of the factors can be found in Indraratna et al. (2012).

The first factor "characteristics of the constituting particles" involves the characteristics of the individual rock particles, including: particle size, particle shape, surface roughness, and particle crushing strength. Large particle sizes, i.e. 1.5 to 3 inches, are typically used in mainline track because it is believed to offer better support and drainage at the expense of reduced contact area and therefore increased inter-particle stresses. Angular particles are preferred because they increase the frictional interlock between individual particles and increase the strength of the ballast matrix. High surface roughness is preferred because increases the frictional resistance between particles. High rock strength is preferred to reduce damage and degradation and is considered the most important individual ballast particle characteristic.

The second factor "bulk properties of the granular assembly" involves the characteristics of the ballast matrix, including: particle size distribution (gradation), void ratio, and degree of saturation. Current standards recommend a poorly graded matrix because it leads to an increase in shear stiffness and permeability. Low void ratios are preferred because a denser ballast matrix suggests higher inter-particle contact areas and lower inter-particle stresses, resulting in more frictional resistance and less breakage. Well drained ballast is also desired to avoid the negative effects of moisture buildup in track.

The third factor "loading characteristics" involves the loading conditions of the ballast matrix, including: confining pressure, deviator stress (loading amplitude), loading frequency, number of load cycles, and load history. The loading characteristics are difficult to measure in-situ and are usually assumed but knowledge of ballast behavior to various loading factors can

help improve design and remediation techniques. Many of these factors will be discussed in subsequent sections.

The fourth factor “particle degradation” involves changes in gradation over time. This will be discussed in detail in Chapter 2.2.3.

2.2.2 New Ballast Behavior

This subsection reviews the fundamental behavior of new ballast, i.e. directly from quarry. While ballast behavior is complicated, an understanding of its basic behavior is necessary before attempting to understand the behavior of reduced-performance ballast (Chapter 2.2.3) or ballast interaction with the track superstructure (Chapter 2.3) and fixed structures (Chapter 2.4). Research on ballast behavior has typically been conducted using either using large-scale triaxial compression tests or ballast boxes. The triaxial cells vary in size but are typically 12 inches in diameters and 24 inches in depth (Indraratna et al. (1998); Mishra et al., 2013). Ballast boxes involve loading a small portion of a timber or concrete tie into a box filled with ballast. The triaxial tests are better at isolating ballast behavior while ballast boxes can better incorporate the interaction between track components.

The ballast response to cyclic loading typically involves an elastic/recoverable deformation and an inelastic/permanent deformation. This can be shown theoretically in Figures 2.3(a) and from results of a cyclic triaxial compression test are shown in Figure 2.3(b). In field track, the elastic/recoverable strain is typically much greater than the inelastic/permanent strain so the transient displacement from each passing wheel is typically represented by the elastic/recoverable strain and the permanent displacement/settlement is represented by the accumulated permanent strain over millions of load cycles.

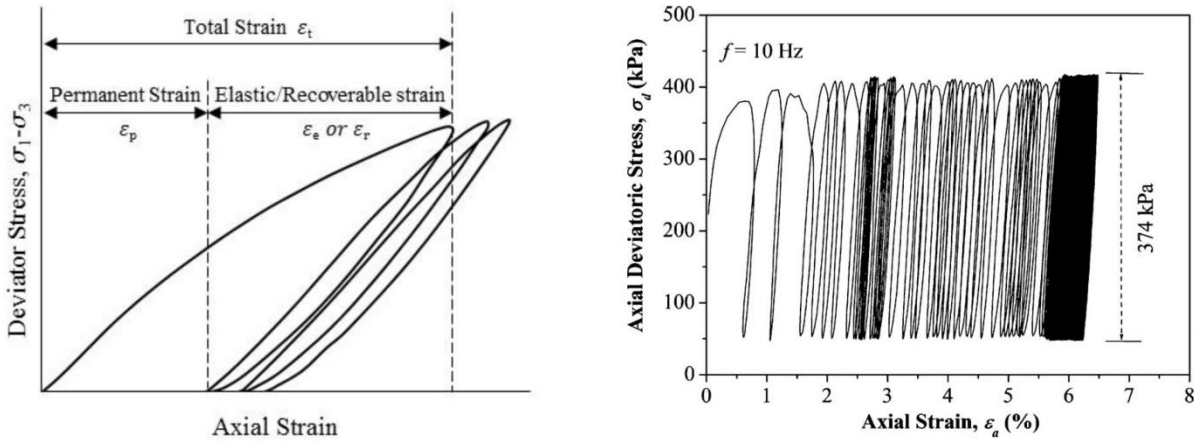

(a) (b)

Figure 2.3: (a) theoretical ballast stress-strain response (from Selig and Waters, 1994) and (b) laboratory data (from Indraratna et al. (2010)).

Defining the ballast stiffness or modulus is important for track analyses because it dictates the track displacement and load distribution. The ballast modulus typically only incorporates the elastic/recoverable strain and is defined as the Resilient Modulus and the equation is shown in Equation 2.1:

$$M_r = \frac{\sigma_1 - \sigma_3}{\varepsilon_r} \tag{2.1}$$

where M_r is resilient modulus, σ_1 is the major principal stress, σ_3 is the minor principal stress, and ε_r is the recoverable strain during load application. The Young's Modulus of ballast can also be determined through penetration tests or seismic waves (Sussmann and Selig, 2000; Nazarian, 2012; Stark et al., 2016).

Ballast settlement, i.e. inelastic/permanent deformation, similar to all granular materials, can occur through changes in gradation and deformation of the ballast matrix. Specifically, this involves multiple mechanisms, including: (1) particle rearrangement, (2) lateral flow, (3) grinding or attrition of asperities (Type I damage), (4) breakage of angular corners or projections (Type II damage), and (5) splitting or crushing of particles (Type III damage) (Mesri and Vardhanabhuti, 2009). Figure 2.4 shows the mechanisms of particle rearrangement, Type II, and Type II damage.

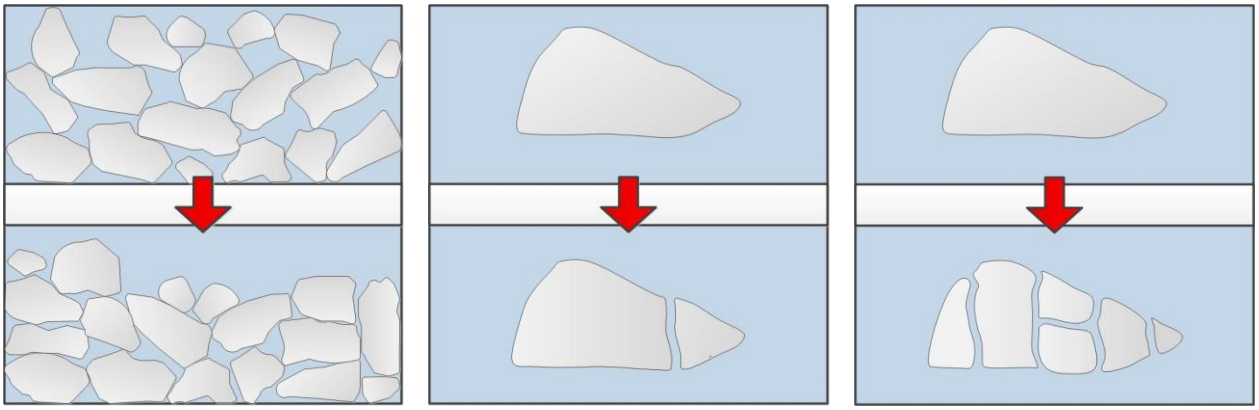

(a) (b) (c)

Figure 2.4: Diagrams of (a) particle rearrangement, (b) Type II damage, and (c) Type II damage mechanisms.

The ballast response is typically separated into two stages: (1) the compaction stage and (2) the post-compaction stage (Selig and Waters, 1994; Indraratna et al. 2010; Indraratna et al. 2012). While the number of cycles that separate the two stages vary, it is often at about 10,000 cycles but can be lower. The first stage often involves rapid ballast settlement from particle rearrangement and Type II damage. This means minimizing ballast settlement at this stage involves attempting to reach the optimum ballast density and using hard ballast.

The second stage typically involves a significant decrease in the rate of ballast settlement than in Stage 1. Ballast settlement may continue at a near-linear rate or even approach zero. This second stage can roughly be viewed as an "equilibrium state" as the external forces and internal resistance are close to stable. Ideal track behavior minimizes Stage 1 settlement and limits Stage 2 settlement.

The reduction in settlement rate with increasing number of load cycles is explained from ballast densification (Selig and Waters, 1994). A secondary factor is that ballast densification increases the ballast inter-particle contact area and therefore reduces contact stresses and ballast breakage. Additionally, increased ballast density will increase the ballast stiffness. A theoretical representation of triaxial test behavior is illustrated in Figure 2.5(a) and an example of laboratory triaxial test results are displayed in Figure 2.5(b). As shown in Figure 2.5(b), the change in ballast settlement rate can be apparent.

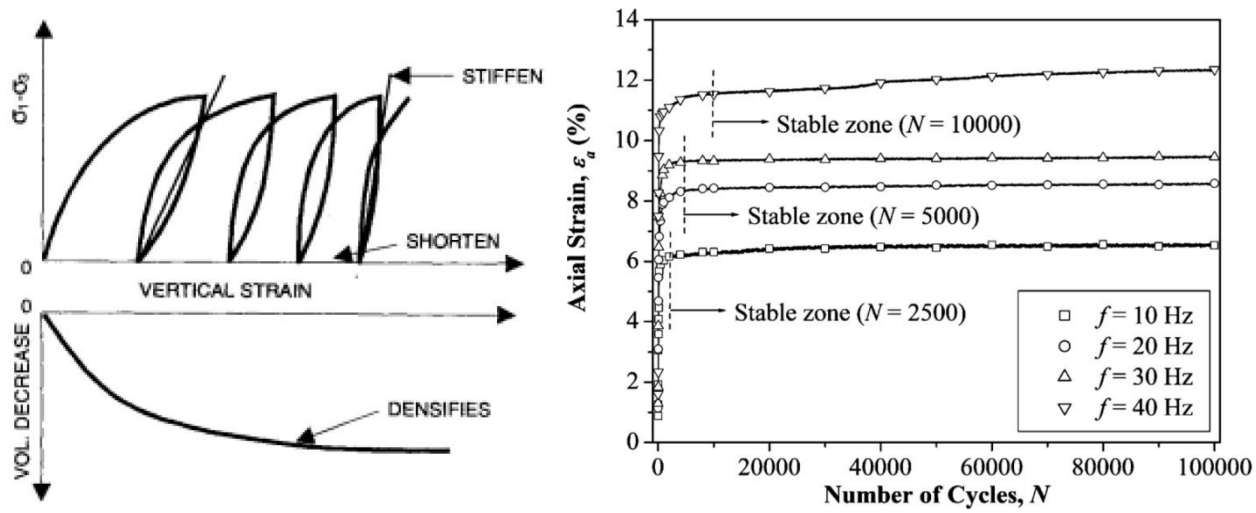

(a) (b)

Figure 2.5: (a) Representation of relation between ballast density, settlement rate, and stiffness (from Selig and Waters, 1994) and (b) laboratory triaxial test results showing change in ballast settlement with increasing load cycles (from Indraratna et al. (2010)).

Some influential factors influencing ballast settlement are the initial density/void ratio, rock type, confinement, loading force, and loading frequencies (Indraratna et al., 2012). Since strong traprock or granite ballast is typically used in mainline ballast and railroad companies prefer larger loading forces and frequencies, ensuring an initial dense state and confinement are potential solutions for reducing ballast settlement. The effects of confinement and loading frequency are discussed below.

To investigate the effect of confinement pressure and deviator stress on permanent axial strain of latite ballast, Lackenby et al. (2007) simulated multiple large-scale (h=24 inches, d=12 inches) cyclic triaxial compression tests. The loading frequency was 20 Hz and wide range of confining pressures (σ'_3) and deviator stresses ($q_{max,cyc}$) were tested. The final axial strains after 1,000,000 cycles are displayed in Figure 2.6(a) and show a significant reduction in final axial strains with increasing confining pressure. Testing of very low confining pressures (<10 kPa) resulted in the ballast not reaching a stable state and continued to settle at high rates.

Additional results show that higher deviator stresses result in higher axial strains, higher confining pressures result in a higher resilient modulus (M_R) (see Figure 2.6b), and there is an optimal confining pressure range to reduce ballast degradation. This range varies depending on the deviator stress, e.g. 25 to 100 kPa for deviator stress of 500 kPa.

Anderson and Fair (2008) also investigated the effect of confinement on axial strain and the results agreed that increasing confining stress reduces axial strain.

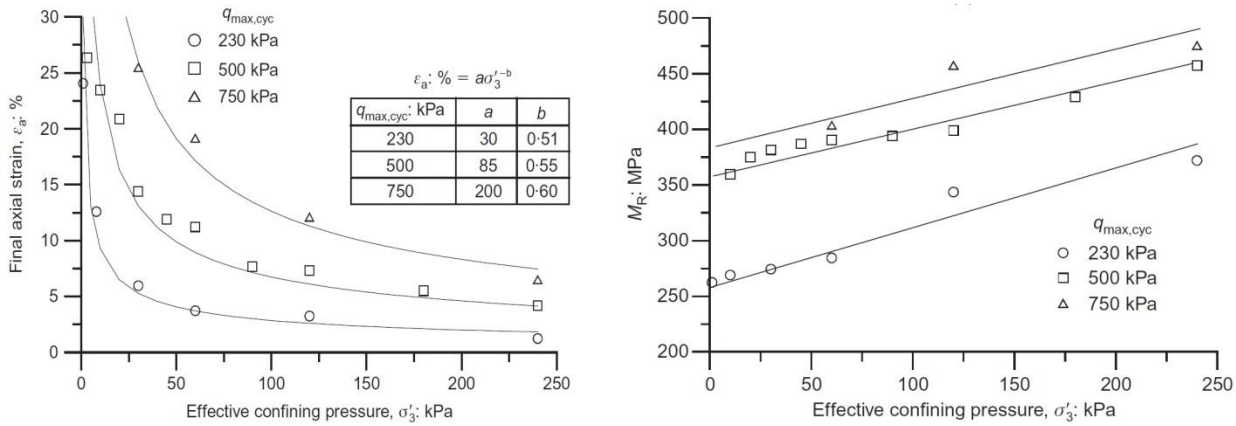

(a) (b)

Figure 2.6: Results showing (a) final axial strains and (b) resilient modulus with effective confining pressure (from Lackenby et al., 2007).

Indraratna et al. (2010) investigated the effect of frequency on axial strains for Latite ballast using large-scale cyclic (h=24 inches, d=12 inches) triaxial compression tests. The confining pressure was 60 kPa and loading frequency varied from 10 to 40 Hz. The axial strains with increasing loading cycles are displayed in Figure 2.5(b) and show an increase in axial strains with increasing loading frequency. Analysis of the ballast particles after testing showed that the majority of settlement occurred from particle rearrangement and Type II damage (angular breakage), however, Type III damage (particle splitting) did occur at higher frequencies.

Discrete Element analyses were also conducted in Indraratna et al. (2010) to investigate how particles were breaking during testing. Results showed that most bond breakage occurred during initial cycles and broken particles move into void spaces and contribute to densification. The breakage also occurred from tensile stresses in the rock particles and breakage occurred in the direction of particle movement (major principal stress).

Sun et al., (2016) also investigated the effects of loading frequency but varied the range from 5 Hz to 60 Hz. Table 2.2 shows the relation between loading frequency and simulated train velocity. Figure 2.7 shows the accumulation of strain from multiple tests and the variation in resilient modulus. The results show minimal difference between 5 and 10 Hz (simulating 23 and 45 mph trains) and then a gradual increase in final strain with increasing loading frequency.

Higher frequency loading also led to unstable ballast settlements in certain situations. A wide range in resilient moduli was also observed (200 to 800 MPa).

Table 2.2: Cyclic loading frequencies and simulated train velocity

Frequency [Hz]	Simulated Train Velocity [km/h]	Simulated Train Velocity [mph]
5	36	23
10	73	45
20	145	90
30	218	136
40	291	181
50	364	226
60	436	271

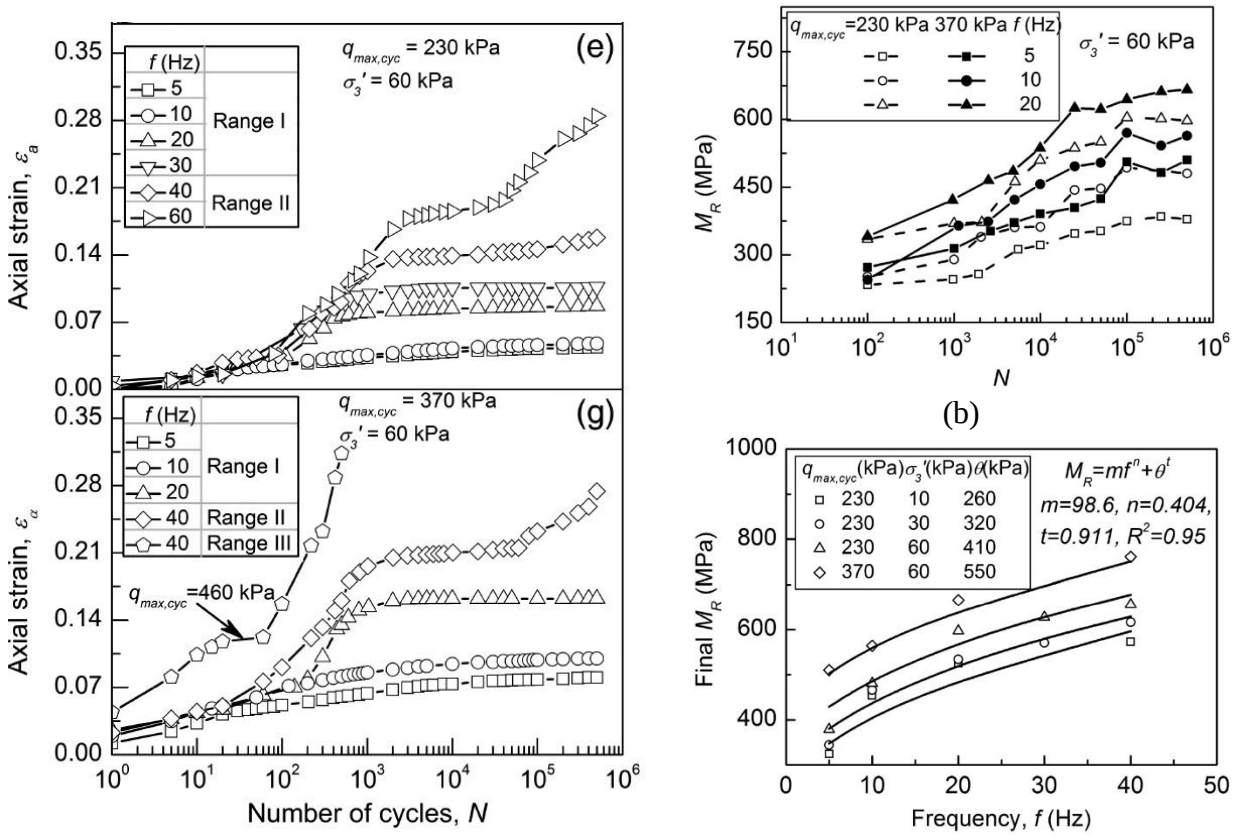

Figure 2.7: Laboratory triaxial test results showing influence of loading frequency on (a) axial strain (b,c) resilient modulus (from Sun et al. 2016).

Thakur et al. (2013) looked into the combined influences of confining pressure and loading frequency by performing large-scale cyclic compression tests on Latite ballast. The loading frequency varied from 10 to 40 Hz and the confining pressure was lowered every 25,000 cycles, starting at 120 kPa, then 60 kPa, then 30 kPa, and finally ending at 15 kPa. The purpose of the tests was to simulate the gradual loss of confinement from lateral ballast flow.

The axial strains are displayed in Figure 2.8(a) and show that the ballast appears to go through the Stage 1 (Compaction Stage) and Stage 2 (Post-Compaction Stage) cycle with each change in external loading condition. For high frequencies, the ballast did not reach Stage 2 and remained unstable until approaching the maximum strain possible for the laboratory test. The change in resilient modulus for all combinations are displayed in Figure 2.8(b) and show a reduction in resilient modulus with increased frequency and decreased confinement.

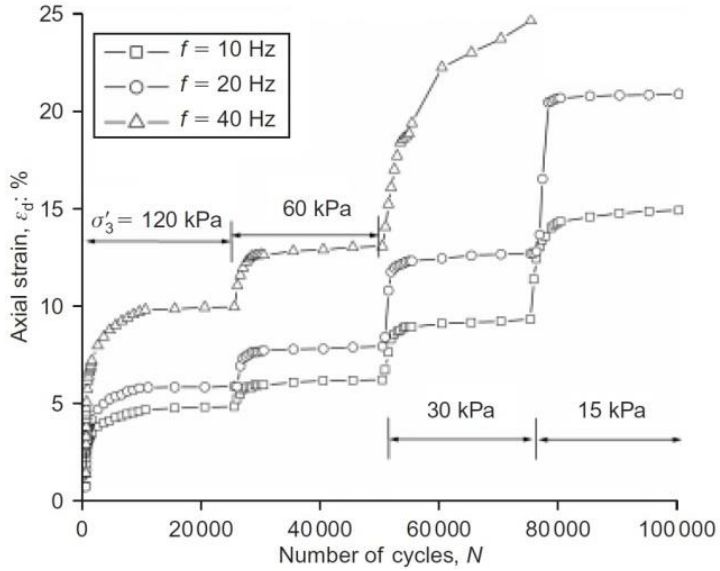

Figure 2.8: Laboratory triaxial test results showing influence of confinement and loading pressure on axial strain.

A summary of new ballast behavior is listed below:

- Ballast behavior varies significantly and depends on particle, ballast matrix, and external loading conditions.
- Ballast typically experiences rapid initial densification followed by a stage of near-linear settlement
- Ballast settlement can be reduced by increasing confinement pressures

- Ballast settlement is increased from low confinement, high-frequency and high-magnitude loadings.
- Ballast often reaches a state of "equilibrium" with external loading conditions; however, a complete loss of stability can occur from low confinement or high-frequency loading.
- A wide range of resilient modulus values have been measured for clean ballast (250 to 750 MPa)

2.2.3 Reduced-Performance Ballast Behavior

This subsection reviews the behavior of reduced-performance ballast. In this thesis, reduced-performance ballast is defined as ballast that has suffered a noticeable reduction in stiffness and support due to changes in internal or external ballast conditions such as gradation changes or increased water content. Gradation changes can occur from degradation of ballast (Type I, Type II, and/or Type III damage) or infiltration of sand-, silt-, or clay-sized particles.

In railroad terminology, sand-, silt-, and clay-sized particles are defined as "fouling particles" and track with noticeable amounts of fouling particles is called "fouled ballast". The behavior of fouled ballast varies significantly depending on degrees of fouling, fouling material and plasticity, and water content (Selig and Waters, 1994; Han and Selig, 1997). Examples of fouling in ballast are shown in Figure 2.9.

(a) (b)

(c) (d)

(e) (f)

Figure 2.9: Photographs of track with various fouling levels (a,e photos courtesy of David Jamieson).

Fouling particles can infiltrate the ballast matrix multiple ways. The percentage of each factor is disputed, but Selig et al. (1992) states the following breakdown: (1) ballast breakdown (73%), infiltration from ballast surface (7%), (3) tie wear (1%), (4) infiltration from underlying granular layers (14%), and (5) subgrade infiltration (5%). However, these percentages can vary significantly from site-to-site.

Multiple indices have been developed to correlate the degree of fouling with track behavior. Percentage Passing and Fouling Index (FI) are introduced because they are simple weight-based indices commonly used within the United States. In the case of coal fouling, common in Australia and South Africa, volume-based indices such as Percentage Void Contamination (PVC) and Void Contamination Index (VCI) can be used (Tennakoon et al. 2012) because the specific gravity of coal (~1.28) is half that of typical geomaterials (~2.76) and fouled ballast behavior is more dependent on volume than weight (Huang et al. 2009).

The Percent Passing index is simply the percentage of material weight that passes a particular sieve. Commonly, that is the No. 4 sieve (4.75 mm) but countries outside the United States have used different sieves as the cutoff. For example, if fouling material is defined as particles passing the No. 4 sieve and the material by weight of a sample passing the No. 4 sieve is 20% of the total sample weight, the "Percent Passing" is 20%. "Percent Passing" is also commonly referred to as "Percent Fouling" (Han and Selig, 1997; Teenakoon et al., 2012) and Percent Passing is useful because it reminds the user/reader to inquire about the grain-size diameter that is being used to define the fouling material.

To emphasize the importance of silt and clay-sized fouling particles (<0.075 mm), Selig and Waters (1994) propose the Fouling Index (FI). This parameter defines "fouling material" as the particles that pass the No. 4 sieve (4.75 mm) and includes the influence of fines content, i.e., particles passing the #200 sieve, because fine-grained particles (<0.075 mm) were observed to reduce ballast performance to a greater extent by weight than coarse-grained fouling particles (0.075 mm to 4.75 mm). As a result, FI is defined in Equation 2.2 by Selig and Waters (1994) as:

$$\mathrm{FI} = \mathrm{P}_4 + \mathrm{P}_{200} \tag{2.2}$$

where P_4 is the percentage of particles passing the No. 4 sieve (4.75 mm) and P_{200} is the percentage of particles passing the No. 200 sieve (0.075 mm) by weight. Therefore, FI reflects the importance of fines content by adding the fines content twice to the FI through P_{200} and P_4. Figure 2.10 (from Sussmann et al., 2012) shows the gradation of various fouling levels.

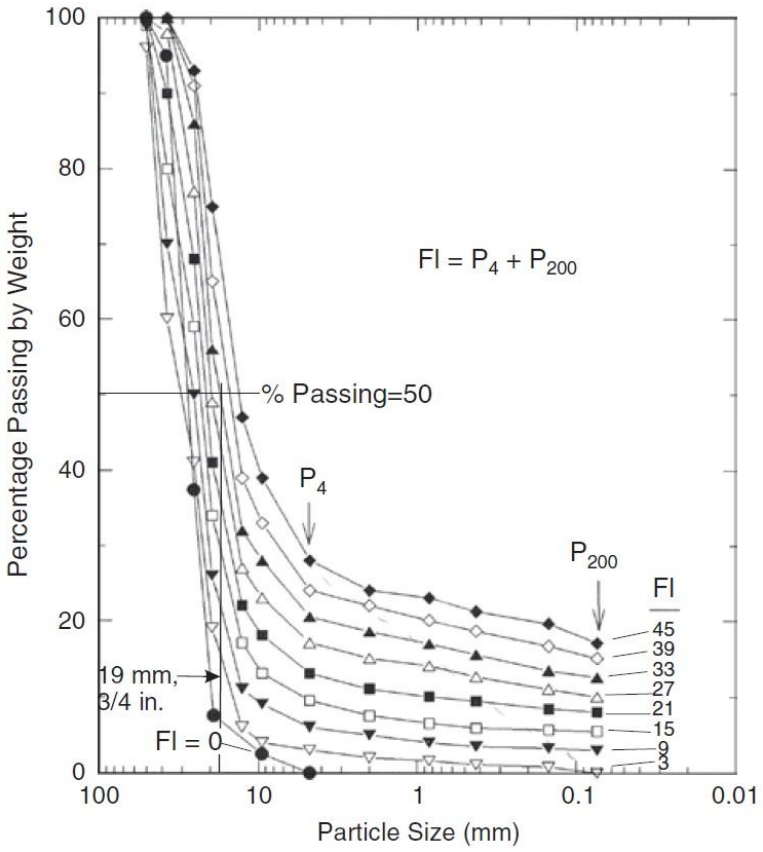

Figure 2.10: Influence of fouling on ballast gradation curves (from Sussmann et al., 2012).

Settlement of degraded/fouled ballast can occur in two ways and the difference is emphasized with large-scale triaxial compression tests of new, degraded but clean, and degraded and fouled ballast Qian et al. (2014). The degraded ballast state was obtained by taking a portion of the new ballast and putting it through a Los Angeles (LA) abrasion test until a FI=40 condition was reached. The degraded ballast was halved and in one portion, all fouling particles removed by sieving (FI=0). In the other half, the fouling particles remained (FI=40).

By comparing identical ballast weights side-by-side in Figure 2.11(a), it is clear that degraded ballast occupies less volume than new ballast. This would translate to ballast settlement from changes in gradation from Type I, II, and III damage and subsequent particle rearrangement, i.e. densification. Secondly, when subject to triaxial compression tests, the degraded but clean ballast (open green squares) recorded about 50% more settlement than the new ballast (red xes) and the degraded and fouled ballast (closed blue squares) exceeded 100% at 10,000 load cycles. This is shown in Figure 2.11(b). This means settlement can occur from the

change in internal structure (gradation change and rearrangement) and reduced support and stiffness from external loading (increased permanent strain).

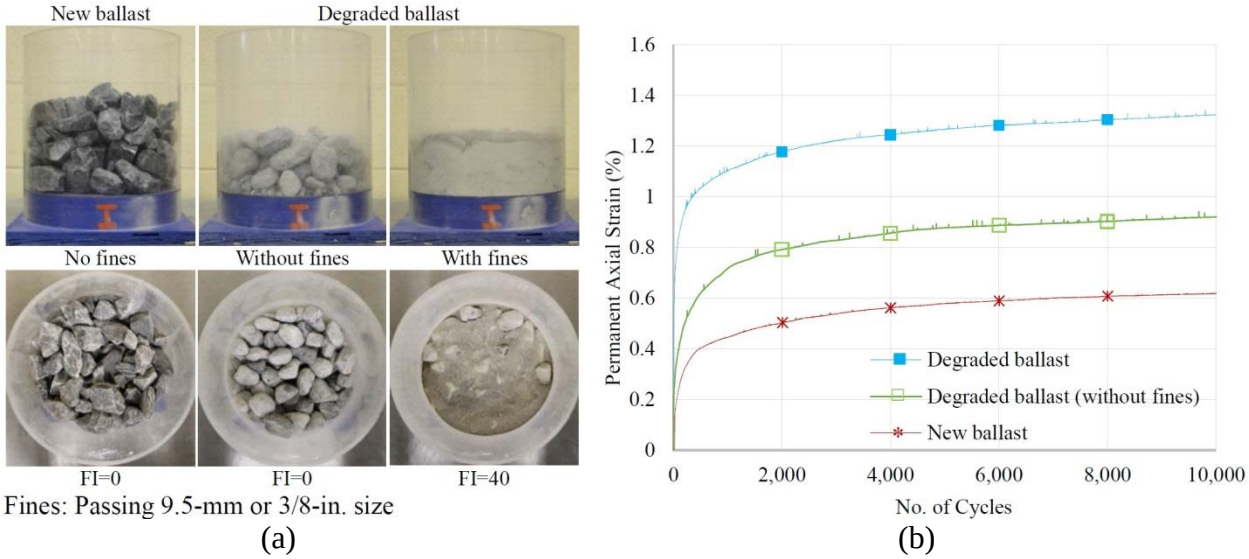

Figure 2.11: (a) Photograph of volume of new and degraded ballast with identical weights and (b) triaxial compression tests of the new, degraded but clean, and degraded ballast (from Qian et al., 2014).

The reduction in fouled ballast performance occurs because when fouling material accumulates on the ballast particles and/or within the ballast voids, the strong frictional contact between the ballast particles is reduced and replaced by a weaker frictional contact between the ballast and/or fouling particles. To further show examples of reduced-performance ballast, ballast box testing by Han and Selig (1997) are displayed in Figure 2.12. These two tests show that (1) a strong relationship is found between ballast settlement and (1) degree of fouling and (2) fouling material, and (3) moisture content under repeated loading.

Figure 2.12(a) illustrates the relationship between ballast settlement and (1) degree of fouling and (2) fouling material by comparing ballast settlement under repeated loading at various fouling levels with the fouling material being a moist silt. For example, the settlement values after 10,000 load cycles at 0%, 10%, 20%, 30%, and 40% fouling are about 0.75”, 1.75”, 2.75”, 3.75”, and 4.75” respectively and represent an almost linear relationship between percent fouling and settlement. Han and Selig (1997) also observed this trend for sand- and clay-sized fouling material and similar behavior was observed for silt- and clay-sized particles but the settlement was lower for ballast with sand-sized fouling particles. The increased settlement from

silt- and clay-sized fouling particles is one justification for using the Fouling Index (FI) parameter. Increases in permanent strain during large-scale triaxial testing of fouled specimens were also observed by Ebrahami et al. (2011). These laboratory tests suggest greater ballast and track settlement will occur as more fouling material infiltrates the ballast voids.

Han and Selig (1997) also investigate the effect of moisture content on fouled ballast settlement by comparing identical clay-sized fouled ballast specimens but in dry, moist, wet states. Figure 2.12(b) illustrates that significantly greater ballast settlement is observed by increasing the moisture content of clay-sized fouled ballast. For example, only slightly greater ballast settlement was observed in the dry clay-sized fouled ballast versus clean ballast (35 vs. 25 mm at 100,000 load cycles) even at a percent passing value of 40%. However, when the clay-sized fouled ballast was wetted, the fouled ballast became unstable and displayed significant settlements (>200 mm) at percent passing values of only 30%. This has important implications because fouled but stable track in dry conditions may rapidly become unstable when wetted.

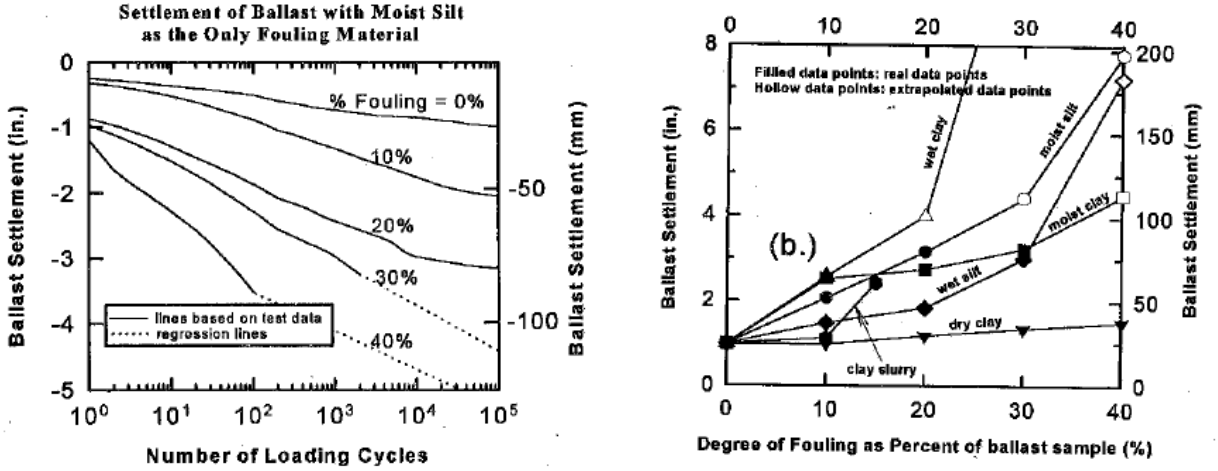

(a) (b)

Figure 2.12: (a) Ballast settlement of moist silt as the only fouling material and (b) Ballast settlement from various moisture contents of silt and clay-sized fouling particles (from Han and Selig, 1997).

The effect of fouling on Young's Modulus in dry- and wet states are compared and presented in Stark et al. (2016). The modulus values were measured from Seismic Surface Wave Testing and are summarized in Table 2.3. The results show that Young's Modulus values are the highest for dry fouled ballast (340 to 380 MPa) and lowest for wet fouled ballast (135 to 170

MPa). Wet and dry clean ballast displayed similar modulus values (200 to 275 MPa). This agrees with the resilient modulus values and the calculated modulus is in-between the dry- and wet fouled states. An explanation for the larger modulus in dry fouled ballast is the dry fouling material results in better gradation and adds cohesion to the fouled ballast material. The fouled ballast becomes soften when soaked with a fire hose because of the softening of the fouling material and a reduction of modulus by a factor of two is observed. This also has significant implications on the variation of track performance when the fouled ballast is in dry- or wet states.

Table 2.3: Comparison of Young's Modulus from seismic testing of different ballast conditions (from Stark et al., 2016)

Ballast Type	Young's Modulus [MPa]	Young's Modulus [ksi]
Clean – Dry and Wet	200 – 275	30 – 40
Fouled – Dry	340 – 380	50 - 55
Fouled - Wet	135 – 170	20 - 25

Selig and Waters (1994) performed laboratory tests on the drainage capabilities of fouled ballast and attempted to relate Fouling Index (FI) with the necessary critical rainfall rate to fully saturate the track. Fully saturated track represents a violation of TSS (2014) and must be avoided. The relationship is presented in Figure 2.13 and shows a significant reduction in critical rainfall rate, i.e. drainage capacity, after an FI of 30 is reached. This reduction in drainage capacity occurs because as the fouling material accumulates within the ballast voids, the available voids for water to pass through decreases. Once the ballast voids become completely filled with fouling material (FI = ~40), the ballast has an inability to drain. This study is important because it shows that track drainage is not only dependent on FI but also the rainfall rate.

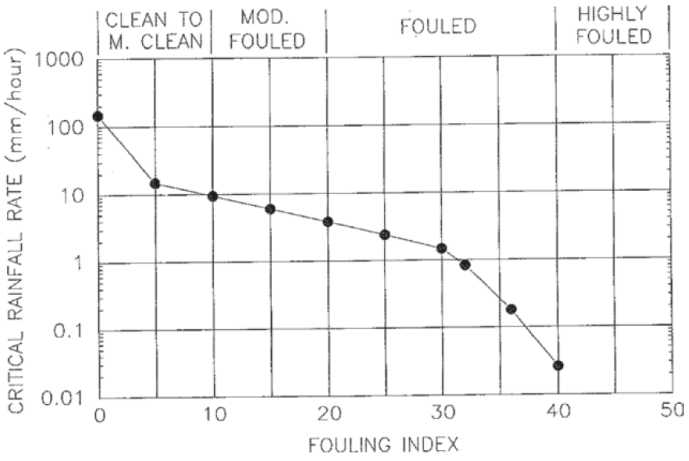

Figure 2.13: Comparison of critical rainfall rate and Fouling Index (from Selig and Waters, 1994).

2.2.4 Tie-Ballast Gaps

This subsection investigates the influence of tie-ballast gaps on ballast settlement. The issue arises because most laboratory ballast testing assumes continuous and intimate contact between the tie and ballast but this often not the case in the field. For example, it is anticipated that about 50% of ties are more or less hanging (Lundqvist and Dahlberg, 2005). An example of sleeper (tie) gaps/voids for 20 consecutive ties are displayed in Figure 2.14. The results show gaps ranging from 0 to 1 mm.

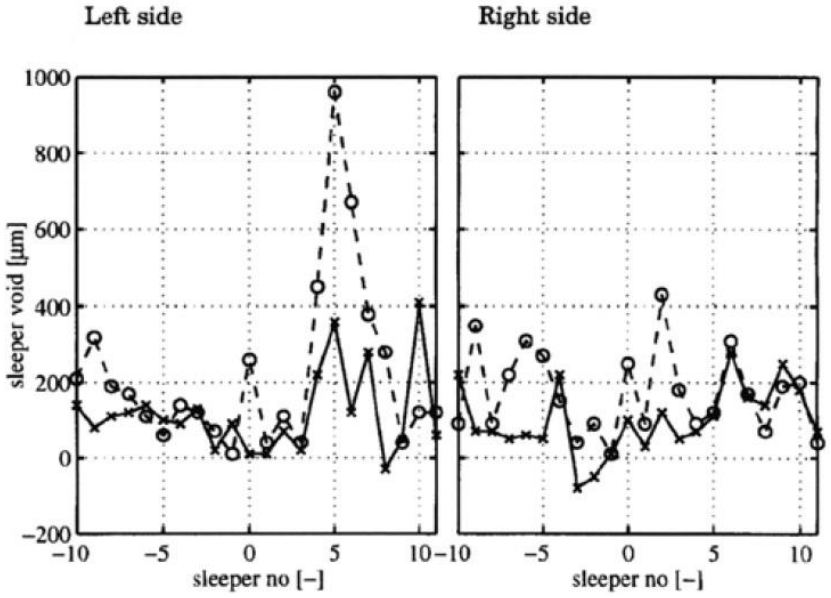

Figure 2.14: Measured gaps under twenty consecutive ties (from Lundqvist and Dahlberg, 2005).

The only laboratory testing the author is aware of involving hanging ties is ballast box testing by Selig and Waters (1994) and the results are shown in Figure 2.15. The study compares ballast settlement for various Fouling Indices assuming no gap and a gap of one to four millimeters, which can be common in track. The results show an order of magnitude greater settlement in situations with tie-ballast gaps than without a gap. Additionally, fouling appears to have a large influenced when coupled with tie-ballast gaps.

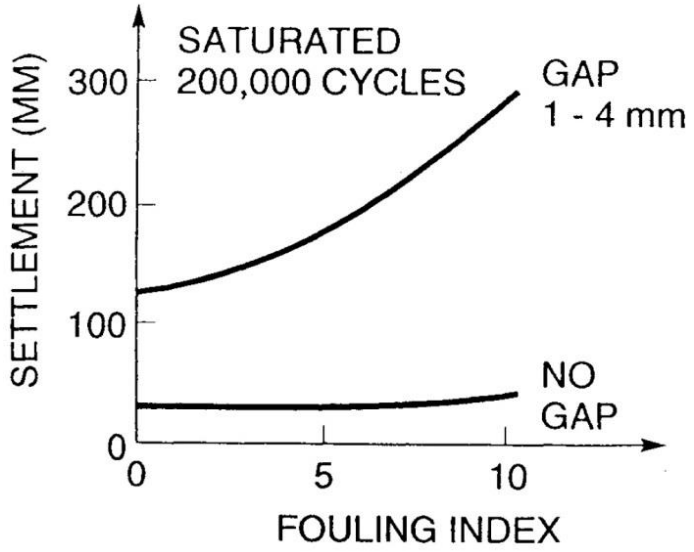

Figure 2.15: Ballast settlement with varying Fouling Indices and Tie-Ballast Gaps (from Selig and Waters, 1994).

Tie-ballast gaps can be an additional problem because they increase the likelihood of tie and fastener cracking (Lundqvist and Dahlberg, 2005).

A summary of ballast behavior is listed below:

- Ballast behavior can vary significantly depending on particle, ballast matrix, and external conditions.
- New ballast with good frictional interlock experiences an initial stage of rapid densification (Stage 1) followed by a stage of near equilibrium with stable/limited ballast settlement (Stage 2).
- Unstable ballast settlement, i.e. no equilibrium, has been shown from high-frequency loading, low confining pressures, and wet fouled ballast.
- The combination of fouled ballast and tie-ballast gaps can increase ballast settlement by up to an order of magnitude.

2.3 Track Behavior and Maintenance Cycle

This subsection reviews short- and long-term behavior of typical railroad track and explains the methods and limits at which track maintenance is required. The ballast behavior introduced in Chapter 2.2 plays a key role in track behavior, as ballast is often the greatest contributor to accumulated track settlement (Selig and Waters, 1994). This section includes (1) theoretical transient track behavior, (2) measured/simulated transient track behavior, (3) measured long-term (permanent) track behavior, (4) track maintenance cycle, (5) tamping, and (6) other resurfacing methods.

The purpose of this section is to introduce fundamental track behavior and explain how track is expected to perform under adequate conditions. Adequate conditions describes track and track components that serve the purposes explained in Chapter 2.1. Essentially, (1) the wheel loads should be evenly dissipated throughout the track structure, (2) similar displacements should be experienced along the track, and (3) minimal relative movement should occur between track components. To clarify, adequate track conditions should not be confused with perfectly ideal behavior as track is inherently non-ideal and will naturally deteriorate over time. Inadequate track conditions is also a highly relative term that has no quantitative definition, but it is usually defined in relation to surrounding track or common maintenance schedules. For example, if a track location requires maintenance at a 25% higher rate than the surrounding track, it may be regarded as problematic and having inadequate track conditions (Davis et al., 2007).

The analytical equations and field studies presented in this section assumes adequate conditions and are representative of the majority of track in service. If these conditions are not realized, track loading and settlement is expected to increase and violate the assumptions of most track design and analysis. Inadequate track conditions, e.g. transition zones, are included in Chapter 2.4.

2.3.1 Theoretical Transient Track Behavior

This subsection introduces theoretical track behavior equations commonly inspiring track design. Two common metrics for evaluating track is loading and displacement. The loads and pressures experienced by track components dictate component selection and can help forecast anticipated substructure settlements. Track displacements are used to predict the magnitude of rail bending

and are also indicators of (1) future substructure settlement as transient displacements and accumulated substructure settlement are generally observed to be related (Hay, 1982) and (2) existing substructure settlements.

Analytical solutions for predicting track superstructure behavior, such as the Beam on Elastic Foundation (BOEF) equations, have been developed since Talbot (1919) and full derivations can be found in Hay (1982) and Kerr (2003). Other methods are available (Nicks, 2009) but track design in the United States is inspired from the BOEF equations and therefore will be introduced (AREMA, 2016). Two important underlying assumptions made while deriving the BOEF equations is that (1) the track structure is homogenous along the track and (2) the track behaves in a linear elastic manner. This means there are no changes in the track super- or substructure and no non-linearity is accounted for. The consequences of these assumptions are introduced in this section but expanded upon in detail in Chapter 2.4.

The BOEF equations are based on the differential equation displayed in Equation 2.3:

$$EI\frac{d^4y(x)}{dx^4} + uy(x) = q(x) \tag{2.3}$$

where EI is flexural rigidity of the beam, y(x) is the vertical deflection of the beam at a location x away from the load, u is track modulus, and q(x) is the distributed load equivalent to the wheel load (Hay, 1982). By solving the problem, the maximum displacement, rail bending moment, and rail seat load can be determined. In this thesis, only the maximum displacement and rail seat load are of interest and are presented in Equation 2.4 and 2.5:

$$Q_o = \frac{Pus}{(64EIu^3)^{1/4}} \tag{2.4}$$

$$Y_o = \frac{P}{(64EIu^3)^{1/4}} \tag{2.5}$$

where Q_o is the rail seat load, Y_o is maximum rail displacement, P is maximum wheel load, u is track modulus, and s is tie spacing. The rail seat load (Q_o), also commonly defined as the tie

load, is the load transferred from the rail to the rail seat/tie. Track modulus is defined as the force required to produce a unit length of track to deflect a unit length (force / length / length). This is distinct from track stiffness which is defined as the force required to produce a unit length of track deflection (force / length) (Plotkin and Davis, 2008). Track modulus is common for design because of its use in the equations above and is independent of rail stiffness while track stiffness is beneficial for track analyses and numerical modeling because of its more tangible meaning.

The equations suggest that rail seat load (Q_o) increases with increasing wheel load (P), track modulus (u), and tie spacing (s) and decreases with increasing rail stiffness (EI). Alternatively, the maximum rail displacement (Y_o) increases with increasing wheel load (P) and decreases with increasing rail stiffness (EI) and track modulus (u). The United States recommends 30 to 50% of the wheel load as the typical range for rail seat load (AREMA, 2016). Variations in rail displacement in adequately performing track is mostly due to variations in track modulus, which is dependent on multiple factors including fastening system, tie type, ballast condition, and type/condition of subballast and subgrade. However, typically, rail displacements range from 1 to 4 mm.

2.3.2 Measured/Simulated Transient Track Behavior

This subsection describes measured or simulated transient track behavior of adequately performing track with a focus on (1) load distribution amongst ties, (2) load distribution amongst a single tie, and (3) load-displacement behavior. In doing so, this subsection presents a benchmark on how track should realistically behave. This is important because while this thesis emphasizes inadequately performing track, e.g. transition zones, successful design and remedial solutions should result in transition zone behavior that resembles the track behavior introduced in this and next subsection.

The first aspect is the distribution of wheel load amongst the underlying ties. This value is rarely measured directly because of instrumentation difficulties but indirect measurements typically show rail seat loads falling within the range of 30 to 50% of the wheel load (Fröhling et al., 1997). Numerical analyses using the software GEOTRACK roughly agrees with AREMA (2016) and estimates about 40% of the wheel load is transferred to the rail seat with 20% of the load transferred to the adjacent ties and 10% to the ties adjacent to those (Chang et al., 1980). A diagram of the typical load distribution is displayed in Figure 2.16. The good agreement between

the theoretical and simulated solutions is not surprising because of the idealized nature of both methods. While skepticism of the 30 to 50% value is not common because the majority of existing track in service is sufficiently designed, deviations from the 30 to 50% are commonly attributed to inadequately performing track and will be explained in Chapter 2.4.

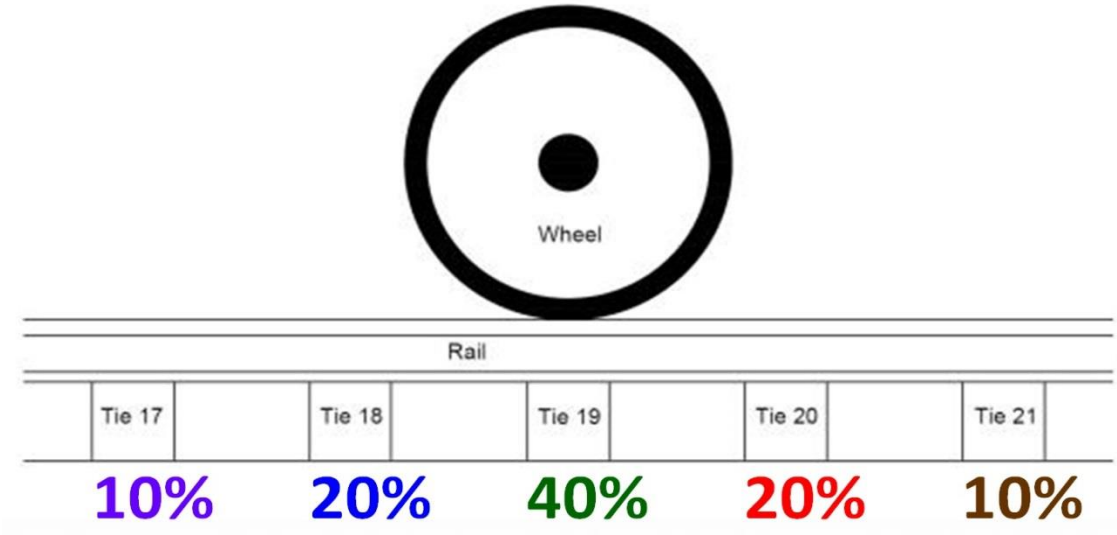

Figures 2.16: Distribution of load to underlying ties under ideal conditions.

A second aspect of load distribution not accounted for in the BOEF equations is the distribution of load throughout the tie. Simple analyses assume homogeneous pressure or that load is transferred along two-thirds of the tie-ballast interface. AREMA (2016) adopted the homogenous pressure assumption while Europe typically uses two-thirds. The exact distribution of load is not known because of the difficulty obtaining tie-ballast pressures but greatest pressures are believed to be located underneath the rail in most scenarios (Selig and Waters, 1994), but it is acknowledge that load distribution depends on support conditions (Talbot, 1919; Gao et al., 2016). Observations of indentations underneath concrete and timber ties after their removal from track suggest the existence of large contact stresses between the ballast particles and tie. A photograph of an indented timber tie is displayed in Figure 2.17.

Figure 2.17: Photographs of indented ties at the tie-ballast interface.

A study by McHenry (2013) investigated the tie-ballast load distribution and contact area by installing multiple pressure sensors underneath concrete ties. Figure 2.18 presents two tie-ballast pressure distribution plots that show varying pressure distributions along the two different ties. This variation is likely due to differing underlying support conditions and local differential ballast settlement. The contact area for a concrete tie with varying ballast materials ranging from sand to new ballast is displayed in Figure 2.19. The results show that new ballast with large angular particles has average contact areas of only 10 to 20% of the available area. The contact area increases with smaller, more degraded, and well graded materials. This suggests that local tie-ballast particle contact stress may be significantly higher than anticipated. This low contact area is likely unintentionally replicated in laboratory and empirical testing (Chapter 2.2 and Chapter 2.3.2) will not affect design but leaves open the possibility of reducing ballast degradation and settlement if the tie-ballast contact area can be increased. This will be discussed in Chapter 2.4.4 with a product called an under-tie pad.

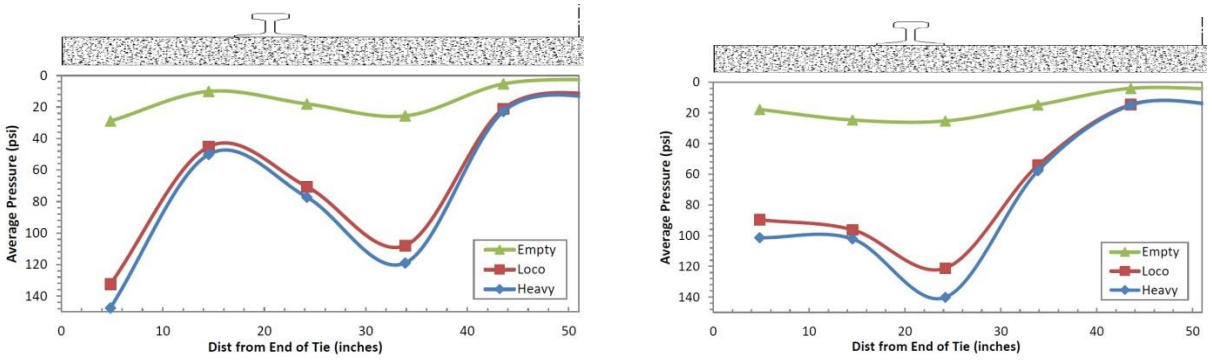

(a) (b)

Figure 2.18: Two example tie-ballast pressure distribution plots (from McHenry, 2013).

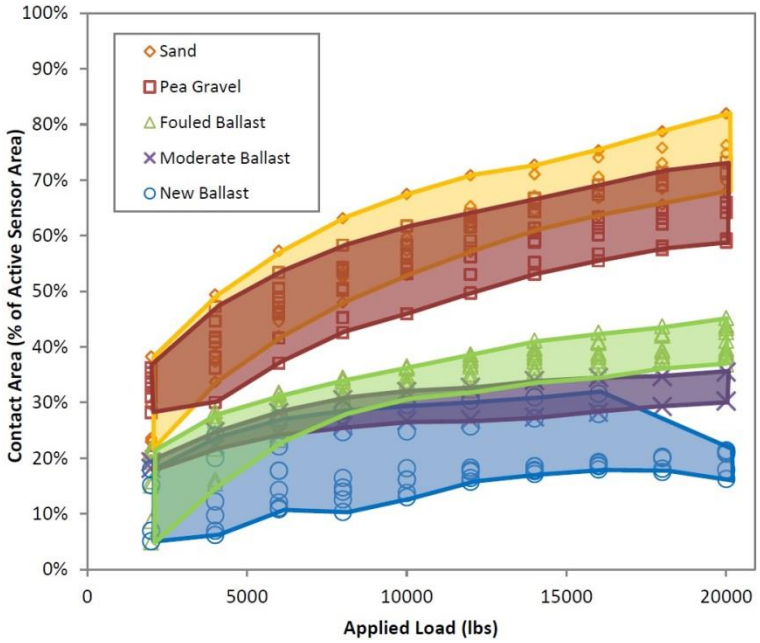

Figure 2.19: Contact area from various ballast materials (from McHenry, 2013).

The third aspect is the transient, i.e. elastic, load-displacement behavior of railroad track. Field measurements to characterize transient track behavior typically involve rail displacements and are sometimes supplemented with wheel loads (Sussmann and Selig, 2000) and less commonly indirect measurements of rail seat loads (Fröhling et al., 1997**).** If both loads and displacements are obtained, track behavior is often portrayed in a load-displacement graph with the wheel or rail seat load on the y-axis and rail displacement on the x-axis. Typical load-displacement behavior is displayed in Figures 2.20 and 2.21.

During initial loading, the track closes any slack or gaps (voids) between the track components such rail-tie gaps or tie-ballast gaps. Additionally, the ballast and subgrade may require some displacement in order to mobilize its full frictional resistance. When all gaps are closed and the substructure materials are fully mobilized, the behavior switches from a non-linear curve to a near-linear increase in displacement within increasing load. The load at which the non-linearity switches to near-linear behavior is defined as the seating load. This is often at wheel loads of 20 to 40 kN (4.5 to 9 kips) or rail seat loads of 8 to 16 kN (1.8 to 3.6 kips). The linear response is expected to continue until the maximum track load is reached. It is unclear whether the linearity will continue near track failure but this is not a focus of the thesis and is not explored. Mathematically characterizing the load-displacement response is not common because of the lack of field measurements and the non-linearity is generally not considered an issue, but Kerr (1986), and Lu et al. (2008) have analytically developed bilinear and cubic models. The influence of rail-tie or tie-ballast gaps is typically not addressed specifically and is generally included within general track "slack".

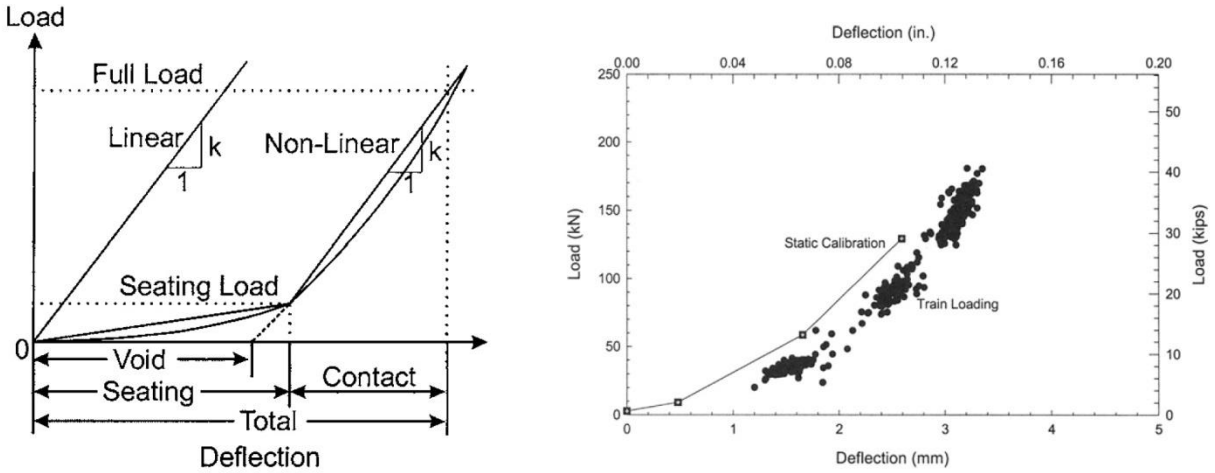

Figure 2.20: Load-displacement curves (a) theoretical (from Sussmann et al., 2001) and (b) field data (peaks only) (from Sussmann and Selig, 2000).

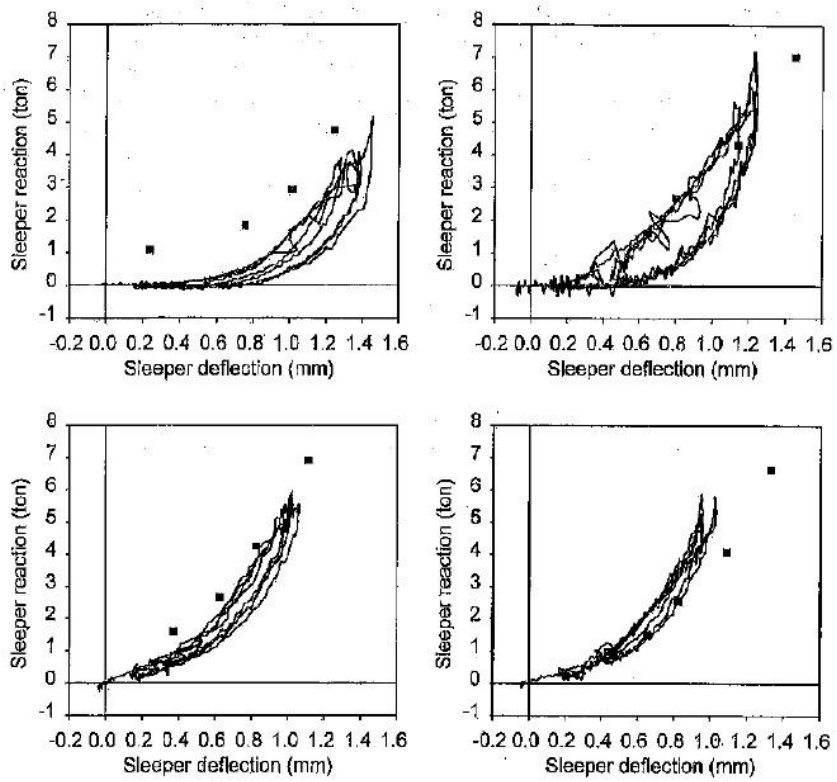

Figure 2.21: Full tie reaction (tie load) – displacement curves (from Fröhling et al., 1997).

In summary, the transient track behavior of adequately performing track generally involves the sufficient distribution of wheel load throughout the track and non-linear behavior at low loads due to the closure of small gaps within the track system and non-linear substructure material behavior. While the behavior is not perfectly ideal, the deviations from the ideal assumptions in Chapter 2.3.1 are acceptable and taken into account during track design.

2.3.3 Measured Long-Term Track Behavior and Track Maintenance Cycle

This subsection focuses on the accumulated settlement of the track structure and the track maintenance cycle. Since the track superstructure consists of manufactured materials and are designed not to exceed plastic limits, the vast majority of track settlement results from settlement of the track substructure. This means track settlement should be a natural extension of ballast settlement (Chapters 2.2.2) and behave similarly. The influence of the track superstructure primarily involves how the load is distributed throughout the track. This is typically not an issue

for adequately supporting track but can be detrimental in cases of inadequately performing track, such as regions with large differential settlements, e.g. transition zones.

As introduced in Chapter 2.2.2, ballast settlement typically involves two stages: (1) compaction stage and (2) post-compaction stage (Dahlberg, 2001; Nimbalkar and Indraratna, 2016). In the compaction stage, the ballast particle will rearrange into a more compact state and asperities will break off. Rapid settlement is often observed at this stage and the magnitude of settlement is dependent largely on how compact the ballast is after tamping. In the post-compaction stage, the ballast continues to rearrange and degrade resulting in gradual settlement.

If the ballast settlement exceeds set thresholds, explained in the next section (Chapter 2.3.4), the track is reset by a process called tamping. The tamping process usually degrades the ballast and therefore the ballast will settle at a quicker rate than in the previous cycle because tamping damages the ballast particles (Selig and Waters, 1994; Douglas, 2013). This process often continues until the ballast must be replaced and the entire cycle repeats itself. This is defined as the track maintenance cycle.

An example of this behavior is displayed in Figure 2.22, in which the permanent deformation, i.e. settlement, of a track is measured over nearly 20 million load cycles. The results show with each tamping event the track experiences a rapid settlement followed by a more stable, linear settlement until resurfacing is required again.

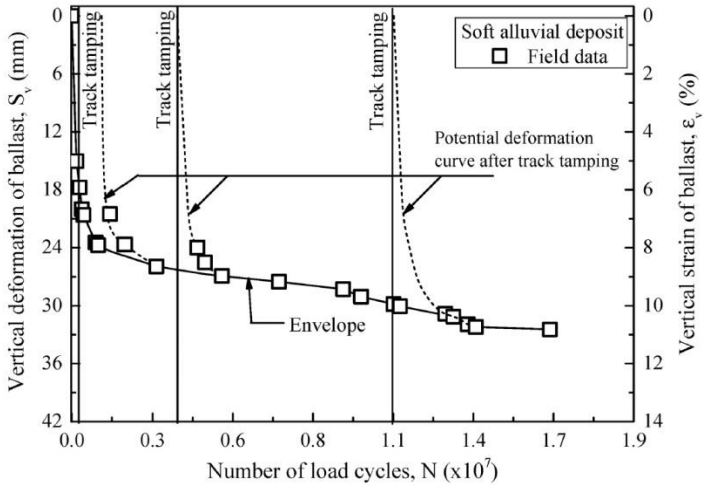

Figure 2.22: Field measured accumulated settlement over three tamping cycles (from Nimbalkar and Indraratna, 2016).

Multiple equations have been developed to mathematically characterize track settlement with increasing load cycles and many of these equations can be referenced (Dahlberg, 2001). These equations were developed either in the laboratory or empirically from open track sites, both of which typically experience good track support and conditions. This explains why these equations are similar or identical to accumulated ballast strain in laboratory tests. If the ballast is initially loose, tie-ballast gaps develop, the ballast degrades and fouls, or there are increased loads from fixed structure – track interaction, all of which are typical in transition zones, these equations will not be representative.

2.3.4 Track Geometry Limits

As introduced in the previous section, repeated train loadings produce substructure settlements therefore the track superstructure will settle with it. Oftentimes, this substructure settlement varies along the track resulting in differential substructure settlements, which produces uneven running surfaces for the train. Uneven running surfaces are a safety issue because train derailments can occur if certain thresholds are exceeded and can force the railroad company to intervene and reset the track structure to an acceptable elevation using a procedure called tamping.

Local differential substructure settlement can produce multiple types of uneven running surfaces. For example, if the substructure settles unevenly under a single tie, one rail may be higher than the other. Alternatively, if a group of ties settle more than the surrounding ties, a local dip may appear along the track. This defect may be isolated to a single location or can be repetitive in the case of increased settlement at evenly spaced rail joints (78 ft. intervals).

In order to quantify these uneven rail surfaces, track geometry deviations are generally categorized into four main geometry defects: crosslevel, alignment, profile, and warp. Crosslevel refers to one rail being at a higher elevation than the other and can result from uneven substructure settlement underneath a single tie. Alignment refers to a lateral deviation of the entire track. Profile refers to the vertical deviation of the track and can result from differential substructure settlement along a stretch of track. Warp refers to the twisting of the track and is measured by comparing the maximum crosslevel difference at various track locations. Examples of crosslevel and profile deviations are illustrated in Figure 2.23.

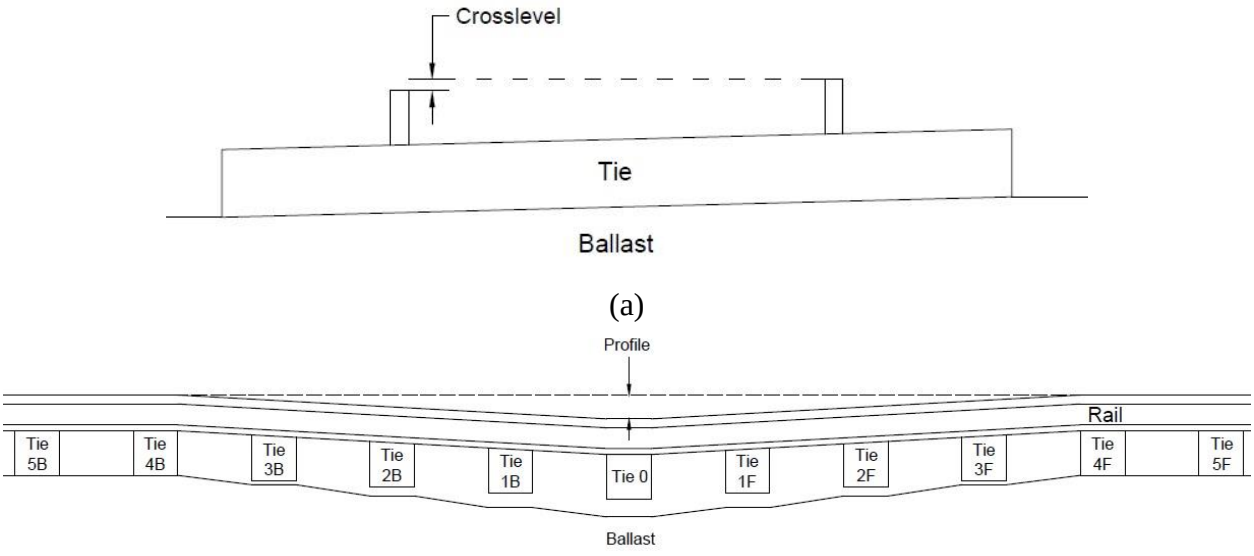

Figure 2.23: Examples of (a) crosslevel and (b) profile deviations.

The Federal Railroad Administration (FRA) has limits on track geometry deviations that is dependent on train speed, i.e. Track Class. Some of these limits are presented in Table 2.4, which shows a reduction in track geometry limit tolerance with increasing train speed. If any of these limits are exceeded, the railroads are forced to intervene or are subject to a monetary fine.

Table 2.4: Track geometry deviations with Track Class

Geometry Defect	Class 1 (10 mph) [in]	Class 2 (25 mph) [in]	Class 3 (40 mph) [in]	Class 4 (60 mph) [in]	Class 5 (80 mph) [in]
Crosslevel	3.00	2.00	1.75	1.25	1.00
Profile	3.00	2.75	2.25	2.00	1.25
Warp	3.00	2.25	2.00	1.75	1.50

Geometry Defect	Class 6 (110 mph) [in]	Class 7 (125 mph) [in]	Class 8 (160 mph) [in]	Class 9 (220 mph) [in]
Crosslevel	1.00	1.00	1.00	0.75
Profile	0.75	1.50	1.25	1.25
Warp	1.50	1.50	1.50	1.50

2.3.5 Tamping

After surpassing track geometry limits, in anticipation of surpassing track geometry limits, or from scheduled maintenance, the railroad track is resurfaced to an acceptable elevation. The most common resurfacing practice in the United States is a procedure called tamping. Automated tamping from a tamping machine essentially raising the rail and attached track superstructure to the desired elevation and fills the underlying gap by squeezing additional ballast underneath the tie (see Figure 2.24). This process is quick and cost-effective, but is criticized for only loosening and damaging the ballast. The loosening explains the rapid settlement immediately after tamping as the ballast is re-compacted from the first few train passes (see Figure 2.22). The term ballast memory is often used to describe how ballast tends to re-compact to the pre-tamping state almost immediately after tamping (Selig and Waters, 1994; Sol-Sanchez et al., 2016a). The process of tamping will also damage and degrade the ballast every resurfacing cycle (McMichael, 1991; Selig and Waters, 1994; Douglas, 2013), resulting in increased settlement rates as explained in Chapter 2.2.3 (Qian et al., 2014).

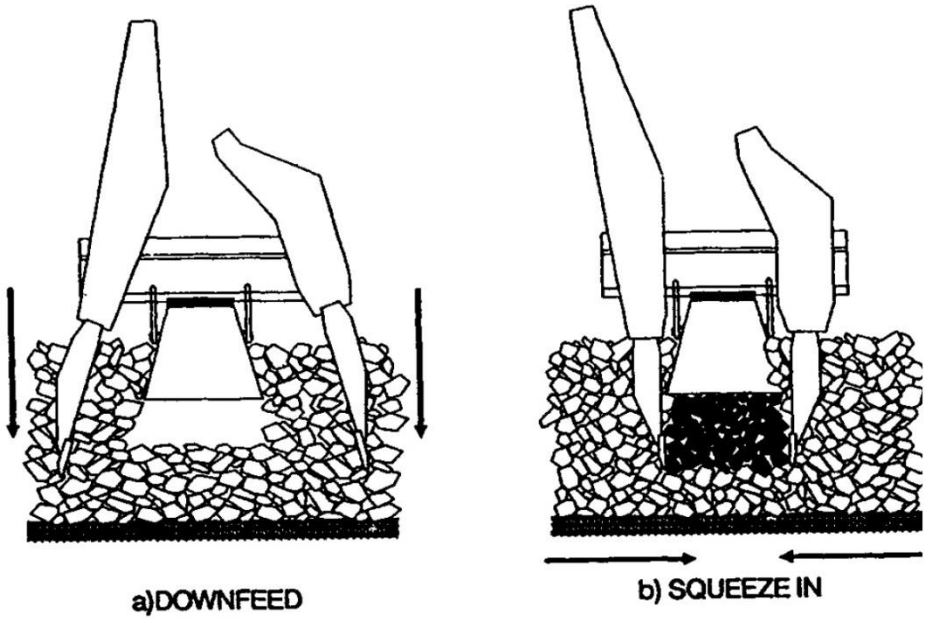

Figure 2.24: Diagram of automated tamping procedure (from Selig and Waters, 1994).

Hand tamping is a second tamping method which requires raising the track to the desired elevation with jacks and pneumatically pushing new ballast underneath the tie. This process

takes longer, is more costly, and results can be highly dependent on the quality of the tamping and the type of tamper.

2.3.6 Other Resurfacing Methods

The rapid track settlement after tamping has led railroads to explore alternative methods of resurfacing. One method popularized in Europe is stoneblowing. Instead of loosening existing ballast to support the track superstructure at its desired elevation, stoneblowing leaves the existing ballast in its equilibrium state and adds new material by "blowing" small stones underneath the ties. The goal is to limit the "compaction phase" immediately after resurfacing. A diagram of the stoneblowing procedure is shown in Figure 2.25. However, the main drawbacks of stoneblowing are that it is expensive, not easily automated, and it can be difficult to judge the volume of stone required to stabilize the track.

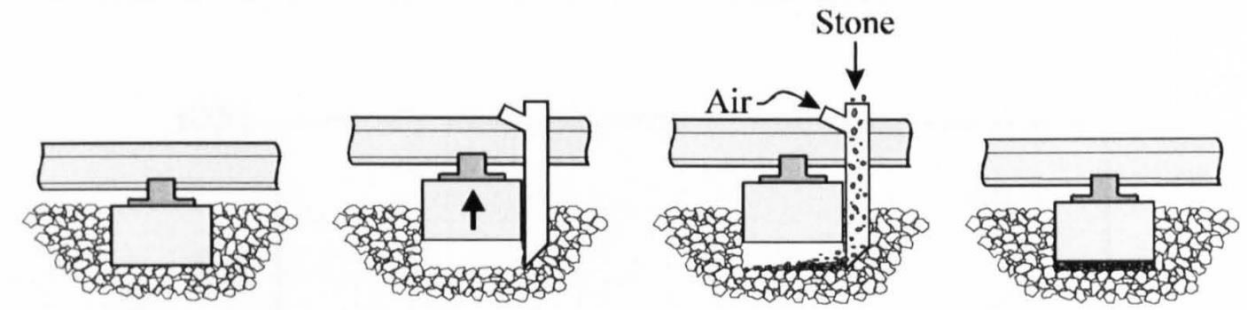

Figure 2.25: Stoneblowing procedure (Fair, 2004; adapted from Selig and Waters, 1994).

A study by British Railroads in the early 1990's looked at the viability of stoneblowing and found a reduction in maintenance when track was resurfaced by stoneblowing instead of tamping (McMichael, 1991). An example of reduction is shown in Figure 2.26. The explanations provided for this reduction are reduced ballast damage and ability to maintain untampable ballast.

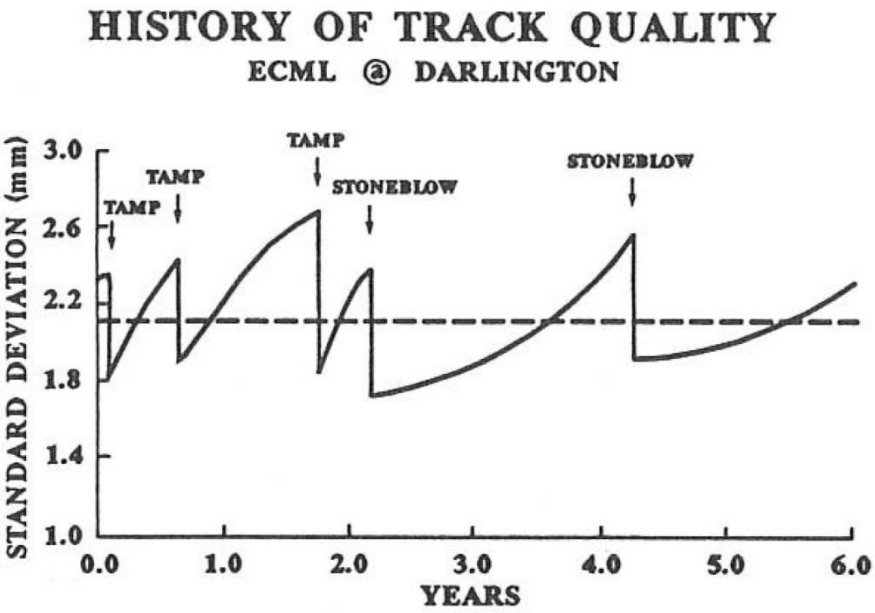

Figure 2.26: History of track quality for track switched from tamping to stoneblowing (from McMichael, 1991).

To better quantify the benefits of stoneblowing, a recent laboratory study by Sol-Sanchez et al. (2016a) compared the effects of tamping and stoneblowing on vertical settlements with both stiff and soft under-sleeper pads (USP), or also known as under-tie pads (UTP) in the United States (see Chapter 2.4.4). The results in Figure 2.27 show the combination of stoneblowing and under-sleeper pads (USP) reduce the vertical settlement after resurfacing by about 70% from 15 mm to about 4.5 mm.

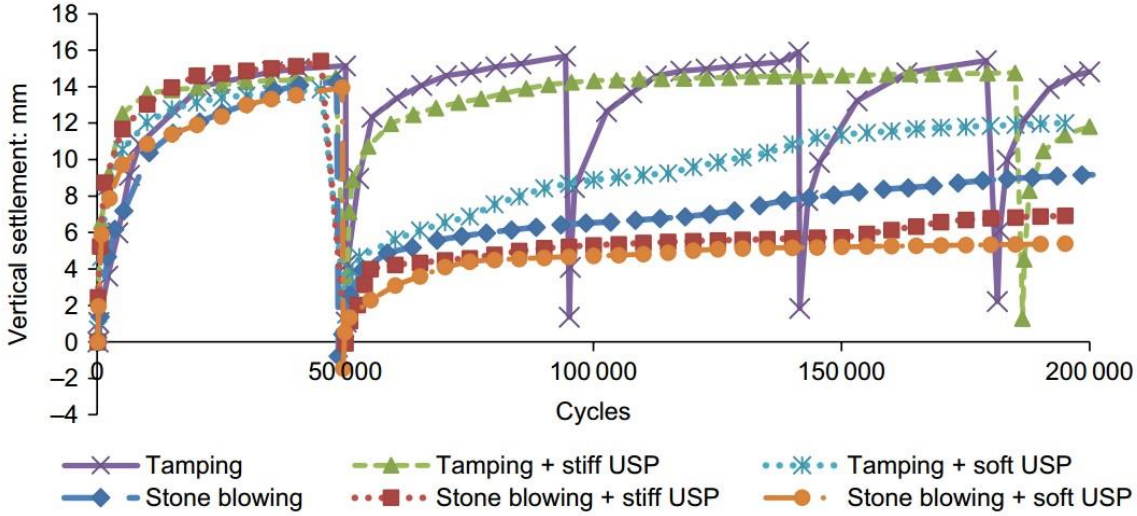

Figure 2.27: Comparison of tamping and stoneblowing on vertical settlement with stiff and soft under-sleeper pads (USP) (from Sol-Sanchez et al., 2016a).

Recent studies have also investigated the potential effectiveness of using different material such as rubber pellets instead of stones for stoneblowing in laboratory ballast box testing (Sol-Sanchez et al., 2016b). Figure 2.28 shows that replacing stones with rubber pellets can be effective in further reducing the ballast settlement after resurfacing by combining the benefits of stoneblowing and USPs. For example, after resurfacing (5,000 cycles), conventional stoneblowing experienced about 9 mm of settlement after 150,000 cycles (200,000 cycles in Figure 2.28), while stoneblowing plus the use of 50% rubber pellets (RP) resulted in about 2.5 mm, about a 70% decrease.

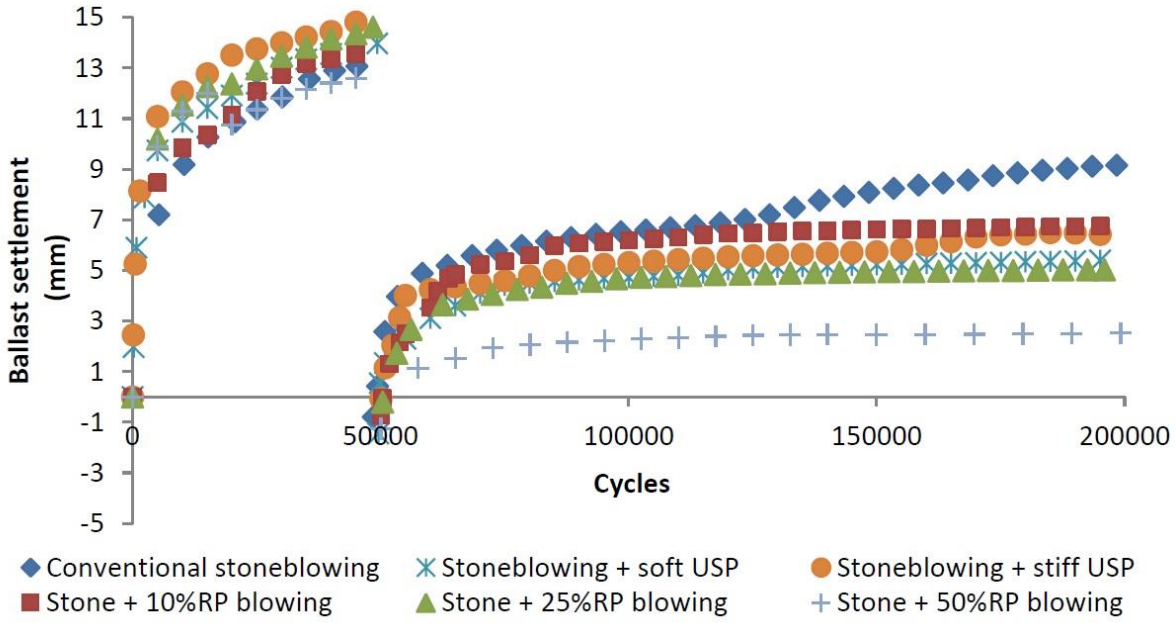

Figure 2.28: Effect of rubber pellets (RB) and under-sleeper pads (USP) on laboratory ballast settlement (from Sol-Sanchez et al., 2016b).

2.4 Transition Zones

The Transition Zone subsection expands upon previous sections by explaining how the interaction between the track structure and fixed structures can increase settlement near the abutment and represents a greater maintenance problem than the surrounding track. The subsection covers the following topics: (1) definitions and examples, (2) transition zone behavior, (3) mechanisms of increased settlement, and (4) design and remedial techniques.

2.4.1 Definition and Examples

Transition zones are generally defined as railroad track locations that experience a rapid change in track structure, often resulting in differential stiffness, settlement, and damping at that location. Examples of transition zones include bridges, asphalt crossings, culverts, transitions from slab to ballasted track, and transitions from concrete crossties to timber crossties. Figure 2.29 displays four various different types of transition zones. This thesis focuses on bridge transition zones as they typically represent the greatest change in track stiffness and damping because the bridge structure is placed on deep foundations and will generally experience little to no movement. However, all track transitions display similar behavioral attributes because of the rapid change in track structure but with varying degrees of severity.

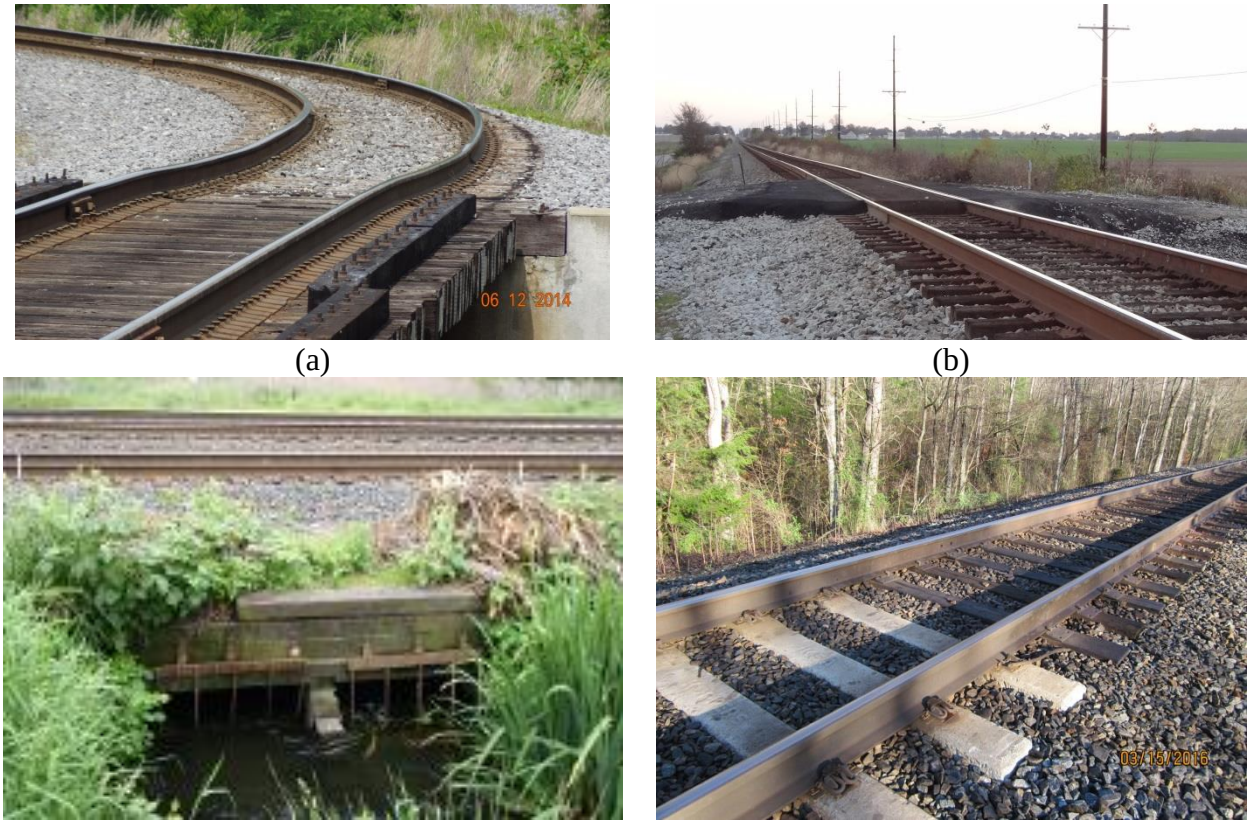

(a) (b)

(c) (d)

Figure 2.29: Examples of transition zones: (a) bridge, (b) asphalt crossing, (c) culvert, and (d) concrete to timber crosstie track. Photograph (c) courtesy of (portlandoregon.gov).

To clarify terminology, the term *transition zone* refers to the region that "transitions" from the open track to the fixed structure. This is typically the first 20 or 30 feet away from the

fixed structure and *open track* is the track beyond that, as illustrated in Figure 2.30. The transition zone a train uses to enter a fixed structure is called the *approach* and the transition zone a train uses to exit a fixed structure is called the *exit*, but is often used interchangeably because in some tracks, trains can move in both directions. The approach transition is typically emphasized, as it is in this thesis, because they usually degrade faster than exits (Mishra et al., 2012). Additionally, the term transition zone can refer to both the region specifically designed to "transition" from the open track to fixed structure, i.e. soil stiffening or larger ties, or the naturally forming "transition", which typically results in increased settlement. The distance of transitions can vary significantly from site to site, e.g. 6 feet to 30 ft.

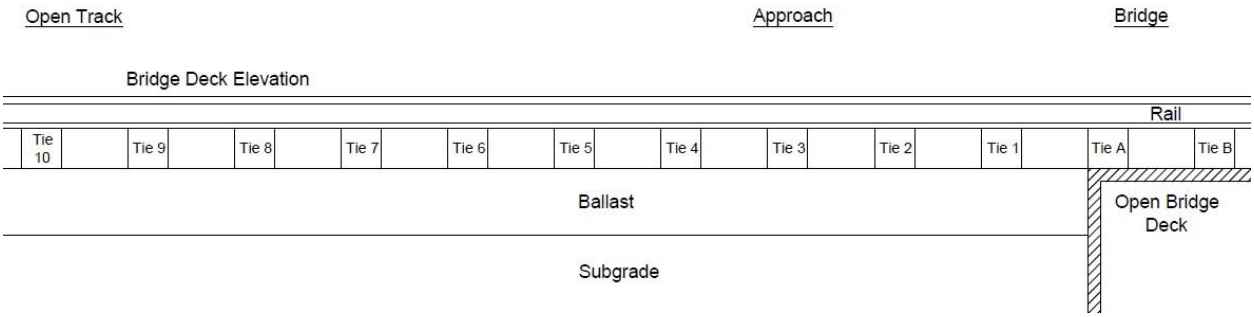

Figure 2.30: Diagram of bridge transition zone.

2.4.2 Transition Zone Behavior

Transition zones are recognized as problematic track locations because they are often associated with reoccurring track geometry problems. Kerr (2003) states about 50% of transition zones experience track geometry problems and Sasaoka and Davis (2005) estimated that in 2005, $200 million is spent annually on track transition maintenance. The track geometry defects often manifests as profile problems (see Chapter 2.3.4) in which greater or accelerated track settlement is observed in the approach region and can produce a "dip" in the track. Two photographs of "dipped" bridge approaches are displayed in Figure 2.31(a) and (b). Diagrams showing the difference between even substructure settlement and uneven substructure settlement within the transition zone are displayed in Figure 2.31(c) and (d). The first example is referred to as a "bump" while the second example is refereed as a "dip" (Nicks, 2009).

For bridges and culverts, the track surrounding the fixed structure will settle from repeated train loading because the track substructure consists of granular and earthen materials (Chapter 2.3.3) while the fixed structure will not because it is placed on deep foundations. This

results in differential settlement at the fixed structure-approach interface. In addition, the differential stiffness and damping between the bridge and surrounding track can increase dynamic loads on the fixed structure and approach track, which degrades track components and increases ballast degradation. Blocked drainage from the bridge abutment can wet and foul the approach ballast. The increased loading, increased degradation of track components and ballast, and increased moisture and fouling of the ballast in the approach can further increase and accelerate the settlement of the approach track and results in the development of a “dip” in the approach region.

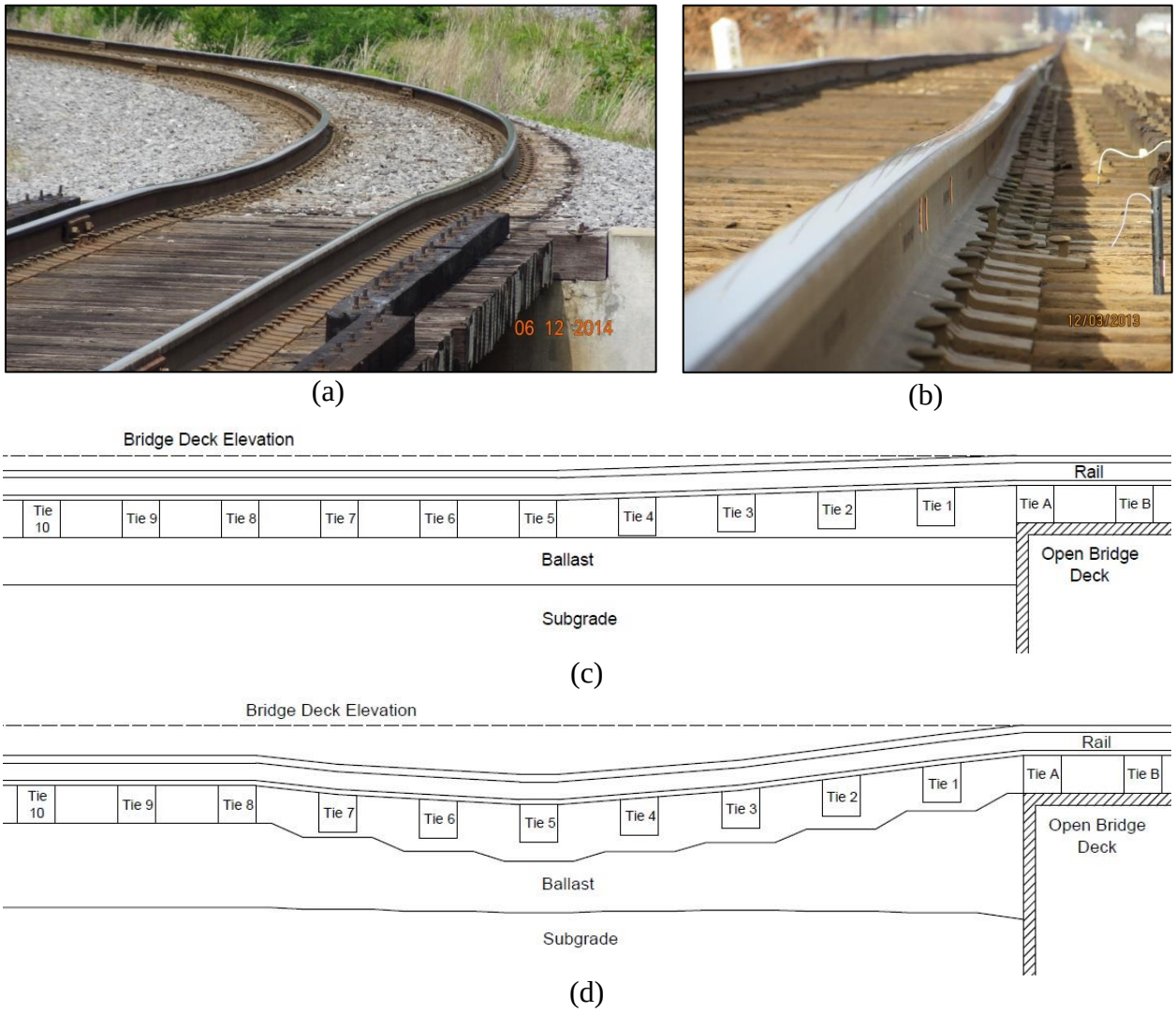

Figure 2.31: **(a,b) two photographs of transition zone settlement and two diagrams of transition zone settlement: (c) no additional settlement in approach and (d) additional settlement in the approach.**

Four examples of measured transition zone behavior are displayed in Figures 2.32 through 2.34. All the presented examples show greater transient displacements, i.e. track deflections from train passage, in the approach than open track. However, the additional displacement is often not apparent from settlement or top-of-rail (TOR) analyses, i.e. rail elevation with no train loading. Figure 2.32 compares the accumulated settlement (long-term, no train loading) and transient displacement (short-term, train loading) of an approach with a hot-mixed asphalt (HMA) ballast underlayment (Li and Davis, 2005). The TOR settlement results show similar or slightly greater settlements in the approach (-2 to -5 meters / -6.5 to 16.5 feet from bridge) while transient displacements in the approach are about two times the displacement of the surrounding track (4 to 6 mm v. 3 to 3.5 mm).

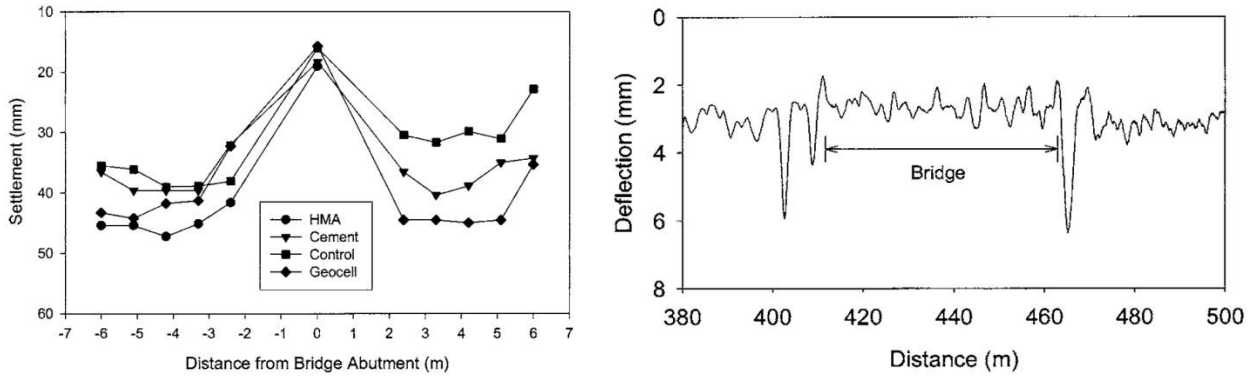

(a) (b)

Figure 2.32: Comparison of (a) settlement profiles and (b) deflection profiles of HMA approach (from Li and Davis, 2005).

Figure 2.33 shows similar behavior at a culvert transition zone with historical track geometry problems. While the measured TOR settlement values are similar in the approach and open track, the approach displacements are almost 6 times the open track value (9 mm v. 1.5 mm) (Coehlo et al., 2011). The study acknowledged the presence and possible influence of hanging ties in the approach.

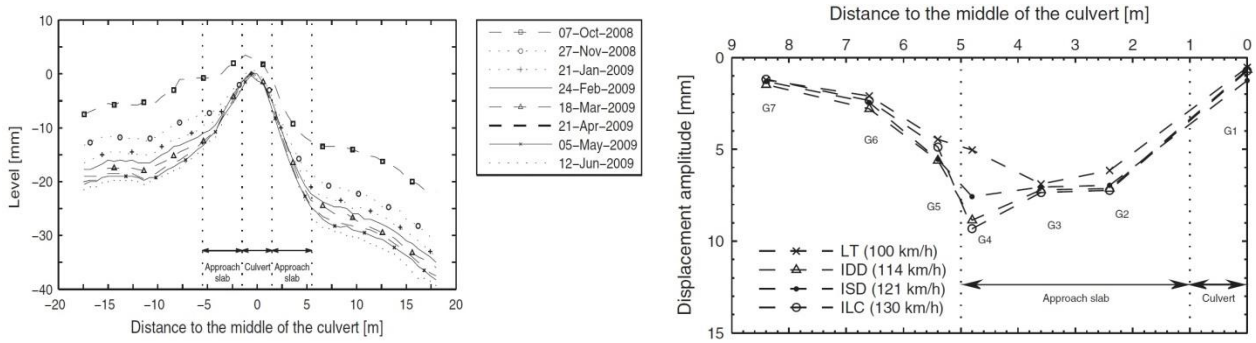

(a) (b)

Figure 2.33: (a) Vertical settlements with time from level-lining and (b) maximum vertical displacements for various train passages (from Coehlo et al., 2011).

Figure 2.34(a) shows an example of an asphalt crossing where the displacement under approach sleepers (ties) 5 and 6 (5 mm) are displacing about five times the magnitude of the open track sleepers/ties (1 mm). Figure 2.34(b) shows a gradual increase then gradual decrease in sleeper (tie) displacement away from a bridge transition zone. The approach experiences about twice the transient displacement magnitude than the open track.

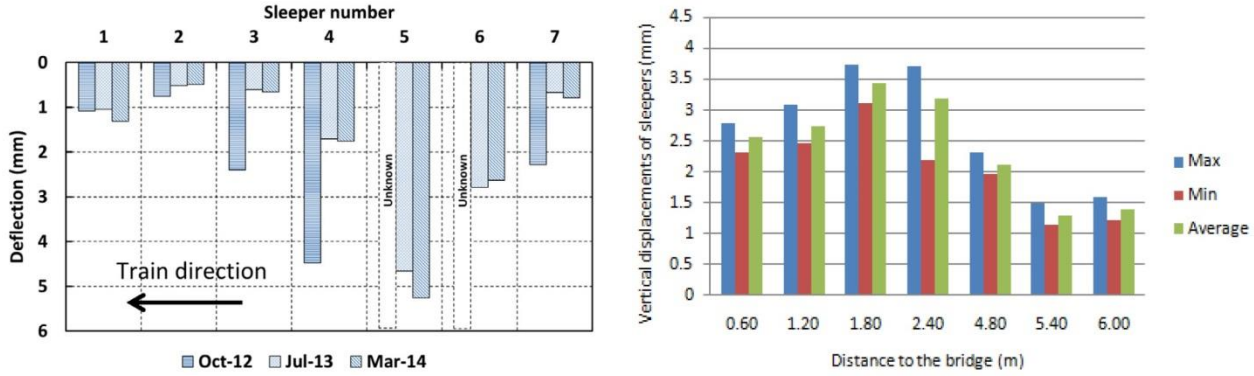

(a) (b)

Figure 2.34: Two examples of transition zone tie/sleeper transient displacements (a) from Le Pen et al. (2014) and (b) Markine et al. (2014).

These examples illustrate that the additional approach displacement can vary in magnitude relative to the open track and that the additional approach ballast settlement may not be apparent from top-of-rail (TOR) analyses because of hanging ties. Hanging ties, also known as unsupported ties, develop in locations with localized approach settlement because the stiff rail is supported from both the fixed structure and open track, which experiences lesser amounts of substructure settlement (see Figure 2.31d). The percentage of transition zones that have

additional approach displacements is unknown but the majority of instrumented problematic transition zones display this behavior.

2.4.3 Mechanisms of Increased Settlement

Multiple mechanisms/root causes are attributed to the accelerated settlement within bridge approaches. While the attributed mechanisms/root causes can vary between researchers (Li and Davis, 2005; Sasaoka and Davis, 2005; Plotkin and Davis, 2008; Nicks, 2009; Hyslip et al., 2009; Li et al., 2009; Coelho et al., 2011), there is a consensus that the mechanisms are site specific. Proposed root causes include: differential track stiffness, differential track damping, differential track modulus, differential ballast settlements, geotechnical issues in the approach, inadequate quality of approach fill, impact loads in the approach, inadequate ballast material, inadequate drainage, abutment type, bridge joints in approach, traffic considerations, and inadequate quality of construction. All these factors can contribute to accelerated settlement of the approach but specific factors and their interaction with other factors can vary significantly by site.

In this thesis, the proposed mechanisms are roughly separated into four main categories to aid understanding:

(a) substructure settlement,
(b) increased loading within the approach,
(c) increased settlement within the approach from reduced-performance substructure materials and conditions, and
(d) construction considerations.

Only the first three categories will be addressed in the thesis. To further clarify, (a) "substructure settlement" refers to settlement that would naturally occur even with no fixed structure, i.e. open track (Chapter 2.3.3), while (c) "increased settlement within the approach" refers to additional approach settlement from primary and secondary effects of the fixed structure. This includes ballast and track component degradation, fouled ballast, blocked drainage, and hanging ties.

2.4.3.1 Substructure Settlement

The first general category of substructure settlement is the expected settlement of the ballast, subballast, and subgrade layers from repeated train loadings. The behavior and settlement magnitudes of ballast are addressed in Chapter 2.3.3. This mechanism is important because differential settlement between the fixed structure and approach will occur to some degree in every transition zone and, if the differential settlement are large enough, is believed to initiate increased loading in the approach and accelerate ballast degradation (Plotkin and Davis, 2008; Nicks, 2009). Therefore, it is desirable to minimize initial substructure settlements around fixed structures to prevent subsequent problems.

One uncertainty related to substructure settlement is the layer in which the majority of substructure settlement occurs. While it is expected to occur in both the ballast and subgrade to some degree, there are disagreements which layer contributes the most settlement. Figure 2.35 show transition zone cross-sections with the majority of settlement occurring the subgrade (Figure 2.35a) and ballast (Figure 2.35b). Determining this is imperative because selecting an effective solution requires knowing the location of settlement. For example, if the majority of settlement occurs in the subgrade, a ballast solution will not solve the problem or vice versa. Unfortunately, measuring the settlement of substructure layers is usually undesirable due to increased effort, cost, and the need to shut down the track for extended periods so little knowledge is available. Measurements from open track sites reported by Selig and Waters (1994) states for existing track the majority of track settlement occurs in the ballast. This is explained by the subgrade being fully compacted from previous train loadings while the ballast must be periodically disturbed from resurfacing to maintain track geometry. Subgrade settlements are often attributed to new track in which the subgrade will compact from train loading. This is often amplified due to the difficulty of compacting fill layers near a fixed structure.

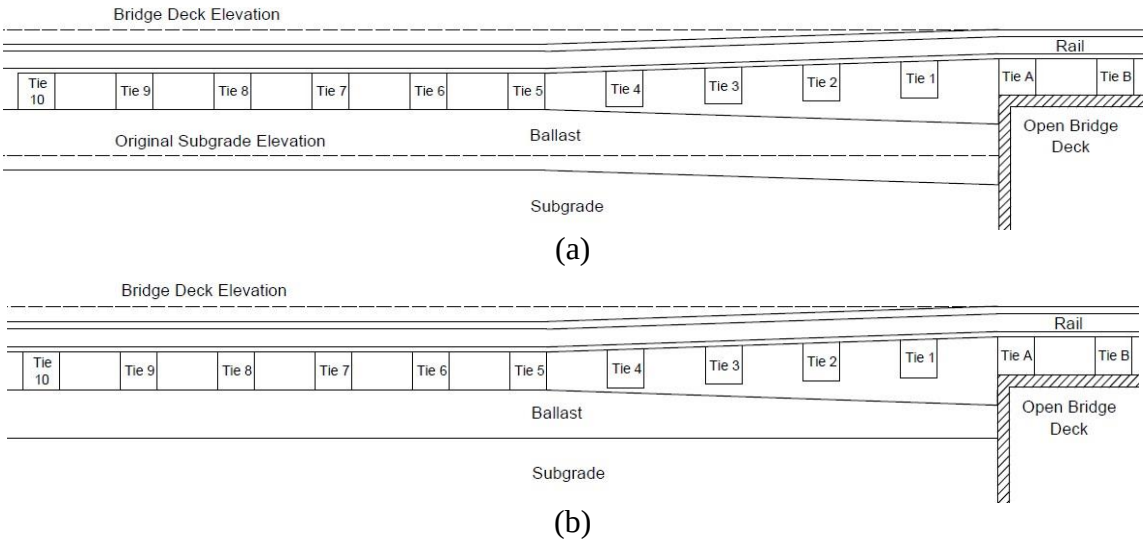

Figure 2.35: Diagrams of settlement occurring in (a) subgrade and (b) ballast.

2.4.3.2 Increased Loads in Approach

The second general category is increased loading within the approach. Increased loading can result from a number of different loading mechanisms, including:

(1) wheel-rail impacts,
(2) train bouncing/oscillations,
(3) rapid change in axle elevation,
(4) tie load concentrations, and
(5) tie-ballast impact.

While these loading mechanisms are not exclusive to transition zones, the conditions within transition zones often increase the occurrence of these five loading mechanisms. The first three mechanisms increase vehicle/wheel loading on the rail while the latter two mechanisms increase tie loading on the ballast. To clarify, ballast settlements respond to tie-ballast pressure and not necessarily the wheel load or even tie load because load is not always evenly distributed throughout the track or tie, especially in cases of differential ballast settlement (see Chapter 2.3.2).

Increased vehicle/wheel loading, i.e. mechanisms (1) through (3), can be measured two ways. The first method involves instrumenting wheelsets with strain gauges and/or accelerometers (see Figure 2.36a). This emphasizes wheelset behavior and records load variations across long stretches of track. Locations with increased loads such as transitions can then be identified by comparing axle load along the distance of track. The second method involves instrumenting the

rail with strain gauges (see Figure 2.36b). This is helpful for determining the load that various track components experience at a single track location and can be used as inputs for settlement analyses and numerical models. Increased tie loading, i.e. mechanisms (4) and (5), have the advantage of physically increasing the load on the ballast and measurement primarily involves placing pressuring plates underneath the tie (see Figure 2.36c), but this also disturbs the track and changes the loading environment. Due to the relative ease of vehicle load monitoring as opposed to tie load monitoring and historic emphasis on vehicle and rail issues over substructure issues, previous work has largely emphasized increased vehicle loads, i.e. loading mechanisms (1) through (3). Additionally, numerical modeling can investigate factors that increase load in both the vehicle and track but much previous work has emphasized vehicle loading over tie loading.

(a) (b) (c)

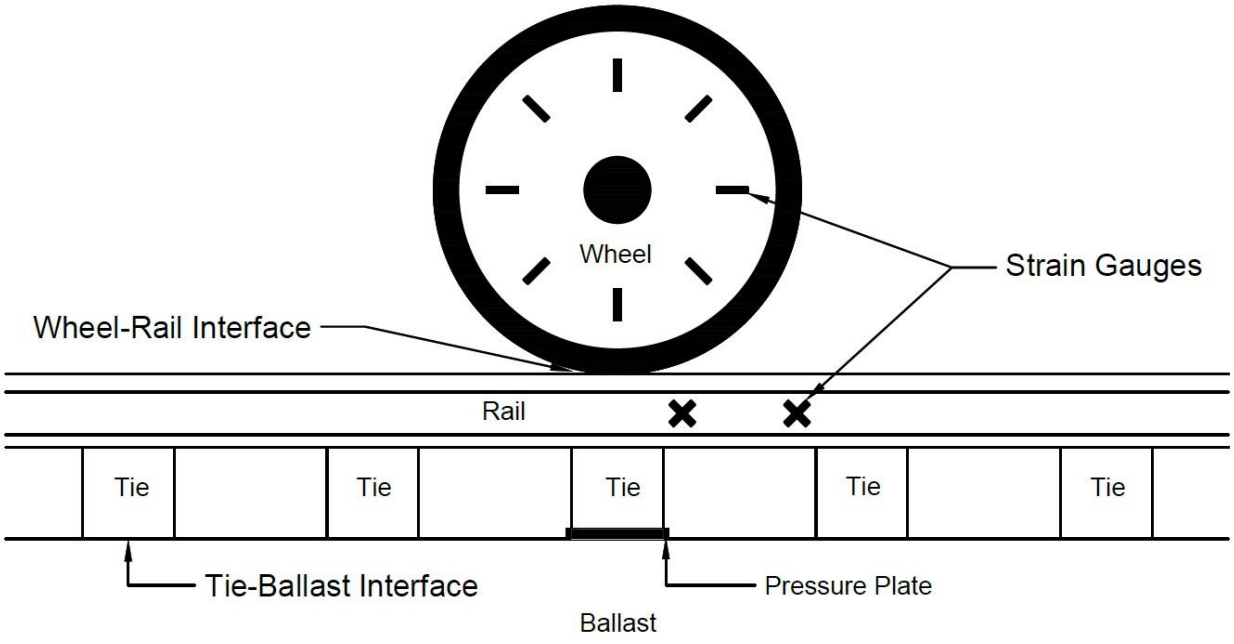

(d)

Figure 2.36: Photographs showing (a) instrumented wheelset (from Plotkin and Davis, 2008), (b) instrumented rail with strain gauges, (c) pressure plates beneath tie, and (d) their location on track.

To explain accelerated bridge approach settlement, increased tie-ballast pressures must be concentrated within the approach and be large enough to have a noticeable effect. Proving this explanation is problematic in a few ways. First, the tie-ballast pressure is difficult to directly measure so the majority of previous work has typically used vehicle-track loading measurements and assumed intimate tie-ballast contact to calculate the tie-ballast load, i.e. tie load = 40% wheel load, and equal pressures along tie-ballast interface (see Chapter 2.3.2). However, it is unclear how often these assumptions hold, especially in transition zones. If this assumption is violated, a wide range of possible wheel load distributions are possible, including the following scenarios:

(1) increased wheel loads and increased ballast pressures, (2) increased wheel loads but no increase in ballast pressure, and (3) no increase in wheel load but increase in ballast pressure. This is illustrated in Figure 2.37 and suggests tie-ballast pressures are generally related to wheel and tie loads, but can be decoupled.

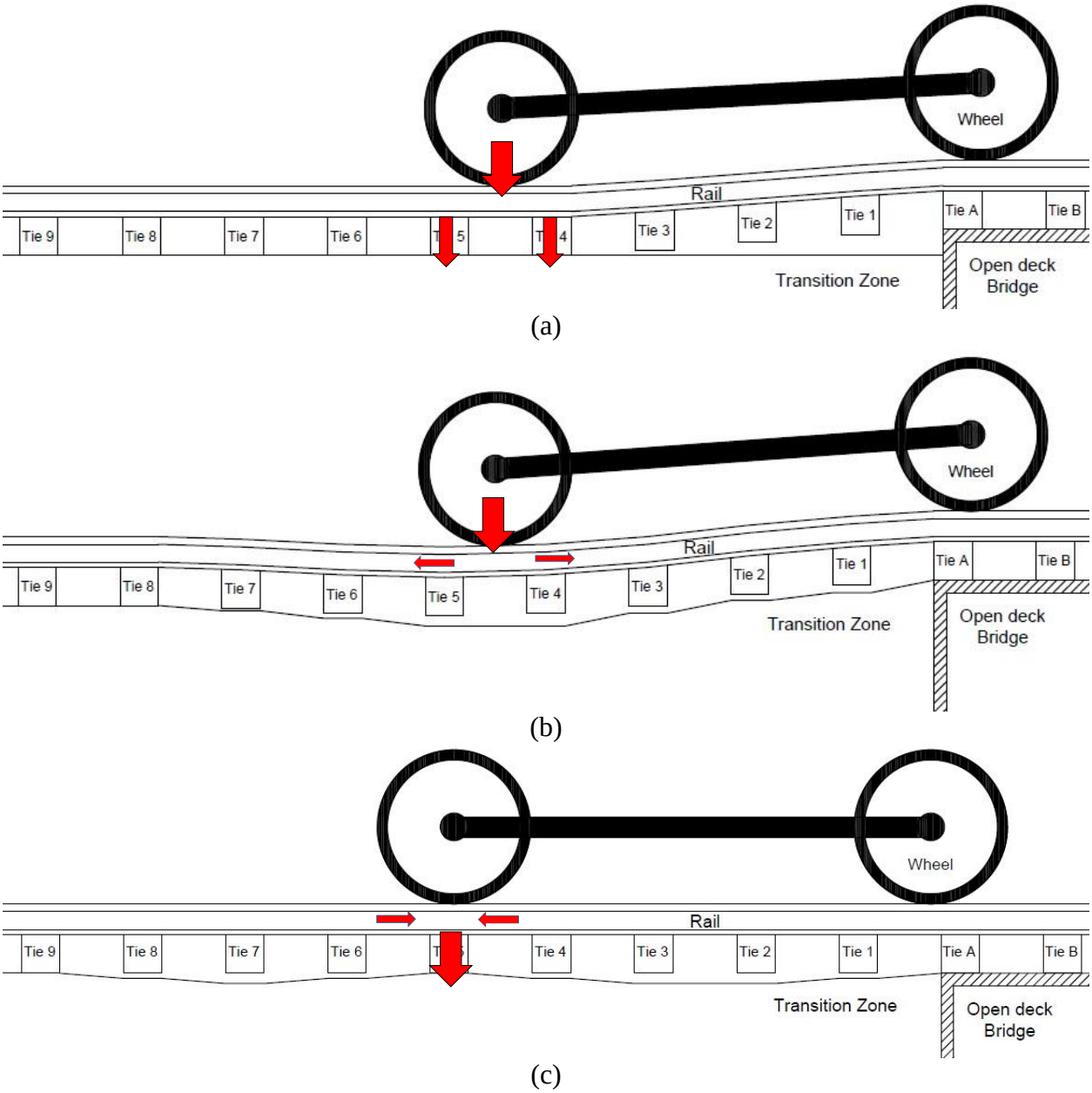

Figure 2.37: Diagrams showing various load paths and potential for increased loads.

Second, the relation between tie-ballast pressure and ballast settlement is highly dependent on the ballast conditions. As shown in Chapter 2.2.3, ballast settlements can vary by over 1000% depending the degree, moisture content, and material of fouling, even with identical loading. Tie-ballast gaps may also significantly increase ballast settlements without increasing loading (Chapter 2.2.4). This means an increase in ballast settlement may be due to either increased loading or reduced-performance ballast and current load measurements, ballast sampling, and testing techniques make it difficult to definitively show which factor controls increased settlement.

Despite these limitations, thresholds are helpful to provide context to increased loading in track. A study by Davis et al. (2007) concluded that a 50% increase in tie-ballast pressure is required to accelerate track settlement by 25%, which is common threshold for defining a problematic track transition location. This threshold assumes similar ballast conditions in the approach and open track but can applicable for transitions with newly laid ballast or similar approach and open track ballast conditions.

With identifying a few uncertainties relating increased loading to increased settlement, a review of the five mechanisms of increased loading are described below:

The first mechanism, wheel-rail impacts, is produced from multiple sources ranging from wheel irregularities to rail joints (Figure 2.38). These impacts are typically considered high-magnitude and high-frequency and often referred in the literature to P1 loading (Remennikov and Kaewunruen, 2008). These impacts are believed to break track components, crack ties, and generally degrade the superstructure (Sasaoka and Davis, 2005). Measurements from Wheel Impact Load Detector (WILD) data by Van Dyk et al. (2016) are presented in Figure 2.39 and show the percentage of impacts expected in track. WILD sites are track locations that detect wheel flats by measuring the peak and nominal dynamic load of each passing wheel. The loads are measured with strain gauges on the rails along six to eight consecutive cribs. If a wheel has a flat spot, at least one of the instrumented cribs should record an increased load. The nominal load is determined by taking an average of all measurement locations and is used as the dynamic wheel load for analysis inputs.

The plot in Figure 2.39 compares the nominal load and the peak load of multiple types of trains in the United States. While the vast majority of wheels show little difference between the nominal and peak loads, i.e. impact factor (IF) = peak/nominal = ~1.0, wheel irregularities can

increase wheel loads by up to five times the static load. Rail joints are another location of increased loading because of unconnected or weak connection of rail joints and welds. AREMA (2016) suggests that rail joints can increase wheel loads be a factor of three.

This mechanism is not exclusive to transition zones and is likely evenly distributed along the track but is important because they can amplify existing increased loads from other sources. For example, a rail joint within a transition zone can add an additional mechanism of increased loading. Additionally, the difference between increased loads from wheel irregularities or other vehicle and increased loads from track structural issues is important for site diagnoses later in the thesis (Chapter 4).

(a) (b)

Figure 2.38: Photograph of wheel flat (TSBC, 2007) and rail joint with joint bar.

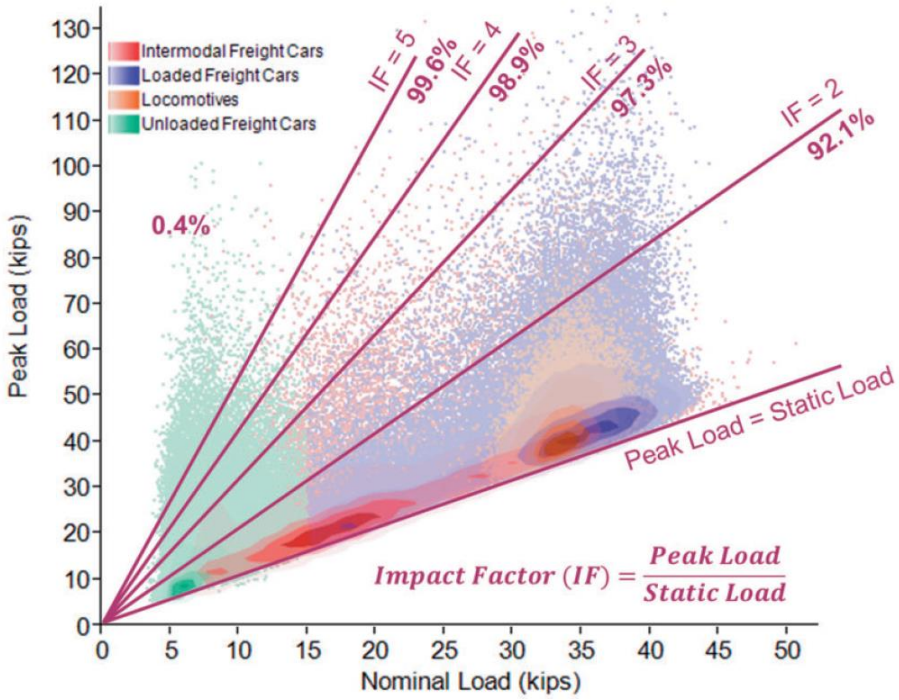

Figure 2.39: Relationship between peak and nominal wheel loads (from Van Dyk et al., 2016).

The second mechanism of train oscillation/bouncing occurs from periodic differential settlement. Examples of this would be evenly spaced rail joints, natural variation in track support, or vehicle dynamics. These loadings are considered lower magnitude and frequency and are referred to as P2 loads in the literature (Remennikov and Kaewunruen, 2008). These loads are generally considered to degrade the ballast and track geometry (Sasaoka and Davis, 2005).

Figures 2.40 and 2.41 from Plotkin and Davis (2008) and Fröhling (1998) illustrate three examples of the natural variation of vertical wheel load in track. Figure 2.40 shows a T-16, a train car with instrumented wheelsets, passing over two ballasted deck bridges at 108 mph near Baltimore, MD. As observed the vertical force varies from about 15 to 20 kips (67 to 89 kN), a 5-kip (22-kN) variation, and appears to have a periodic oscillation. As a note, the bridge approaches did not show any significant rail profile deviations and increased loads were not observed. Figure 2.41 shows the dynamic wheel load from an instrumented car in South Africa. The results show about a 10-kip (45-kN) variation between 28 to 38 kips (125 to 170 kN). These studies suggest that track load naturally varies by about 15%.

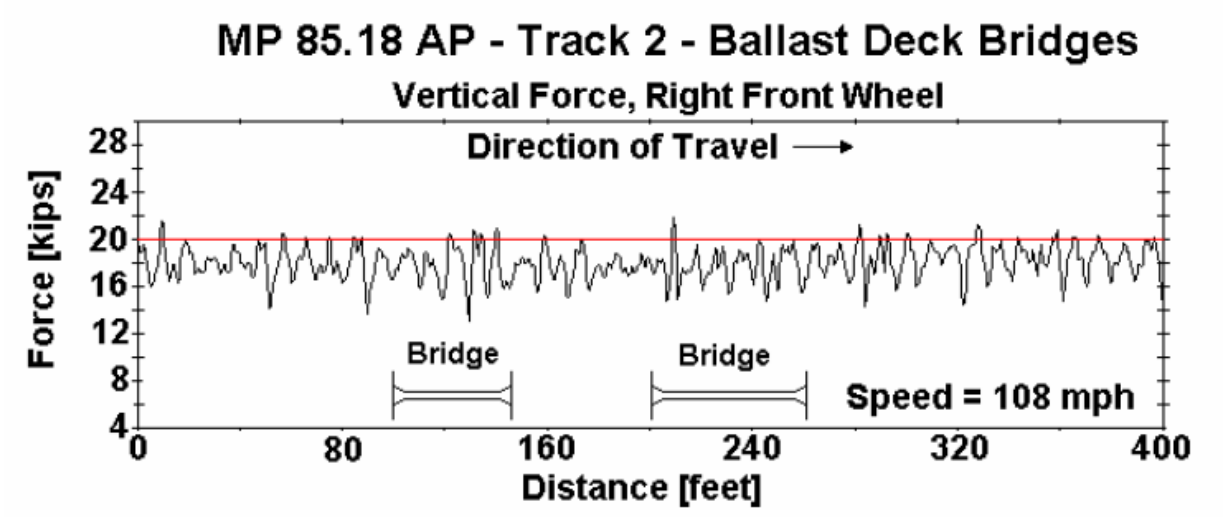

(a)

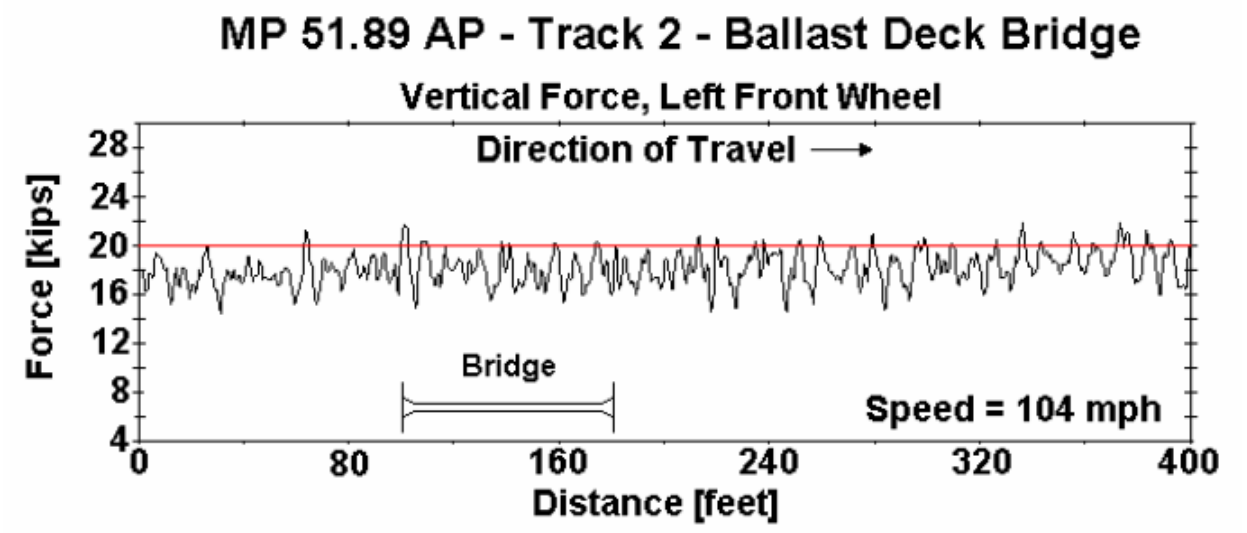

(b)

Figure 2.40: Two examples of natural variation in vertical wheel force in track (from Plotkin and Davis, 2008).

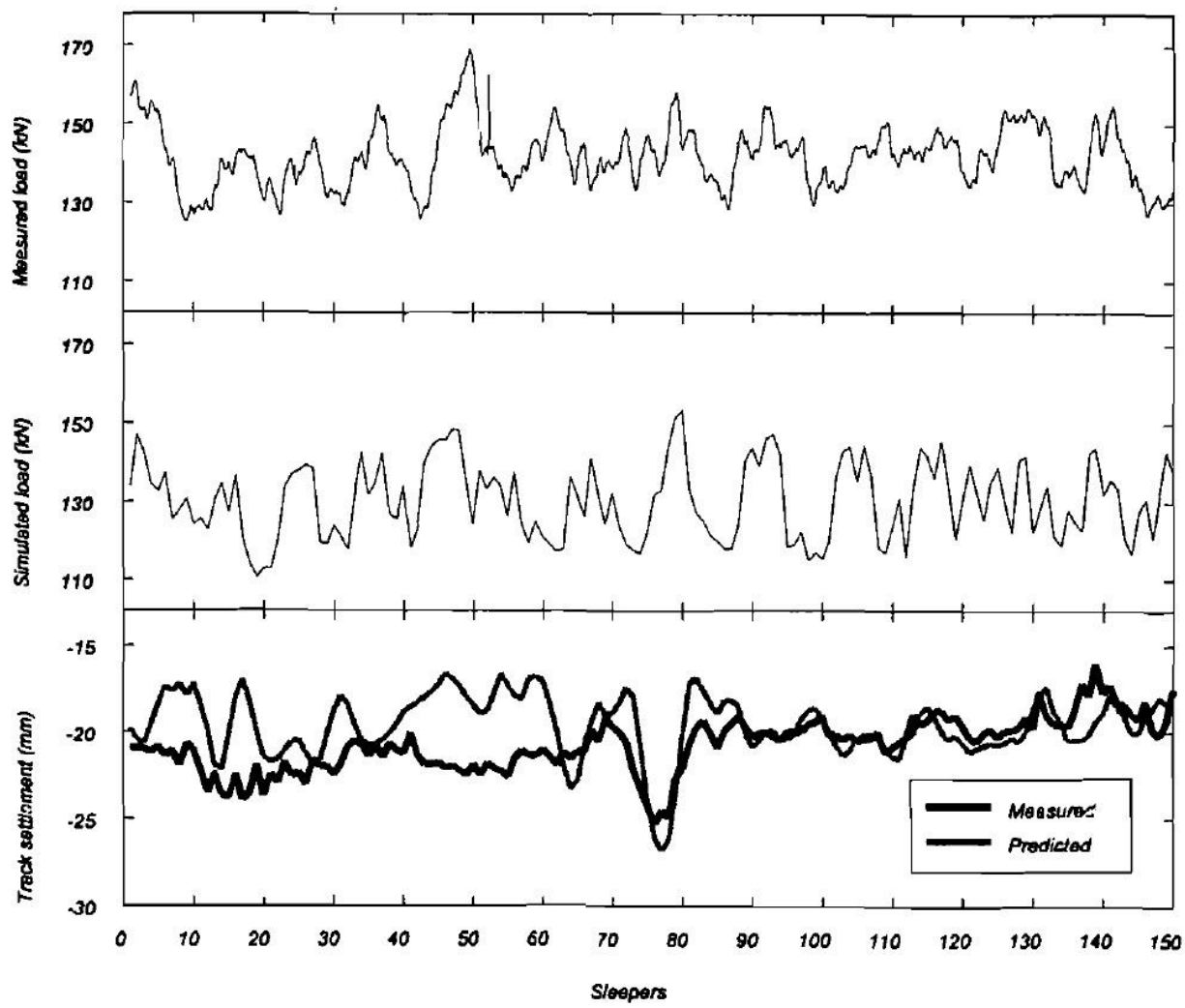

Figure 2.41: Example of natural variation in load and stiffness in track (from Fröhling, 1998).

Presenting this mechanism is important to emphasize that variations and increased loads are expected naturally in track and should serve as a minimal threshold before considering the influence of increased loads from subsequent mechanisms. For example, if a 15% variation of wheel load is expected in all track, a 10% increase in wheel load from a bridge approach will likely not explain the accelerated track settlement in that region because it is inside the expected natural variation.

Additionally, train oscillation/bouncing have been suggested as a potential accelerant of transition zone settlement in tangent track at locations with multiple closely spaced bridges (Kerr and Bathurst, 2001). When the train leaves one bridge, the differential stiffness and settlement

between the bridge and exit track can produce train load oscillations that then can acceleration degradation of subsequent approaches.

The third mechanism, rapid change in axle elevation, produces increased vehicle/wheel loads from rapid changes in rail elevation and is one of the commonly investigated explanations for increased loads at bridge approaches. For example, if the front axle elevates when entering a bridge, a temporary increase in load on the bridge and the back axle will follow (Figure 2.42). In the opposite manner, if the vehicle exits the higher elevated bridge to lower elevated exit, the front axle will "fall off" the bridge (Figure 2.42). The location and magnitude of the temporary increase in load will depend on train speed, axle distance, and difference in axle elevation (Nicks, 2009). Unlike the previous two vehicle mechanisms, this mechanism is typically experienced at track locations with poor track geometry or rapid changes in stiffness or rail elevation, and therefore will be concentrated in transition zones.

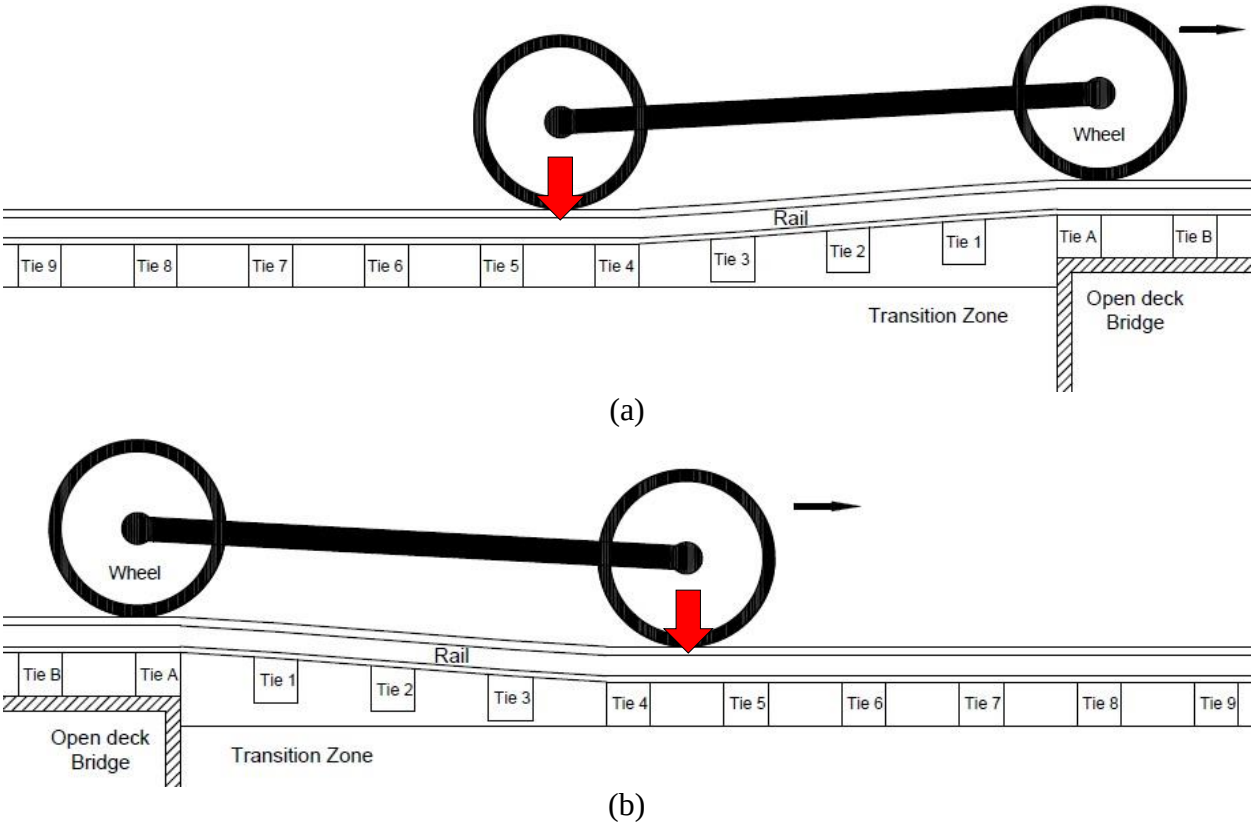

Figure 2.42: Diagrams of train truck (a) entering and (b) exiting bridge.

While often considered separate mechanisms, increased loads from differential stiffness and settlement are incorporated into the same mechanism of rapid change in axle elevation because the underlying mechanism is the same. To initially summarize the results presented below, the majority of previous analyses has emphasized the effect of differential stiffness but results rarely show a significant increase in load (<15% increase). However, the increase in load from differential settlement has been shown to have a potential effect (>50% increase). This bolsters the argument that natural track settlement (category a) can initiate increased loading in the approach (category b).

For bridge approaches, there are two locations of increased load from the rapid change in axle elevation mechanism: (1) front of bridge from the front axle and (2) approach from the back axle. The increased load on the (1) front of the bridge has been shown observationally from broken track components (Kerr and Moorony, 1993; Cantrell and Bourgonje, 2014) and numerically from various numerical models (Kerr and Moorony, 1993; Hunt, 1997; Banimahd et al., 2011). While this is important for bridge structures, it is not relevant to bridge approach settlement analyses. This means numerical analyses investigating this mechanism must simulate the entire train truck, i.e. secondary suspension system, and not just a single axle (see Figure 2.42).

To emphasize this point, Hunt (1997) used a Winkler model to investigate the progressive settlement of a transition zone and its effect on axle and tie loads. The majority of the analysis was simulated using a single moving axle. The analysis began with 2 mm of differential settlement between the bridge and approach to represent the rapid settlement after tamping and then the differential elevation increased with increasing load cycles (see Figure 2.43a). Figure 2.43b displays the variation in tie (sleeper) force over the course of the analysis. The first cycle (N=1) shows a greater load on the front of the bridge (2 m) but then reduces over time, and the approach region (+2 to -4 m) did not show increased loads during the analyses. The lack of increased loads is likely due to the ballast settling in a manner to reduce tie loads and the lack of coupling from front and back axles may have prevented any increased load in the approach. However, the analysis did show the development of hanging ties in the approach.

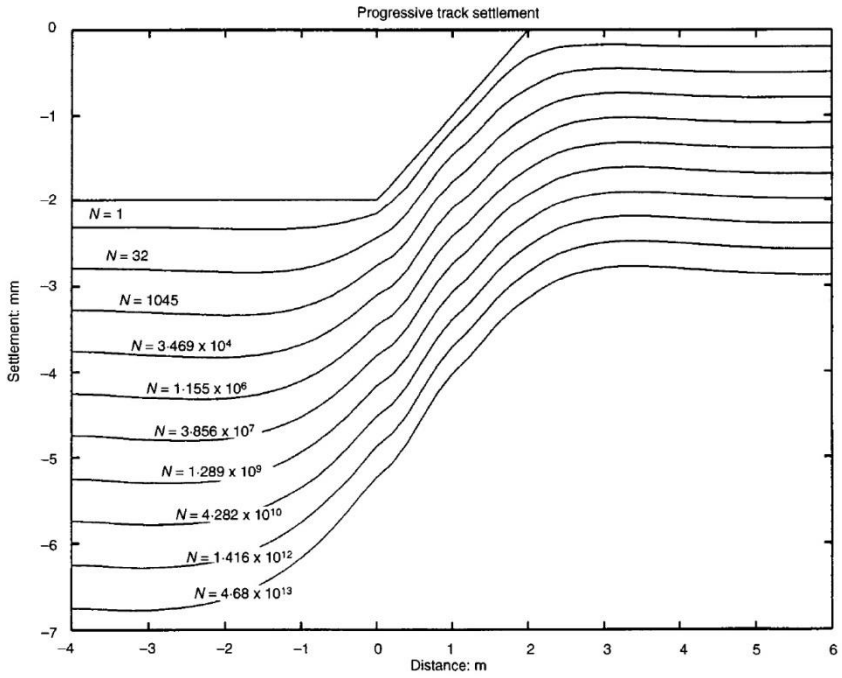

(a)

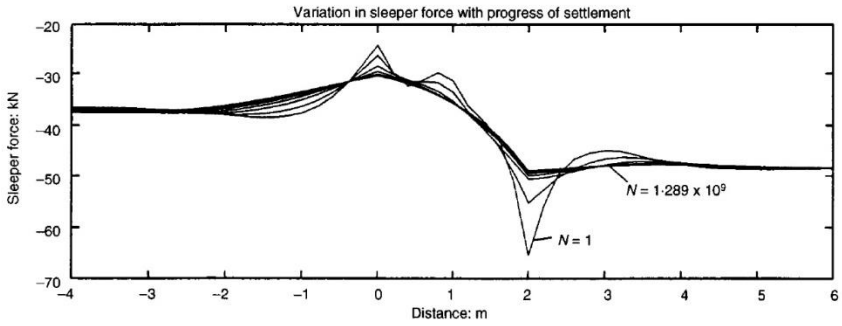

(b)

Figure 2.43: Progressive settlement analysis showing (a) rail elevations and (b) sleeper (tie) loads with increasing load cycles (from Hunt, 1997).

This mechanism of increased loads in the approach from the back axle is often investigated using numerical modeling techniques because it gives the user flexibility to isolate and vary multiple parameters, i.e. track stiffness, and allows the user to know all variables with certainty. Common studies involve simulating the increased load from stiffness and settlement differentials between the approach and bridge and determining which situations are detrimental and explain accelerated approach settlement.

Nicks (2009) performed an in-depth numerical analysis investigating increased loads from stiffness differences (Figure 2.30), bumps (Figure 2.31a), and dips (Figure 2.31b) at bridge approaches. For all three situations, loaded rail elevation difference and coupling from the front

and back axles produced increased back axle loads in the approach. The vehicle, representing a single train truck or secondary suspension system, moved at velocities of 50 mph. For the stiffness difference only analysis, the wheel load increased by 14%. For a bump consisting of a 1:150 slope (5.1 meters in length and 33 mm in height), the wheel load increased by 28%. For a dip consisting of a 1:150 slope is simulated (exact dimensions were not given but the dip appears to be 28 mm in depth), the wheel load increased by 45%. Figure 2.44(a) and (b) shows the wheel/rail reaction force in the case of stiffness differences and a dip.

A parametric analysis was also performed and some key remarks are: higher wheel loads were observed in the approach than in the exit, higher velocities resulted in higher wheel loads (up to 300% increase at 100 mph), and higher bump/dip slopes resulted in higher wheel loads (up to 360% increase at 1:50 bump slope).

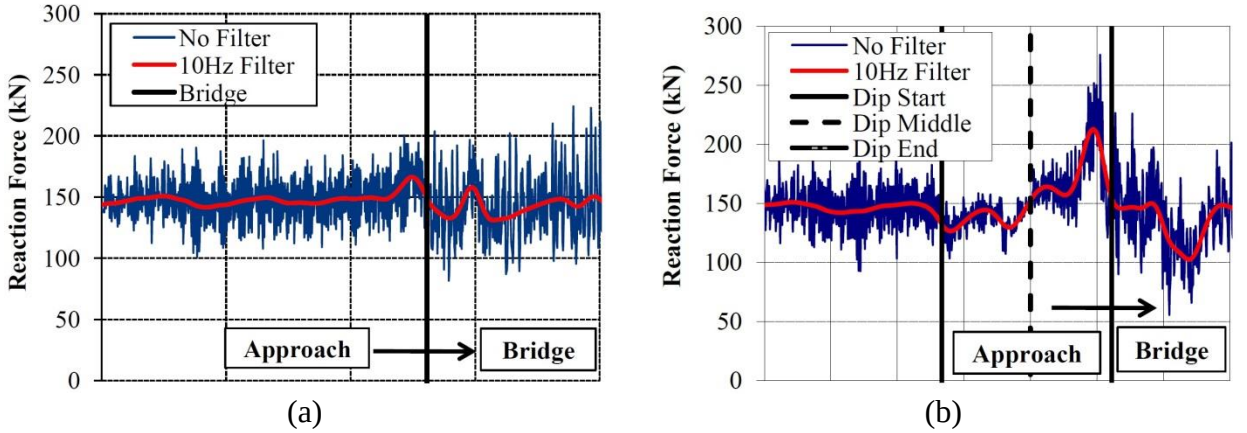

Figure 2.44: Back axle wheel/rail reaction force with (a) just stiffness difference and (b) a dip (from Nicks, 2009).

Wang et al. (2015) used a FEM model to show variations in wheel load, ballast pressure, and train body acceleration from variations in stiffness and settlement at a bridge approach. The results showed the load remained within the natural variation from only differential stiffness (no settlement) but fairly significant increases in wheel load and ballast pressures from 2 mm of settlement in the approach and exit. With 2 mm of settlement, wheel loads increased by 150% on the bridge and 75% in the approach (Figure 2.45a) while ballast pressure increased by 57% in the approach (Figure 2.45b).

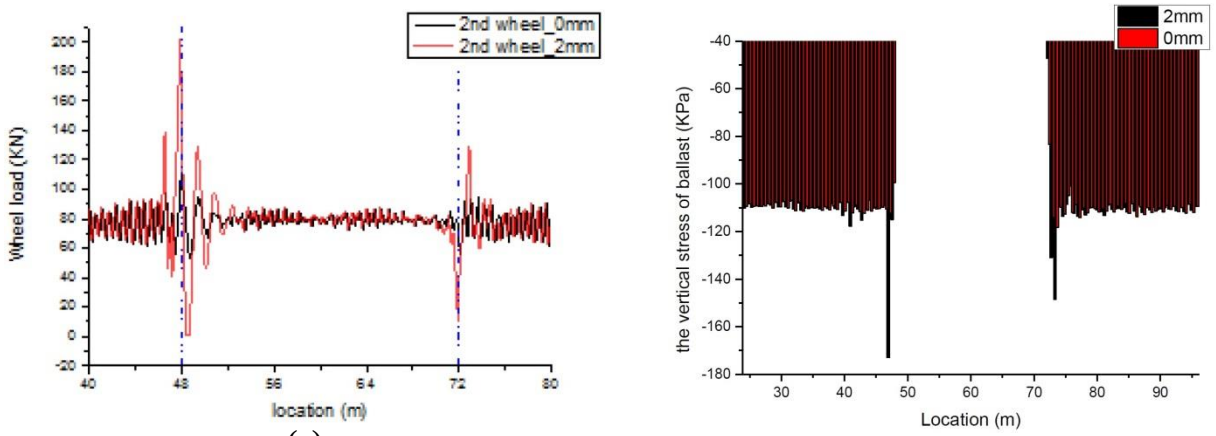

(a) (b)

Figure 2.45: Back axle (a) wheel loads and (b) ballast pressures from differential stiffness only (black) and 2 mm of differential settlement (red) (from Wang et al., 2015).

In 2008, Plotkin and Davis (2008) used five different methods in addition to a literature review to determine the potential effect of track stiffness on increased loads at transition zones. The methods included: (1) analysis with the NUCARS track/train dynamics computer program, (2) examination of vertical force and carbody acceleration data collected with instrumented wheelsets, (3) examination of settlement and top-of-rail profile data at bridge approaches, (4) simple beam defection equations and BOEF track defection theory, and (5) a train ride test. The investigation did not find any evidence that rapid changes in track stiffness produced applied loads great enough to explain the differential settlement at transition zones. The assumed benchmark of the study was a 50% increase in load to accelerate track settlement by 25% (Davis et al., 2007). This conclusion agrees with later numerical analyses by Nicks (2009) and Wang et al. (2015). The report suggests that track support and uneven tie loading may be influential and should be investigated in the future.

In summary, the third mechanism of "rapid change in axle elevation" appears to be significant when differential settlement between the bridge and approach already exist. Increased loads from differential stiffness is a commonly attributed to increased loads in the approach but no evidence appears to support this claim. This supports the claim that natural track settlement (category a) initiates increased loading in the approach (category b).

The fourth and fifth mechanisms of uneven tie loads and tie-ballast impacts have been mostly speculative (Plotkin and Davis, 2008; Nicks, 2009) because of the difficulty to directly

measure or numerically simulate increased tie loading. These mechanisms may be influential because they directly involve increased tie-ballast pressures.

A few numerical modeling simulations have investigated increased loading from unsupported ties. Lundqvist and Dahlberg (2005) investigated the potential increased loads from unsupported ties in open track. The results suggest that the load is transferred from the unsupported ties (sleepers) to the adjacent better supported ties (sleepers) and can increase (concentrate) loads from uneven load distribution. If a tie is completely unsupported, 1.0 mm gap underneath Tie 15 (middle row) in Figure 2.46, the unsupported tie will receive zero load and the load shifts to the adjacent tie load (Tie 16 / bottom row). This can increase tie loads on adjacent ties by up to 66% (50 kN to 83 kN). This increase in the adjacent tie load will increase with increasing train velocity and number of unsupported ties.

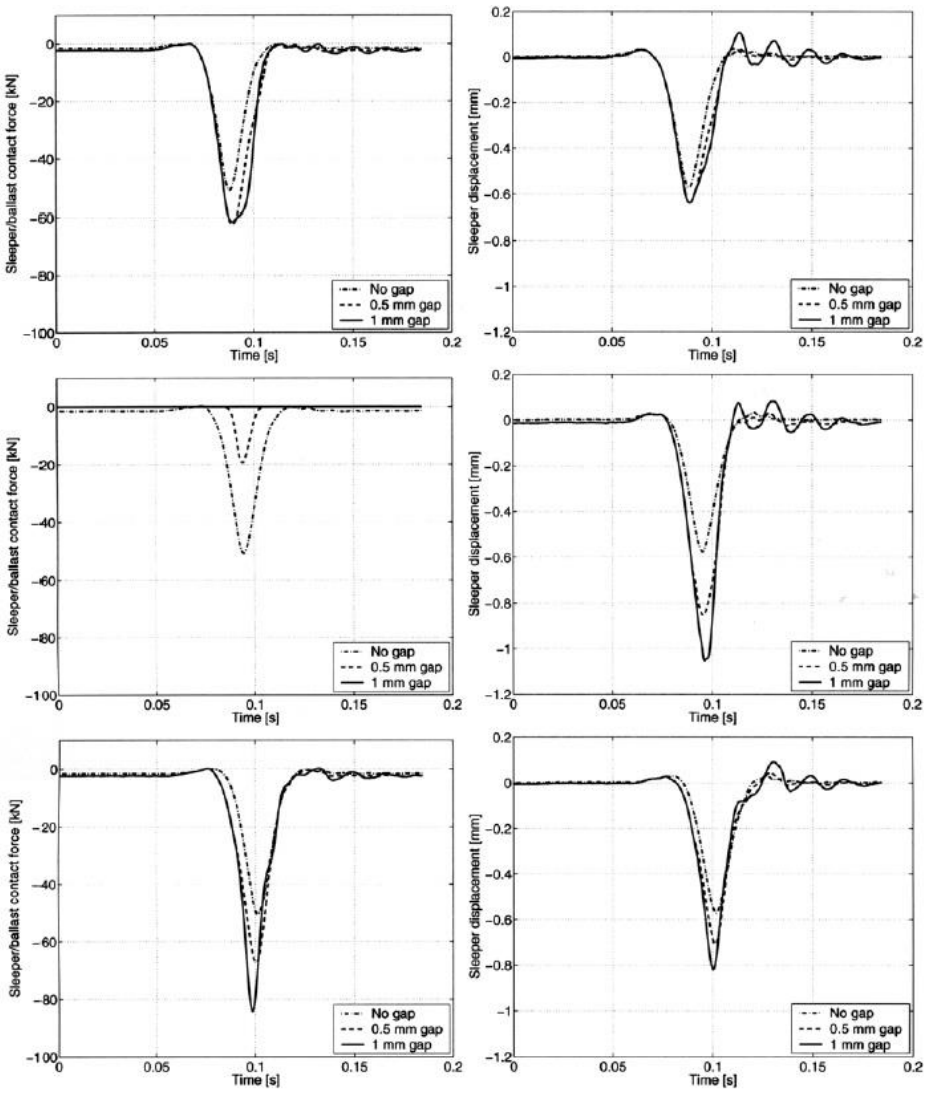

Figure 2.46: Sleeper load (left) and sleeper displacement (right) for Sleeper 14 (top), Sleeper 15 (middle), and Sleeper 16 (bottom), in which Tie 15 is unsupported.

Numerical simulations by Varandas et al. (2011) attempt to numerically replicate the loading and displacement of a culvert transition zone instrumented by Coelho et al. (2011). The model incorporated non-linear tie-ballast behavior and the development of a tie-ballast gap. The results in Figure 2.47 show the development of tie-ballast gaps (voids in Figure 2.47a) and uneven tie loads (Figure 2.47b) with the load transferring from the unsupported ties to surrounding better supported ties. For examples, Ties -2, -6, and -11 have high loads and are adjacent to ties with larger tie-ballast gaps. This means the load that would normally be distributed to Ties -3 and -4 are transferred to Tie -2 and increases the tie load by 150%. In

Figure 2.47(b), TR is defined as the tie load divided by the static wheel load and a TR of 40% is considered typically for well-supported tie (Chang et al., 1980; AREMA, 2016).

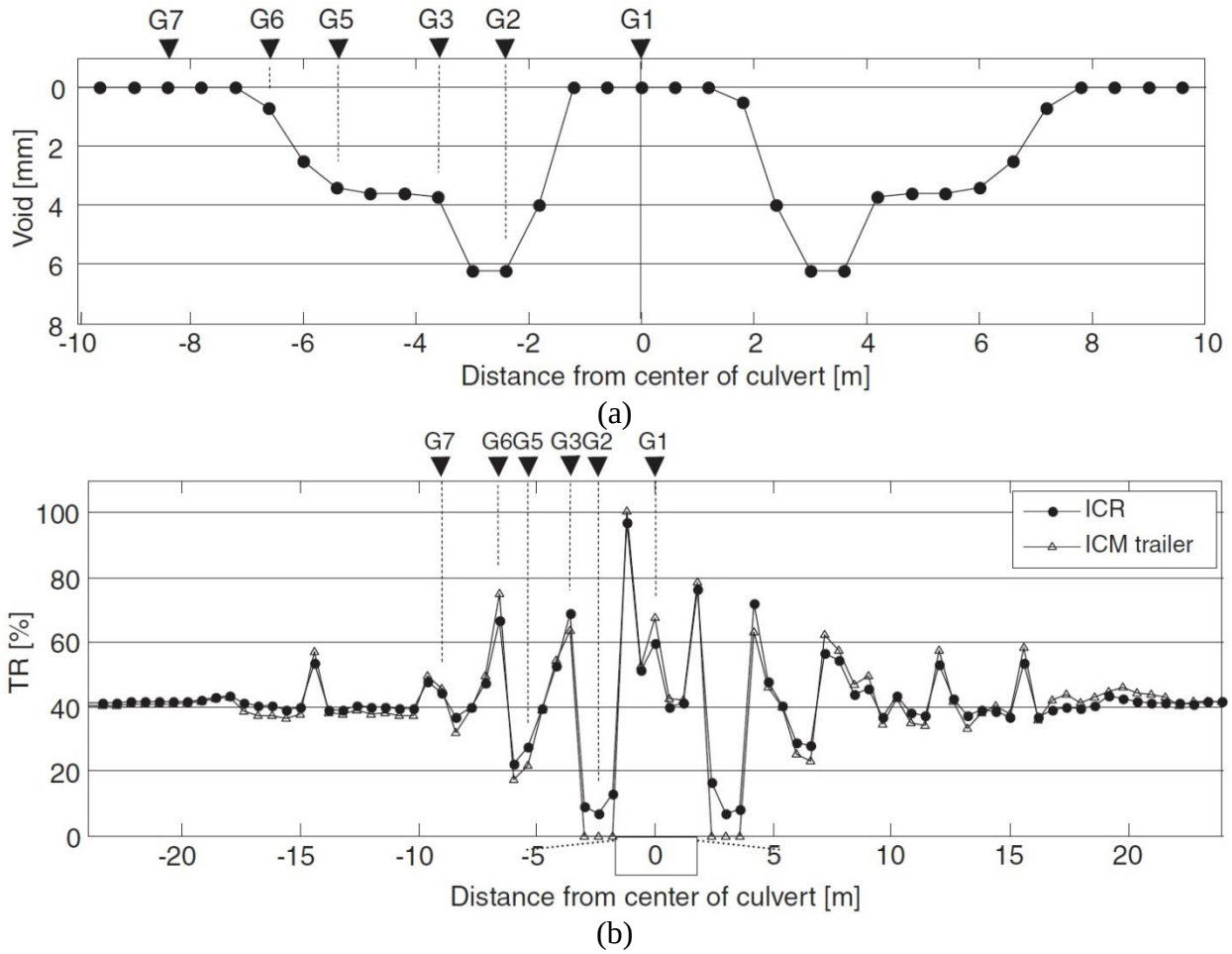

Figure 2.47: Results showing the (a) back-calculated tie-ballast voids and (b) resulting load distribution (TR = 40% is standard for tie with good contact) (from Varanadas et al., 2011).

The author is unaware of any measurements of increased impact loads from unsupported ties but the reasoning is Newton's Second Law of Force = Mass * Acceleration, in which an increased load can result from the rapid change in velocity of a moving tie contacting the ballast. Measuring tie pressures with pressure plates is a difficult procedure and requires intimate contact between the tie and ballast so it cannot be used to measure loads if a discontinuity between the tie and ballast exist, i.e. tie-ballast gap. This means evidence will likely be obtained from indirect measurements or from numerical simulations.

In summary, a literature review of field measurements and numerical simulations on increased loading show the following:

- Wheel flats and joints can increase loads by up to five and three times the static value, respectively
- Loads are expected to naturally vary by about 15%
- No evidence of significant increases in load from differential stiffness exists (<15% increase), however, there is evidence of significant increases in load from existing differential settlement (>50% increase)
- Unsupported ties can increase the tie load of surrounding, more well-supported ties up to 66% in open track situations and 150% in transition zone situations.
- All evidence of increased loads are attributed to situations in which there is (1) differential settlement between the approach and bridge, and/or (2) differential settlement within the approach.

2.4.3.3 *Increased Settlements in Approach*

The third category is increased settlement in the approach. This incorporates conditions within the ballast or subgrade that causes the ballast or subgrade to settle at greater rate than the surrounding track, even with identical loadings. Ballast degradation, fouling, track component degradation and tie-ballast gaps are previously mentioned examples. Lack of compaction during subgrade fill placement, tamping, and increased moisture from blocked drainage are additional scenarios that can occur because of the influence of bridge abutments. Figure 2.48 shows some examples of wet, fouled ballast and broken track components in approaches.

The behavior of the reduced-performance ballast is presented in Chapter 2.2.3 which describes how reduced-performance conditions can increase ballast settlement, even exceeding 10x the typical levels in cases of wet, fouled ballast. Therefore, increased loads are not necessary for track to experience accelerated ballast settlements. The influence of reduced-performance ballast as a cause for differential settlements has been mentioned (Li and Davis, 2005) but has not been emphasized in most transition zone assessments.

(a) (b) (c) (d) (e)

Figure 2.48: Photographs of (a,b) wet, fouled ballast and (c,d,e) broken track components in approaches.

In summary of Chapter 2.4.3, it appears that, if large enough, the inevitable differential settlement between the approach and bridge can produce increased loading and reduced-performance ballast. This can initiate a self-perpetuating cycle that is unlikely to be stopped from

resurfacing methods such as tamping because the loose freshly tamped ballast will quickly settle back to its previous elevation and the degraded, fouled ballast will settle at greater rates than the surrounding track. Broken track components from increased loading and poor tie support also amplify the problem.

2.4.4 Design and Remedial Techniques

This subsection reviews design and remedial techniques proposed and implemented by a variety of researchers and railroad companies. While many possibilities exist, desirable characteristics of bridge approach solutions include: being effective, low cost, minimal disruption, and the track should remain in place (Hyslip et al., 2009).

Transition zone design and remediation philosophy has slowly evolved over recent years. For much of railroad history, the primary actionable root cause of differential movement at transition zones was the differential stiffness between the approach and bridge. This was believed to increase the dynamic loads in the approach so the majority of transition zone solutions and remediation have emphasized matching the stiffness between the approach and bridge. Many new techniques have emphasized increasing track support and reducing substructure settlement.

Multiple transition zone design and remedial solutions have been proposed and implemented and can be categorized in the following way:

(1) stiffening of approach superstructure,
(2) stiffening of approach substructure,
(3) softening of bridge, and
(4) mixed solutions

The first category, stiffening of approach superstructure, is one of the simplest fixes and can be accomplish using multiple techniques. The underlying assumptions of this philosophy is that by gradually increasing the approach superstructure stiffness, the stiffness disparity at the bridge abutment, and therefore increased loads in the approach would be reduced. Kerr and Moorony (1993) proposed multiple superstructure fixes including decreased tie spacing, increased tie length, and adding additional rails in the approach. Read and Li (2006) suggest that most investigated superstructure fixes had minimal effects and GEOTRACK analyses have

shown little increase in stiffness from modifications of the superstructure. While these solutions are widely implemented, there is little evidence of their success.

The second category, stiffening of approach substructure, is more difficult and expensive as the track must be removed but GEOTRACK analyses show the greatest increase in stiffness from modifications of the subgrade (Read and Li, 2006). Both ballast and subgrade stiffening techniques are available and, as previously mentioned, it is important to identify the location of settlement so the problematic location can be targeted. Ballast stiffening techniques included using polyurethane grout (Woodward et al., 2012). Stiffening techniques at the ballast-subgrade include installing hot-mixed asphalt (HMA), geoweb, or geocells underneath the ballast (Rose, 2013; Li and Davis, 2005). Subgrade stiffening techniques include cement grout, geopiers, driven piles (Hyslip et al., 2009; Nicks, 2009).

Li and Davis (2005) investigated the causes of transition problems and attempted to remediate three bridge using subgrade stiffening remediatons. The existing bridges were ballasted-deck bridges and annual tonnage was approximately 180 MGT. The three remediations included: (1) 8-in HMA layer underneath the ballast extending 100-ft from the bridge, (2) an 8-in geocell confined subballast layer extending 100-ft from the bridge, and (3) 6.75-ft deep, 10-ft long cement stabilized with a 2:1 taper upwards. A fourth similar bridge approach was used as a control. The settlement over time showed no improvement of the remediated approaches over the control approach (see Figure 2.49). The presented explanation for the similar behavior was the bridge was still much stiffer than the remediated track therefore could still result in increased loading.

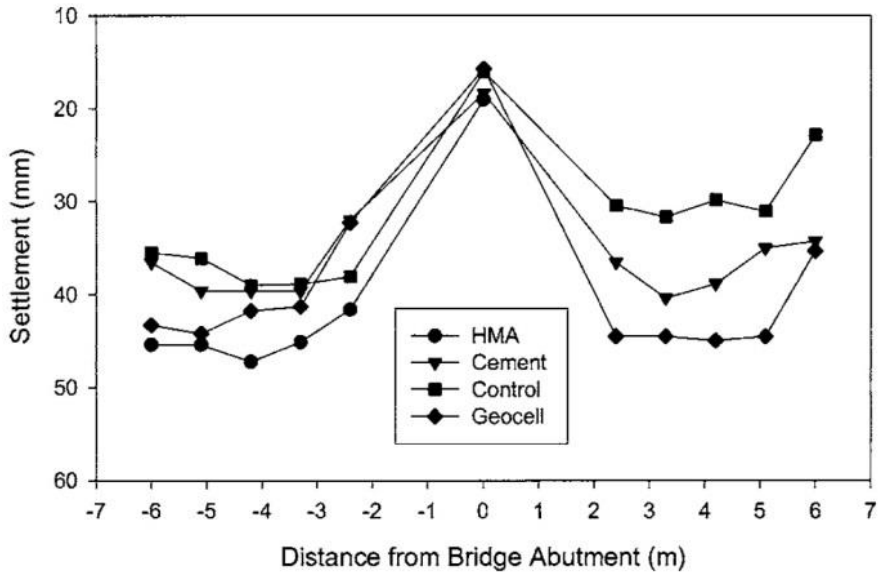

Figure 2.49: Track settlement from three remediations and control site.

An example of a seemingly successful bridge approach design is a wedge-shaped transition zone (Paixão et al., 2015a). A diagram is displayed in Figure 2.50 in which CBGM stands for cement bonded granular material and UGM standards for unbonded granular material. Wing walls, not shown in the diagram, were also included to confine the approach and prevent lateral movement. The purpose of the transition is to gradually increase the stiffness and support of the transition zone until the culvert is reached. Much emphasis was placed on compacting the ballast and subgrade material and no significant settlements have occurred over three years of service.

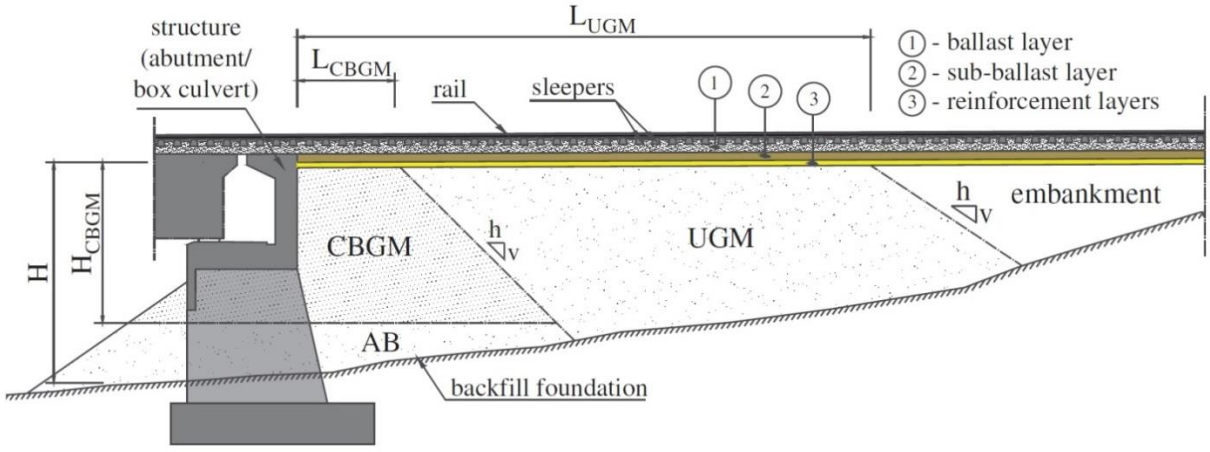

Figure 2.50: Schematic design of a wedge-shaped transition zone (from Paixão et al., 2015a).

The third category, softening of bridge, has had multiple attempts in recent years and can range widely in cost. The most common technique is by switching from an open-deck bridge to a ballasted-deck bridge. An open-deck bridge is a bridge in which the timber ties are directly supported on the bridge structure and have high stiffness. Ballasted-deck bridges have the concrete or timber ties supported on a typically 12-in thick layer of ballast that is supported by a precast concrete deck. The additional ballast softens the bridge and allows for some settlement over time. Figure 2.51 shows examples of open-deck and ballasted-deck bridges. The conversion is a common but expensive fix and requires a lowering in clearance underneath the bridge, which is sometimes restricted.

(a) (b)

Figure 2.51: Photographs of an (a) open-deck bridge and (b) ballasted-deck bridge.

While upgrading to ballasted-deck bridges have been shown to temporarily alleviate track geometry problems, the differential settlement often returns after a brief delay. For example, Hyslip et al. (2009) published a paper investigating potential improvements from the upgrade of two open-deck bridges on a Norfolk Southern (NS) freight line to ballasted-deck bridges. The results show a significant improvement for about a year after installation at Bridge 352.2 but some degradation at BR352.8 (see Figure 2.52). However, these bridges began to degrade sometime after publication, as they are two of the five bridges that are analyzed in Chapter 3.

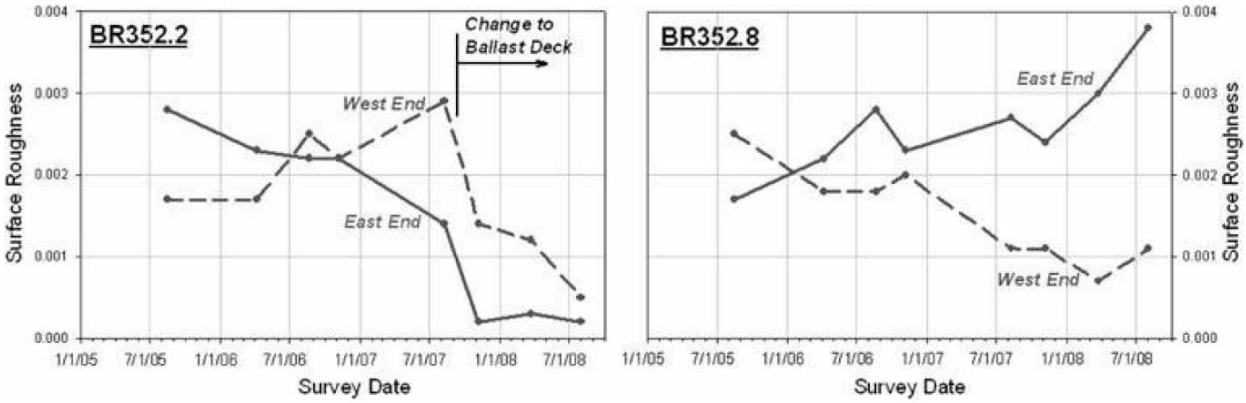

Figure 2.52: Surface roughness of two converted bridge approaches (from Hyslip et al., 2009).

If a bridge cannot be lowered because of clearance issues, rubber pads at the rail-tie interface can soften and dampen the track on the bridge. As an example of rail pads, Kerr and Bathurst (2001) installed matched pads on multiple open-deck bridges along Amtrak's Northeast Corridor (NEC) near Chester, Pennsylvania. The purpose of the matched pads was to lower the bridge track modulus to match the approach and eliminate the need for transition sections in the approach. The pads were selected over other options because pads represent a cheaper and less labor intensive option than stiffening transition sections. The initial installation appeared to reduce track geometry within the transition and after two-weeks, fine ballast was shovel-packed underneath the first six approach ties to improve track support. Track geometry measurements showed additional but temporary improvements after shovel-packing. Matched pads were also installed on a Norfolk Southern (NS) line and track geometry deviations were reduced by 25% about a year after installation. The long-term benefits of the matched pads are not clear, as the remediated bridges were instrumented, or were considered for considered for instrumentation, in a project presented in Chapter 3.

Another successful implementation of bridge softening techniques by Li and Maal (2015) involved rubber pads or ballast mats on ballasted-deck bridges. The rubber pads are thin pads placed underneath the concrete ties (see Figure 2.53a) and ballast mats are thin rubber mats that are placed underneath the ballast in ballasted-deck bridges (see Figure 2.53b). The purpose was to compare the combined effects of rail pads and ballasted-deck bridges against the combined effects of ballast mats and ballasted-deck bridges. Additionally, drainage systems were installed in the approach to facilitate drainage. The results showed improved track geometry three to five

years after installation (see Figure 2.53c). Other options for softening the bridge are plastic ties (Hyslip et al., 2009).

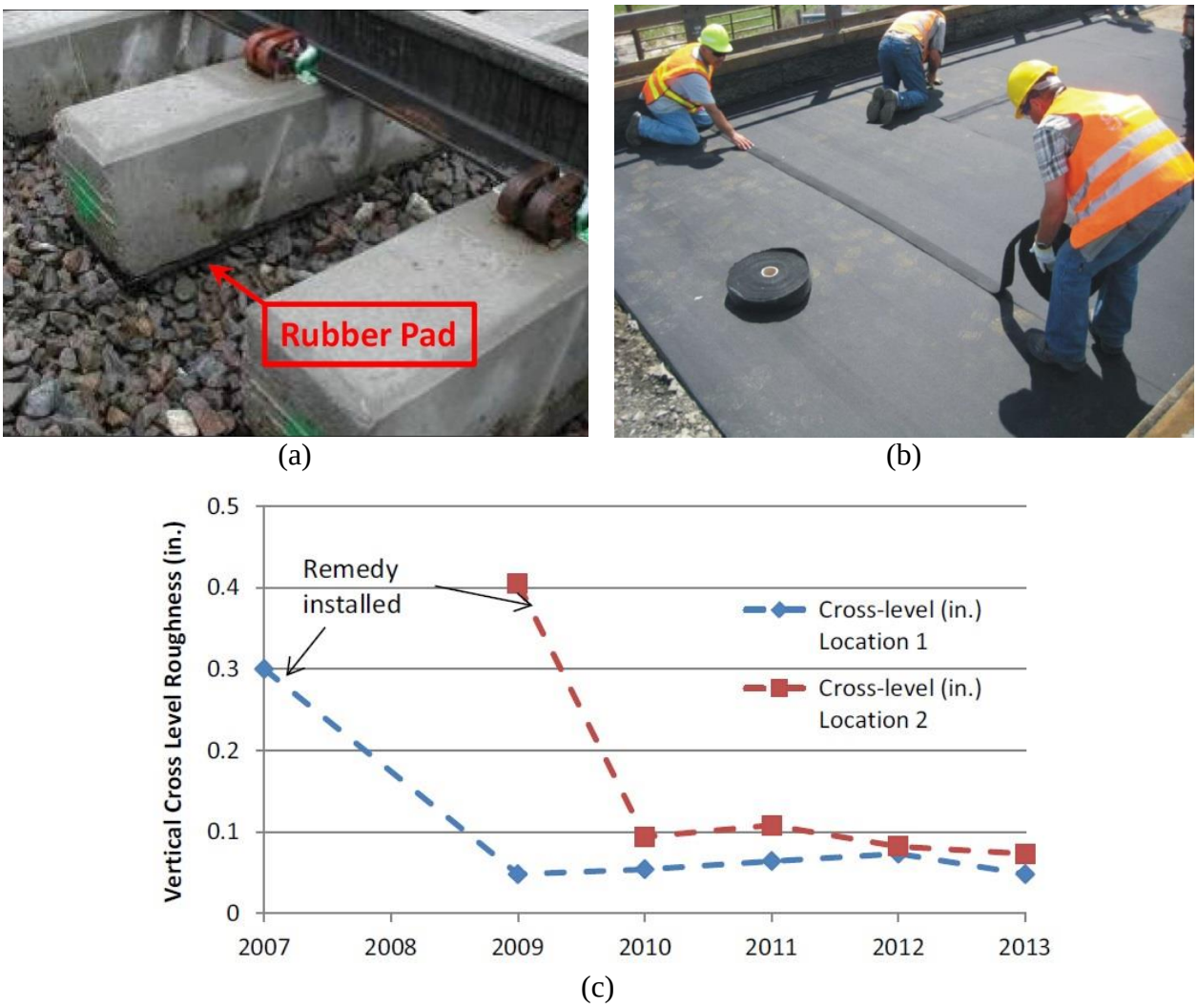

Figure 2.53: Photographs of (a) rubber pads under tie, (b) ballast mats, and (c) reduction in crosslevel roughness (from Li and Maal, 2015).

The fourth category, mixed solutions, is typically the most successful because they incorporate multiple philosophies into a single design or remediation. For example, this could involve both softening the bridge and stiffening and supporting the approach.

One example is a bridge in Alabama that was remediated by installing a 1475-ft long ballasted-deck bridge with concrete wing walls to restrict lateral movement and HMA underneath the ballast (Rose, 2013). This bridge was placed in service in 1998 and has required

minimal maintenance since. This bridge approach was analyzed in Chapter 4 and more details can be referenced there.

An example of stiffening both the superstructure and substructure is presented by Patel and Jordan (1996). Metropolitan Atlanta Rapid Transit Authority (MARTA) installed gradually increasing ties along with a 20-ft long concrete transitional slab in the ballast track approach. The study found that maintenance was reduced by a factor of three when the combined approach was compared against approaches with only the concrete transitional slab.

2.5 Summary

A literature review of ballast, track, and transition zone behavior shows a complicated system in which the performance is dependent on the behavior of individual track components and the interaction between the track structure and a fixed structure. Additionally, there are many constraints regarding sampling and direct measurement so most explanations of transition zone behavior and solutions are inferred from field observations and modifying idealistic track scenarios.

A summary of the review is below:

- Laboratory ballast testing shows two main stages of settlement for clean ballast. First, an initial compaction stage in which the ballast particles rearrange (densify) and breakage of particle corners occurs. Second, a post-compaction stage, which is identified by lower settlement rates.
- Laboratory ballast testing shows increased ballast settlements can occur from the following factors: increased loads, increased loading frequencies, decreased confinement, increased ballast degradation, increased fouling and moisture content, and inclusion of tie-ballast gaps.
- Transition zones often experience accelerated settlement with regard to the surrounding track and prior investigations have shown the existence of a “dip” within the bridge approach region.
- The accelerated approach settlement is commonly attributed to increased loads within the approach and to a lesser extent, fouled and degraded ballast (reduced-performance ballast) in the approach.
- Direct measurements of increased approach loads are rare and evidence is typically inferred from numerical models and modified analytical solutions. Numerical models show potential increased loads by 150% in situations of differential settlement between the bridge and approach.

- Recent studies suggest that increased approach loads that are detrimental to the track can occur either from differential settlement between the approach and bridge or from differential settlement within the approach. This implies initial settlement is required to initiate increased loading.
- Mixed transition zone solutions that soften the bridge and better support the approach appear to be the most successful.

CHAPTER 3

TASK I: HIGH-SPEED PASSENGER AND FREIGHT MONITORING

3.1 Introduction

The first task involves the instrumentation and analysis of ten sites located on both high-speed passenger and freight lines to study the behavior of transition zones. While multiple root causes of transition zone settlement have been proposed prior to this study, the impetus for this investigation comes from the need to quantify track behavior with depth and determine the layer at which the movement is occurring so remedial measures can address that specific layer. The instrumentation measures wheel loads, tie reaction, and permanent and transient displacement with depth with the purpose of determining the problematic locations in transition experiencing reoccurring track geometry problems.

The objectives of Task I are to:

(1) determine the depth at which the majority of permanent and transient displacements are occurring, and
(2) determine the root cause(s) of differential movement at the ten instrumented high-speed and freight lines.

Additional aspects of the project are numerically simulating track and transition zone behavior and recommending potential design and remedial techniques to prevent differential transition displacements from occurring. These aspects are addressed in Task III and IV (Chapters 4 and 5).

In this thesis, the results will be displayed in metric units because for comparison with previous testing and widespread use within railroad studies. However, Imperial units are used for train velocities and site locations, e.g. 15 ft. from bridge abutment, because the audience is primarily from the United States.

This chapter first introduces the site location and instruments in Chapter 3.2. The results of the permanent vertical displacements, wheel loads, tie reactions, and transient vertical displacements are presented in Chapters 3.3 through 3.6. Observations from site visits are listed in Chapter 3.7. Chapter 3.8 relates the multiple variables determined from Chapters 3.3 to 3.6

and propose a root cause for the monitored transition zones. Chapter 3.9 summarizes the work from Task I.

3.2 Instrumented Bridge Transitions

3.2.1 Instrumented Site Selection

To determine the causes of differential movement at railway bridge transition zones, multiple transition were instrumented to measure track behavior and compare behavior between sites. To get variations in behavior and cause, three bridges along a high-speed passenger line and two bridges along a freight line were selected. Four of the five bridges involve instrumenting both the approach and open track and one involved instrumenting opposite sides of the same tie.

Typically, the instrumented transition tie is the location of the greatest track geometry deviation, e.g. bottom of dip, and is the worse-case location. The open track location is typically used as a control. Details of the high-speed passenger and freight site locations are discussed in the subsequent subchapters.

3.2.1.1 High Speed Passenger Site Selection

The high-speed passenger site was selected along Amtrak's North East Corridor (NEC) located south of Philadelphia in Chester, Pennsylvania. This segment of the NEC comprises of a long stretch of straight raised track with a number of closely spaced bridges that experience differential movement at the bridge/approach fill interfaces that are causing ride quality and safety concerns. This has been a historically difficult region to maintain track geometry and serves as a common testing location for possible transition zone remediation techniques (Kerr and Bathurst, 2001; Chapter 2.4.4). The line at this location has four tracks, with the middle Tracks #2 and #3 being utilized for high-speed passenger trains, e.g., Acela Express, which usually operate at 110 mph.

Figure 3.1: Photograph on Upland Avenue Bridge on Track #2.

Based on pre-existing track geometry data, the following Amtrak bridge approaches were selected for field instrumentation during this project:

Table 3.1: List of instrumented sites along Amtrak's NEC

Bridge	Street	Rail	Distance from Abutment [ft]	Reference in Text
1	Upland Avenue	West	15	Upland (15 ft.)
		West	60	Upland (60 ft.)
2	Madison Avenue	West	12	Madison (12 ft.)
		West	60	Madison (60 ft.)
3	Caldwell Avenue	East	80	Caldwell (East)
		West	80	Caldwell (West)

The track superstructure consists of welded rail joints, 136-RE rail, concrete ties at about 24-in spacing, and spring clip fastening system. The substructure is interpreted from borings and is described in Figures 3.2 to 3.4. As a note, the ballast layer for all sites is 12 inches and the concrete ties are 7 inches in height.

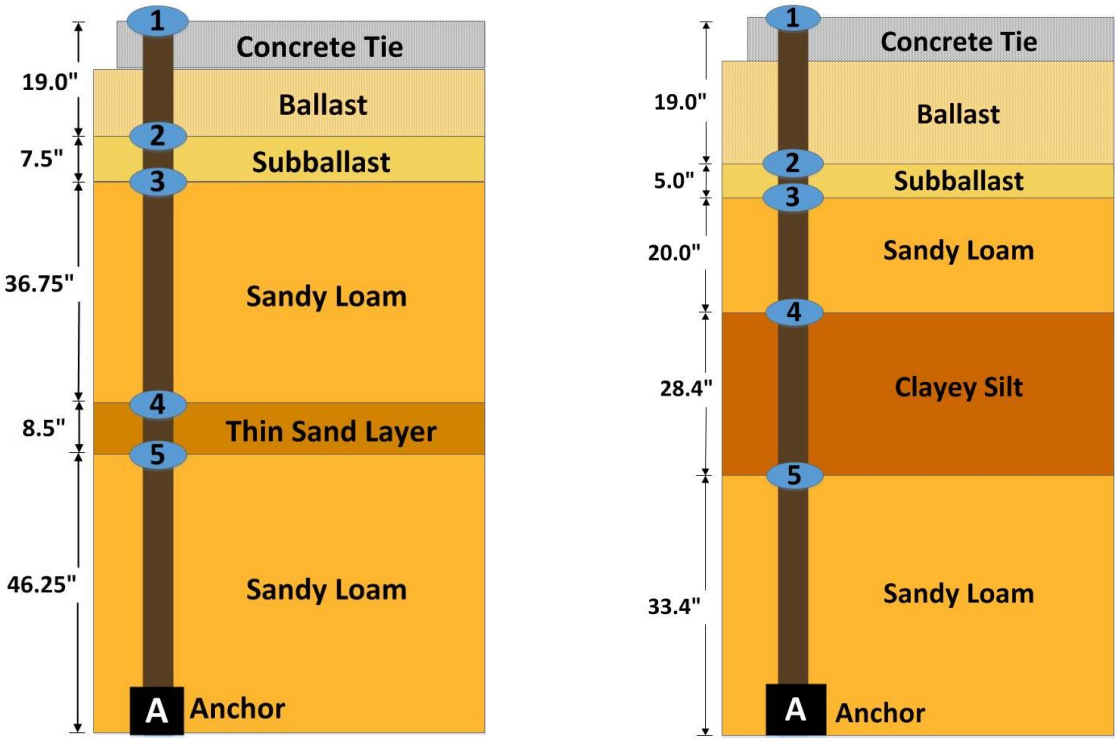

Figure 3.2: Subsurface profile for (a) Upland (15 ft.) and (b) Upland (60 ft.).

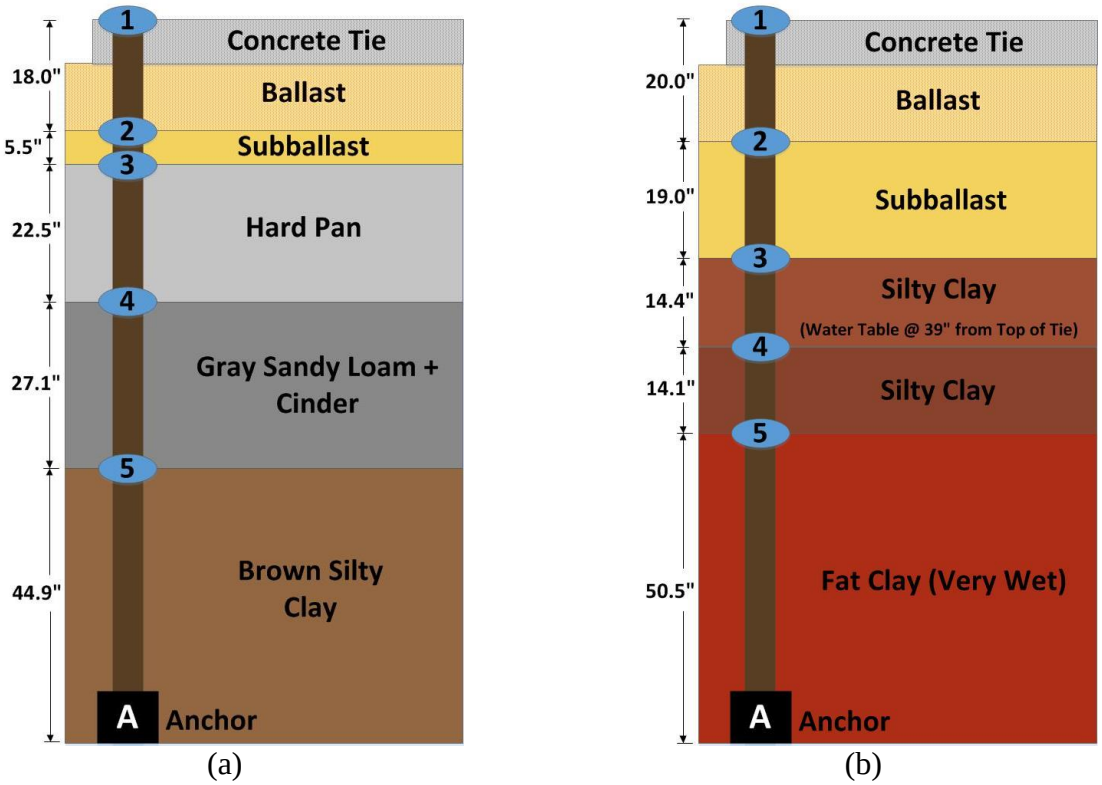

Figure 3.3: Subsurface profile for (a) Madison (12 ft.) and (b) Madison (60 ft.).

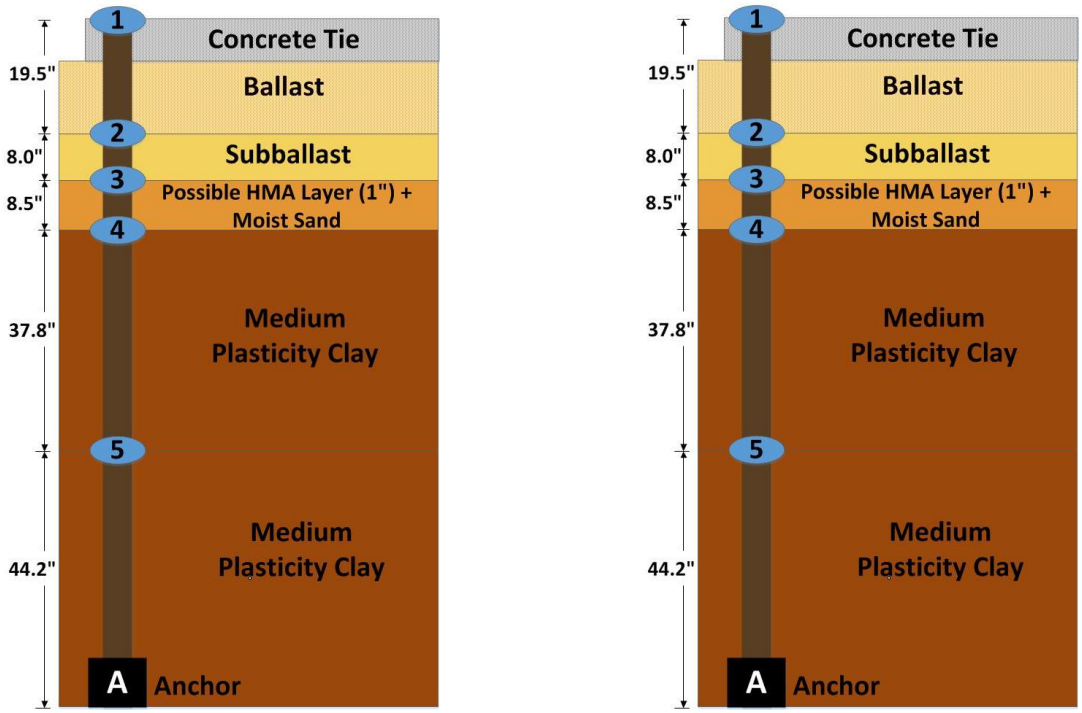

Figure 3.4: Subsurface profile for (a) Caldwell (East) and (b) Caldwell (West).

3.2.1.2 *Freight Site Selection*

The freight site was selected along Norfolk Southern's (NS) N-Line located between Roanoke, Virginal and Bluefield, West Virginia. The bridge at MP 352.2 is located on a 10-degree curve and on a 1.1% grade, and the bridge at MP 352.8 is located on a 9.7-degree compound curve on a 0.9% grade. An aerial photograph is provided in Figure 3.5. Track speed in the region is commonly 25 mph as loaded trains move downhill from west to east with full dynamic brake and often with air brakes applied. This track section is subjected to heavy axle load train operation with an annual tonnage of approximately 55 MGT (million gross tons). However, the track also carries empty or light weight cars, providing a range of wheel loads and track response.

Figure 3.5: Aerial view of NS instrumentation locations near Bluefield, West Virginia.

Based on pre-existing track geometry data, the following NS bridge approaches were selected for field instrumentation during this project:

Table 3.2: List of instrumented sites along Norfolk Southern's N-Line

Bridge	Location	Curve	Grade	Distance from Abutment [ft]	Reference in Text
1	MP 352.2	10°	1.1%	13	MP 352.2 (13 ft.)
				31	MP 352.2 (31 ft.)
2	MP 352.8	9.7	0.9%	11	MP 352.8 (11 ft.)
				29	MP 352.8 (29 ft.)

The bridge has a ballasted-deck bridge that was installed in 2008 (Hyslip et al., 2009, Chapter 2.4.4), and the track superstructure consists of welded rail joints, concrete ties, and spring clip fastening systems. The substructure is interpreted from borings and is described in Figures 3.6 and 3.7. As a note, the ballast layer varies at each location and the concrete ties are 7 inches in height.

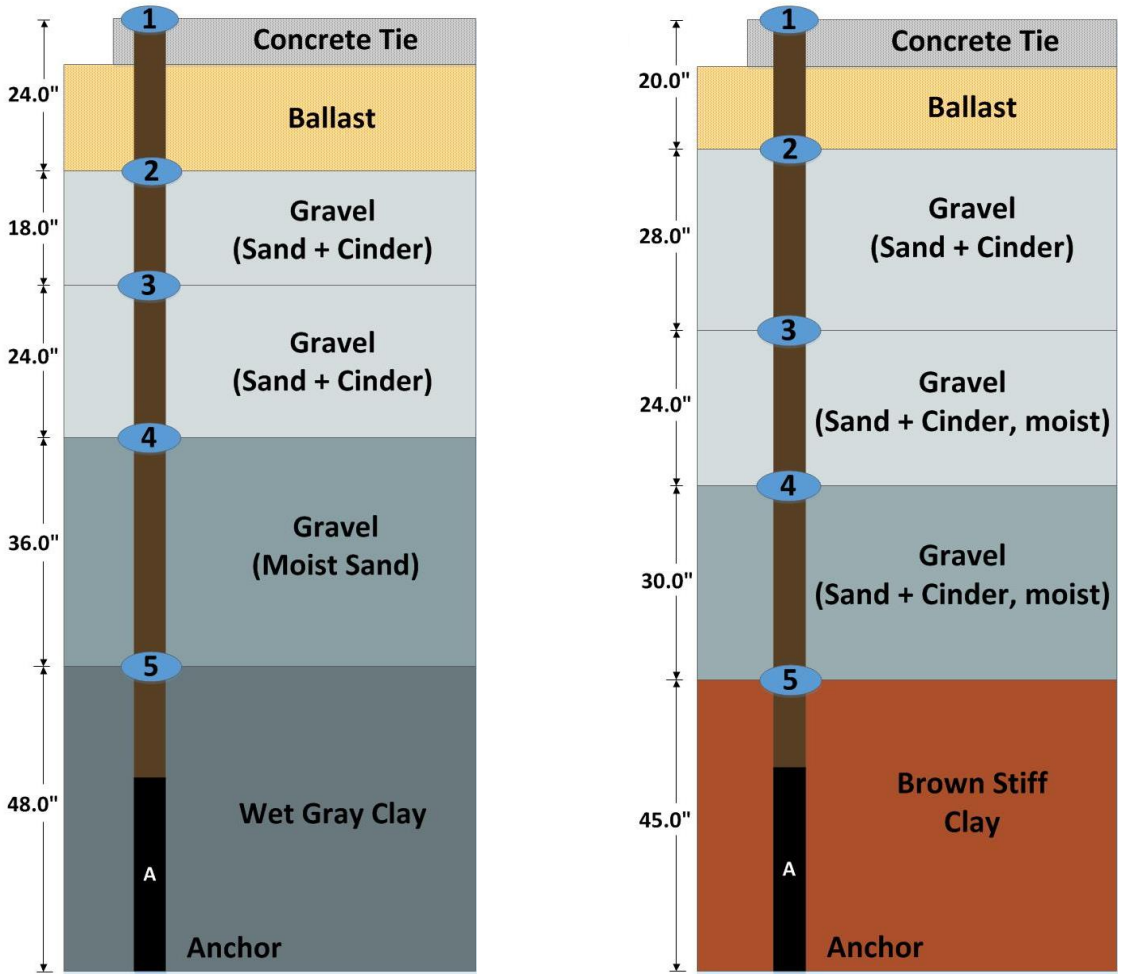

Figure 3.6: Subsurface profile for (a) MP 352.2 (13 ft.) and (b) MP 352.2 (31 ft.).

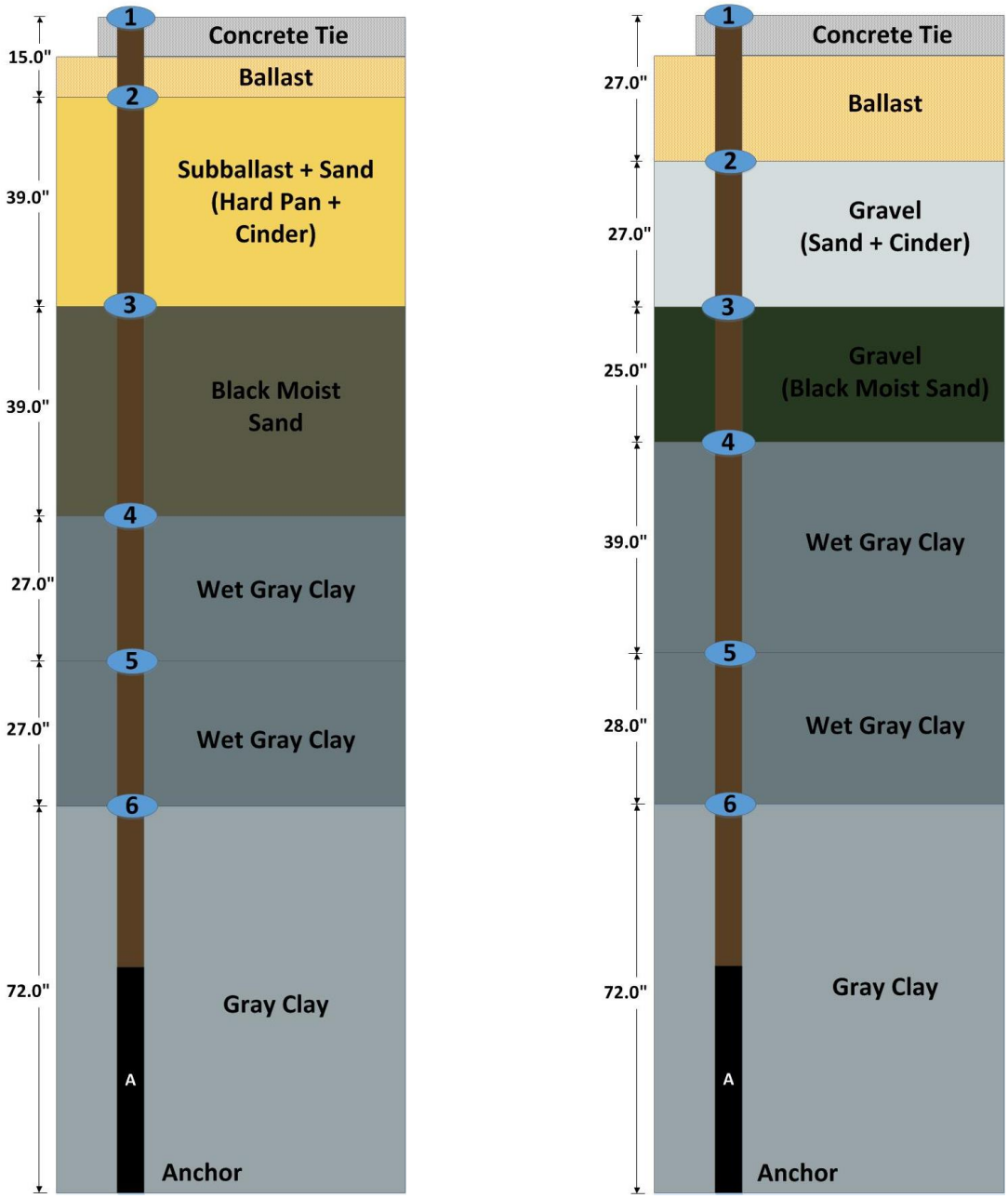

Figure 3.7: Subsurface profile for (a) MP 352.8 (11 ft.) and (b) MP 352.8 (29 ft.).

3.2.2 Instrumentation

Two types of instrumentation were used to monitor the ten installation locations: strain gauges on the rail and multi-depth deflectometers (MDDs) installed in the subgrade. The purpose of each instrumentation and its outputs are described in the subsequent two subchapters.

3.2.2.1 Strain Gauges

The strain gauges were installed on the rails by Mike Tomas of AMTRAK and are used to collect wheel loads and tie reactions. A total of eight (8) strain gauges, four on each side of the rail, were installed at each instrumentation location. Figure 3.8 shows the instrumented rail with four strain gauges at Upland (15 ft). The two leftmost strain gauges in Figure 3.8 are located in the crib area and are used to estimate applied wheel load and the two rightmost strain gauges are located above the tie and are used to estimate the tie reaction, i.e. load distributed to the tie. Wheel load results are presented in Chapter 3.4 while the tie reaction results are presented in Chapter 3.5.

Figure 3.8: Photograph showing two strain gauges in crib area for vertical wheel load and two strain gauges above the tie for tie reaction.

3.2.2.2 Multi-Depth Deflectometers

The second type of instruments are multi-depth deflectometers (MDDs) and used to measure the permanent and transient displacements of multiple layers in the substructure (DeBeer et al., 1989; Sussmann and Selig, 1998; Billow and Li, 2005). MDDs were selected to measure subsurface vertical displacements based on the one-dimensional nature of the track movements at the Amtrak's NEC locations. An MDD consists of Linear Variable Differential Transformers

(LVDTs) installed at various depths to measure displacements with depth due to the applied loads.

The vertical movements at the Caldwell, Madison, and Upland Avenue bridges along the NEC are expected to be vertical because the track in this area is essentially straight and the elevated railways are confined by large masonry walls (see Figure 3.9). This is important because MDDs can only measure vertical displacements. If lateral displacements were occurring, the LVDTs would not be able to measure the lateral displacements and might under represent the actual field displacements.

Figure 3.9: Photograph of masonry walls at Upland Avenue below the Upland (15 ft) MDD location with Mike Tomas collecting MDD cables.

The instrumented NS N-Line sites are located on horizontal curves and the movements at these locations will likely involve both vertical and lateral displacements. One limitation of using MDDs at these locations is that only the vertical displacements were measured and the effect of lateral forces/movements are not known.

The clamping nut at the top of an LVDT (see Figure 3.10) is tightened to displace the washer and steel balls of the loading washer out radially and secure the LVDT to the inside wall of the borehole casing or tubing at the desired depth. As the layer deforms under train loading, the LVDT registers the vertical displacement with respect to the bottom of the MDD string. The

bottom of the MDD string is frequently referred to as the anchor point but this point can undergo vertical displacement if not founded in rock or another unyielding material. The MDDs are installed using hand operated drill equipment so the depth of the anchor is limited, i.e., usually less than fifteen feet. As a result, there is potential for the anchor point to move due to settlement of the underlying layers.

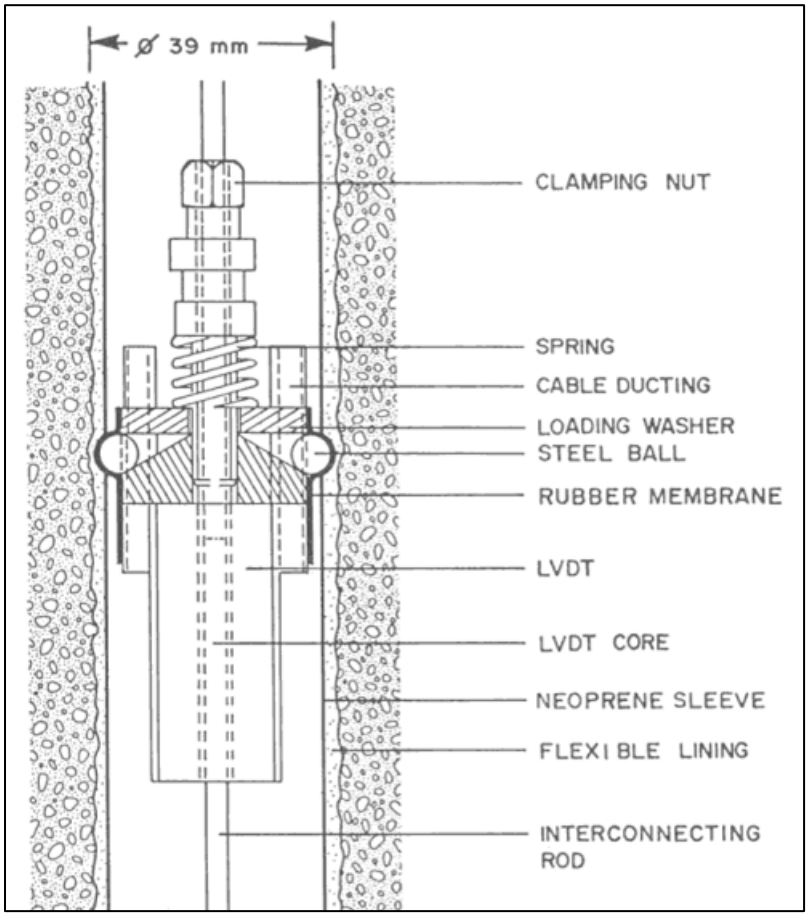

Figure 3.10: Schematic of a Multi-depth Deflectometer (MDD) Module from DeBeer et al. (1989).

The five LVDTs in each MDD string installed at the instrumented sites were placed at depths that roughly correspond to the following track features: (1) top of cross-tie, (2) bottom of ballast layer, (3) bottom of subballast layer, (4) within upper approach fill layer, and (5) within the lower approach fill layer. An anchor was also placed at the bottom of the approach fill layer. The individual LVDT locations at each site can be referenced in Figures 3.2 to 3.4 and Figures 3.6 and 3.7. The transition from one layer to another layer was determined during the hand

drilling process by Mike Tomas of AMTRAK and roughly correspond to changes in the materials or properties within the track substructure system.

The approach fill below the fifth LVDT in the elevated track sections in Chester, PA, see Figure 3.9, can settle so the total measured vertical displacement could be greater than the measured values. In this system each LVDT serves as the anchor for the LVDT immediately above it. This concept is schematically shown in Figure 3.11 and the inner core for LVDT #5 (attached to MDD module # 5) is mounted on the bottom anchor or Core #5. The core for LVDT # 4 (attached to MDD # 4) is then mounted on module #5. This configuration is repeated for LVDTs #3, #2, and #1. It is assumed that LVDTs 1 through 4 have movable anchors while the anchor for LVDT #5 (Core #5) is assumed to be stationary. As a result, the deflection value measured by each LVDT represents the deflection in that particular layer, i.e., the distance between the two LVDTs. For example, the deflection of LVDT #2 corresponds to the deformation of the 2^{nd} layer (d_2 or distance between LVDTs 2 and 3) or Core #2 shown in Figure 3.11. The vertical movement of each LVDT is measured and used to describe the vertical displacement of the corresponding layer. If the bottom of the MDD string is assumed to be stationary, the total vertical displacement of the MDD string can be calculated by adding all of the LVDT readings together. The MDD strings installed along the NEC terminate at a depth of 3.0 m (118 inches) below the top of the concrete cross-tie, which places the "anchor" within the approach fill. The vertical walls confining the elevated track in Chester, PA are approximately 12.5 ft (150 inches) high (see vertical clearance sign in Figure 3.9). Therefore, the anchor point is well above the bottom of the wall in the approach fill material.

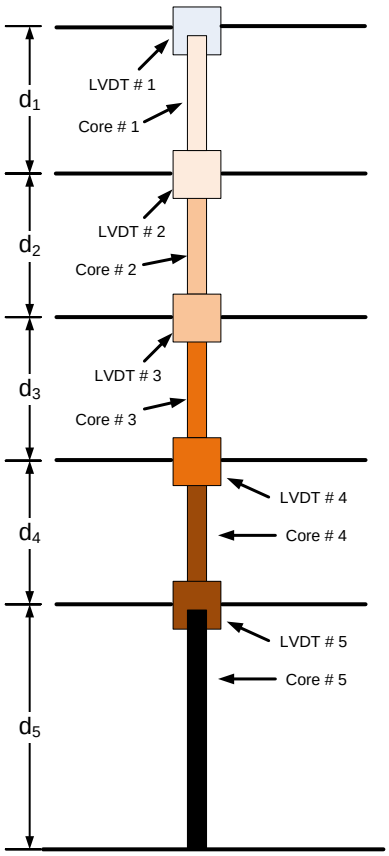

Figure 3.11: Schematic showing five LVDTs in an MDD string with the bottom founded on an unyielding layer (after Tutumluer et al., 2012).

3.2.3 Installation and Data Collection

Installation of the six Amtrak sites were completed on 1 August 2012 and the installation of the four NS sites were completed on 2 November 2013. Forty-two (42) passing trains were recorded at the ten instrumented sites at Amtrak and NS. Thirty-four (34) of the trains are high-speed passenger trains at Amtrak and eight (8) are freight trains at Norfolk Southern. A breakdown of the number of trains recorded on each particular day at each site is displayed in Tables 3.3 (Amtrak) and 3.4 (Norfolk Southern).

Table 3.3: Number of Data Measurements at the NEC Instrumented Sites

AMTRAK Site	6,7 August 2012	5 November 2012	29 January 2013	25 June 2013	4 September 2013	Total
Caldwell	2	2	5	3	0	12
Madison	2	3	3	2	2	12
Upland	2	2	2	2	2	10

Table 3.4: Number of Data Measurements at the N-Line Instrumented Sites

NS Site	1 November 2013	19 March 2014
352.8 (11 ft.)	1	1
352.8 (29 ft.)	0	2
352.2 (13 ft.)	1	1
352.2 (31 ft.)	1	1

3.3 Measured Permanent Vertical Displacements

This section presents the analysis of the permanent vertical displacements measured at the various MDD locations along Amtrak's NEC and NS lines. The two main objectives of instrumenting these sites are to: (1) locate the depth(s) at which the majority of the permanent vertical displacements are occurring and (2) determine which instrumented sites exhibit the largest permanent vertical displacement. To accomplish these objectives, the permanent vertical displacements of each Amtrak LVDT were measured periodically between 2 August 2012 and 18 December 2013. Only data from two NS sites between 1 November 2013 and 19 March 2014 are available. The permanent vertical displacements were measured when no train was passing each instrumentation site.

In Task I, the terms "permanent vertical displacement*"* and "settlement" are both used to describe plastic deformation of various substructure layers. However, the two terms are not used interchangeably. The term "permanent vertical displacement" signifies a measured value from this particular instrumentation setup while "settlement" is used as a general term. Additionally, the term "transient vertical displacement" signifies the measured short-term or essentially elastic deformation of the various substructure layers and the term "displacement" is used as a general term.

3.3.1 Depth of Permanent Vertical Displacements

To determine the depth at which the majority of settlement is occurring at the Amtrak and NS sites, the permanent vertical displacements of all LVDTs are compared over time. Data over a period of 446 days is analyzed for all six Amtrak sites while data for a period of 138 days at only two NS sites were analyzed because of limitations in data availability.

The first two months (57 days) of data were omitted from the Amtrak data set because some LVDTs may displace after installation as the tube and foam around the tubing compress due to the weight of the MDD string and/or the tubing becomes fully engaged in the ballast and underlying materials. Figures 3.12 (a) and (b) show the full 503 days data set (446 + 57 days) for Caldwell (East) and Madison (12 ft.), respectively. At Caldwell (East), about half of the LVDT #1 permanent vertical displacement occurs within the first week then proceeds at a constant rate for the remainder of data collection. At Madison (12 ft.), tamping of the MDD site occurred sometime between 18 and 26 days after MDD installation which raises and loosens the ballast (Figure 3.12b) and higher rates of permanent vertical displacements is anticipated for a short period of time as the ballast recompacts (see Chapter 2.3.3). In the 18 days prior to tamping, 5.7 mm of permanent vertical displacement was measured while 216 days after tamping were required to reach a value of 5.9 mm. The four other sites display similar behavior with large initial permanent vertical displacements in the first two months but to a lesser degree. Therefore, to avoid the possible influence of the MDDs on results and to avoid the influence of tamping from the Madison (12 ft.) site, the first two months (57 days) are omitted from the analysis.

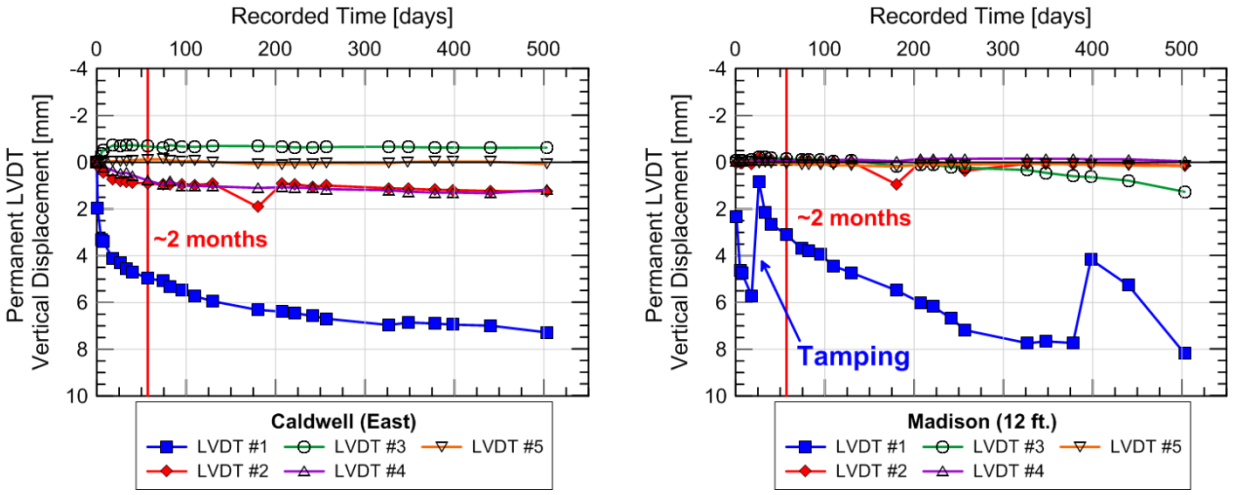

(a) (b)

Figure 3.12: Permanent vertical displacement with first two months of data included at (a) Caldwell (East) and (b) Madison (12 ft.).

Figure 3.2 shows the permanent vertical displacements of each LVDT with time for all six MDD instrumentation sites for a period of 446 days from 27 September 2012 to 18 December 2013. At all six site locations, the greatest permanent vertical displacement occurs in LVDT #1, implying the majority of settlement is occurring in the ballast at the Amtrak sites. This matches

with previous observations from Selig and Waters (1994) that the majority of settlement occurs in the ballast for existing track.

The noticeable increase in permanent vertical displacement of LVDT #2 in January 2013 (123 days) at Upland (15 ft.), Madison (12 ft.), and Caldwell (West) (see Figures 3.2(a), (c), and (f)), is probably caused by high precipitation at or before the measurement time, equipment error, and/or the LVDT undergoing more permanent vertical displacement due to muddy conditions but rebounding after loading. This increase is temporary and the LVDT returned to about its original position shortly thereafter.

Tamping is observed between 1 April 2013 and 16 April 2013 (185 to 200 days) at Upland (15 ft.) (see Figure 3.2a). The negative reading on 16 April 2013 (200 days) is likely due to the "zero" reading not corresponding to the rail elevation immediately after tamping. Tamping also occurred sometime between 15 August 2013 and 4 September 2013 (321 and 341 days) at Madison (12 ft.) (see Figure 3.2c).

Conversely, it appears the permanent vertical displacement at LVDT #3 at Madison (12 ft.) and LVDT #2 at Caldwell (East) appear to be increasing with time. LVDT #3 at Madison (12 ft.) measures a subsurface layer described as Hard Pan (see Figure 3.3a) while the LVDT #2 layer at Caldwell (East) measures the subballast layer. This suggests that while the majority of settlement occurs in the ballast layer, non-negligible settlement can sometimes occur at other depths as well.

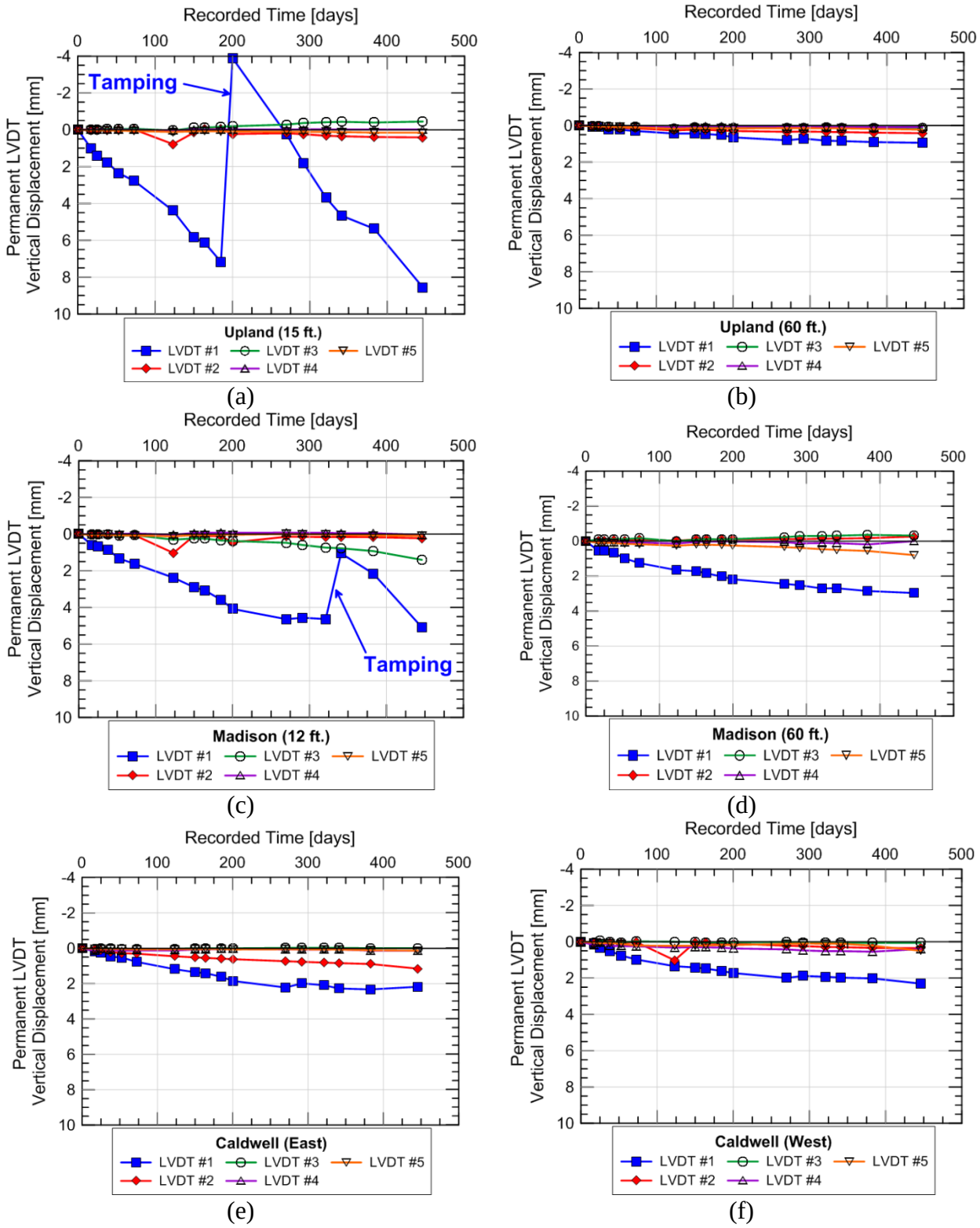

Figure 3.13: **Permanent vertical displacement with first two months of data omitted at (a) Upland (15 ft.), (b) Upland (60 ft.), (c) Madison (12 ft.), (d) Madison (60 ft.), (e) Caldwell (East), and (f) Caldwell (West).**

The rates of permanent vertical displacements for the five LVDTs at each instrumented site are compared in Table 3.5. The permanent vertical displacements span a total of 185 days starting from 27 September 2012 to 1 April 2013. During this time period, no tamping occurred and the influence of LVDT drift occurred is believed to be minimal. The results clearly show the more of permanent vertical displacements occurred in LVDT #1 while the remaining depths were minimal.

Table 3.5: Permanent vertical displacement rates of each LVDT at the six MDD Locations from 27 September 2012 until 1 April 2013

	Upland		Madison		Caldwell	
LVDT	**15 ft.**	**60 ft.**	**12 ft.**	**60 ft.**	**East**	**West**
	[mm/yr]	**[mm/yr]**	**[mm/yr]**	**[mm/yr]**	**[mm/yr]**	**[mm/yr]**
1	14.1	1.03	7.06	3.99	3.18	3.18
2	-0.06	0.53	0.24	-0.18	0.30	1.16
3	-0.32	0.26	0.69	-0.22	0.08	-1.99
4	-0.04	0.06	-0.16	0.04	0.63	0.08
5	0.45	0.30	0.08	0.45	0.34	0.08

Permanent displacement data is limited at the NS site with only two data points at MP 352.2 being available. The permanent vertical displacements at MP 352.2 (13 ft.) are displayed in Figure 3.14(a) and show similar behavior to the Amtrak sites in which the permanent LVDT #1 displacement is greatest contributor to overall settlement. The rate of LVDT #1 permanent displacement at MP 352.2 (13 ft.) appears to be about equal to Upland (15 ft.) with a value of 15.9 mm/yr. However, it should be noted that the first two months of data could not be omitted due to a lack of data so the MP 352.2 (13 ft.) value is likely lower and direct comparisons between the Amtrak and NS sites cannot be made. The results at MP 352.2 (31 ft.) displayed in Figure 3.14(b) show the greatest permanent displacement occurring in LVDT #3. This soil was described as a gravel with moist sand and cinder from the boring logs (see Figure 3.6b) but there is no indication of why the greatest settlement occurs in this layer. Both physical and initial LVDT displacements that would have been omitted with more data are possible reasons. This

also suggests that the subgrade may experience greater settlement at some track locations than others.

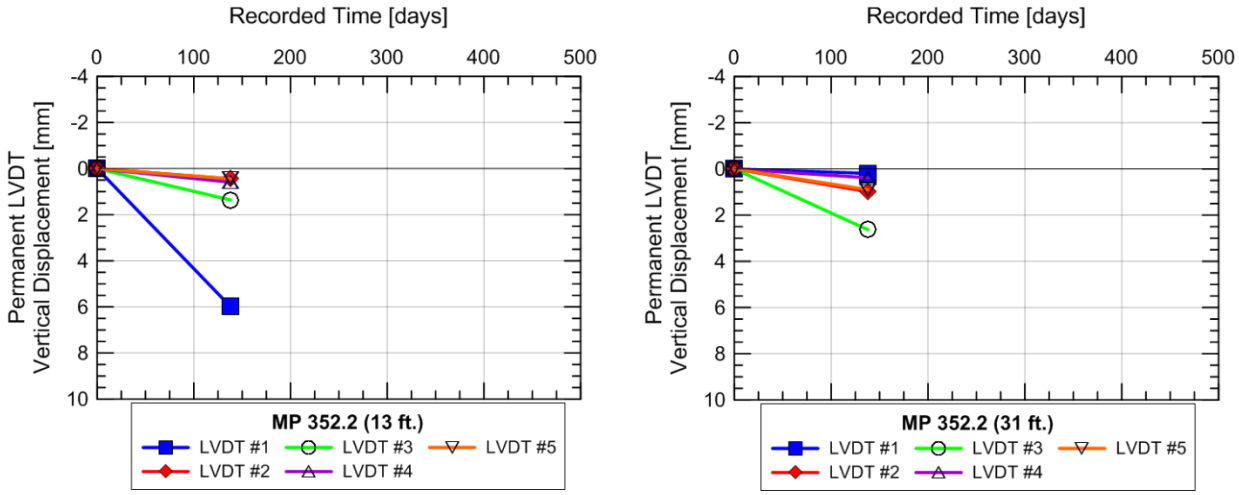

(a) (b)

Figure 3.14: Permanent vertical displacement at (a) MP 352.2 (13 ft.), (b) MP 352.2 (31 ft.).

3.3.2 Location of Permanent Vertical Displacements

The largest magnitude and variation in permanent vertical displacement occurs in LVDT #1, i.e., top of the concrete tie to the bottom of the ballast layer. All measured sites are compared and knowledge from laboratory tests introduced in Chapter 2.2 are used to potentially explain increased permanent LVDT #1 vertical displacements.

A comparison of the LVDT #1 permanent vertical displacements for all six MDD sites at the Amtrak site is shown in Figure 3.15. The largest permanent vertical displacement in LVDT #1 occurred at Upland (15 ft), followed by Madison (12 ft). Upland (15 ft) and Madison (12 ft) are located within the transition zone at each bridge and are expected to exhibit the greatest permanent vertical settlement. Caldwell (East), Caldwell (West), and Madison (60 ft) represent an "open track" condition and exhibit similar permanent vertical displacement rates but less permanent vertical displacement than Upland (15 ft) and Madison (12 ft). The Upland (60 ft) location is also an "open track" condition and exhibits the smallest permanent vertical displacement.

Comparing the permanent LVDT #1 vertical displacement results to laboratory ballast testing (see Chapter 2.2) suggests that the ballast settlement at the four open track sites are

similar to post-compaction stage ballast conditions. In this stage, the ballast settles at a decreasing rate from increasing ballast density and is approaching a stage of "equilibrium". The transition zone locations show continual permanent LVDT #1 vertical displacement, which is similar to laboratory ballast testing with low confinement, high frequencies, high degrees of wet, fouled ballast, or tie-ballast gaps. Both fouled ballast in the approach (Chapter 3.7) and tie-ballast gaps (Chapter 3.8) were observed in the transition zone location and are leading explanations for the accelerated ballast settlements because loading frequency and confinement are expected to be similar to the open track sites. Increased loads are a second possible explanation that is discussed later in the thesis.

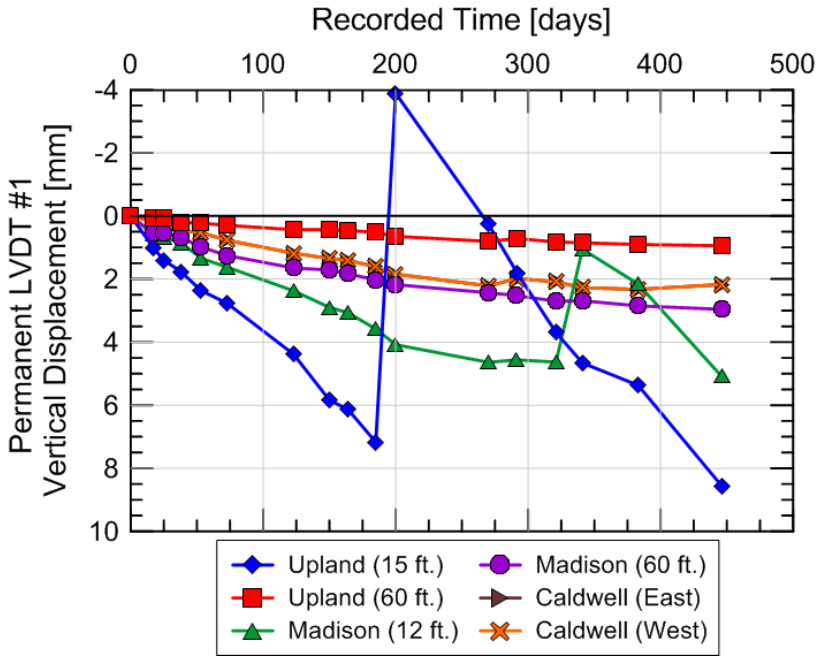

Figure 3.15: Comparison of permanent vertical displacements for LVDT 1 at all six MDD instrumentation sites with first two months of data omitted.

Table 3.6 displays the rates of permanent LVDT #1 vertical displacements for the initial 185 days (27 September 2012 to 1 April 2013) and the entire 446 days (27 September 2012 to 18 December 2013) of monitoring. Additionally, the rates prior and after tamping for Madison (12 ft.) and Upland (15 ft.) are also included.

The data shows that the rates of permanent vertical displacements generally decrease over time. This agrees with observations made earlier that the ballast is increasing in density and reaching a state of "equilibrium". Increases in rates of permanent vertical displacements were

observed for both Madison (12 ft.) and Upland (15 ft.) after tamping. This may be due to inadequate ballast compaction after tamping or increased ballast degradation and fouling from ballast damage during the tamping process.

Table 3.6: Permanent vertical displacement rate of LVDT #1 at the six MDD locations

Time Frame	Caldwell		Madison		Upland	
	East	West	12 ft.	60 ft.	15 ft.	60 ft.
	[mm/yr]	[mm/yr]	[mm/yr]	[mm/yr]	[mm/yr]	[mm/yr]
10/27/12 – 4/1/13	3.18	3.18	7.06	3.99	14.1	1.03
10/27/12 – 12/18/13	1.89	1.78	-	2.42	-	0.77
Pre-tamping	-	-	5.30	-	14.1	-
Post-tamping	-	-	14.0	-	18.5	-

Comparisons of permanent LVDT #1 displacement between the MP 352.2 (13 ft.) and MP 352.2 (31 ft.) are displayed in Figure 3.16 and show significantly greater permanent displacement in the transition zone than open track. This also agrees with the conclusions from the Amtrak sites. The first two months were not omitted because only a single measurement after installation was recorded.

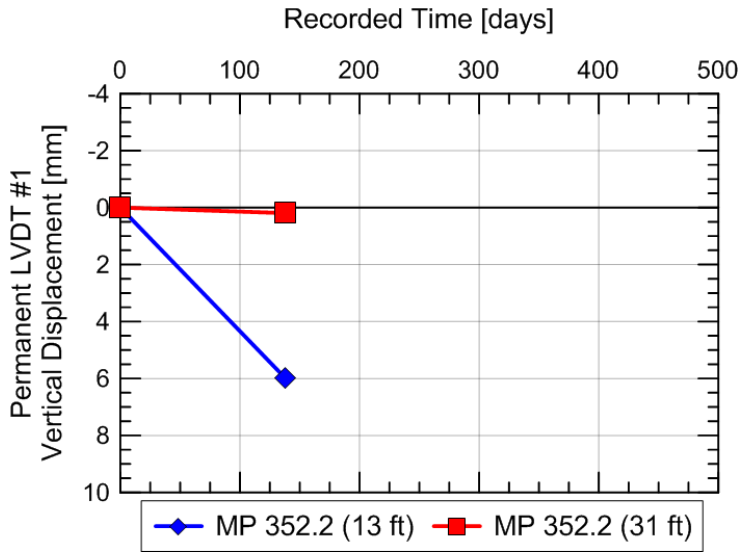

Figure 3.16: Comparison of permanent vertical displacements for LVDT 1 at MP 352.2 (13 ft.) and MP 352.2 (31 ft.).

3.3.3 Summary of Permanent Vertical Displacements

A primary objective of the instrumentation setup was to quantify the depths and trends of substructure settlement at sites that experience historical track geometry problems. The following remarks are made:

- The majority of permanent vertical displacement occurred in LVDT #1, which represents the ballast layer for all but one site. This suggests that ballast settlement is the main contributor to the transition zone track geometry problems at these sites and likely for most existing lines.
- Permanent vertical displacements of a few specific subballast or subgrade layers appear to contribute to track settlement but the data is not conclusive.
- Permanent LVDT #1 vertical displacement was greatest at all transition zone sites.
- The permanent LVDT #1 vertical displacement behavior for open track sites resembled post-compaction stage laboratory ballast behavior in which the ballast appears to be approaching a state of equilibrium.
- The permanent LVDT #1 vertical displacement behavior for transition zone sites resemble laboratory behavior experiencing wet and fouled ballast, tie-ballast gaps, or high-load environments. Site observations suggests all three factor may contribute.

3.4 Dynamic Wheel Loads

Wheel loads are defined as the load transferred at the wheel-rail interface and is a commonly measured value in track analyses. The wheel load then gets distributed amongst the underlying ties (rail seat / tie load) and then further distributed along each tie-ballast interface. This distribution can be assumed to relate ballast pressure and settlement or ballast settlement can be related directly to wheel load.

The wheel loads are compared in this section to determine the following:

- The magnitude and range of wheel load experienced at each site
- Whether increased wheel load explains increased settlements in the approach

The wheel loads are important for characterizing the load-displacement material behavior of the substructure materials and will be used in subsequent chapters. For those analyses, only peak values are necessary.

This analysis can also determine whether increased wheel loads at a particular location explain the increased permanent vertical displacements at each tie location. However, this setup cannot disprove the existence of increased wheel loads in the approach because only a single location is measured. The entire approach or an instrumented wheelset (Chapter 2.4.3) would be necessary to determine if the "rapid change in axle elevation" mechanism introduced in Chapter 2.4.3 is influential at these site locations.

Additionally, the influence of train velocity and dynamic wheel load is not considered. Recent studies suggest the influence of train velocity is lower than initially anticipated (Van Dyk et al., 2016). Additionally, train velocity is not believed to be high enough for seismic waves to be influential and the lack of variation in train velocity prohibit direct comparisons.

3.4.1 Measured Wheel Loads

As mentioned in Chapter 2.4.3, wheel loads can be measured using multiple methods. The method selected for this instrumentation setup involves installing strain gauges on the rail and relating applied wheel load to rail bending. This subsection describes the setup, calibration, and data interpretation.

Wheel loads are measured by installing stain gauges on the rail above the crib (see Figure 3.8). It is necessary to install the strain gauges above the crib because rail bending can be measured without influence from ties and tie support. To field calibrate these gauges, a load-frame is used (Figure 3.17). The load applied is measured with a load cell at the base of the load-frame and this is correlated with the rail bending measured using the two strain gauges. Therefore, when a train passes, the stain gauges measure the strain of the rail due to bending and the result is converted to applied load using the conversion factor shown below. The calculated load from the strain gauges is directly proportional to the amount of rail bending. The stain gauges installed above the tie (see Figure 3.8) uses the same principals.

$$Measured\ Load\ (kN) = 0.0818 * Voltage\ from\ Strain\ Gage \tag{3.1}$$

Figure 3.17: Photo of load-frame used to calibrate strain gauges and MDDs on Amtrak NEC by Marty Perkins and Carl Walker (photo courtesy of Deb Mishra).

A set of measured wheel load data for a passing Acela high-speed passenger train on Amtrak's NEC at Upland (60 ft.) on 7 August 2012 at 11:18 AM is shown in Figure 3.18. The train consists of two heavy power cars and seven lighter passenger cars with four axles per car. The first and last set of four measured wheel loads clearly shows the heavier power cars.

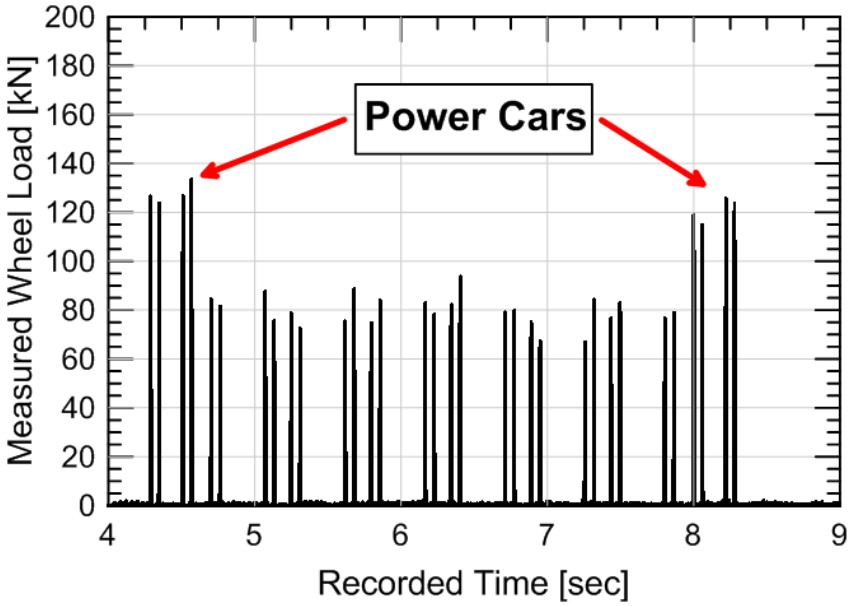

Figure 3.18: Measured passing wheel load at Upland (60 ft.) on 7 August 2013 at 11:18 AM.

A set of measured wheel load data for a passing freight train at NS MP 352.2 (13 ft) site on 2 November at 8:43 AM is shown in Figure 3.19. The train consists of engines and both loaded and unloaded freight cars, resulting in significant variations of applied load within a single train. This variation in load is helpful in subsequent analyses to characterize ballast and subgrade behavior.

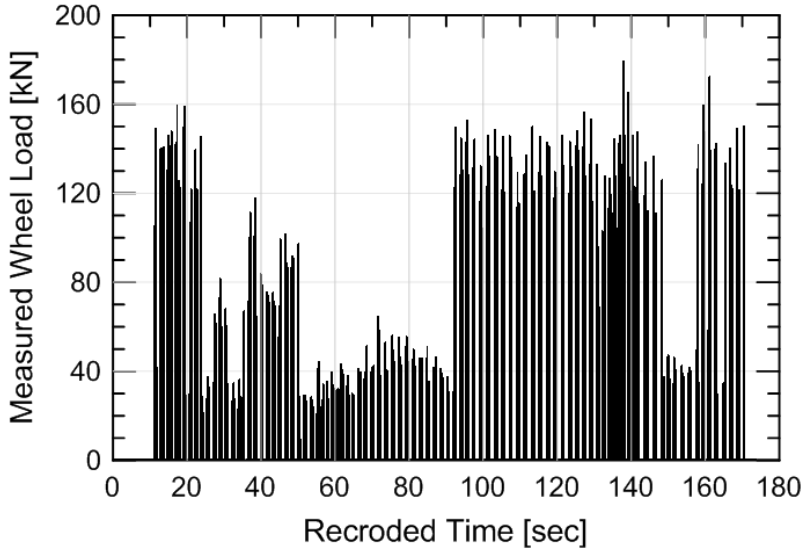

Figure 3.19: Measured passing wheel load at MP 352.2 (13 ft) on 2 November 2013 at 8:43 AM.

To emphasize the differences between passenger and freight trains, Figure 3.20 compares the measured wheel load time histories. The passenger train data was measured at Upland (15 ft.) on 7 August 2012 at 11:18 AM while the freight train data was measured at MP 352.2 (13 ft) on 2 November 2013 at 8:43 AM. Figure 3.20 shows the freight trains are much longer and move at a much slower speed than the passenger trains. The nine car Acela train passes in less than five seconds while the freight trains pass over the instrumented tie for several minutes. Figure 3.20 also shows similar maximum wheel loads for freight and passenger cars, which implies the underlying components experience similar loads for both freight and passenger trains but with different durations.

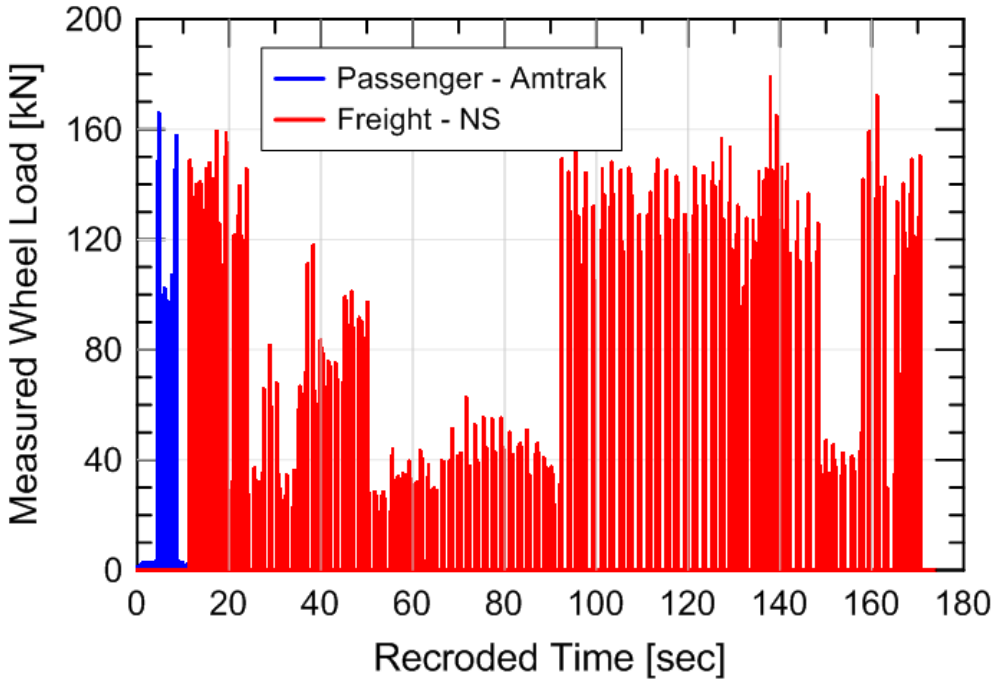

Figure 3.20: Comparison of passenger vs. freight wheel load measurements. Passenger train is Upland (15 ft.) on 7 August 2013 at 10:17 AM and freight train is at 352.2 (13 ft) on 2 November 2013 at 8:43 AM.

3.4.2 Amtrak Wheel Loads

The peak force measured from each passing wheel is the most useful parameter for this analysis. This data permits comparison of wheel loads between instrumented sites and help explain potential increased loads at various track regions. The average peak wheel loads for all six instrumented NEC sites are displayed in Table 3.7, which shows the highest wheel loads

correspond to the transition zones at Upland (15 ft.) and Madison (12 ft.). These tests sites also have the largest permanent vertical displacement in Figure 3.15.

The results show some variation between site locations with both transition zone locations experiencing greater wheel loads than the open track. Upland (15 ft.) experiences a wheel load 13% greater than Upland (60 ft.) and Madison (12 ft.) experiences a 4% increase. Without data at different site locations, it is unclear whether the transition is experiencing greater loads or whether the variation is simply the 15% variation that track is naturally expected to experience (see Chapter 2.4.3). Either way, a 13% increase, while notable, would not explain the 14x greater permanent LVDT #1 vertical displacements.

Caldwell (West) experiences an 11% greater average peak wheel load than Caldwell (East). The tie cross level was measured and found the west rail being one-eighth of an inch (1/8") lower than the east rail. The lower tie may be attracting more of the load because it is "downhill" from the east end of the tie.

Table 3.7: Average peak wheel loads at NEC instrumented sites

Upland Avenue		**Madison Avenue**		**Caldwell Avenue**		**All Sites**
15 ft. [kN]	**60 ft. [kN]**	**12 ft. [kN]**	**60 ft. [kN]**	**East [kN]**	**West [kN]**	**[kN]**
96.3	83.3	93.2	89.5	75.6	85.7	86.7

Figure 3.21 compares the peak wheel loads between the two locations at each of the three bridges. The data shows fairly consistent greater wheel loads at Upland (15 ft.) and Caldwell (West) and more scatter at the Madison Avenue site. This suggests a physical mechanism is consistently causing the greater wheel loads at Upland (15 ft.) and Caldwell (West) while the Madison Avenue loads appear more random. Additionally, the averages do not appear to change much with time.

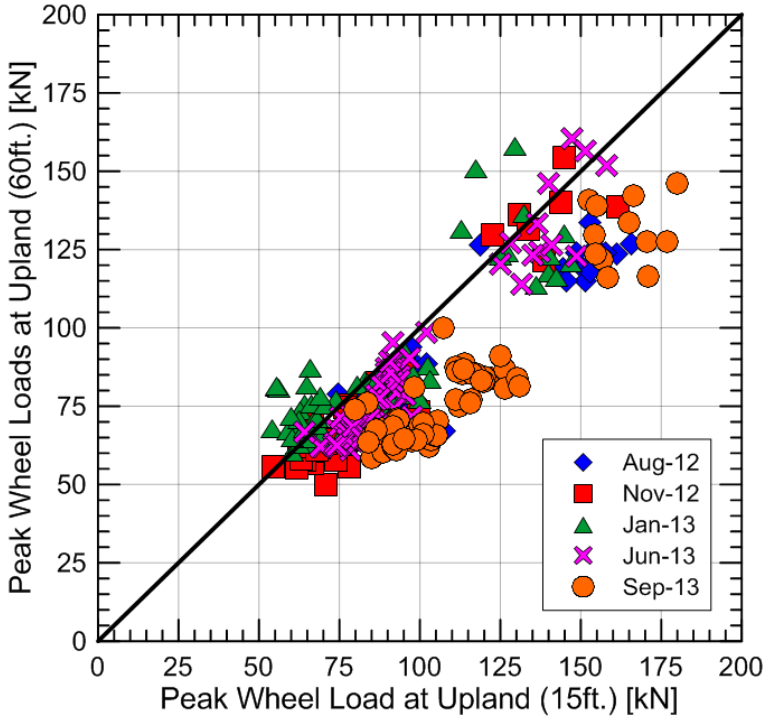

(a)

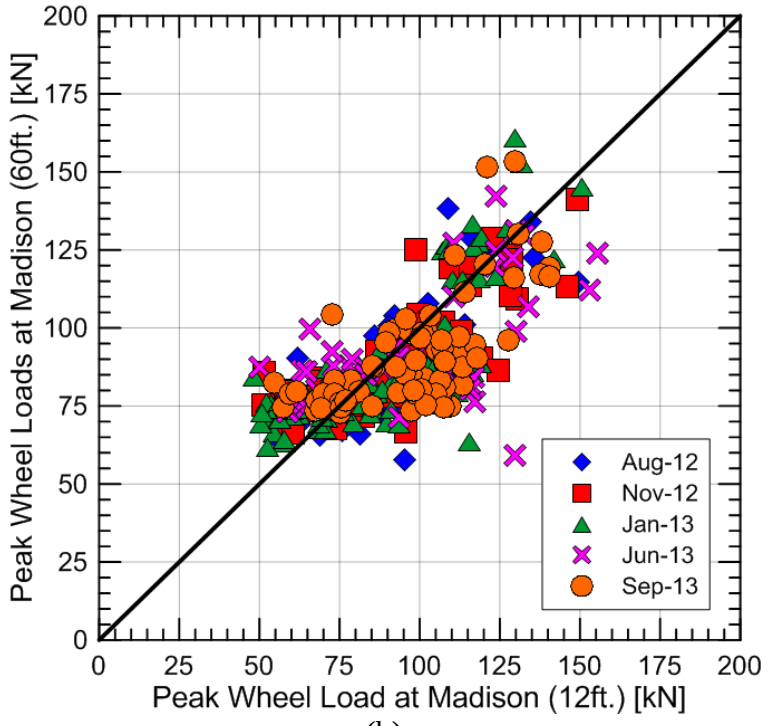

(b)

Figure 3.21 (cont.)

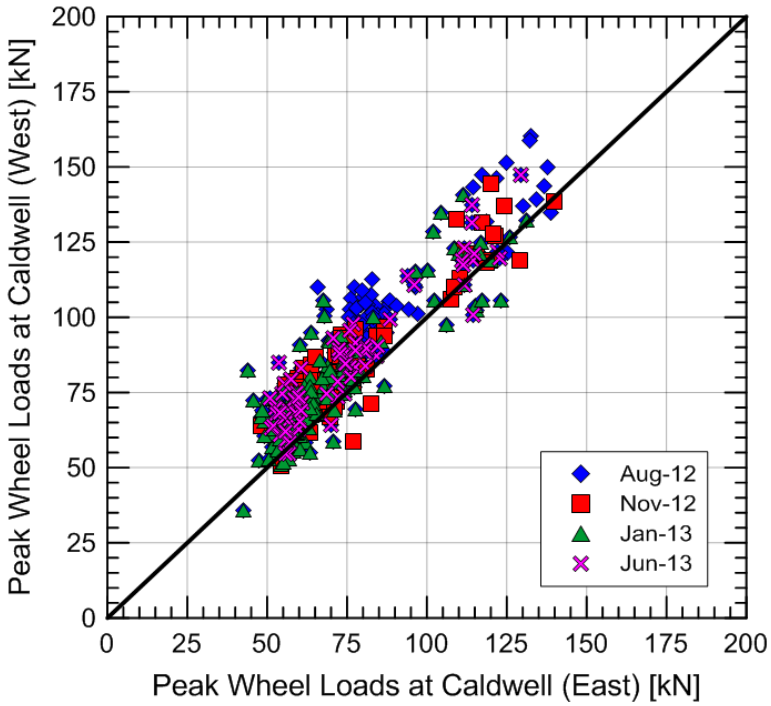

(c)

Figure 3.21: Comparison of wheel loads at (a) Upland Avenue, (b) Madison Avenue, and (c) Caldwell Avenue with 1:1 trend line.

Figure 3.22 compares the peak wheel load distribution of all Amtrak NEC sites by displaying the percentage of measured peak wheel loads exceeding the given value. Figure 3.22 verifies that Upland (15 ft.) and Madison (12 ft.) experience the largest peak wheel loads and Caldwell (East) experiences the smallest peak wheel load. However, the peak wheel load distributions are very similar at all sites.

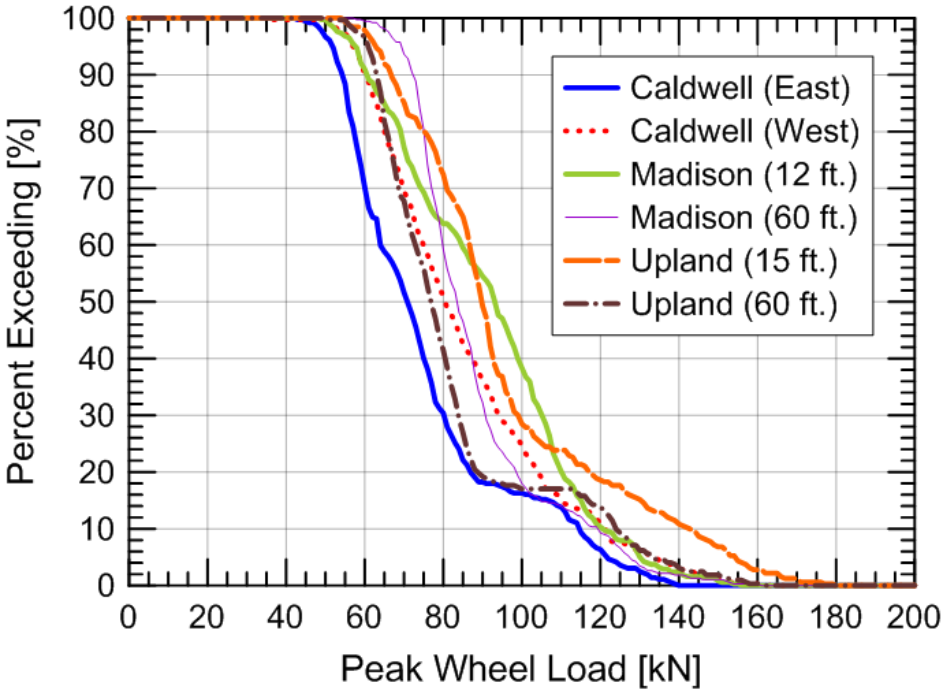

Figure 3.22: Comparison of load distributions for the six Amtrak NEC sites.

3.4.3 NS Wheel Loads

Unlike the Amtrak sites, each train comprises of some possible mixture of unloaded, partially loaded, and unloaded cars, resulting in trains that vary significantly in loading, and only a single NS train was measured per site. This makes direct comparisons between sites impossible but the peak wheel load analysis is completed because of its importance to characterizing the load-displacement material behavior of the substructure.

The average peak wheel load of the eight measured freight trains along the NS track is calculated and displayed in Table 3.8. Table 3.8 shows a wide range of peak wheel loads, which should be expected because some of the freight cars may be unloaded, partially loaded, or fully loaded. For example, two fully loaded freight trains passed over MP 352.2 (31 ft.) during recording, explaining the greater wheel loads, while mostly unloaded and mixed trains passed over the remaining three sites. The load distribution of all four recorded NS freight trains is displayed in Figure 3.23.

Table 3.8: Average peak wheel loads at NS N-Line sites

MP 352.2 (31 ft) [kN]	MP 352.2 (13 ft) [kN]	MP 352.8 (11 ft) [kN]	MP 352.8 (29 ft.) [kN]	All Sites [kN]
141.5	53.5	66.9	50.7	79.0

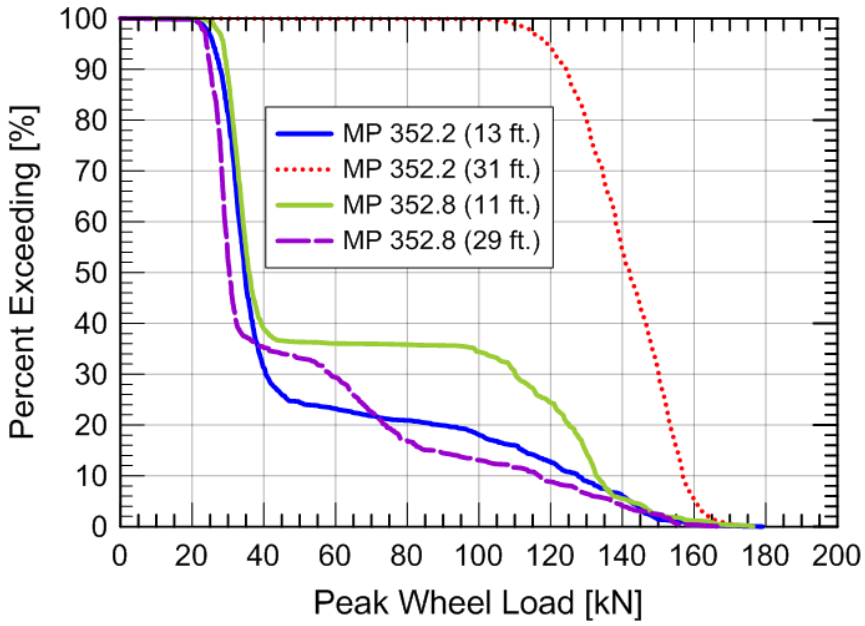

Figure 3.23: Comparison of load distributions for the four NS N-Line sites.

3.4.4 Summary of Wheel Loads

Analyzing dynamic wheel load is important for determining the load transferred at the wheel-rail interface and served as an important input for analysis. The following is a summary of the wheel load analysis:

- Peak dynamic wheel loads for all ten sites were similar with maximum values of about 180 kN (40 kips).
- Upland (15 ft.) consistently showed about a 13% greater average peak wheel load than Upland (60 ft.). This suggests some physical mechanism is producing the increased load but is it is not considered a cause of accelerated settlement because the value below the naturally expected variation in track (15%).
- Caldwell (West) consistently experienced about a 11% greater average peak wheel load than Caldwell (East) and is explained by the east rail being 1/8" higher than the west rail.
- Additional locations or an instrumented wheel set would be necessary to prove or disprove the anticipated "increase in axle elevation" mechanism so no conclusions can be made from this instrumentation setup.

3.5 Tie Reaction

Tie Reaction is defined as the load transferred at the rail-tie interface and is commonly referred to as rail seat load or tie load. This metric is less common in analyses but can give valuable insight into the distribution of wheel load amongst underlying ties, the load transferred to the underlying ballast, and can be used for characterizing the load-displacement material behavior of the substructure layers.

The tie reactions are compared in this section to determine the following:

- The magnitude and range of tie reactions experienced at each site.
- The range and characterization of tie support conditions
- Whether increased tie reactions explains increased settlements in the approach.

As introduced in Chapter 2.3.2, the peak tie reaction value is expected to be about 30 to 50% of the wheel load for track conditions in which the displacement is homogenous along the track and the track structure response is linear. Calculating peak tie reaction values can indicate whether or not the track conditions are holding to these assumptions. If the tie is unsupported, i.e. non-linear behavior, or if track conditions are heterogeneous, the tie reaction values are anticipated to be lower or higher in the case where all surrounding ties are unsupported so the majority of load is transferred to the instrumented tie.

3.5.1 Calculating Tie Reaction

Calculating tie reactions involves subtracting the load measured by the strain gauges above the tie from the load measured by the strain gauges above the crib, i.e. track in-between ties, as shown below. It is assumed that the load measured above the crib is the actual wheel load which is usually greater than the tie load because the tie is not rigidly supported. The tie reaction is calculated using the expression in Equation 3.2:

$$Tie\ Reaction = Load\ above\ crib - Load\ above\ tie \tag{3.2}$$

The strain gauges above the tie use the wheel load calibration factors and are assumed to measure bending in an identical manner. Below is an explanation on how rail bending can be used to indirectly measure tie reaction and serve as an indicator for tie support.

- If a perfectly rigid tie lies on a perfectly rigid foundation, 100% of the wheel load will be transferred from the rail to the tie when the wheel is directly above the tie. Physically, this means the rail bending strain above the tie will be zero. Therefore, the tie reaction value will equal the wheel load (load above crib).
- If a tie is completely unsupported, 0% of the wheel load will be transferred from the rail to the tie when the wheel is directly above the tie. Physically, this means the rail bending strain above the tie will be equal to the rail bending strain above the crib. Therefore, the tie reaction value will be zero.
- If a tie is well-supported, about 40% of the wheel load will be transferred from the rail to the tie when the wheel is directly above the tie (AREMA, 2013; Chang et al., 1980). Physically, this means the rail bending strain above the tie will about 60% of the rail bending strain above the crib because the rail will experience some displacement from fastener, tie, and substructure deformation. Therefore, the tie reaction value will be about 40%.

Figure 3.24 compares the measured wheel load above the crib and tie for Upland (60 ft) and Upland (15 ft) on 7 August 2012 at 10:17 A.M, respectively. At Upland (60 ft.), the load above the tie is noticeably lower than the load above the crib, indicating good tie support, while the loads above the crib and tie are near equal at Upland (15 ft.), indicating poor tie support.

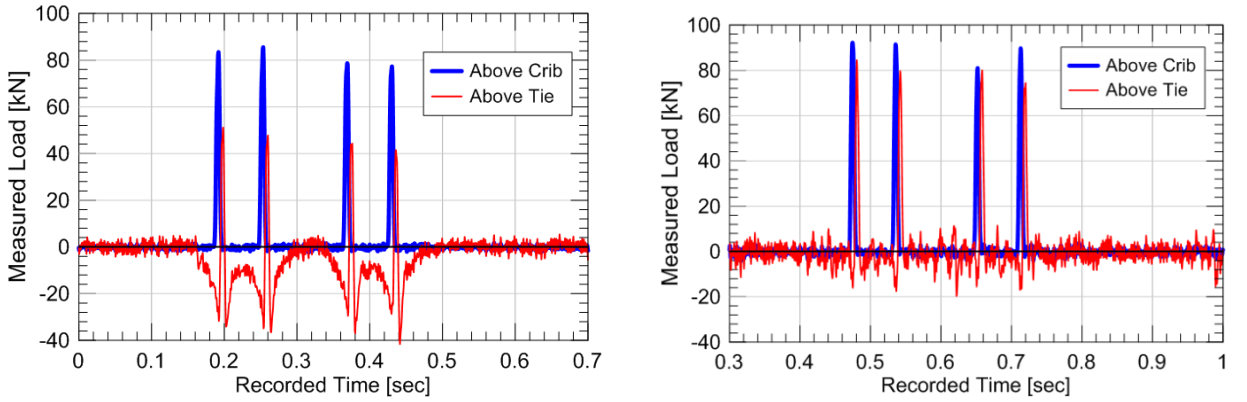

(a) (b)

Figure 3.24: Measured load above crib (wheel load) and tie at (a) Upland (60 ft.) on 7 August 2012 showing good tie support and (b) Upland (15 ft.) on 7 August 2012 showing poor tie support.

Tie reaction for both scenarios is calculated and plotted in Figure 3.25. Despite the scatter, the tie reaction time history is recognizable for Upland (60 ft.) with the tie reaction about 50% of the peak wheel load values. At Upland (15 ft.), the peak tie reaction is barely recognizable with tie reactions values being about 20% of the peak wheel load values. This suggests that the Upland (15 ft.) tie is experiencing poor tie support.

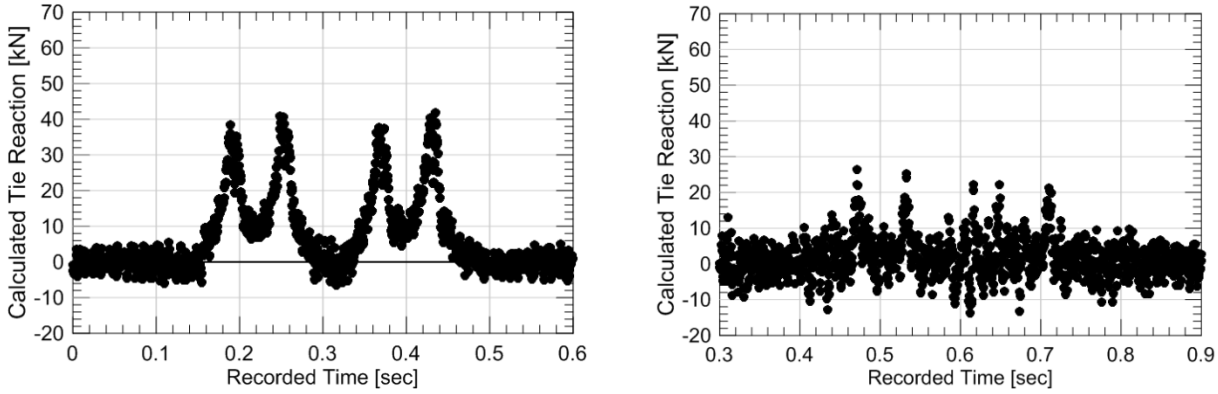

(a) (b)

Figure 3.25: Tie reaction loading at (a) Upland (60 ft.) on 7 August 2012 showing good tie support and (b) Upland (15 ft.) on 7 August 2012 showing poor tie support.

3.5.2 Tie Load Ratio

To quantify the quality of tie support, the term "tie load ratio" was developed. Tie load ratio is the ratio between the peak measured tie reaction and peak measured wheel load in the crib. A value of 100% indicates full and rigid tie support while 0% indicates zero support, i.e. a hanging tie. Values around 40% are often associated with good tie-ballast support (Chang et al., 1980) while values below 30% are associated with poor tie support.

$$Tie\ Load\ Ratio = \frac{Tie\ Reaction}{Wheel\ Load} = \frac{Load\ above\ crib - Load\ above\ tie}{Load\ above\ crib} \tag{3.3}$$

Figure 3.26 shows the tie load ratio at the six Amtrak NEC instrumented locations for each measured passing wheel. Each plot has a green line at 40% to indicate the value corresponding to good tie support. Table 3.9 displays the average tie load ratio at each NEC site. The average tie load ratio is calculated by taking the average and standard deviation tie load ratio

from all passing wheels at a particular site. From the data in Figure 3.26 and Table 3.9, the following observations of track behavior can be made:

- The tie load ratios roughly inversely correlates with permanent vertical displacements. For example, Upland (60 ft.), which experienced the least amount of permanent vertical displacement, shows the best tie support and has an average tie load ratio of 44%. Conversely, Upland (15 ft.), which experienced the greatest amount of permanent vertical displacement, shows the worse tie support and has an average tie load ratio of only 3%. The other sites have average tie load ratios between these two extremes (44% and 3%).
- The two transition zone sites, Upland (15 ft.) and Upland (60 ft.) experience more inconsistent tie load ratio values (17% and 18% standard deviation) than the four open track sites (13% and 8% standard deviation). This range and variation of tie load ratio from one wheel to another in the same train implies that wheel loads are being distributed in an inconsistent manner between adjacent ties. These erratic tie load ratios within the same time period can be attributed to poor tie support at the instrumented and surrounding ties and damaged ties. If support conditions change during the passing of a train, e.g., development of pore-water pressures in wet fouled ballast, this load redistribution will change as well.
- Negative tie load ratios can be explained by defects in wheels, rails, or bouncing of the wheel, all of which cause higher wheel loads over the tie than the crib. However if this is the case, the negative tie load should be random and occur only sparingly. At Madison (12 ft.) and Upland (15 ft.), the negative tie load ratios are much more consistent, implying that this is likely not the case. The negative tie load ratios are then possibly due to wheel bouncing from broken or damaged ties near the instrumented tie. This could result in consistently greater rail bending above the tie than rail.

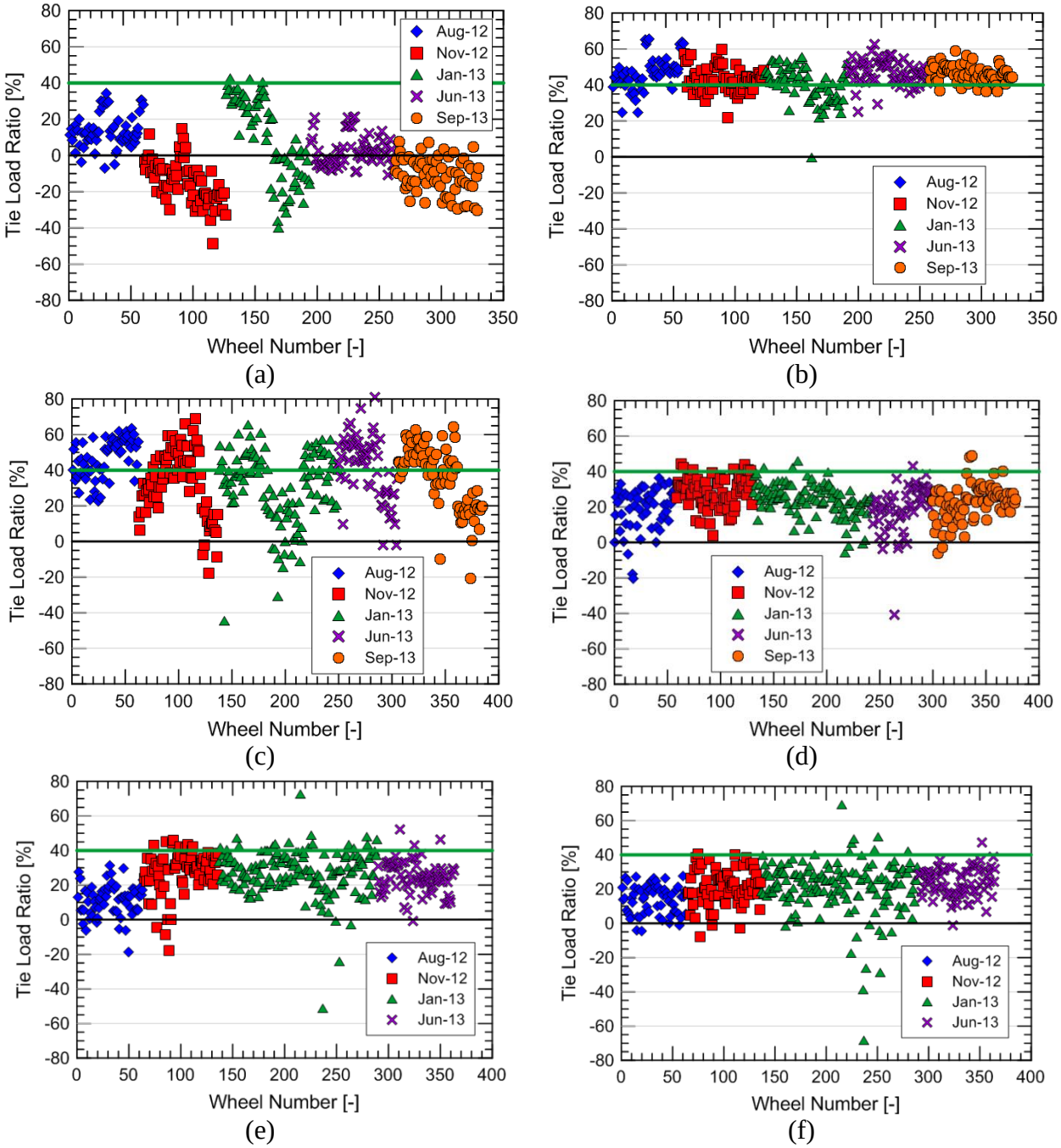

Figure 3.26: **Tie load ratio for each passing wheel at (a) Upland (15 ft.), (b) Upland (60 ft.), (c) Madison (12 ft.), (d) Madison (60 ft.), (e) Caldwell (East), and (f) Caldwell (West).**

Table 3.9: Average and Standard Deviation of tie load ratio at the six Amtrak NEC sites

	Upland		Madison		Caldwell	
	15 ft.	**60 ft.**	**12 ft.**	**60 ft.**	**East**	**West**
Average	3%	44%	36%	23%	24%	21%
Standard Deviation	17%	8%	18%	13%	13%	13%

The tie load ratios of each passing wheel load at each NS site are shown in Figure 3.27 and the average tie load ratios is displayed in Table 3.10. The average and standard deviation are not taken because, as presented in the next analysis, tie load ratio is dependent on the wheel load so results will not be representative.

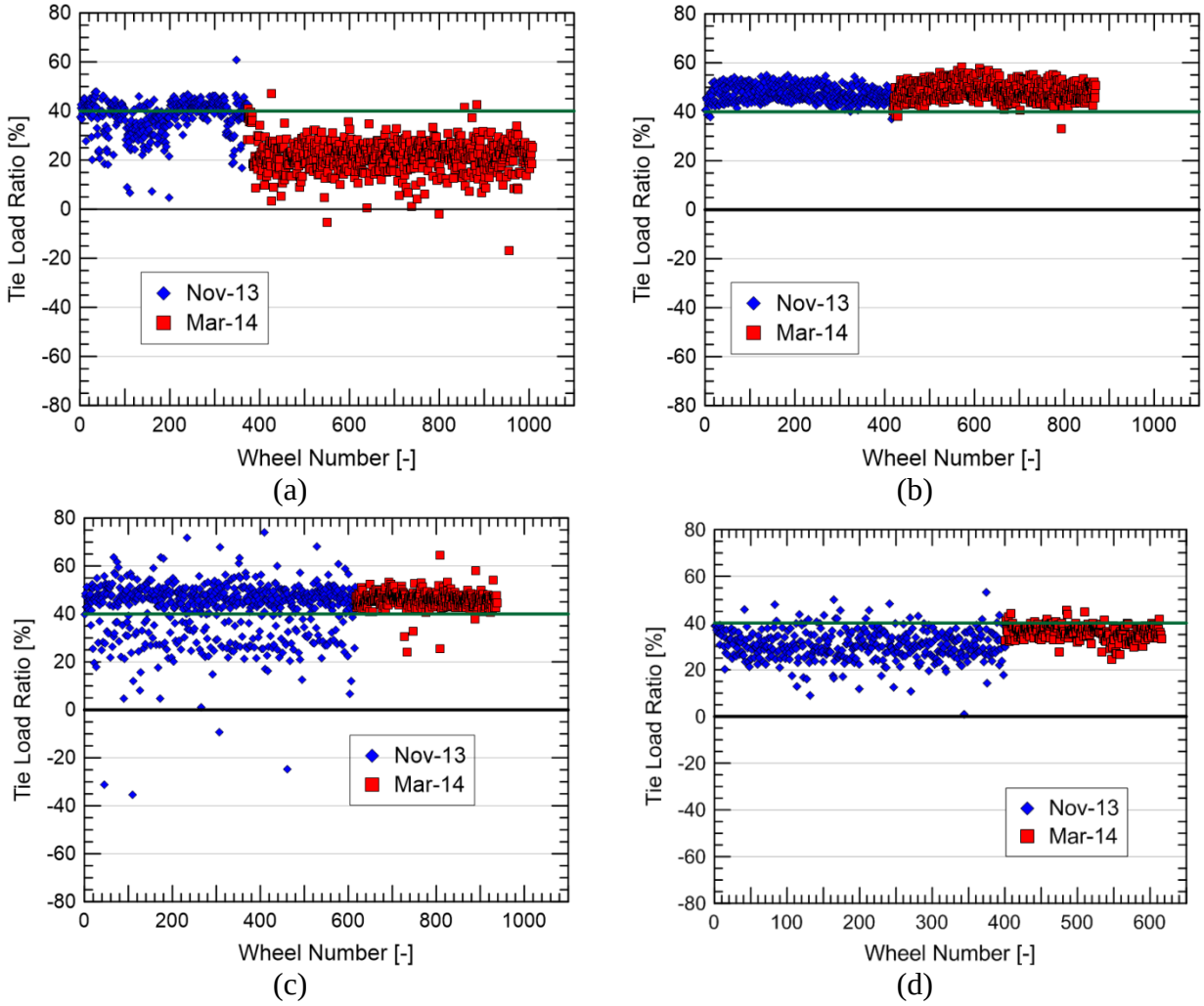

Figure 3.27: Tie load ratio for each passing wheel at (a) MP 352.2 (13 ft.), (b) MP 352.2 (31 ft), (c) MP 352.8 (11 ft.), and MP 352.8 (29 ft.).

3.5.3 Tie Load Ratio v. Wheel Load

A different perspective on tie support can be obtained by plotting the tie load ratio as a function of wheel load. Good tie support is indicative of a relatively constant tie load ratio with increasing wheel load. Conversely, if the tie load ratio is initially low and increases with increasing wheel load, this indicates poor tie support at low wheel loads and increasing tie support as the wheel load increases because the tie requires greater wheel load to close the tie-ballast gap. Figure 3.28 show the comparison of tie load ratio and wheel load at all six Amtrak instrumented sites. The green line at a tie load ratio of 40% in each plot represents good tie support conditions.

Upland (60 ft.), Figure 3.28(b), shows relatively good tie support because the tie load ratio is relatively constant with increasing wheel load. Comparing the tie load ratio with applied wheel loads shows that Upland (15 ft.) and Madison (12 ft.) display poor tie support behavior in Figure 3.28(a) and (c), respectively. These locations also experience the greatest permanent LVDT #1 vertical displacements. The other four sites display more constant tie loads with increasing wheel load, implying good or consistent support behavior.

Figure 3.29 compares the tie load ratio for the corresponding wheel load at the four recorded NS bridge sites. The plots show similar behavior for all four sites, in which tie support is around 40% for all peak wheel loads about 50 kN and drops significantly as peak wheel load decreases. This suggests that the about 50 kN is required to close any gaps within the track system and fully mobilize the substructure materials (see Chapter 2.4.3). The trend is not apparent at MP 352.2 (31 ft.) because only loaded train cars were measured so behavior from unloaded cars is not known. The low tie load ratio values below 50 kN imply non-linearity but it difficult to discern closure of gaps within the track system from mobilization of substructure materials, as both contribute to non-linearity.

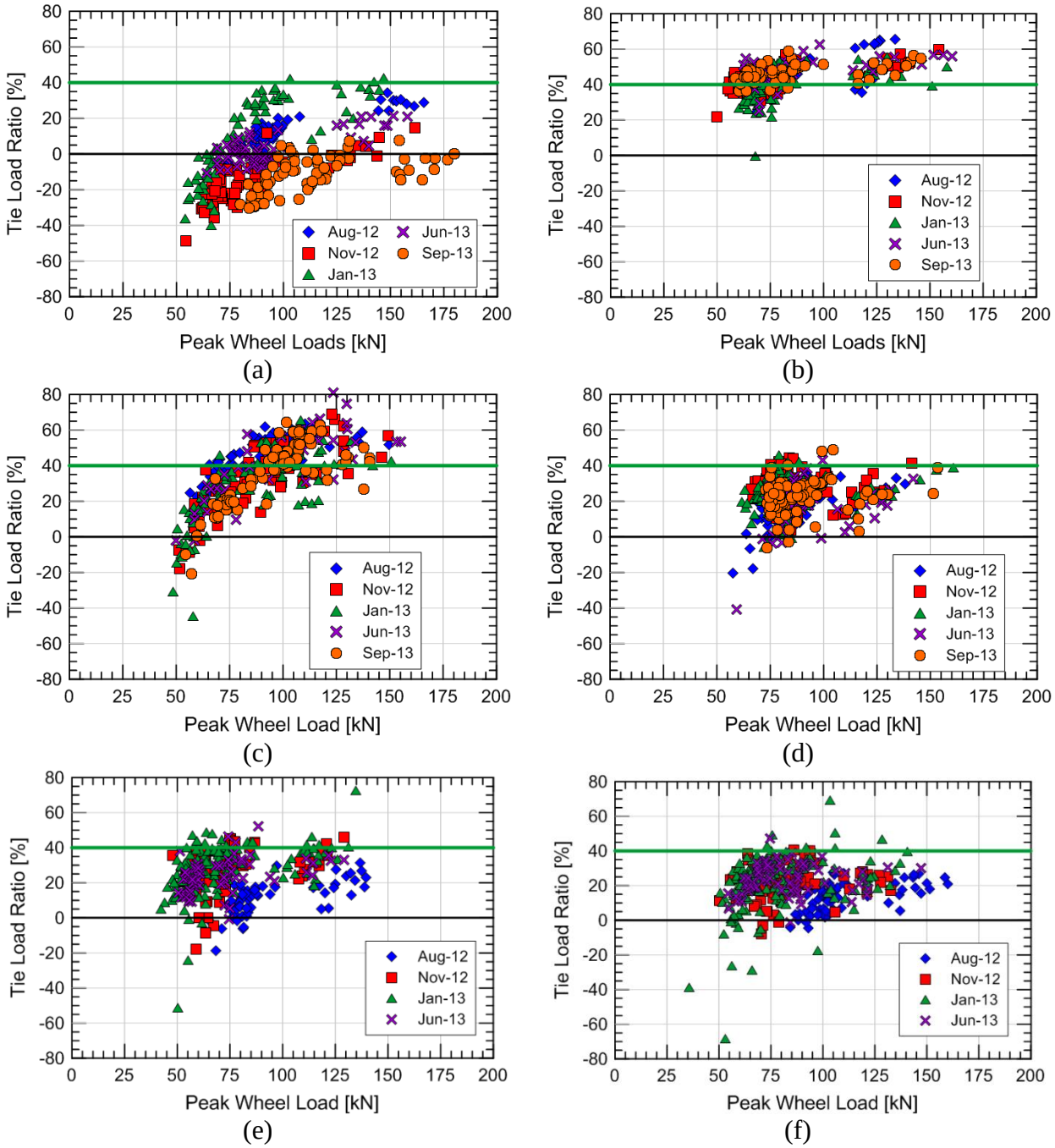

Figure 3.28: Comparison between tie load ratio and wheel load for each passing wheel at (a) Upland (15 ft.), (b) Upland (60 ft.), (c) Madison (12 ft.), (d) Madison (60 ft.), (e) Caldwell (East), and (f) Caldwell (West).

Additionally, this suggests that all four sites are generally well supported at load about 50 kN and differences in average tie load ratio are more reflective of the number of empty freight cars than tie support conditions.

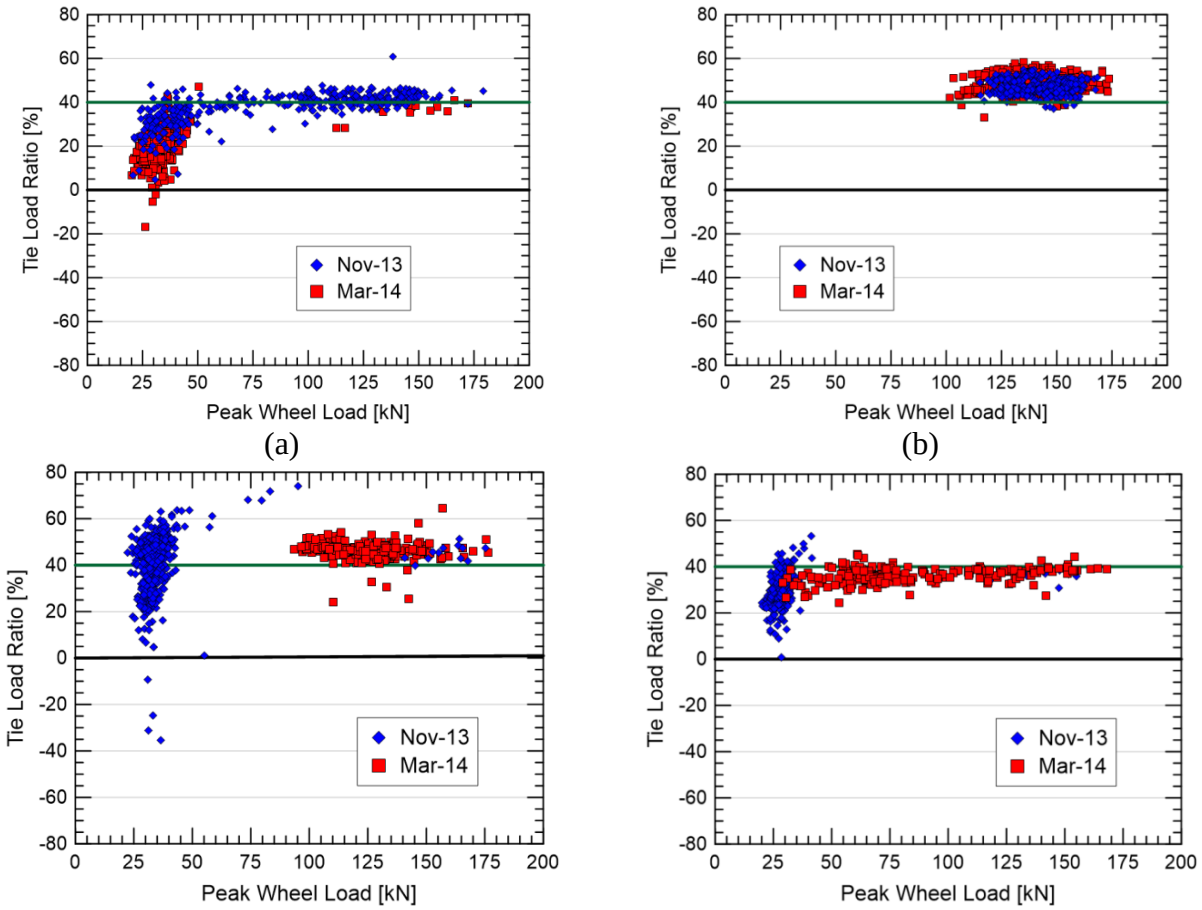

Figure 3.29: Comparison between tie load ratio and wheel load for each passing wheel at (a) MP 352.2 (13 ft.), (b) MP 352.2 (31 ft), (c) MP 352.8 (11 ft.), and MP 352.8 (29 ft.).

3.5.4 Discussion of Tie Reaction Results

The tie reaction measurement has the potential to be informative because it indirectly measures the load transferred from the rail to the rail seat via rail bending. However, the results suggest that tie reaction is more indicative of tie support than measurable tie load.

First, the Amtrak results show a rough inverse correlation between tie load ratio and permanent LVDT #1 vertical displacement rates. This is surprising as tie load and ballast settlement should be related. For example, taking the average wheel load, tie load ratio, and permanent LVDT #1 vertical displacement rates, a tie load of 36.7 kN produces 1.03 mm/yr permanent vertical displacement at Upland (60 ft.) while a tie load of 2.8 kN produces 14.1 mm/yr permanent LVDT #1 vertical displacement at Upland (15 ft.). Assuming linear settlement behavior, this suggests that 180 times the tie load at Upland (60 ft.) is required to produce

identical permanent LVDT #1 vertical displacements. This claim is contested by almost all laboratory and empirical data and makes little sense conceptually.

Secondly, tie reaction measures rail bending and not load or pressure transfers. It is anticipated that for highly non-linear load-displacement conditions from tie-ballast gaps or unmobilized substructure materials, high tie displacement can occur while still transferring significant load. Additionally, impacts from closure of tie-ballast gaps (see Chapter 2.4.3) or degradation of ballast from continual impact (see Chapter 2.2.4) can contribute to increased load and settlement and would not necessarily affect rail bending.

Therefore, tie reaction analysis is likely more indicative of support conditions than the transfer of load throughout the tie. This conceptually is unsurprising as unsupported ties are anticipated in transition zones experiencing track geometry problems because the differential settlement between the bridge and approach produces hanging ties (see Chapter 2.4.2).

3.5.5 Summary of Tie Reaction

In summary, tie reaction and tie load ratio can be used to estimate the quality of tie support and possibly the load being applied to the tie in well-supported conditions. The following is a summary of the wheel load analysis:

- Tie load ratios at the Amtrak sites appear to roughly inversely correlated with permanent LVDT #1 vertical displacements. This suggests that tie load ratio indicates poor tie support and not load transfer.
- The NS sites show low tie load ratios below 50 kN and about 40% above 50 kN. This suggests that 50 kN is required to close all gaps within the track system and mobilize resistance from the substructure materials. The 50 kN threshold can be referred to as the seating load.

3.6 Measured Transient Vertical Displacements

This section presents the analysis of the transient vertical displacements measured at the various instrumented locations along the Amtrak and NS sites. The main objectives are to: (1) locate the depth at which the majority of the transient vertical displacements are occurring, (2) determine which instrumented sites exhibit the largest transient vertical displacements, and (3)

mathematically characterize the LVDT behavior to correlate with permanent vertical displacement rates (Chapter 3.3) and for use in analyses and numerical modeling (Chapter 5).

3.6.1 Transient Substructure Behavior

This section introduces the transient vertical displacement time history records of passing trains from various sites to describe behavior and traits of the time history that may not be apparent from analyzing peak values.

A typical set of wheel loads and corresponding measured transient LVDT vertical displacements from a passing Acela high-speed passenger train are shown in Figure 3.30. The data set was measured at Upland (60 ft.) on 7 August 2012 at 10:17 AM and shows that the transient response of the LVDTs matches the wheel loads for the entire train. As each wheel passes over the instrumented tie, the loaded tie displaces the underlying LVDTs. Some notable features are that the peak LVDT displacements increase with increasing load and that while LVDT #1 is the largest displacement component for the lower weight passenger cars, LVDT #3 and #4 are the largest displacement component for the heavier power cars. This is due to non-linearity in LVDT #1 that is described in detail in subsequent sections.

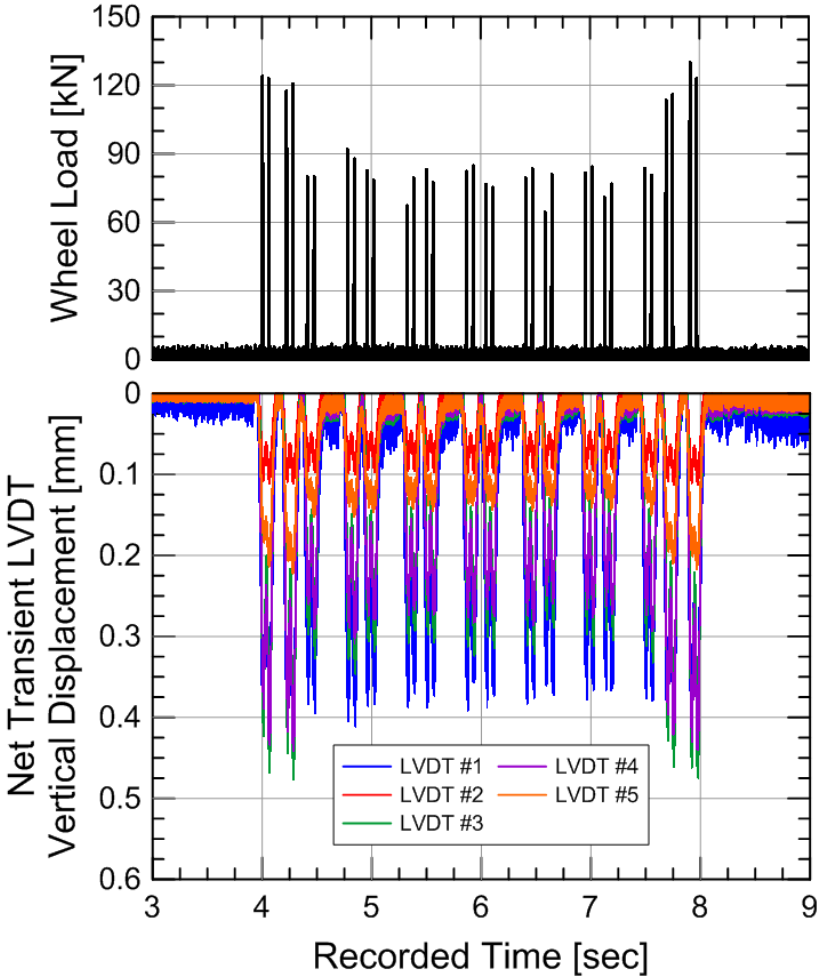

Figure 3.30: **Measured Wheel Loads and corresponding transient vertical displacements time histories at Upland (60 ft.) on 7 August 2013 at 10:17 AM.**

Figure 3.31 presents a more focused view on the transient substructure displacement response from four wheels of a passing high-speed Acela train at Upland (60 ft.) and Upland (15 ft.) on 7 August 2012. Upland (60 ft.) and Upland (15 ft.) were chosen as examples because they exhibit the smallest and largest permanent LVDT #1 vertical displacement, respectively. The vertical axes of Figure 3.31 are scaled differently to emphasize the different behavior of these two sites.

Figure 3.31(a) shows the tie reaction and LVDT response at Upland (60 ft.). As the passing wheels imparts load through the tie and into the substructure, the underlying LVDTs displace downwards. Eventually each LVDT reaches a peak value and returns to, or near, its original position when unloaded. Due to the close proximity of the wheels on the same truck (≈ 9

ft.), the substructure reloads before reaching its original unloaded position, i.e., a transient displacement equal to zero (0), resulting in two local peaks for each passing truck.

Notable features of the Upland (60 ft.) time history are that the tie reaction and all five LVDT displacements appear to move in unison and in a smooth fashion. This implies a smooth distribution of load throughout the track and minimal relative movement between track components. This represents an ideal response for track.

Many differences exist between the measured transient vertical displacements at the Upland (60 ft.) and Upland (15 ft.) sites. The following summarize some of these differences between these transition and open track sites:

- The peak transient vertical displacement of LVDT #1 at Upland (15 ft.) is much greater than Upland (60 ft.), i.e., 1.5 mm versus 0.4 mm, which is evident by comparing the different vertical axes in Figure 3.31.
- At Upland (60 ft.), all five LVDT vertical displacements began recording displacements at the same time while at Upland (15 ft.), the vertical displacements for LVDTs #2 through #5 were recorded after LVDT #1. This shows a delay in the load transfer from the tie to the underlying materials at Upland (15 ft.) and is believed to be from the presence of a tie-ballast gap.
- While the vertical displacements in LVDT #1 are smooth at Upland (60 ft.), a more erratic response is observed in LVDT #1 at Upland (15 ft.) including a few “bumps” at a vertical displacement of 1 mm. This is believed to be instant in which the unsupported tie makes contact with the underlying ballast.
- A significant amount of vertical rebound (upwards displacement) is measured at Upland (15 ft.) while there appears to be little to no rebound at Upland (60 ft.).

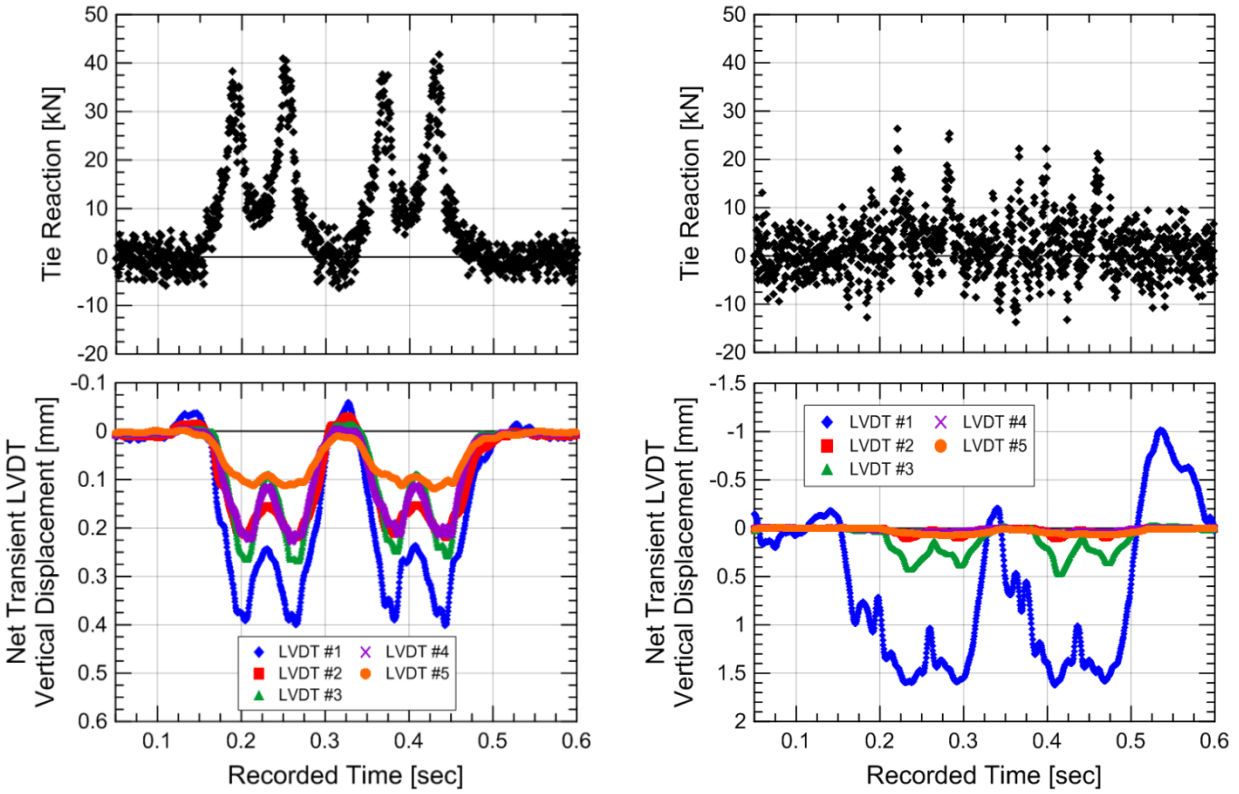

Figure 3.31: Tie reaction and transient LVDT vertical displacement response (note different axes) at (a) Upland (60 ft.) and (b) Upland (15 ft.) on 7 August 2012.

These observations all indicate Upland (15 ft.) is unsupported while Upland (60 ft.) has good tie support and is behaving adequately. If the Upland (15 ft.) tie is unsupported, LVDT #1 will experience displacement as the tie-ballast gap closes and the tie establishes contact with the ballast. This is believed to occur at about 1.0 to 1.3 mm. Once the tie is in contact with the ballast, load transfer commences and the substructure materials mobilize frictional resistance to counter tie penetration. The transient response after substructure mobilization will then be similar to the well supported tie at Upland (60 ft.) in Figure 3.31(a). When observed visually, the tie movement at Upland (15 ft.) during train passage is obvious and this erratic movement is often referred to as a "dancing tie".

Figure 3.32 presents transient data from MP 352.2 (31 ft) and 352.2 (13 ft). Figure 3.32(a) shows nine passing wheels at bridge MP 352.2 (31 ft) while Figure 3.32(b) shows eight passing wheels at bridge MP 352.2 (13 ft). As with Figure 3.31 for Upland (60 ft.) and (15 ft.), respectively, the transient vertical displacement axes are scaled differently to emphasize the

transient behavior. The corresponding measured wheel load time histories are also included for reference purposes.

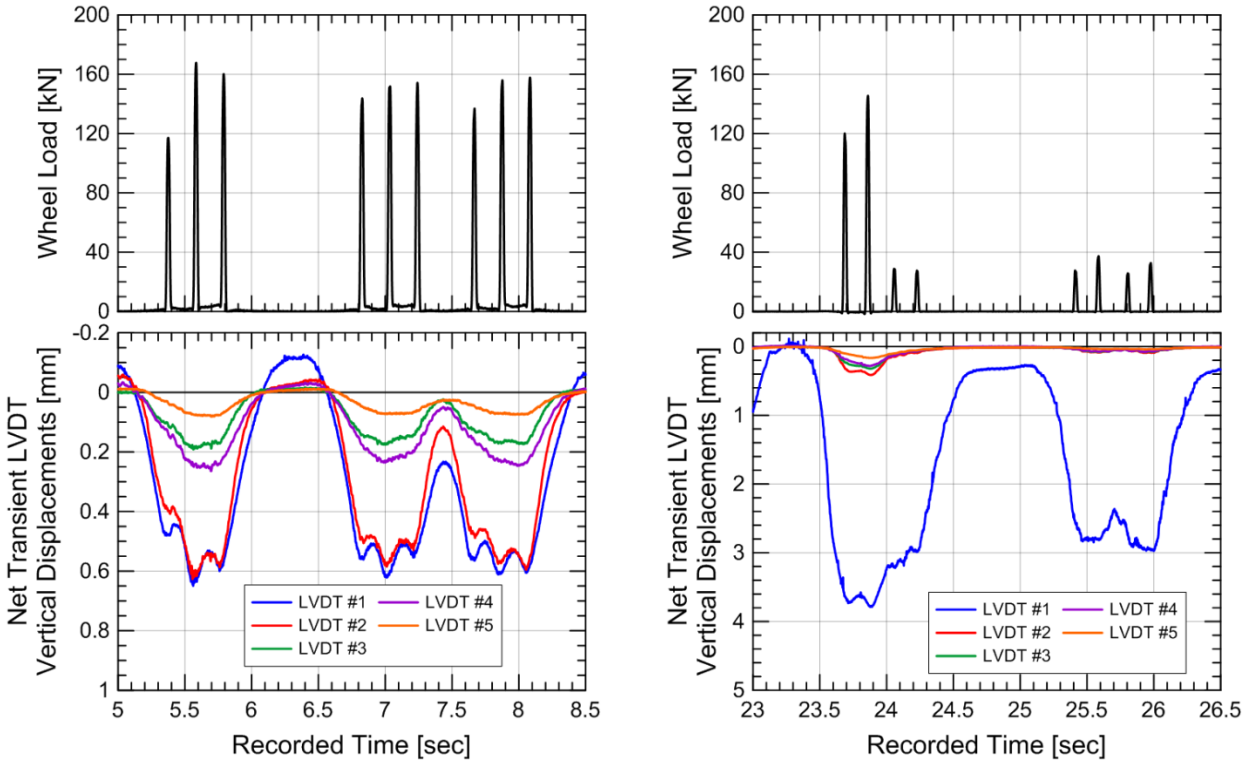

Figure 3.32: Transient LVDT displacement response at (a) NS bridge MP 352.2 (31 ft) and (b) NS bridge MP 352.2 (13 ft) on 2 November 2013.

Both the open track and the bridge transition measurements at MP 352.2 display behavior similar to Upland Avenue measurements. The open track displays smooth behavior in which all the LVDT displacements appear to move in unison. For the bridge transition location (MP 352.2, 13 ft.), the peak transient LVDT #1 vertical displacement is much greater than MP 352.2 (31 ft), i.e., 3.8 mm versus 0.6 mm. Additionally at MP 352.2 (13 ft), LVDTs #2 through 5 are delayed, which indicates the presence of a tie-ballast gap. This is another sign of poor tie support at MP 352.2 (13 ft.).

Differences in transient response between the high-speed passenger trains and slow-moving freight trains are evident by comparing the Amtrak and NS data and these differences are summarized below:

- The greater depth of LVDTs #3 through #5 at MP 352.2 sites results in a single peak displacement for a group of three or four passing wheels instead of a single peak per passing wheel observed at the NEC sites. This reduced response with depth is due to stress distribution with depth.
- Despite suspected unsupported behavior at MP 352.2 (13 ft), LVDT #1 does not display erratic behavior or rebound after a passing wheel set. This is likely due to the slower velocity of the passing freight wheels compared to Amtrak. This implies that transient behavior becomes more erratic as train velocity increases.

In summary, comparing the open track and bridge approach transient vertical displacement time histories at select Amtrak and NS instrumentation sites shows a difference between suspected supported and unsupported tie behavior. Suspected unsupported ties at the bridge approach display much larger peak transient LVDT #1 displacements and a delay in response time between LVDT #1 and #2 as the tie-ballast gap closes with the applied load. The peak values are emphasized in subsequent sections because of the ease of computing but viewing the behavior prior to analysis gives insight into causes of settlement at the transition locations.

3.6.2 Peak Transient LVDT Vertical Displacements

To gain an understanding of the depth and site locations at which the majority of the transient vertical displacement occurs, the peak transient vertical displacement of each LVDT from each recorded wheel is located and compared in this section. The analysis looks at changes in peak transient vertical displacements between LVDTs, between sites, and over time. The peak transient LVDT vertical displacement values are not used for analyses because they are influenced by the wheel load. Methods to eliminate the influence of wheel load are introduced in subsequent sections.

The peak transient vertical displacement value of each LVDT at all six Amtrak sites is displayed in Figure 3.33. The y-axes are scaled differently to emphasize which LVDTs are experiencing the largest peak transient vertical displacement at each particular instrumented site. In each plot, the data are separated by the month it was recorded, e.g., August 2012, November 2012, January 2013, and June 2013. Due to calibration issues, the data for LVDT #2 during the January 2013 recording of Madison (12 ft.) is not included in Figure 3.33(c). Tables 3.11 and 3.12 show the average transient vertical displacement of each LVDT expressed as a displacement value in mm in Table 3.11 and as a percentage of cumulative LVDT displacement in Table 3.12.

A few trends can be observed from the responses displayed in Figure 3.33. First, as with permanent vertical displacements, the largest contributor to transient displacement is LVDT #1, which measures from the top of the concrete tie to the bottom of the ballast layer. Upland (60 ft.) is the only site in which the average peak LVDT #1 displacement is close to subgrade layer displacements (29% in LVDT #1 v. 26% in LVDT #3 v. 23% in LVDT #4). In all other sites, LVDT #1 represents over half the cumulative peak transient displacement.

Second, the greatest variation in peak transient values is within LVDT #1. The sites of Upland (15 ft.), Madison (12 ft.), Madison (60 ft.) all show significant changes in peak transient LVDT #1 vertical displacement with time. For example, Upland (15 ft.) displays about 1.5 mm of peak transient LVDT #1 vertical displacement in January 2013 and then about 4.9 mm in June 2013. Due to discrete measurements, it is unclear how the variation changes daily, weekly, or seasonally. Additionally, the results show no clear effect of tamping or weather.

Third, the peak transient LVDT #1 vertical displacement values roughly correlate with the permanent LVDT #1 vertical displacement rates measured and displayed in Chapter 3.3. Upland (15 ft.) displays the greatest, followed by Madison (12 ft.), and with Upland (60 ft.) at the lowest value. The two Caldwell sites and Madison (60 ft.) are similar in value and are in-between Madison (12 ft.) and Upland (60 ft.). As explained in previous sections, larger peak transient LVDT #1 vertical displacements are an indicator of unsupported ties so these results agree with the tie reactions trends observed in Chapter 3.5.

Referencing back to Chapter 3.3, permanent vertical displacement rates appeared near the end of the analysis in LVDT #3 at Madison (12 ft.) and LVDT #2 at Caldwell (East). No evidence of increased transient vertical displacements at these locations are observed.

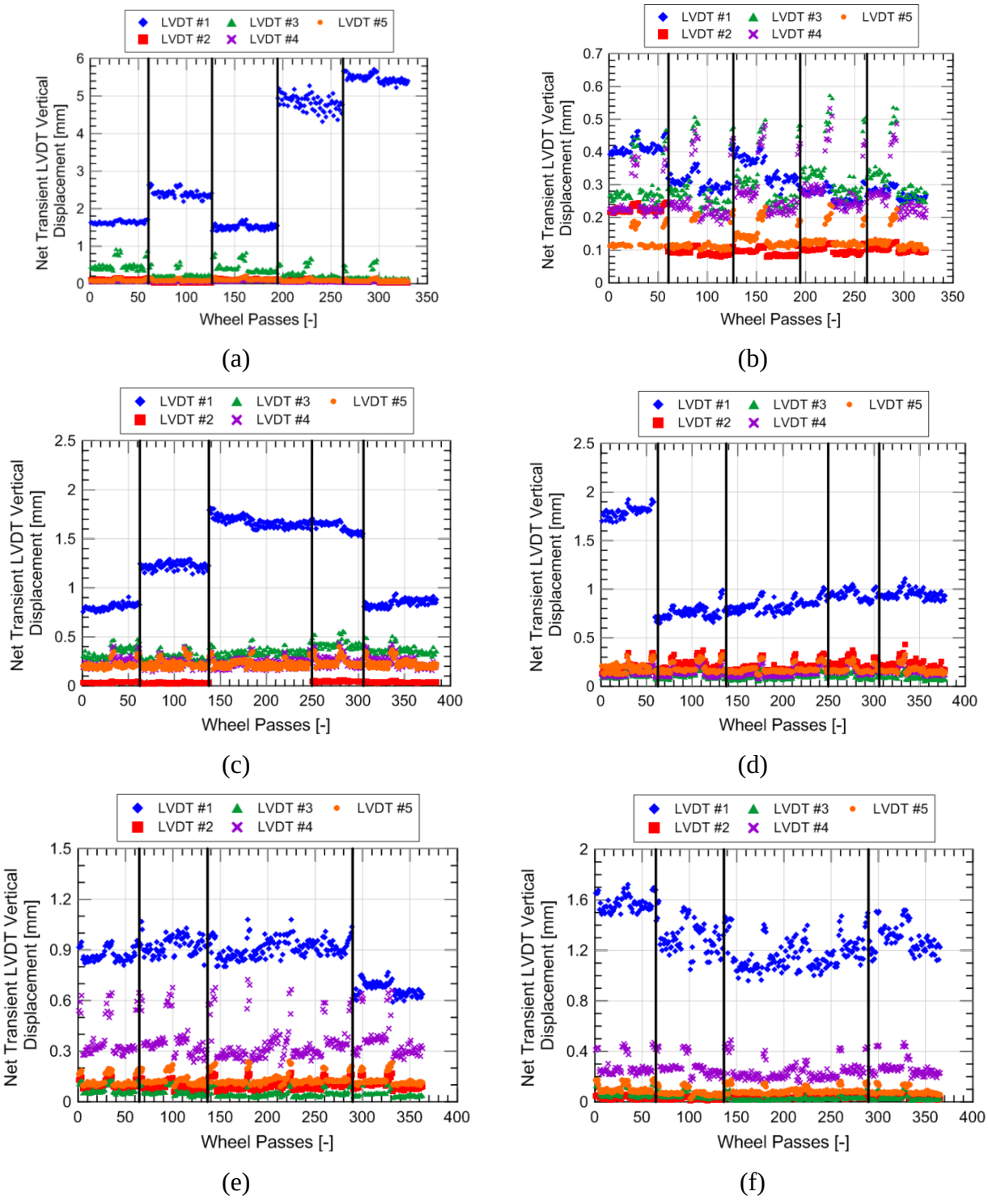

Figure 3.33: **Comparison of peak transient vertical displacements for all subsurface LVDTs at (a) Upland (15 ft.), (b) Upland (60 ft.), (c) Madison (12 ft.), (d) Madison (60 ft.), (e) Caldwell (East), and (f) Caldwell (West).**

Table 3.11: Average transient vertical displacement of each LVDT for all Amtrak sites

Instrumented Site	LVDT #1 [mm]	LVDT #2 [mm]	LVDT #3 [mm]	LVDT #4 [mm]	LVDT #5 [mm]	Total [mm]
Upland (15 ft.)	2.624	0.088	0.356	0.058	0.091	3.216
Upland (60 ft.)	0.332	0.124	0.308	0.269	0.131	1.165
Madison (12 ft.)	1.377	0.035	0.347	0.237	0.224	2.220
Madison (60 ft.)	1.019	0.204	0.103	0.138	0.180	1.643
Caldwell (East)	0.859	0.097	0.055	0.362	0.129	1.502
Caldwell (West)	1.293	0.032	0.042	0.264	0.087	1.718

Table 3.12: Average transient vertical displacement of each LVDT as a percentage of total transient vertical displacement for all Amtrak sites

Instrumented Site	LVDT #1 [%]	LVDT #2 [%]	LVDT #3 [%]	LVDT #4 [%]	LVDT #5 [%]
Upland (15 ft.)	82	3	11	2	3
Upland (60 ft.)	29	11	26	23	11
Madison (12 ft.)	62	2	16	11	10
Madison (60 ft.)	62	12	6	8	11
Caldwell (East)	57	6	4	24	9
Caldwell (West)	75	2	2	15	5

A similar analysis was performed for the four NS sites and results are displayed in Figure 3.34 and Tables 3.13 and 3.14. As with the Amtrak sites, the y-axis is different at each location to emphasize variations in LVDT displacement and the black line separates the two trains recorded at each site. LVDT #1 was not working properly at MP 352.8 (11 ft.) so data from LVDT #1 was omitted.

The results show large LVDT #1 displacements at MP 352.2 (13 ft.) while the other three sites showed LVDT #1 displacements of less than 1.0 mm. Additionally, average peak displacement values show 89% of transient displacement occurring in LVDT #1 while the other three sites are about 50%.

While it appears significant variation in LVDT displacements occurred at both MP 352.8 sites, this difference is due to the difference response of unloaded and loaded trains. Train #1 was unloaded for both MP 352.8 sites and therefore the displacement will be lower. Train #2 was

loaded and therefore the displacements are higher. However, the locomotive of Train #1 matches the response of the loaded cars of Train #2, indicating a similar response. This shows the influence of wheel load on peak transient LVDT values so methods at eliminating the influence of wheel load will be introduced and used in subsequent sections.

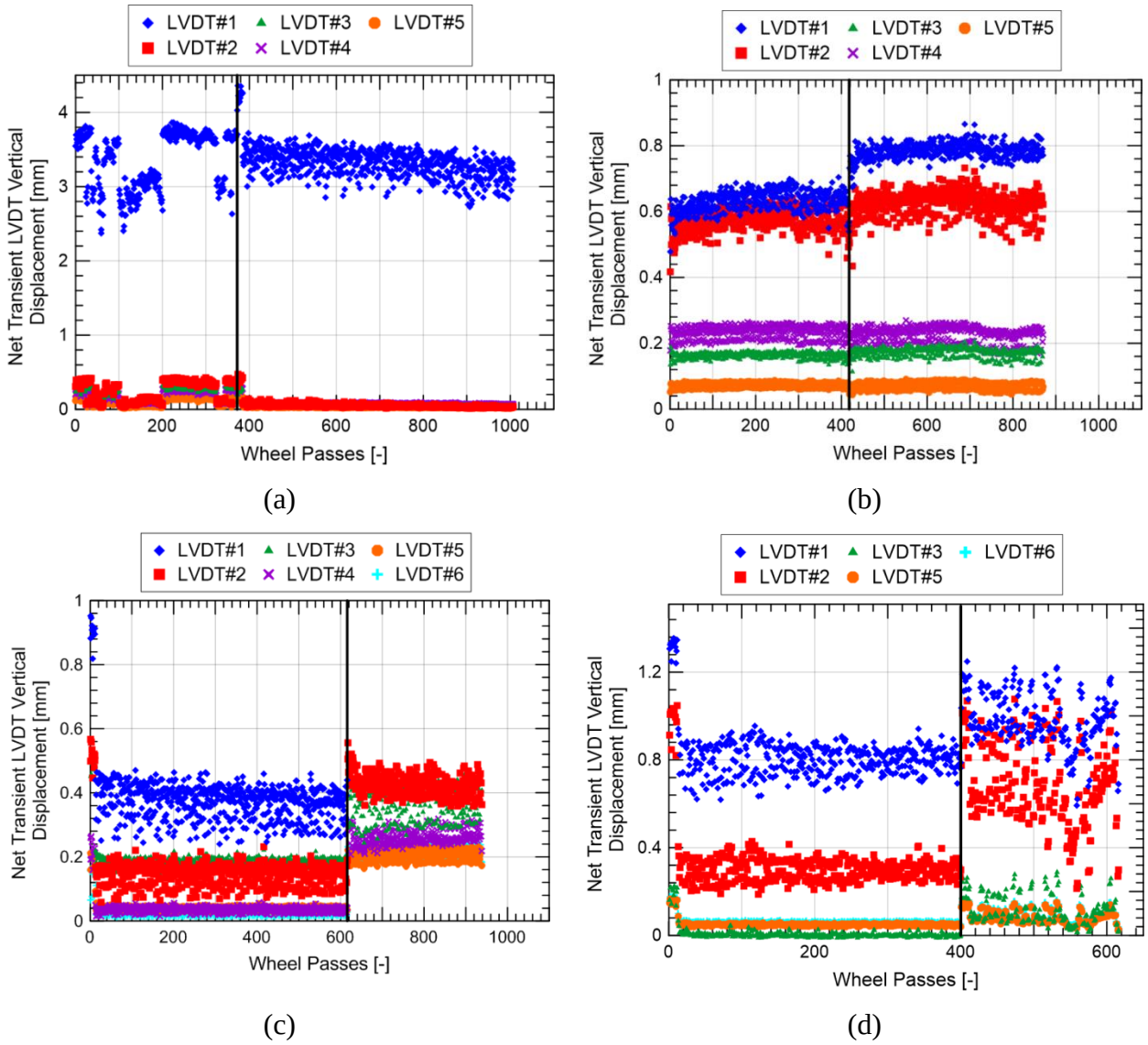

Figure 3.34: Comparison of peak transient vertical displacements for all subsurface LVDTs at (a) MP 352.2 (13 ft.), (b) MP 352.2 (31 ft), (c) MP 352.8 (11 ft.), and MP 352.8 (29 ft.).

Table 3.13: Average transient vertical displacement of each LVDT for all NS sites

Instrumented Site	LVDT #1 [mm]	LVDT #2 [mm]	LVDT #3 [mm]	LVDT #4 [mm]	LVDT #5 [mm]	LVDT #6 [mm]	Total [mm]
MP 352.2 (31 ft.)	0.711	0.598	0.168	0.231	0.074	-	1.782
MP 352.2 (13 ft.)	3.345	0.130	0.113	0.116	0.056	-	3.760
MP 352.8 (29 ft.)	0.877	0.451	0.046	-	0.063	0.073	1.150
MP 352.8 (11 ft.)	0.384	0.153	0.189	0.040	0.043	0.035	0.844

Table 3.14: Average transient vertical displacement of each LVDT as a percentage of total transient vertical displacement for all NS sites

Instrumented Site	LVDT #1 [%]	LVDT #2 [%]	LVDT #3 [%]	LVDT #4 [%]	LVDT #5 [%]	LVDT #6 [%]
MP 352.2 (31 ft.)	40	34	9	13	4	-
MP 352.2 (13 ft.)	89	3	3	3	2	-
MP 352.8 (29 ft.)	58	30	3	-	4	5
MP 352.8 (11 ft.)	46	18	22	5	5	4

In summary, the following observations can be made:

- The greatest contributor to transient displacement is LVDT #1 for all sites
- The greatest variation in transient displacement over time in LVDT #1.
- Peak transient LVDT #1 vertical displacement values roughly correlate to permanent LVDT #1 vertical displacement rates and inversely correlate with tie reaction values. This suggests a possible relation between poor tie support and ballast settlement.
- Peak LVDT values are influenced by wheel load so average values can be unrepresentative if sites experience varying wheel loads.

3.6.3 LVDT #1 Load-Displacement Characterization (Amtrak Sites)

The previous section showed the greatest contributor to transient displacement is LVDT #1 and a possible link between transient and permanent LVDT #1 movements. This chapter attempts to further analyze transient LVDT #1 behavior by characterizing the load-displacement behavior at the six Amtrak sites and the next section characterizes the NS sites.

The benefit of characterizing the load-displacement behavior is to make the mathematical models a function of wheel load, therefore eliminating its contribution. This can be accomplished

by a developing a representative stiffness value for each material layer. This value will then be used for correlations in Chapter 3.8 and numerical modeling in Chapter 5.

To characterize the load-displacement behavior, the peak wheel loads and peak transient LVDT #1 vertical displacement values from each passing wheel are recorded and compared. While ideally both wheel loads and tie reactions could be used as load inputs, the uncertainty on how well tie reaction represents tie load (Chapter 3.5) prevented a reliable tie reaction analysis and therefore peak wheel loads are used. If the tie reaction values can be trusted, i.e. Upland (60 ft.), the load and unloading curves can also be characterized.

As mentioned previously, LVDT #1 measures the displacement from the top of the tie to the bottom of the ballast layer. Therefore, transient LVDT #1 displacement can be divided into the following four main components:

1. Vertical deformation of the concrete tie,
2. Closure of any gap between the tie bottom and ballast surface (δ_{gap}),
3. Initial non-linear behavior of the ballast referred to as seating deformation (δ_{seat}), and
4. Displacement of the ballast layer due to the applied load ($\delta_{mobilized}$).

Concrete ties are much stiffer than ballast and therefore their displacement can be considered negligible. This leaves closure of a gap (δ_{gap}), non-linear seating displacement (δ_{seat}), and mobilized ballast vertical displacements ($\delta_{mobilized}$) as the three main components of transient LVDT #1 vertical displacement. The conceptual model for these three components is shown in Figure 3.35, which displays the theoretical transient displacement behavior of a tie with a gap between the tie and the ballast.

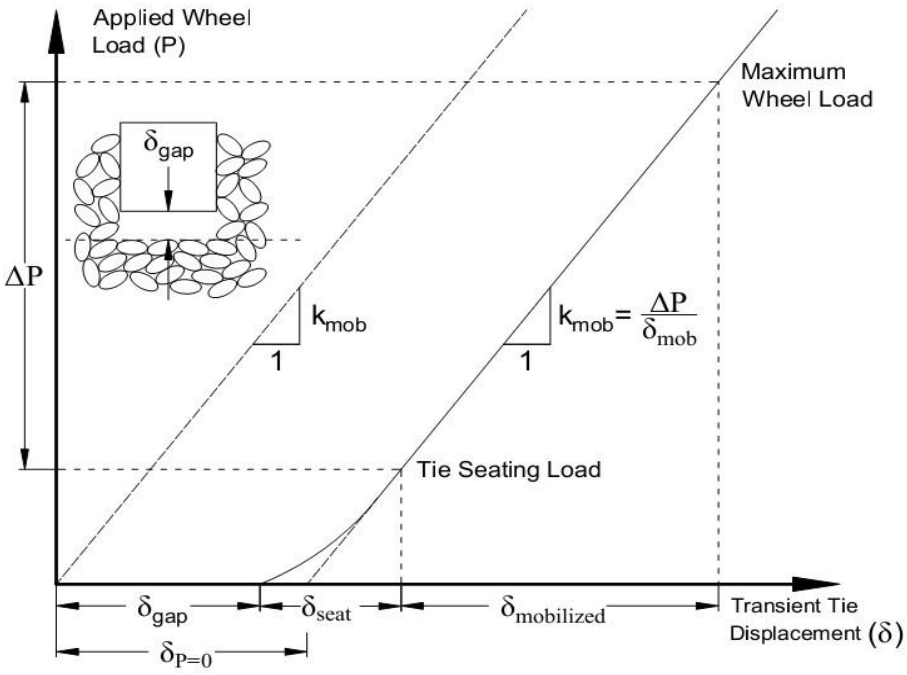

Figure 3.35: Theoretical tie displacement behavior of a tie with a gap.

The solid line represents the theoretical tie displacement behavior. Prior to loading, a gap between the tie and ballast is assumed to exist (δ_{gap}). As the tie is loaded, the gap closes and the ballast resists the tie by mobilizing shear resistance from particle friction and interlocking. The tie displacement during the shear mobilization of the ballast is represented by δ_{seat} and the load that fully mobilizes the ballast is called the tie seating load. Any tie displacement after tie seating ($\delta_{mobilized}$) is due to displacement of the ballast and underlying soils. The tie should displace linearly with increasing applied load in accordance with the mobilized stiffness (k_{mob}) of the ballast and underlying soils.

For analysis of LVDT #1, it is imperative that the tie-ballast gap (δ_{gap}) be separated from the mobilized ballast displacement ($\delta_{mobilized}$) to determine which component is problematic. To overcome this, the tie-ballast gap is estimated by extrapolating k_{mob} to the unloaded condition (P=0). This estimated "gap" is represented as $\delta_{P=0}$. One issue that arises when separating components is determining the tie-ballast gap (δ_{gap}) and seating displacement (δ_{seat}) because measurements below the tie seating load are rarely obtained from analyzing peak values. While this method overestimates the actual tie-ballast gap, the seating displacement (δ_{seat}) is expected to be small because the ballast will be compacted due to prior tie displacements. The transient

ballast displacement can then be calculated by subtracting the estimated tie-ballast gap ($\delta_{P=0}$) from the peak transient LVDT #1 vertical displacement value.

To determine the estimated tie-ballast gap ($\delta_{P=0}$) at each instrumented site, the peak wheel load and corresponding peak transient LVDT #1 vertical displacement is recorded for each passing wheel. Caldwell (East) during the 26 January 2013 measurement is used as an example in Figure 3.36. The linear mathematical relationship in Equation 3.4 can be fitted to the field data to represent the transient LVDT #1 vertical displacement behavior:

$$\delta_{LVDT\#1} = \delta_{P=0} + \frac{P}{k_{mob}} \tag{3.4}$$

with the inverse of the slope representing the mobilized ballast stiffness (k_{mob}). This characterization produces a non-linear load-displacement response in which negligible load is required to close to the estimated tie-ballast gap ($\delta_{P=0}$) and a linear response follows. Additionally, larger estimated tie-ballast gap values will result in a greater degree of non-linearity in the track system. Knowning the degree of non-linearity is important because linear behavior is a common assumption in analytical and numerical track analyses (Chapter 2.3.1).

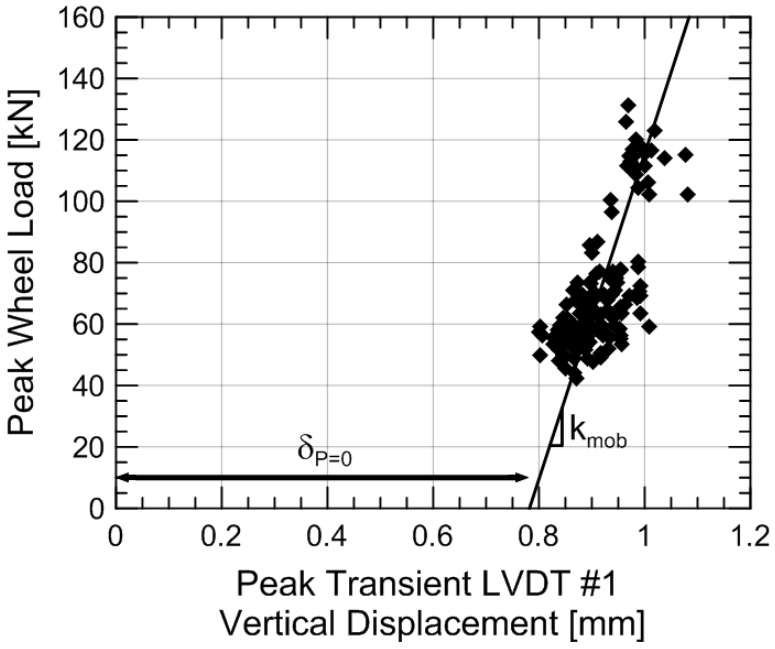

Figure 3.36: Transient LVDT #1 vertical displacement behavior at Caldwell (East) on 26 January 2013.

Another method of determining the tie-ballast gap is by using the entire tie reaction time history (Method B) instead of peak wheel loads (Method A). Figure 3.37 contrasts the load-displacements behavior using Method A and Method B. The benefit of using Method B is the full load-displacement curve can be obtained because every data point is used. The entire non-linear seating curve can be observed in Figure 3.37(b) and the actual gap ($\delta_{P=0}$) appears to be at 0.2 mm, close to the estimated gap ($\delta_{P=0}$) of 0.26 mm. However, the drawback of using Method B is that tie reactions do not appear to replicate tie loads for unsupported ties so only Upland (60 ft.) can consistently be used. This suggests Method A is sufficient for estimating tie-ballast gaps.

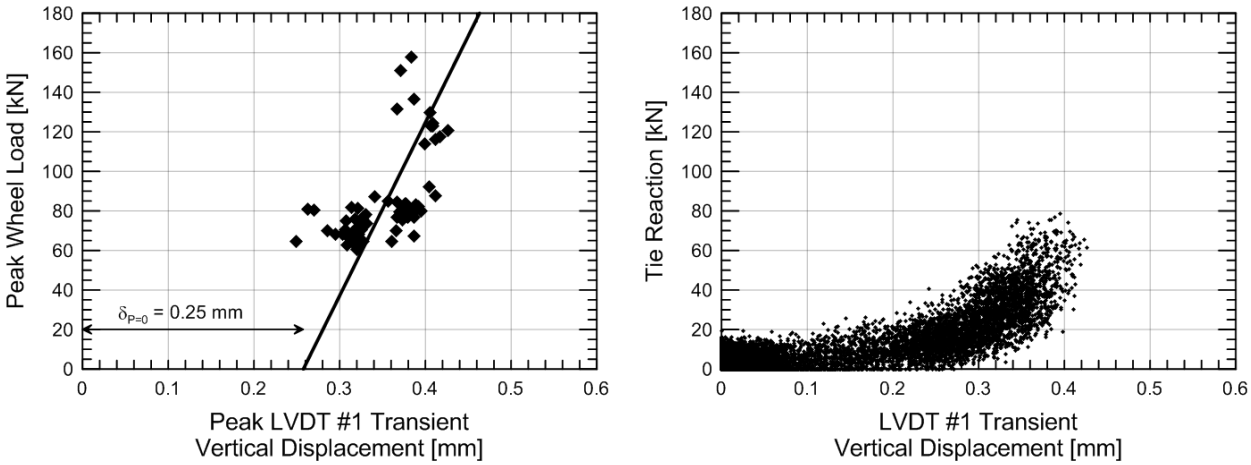

(a) (b)

Figure 3.37: Measured load-displacement behavior of LVDT #1 at Upland (60 ft.) on 29 January 2013 using (a) Method A: peak wheel loads and (b) Method B: tie reaction.

It was determined that the load-displacement behavior at LVDT #1 (and LVDTs #2 through 5) is similar for multiple trains recorded on the same day. This is expected because the ballast and underlying soil behavior should not change significantly from trains passing within the same hour. To show this, Figure 3.38 displays the load-displacement results from five recorded trains at Caldwell (East) measured on 26 January 2013.

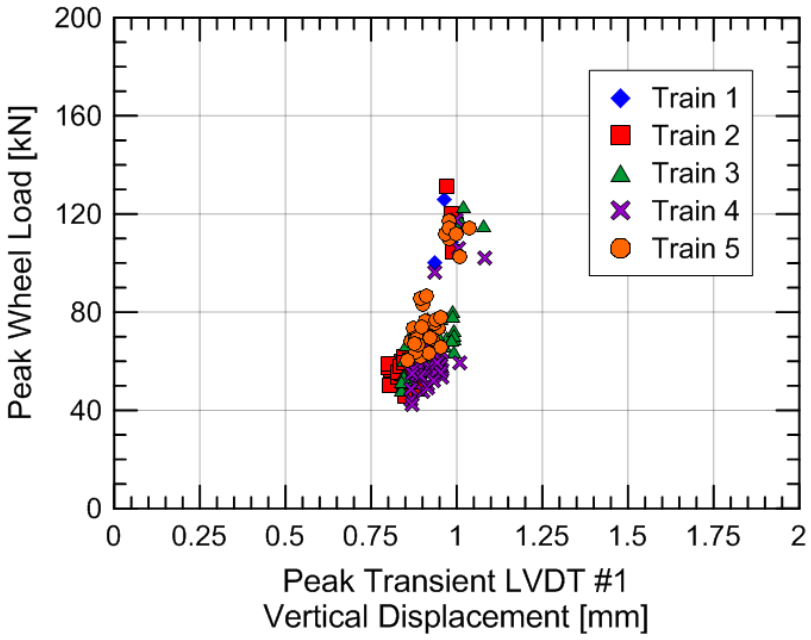

Figure 3.38: Transient LVDT #1 vertical displacement behavior at Caldwell (East) on 26 January 2013.

Figures 3.39 through 3.41 compare the load-displacement behavior at LVDT #1 for both instrumented sites at the three bridge approaches on 26 January 2013. Figure 3.39 compares Upland (15 ft.) with Upland (60 ft.), which are also both located on the west end of the ties. Figure 3.40 compares Madison (12 ft.) and Madison (60 ft.), which are both located on the west end of the ties. Figure 3.41 compares Caldwell (East) and Caldwell (West), which are located on the same tie about 80 ft. away from the abutment. The numerical values of estimated tie-ballast gap ($\delta_{P=0}$), mobilized ballast stiffness (k_{mob}), and the ballast Young's Modulus estimated using FLAC3D (see Chapter 5.3) are displayed in Table 3.15. All three values are an average of four data trips. For comparison purposes, the values of ballast modulus measured using seismic testing range from 140 to 380 MPa (Stark et al., 2016). This includes clean, dry fouled, and wet fouled ballast.

The difference in estimated tie-ballast gap is greatest at the Upland site with a 0.26 mm gap at Upland (60 ft.) and 1.42 mm at Upland (15 ft.). This also validates previous observations that Upland (60 ft.) displays good tie support while Upland (15 ft.) has poor tie support. The stiffness at both Upland sites is similar, suggesting ballast stiffness may not have a large contribution to settlement in this studied case.

At the Madison site, the estimated tie-ballast gap is much greater at Madison (12 ft.) than Madison (60 ft.), with gap heights of 1.61 mm and 0.62 mm, respectively. This matches up with past observations from other indicators, tie reaction and transient vertical displacement, that Madison (12 ft.) has less tie support than Madison (60 ft.). The stiffness is greater at Madison (12 ft.) than Madison (60 ft.) and may be due to greater compaction of the ballast.

The estimated tie-ballast gap ($\delta_{P=0}$) is similar at both Caldwell sites (0.78 mm and 0.76 mm) however the stiffness at Caldwell (East) is greater than at Caldwell (West). Due to the similar tie ballast gap at both ends of the tie, it can be inferred that the gap under the tie is likely uniform. The differing ballast stiffness at Caldwell (80 ft.) could be the result of multiple factors including: greater wheel loads on the west rail due to the west rail being 1/8" lower than the east rail, different ballast conditions, and differences in drainage.

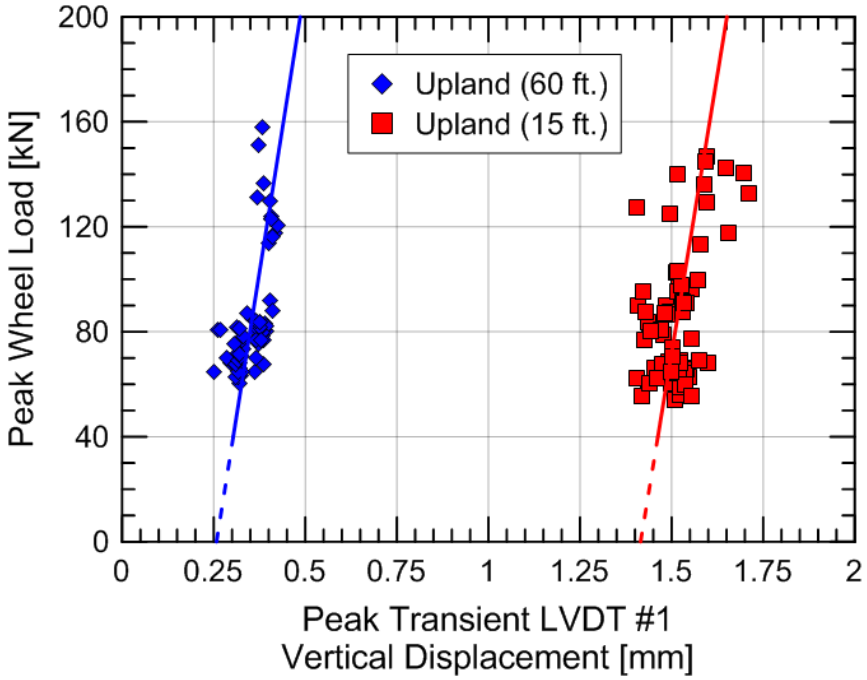

Figure 3.39: Comparison of transient LVDT #1 vertical displacement behavior at Upland (15 ft.) and Upland (60 ft.) on 26 January 2013.

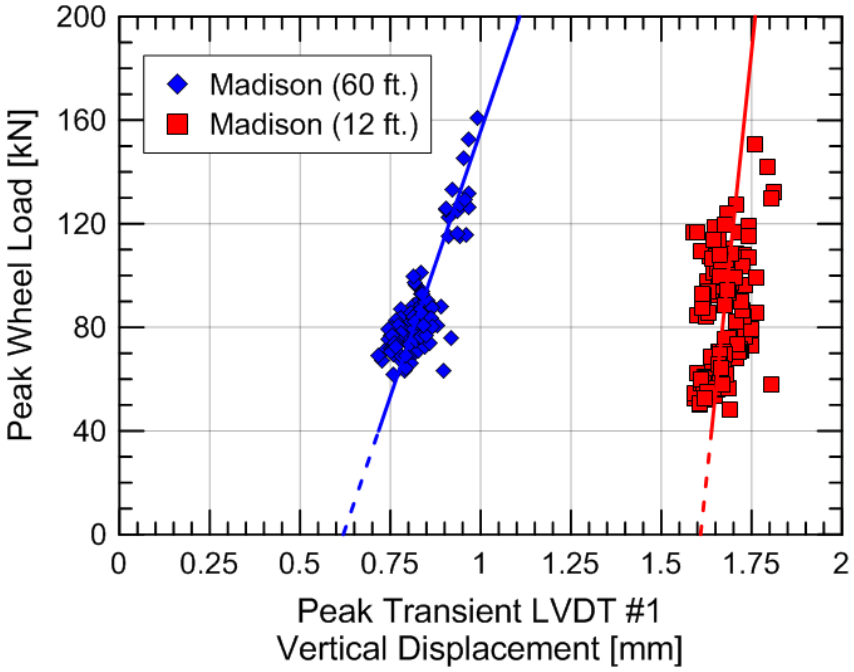

Figure 3.40: **Comparison of transient LVDT #1 vertical displacement behavior at Madison (12 ft.) and Madison (60 ft.) on 26 January 2013.**

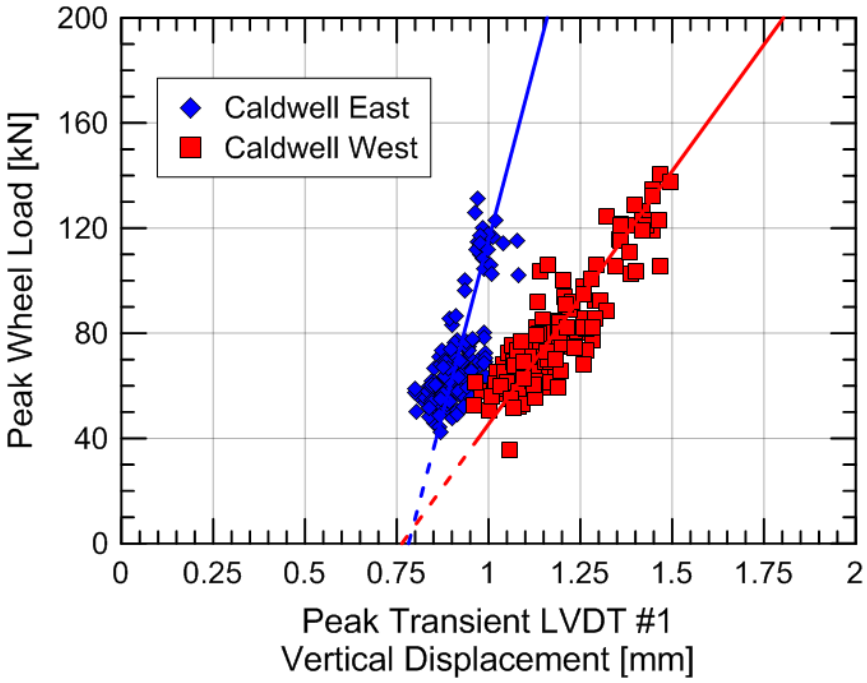

Figure 3.41: **Comparison of transient LVDT #1 vertical displacement behavior at Caldwell (East) and Caldwell (West) on 26 January 2013.**

Table 3.15: Values of estimated tie-ballast gap, mobilized ballast stiffness, and Young's modulus at all six instrumented sites for 26 January 2013

Instrumented Site		Upland		Madison		Caldwell	
		15 ft.	60 ft.	12 ft.	60 ft.	East	West
$\delta_{P=0}$	[mm]	2.35	0.26	1.24	0.89	0.71	0.95
k_{mob}	[kN/mm]	848	876	1322	410	530	192
E via FLAC3D	[MPa]	200	202	271	110	132	51

Figure 3.42 displays the change in estimated tie-ballast gap for the four recorded days used for the average in Table 3.15. The results show most variability at Upland (15 ft.) and fairly consistent values for the remaining sites.

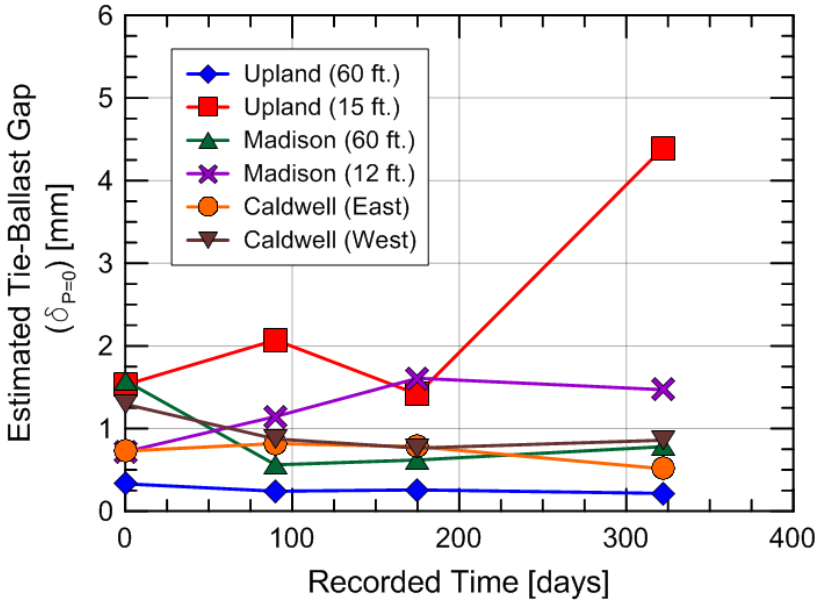

Figure 3.42: Estimated tie-ballast gap values over time.

In summary, this section presents a method for separating peak transient LVDT #1 vertical displacement values into estimated tie-ballast gap ($\delta_{P=0}$) and mobilized ballast displacement components (δ_{mob}). This is accomplished by assuming a non-linear load-displacement curve and determining the estimated tie-ballast gap by extrapolating the best-fit LVDT #1 load-displacement response to a condition of zero load. This eliminates the influence of wheel load and allows for the representation of non-linear substructure behavior. The results show the following significant variations in both estimated tie-ballast gaps and mobilized ballast stiffness

between sites and over time. The estimated tie-ballast gap ($\delta_{P=0}$) and mobilized ballast stiffness values (k_{mob}) will be used for correlations (Chapter 3.8) and numerical modeling (Chapter 5).

3.6.4 LVDT #1 Load-Displacement Characterization (NS Sites)

The previous section separated the transient LVDT #1 vertical displacement measurement into multiple components. In the Amtrak case, the range in peak wheel loads were limited and estimates of the tie-ballast gap ($\delta_{P=0}$) could only be determined by extrapolating the linear "best-fit" line to zero wheel load (P=0) which estimates but overpredicts the actual tie-ballast gap (δ_{gap}).

In this section, the NS data is used to separate the transient LVDT #1 vertical displacement measurement into multiple components and fully characterize the non-linear load-displacement relationship. This can be accomplished because the NS sites experiences a wide range of recorded peak wheel loads because the trains often consist of both loaded and unloaded freight cars. This produces a wider range of data that can be used to characterize the load-displacement relationship.

To illustrate the non-linear load-vertical displacement behavior of LVDT #1, the freight train measured at MP 352.2 (13 ft) on 2 November 2013 at 8:43 AM is used as an example in Figure 3.43. The range of data in Figure 3.43 is sufficient to delineate the seating load, which is the load that establishes good contact between the tie and ballast. The seating load for the freight train on 2 November 2013 is about 60 kN. This is similar to the 50 kN value estimated from the tie reaction measurements in Chapter 3.5. Above the seating load, the response is nearly linear and thus similar to the measured response at the Amtrak NEC sites in Figures 3.39 through 3.41. Below the seating load, the LVDT #1 response is also non-linear as observed with the NEC sites.

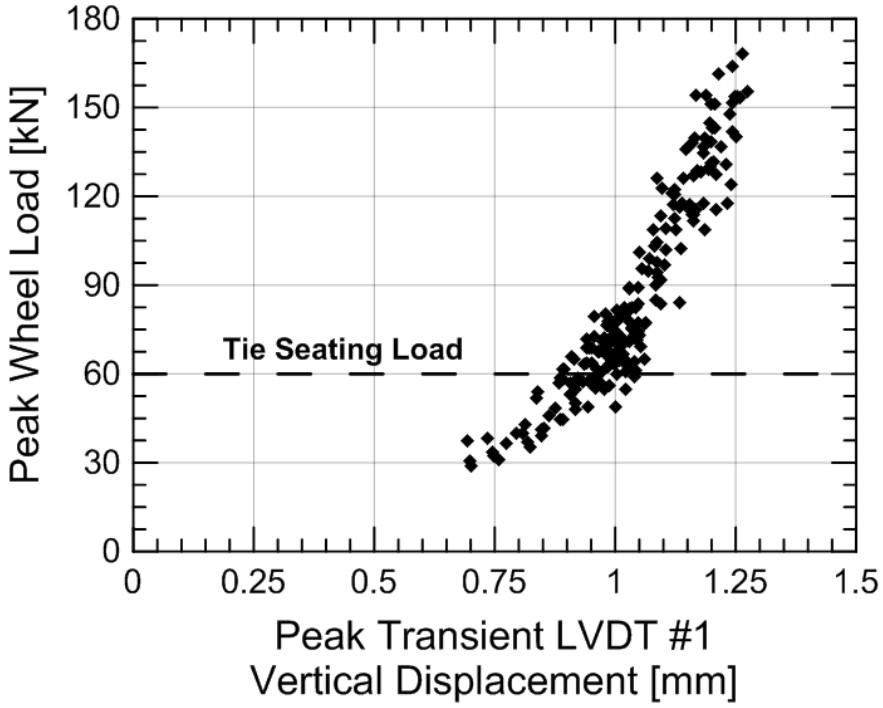

Figure 3.43: Non-linear transient LVDT #1 vertical displacement behavior at MP 352.2 (13 ft) on 2 November 2013.

Studying the non-linear response below the seating load, it is now possible to determine the following three displacement values for the conceptual model presented in Figure 3.44: δ_{gap}, δ_{seat}, and $\delta_{P=0}$. The lowest recorded peak wheel load is 30 kN so the non-linear relationship still must be extrapolated to the zero wheel load (P=0). To do this, two non-linear relationships, bi-linear and cubic, are used to approximate the data. Logarithmic, exponential, power, parabolic, and higher order relationships also were considered but none represent the data trend better than bi-linear and cubic functions.

The equations for a bi-linear representation of the data in Figure 3.43 are shown in Equations 3.5 and 3.6as follows for above and below the seating load in Figure 3.43, i.e., P_{seat}:

$$\delta_{LVDT\#1} = \delta_{P=0} + \frac{P}{k_{mob}} \qquad if\ P \geq P_{seat} \tag{3.5}$$

$$\delta_{LVDT\#1} = \delta_{gap} + \frac{P}{k_{seat}} \qquad if\ P < P_{seat} \tag{3.6}$$

where the linear portion above the seating load is the same as shown for the Amtrak data where k_{mob} is the stiffness of the ballast underlying the tie. Below the seating load, δ_{gap} represents the tie-ballast gap and k_{seat} represents the stiffness of the unmobilized ballast.

The equation for a cubic representation of the data in Figure 3.43 is:

$$\delta_{LVDT\#1} = a_1 P^3 + a_2 P^2 + a_3 P + a_4 \tag{3.7}$$

where a_1, a_2, a_3, and a_4 are best fit parameters. The last best fit parameter (a_4) equals the tie-ballast gap (δ_{gap}).

The seating displacement, δ_{seat}, is calculated by subtracting the tie-ballast gap from the LVDT #1 displacement at the seating load.

$$\delta_{seat} = \delta_{LVDT\#1}(P_{seat}) - \delta_{gap} \tag{3.8}$$

The graphical representations for the bi-linear and cubic models are shown in Figure 3.44 with the NS field data. The parameter values for each model are displayed in Table 3.16. Figure 3.44 shows that both models fit the data reasonably well within the range of measured peak wheel loads (30 kN < P < 160 kN). However, the cubic model appears to provide a better representation at low peak wheel loads, i.e., less than 40 kN, than the bi-linear model. The greater non-linearity of the cubic relation results in a smaller estimate of δ_{gap} than the bi-linear model which is similar to the extrapolation used for the Amtrak data. However, when extrapolating to wheel loads larger than the measured values, the cubic model curves away from the measured data resulting in lower tangent stiffness values at high loads. Conversely, the bi-linear model assumes the stiffness remains constant for peak wheel loads greater than 80 kN, i.e., P_{seat}.

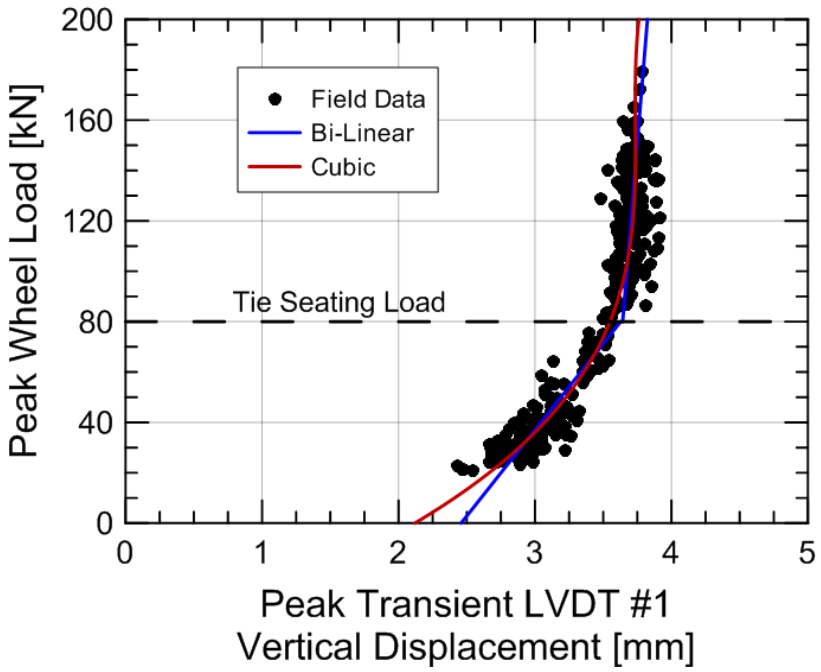

Figure 3.44: **Mathematical representation of transient LVDT #1 vertical displacement behavior at MP 352.2 (13 ft) on 2 November 2013.**

Table 3.16: **Best-fit parameters for bi-linear and cubic models for NS data**

Bi-linear		Cubic	
k_{mob}	568	a_1	6.50×10^{-7}
$\delta_{P=0}$	3.46	a_2	2.59×10^{-4}
k_{seat}	65	a_3	0.0356
δ_{gap}	2.41	a_4	2.01

Table 3.17 displays the values of δ_{gap}, δ_{seat}, and $\delta_{P=0}$ and shows a seating displacement, δ_{seat}, of 1.2 to 1.5 mm is predicted by the bi-linear and cubic models. The $\delta_{P=0}$ value is determined using the method presented in the previous section (Chapter 3.6.3) and is included for comparison purposes. This means the value of $\delta_{P=0}$ will be constant regardless of which non-linear model is used to determine δ_{gap} and δ_{seat}. The contribution of seating does appear to have greater effect on MP 352.2 (13 ft.) and Upland (60 ft.), which is likely due to the lack of intimate contact. Without more data, the estimated tie-ballast gap is still considered sufficient because it still incorporates both non-linear components and allows for the comparison with Amtrak values. However, cubic or bi-linear models would be more representative of behavior if more complex models are required.

Table 3.17: Values of estimated tie-ballast gap, actual tie-ballast gap, and seating displacement at MP 352.2 (13 ft) on 2 November 2013

Fitting Model	$\delta_{P=0}$ [mm]	δ_{gap} [mm]	δ_{seat} [mm]
Bi-Linear	3.46	2.41	1.19
Cubic	3.46	2.01	1.52

As with the Amtrak sites, the transition zone and open track load-displacement behaviors are compared in Figure 3.45. While the full load-displacement curve at MP 352.2 (31 ft.) cannot be characterized because only loaded trains were measured, the difference between the two sites is apparent and validates claims that MP 352.2 (13 ft.) is unsupported.

The load-displacement responses of the four sites for all train passes are displayed in Figure 3.46. LVDT #1 was not working properly for MP 352.8 (11 ft.) in March 2014 so the data is omitted. The results seem to be fairly consistent over time and all sites besides MP 352.2 (13 ft.) appear to be fairly well supported with tie-ballast gaps less than 1.0 mm. The permanent LVDT #1 displacement are not known to compare with tie-ballast gap values.

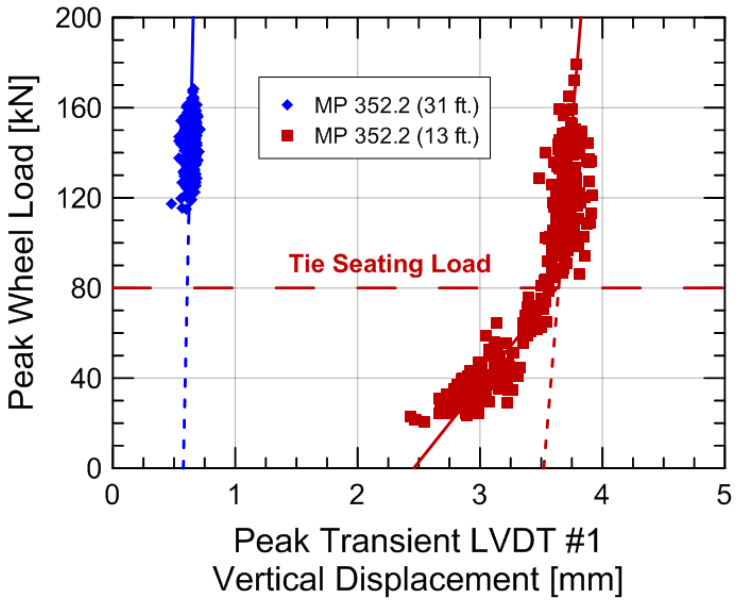

Figure 3.45: Comparison of transient LVDT #1 vertical displacement behavior at MP 352.2 (31 ft) and MP 352.2 (13 ft) on 2 November 2013.

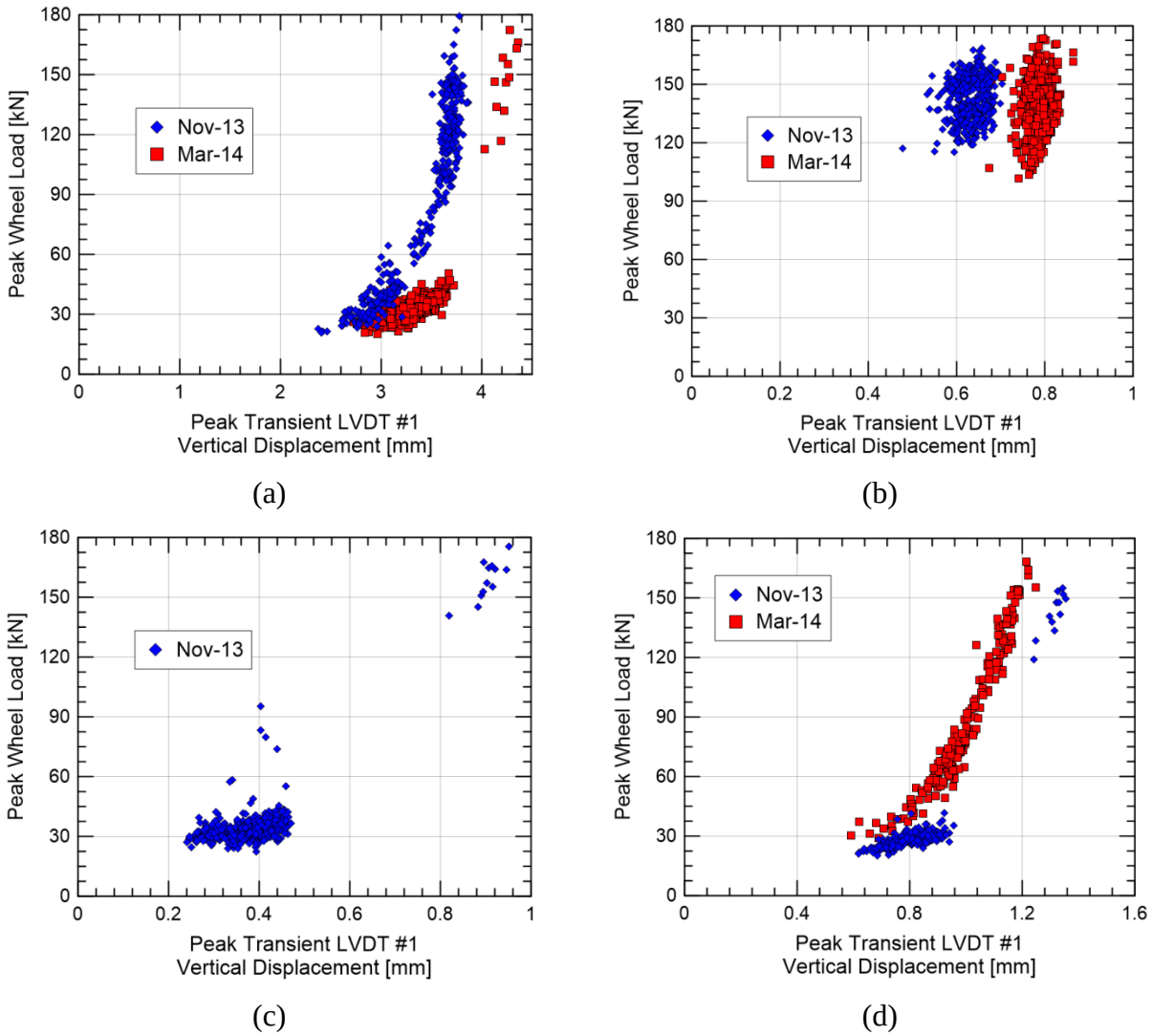

Figure 3.46: Transient LVDT #1 vertical displacement behavior at (a) MP 352.2 (13 ft.), (b) MP 352.2 (31 ft.), (c) MP 352.8 (11 ft.), and MP 352.8 (29 ft.).

Table 3.18 compares the values of mobilized ballast stiffness and tie-ballast gap for the Upland Avenue and MP 352.2 locations. These values of ballast stiffness are in agreement with the values for Upland Ave. (15 ft) and (60 ft) also shown in Table 3.18.

Table 3.18: Values of estimated tie-ballast gap and mobilized ballast stiffness for the Amtrak Upland Avenue sites and NS MP 352.2 sites

Instrumented Site		Upland		MP 352.2	
		15 ft.	60 ft.	13 ft.	31 ft.
$\delta_{P=0}$	[mm]	1.42	0.26	3.46	0.48
k_{mob}	[kN/mm]	848	876	568	1018

In summary, this section presents methods for separating the three LVDT #1 components: tie-ballast gap, tie seating displacement, and mobilized displacement. This is accomplished by assuming a bi-linear and cubic fit to the data. While the model in Chapter 6.3 will be used for the remainder of this study, the bi-linear and cubic models are more representative and can be used with more complex models. The load-displacement curves show MP 352.2 (13 ft.) has a greater tie-ballast gap than the remaining three sites, potentially explaining the greater permanent LVDT #1 vertical displacement rates at that location.

3.6.5 LVDT #2 through #5 Load-Displacement Characterization (Amtrak)

As with LVDT #1, quantifying substructure behavior into mathematical parameters is important for track analysis and modeling. The stiffness values derived in this section will be used for substructure and numerical analyses in Chapter 5. This section has two parts with the first part characterizing the substructure behavior into mathematical parameters and the second part comparing the transient displacement of each site with depth.

The methodology to determine the behavior of LVDTs #2 through 5 is similar to that of LVDT #1 for the Amtrak sites. For each passing wheel, the peak wheel load and peak transient LVDT vertical displacement is recorded and plotted against each other. Two examples, LVDT #3 at Madison (12 ft.) on 7 August 2012 and LVDT #4 at Upland (60 ft.) on 29 January 2013, are shown in Figure 3.47.

Unlike LVDT #1, a physical gap can not present in-between substructure layers however slight non-linear behavior of the material prevents the best-fit trend line from passing through the origin. Therefore, $\overline{\delta_{P=0}}$ does not represent a physical gap but non-linearity in the form of an "apparent gap" for LVDTs #2 through 5. Also, the results from Figure 3.47 shows the "apparent gap" ($\overline{\delta_{P=0}}$) can either be positive or negative.

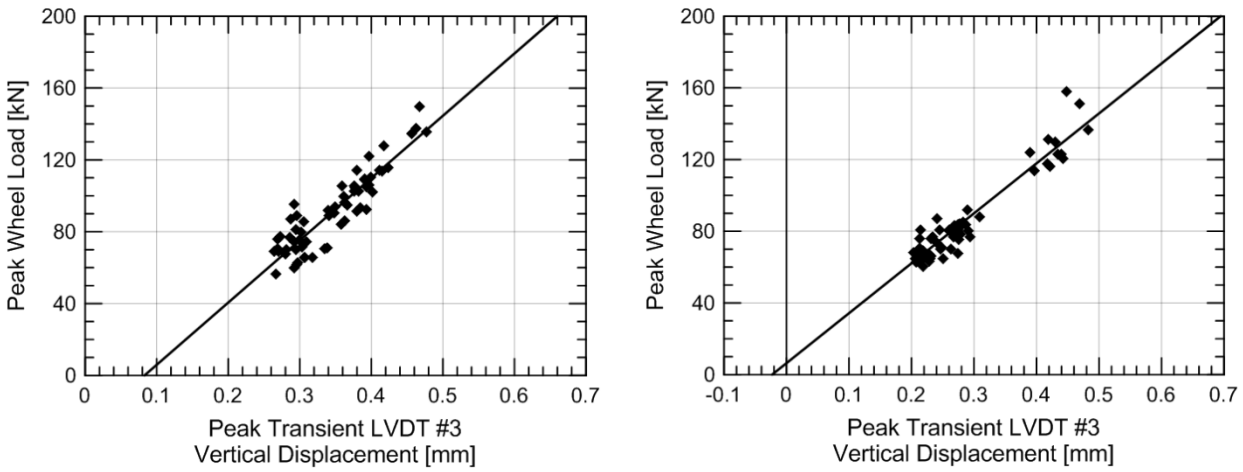

Figure 3.47: (a) Transient LVDT #3 vertical displacement behavior at Madison (12 ft.) on 7 August 2012 and (b) transient LVDT #4 vertical displacement behavior at Upland (60 ft.) on 29 January 2013.

Using the same terminology as LVDT #1, the mathematical representation of LVDT #2 through 5 behavior is displayed in Equation 3.9:

$$\delta_{LVDT\#2-5} = \overline{\delta_{P=0}} + \frac{P}{k_{mob}} \tag{3.9}$$

however $\overline{\delta_{P=0}}$ does not represent a gap but considers non-linear behavior into account in the form of an "apparent gap".

Using this mathematic representation, the "apparent gap" ($\overline{\delta_{P=0}}$) and mobilized LVDT stiffness (k_{mob}) can be determined by applying a best fit line to the data. The average values from all measured trains are displayed in Tables 3.19 and 3.20 as well as LVDT #1 for completeness.

Table 3.19: Average mobilized LVDT stiffness (k_{mob}) values for the NEC sites

Instrumented Site	LVDT #1 [kN/mm]	LVDT #2 [kN/mm]	LVDT #3 [kN/mm]	LVDT #4 [kN/mm]	LVDT #5 [kN/mm]
Caldwell (East)	609	809	825	166	566
Caldwell (West)	243	1415	737	245	645
Madison (12 ft.)	1041	3068	351	364	400
Madison (60 ft.)	464	307	548	411	404
Upland (15 ft.)	575	964	165	1875	886
Upland (60 ft.)	1211	2340	286	307	694

Table 3.20: Average tie-ballast gap (LVDT #1) and apparent gap (LVDTs #2 – 5) values for the NEC sites

Instrumented Site	LVDT #1 [mm]	LVDT #2 [mm]	LVDT #3 [mm]	LVDT #4 [mm]	LVDT #5 [mm]
Caldwell (East)	0.711	0.000	-0.039	-0.086	-0.019
Caldwell (West)	0.948	-0.032	-0.083	-0.094	-0.052
Madison (12 ft.)	1.236	0.004	0.086	-0.012	-0.003
Madison (60 ft.)	0.885	-0.099	-0.062	-0.085	-0.051
Upland (15 ft.)	2.353	0.008	-0.125	-0.008	-0.010
Upland (60 ft.)	0.262	0.091	0.013	-0.006	0.008

With the field measured substructure behavior mathematically characterized into simple parameters, these parameters can be used for analysis or modeling purposes. The second part of this section analyzes the change in transient vertical displacement with depth using these calculated parameters. Comparing all six instrumented sites gives insight into potentially stiff or soft layers at particular locations.

The cumulative transient displacements are calculated using the following method.

a) First, the net transient vertical displacement of each LVDT is determined using the formula below assuming a load (P) of 100 kN. This load is used because it is close to the average peak wheel load of the NEC sites.

$$\delta_{LVDT\#2-5} = \delta_{P=0} + \frac{P}{k_{mob}} \tag{3.10}$$

b) Second, the cumulative transient displacement of a particular LVDT equals the sum of the transient LVDT displacement and any transient LVDT displacement below it. For example, the cumulative transient displacement of LVDT #4 is the sum of the net transient displacement of LVDT #4 and #5. The cumulative transient displacement of LVDT #1 is the sum of all five net transient LVDT displacements. The cumulative transient displacements with depth are shown in Figure 3.48.

c) Third, because the tie-ballast gap is large component of transient LVDT #1 displacement and therefore cumulative transient displacement, it is included in Figure 3.48(a) and excluded in Figure 3.48(b) for comparison purposes. The calculated total cumulative transient displacement, e.g. a depth of zero, is displayed in Table 3.21 for situations where the tie-ballast gap is included and not included.

If the tie-ballast gap is excluded from the analysis (Figure 3.48(b)), the substructure behavior is similar for all six Amtrak sites. LVDT #2 and #3 appear to be stiffer at Caldwell (West), however the difference is not significant. This further suggests that for the six instrumented NEC sites, the tie-ballast gap is primary difference between sites and not the stiffness of the substructure materials.

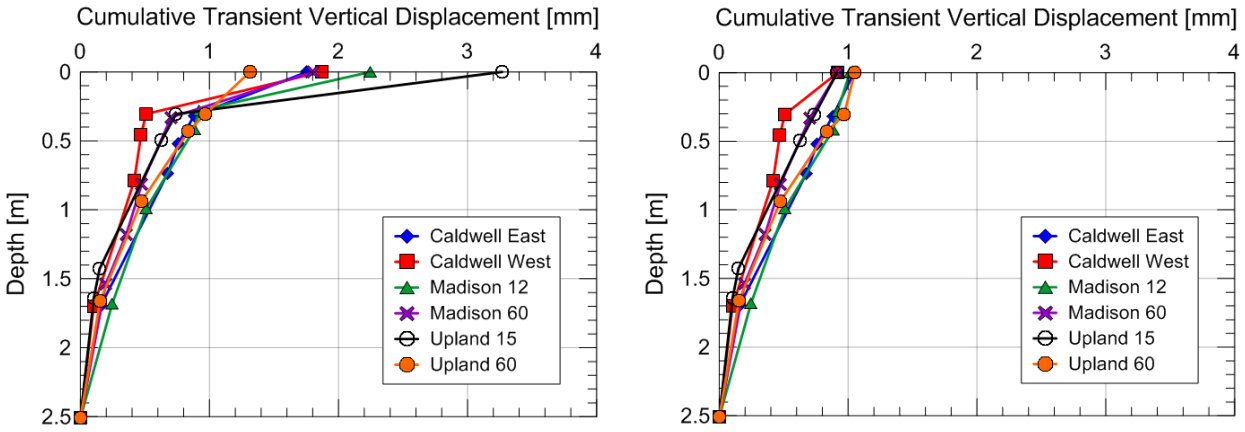

Figure 3.48: Comparison of cumulative transient vertical displacement at the six NEC sites when (a) tie-ballast bap is included and (b) tie-ballast gap is not included.

Table 3.21: Total cumulative transient displacement values for the six NEC sites

Instrumented Site	Caldwell		Madison		Upland	
	East [mm]	West [mm]	12 ft. [mm]	60 ft. [mm]	15 ft. [mm]	60 ft. [mm]
$\delta_{P=0}$ Included	1.76	1.87	2.25	1.80	3.27	1.31
$\delta_{P=0}$ Excluded	1.05	0.92	1.01	0.92	0.92	1.05

In summary, this section introduces a process to characterize transient LVDT displacement behavior with the use of two mathematical parameters: "apparent gap" ($\overline{\delta_{P=0}}$) and mobilized LVDT stiffness (k_{mob}). From the Amtrak NEC data, the subgrade stiffness is similar for all six instrumented sites and the tie-ballast gap is the primary difference between sites.

3.6.6 LVDT #2 through #5 Load-Displacement Characterization (NS)

The behavior of LVDT #2 through #6 at the NS sites is expected to be similar to the Amtrak locations and the same process for determining the cumulative transient vertical displacements is used. Table 3.22 displays the estimated tie-ballast gap and the mobilized LVDT stiffness. The "apparent gap" value was not used in this analysis because the lack of variety in wheel loads, i.e. only loaded trains were recorded at some sites, prevented any meaningful non-linear trend to be characterized. Therefore, only the origin could be used a reference for trend lines. As with the Amtrak results, the NS results show a wide range of stiffness values with little variation between sites besides MP 352.8 (11 ft.), which appears to have a softer subgrade. LVDT #4 of MP 352.8 (29 ft.) did not work during measurements so a value could not be obtained or used in substructure analyses.

Table 3.22: Average mobilized LVDT stiffness (k_{mob}) values for the NS sites

Instrumented Site	$\delta_{P=0}$ [mm]	LVDT #1 [kN/mm]	LVDT #2 [kN/mm]	LVDT #3 [kN/mm]	LVDT #4 [kN/mm]	LVDT #5 [kN/mm]	LVDT #6 [kN/mm]
352.2 (31 ft.)	0.655	2500	200	741	476	1485	-
352.2 (13 ft.)	3.600	444	313	500	435	909	-
352.8 (29 ft.)	0.765	308	126	769	-	1000	870
352.8 (11 ft.)	0.320	271	274	400	526	645	645

Comparisons of the transient vertical displacement with depth between the four NS sites are displayed in Figures 3.49. Figure 3.49(a) includes the tie-ballast gap and shows significantly greater surface displacements for MP 352.2 (13 ft.), due to the large tie-ballast gap at that location. When the tie-ballast gap is excluded, the surface displacements are similar, and reminiscent of the Amtrak results in Figure 3.48. The majority of subgrade transient displacement occurs in the upper two meters. As mentioned, MP 352.8 (11 ft.) has a softer subgrade but stiffens near the surface. The total cumulative transient displacement values, i.e. surface displacements, are displayed in Table 3.23.

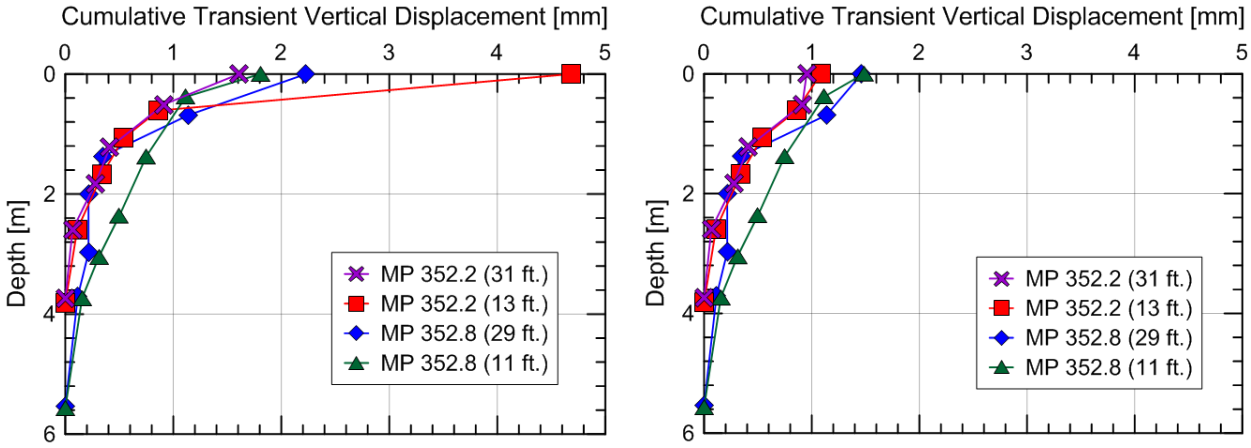

Figure 3.49: Comparison of cumulative transient vertical displacement at the four NS sites when (a) tie-ballast bap is included and (b) tie-ballast gap is not included.

Table 3.23: Total cumulative transient displacement values for the four NS sites

Instrumented Site	MP 352.2		MP 352.8	
	13 ft. [mm]	31 ft. [mm]	11 ft. [mm]	29 ft. [mm]
$\delta_{P=0}$ Included	4.68	1.61	1.80	2.23
$\delta_{P=0}$ Excluded	1.08	0.95	1.48	1.46

In summary, this section uses the process to characterize substructure transient LVDT displacement behavior on the NS data. The results show similar response to the Amtrak sites and with the majority of subgrade displacement occurring in the upper meters.

3.6.7 Tie Frequencies

This section investigates the common frequencies experienced by the ballast during tie loading. While this is not imperative for the analysis of transition zones, it can validate or give insight into which loading frequencies should be used during laboratory testing. This topic is introduced in Chapter 2.2.2 and previous laboratory results show that ballast settlement increases with increasing tie frequencies after a threshold of 10 Hz is surpassed.

Figure 3.50 presents 0.3 seconds of LVDT #1 displacement at both Caldwell (80 ft.) sites along with the record in the frequency domain. The time history shows the response of two train trucks with two wheels per train truck. At both sites, three sine frequencies in the time domain are fitted to the time history response to show the frequencies of tie loading. Only the peak regions are fitted because the displacement frequencies at lower displacement values are likely from gap closure/opening and mobilization or unloading of the ballast and therefore unrepresentative of laboratory testing conditions. Laboratory testing typically keep a seating load at all times to ensure the ballast is mobilized and therefore the non-linear contributions are not represented. This is also a potential reason why laboratory tests of ballast settlement may not represent field locations with unsupported ties.

From comparing the fitted response in the time histories and frequency domain plot, it is apparent that the majority of frequencies from tie displacement represent motions other than tie loading. For example the tie loading frequencies from the time histories are 11.1 Hz, 12.9 Hz, and 16.6 Hz. These frequencies are represented in the frequency domain plot but at much lesser magnitudes than the frequencies of 1.8 Hz or 5.2 Hz, which could represent the unloading and loading between train trucks. Therefore, trying to determine the tie loading frequencies from the frequency domain plots can be deceptive and is not suggested.

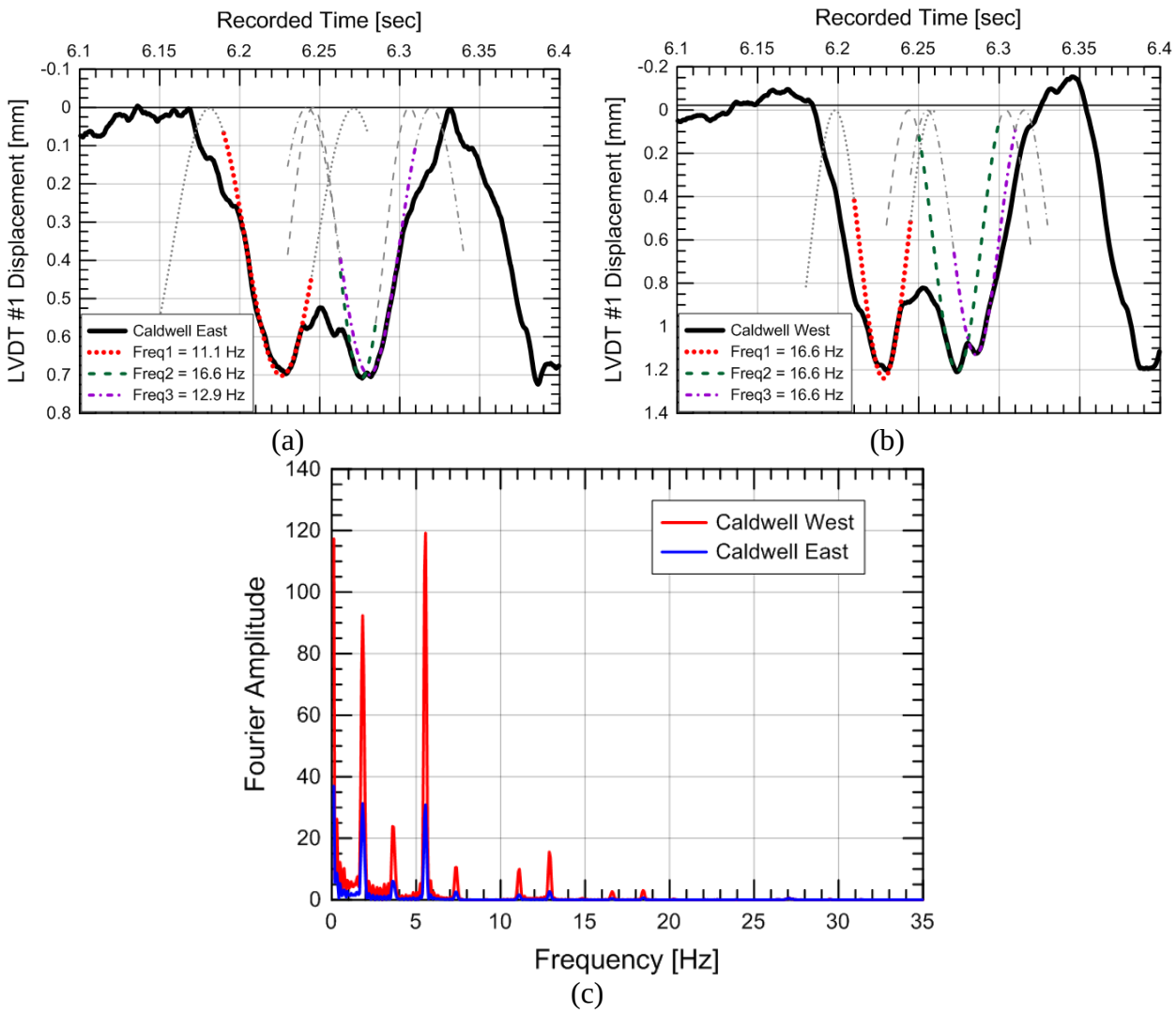

Figure 3.50: Time histories with fitted frequencies at (a) Caldwell (East) and (b) Caldwell (West) along the (c) frequency domain plot.

Figure 3.51 presents sample responses from Madison (12 ft.) and both Upland sites. The results show a wide range of frequencies ranging from 11 Hz to 35 Hz. This suggests that tie loading frequencies can vary significantly between sites and may contribute to increased ballast settlements at particular regions. However, there does not appear to be a trend between ballast displacement frequency and permanent vertical displacement rates.

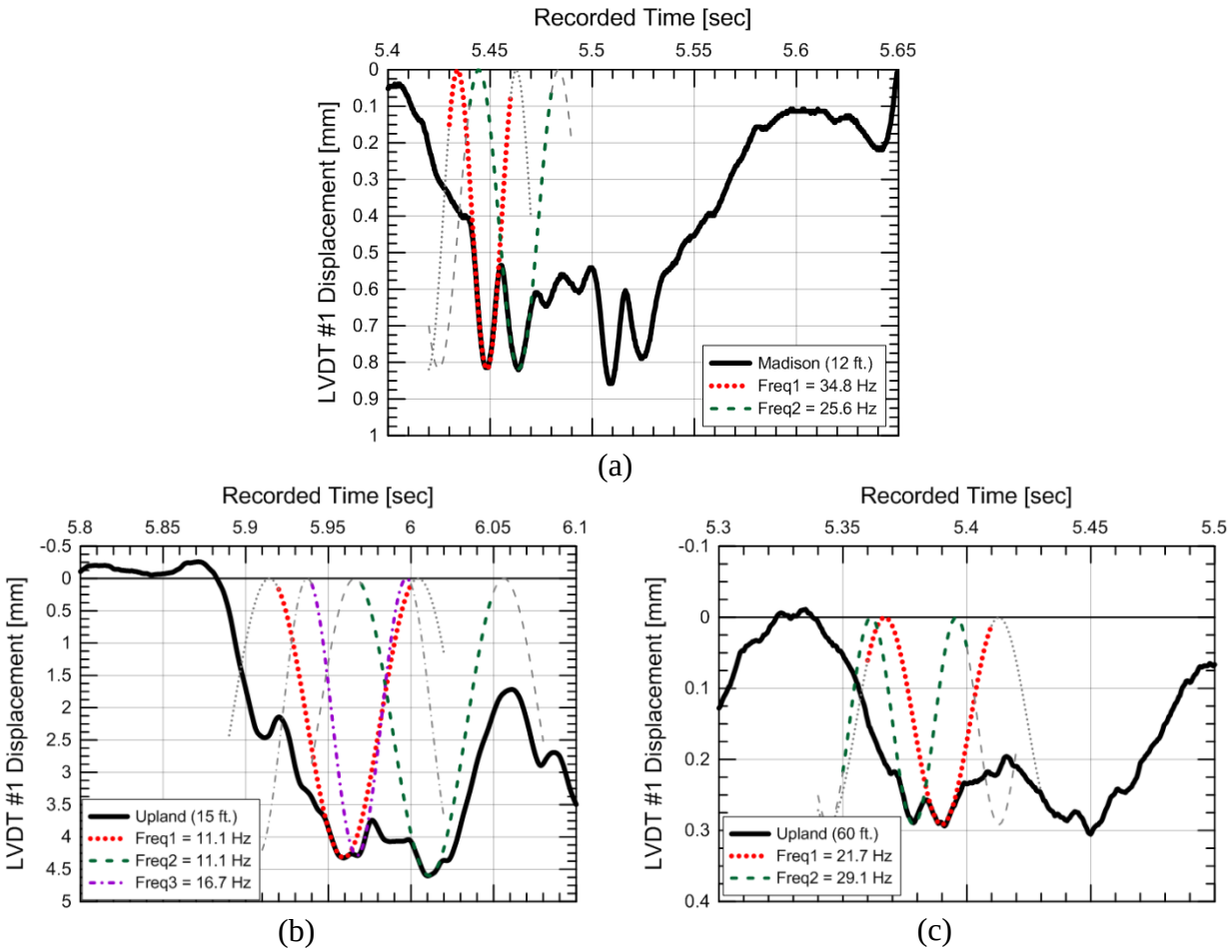

Figure 3.51: Time histories with fitted frequencies at (a) Madison (12 ft.), (b) Upland (15 ft.), and (c) Upland (60 ft.).

Figure 3.52 presents two sample NS responses in which two train trucks are shown but each train truck has three wheels instead of two. The ballast frequencies are much lower for the 25 mph trains and range from about 0.75 to 2.25 Hz.

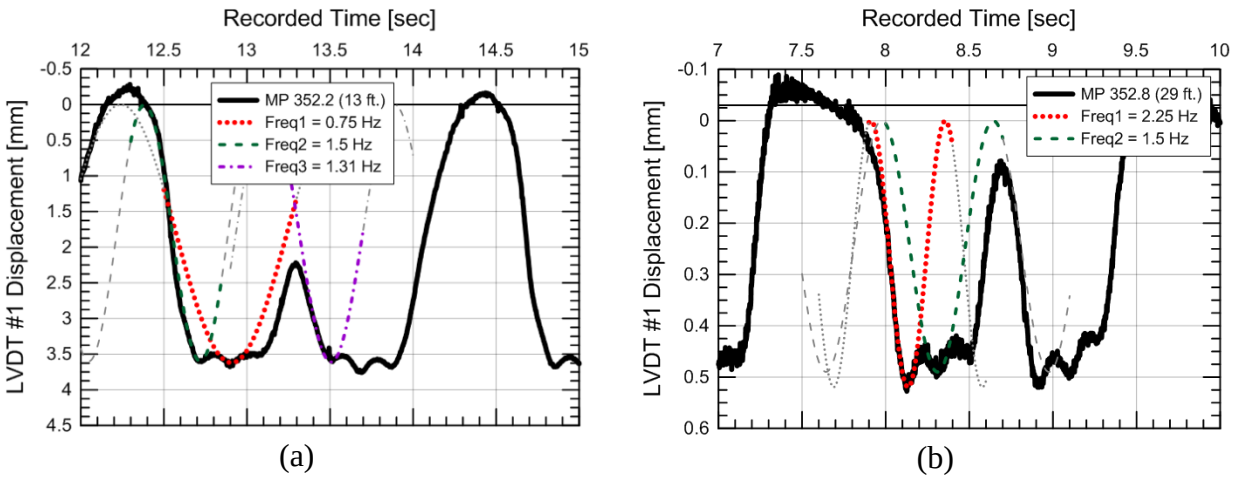

(a) (b)

Figure 3.52: Time histories with fitted frequencies at (a) MP 352.2 (13 ft.) and (b) MP 352.8 (29 ft.).

Comparisons with the loading frequencies used in laboratory tests show fairly good agreement. The recommended loading frequency for representing a 110 mph train is 25 Hz and field results show a range from 10 to 35 Hz. The recommended loading frequency for representing a 25 mph train is 5 Hz and the results show a range of about 0.75 to 2.25 Hz. While the recommended value overestimates the field results at the NS site, laboratory results show similar ballast settlement behavior for loading frequencies below 10 Hz so the difference between 2 and 5 Hz will not affect results.

3.6.8 Transient Displacement Summary

The final section in Chapter 3.6 provides a general overview of the various transient displacement components, including the estimated tie-ballast gap, mobilized ballast displacement, and subgrade displacement. The purpose is to solidify the contributions from each component and their variation between sites and over time.

Figure 3.53 presents the components for all six Amtrak sites for all site visits. In the previous analyses, only the first four day of recorded were included to match the transient components with the permanent vertical displacement rates obtained in Chapter 3.3. This analysis includes the results of all recorded days to give a full overview. The results show fairly similar displacement contributions from the subgrade of about 1 mm and a small contribution from the mobilized ballast displacement. These factors so not appear to change with time and are

fairly consistent. The primary variation between sites and time occurs within the estimated tie-ballast gap component.

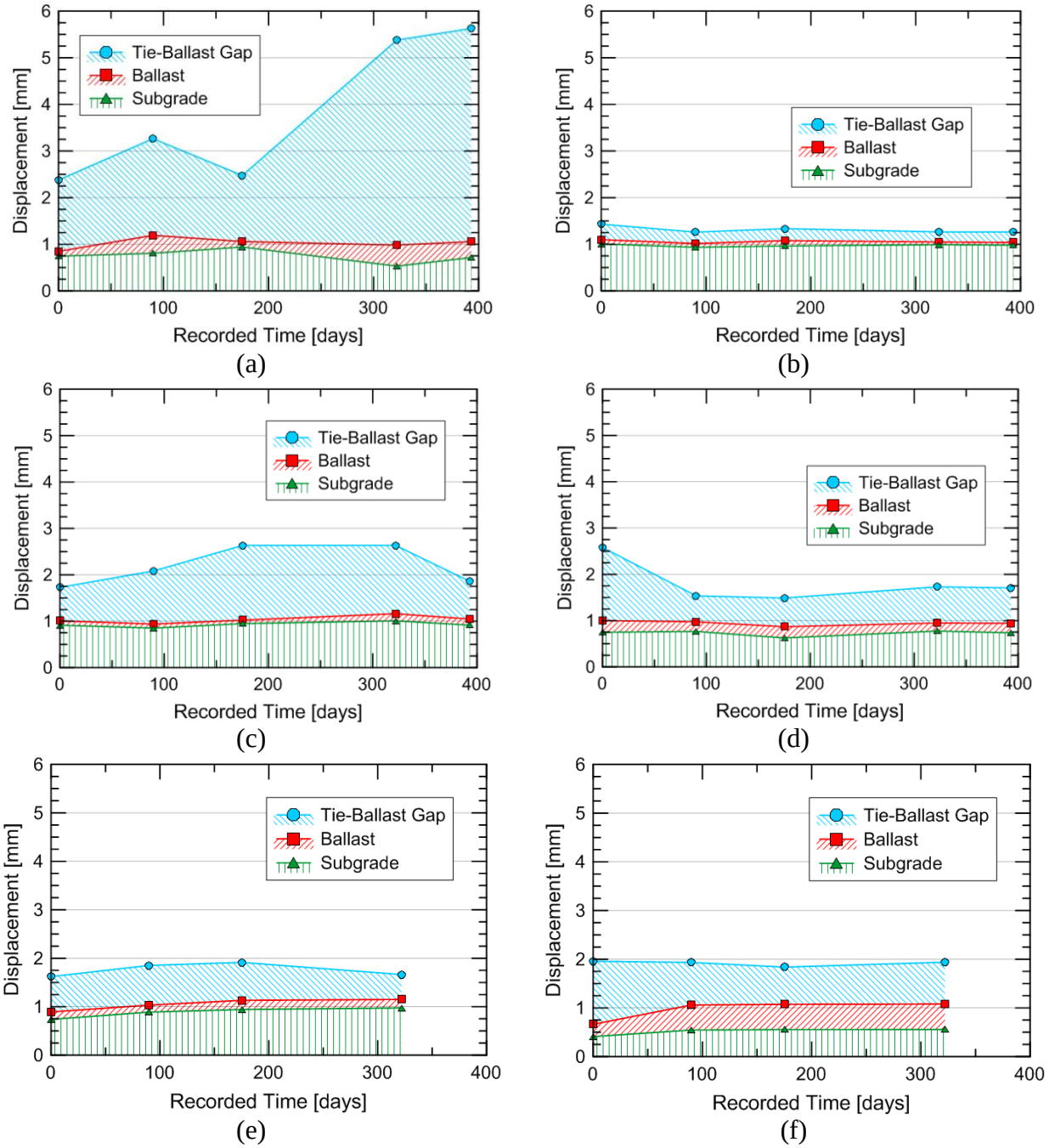

Figure 3.53: Comparison of transient vertical displacements at (a) Upland (15 ft.), (b) Upland (60 ft.), (c) Madison (12 ft.), (d) Madison (60 ft.), (e) Caldwell (East), and (f) Caldwell (West).

Figure 3.54 presents the components for all four NS sites. The results are similar with about 1 mm of subgrade displacement, small ballast contributions, and the majority of variation occurring within the estimated tie-ballast gap component.

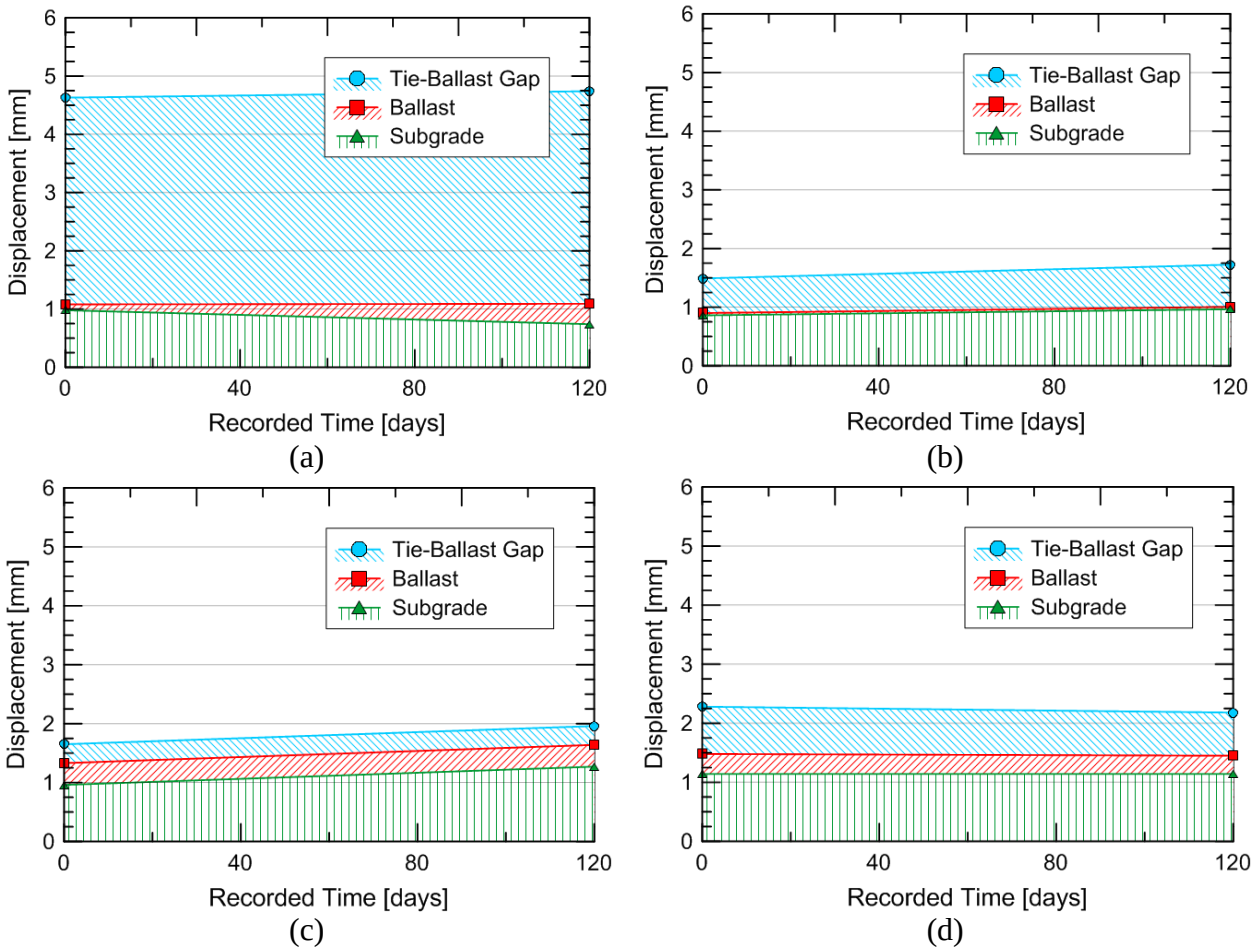

Figure 3.54: Comparison of transient vertical displacements at (a) MP 352.2 (13 ft.), (b) MP 352.2 (31 ft.), (c) MP 352.8 (11 ft.), and MP 352.8 (29 ft.).

After analysis of the ten instrumented sites, the following remarks can be made:

- Contributions from the subgrade appear to fairly consistent for all instrumented track locations and produce about 1 mm of transient displacement during train passage for a 100 kN wheel load.
- The main variation in the instrumented railroad track locations appears to be within the estimated tie-ballast gap. This component incorporates both the actual tie-ballast gap and non-linear seating displacement. The magnitude of the estimated tie-ballast gap is dependent on support conditions of the instrumented and surrounding tie and ballast density after unloading.

- The results suggest that track conditions are fairly consistent at site locations that experience low levels of settlement while track conditions are inconsistent at locations that experience high levels of settlement. Rapidly changing track conditions may result in increased loads and ballast degradation.
- Ideal track appears to experience about 1 to 2 mm of transient displacement.

3.7 Field Investigations

Field investigations are an important aspect of any site analysis and the Amtrak NEC instrumentation sites were visited twice to assess the condition of the track and transition zones. Unfortunately, the author was unable to visit the Norfolk Southern instrumentation sites in West Virginia. The main observations from the two Amtrak NEC site visits relate to damaged ties and wet, fouled ballast in the approach.

3.7.1 Tie Condition

Damaged ties are an important consideration during data analysis because of the effect of these ties on the load distributed to the tie and the load transferred to the ballast. If a tie is damaged, e.g., missing, broken, or hanging, a redistribution of load occurs from the damaged tie to adjacent ties. This may overload the adjacent ties, leading to further damaged ties, and further redistribution of load to adjacent ties. Impact loads and wheel bouncing are other potential consequences of damaged ties because of the transient vertical displacement required to mobilize some tie support. Figures 3.55 and 3.56 show damaged ties around the instrumentation locations of Madison (12 ft.) and Upland (15 ft.), respectively, which experienced the largest measured permanent vertical displacements during this study.

Figure 3.55: **Photograph of damaged tie to the left of the MDD instrumentation location (see red arrow) at Madison (12 ft.) on 4 September 2013.**

Figure 3.56: **Photo of two damaged ties near the Upland (15 ft.) instrumentation location (see red arrows). Damaged ties are three ties to the left and one tie to the right of the instrumented tie which have been replaced as of July 2013. (Photo taken by Deb Mishra.)**

Damaged ties surrounding the Madison (12 ft.) and Upland (15 ft.) sites may be increasing the applied load on the instrumented tie and be a factor in the large permanent vertical displacements being measured at these sites. The ties around the open track sites, i.e., Upland (60 ft.), Madison (60 ft.), and Caldwell (80 ft.), do not show as much tie damage as shown in Figures 3.55 and 3.56. Ties loads appear greater at track transition locations resulting in greater damage to the ties.

Damaged ties can be produced from increased tie load or poor tie loads. Both of which are likely present to some extent in both transition zones.

3.7.2 Fouled Ballast

Fouled ballast and inadequate drainage conditions can lead to a decrease in stiffness and shear strength of the ballast and promotes additional ballast fouling, ballast erosion, and mud pumping. The effects on ballast settlement is covered in Chapter 2.2.3, and previous laboratory studies show up to ten times the increase in settlement when the ballast is wet and fouled. This suggests the track displaying wet fouled ballast may settle at greater rates than track displaying clean ballast, even with identical loads.

Figure 3.57(a) shows water splashed up on the side of a tie near Madison (12 ft.) and Figure 3.57(b) shows water ponded near the bottom of this concrete tie on 4 September 2013. Figure 3.58 shows mud covering the ballast and several ties near Madison (12 ft.). Figure 3.59(a) shows seepage of water out of the abutment at the Upland Bridge and Figure 3.59(b) shows seepage from the north-south trending wall north of the Upland Avenue Bridge near Upland (15ft.). Some seepage from the abutment wall was also observed at the bridges near the Upland (15 ft.) and Madison (12 ft.) instrumentation sites. Water was observed flowing from the masonry wall shortly after a precipitation event in January 2013 and splashing on ties from the ballast during train passage in January 2013.

In summary, the fouling and inadequate drainage at the transition zone locations, e.g. Upland (15 ft.) and Madison (12 ft.), may contribute to the increased settlements at that region. Promoting drainage by removing fouling particles within the ballast and improving the drainage at the abutments may result in improved behavior and avoid the negative effects of wet fouled ballast.

(a)

(b)

Figure 3.57: Water collecting (a) on and (b) below (see red arrow and blue pen for scale) concrete tie on 4 September 2013.

Figure 3.58: **Fouling material covering ballast and concrete ties on Track #1 at Madison (12 ft) on 4 September 2013.**

(a) (b)

Figure 3.59: **Water seeping from (a) masonry abutment wall under Upland Avenue Bridge and (b) north-south trending masonry wall north of Upland Avenue Bridge on 8 August 2013.**

3.8 Correlations with Permanent LVDT #1 Vertical Displacement

This section aids understanding of relationship between various metrics and permanent vertical displacement rates by correlating the various calculated values determine in previous sections. Once a relationship is established, the potential reason for the relationship can be determined, if one does exists. Averages of the four measurement days in August 2012, November 2012, January 2013, and June 2013 are compared against the 185-day permanent vertical displacement rate presented in Table 3.5. Therefore, only a single value per site is taken. Additionally, only Amtrak data is used because of the lack of permanent vertical displacement measurements at the NS locations.

The metrics to compare against permanent vertical displacement rates are the following:

- Wheel Loads (Chapter 3.4)
- Tie Load Ratios (Chapter 3.5)
- Subballast Displacement (Chapter 3.6.5)
- Subgrade Displacement (Chapter 3.6.5)
- Ballast Stiffness (Chapter 3.6.3)
- Estimated tie-ballast gap (Chapter 3.6.3)

The first relationship compares permanent vertical displacement rate with the peak wheel loads that were determined in Chapter 3.4. Figure 3.60 shows a weak relationship with slightly greater wheel loads at the transition zone locations. However, the Upland (15 ft.) average peak wheel load value is only 13% greater than average and likely not an explanation for the increased permanent vertical displacement rates at that location.

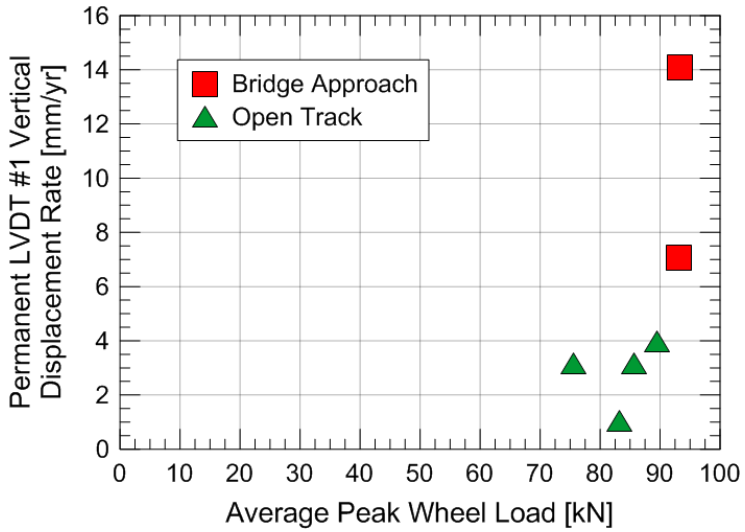

Figure 3.60: Relationship between average peak wheel load and permanent LVDT #1 vertical displacement rates at all six instrumentation sites.

The second relationship is with the peak tie load ratios that were determined in Chapter 3.5. Figure 3.61 shows an inverse relationship between the metrics. The explanation is that tie load ratio actually indicates tie support and does not represent tie load in unsupported cases. Therefore, Figure 3.61 suggests that sites with unsupported ties tend to display higher rates of permanent LVDT #1 vertical displacement.

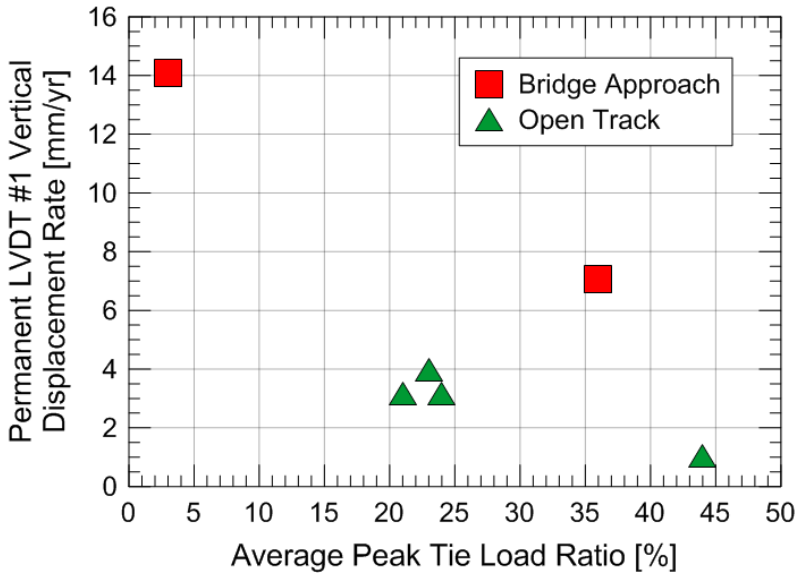

Figure 3.61: Relationship between average peak tie load ratio and permanent LVDT #1 vertical displacement rates at all six instrumentation sites.

The third and fourth relationship is with the subballast and subgrade displacements determined in Chapter 3.6.5. The subballast displacement is represented by the average transient LVDT #2 displacement and shown in Figure 3.62(a). The subgrade displacement is represented by the cumulative transient LVDT #3 through #5 displacement and is displayed in Figure 3.62(b). The data does not support and relationship between the various parameters. This is unsurprising since it is unlikely that a soft subballast or subgrade will result in increased ballast settlements.

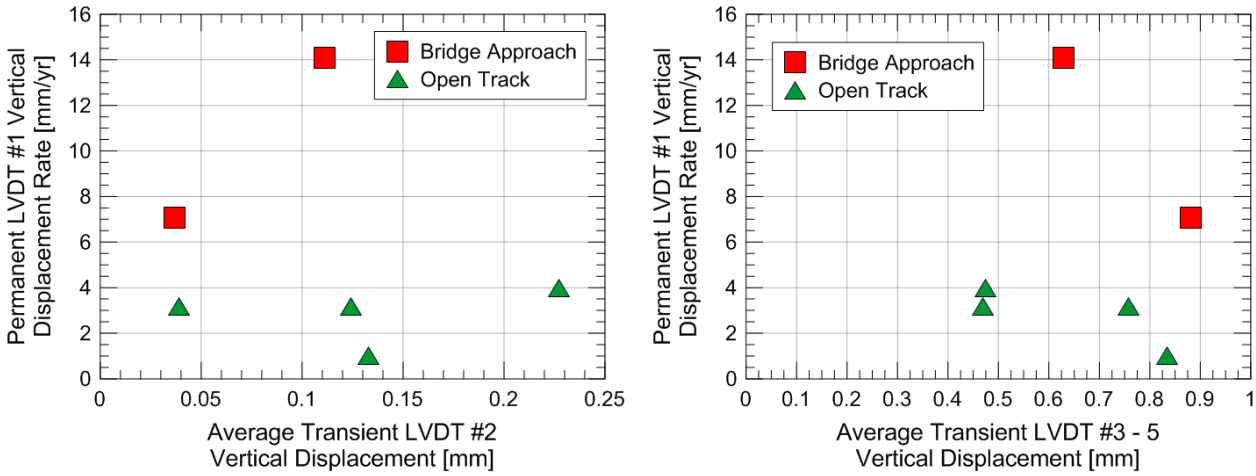

(a) (b)

Figure 3.62: Relationship between average transient (a) LVDT #2 and (b) LVDT #3 through #5 vertical displacement and permanent LVDT #1 vertical displacement rates at all six instrumentation sites.

The fifth relationship is with the mobilized ballast stiffness values determined in Chapter 3.6.3 and is displayed in Figure 3.63. Average mobilized ballast stiffness is used to isolate the influence of tie-ballast gaps and seating displacements. The argument for this relationship is that lower stiffness ballast will likely settle to a greater degree than stiff ballast. This is especially true if the ballast is wet and fouled.

The results suggest a potential relationship if the open track and bridge approach sites are separated. Potential explanations for this relationship are fouling or ballast degradation but samples were not obtained from the sites so this cannot be verified.

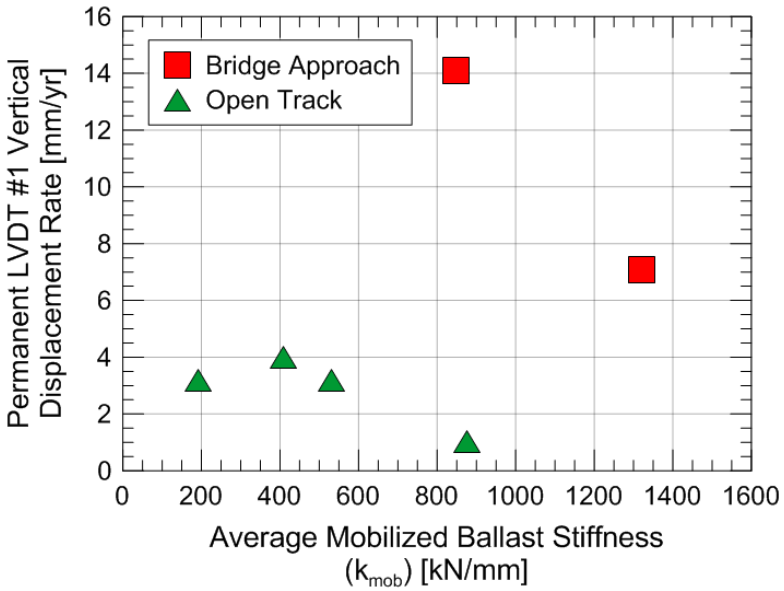

Figure 3.63: Correlation between average mobilized ballast stiffness and net permanent LVDT #1 vertical displacement rates.

The last relation is between the average estimated tie-ballast gap and permanent LVDT #1 vertical displacements. The tie-ballast gap is plotted against permanent LVDT #1 vertical displacement rates in Figure 3.64(a) and the value after 185-days in Figure 3.64(b). The results show a strong empirical relationship between the two factors and suggest a connection. If a connection exists, it appears that 1 mm could be a potential threshold to separate track with potential track geometry problems and track that will not experience issues.

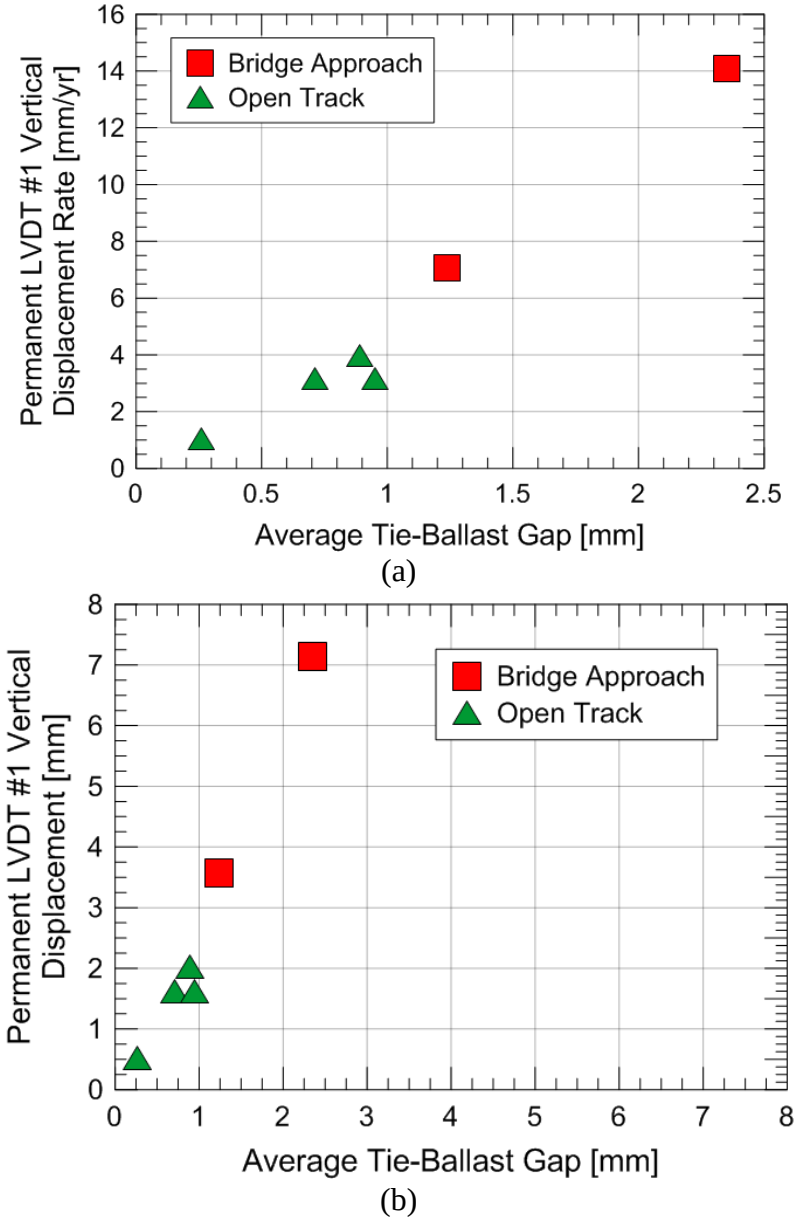

Figure 3.64: **Correlation between average tie-ballast gap height and (a) net permanent LVDT #1 vertical displacement and (b) permanent LVDT #1 vertical displacement rate.**

Two potential explanations for the connection exist:

- The differential rail elevation resulting from inevitable ballast settlement and reduced-performance ballast in the approach naturally produces tie-ballast gaps within the approach and, therefore, the tie-ballast gaps are a result and not a driver of ballast settlement at bridge transition zones.
- The tie-ballast gaps increase ballast settlement from ballast degradation and increased loads and, therefore, is a driver of ballast settlement at bridge transition zones.

The first explanation suggests that increased ballast settlements in the approach from unrelated reasons would cause tie-ballast gaps to develop and produce the empirical relationship. Reduced-performance ballast from fouling and blocked drainage could be potential explanations. The second explanation suggests that tie-ballast gaps directly or indirectly contribute the increased ballast settlements. This could be from increased loads from load redistribution and impacts or increased ballast degradation from the relative movement between the tie and ballast. A combination of both explanations is also possible and likely.

From the available instrumentation, no additional insight can be gained about which explanation has a greater influence. With regards to the first explanation, laboratory tests show the following factors can increase ballast settlement: increased wheel loading, increased loading frequency, decreased confinement, and increased ballast degradation and fouling (See Chapter 2.2). There was no evidence of significant increased wheel loading in Chapter 3.4, and no evidence of increased loading frequency in Chapter 3.6.7. No information on ballast confinement is available but it is unlikely that a dramatic reduction in ballast confinement occurred because of the surrounding tracks. The remaining and most likely possibility is the existence of ballast degradation and fouling. No ballast samples were taken so the gradation curves and degree of fouling were not identified; however, visual observations of fouling were noted in Chapter 3.7. An additional explanation is that the blocked drainage near the approach in conjunction with ballast fouling could produce the increased settlements. Contrarily, the mobilized ballast stiffness does not strongly support the fouled ballast argument if stiffness is used as an indicator.

With regards to the second explanation of tie-ballast gaps directly or indirectly producing the increased rates of permanent vertical displacement, the strongest supporting evidence is a single laboratory test that shows tie-ballast gaps can increase ballast settlements without increased ballast pressures or reduced-performance ballast. Additionally, the available instrumentation would not pick up increased loads from load redistribution and impacts so further study is required.

Realistically, both explanations likely play a role. A more detailed framework is presented in Chapter 6 explaining the chain of events during transition zone settlement.

3.9 Summary

The first task presents the data, analyses, and interpretations of the field measurements of the monitored railway transitions along the Amtrak Northeast corridor (NEC) near Chester, Pennsylvania and the Norfolk Southern (NS) N-line bridges in southern West Virginia. The stated objectives of Task I are the following:

(1) determine the depth at which the majority of permanent and transient displacements are occurring, and
(2) determine the root cause(s) of differential movement at the ten instrumented high-speed and freight lines.

3.9.1 Summary of Results

The first objective involved determining the depth at which the majority of permanent and transient displacements are occurring because the depth is often subject to much debate and is required knowledge for successful remediation. This is addressed in Chapter 3.3 and Chapter 3.6. A summary is listed below:

- Analyzing the permanent vertical displacement response of all LVDTS show the majority of permanent vertical displacements occurs in LVDT #1, which measures from the top of the concrete tie to the bottom of the ballast layer. This suggests the majority of settlement occurs in the ballast layer.
- The largest permanent LVDT #1 vertical displacement occurred at the three transition zone locations, confirming historical records.
- For all sites, the largest transient vertical displacements occurred in LVDT #1 and were greater for the transition zone locations.
- Separating the LVDT #1 displacement into individual components shows the majority of transient vertical displacement involves the closure of tie-ballast gaps and not ballast displacement.

The second objective involved determining the root cause(s) of differential movement at the high-speed and freight lines so remediation efforts can try to address the root cause of the problem. The collected data was analyzed in Chapters 3.3 to 3.6 and empirical relations were plotted in Chapter 3.8. The results of a site visit are presented in Chapter 3.7. A summary is listed below:

- The strongest correlation with permanent LVDT #1 vertical displacement was the estimated tie-ballast gap height. Ballast stiffness and tie support showed potential correlations but to a lower extent. The wheel loads, subballast, and subgrade were not considered influential factors.
- Site observations showed damaged ties and wet fouled ballast in the approach regions. This suggests potential increased loads and reduced-performance ballast conditions.
- Increased loads and ballast degradation from tie-ballast gaps and reduced-performance ballast from degraded and wet, fouled ballast are proposed as the root causes of differential movements at the monitored railroad bridge transition zones.
- These observations suggest remediation focus on the ballast layer and/or reducing tie-ballast gaps in transition zone locations.

3.9.2 Lessons Learned and Future Work

The instrumentation setup for the high-speed and freight sites involved measuring wheel loads, tie reactions, and permanent and transient displacement with depth. While this instrumentation was successful at determining the depth at which the majority of movement was occurring, the goal of this setup, it was not able to provide conclusive evidence on the causes for the movement. Suggestions for future instrumentation setups are listed below:

- It is recommended that future setups put more emphasis on characterizing a single bridge approach instead of spreading the instrumentation amongst multiple transitions. The track behavior at poorly performing transition zones vary along the track and is difficult to diagnose problems with only a two instrumentation locations at a single bridge approach. For example, instrumentation at 2-ft, 6-ft, 10-ft, 15-ft, 20-ft, and 60-ft would be very informative about varying track conditions and how tie-ballast gaps form and change over time.
- It is recommended that instrumentation increase focus on the tie-ballast interface to evaluate potential increased tie loading.
- It is recommended that future setups collect permanent and transient records to clearly define the change in behavior after tamping. For example, collect train measurements for the four or five trains immediately after tamping, two the next day, and two the following day. Multiple permanent measurements should be taken within that time-frame as well. The will provide essential information on the benefits and effectiveness of tamping.
- It is recommended that future setups attempt to collect data showing the variation in behavior on a daily, weekly, and seasonal time-frame. This would give insight whether the observed variations with time are long-term trends or just artifacts of weekly or seasonal trends.

- It is recommended that future setups better define the ballast and subgrade properties. This includes gradation, fouling index, and plasticity index if possible. This will give better insight into whether reduced-performance ballast exists and its influence on track behavior.

Many of these recommendations are incorporated into a newly developed instrumentation setup presented in Task II (Chapter 4). Additionally, Chapters 4 and 5 attempt to investigate whether increased loads are present at unsupported ties using accelerometers and finite element models. This will provide additional information that can be used to diagnose the root causes and improve remedial recommendations.

CHAPTER 4

TASK II: NON-INVASIVE INSTRUMENTATION

4.1 Introduction

Task I presented an in-depth instrumentation setup and analysis of ten track locations in the United States and drew the following conclusions:

- at the instrumented sites, the majority of permanent settlement occurred in the ballast layer,
- the primary transient tie displacement component in transition zones involved the closure of tie-ballast gaps, and
- a strong correlation was found relating tie-ballast gap height and permanent track settlement suggesting possible increased loading and ballast degradation from impacts due to the closure of tie-ballast gaps.

Direct or indirect evidence of increased loads and ballast degradation were not obtained from the Task I instrumentation and lessons learned suggest future instrumentation should measure multiple tie locations in a single approach and emphasize the tie-ballast interface. This indicates the need to develop a different instrumentation system to gain insight into potential increased loads from tie-ballast gaps and is capable of non-invasively evaluating track performance within a few hour time-frame. Additionally, a means of quantitatively measuring general track performance is desired for inspection and can be used to compare the performance of various transition zone designs. This shapter introduces and discusses this instrumentation program.

The primary objectives of Task II are the following:

(1) develop non-invasive monitoring system to evaluate the tie-ballast interface,
(2) use track instrumentation to gain evidence of increased loads in transition zones, and
(3) compare the performance of various transition designs.

To evaluate the tie-ballast interface, the metrics of tie displacement and tie acceleration were selected because they give complementary information about the tie-ballast interface and installation and data collection at multiple sites can occur within a single day. Further

improvements in techniques and analysis are required before strong conclusions and correlations can be made, but this preliminary instrumentation can provide direction and insight for future work.

This chapter first introduces the instrumentation and data analysis methods used in Chapter 4.2. A list and overview of the eight instrumented sites are listed in Chapter 4.3. Analysis of the eight visited sites is presented in Chapter 4.4. Chapter 4.5 summarizes the work from Task II.

4.2 Instrumentation

To evaluate the tie-ballast interface, the metrics of tie displacement and tie acceleration were selected because they give complementary information about the tie-ballast interface and require minimal installation and data interpretation effort. The instruments selected to measure tie displacement and tie accelerations are high-speed video cameras and piezo-electric accelerometers. This section introduces the two instruments of (1) high-speed video cameras and (2) accelerometers and follows by introducing the processing techniques of (3) filtering and (4) double-integration.

The objective of the instrumentation setup is to collect information indicating increased displacements and/or accelerations in a manner that is non-invasive, capable of being set-up in less than 30 minutes, and requires minimal post-processing. The instruments and methods selected are shown to fulfill the above requirements and while the measurements will not be as accurate as other existing methods, it is believed the reduced setup and processing time makes up for the reduced accuracy. Track time is a limited and highly sought resource that cannot be wasted and long setup and processing times are inconvenient and costly for railroad companies. Additionally, the rapid upgrade in technology and processing power allows the current setup to be upgraded and improved over time.

4.2.1 High-Speed Video Cameras

This subsection introduces various methods of measuring rail and tie displacement, benefits of high-speed video cameras, image processing techniques, and a brief discussion of capabilities and limitations.

Measuring rail and tie displacement is a beneficial metric for evaluating track performance because it is easily understood and empirically correlates with permanent settlement. Many methods are available but optical techniques, typically lasers or high-speed video cameras, are becoming increasing popular because they directly and non-invasively measure rail and tie displacement. For example, laser measurements are highly accurate and can accommodate sampling rates of over 1,000 Hz (Pinto et al., 2015). Lasers have been used to measure open track tie displacements in Brazil and transition zone rail displacements in Portugal (Silva and Logistica, 2007; Pinto et al., 2015). The primary disadvantages of lasers are safety concerns of a laser near traffic and only a single location can be measured with each individual laser, therefore requiring a stable base. Alternatively, high-speed video cameras can be used for stationary measurements and can monitor multiple locations without laser related safety concerns. Vertical displacements can be derived from video camera recordings using Particle Image Velocimetry (PIV) or Direct Image Correlation (DIC) to track targets attached to the rail and ties (Murray et al., 2012; Priest et al., 2010; Le Pen et al., 2014). High-speed video cameras are capable of measuring multiple targets in a single shot, do not require a completely stable foundation, and provide a visual account of the moving track. The disadvantages include more complicated image processing and typically lower accuracy or sampling rates than lasers. Advances in both laser and high-speed video technology in the past decade have made both of these methods more practical to use and analyze.

Consumer high-speed video cameras (Figure 4.1a) were selected to directly and non-invasively measure transient rail and tie displacements. The high-speed cameras are capable of measuring two rail and tie locations in a single shot and sampling frequencies of 240 frames per second (fps) were used. The literature indicates that camera monitoring initially used 30 fps (Priest et al., 2010) but higher values of 100 fps (Murray et al., 2012) to 500 fps (Le Pen et al., 2014) are now typical because of advancements in camera technology. The cameras have a resolution of 448 x 336 pixels and are typically placed about 15 to 20 feet from track.

To convert the video to displacement time histories, a MATLAB code was modified from an open source code that tracks the movement of the targets attached to the rail and tie. The technique used is often defined as a “blob analysis” and tracks large moving targets that can be easily identified. For the analysis, an orange target color is used because it is distinct from common background colors and can be isolated during post-processing (Figure 4.1b). The code

locates the targets by creating a binary image in which all pixels with the pre-selected orange color are converted to white while all non-orange pixels are converted to black. Secondly, the code calculates the centroid of each target, i.e. white pixels, in each frame and produces a time history by tracking the centroids during the course of the video. The influence of ground vibrations are minimized by also tracking a target attached to an 18-inch stake that is driven into the ballast shoulder about 1-ft from the tie edge and subtracting the stake time history from the rail and tie time histories. This method reduces setup and image processing time compared to established PIV, DIC, and lasers methods (Pinto et al., 2015; Silva and Logistica, 2007; Murray et al., 2012; Priest et al., 2010; Le Pen et al., 2014) but sacrifices accuracy if low displacement values (<0.50 mm, <0.02 in) are desired. The video cameras are capable of tracking both transient vertical and longitudinal displacements but only vertical results are presented herein.

Figure 4.2 shows photographs of the steps within the MATLAB code. Figure 4.2(a) shows a .jpeg obtained from the video file showing one rail, four tie, and one stake target. The first step of the code is to isolate one target, stake target in Figure 4.2(b), and select a color. The entire shape does not need to be outlined; just the desired color has to be within the selected region. Next, the code binarized the target for each .jpeg (Figure 4.2c and d) and takes the centroid. These centroids are outputted into a .txt file and can be used as time histories.

(a) (b)

Figure 4.1: Photographs of (a) consumer high-speed video cameras and (b) orange targets attached to rail, timber tie, and stake locations.

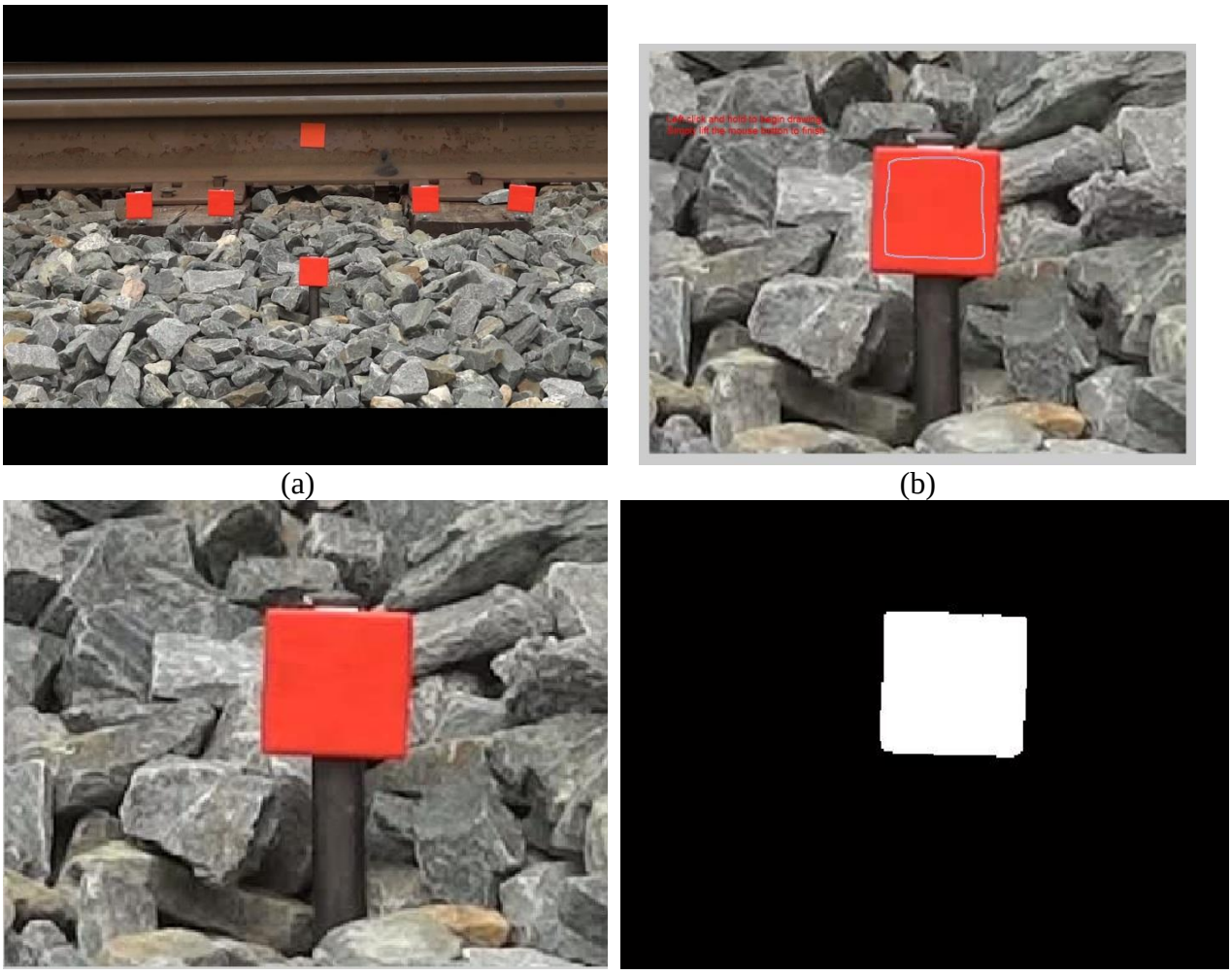

Figure 4.2: Photographs showing (a) sample video jpeg, (b) selection of target color, and comparison between (c) color and (d) binarized target.

The next step of the process is reduce the influence of camera translation from wind or ground vibrations. This is accomplished by subtracting the stake time history from all rail and tie time histories. An example of this process is displayed in Figure 4.3 in which the stake and uncorrected time histories are displayed in Figure 4.3(a). Some downward movement, which is common, is seen in the first few seconds, possibly from wind movement of the passing train. The stake time history is subtracted from the uncorrected rail and the corrected rail history is displayed in Figure 4.3(b).

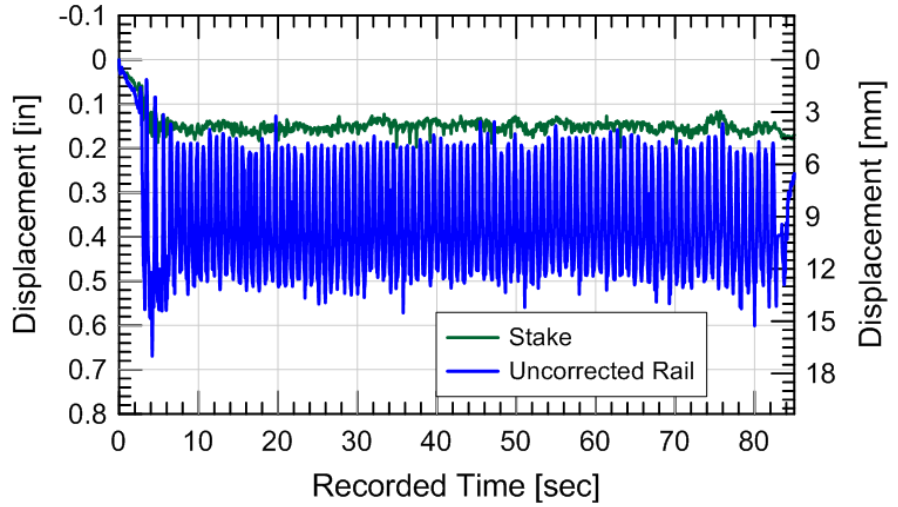

(a)

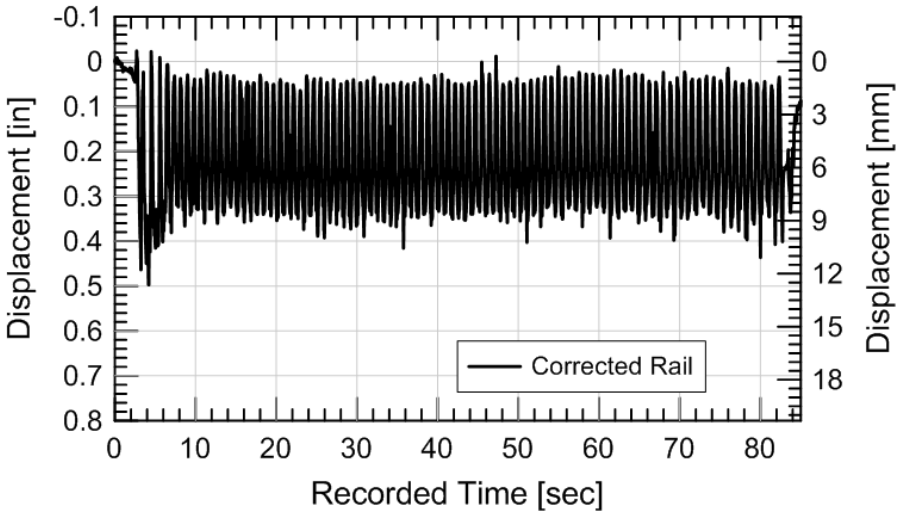

(b)

Figure 4.3: Rail displacement time histories from video images showing (a) raw and (b) corrected values.

4.2.2 Piezo-electric Accelerometers

This subsection introduces the piezo-electric accelerometers, their benefits and capabilities, and lists the various mechanisms that produce tie accelerations.

The second metric for evaluating the tie-ballast interface is tie accelerations. Tie acceleration time histories can be informative of track performance because any impact or movement of the tie is recorded by the accelerometer. While load is not measured directly, increased tie accelerations can be indicative of increased loading within the track system. Piezo-electric accelerometers are selected because they can have a sensitivity of 10 mV/g, large

measurement range (+/- 500g), large frequency range (1 to 10,000 Hz at 5%, 0.75 Hz to 20,000 Hz at 10% or 0.35 to 30,000 Hz at 3dB), and are small and easy to attach to the ties.

Additional devices required to collect data are signal conditioners, data-acquisition (DAQ) systems, and a laptop to record data. The signal conditioners power the accelerometers and are capable of amplifying and filtering the signal while the DAQ converts the data from an analog signal to a digital signal. The laptop collects the data. The setup with the additional devices is displayed in Figure 4.4.

Besides the time history, the tie response is also analyzed in the frequency domain to understand which frequencies are most predominant in the sample. This study does not compared between sites. To convert to the frequency domain, the time history is split into about 20 to 30 equal parts and zero padded until reaching 262,144 data points. This is performed to clean up the frequency response.

(a) (b)

Figure 4.4: Photographs of (a) an accelerometer attached to a timber tie, and (b) the roadside accelerometer setup including signal conditioners, DAQ, and laptop.

Railroads produce a complex loading environment and multiple loading/vibration mechanisms can produce tie accelerations, including:

(1) wheel-rail impacts,
(2) wheel-rail vibrations,
(3) superstructure impacts,
(4) tie vibrations,
(5) train loading,
(6) tie-ballast impacts, and
(7) tie displacements.

A discussion of each mechanism and indicators on how to identify each mechanism is provided below.

The first mechanism, wheel-rail impacts from wheel flats or other wheel irregularities, are high-magnitude short-duration impacts can produce tie accelerations exceeding 400g. While these impacts are vehicle issues, the impact can increase wheel loads by five times the static load and can damage track components (see Chapter 2.4.3). These impacts can be identified as inconsistent, single peaks in tie acceleration. The wheel flats are also noticeable during recording by the loud periodic “clanking noise” as the wheel flat impacts the rail every wheel rotation and be noted and correlated to the tie acceleration data. Figure 4.5 shows a distinct wheel flat impact that approaches tie acceleration magnitudes of 400g at about 38 seconds in the recorded time history. The frequency of the wheel flats can vary from about 100 to 1000 Hz. This high-frequency motion is usually believed to be attenuated by the superstructure and generally not passed to the ballast but his has been disputed by field measurements (Indraratna et al., 2010). Therefore, the influence of wheel flats on ballast degradation is unclear.

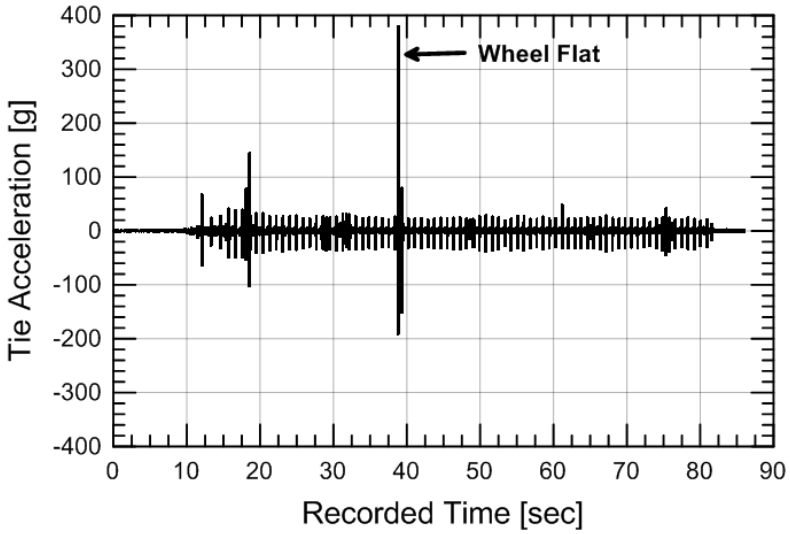

Figure 4.5: Acceleration time history showing a peak from a wheel flat. Data are from Site #6, Train#6-2-7, Accel #6.

The second mechanism, wheel-rail vibrations from braking, are medium-magnitude high-frequency vibrations that produce sudden tie acceleration and can drown out tie vibrations from other mechanisms. These vibrations are not considered a track issue and it is preferred that this mechanism is avoided. The wheel-rail vibrations can be identified by sudden medium-magnitude and high-frequency tie accelerations that dominate tie acceleration records. An example of the influence of braking is displayed in Figure 4.6. The time history shows near-continuous braking and is clearly identified at about 15.8 seconds in which 15g high-frequency vibrations suddenly appears and slowly decrease in magnitude until 18.5 seconds, in which the breaking is applied again. Despite drowning out other acceleration mechanics, due to the high-frequency nature of these vibrations, filtering methods (Chapter 4.2.3) can be used to reduce their influence. As with wheel flats, the high-frequencies are generally assumed to be attenuated before reaching the ballast but the authors are not aware of any field evidence that supports or disputes this.

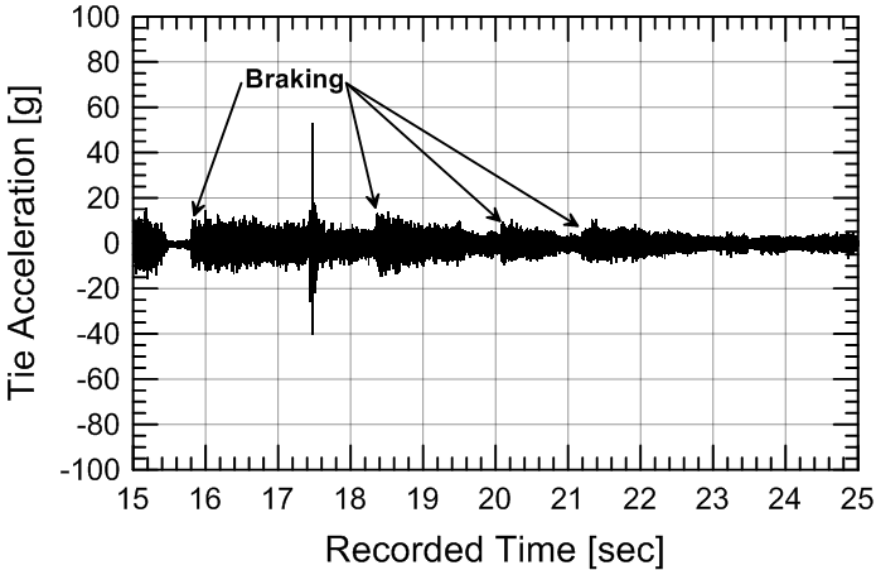

Figures 4.6: Acceleration time history showing the influence of braking. Data are from Site #2, Train #2-3, Accel #6.

The third mechanism, superstructure impacts, occurs when an impact or some sudden acceleration is produced from the superstructure. This may be the result of a damaged rail, slippage of the fastening system, or relative movement between the rail and tie that results in the rail impacting the tie during every wheel or bogie passage. This impact has a short duration and can range significantly in magnitude depending on how the impact is produced. The impacts can be identified because they are consistent and occur every wheel passage or once every during a set of train trucks. Figure 4.7 shows an example of a superstructure impact, in which an impact is produced during the passage of two train trucks (back truck and front truck of next train car). The impacts produce distinct acceleration peaks every wheel pass (four wheels every acceleration "burst") ranging from 50 to 200g (note scale difference). The frequencies of the impacts range from about 150 to 200 Hz. The exact cause and location of impact is unknown but is likely from the wheel-rail or rail-fastening system interface because metal-on-metal contact is expected to produce higher accelerations than metal-on-timber contact. This would be considered a track structural issue because the peak is consistent with each passing wheel and therefore causes by the track itself.

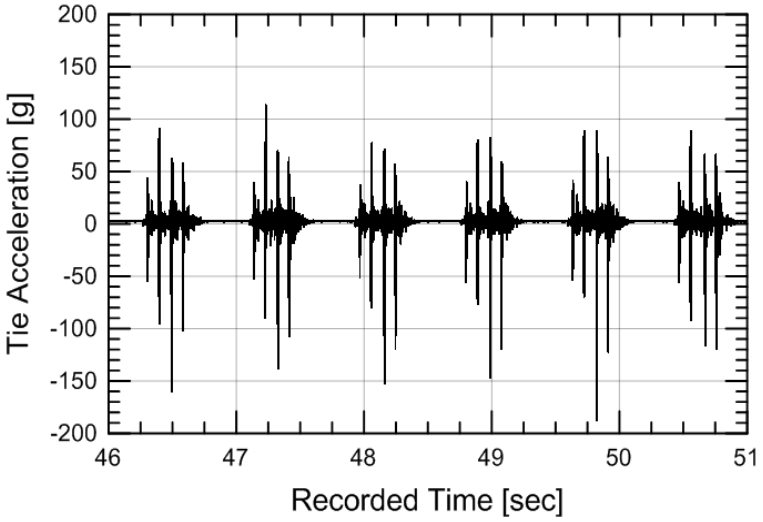

Figure 4.7: Acceleration time histories showing superstructure impacts. From Site #6, Train#6-3-2, Accel #7.

The fourth mechanism, tie vibrations, is produced from unsupported concrete ties. Ballast typically provides restraint and damping to the concrete tie so a lack of ballast surrounding the tie causes the tie to freely vibrate at its natural bending modes (see Figure 4.8a). For concrete ties, the first three vibration modes are about 100 to 150 Hz, 330 Hz, and 630 Hz but vary depending on the type of concrete tie (Harrison et al., 1984; Remennikov and Kaewunruen, 2006; Taherinezhad et al., 2013). This vibration can be identified when viewing the tie acceleration time history in the frequency domain and observing dominate frequencies that correspond to the expected bending modes of the tie. Figure 4.8(b) compares an unsupported tie (Accel #3) with a supported tie (Accel #5) in the frequency domain to illustrate the bending modes. As observed, the bending modes of Accel #3 roughly agree the first three vibration modes with values of 110 Hz, 300 Hz, and 585 Hz.

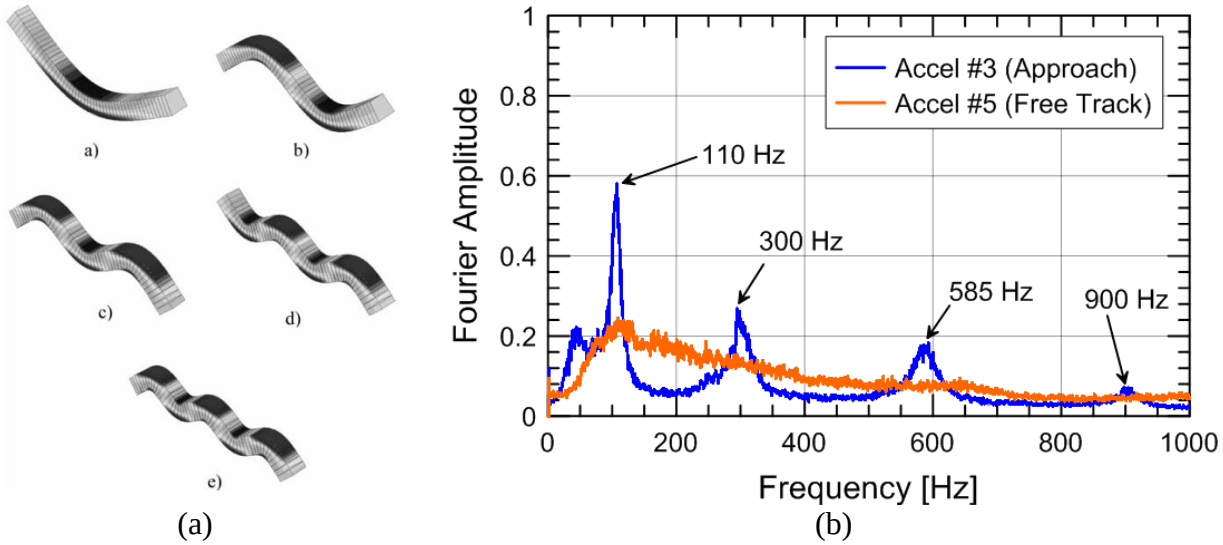

(a) (b)

Figure 4.8: Diagram showing the physical motions of the first five vibration modes (from Kaewunruen and Remennikov, 2007) and (b) relative frequency domain plot showing the first four vibration modes of an unsupported tie. From Site #3, Train# 3-2, Accels #3&5.

The fifth mechanism, train loading, is the most general tie acceleration mechanism and will occur during every train passage. The magnitudes can vary depending on train weight, velocity, car type, tie support, and many other factors. During measurements, values are generally consistent for homogenous trains but can also vary for heavier coal trains. For example, Figure 4.9 illustrates the tie acceleration time history from a passing empty train. Each "burst" of tie acceleration corresponds to two train trucks (back truck and front truck of next train car). The tie acceleration magnitudes are typically 3 to 4g but inconsistent peaks of 5 to 15g can sometimes appear and are likely vehicular issues such as wheel irregularities or impacts between the wheel flange and rail. The frequency varies but is typically between 50 to 300 Hz. This mechanism can be identified by consistent "burst" of tie acceleration every wheel, train truck, or two consecutive train trucks, depending on rail-tie contact.

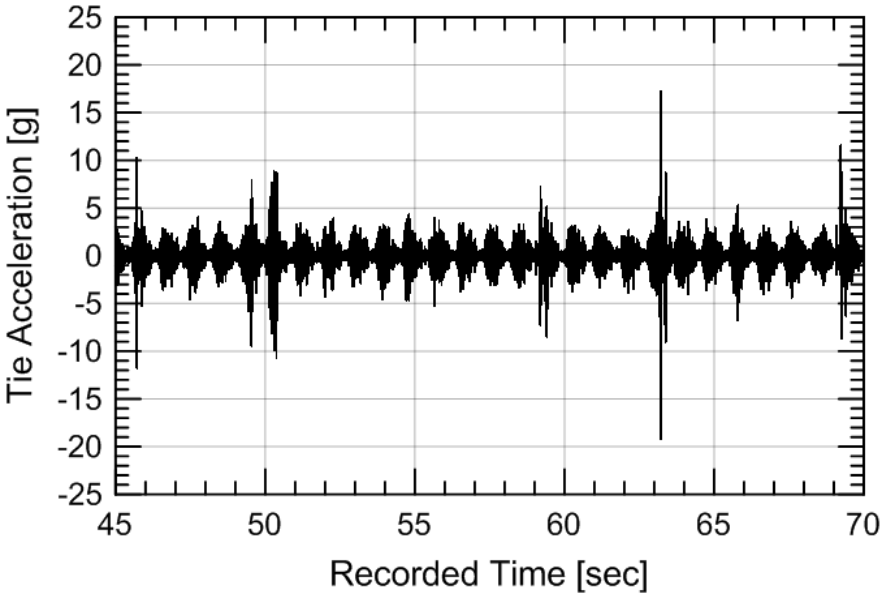

Figure 4.9: Acceleration time history showing fairly consistent tie load. From site not introduced.

The sixth mechanism, tie-ballast impacts, occurs when an unsupported tie impacts the ballast during train loading. This impact has a short duration and ranges from about 20 to 40g, depending on the height of the tie-ballast gap. The impact can be identified by a sudden tie acceleration peak at the beginning of an acceleration loading and has frequencies ranging from 50 to 100 Hz. It will also typically be located at the beginning of an acceleration "burst" because the tie will impact the ballast prior to the train loading mechanism. Figure 4.10 shows an example of a tie-ballast impact, in which the impact produces a 25 to 30g load every passing double train truck (back truck and front truck of next car).

The direct impact between the tie and ballast is not only believed to increasing ballast loading but also increase ballast degradation. This is backed by ballast box testing from Selig and Waters (1994) and is described in Chapter 2.2.4.

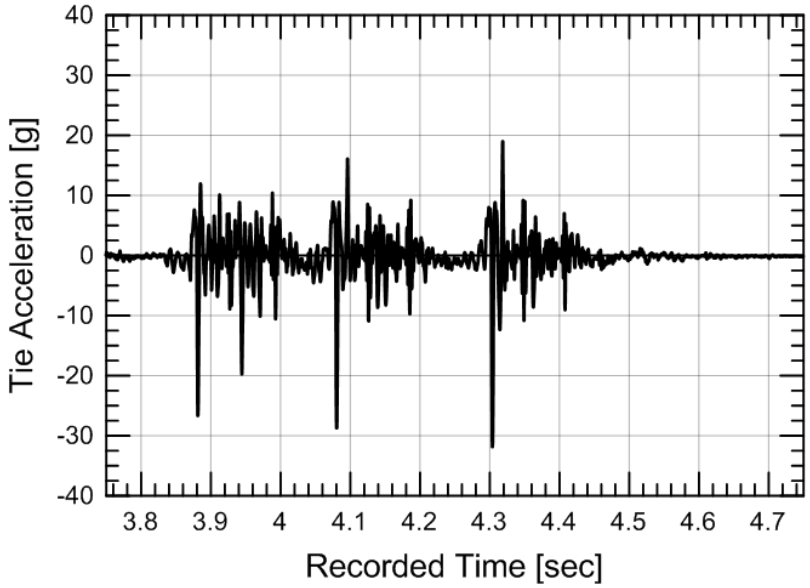

Figure 4.10: Time history showing impacts from tie-ballast contact. From Site #5, Train #5-1, Accel #3 (15 ft.)

The seventh mechanism, tie displacement, is the tie acceleration that occurs from the displacement of the tie. This is different from previous mechanisms which are produced from the stress wave from an impact or vibrations. Tie displacement accelerations are long duration (0 to 30 Hz) and produce low acceleration magnitudes (<2g). This means the tie accelerations from tie displacement are typically overpowered by the previous six mechanisms; however, the tie displacement mechanism can be isolated by filtering out high-frequency vibrations (>30 Hz).

To emphasize the low-frequency low-magnitude nature of the tie displacement mechanism, a tie acceleration record is presented in Figure 4.11 that isolates the tie displacement accelerations. An in-depth explanation of filtering is presented in the next subsection and tie displacement accelerations are used for the double-integration procedure explained in the subsection after filtering.

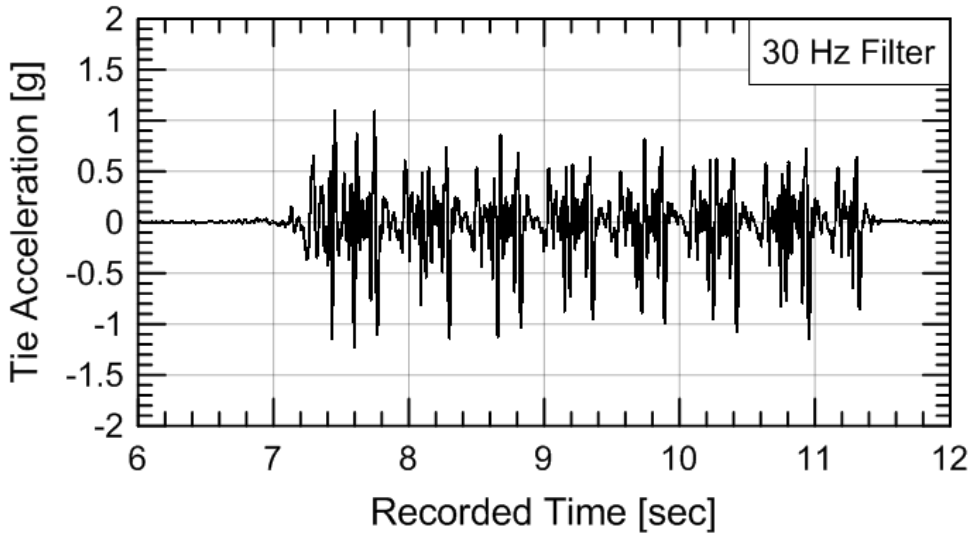

Figure 4.11: Time history of tie accelerations from tie displacement (low-pass 30-Hz Butterworth Filter). From Site #7, Train #7-8, Accel #2.

An additional signal that is present in all measurement records is noise. Noise can be produced from multiple sources, including the instrument, signal conditioners, data-acquisition (DAQ) systems, electrical inputs, and many others. Prior to processing, it generally beneficial to identify noise within the instrumentation system so this noise can be reduced or eliminated. For the piezo-electric accelerometers, noise is more prevalent at low-frequencies (<0.75 Hz) but also exists at lower magnitudes along all frequencies. Figure 4.12(a) shows an example of a time history that connected to railroad tie but with no load. Figure 4.12(b) shows the frequency domain to emphasize the low-frequency noise.

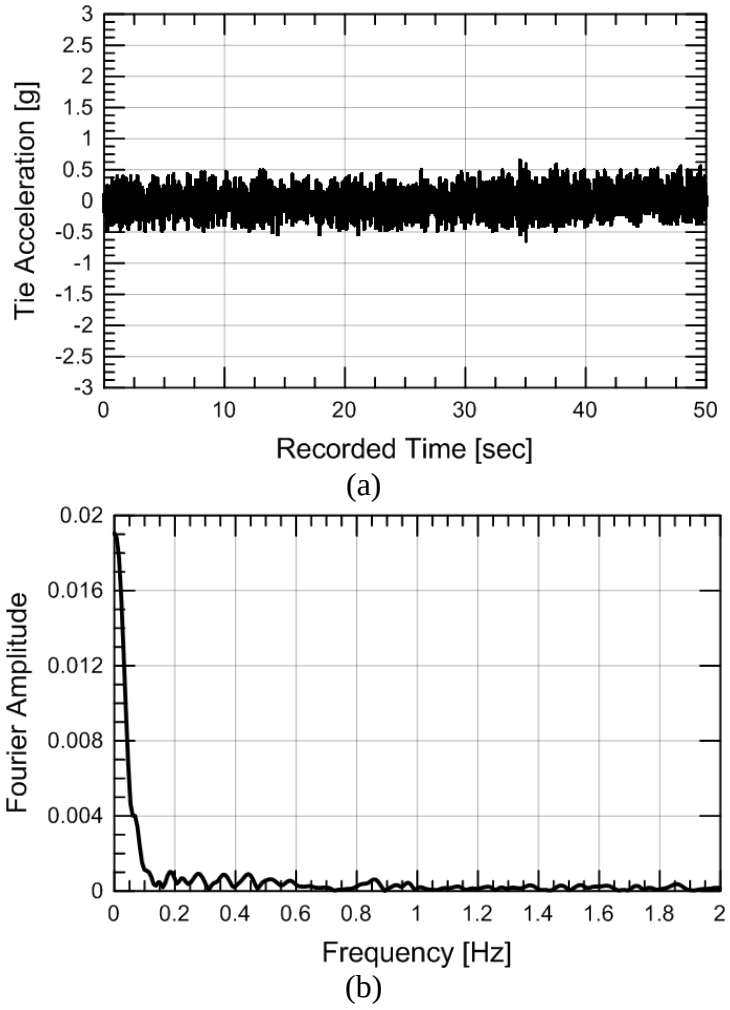

Figure 4.12: Tie response with no loading (noise only) in (a) time domain and (b) frequency domain.

This low frequency noise is relevant to acceleration analyses because if a train is moving slower than 25 mph, the tie displacement frequencies are typically less than 0.75 Hz and makes it difficult, if not impossible, to isolate the tie displacement frequencies from the noise. This is further explained in the next two subsections.

Analysis and interpretation of acceleration time histories tends to be less straight-forward than wheel loads or displacements because of the multiple mechanisms producing tie accelerations, variation of peak values every passing train truck, influence of noise and high-frequency peaks, and lack of a clearly defined peak for automated analyses. For these reasons, automated methods to analyze peak tie accelerations were not used and interpretation relied on user judgement.

To summarize, seven mechanisms that can produce tie accelerations and are listed in Table 4.1.

Table 4.1: Summary of tie acceleration mechanisms

Mechanism	Magnitude [g]	Frequency [Hz]	Description
Wheel-rail impact	Up to 400+	100 to 1000	Inconsistent single peaks
Wheel-rail vibration	20 to 40	>500	Continuous high-frequency noise
Superstructure impacts	Up to 200+	150 to 200	Peaks every wheel passing
Tie vibrations	-	100-150, 330, 630	Dominant frequencies
Train loading	1 to 20	50 to 300	Consistent acceleration "bursts"
Tie-ballast impacts	Up to 40	50 to 100	Single peak before train loading
Tie displacement	<2	<30	Low-frequency, Need filtering

To clarify, accelerometers attached to railroad ties provide much information about impacts, vibrations, movement occurring within the track structure. Diagnosing the cause of these tie accelerations can be difficult but is possible if written records and videos are recorded during train passage. In that way, tie accelerations are viewed as complementary to tie displacements because they give additional insight into the track response.

Tie accelerations are also expected to indicate potential increased loads in the track structure but no correlation yet exists to directly compare the two metrics. This means that a 30g impact from the closure of a tie-ballast gap could have different implications than a 30g impact from the superstructure. More studies are required to answer these questions. If the tie displacement magnitude is isolated, it is expected to correlate with tie displacement because the two values are directly related.

4.2.3 Filtering

A signal processing technique used for both the video camera and accelerometer records is filtering. The purpose of filtering is to eliminate noise within the signal records or isolate particular frequencies. This subsection will give a general overview of filtering methods and the procedures.

The filtering methods herein are described by the mathematical filter and frequency range the filter passes. Multiple types of mathematical filters exist and differ based on the mathematical equation used to smooth the transition from the filtered and non-filtered range. The

Butterworth filter is selected for analyses because it is simple to use and sufficiently filters the signal. The primary drawback is the transition from the filtered to non-filtered frequencies is not as steep as other filters but this has generally not been an issue. Elliptical filters can also be used and will have a steeper slope but will generally yield identical results.

The frequency range is specified by selecting one of three types of filters: low-pass, high-pass, or band-pass. Low-pass filters allow frequencies lower than the frequency cutoff and attenuate higher frequencies. High-pass filters allow frequencies higher than the frequency cutoff and attenuate lower frequencies. Band-pass filters allow frequencies between two frequency cutoffs and attenuate frequencies outside the cutoff range. The order of the filter relates to how many variables are used to develop the mathematic filter and essentially a higher order filter means a steeper transition from passed and attenuated frequencies. An example of a 3^{rd}-order bandpass Butterworth filter with cutoffs at 0.75 and 500 Hz and its effect on the time and frequency domain response is displayed in Figure 4.13.

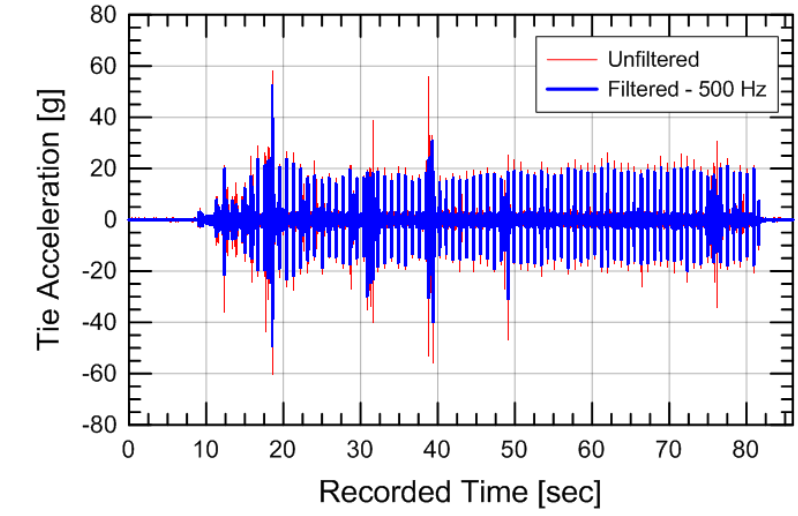

(a)

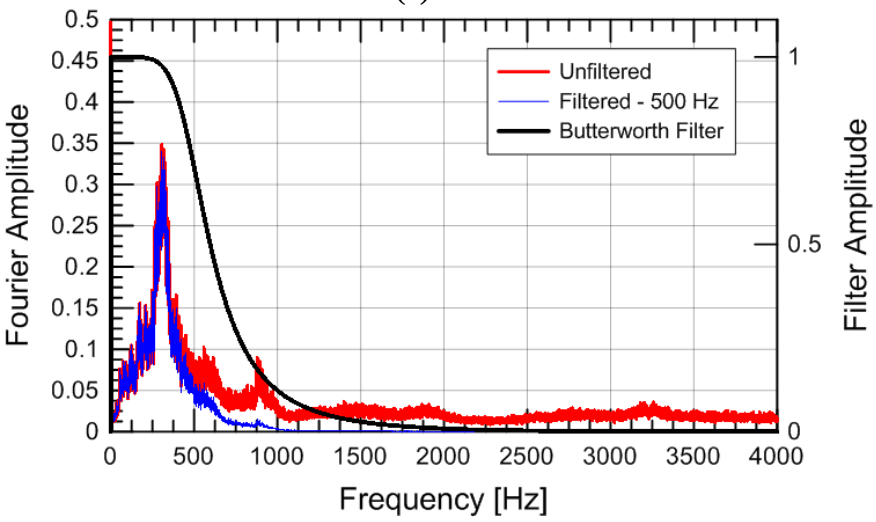

(b)

Figure 4.13: Examples of 3rd-order bandpass Butterworth filter with frequency cutoffs at 0.75 and 500 Hz in (a) time and (b) frequency domain.

The filtering method used for the video cameras is an 8th-order low-pass Butterworth filter with a frequency cutoff at 12 Hz. This removes much of the noise and isolates the primary displacement frequencies ranging from 1 to 5 Hz. However, it is good practice to view the frequency domain prior to filtering to ensure that no important frequencies are attenuated. An example of an unfiltered and filtered video camera time history is displayed in Figure 4.14(a) and the frequency domain in Figure 4.14(b). The results show the filtering has minimal effects on peak values and that the majority of displacement information is contained within about 1 to 5 Hz.

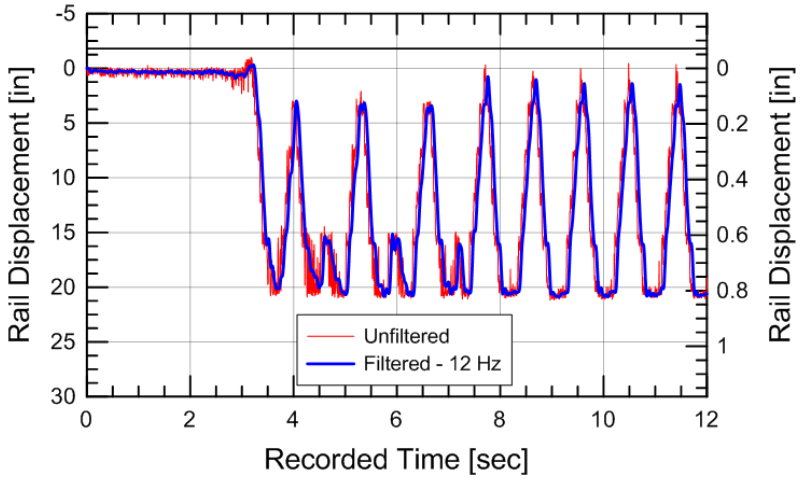

(a)

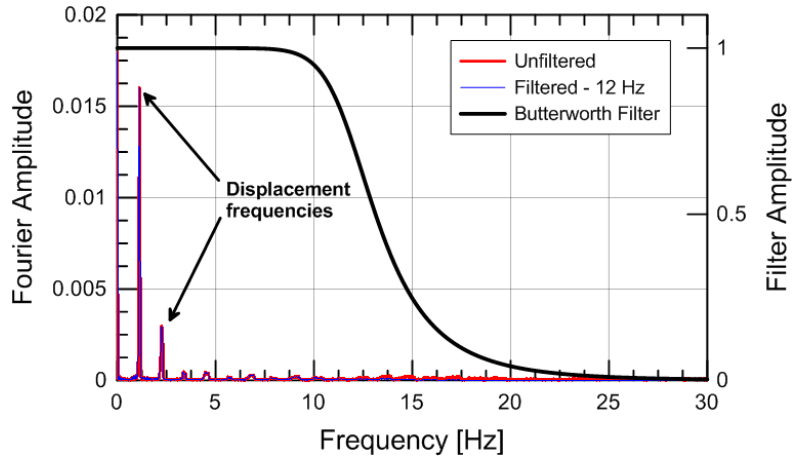

(b)

Figure 4.14: 12 Hz 8th-order low-pass Butterworth filtered and unfiltered response in (a) time domain and (b) frequency domain.

The filtering method used for accelerometers is a 3rd-order bandpass Butterworth filter with a frequency cutoff at 0.75 Hz and 500 Hz. This eliminates the majority of low-frequency noise within the acceleration record and high-frequency vibrations. Generally, the unfiltered and filtered records are similar with little change in acceleration magnitudes. However, it is advised to study the acceleration record in the frequency domain to better understand what mechanisms are filtered. For coal trains, high magnitude vibrations from train loading are common at the 500 to 700 Hz range and can be significantly reduced by filtering at 500 Hz. The effect of this vibration range on the ballast is currently unclear but it is an important factor to note. An example of the effect of the bandpass filter is displayed in Figure 4.13 and shows little difference in the majority of peak tie accelerations. The reduced values appear to be wheel flat impacts,

which commonly have higher frequency values than the other peaks impacts. The remaining peaks appear to be from superstructure impacts.

To isolate the tie displacement accelerations for analysis or double-integration (next section), a 3rd-order bandpass Butterworth filter with a frequency cutoff of 0.75 Hz and 30 Hz is used. The low frequency (high-pass component) filter is displayed in Figure 4.15 and shows a reduction in noise but not the tie displacement frequencies.

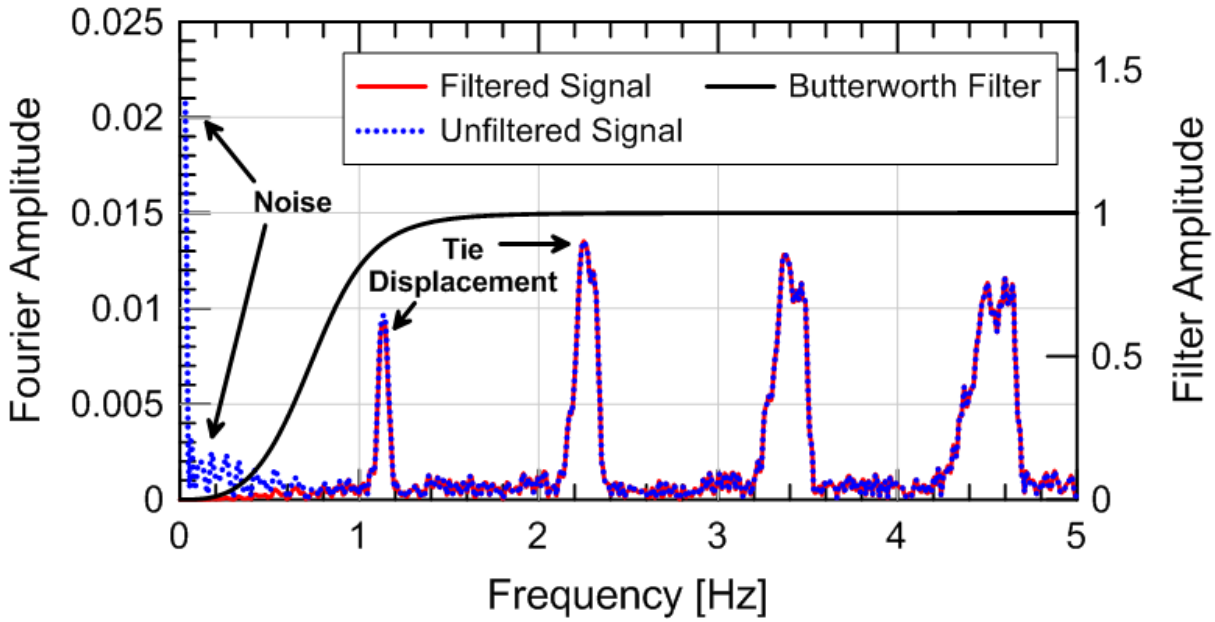

Figure 4.15: High-pass Butterworth filter with a cutoff frequency of 0.75 Hz applied to a tie acceleration time history presented in frequency domain.

4.2.4 Double-Integration

This section introduces the procedure used for double-integrating tie acceleration records. This method is not expected to produce tie displacement magnitudes as accurate as video cameras, but double-integration can be useful to estimate displacements in regions that are not measured by the video cameras. The procedure can only be used if the tie displacement frequencies are not attenuated when filtering the system noise. This limits the analysis to trains moving faster than about 25 mph and ties with consistent displacements over about 4 mm. Other types of accelerometers, e.g. DC accelerometers, which are better at reducing noise while sacrificing magnitude and high-frequency measurement range are also available but not used in this analysis (Lamas-Lopez et al., 2014).

The double-integration procedure includes the following steps:

1. Passing the acceleration time history through a 3rd-order bandpass Butterworth filter (0.75 to 30 Hz) to eliminate low-frequency noise and high-frequency motions. The lower frequency cutoff is set by the accelerometer while the upper limit is more arbitrarily set because high-frequency tie accelerations (>30 Hz) have negligible effect on the calculated tie displacements. An upper limit value of 30 Hz was selected because it removes the high-frequency motion and generally isolates the tie displacement component.
2. Integrating the acceleration time history using the trapezoidal method to obtain a velocity time history;
3. Passing the velocity time history through a 3rd-order high-pass Butterworth filter (0.75 Hz) to remove residual noise from the integration process;
4. Integrating the velocity time history using trapezoidal method to obtain a displacement time history.

This procedure is illustrated in Figure 4.16, which shows the unfiltered and filtered tie acceleration time histories, the integrated tie velocity time history, and double-integrated tie displacement time history. The significant reduction in acceleration magnitudes (~10g to ~1g) when the unfiltered acceleration time history is passed through the band-pass filter isolates accelerations for the tie displacement mechanism. The acceleration spikes greater than 30g are inconsistent and likely from passing wheel flats while the consistent 10 to 15g accelerations are likely from superstructure impact within the track system during wheel loading and therefore are not associated with vertical tie displacements. These loading mechanisms have frequencies much greater than 30 Hz so will be attenuated and will not contribute to tie displacement magnitudes. The tie velocity and displacement time histories show consistent values which is expected from a passing train and can be used to estimate peak-to-peak tie velocity and displacements. This means the difference between the minimum and maximum tie displacements from the double integration procedure should be comparable to the difference between the minimum and maximum tie displacement from the high-speed video camera.

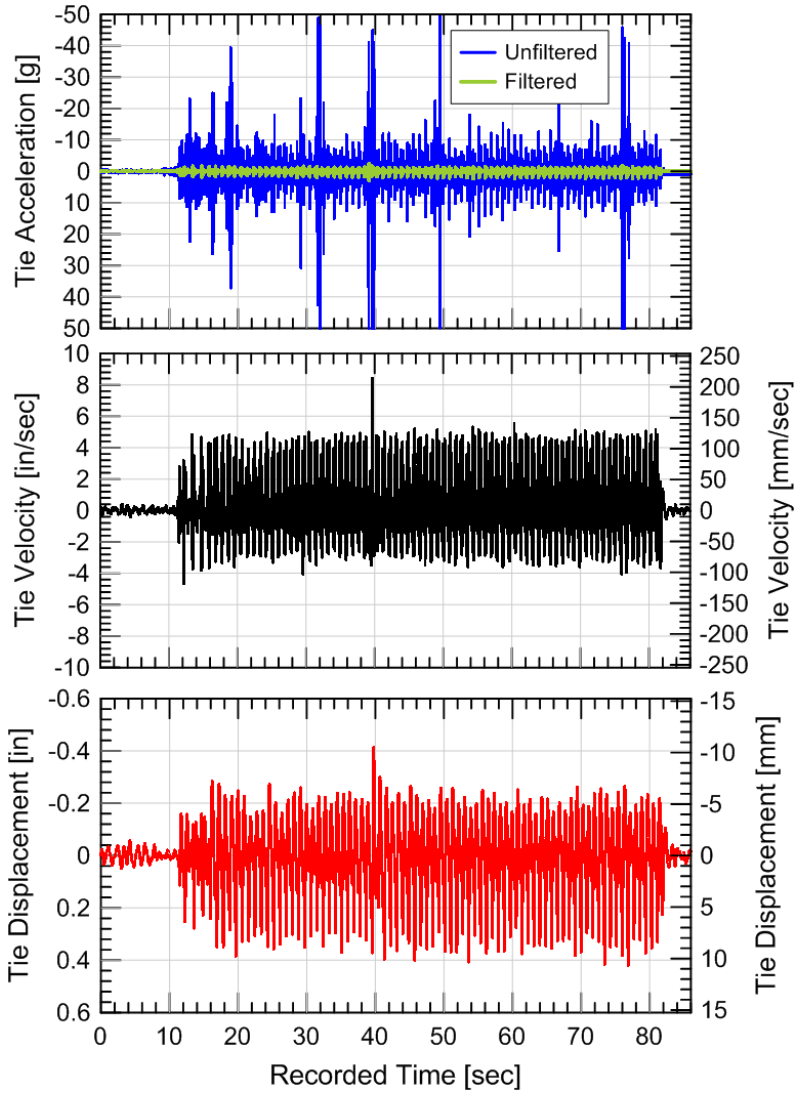

Figure 4.16: Comparison of unfiltered and filtered tie acceleration (top), integrated velocity (middle), and double-integrated displacement (bottom) time histories.

Tie displacement time histories from a high-speed video camera and double-integrated accelerometer time histories are compared using the procedures explained above. Figure 4.17 compares the high-speed video camera and double-integrated displacement time histories for a loaded coal train moving at a velocity of 39 mph. Figures 4.17(a) and (b) compare the full time histories while Figures 4.17(c) and (d) display only ten seconds of this time history to facilitate comparison of the displacement signatures. The peak-to-peak tie displacement values of the high-speed video camera (12.75 to 14 mm or 0.5 to 0.55 inches) and accelerometers (12.75 to 15.25 mm or 0.5 to 0.6 inches) are comparable. A key difference in the time histories is the high-

speed video camera data (Figures 4.17a and c) show the tie moving downward (downward displacement is positive) from the origin while the double-integrated time history is more "symmetric" about the origin. The lack of "symmetry" in the video camera data is caused by the existence of low-frequency movements (<0.05 Hz) that are filtered out in the accelerometer signal (Figures 4.15 and 4.16). The 10-second data in Figures 4.17(c) and (d) shows the exact signature is not matched well but this is expected when comparing filtered and double-integrated data from piezo-electric accelerometers.

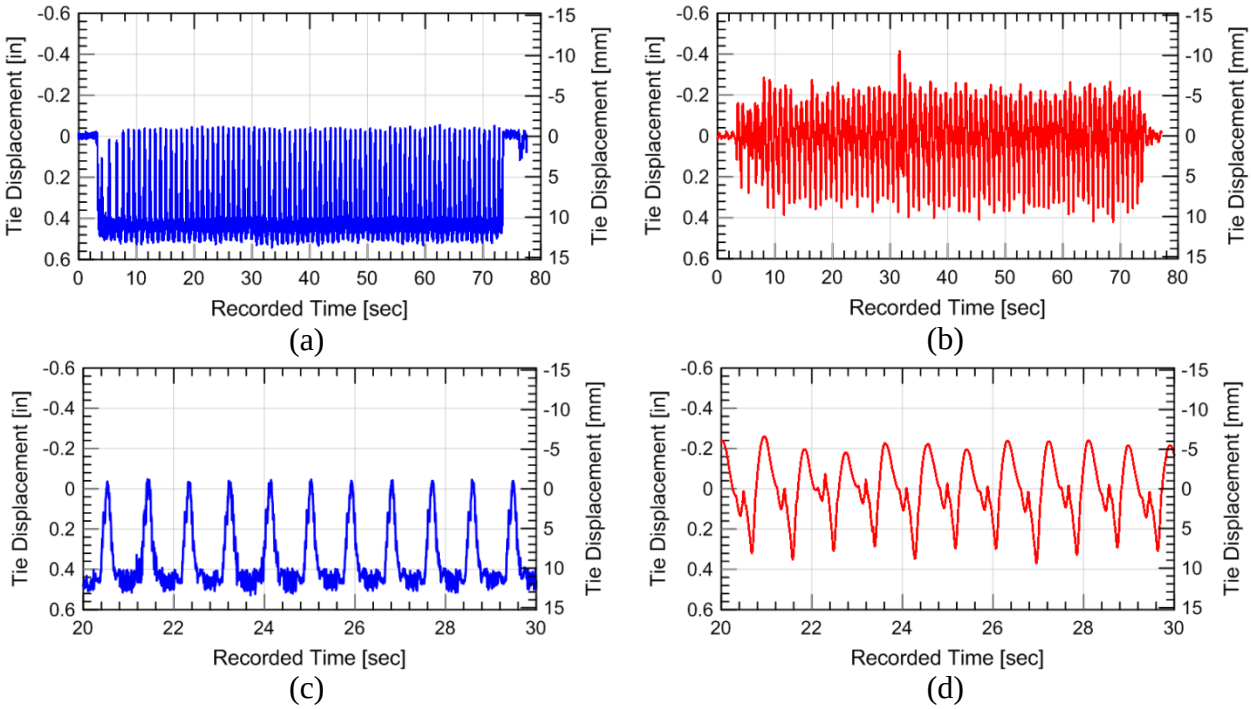

Figure 4.17: Corrected tie displacement time histories of passing coal train with a velocity of 39 mph: (a) entire train with high-speed video camera, (b) entire train with double-integrated accelerometer, (c) 10-seconds of high-speed video cameras, and (d) 10-seconds of double-integrated accelerometer.

4.3 Site and Instrument Location

This section introduces the eight instrumented sites, the reasons for their selection, and strategies implemented for exact instrument location.

The selected sites typically represent the extreme differences of track behavior including both well-performing transitions and transitions that require regular track geometry maintenance.

This bounds the problem and allow for data to be obtained for a wide range of conditions. Future instrumentation trips are expected to collect data of sites in-between the two extremes. Additionally, track time and access is a limited resource so locations are often restricted to what is available and while multiple site visits are desirable, are often not possible for a variety of reasons.

Table 4.2 lists all eight primary sites with the factors: (1) reoccurring geometry problems (Yes/No), bridge deck (Open/Ballasted), Wing Walls (Length or N/A), underlayment or other design measure (HMA/Geowebl/UTPs/N/A), and ballast conditions (Clean/Fouled/Unknown).

Table 4.2: List of sites tested in Task II

Site	Geometry Problems	Bridge Deck	Wing Walls [ft]	Underlayment	Ballast Condition
#1	No	Ballasted	27	HMA	Clean
#2	No	Ballasted	24	HMA	Clean
#3	No	Ballasted	17 (1 side)	HMA	Clean
#4	Yes	Open	6	N/A	Unknown
#5	Yes	Open	N/A	N/A	Fouled
#6	Yes	Open	N/A	N/A	Fouled
#7	Unknown	Open	N/A	UTP	Clean
#8a	Unknown	Ballasted	9	Geoweb	Clean
#8b	Unknown	Ballasted	7	HMA	Clean
#8c	Unknown	Ballasted	N/A	Geoweb	Clean
#8d	Unknown	Ballasted	7	Soil Grout	Clean

The site locations and railroad companies that own the track are not listed to keep sites anonymous unless publishing permission was obtained. Additionally, Site #8 has multiple bridges and is included as a single site to compare the various remedial techniques. Descriptions of what is expected to be learned for each of the eight instrumented sites are listed below:

- The objectives of instrumenting Site #1 are to: (1a) measure the behavior along the track for a well-performing transition zone, (1b) compare the response from unloaded and loaded trains, and (1c) investigate the tie acceleration response from wheel flats.
- The objectives of instrumenting Site #2 are to: (2a) compare the behavior along the track for well-performing transition zones, (2b) compare the behavior between Site #1 and Site #2, (2c) compare the response of opposite ends of a single tie, and (2d) investigate the influence of welded rail joints.
- The objectives of instrumenting Site #3 are to: (3a) compare the behavior of opposite ends of the same bridge with different transition designs and subgrade, (3b) compare the

response of opposite ends of a single tie, and (3c) investigate the influence of unsupported ties on tie acceleration and vibration.

- The objectives of instrumenting Site #4 are to: (4a) compare the behavior along the track for a transition zone requiring regular maintenance, (4b) compare the behavior of entrance and exit runs, and (4c) investigate the influence of train velocity on tie acceleration.
- The objectives of instrumenting Site #5 are to: (5a) investigate the influence of tie-ballast impacts on tie acceleration, (5b) compare the behavior along the track for a transition zone requiring regular maintenance, (5c) compare the tie accelerations with time and tie-ballast gap height.
- The objectives of instrumenting Site #6 are to: (6a) gain a general overview of the tie acceleration environment of a site requiring regular maintenance, (6b) investigate the effect of tamping, (6c) investigate the change in displacement within the approach, and (6d) investigate the change tie accelerations at an exit transition.
- The objectives of instrumenting Site #7 are to: (7a) compare various displacement measurements, (7b) investigate the displacement and acceleration behavior along the track, and (7c) investigate the contributions of under-tie pads on approach behavior.
- The objectives of instrumenting Site #8 are to: (8a) compare the displacement behavior along the track at four transition zone locations, (8b) compare the displacement behavior at a transition zone remediated with HMA with time, and (8c) compare the acceleration behavior along the track for a transition zone remediated with Geoweb and HMA.

The selected instrumentation location for each site is dependent on the purpose of the instrumentation for each site. For well-performing sites that have little difference in transient track displacement along the track, it is desirable to compare bridge, transition, and open track behavior. The exact instrumentation location is not expected to have much influence as the response should be homogeneous along the track.

For track with poor support, a single train is usually allowed to pass before selecting instrumentation locations in order to observed track behavior. That way, locations of high transient displacements or potential impacts can be identified and instrumented. Usually one or two locations of interest are targeted along with well-supported locations for comparison.

4.4 Site Analysis

This section presents the analysis of the eight instrumented sites.

4.4.1 Site #1

The first instrumented site provides a near-ideal example of the performance of a well-designed transition zone. The objectives of the site analysis are to: (1a) measure the behavior along the track for a well-performing transition zone, (1b) compare the response from unloaded and loaded trains, and (1c) investigate the tie acceleration response from wheel flats.

Site #1 consists of a bridge transition zone that accommodates freight traffic with train velocities of about 25 mph, an annual traffic of about 7 MGT, and was constructed with transition designs that have resulted in minimal track geometry maintenance since being placed in service in 2009 (~6 years of service from instrumentation date). The track superstructure consists of 140-RE rail, timber ties at 19.5-in spacings, and cut spike fastening system. The substructure consists of a 12-in granite ballast layer, a 6-in HMA underlayment, and a 75-ft compacted fill embankment. The track is considered Class III for operations (maximum train velocity of 40 mph) but the operating speed is only about 25 mph because the train is near its destination.

The transition designs include the major features:

(1) ballasted bridge deck reduces the load-displacement differences between the approach and bridge deck by increasing track displacement and settlement on the bridge,
(2) a 6-in HMA layer that extends for 2,000-ft that creates a higher ballast modulus, spreads the train loads over the approach fill, confines the ballast laterally, and provides an infiltration barrier between the ballast and subgrade to reduce softening of the approach fill, all of which reduce settlement in the approach (Rose and Lees, 2008; Anderson and Rose, 2008),
(3) 27-ft long perpendicular concrete wing walls provide confinement to the ballast and subgrade which reduces vertical and lateral ballast settlements in the approach,
(4) wetting and hydrocompression of the 75-ft approach fill for five years prior to track construction reduces future approach fill (subgrade) settlement due to train and environmental loadings, and
(5) drains installed at regular intervals along the concrete abutment and wing walls reduce moisture build up in the approach.

On 12 June 2014, seven accelerometers were installed at various regions of the track to monitor the transition response (see Figure 4.18c). All accelerometers were located on the east-

end of the tie and multiple ties were selected on the bridge, transition zone, and open track to compare the response along the track. The sampling rate of the accelerometers was set to 4,000 Hz and the response was put through a 3rd-order bandpass filter with cutoffs at 0.75 and 500 Hz.

Two trains were recorded and include an unloaded coal train moving at a velocity of 25 mph onto the bridge (north) and a loaded coal train moving at a velocity of 25 mph off of the bridge (south). The trains are labeled Train #1-1 and Train #1-2 respectably and the wheel loads are anticipated to range from 5 to 15 kips (22 to 67 kN) for Train #1-1 and 35 to 40 kips (156 to 178 kips) for Train #1-2 (Van Dyk et al., 2016). Due to the good track support, the train direction is not anticipated to influence the response and many loud wheel flats were audible during the passage of Train #1-2. Wheel flats are wheel irregularities that produce a wheel-rail impact during every wheel rotation and can be detected from loud, periodic clanking from the wheel flat impacting the rail. Van Dyk et al. (2016) shows wheel flats can produce loads up to five times the static value.

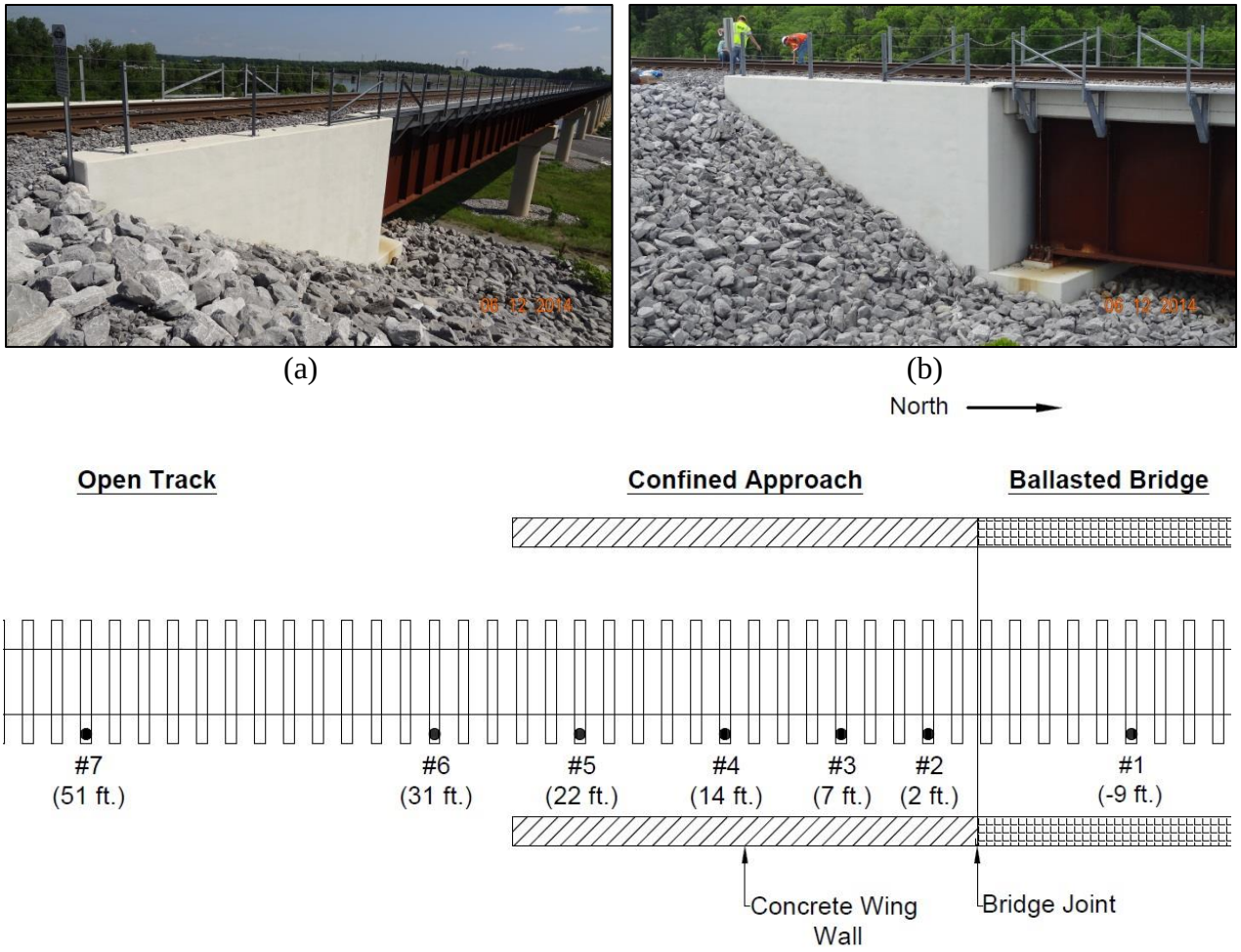

Figure 4.18: (a,b) Photographs of transition zone and (c) instrumentation layout for Site #1.

Figure 4.19 shows the recorded tie acceleration time histories for Accel #3 (7 ft.) and Accel #7 (51 ft.) from Train #1-2. Figure 4.19(a) and (b) show the full time history and many peaks exceeding 50g are observed. Upon inspection, these peaks are attributed to wheel flats as they are not repetitive and these peaks were observed during recording immediately after wheel flats were audibly heard passing the accelerometers. These peaks regularly exceed 50g and approach 200g in a single instance. The exact effect and load from these wheel flats on the track structure are not known but are attributed to increased track superstructure component degradation.

To focus on the track structure, the 10 second timeframe from 80 to 90 seconds is emphasized because no wheel flats were present during this stretch of the train. Each discrete

response is associated with the trailing train truck of a car and the following leading train truck of the subsequent car. This means each discrete response corresponds to four wheels. The results show average peak tie accelerations of about 2 to 3g at both locations with Accel #7 (51 ft.) displaying a small impact of about 6g during the passing of every second train truck. The cause of the acceleration peak is not known but is possibly some rotation or small impact within the tie plate-crosstie interface and is not considered detrimental to the track.

The average peak tie accelerations for Trains #1-1 and #1-2 are displayed in Figure 4.20 and show: (1a) little discernable difference between the bridge, transition zone, and open track and (1b) only a small increase in tie acceleration from an increase in wheel load. The similar tie acceleration response suggests there is minimal differential displacement along the track, likely due to the influence of the transition design features. The small increase in tie acceleration from higher wheel loads suggests that the track is well-supported and smoothly transfers the wheel load from the rail to the ballast with minimal relative movement between track components. For poorly-supported track, wheel load is expected to play a significantly greater influence.

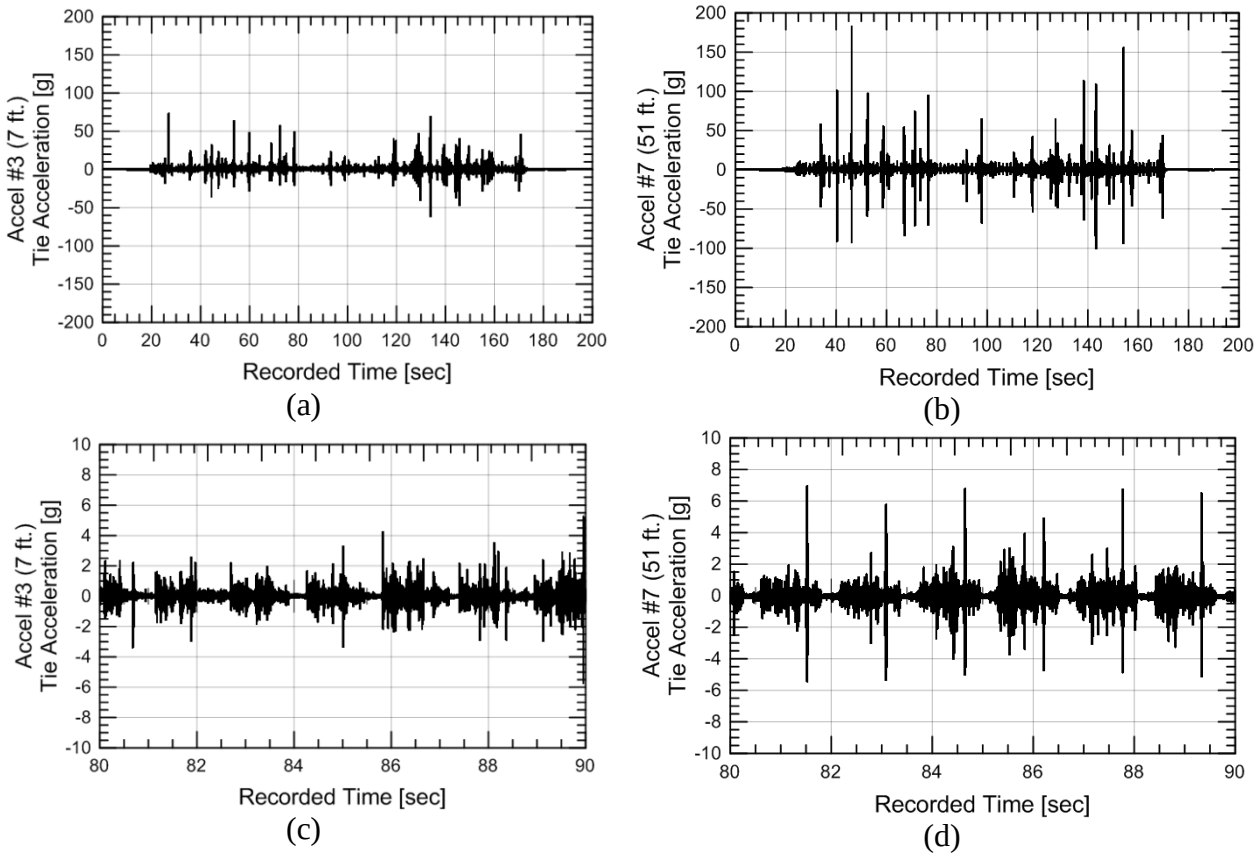

Figure 4.19: **Tie acceleration time histories from Train #1-2 showing the full time histories of (a) Accel #3 (7 ft.) and (b) Accel #7 (51 ft.) and 10 seconds of train passage with no wheel flats of (c) Accel #3 (7 ft.) and (d) Accel #7 (51 ft.).**

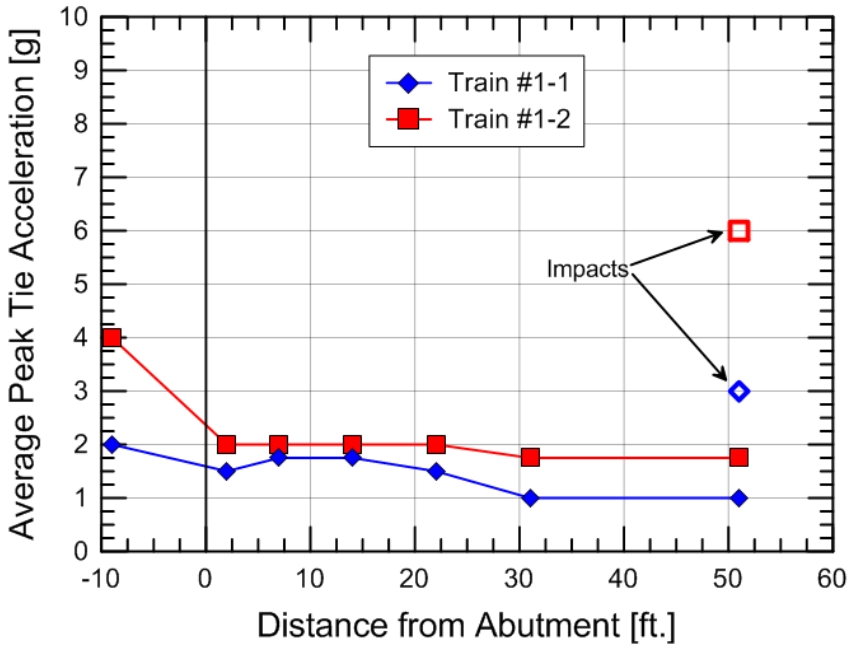

Figure 4.20: Average peak tie acceleration values along the track for Train #1-1 and Train #1-2.

A summary of results from Site #1 are the following:

- The five transition design techniques of (1) ballasted-deck bridges, (2) 27-ft long concrete wing walls, (3) 6-in thick HMA underlayment, and (4) pre-compressed fill and (5) approach drainage appear to limit differential movement along the track.
- Tie accelerations from round wheels were less than 10g at all track locations and little variation was observed between unloaded and loaded trains.
- Wheel flats or out-of-round wheels produce tie accelerations exceeding 50g and approached 200g.

4.4.2 Site #2

The second instrumented site provides a second example of a well-designed transition zone. The objectives of the site analysis are to: (2a) compare the behavior along the track for well-performing transition zones, (2b) compare the behavior between Site #1 and Site #2, (2c) compare the response of opposite ends of a single tie, and (2d) investigate the influence of welded rail joints.

Site #2 consists of a west bridge end transition zone that accommodates freight traffic with train velocities of about 25 mph, an annual traffic of about 70 MGT, and was constructed with transition designs that have resulted in minimal track geometry maintenance since being

placed in service in 1998 (~17 years of service from instrumentation date). The track superstructure consists of 136-RE rail, concrete ties at 24-in spacings, and spring clip fasteners. The substructure consists of a 12-in granite ballast layer, a 6-in HMA underlayment, and a well-compacted subgrade previously described as a red clayey material. The bridge is 1470-ft long and was originally constructed in 1851 but has since been renovated multiple times.

The transition designs include three major features (see Figure 4.21) that were present in Site #1:

(1) ballasted concrete bridge deck,
(2) a 6-in HMA layer that extends for 500-ft, and
(3) 24-ft. long concrete wing walls that are parallel to the track.

The main differences between Site #1 and Site #2 are the following: (1) Site #2 has concrete ties with spring clip fastening system instead of timber ties with cut spike fastening systems, (2) Site #2 experiences about 10x the annual tonnage of Site #1 and has been in service for 11 years longer, (3) the concrete wing wall at Site #2 confines the subballast and subgrade but not the ballast unlike Site #1 in which the concrete wing walls confines the entire approach substructure. This allows the comparison of various tie and fastening system types and better insight into transition performance that has experienced greater amounts of tonnage.

On 28 July 2014, eight accelerometers were installed at various regions of the track to monitor the transition response. The first six accelerometers were placed on opposite ends of the three ties, the seventh was placed near a rail joint, and the eighth in the open track. Besides comparing the response of Site #2 with Site #1, differential response at the same tie and the effect of rail joints were also investigated. The sampling rate of the accelerometers was set to 4,000 Hz and the response was put through a 3rd-order bandpass filter with cutoffs at 0.75 and 500 Hz.

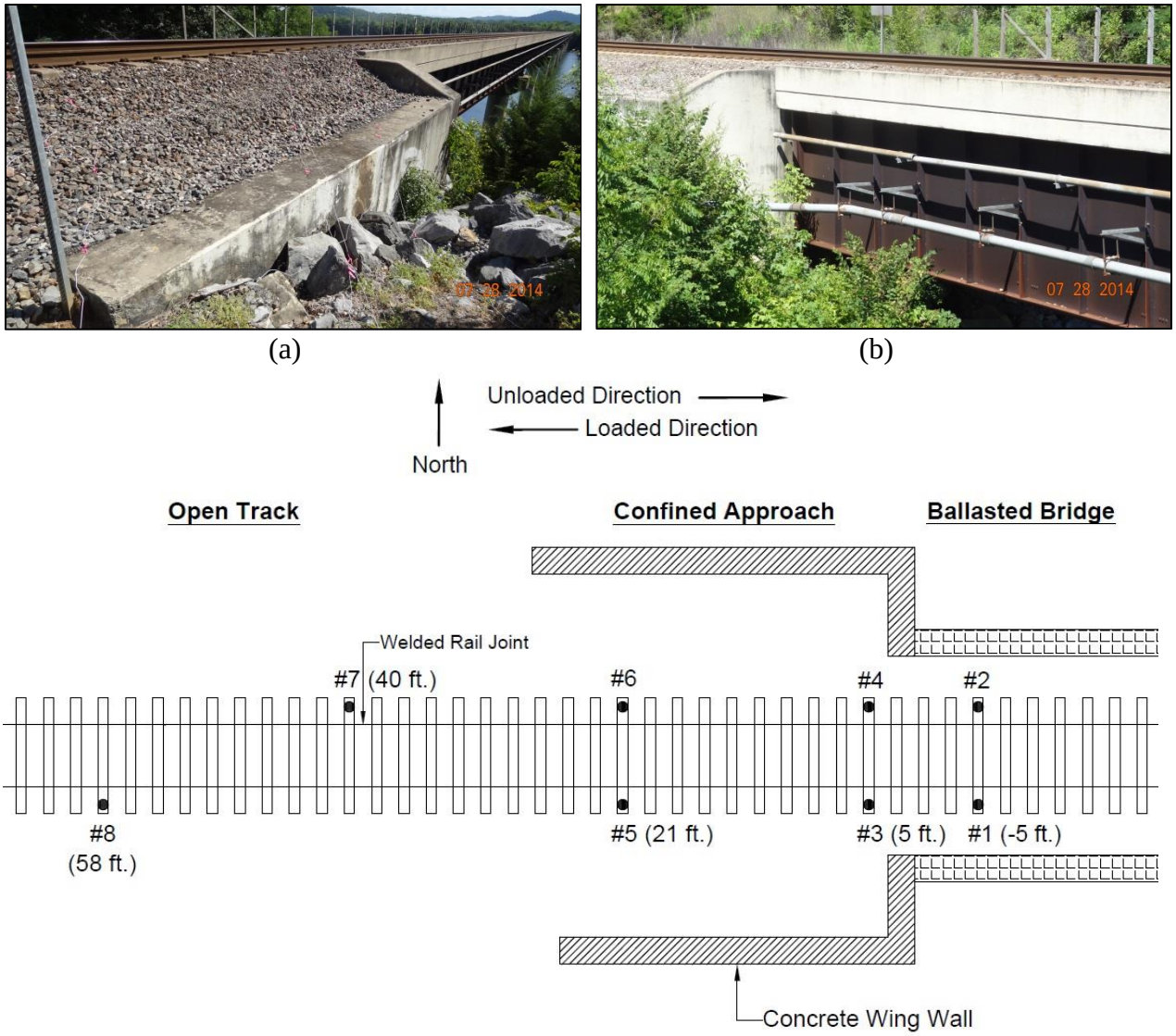

Figure 4.21: **(a,b) Photographs of transition zone and (c) instrumentation layout for Site #2.**

Five trains were recorded and include a variety of trains types and directions and are labeled as Trains #2-1 through 2-5, as shown in Table 4.3. Typically, the trains entering the bridge were unloaded or mixed while the trains exiting the bridge were loaded. Unfortunately, the loaded trains exiting the bridge were braking during the majority of recording, which added vibrations that are difficult to discern from the loading acceleration. Filtering at 500 Hz was able to remove the majority of high-frequency braking vibrations (200 to 2000+ Hz) but not all.

Table 4.3: List of trains recorded at Site #2

Train	Time (EST)	Direction	Train Type	Train Velocity [mph]
2-1	9:50 AM	NB, Entrance	Mixed	~25
2-2	10:33 AM	SB, Exit	Autorack – Loaded	25
2-3	10:52 AM	NB, Entrance	Unloaded Coal	25
2-4	12:52 PM	NB, Entrance	Single/Double Stack, Empty	20
2-5	2:09 PM	SB, Exit	Loaded Coal	25

The average peak tie accelerations for Trains #2-1 through #2-5 are presented in Figure 4.22. Ties with two accelerometers have both data points at the same distance and a dotted line is used to signify the tie accelerations at the welded rail joints because the results are exceptions and not representative of the track. The results show: (2a,b) the majority of average peak tie accelerations at all track locations are below 10g, similar to Site #1, (2c) the north and south ends of the measured ties experienced similar response, and (2d) the average peak tie accelerations at the welded rail joint (Accel #7, 40 ft.) are about three times greater than the surrounding track.

The homogenous tie accelerations along the track, along single ties, and similarities with Site #1 are unsurprising for well-supported track because the loads and displacements are expected to be similar. This is likely attributed to the smooth load distribution throughout the track, which minimizes any differential behavior and potential tie material influence. The average peak tie accelerations from the loaded coal train (Train #2-5) is greater than the remaining trains and appears to be from the influence of high-frequency vibrations (>300 Hz). The influence of this is unknown at the time. The greater tie accelerations at the rail joint are unsurprising because of the rapid change in rail stiffness but the lack of track component damage around the joint suggests the three times increase in tie acceleration (10 to 30g) does not necessarily correlate with three times greater load.

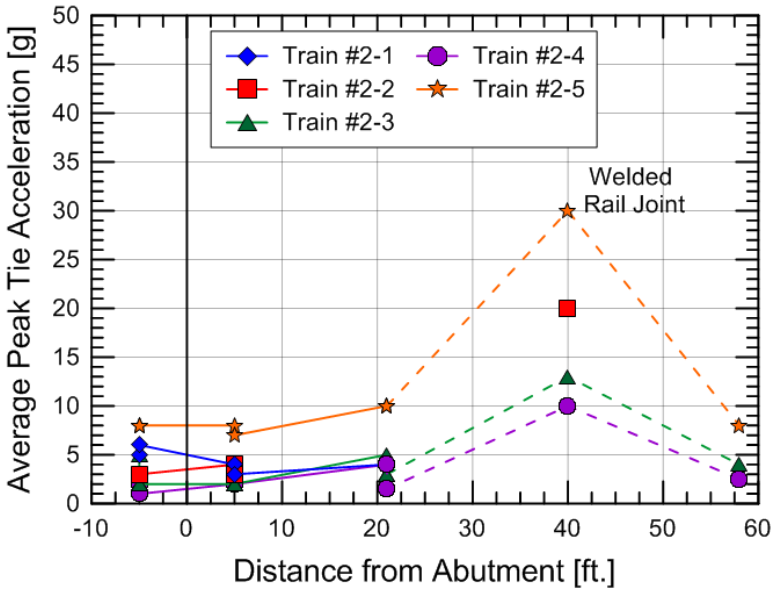

Figure 4.22: Average peak tie acceleration values along the track for Site #2.

A summary of results from Site #2 are the following:

- The three transition design techniques of (1) ballasted-deck bridges, (2) 24-ft long concrete wing walls, (3) 6-in thick HMA underlayment appear to limit differential movement along the track.
- Tie accelerations were less than 10g for all locations along the track and along a single tie, suggesting homogenous displacement and load distribution.
- No conclusive difference between concrete (Site #2) and timber (Site #1) ties could be observed for well-performing track.
- An instrumented rail joint experienced about three times greater tie acceleration than the surrounding track. However, the lack of track component damage suggests the loading is not three times greater.

4.4.3 Site #3

The third instrumented site provides a third example of a well-designed transition zone. The objectives of the site analysis are to: (3a) compare the behavior of opposite ends of the same bridge with different transition designs and subgrade, (3b) compare the response of opposite ends of a single tie, and (3c) investigate the influence of unsupported ties on tie acceleration and vibration.

The transition is the opposite (east) end of the bridge at Site #2, includes three design techniques, and has also required minimal track maintenance since being put into service. The

primary difference between Site #2 and Site #3 is Site #3 only has a single shorter 17-ft wing wall on the south end and just an embankment consisting of natural soil previously described as loamy silty material on the north end.

On 28 July 2014, six accelerometers were installed on opposite ends of three ties on the bridge, approach, and open track. Photographs of the site and the track layout is presented in Figure 4.23. During train passage, it was clear from visual observation that Tie #3&4 (5 ft) and adjacent ties were unsupported and experienced greater tie displacement than ties in the open track. It is unclear whether the substructure settlement that produced the hanging ties occurred in the ballast or subgrade. Unfortunately, the train was moving too slow for double integration techniques to be used to estimate tie displacements. The sampling rate of the accelerometers was set to 4,000 Hz and the response was put through a 3rd-order bandpass filter with cutoffs at 0.75 and 500 Hz.

Three trains were recorded and include a variety of trains types and directions and are labeled as Trains #3-1 through 3-3, as shown in Table 4.4. Opposite to Site #2, the trains entering the bridge were loaded while the trains exiting the bridge were unloaded or mixed. The entrance trains applied breaking for much of the recording, making the collected acceleration records unusable. Therefore, only Train #3-2 is analyzed.

Table 4.4: List of trains recorded at Site #2

Train	Time (EST)	Direction	Train Type	Train Velocity [mph]
3-1	3:12 PM	SB, Entrance	Loaded Auto Rack	13
3-2	3:40 PM	NB, Exit	Mixed	~20
3-3	4:04 PM	SB, Entrance	Double Stack	20 to 0

(a) (b)

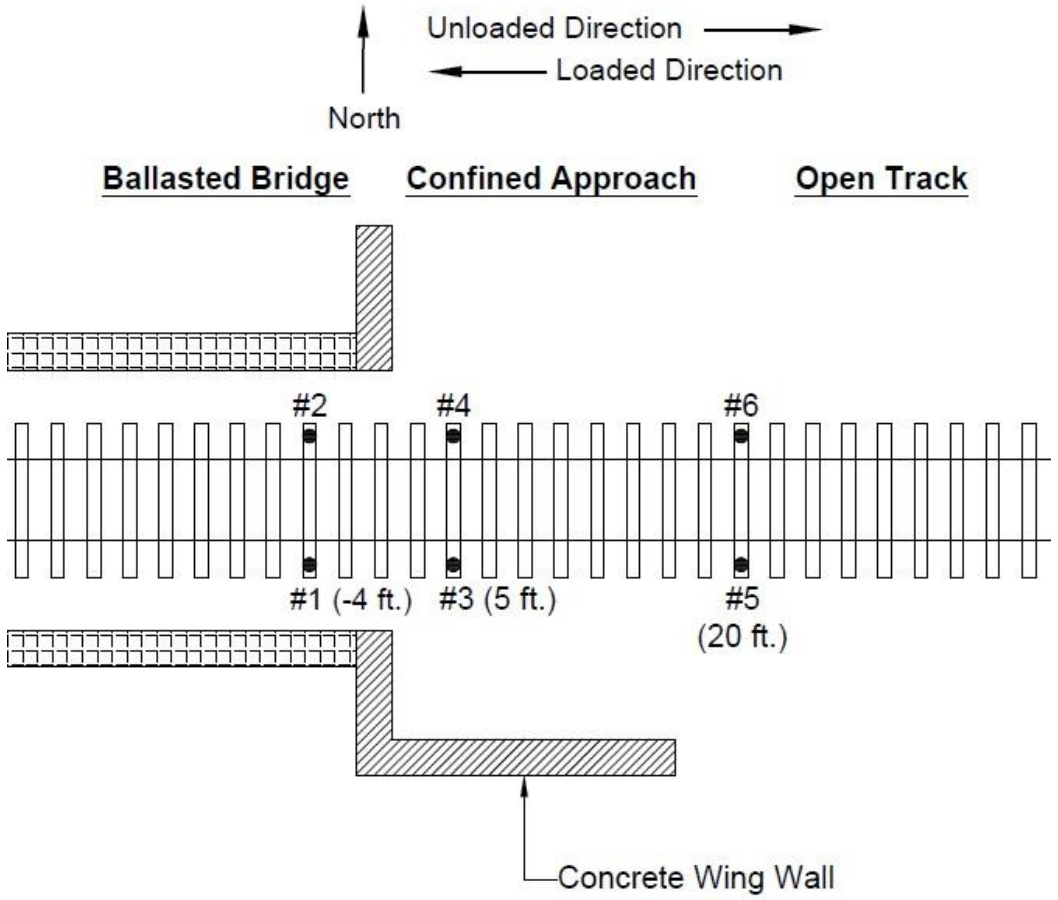

(c)

Figure 4.23: (a,b) Photographs of transition zone and (c) instrumentation layout for Site #3.

The average peak tie accelerations for Train #3-2 is presented in Figure 4.24(a). The results show: (3a) possible greater tie accelerations in the approach and open track, (3b) unclear differences between Site #2 and Site #3, and (3c) greater tie accelerations on the north tie ends than south.

With only three ties recorded, it is difficult to conclude if there are any differences in acceleration magnitude response along the track. However, it does appear the north tie end experiences greater accelerations than the south end. This may be due to reduced confinement or lateral substructure movement from the lack of wing wall on the north end. Instrumenting additional ties would have made this clearer.

Additionally, the frequency response from Tie #3 (5 ft.) and Tie #5 (20 ft.) are compared in Figure 4.24(b). The supported tie (Tie #5, 20 ft.) shows only a single dominant vibration frequency of about 110 Hz, which is the first vibration mode of a concrete tie (Harrison et al., 1984; Remennikov and Kaewunruen, 2006; Taherinezhad et al., 2013). The poorly supported tie (Tie #3, 5 ft.) shows four dominant frequencies of vibration at 110 Hz, 300 Hz, 585 Hz, and 900 Hz, which are the first four vibration modes of concrete ties. The additional vibration modes in the poorly supported tie are explained by the lack of damping and confinement from the ballast which allows the concrete tie to freely "ring" during every wheel loading. This also shows how accelerometers can be used to identify poorly supported concrete ties.

Possible explanations for the unsupported tie include the following: increased ballast settlement from reduced north end confinement, lateral substructure movement towards the unconfined north embankment, local or homogenous substructure settlement from poorly compacted materials. The influence of the subgrade is possible but not expected because the line has been in service for over 150 years and is likely fully compressed.

Either way, this indicates that small groups of unsupported ties can exist without leading to accelerated substructure settlements and repetitive track geometry maintenance. Numerical analysis results in Chapter 5.7 suggest tie loads can still be evenly distributed with the existence of unsupported ties if the substructure materials are homogenous and lack ballast degradation.

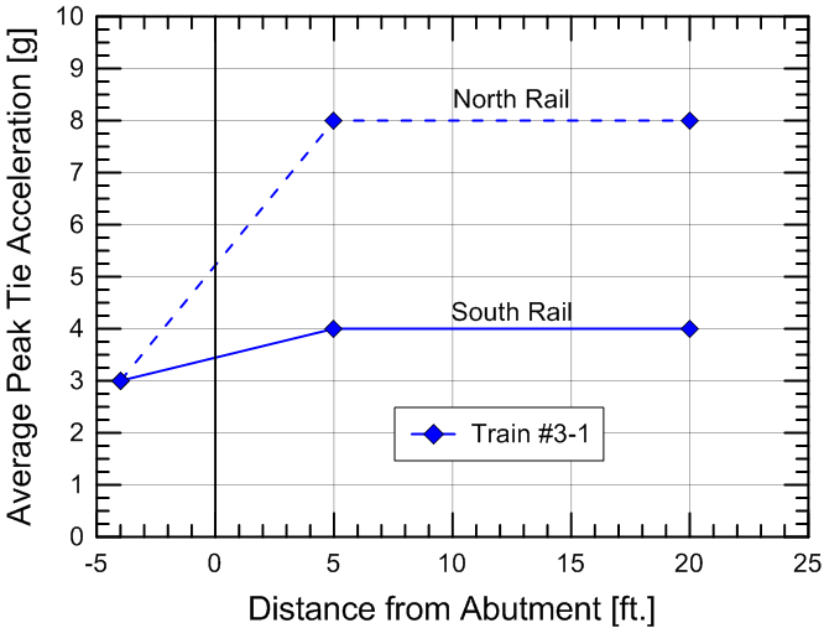

(a)

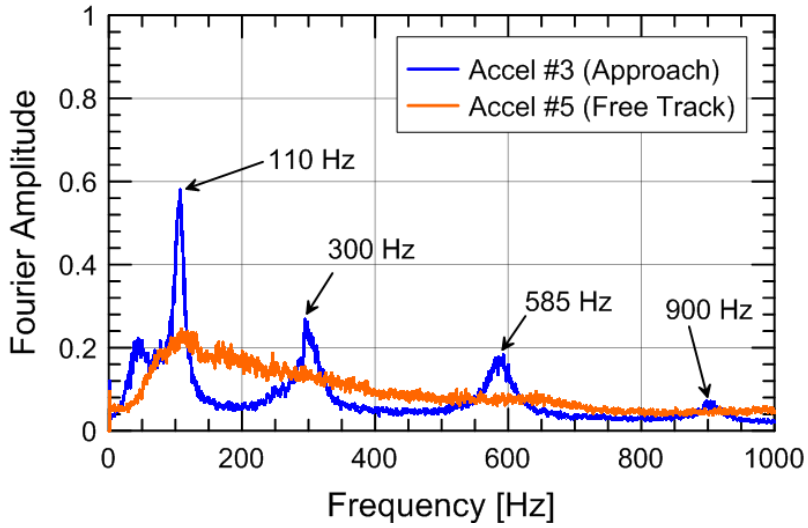

(b)

Figure 4.24: **(a) Average peak tie acceleration values along the track for Site #3 and (b) frequency response of unsupported and supported ties.**

A summary of results from Site #3 are the following:

- The three transition design techniques of (1) ballasted-deck bridges, (2) a single 17-ft long concrete wing wall, (3) 6-in thick HMA underlayment appear to limit differential movement along the track enough to prevent maintenance but not the formation of a small group of unsupported ties in the approach.
- Small groups of unsupported ties can exist without leading to track maintenance.

- Reduced confinement on the north end possibly led to higher tie accelerations on the north tie end.

4.4.4 Site #4

The fourth instrumented site provides an example of a transition zone with poorly supported ties. The objectives of the site analysis are to: (4a) compare the behavior along the track for a transition zone requiring regular maintenance, (4b) compare the behavior of entrance and exit runs, and (4c) investigate the influence of train velocity on tie acceleration.

Site #4 consists of a bridge transition zone on spur track that accommodates freight traffic with train velocities of about 10 mph and was constructed with the only transition design being 6-ft concrete wing walls. The site experienced reoccurring track geometry problems and the primary mitigation attempt being the installation of seven 10-ft ties in the approach. This technique is discussed in Chapter 2.4.4 and attempts to decrease tie-ballast pressure by increasing the tie-ballast contact area. However, this did not mitigate the reoccurring track geometry problems.

The track superstructure consists of welded rail joints, timber ties at about 21-in spacings, and cut spike fasteners. The substructure is unknown but the surface contained seemingly intact and clean granite ballast. Fouled ballast was observed in nearby track so it is possible that fouled ballast exists below the surface and the subgrade is unknown. The bridge is a short-span open deck timber bridge. The track is considered Class I (maximum train velocity of 10 mph).

On 29 July 2014, eight accelerometers were installed at various regions of the track to monitor the transition response. The first four accelerometers were placed on opposite ends of the first two approach ties with the remaining ties installed at different approach and open track locations. Accelerometer #8 was placed near a welded rail joint. The sampling rate of the accelerometers was set to 4,000 Hz and the response was put through a 3rd-order bandpass filter with cutoffs at 0.75 and 500 Hz.

To measure the track response, a single locomotive passed over the transition five times at various speeds ranging from 2 mph to 10 mph. The trains number, direction, and velocity are shown in Table 4.5. The various directions and speeds allowed train analysis with direction and speed. Photographs of the transition zone, the locomotive, and the instrumentation layout are presented in Figure 4.25.

Table 4.5: List of trains recorded at Site #4

Train	Direction	Train Velocity [mph]
4-1	Entrance	2
4-2	Exit	6
4-3	Entrance	10
4-4	Exit	10
4-5	Entrance	10
4-6	Exit	10
4-7	Entrance	6
4-8	Exit	6
4-9	Entrance	10
4-10	Exit	10

(a) (b)

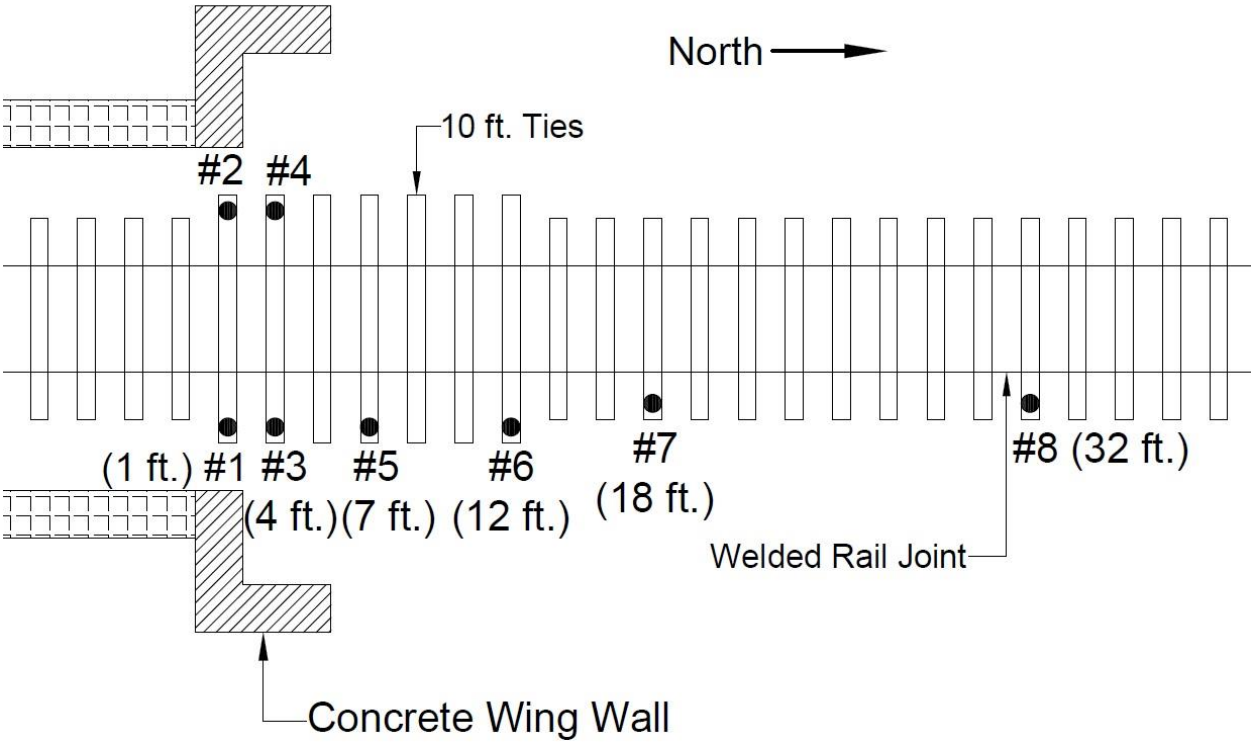

(c)

Figure 4.25: (a,b) Photographs of transition zone and (c) instrumentation layout for Site #4.

The visually observable tie displacement response during locomotive passage was similar along the track and estimated to be about 6 to 12 mm (0.25 to 0.5 inches) with possibly greater displacements near the approach. This is much greater than the displacements at Site #1 and #2, which were estimated to be 1 to 2 mm (0.04 to 0.08 inches). The homogenous response along the track suggests the displacement is from low stiffness ballast or a soft subgrade. The ballast conditions on the surface are clean but this does not guarantee the ballast directly below the surface is not degraded, wet, and highly fouled.

The average peak tie accelerations for Trains #4-2 through #4-10 are presented with distance and velocity in Figures 4.26(a) and (b). A few train passes what appeared to be vehicular or superstructure impacts at Accel #5 (7 ft.) but were not included because of the inconsistency at which they appeared so it is assumed to be vehicular. Due to the variability in track response for each train and to make trends easier to observe, an average value for each tie is calculated and the average trend is plotted as a thick black line. The difference between the entrance and exit averages was not included because they essentially plot on top of each other.

The results show: (1) slightly greater tie accelerations are experienced in the approach (1.5g v. 0.5 to 1.0g), (2) little difference in response is recorded between entrance and exit response, and (3) a clear increase in peak tie acceleration is observed with increasing train velocity. A discussion of these observations and trends is presented below.

Slightly greater tie accelerations in the approach are apparent from the average response of all the trains (black line in Figure 4.26a). Due to low train speeds, it is difficult to determine the mechanism causing the increased tie accelerations. The 5- to 7-ft distance appears to be where the upward rail bend begins, i.e. beginning of bump or middle of dip, so two possibilities could be poor tie support or higher reactionary forces required to raise the wheel elevation.

An increase in tie acceleration from increased train velocity is apparent from averaging the responses. If all ties are included, the increase is about 0.1g/mph. The smallest increase is observed at Accel #1&2 (1 ft.) at about 0.05g/mph and the remaining ties average at about 0.13g/mm. No trend difference is observed between the approach and open track ties.

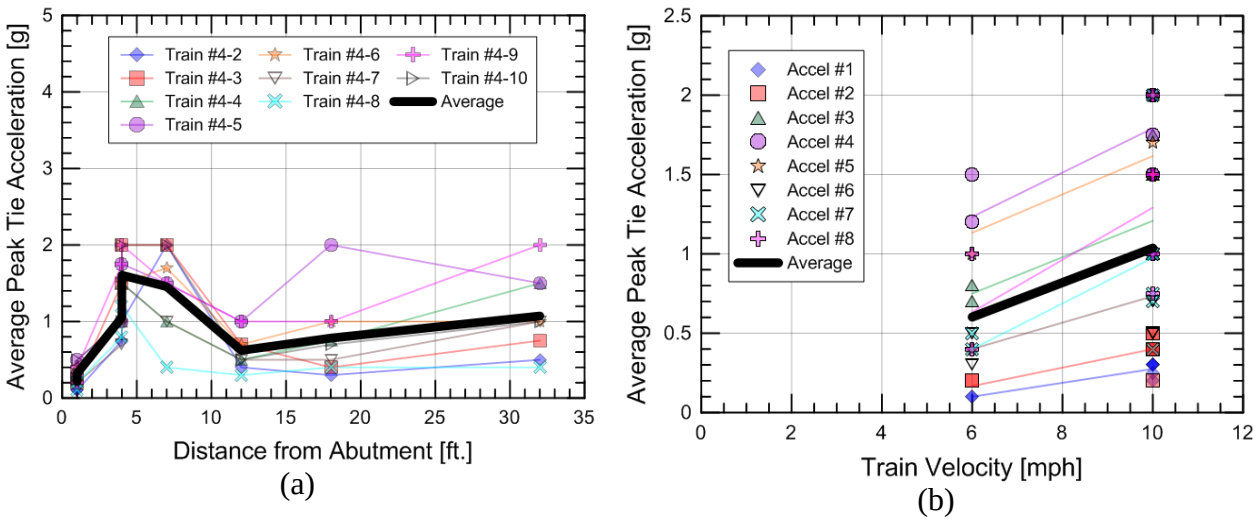

Figure 4.26: Average peak tie accelerations with (a) distance and (b) velocity at Site #4.

A summary of results from Site #4 are the following:

- Six foot concrete wing walls and ten foot timber ties did not arrest reoccurring track settlement at Site #4. The problematic location is likely from reduced-performance ballast underneath the top layer of ballast or from soft subgrade due to high transient displacements in both approach and open track.
- Higher tie accelerations were observed near the approach and with increasing train velocity.

4.4.5 Site #5

The fifth instrumented site provides a second example of a transition zone with poorly supported ties. The site analysis compares the accelerometer responses with the displacement from the LVDT installation introduced in Task I. The objectives of the site analysis are to: (5a) investigate the influence of tie-ballast impacts on tie acceleration, (5b) compare the behavior along the track for a transition zone requiring regular maintenance, (5c) compare the tie accelerations with time and tie-ballast gap height.

Site #5 consists of a bridge transition zone at Upland Street on Amtrak's high speed line near Chester, PA that was instrumented in Task I. Train velocities at the train location are 110 mph and the approach did not have any designs to mitigate against the reoccurring track geometry problems.

The track superstructure consists of welded rail joints, 136-RE rail, concrete ties at 24-in spacings, and spring clip fasteners. The substructure is detailed in Task I and fouled ballast is observed in the approach. The bridges are a short-span open deck timber bridges.

The site was instrumented at two different times. The first instrumentation occurred on 4 September 2013 and involved installing four accelerometers at locations #2, #3, #4, and #6 in Figure 4.27. The accelerometers were PCB B31, which has similar characteristics to the PCB 353B16, and was supplied by Mike Tomas from Amtrak. Two 110 mph high-speed passenger trains were recorded and are referenced as #5-1-1 and #5-1-2. The second instrumentation trip occurred on 1 July 2014 and seven accelerometers were installed; however, Accel #1&2 (7 ft.) had to be discarded due to poor data. Only a single 110 mph train record was obtained, referenced as #5-2-1, because of poor quality data from unknown reasons. The sampling rate of the accelerometers was set to 4,000 Hz and the response was put through a 3rd-order bandpass filter with cutoffs at 0.75 and 500 Hz.

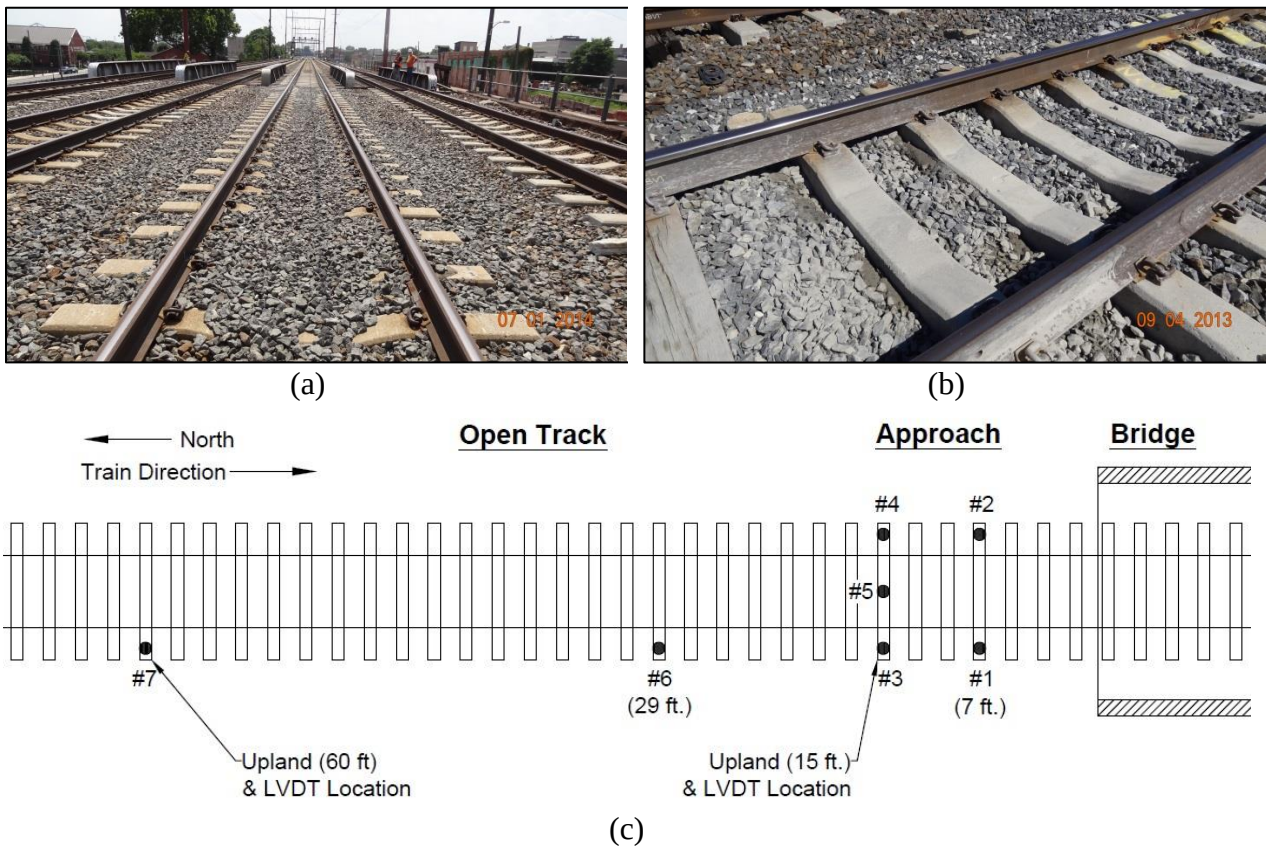

Figure 4.27 **(a,b) Photographs of transition zone and (c) instrumentation layout for Site #5.**

As mentioned previously, Site #5 involved three analyses that are discussed below:

(5a) investigate the influence of tie-ballast impacts on tie acceleration,
(5b) compare the behavior along the track for a transition zone requiring regular maintenance,
(5c) compare the tie accelerations with time and tie-ballast gap height.

The first analysis, (5a) investigate the influence of tie-ballast impacts on tie acceleration, illustrates the impact that occurs from closure of tie-ballast gaps. The data was obtained during the 1 July 2014 trip and involved Accel #3 (15 ft.) because the acceleration record can be directly compared to the LVDT #1 time history. In Figure 4.28, the last three train trucks of a high-speed passenger train are displayed. At recorded times 3.88, 4.08, and 4.30 seconds, a sharp change in tie displacement (top graph) occurs and this is attributed to the tie contacting the ballast. At these same times, peak accelerations ranging from 25 to 30g can be observed. This indicates that the peak in acceleration occurs from the rapid change of tie momentum during impact with the ballast. The exact loading cannot be determined from F=ma because of the mass is highly dependent on influence of the surrounding track but this does indicate potential increased loading and ballast degradation.

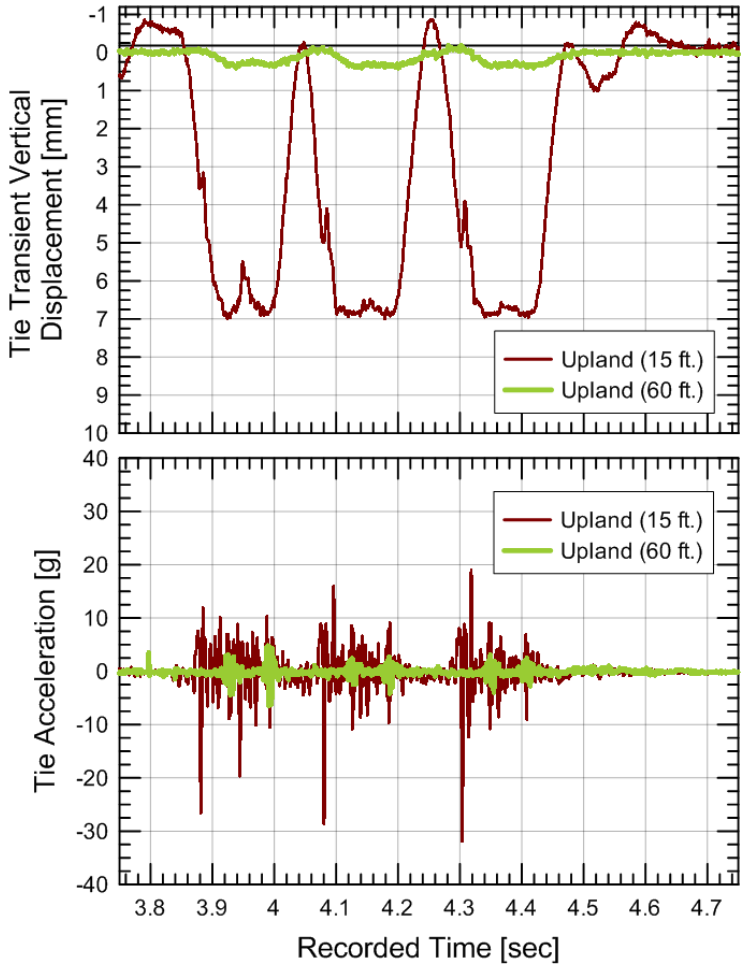

Figure 4.28: Tie displacement and acceleration response from a passing high-speed passenger train at Upland (15 ft.) and Upland (60 ft.) on 1 July 2014.

The second analysis, (5b) compare the behavior along the track for a transition zone requiring regular maintenance, determines how tie acceleration changes with distance. From Task I, it is known from LVDT measurements that the Upland (15 ft.) location experiences greater tie displacements than Upland (60 ft.). One interest of this instrumentation is to determine if this applies to tie accelerations as well. Figure 4.29(a) shows the average peak tie accelerations on the west tie end accelerometers and Figure 4.29(b) displays the average peak tie acceleration on the east tie end accelerometers. The results show about double the tie acceleration magnitudes on the east tie end than west tie end, double the tie acceleration magnitudes at 15-ft than 7-ft at both ends of the same tie, and five times greater tie acceleration magnitudes at 15-ft than the open track locations.

Visual observations of the track showed little displacement at the Accel #1&2 (7 ft.) tie and greater displacement at the Accel #3&4 (15 ft.) tie. It is unclear from the video whether the 7-ft tie is the lone supported tie or if the first four approach ties are supported. Additionally, it appears that the east tie end displaced more than the west, agreeing with the peak tie acceleration measurements.

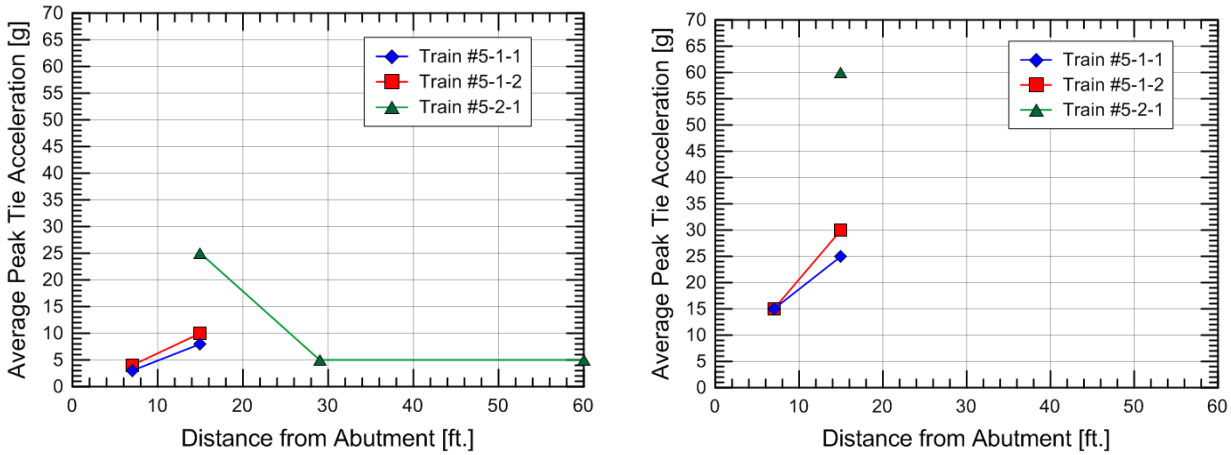

Figure 4.29: Average peak tie accelerations with distance at (a) west and (b) east tie ends at Site #5.

The third analysis, (5c) compare the tie accelerations with time and tie-ballast gap height, investigates the relationship between tie-ballast height and impact tie accelerations. The location Accel #3 (15 ft.) is used because it has two tie displacement and acceleration records. Figure 4.30 shows a correlation between the two values with an increase in peak tie acceleration from 10 to 25g from an increase in estimated tie-ballast gap from 5.08 to 6.74 mm. While a relation between the two factor likely exists, it is not clear how the relation can be characterized or what additional factors, such as the support of surrounding ties, affect the impact. For example, an impact will be more likely when a group of ties are unsupported and can move up and down together so the ability of a single tie to impact the ballast is dependent on the support conditions of the surrounding ties. More analyses would be required before coming to any definite conclusions.

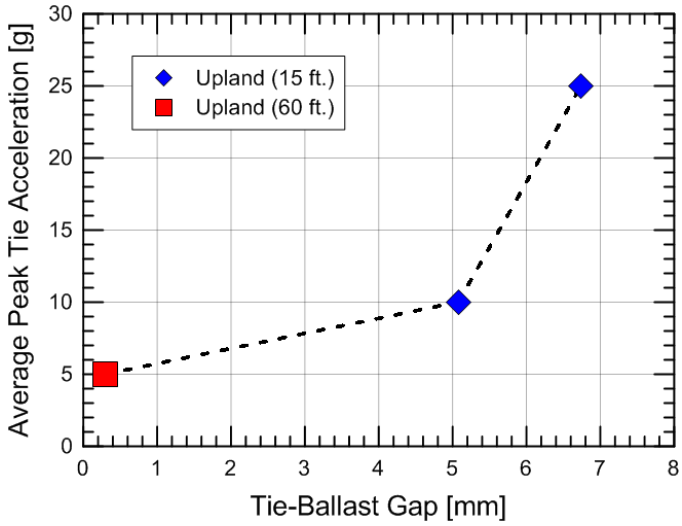

Figure 4.30: Relation between tie-ballast gap and average peak tie accelerations at Upland (15 ft.) at Site #5.

A summary of results from Site #5 are the following:

- Previous instrumentation showed accelerated settlement in the approach the existence of an unsupported tie at the 15-ft tie in the approach.
- High tie accelerations were observed at the moment when unsupported ties contact the ballast, indicating the possible existence of impact loads.
- Increased tie accelerations were correlated with increased tie displacement from measured values and visual observations.

4.4.6 Site #6

The sixth instrumented site provides a third example of a transition zone with poorly supported ties. This site is the most extensively instrumented with five site visits, sixteen accelerometer locations, and four displacement locations instrumented. This allowed multiple types of analyses to be performed. The objectives of the site analysis are to: (6a) gain a general overview of the tie acceleration environment, (6b) investigate the effect of tamping, (6c) investigate the change in displacement within the approach, and (6d) investigate the change tie accelerations at an exit transition. For (6a), the tie accelerations are compared with distance and time, the influence of train velocity is investigated, and the effect of load, train type, and train direction are investigated.

Site #6 consists of a double transition zone with a 75-ft region of track surrounded by a bridge and asphalt crossing. The track accommodates freight traffic with train velocities up to 60

mph and was constructed with minimal transition designs. The site experienced reoccurring track geometry problems and the primary mitigation attempt being the installation of ten ten-foot ties in the approach. As with Site #4, this did not mitigate the reoccurring track geometry problems.

The track superstructure consists of welded rail joints, 141-RE rail, timber ties at about 19.5-inch spacings, and cut spike fasteners. The substructure is unknown but fouling is prevalent within the entire transition zone region. The substructure material about 4 to 6 inches below the surface is primarily sand-sized particles. Mud spots were sporadically observed near the asphalt crossing and within the middle of the transition. The bridge is a short-span open deck timber bridge originally constructed in 1923. The track is considered Class 4 (maximum train velocity of 60 mph).

Figure 4.31 shows multiple photographs of the site. Figure 4.31(a) and (b) show the bridge and the double transition section. Figure 4.31(b) shows the dip that forms within the bridge approach. Figure 4.31(c) and (d) shows fouling locations at Tie #27 (42 ft.) from the bridge and at the asphalt crossing. Figure 4.31(e) shows a single layer of degraded ballast underneath the tie with highly fouled ballast underneath.

(a)

(b)

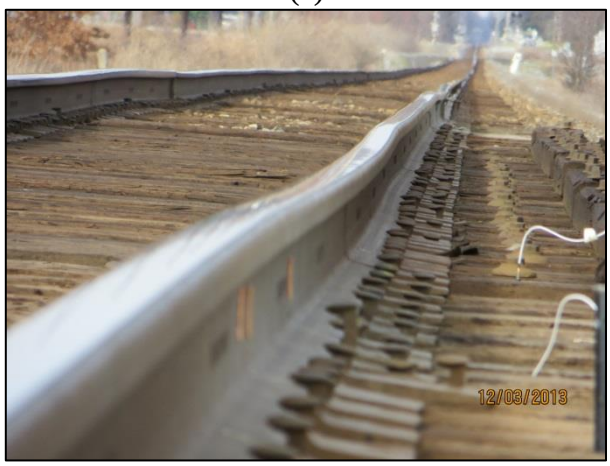

(c)

(d)

(e)

(f)

Figure 4.31: Photographs of Site #6.

Five days of testing were completed at Site #6, including: (1) 21 October 2014, (2) 22 October 2014, (3) 3 December 2014, (4) 10 June 2015, and (5) 11 November 2015. Both video cameras and accelerometers were used at the site and often placed at different locations on

different days. A list of all recorded trains is listed in Table 4.6 and Figure 4.32 displays the locations of the video cameras and accelerometers for all five tested days. The sampling rate of the accelerometers varied between 4,000 and 8,000 Hz and the response was put through a 3rd-order bandpass filter with cutoffs at 0.75 and 500 Hz. The video cameras collected data at 240 fps and the response was put through a 8th-order low-pass filter with a cutoff of 13 Hz.

Table 4.6: List of trains recorded at Site #6

Train	Day	Time (EST)	Direction	Train Type	Weight	Velocity [mph]
6-1-1	21 Oct 2014	10:55 AM	NB, Entrance	Coal	Loaded	25 to 32
6-1-2	21 Oct 2014	2:00 PM	SB, Exit	Autorack	Loaded	49
6-1-3	21 Oct 2014	4:20 PM	SB, Exit	Intermodal	Loaded	58
6-1-4	21 Oct 2014	4:42 PM	NB, Entrance	Intermodal	Mixed	58
6-1-5	21 Oct 2014	5:15 PM	NB, Entrance	Freight	Mixed	44
6-2-1	22 Oct 2014	10:18 AM	NB, Entrance	Autorack	Loaded	25
6-2-2	22 Oct 2014	10:44 AM	NB, Entrance	Mixed	Mixed	25
6-2-3	22 Oct 2014	11:39 AM	SB, Exit	Intermodal	Mixed	42
6-2-4	22 Oct 2014	12:05 PM	NB, Entrance	Mixed	Loaded	25
6-2-5	22 Oct 2014	12:23 PM	SB, Exit	Mixed	Loaded	40
6-2-6	22 Oct 2014	12:37 PM	SB, Exit	Mixed	Loaded	33
6-2-7	22 Oct 2014	2:18 PM	NB, Entrance	Intermodal	Mixed	52
6-3-1	3 Dec 2014	11:57 AM	SB, Exit	Intermodal	Loaded	36
6-3-2	3 Dec 2014	12:32 PM	SB, Exit	Freight	Mixed	36
6-3-3	3 Dec 2014	2:18 PM	NB, Entrance	Intermodal	Mixed	50 to 20
6-3-4	3 Dec 2014	2:55 PM	NB, Entrance	Intermodal	Mixed	59
6-3-5	3 Dec 2014	3:21 PM	SB, Exit	Grain	Loaded	36
6-3-6	3 Dec 2014	3:34 PM	SB, Exit	Auto Rack	Mixed	31
6-3-7	3 Dec 2014	4:00 PM	SB, Exit	Coal	Loaded	39
6-3-8	3 Dec 2014	4:13 PM	SB, Exit	Grain	Loaded	30
6-4-1	10 June 2015	12:40 PM	SB, Exit	Autorack	Mixed	47
6-4-2	10 June 2015	2:25 PM	NB, Entrance	Hopper	Unloaded	47
6-4-3	10 June 2015	2:45 PM	NB, Entrance	Mixed	Mixed	48
6-5-1	11 Nov 2015	10:46 AM	SB, Exit	Inter Modal	Mixed	45
6-5-2	11 Nov 2015	11:55 AM	SB, Exit	Freight	Mixed	40

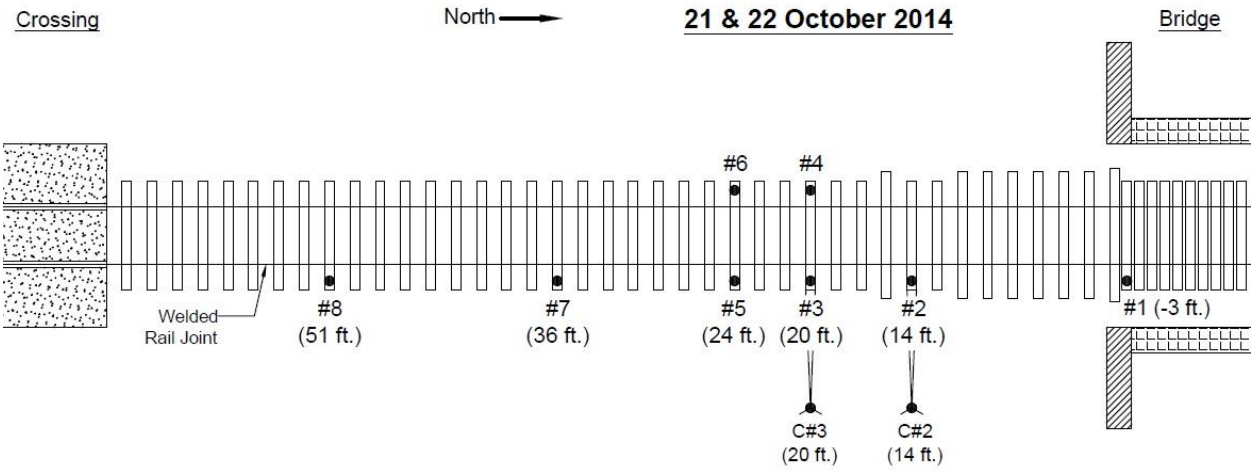

(a)

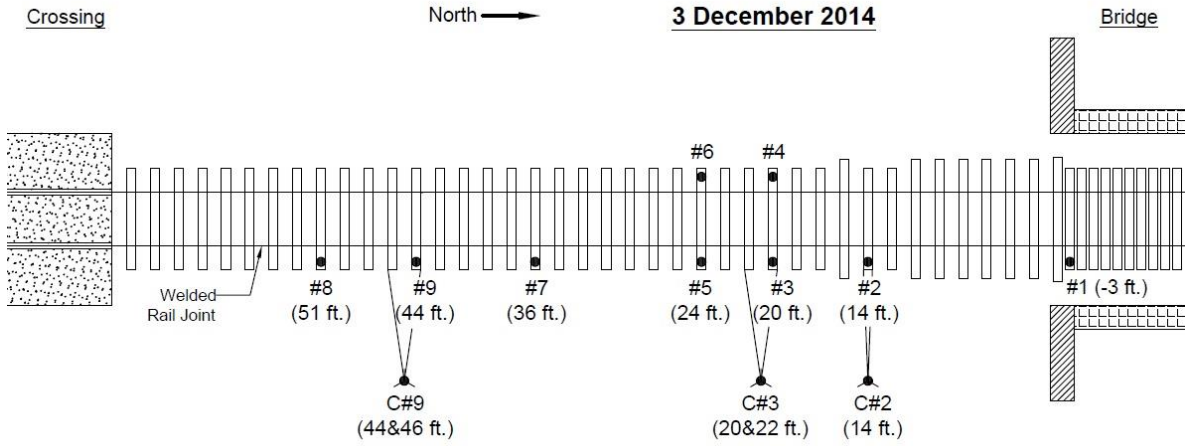

(b)

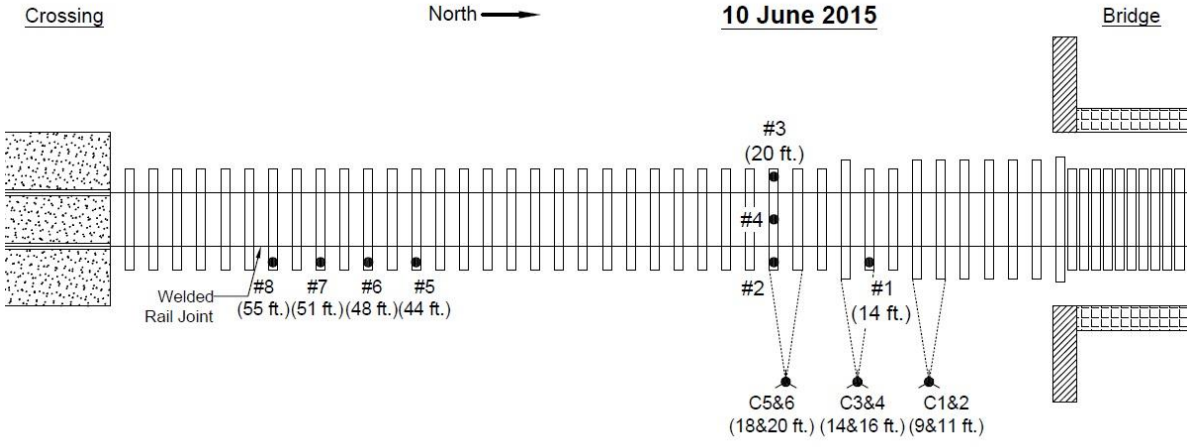

(c)

Figure 4.32 (cont.)

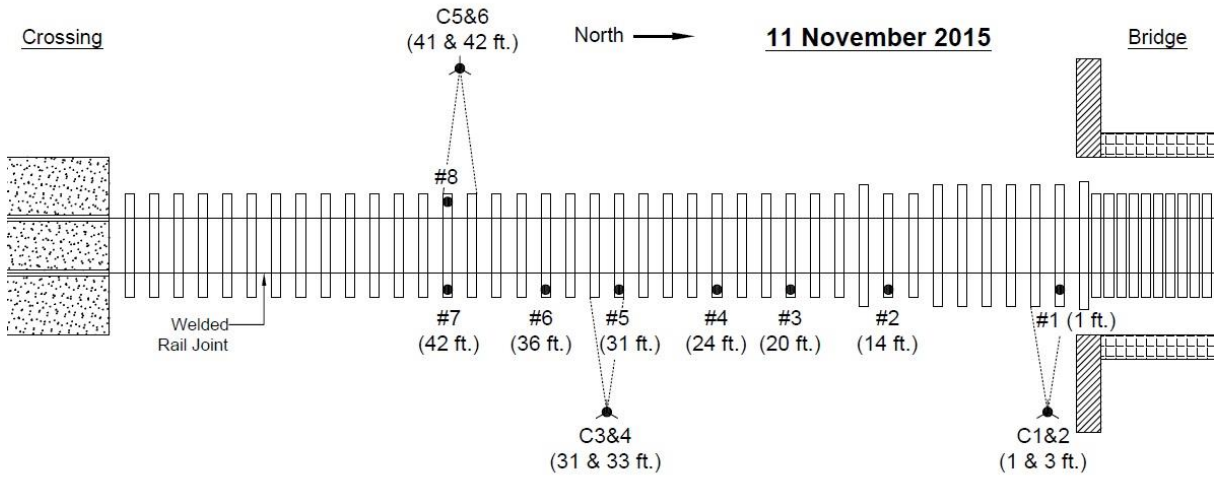

(d)

Figure 4.32: Instrumentation layout for (a) 21 and 22 October 2014, (b) 3 December 2014, (c) 10 June 2015, and (d) 11 November 2015.

The multiple site visits and variety of trains allowed Site #6 as a testing site to assess multiple aspects of transition zone behavior. The primary analyses at Site #6 are:

(6a) general overview of accelerations,
(6b) effect of tamping,
(6c) change in displacements in approach
(6d) change in accelerations at exit

Descriptions of each analysis are below.

Analysis #1: General overview of accelerations

The first analysis presents a general investigation into the overall track behavior at Site #6 and how tie accelerations change with distance, time, and train characteristics. Three investigations were performed: (1) comparing the behavior along the track for all five testing days, (2) investigate the influence of train velocity on tie acceleration, and (3) investigate the influence of load, train type, and train direction on tie acceleration. The results are presented below.

The first investigation compares the change of tie acceleration behavior with distance along the track and with time. For each recorded train, two average peak acceleration were recorded, one disregarding impacts and one including impacts. The purpose of disregarding impacts is an attempt to isolate the train loading mechanism. As a note, isolating the average

peak locomotive tie acceleration produced similar values to the average peak tie acceleration disregarding impacts.

It was discovered that by averaging the peak tie accelerations of all trains for each tie during a single day, a general representation of train behavior with distance for that particular day could be obtained. Figure 4.33 presents the average peak tie acceleration values with distance for the five days of testing along with the average of all five days. Figure 4.33(a) displays the average peak value without impacts while Figure 4.33(b) displays the values with impacts.

The results show much variation with both distance and time. Referencing both the overall average peak tie acceleration and the average of each day, tie accelerations appear to oscillate with distance. This suggests that tie support is varying and some ties are receiving more load than others. For example, Tie #8 (14 ft.) typically experiences the lowest tie acceleration (2 to 3g in Figure 4.33(a)). The low acceleration at Tie #8 (14 ft.) is due to the large rail-tie gap at the site location (reference Analysis #3) so little load is transferred to the tie. The main exception is the day after tamping (reference Analysis #2), in which the tie experienced loading for a few trains before eventually returning to the pre-tamping condition.

However, some ties show significant variation with each recorded day. Tie #15 (24 ft.) shows variation depending on the day (3g v. 8g). Additionally, some days, e.g. 3 December 2014, show lower overall response than other days, e.g. 21 October 2014. This suggests the track behavior changes with time and does not appear to find a state of equilibrium.

An explanation for this behavior is that the unsupported ties in the approach redistribute the wheel loads to ties further from the bridge abutment. For example, the load that should be transferred to Tie #8 (14 ft.) is redistributed to Tie #12 (20 ft.). This increases the load on Tie #12 (20 ft.) and, if the train is exiting the bridge, the train will “bounce” or “gallop” causing the ties immediately after, e.g. Tie #19 (31 ft.), to receive less load and then increase the load on further ties, e.g. Tie #22 (36 ft.). However, over time, the increased load increases the settlement under Tie #12 (20 ft.) and redistributes the load to ties even further from the abutment. This increases the load on other ties and shifts the entire load distribution further along the track. Numerical modeling in Chapter 5.6 shows how the load can be transferred to tie further from the abutment if unsupported ties exist in the approach. The influence of the asphalt crossing likely

causes the same mechanism in the opposite direction. This likely produces a rapidly shifting load environment that cannot obtain a state of equilibrium.

The peak tie accelerations from impacts in Figure 4.33(b) show similar behavior as Figure 4.33(a) but with significantly greater values further from the bridge abutment (see y-axis). It is unclear the exact mechanisms that produce the impact and their influence on track behavior, but it is likely within the superstructure and should be further investigated.

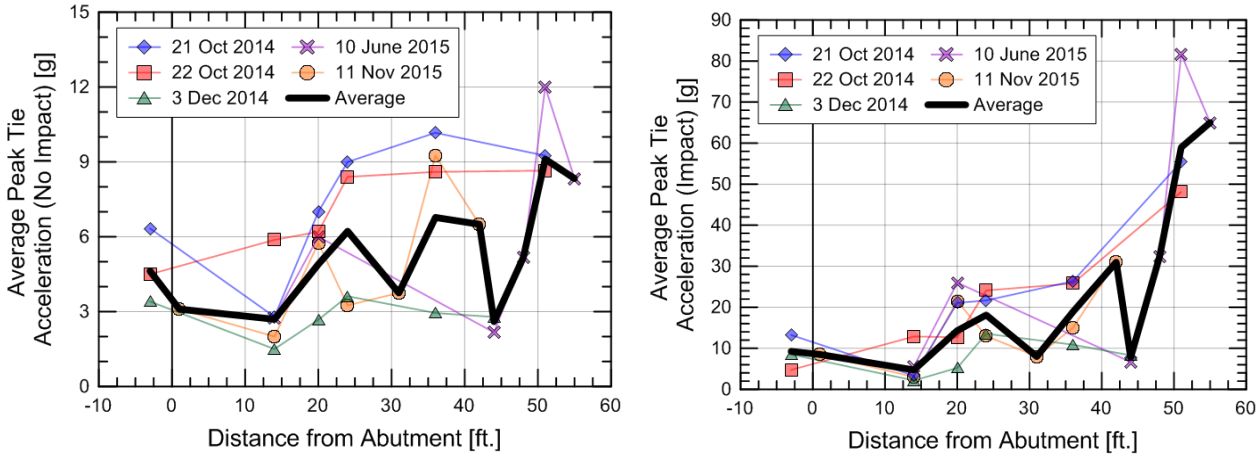

Figure 4.33: Average peak tie accelerations with distance (a) excluding impacts and (b) including impacts at Site #6.

The second investigation studies the influence of train velocity on tie accelerations. For this analysis, the average peak tie acceleration at each location is averaged for each train and is plotted with train velocity in Figure 4.34. The data is separated by the type of train for help in the third investigation. By fitting a trend line through the data, a clear influence of train velocity appears. For the data without impacts, the slope of the trendline is 0.12g/mph. This is similar to the slope from Site #4. This reinforces that train velocity influence tie acceleration values and increases tie accelerations by about 0.1 to 0.15g/mph. For the data with impacts, the slope of the trendline is 0.41g/mph.

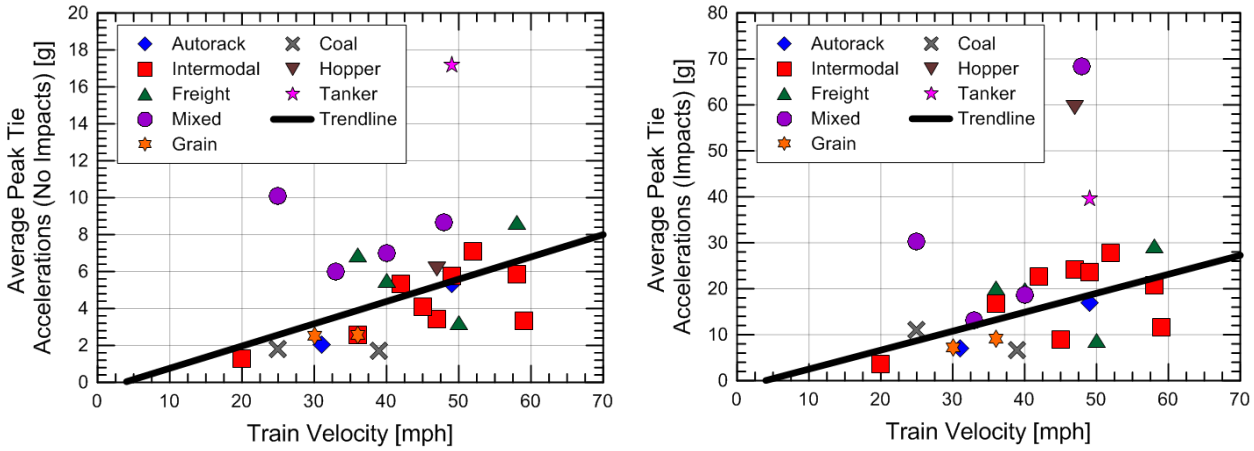

Figure 4.34: Average peak tie accelerations with velocity (a) excluding impacts and (b) including impacts at Site #6.

The third investigation studies in influence of load, train type, and train direction on tie accelerations. To eliminate the influence of train velocity, the average peak tie acceleration for each train is corrected by subtracting each value from the trendline in Figure 4.34. No apparent trend was observed for load or train direction. For train type, it appears in Figure 4.34(a) that measured tanker cars displayed much greater tie acceleration without impacts (~17g) than the average tie acceleration at 49 mph (5.5g). Mixed cars seem to display higher than average tie acceleration magnitudes but more data is required before definite conclusions can be made. An explanation for the lack of trend with load is that the label of loaded, mixed, or unloaded were determined from visual observations and may not directly correlate with the actual loading. Further analysis that isolates the effect of load is required before definite conclusions can be made.

Analysis #2: Effect of tamping

On 22 October 2014, the Site #6 location was pneumatically tamped and the behavior immediately after tamping was investigated. The track behavior of the five trains the day prior to tamping (21 October 2014) and the seven trains immediately after tamping was measured. The objectives were to determine the amount of settlement occurring immediately after the first train pass and how long it took to revert back to the pre-tamping behavior.

This analysis concentrates on the rail and tie displacements at Tie #8 (14 ft.) and contrasts the behavior pre-tamping, immediately after tamping, and post-tamping. The pre-tamping rail

and tie displacements of Tie #8 (14 ft.) and Tie #12 (20 ft.) are compared in Figure 4.35. The train measured at Tie #8 (14 ft.) consists of a northbound (approach) intermodal train moving at a velocity of 58 mph (Train #6-1-4) while the train measured at Tie #12 (20 ft.) consists of a southbound (exit) loaded autorack train moving at a velocity of 49 mph (Train #6-1-2).

Only two seconds of the time histories are shown to better illustrate the differences in track behavior. The rail-tie gap location (Tie #8, 14 ft.) only shows significant peak displacement of the rail (0.4 in/~10 mm) while the peak displacement of the tie is insignificant (0.05 in/~1.25 mm). This is expected because the rail-tie gap limits the amount of loading the rail applies to the tie and is expected to redistribute to surrounding ties. The tie-ballast gap location (Tie #12, 20 ft.) shows peak rail displacement of 0.2 inches (5.0 mm) and tie displacements of 0.25 inches (6.4 mm). It is typically expected that the rail displaces more than the tie but due to a potential centerbound tie condition, the end of the tie bends when loaded resulting in greater displacement at the end of the tie. Additionally, the rail-tie gap location (Tie #8, 14 ft.) experiences more rail displacement than the tie-ballast gap location (Tie #12, 20 ft.), which is expected because the rail-tie gap location (Tie #8) is closer to the bridge abutment and likely experienced greater substructure settlements.

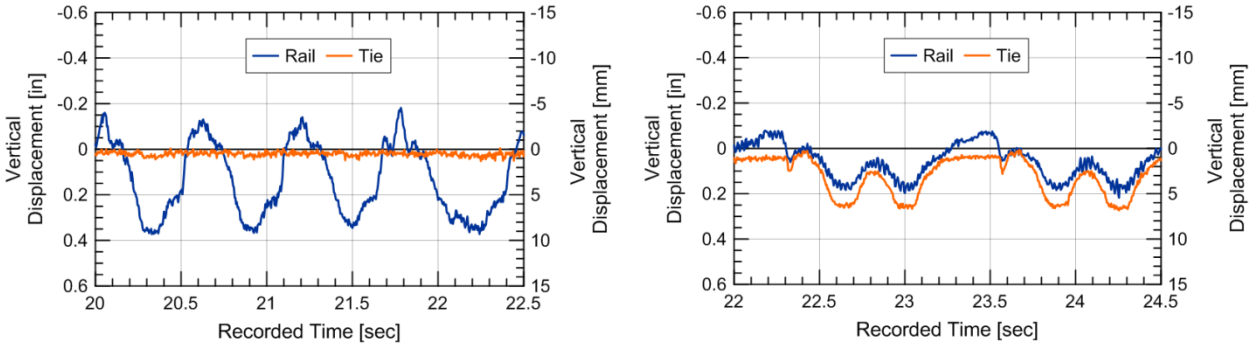

Figure 4.35: Rail and tie displacements at: (a) Tie #8 (14 ft.) and (b) Tie #12 (20 ft.).

On the morning of the second day, the transition zone was resurfaced using a pneumatic tamper. The rail was lifted about 7/8 of an inch at Tie #8 (14 ft.) and was resurfaced with an overlift, e.g. rail elevation in the transition zone was slightly higher than on the bridge, with the hope that the ballast would eventually equalize so the rail elevation in the transition zone would end up being about the same as the elevation of the rails on the bridge deck. After tamping, the rail and tie displacements at Tie #8 (14 ft.) from the first passing train, a northbound (approach)

loaded autorack train moving at a velocity of 25 mph (Train #2-1-1), was measured and the first 18 seconds (13 train trucks) are displayed in Figure 4.36. Tie #12 (20 ft.) was not able to be measured because of a maintenance vehicle blocking the view.

Figure 4.36 illustrates that the loading from the first train truck results in significant settlement of the rail and tie. The tie settles about 0.5 inches (13 mm) after the first truck and eventually reaches 0.7 inches (18 mm) by the end of the train. The rail shows about 0.45 inches (11 mm) of settlement by the end of the train. The reason the tie settles more than the rail is that a gap develops between the rail and tie because the upward reaction force of the rail after unloading pulls the spikes from the ties. As more trains pass and the ballast settles further, this repeated upward reaction force will continue to pull the spike from the tie and increase the rail-tie gap.

The initial truck loading produced about 0.7 to 0.8 inches (18 to 20 mm) of ballast settlement and video of the train shows ballast particles pushed out from underneath the tie. One explanation for this large initial settlement is not enough ballast particles were supporting the tie and rail to the specified elevation and therefore were not able to withstand the entire train loading. This caused the few ballast particles to either be pushed into the underlying ballast, pushed outside of the tie, or suffer particle breakage. The presence of ballast fouling may have facilitated this process. The magnitude of ballast settlement may also be related to the pre-tamping ballast condition because ballast after tamping is observed to have a “memory” of its pre-tamping state. This is discussed in Chapter 2.3.5. Either way, the first train immediately compacted and re-densified the ballast and resulted in about 0.8 or 0.9 inches (20 to 23 mm) of substructure settlement which can then cause the concentration of train loads and reinstitute the track deterioration process.

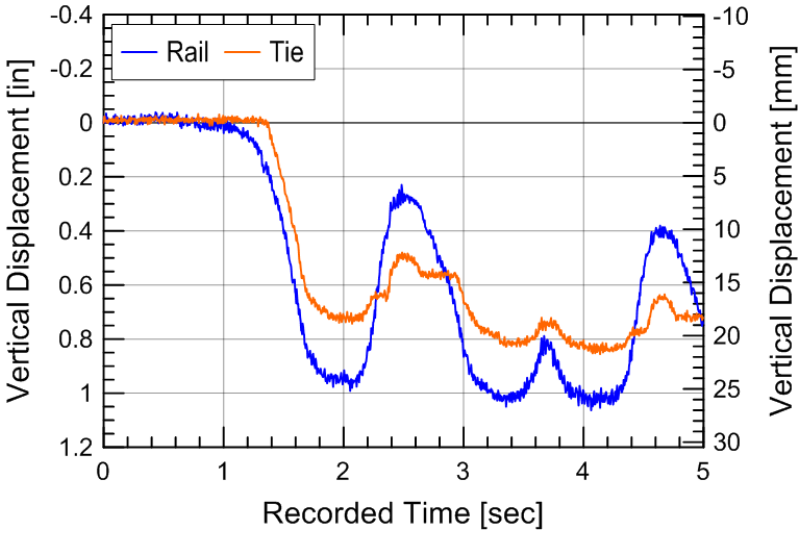

Figure 4.36: Rail and tie displacements at Tie #8 (14 ft.) after pneumatic tamping on 22 October 2014.

The first train produced the greatest amount of track settlement and the track seemed to reach equilibrium after about three to four trains. To evaluate how the track behaved after reaching equilibrium, the rail and tie displacement time histories from the sixth train after tamping is measured at Tie #8 (14 ft.) and displayed in Figure 4.37(b). This train is a southbound (exit off the bridge) loaded train moving at a velocity of 33 mph (Train #6-2-6). By comparing the (a) pre-tamping and (b) post-tamping states, it is clear that post-tamping transient behavior quickly returns to its pre-tamping behavior after a few passing trains. Due to the continual upward force of the rail pulling the spike from the ties, the rail-tie gap reaches about 0.3 inches (8 mm) and will likely eventually increase to the 0.4 inch (10 mm) gap that existed pre-tamping.

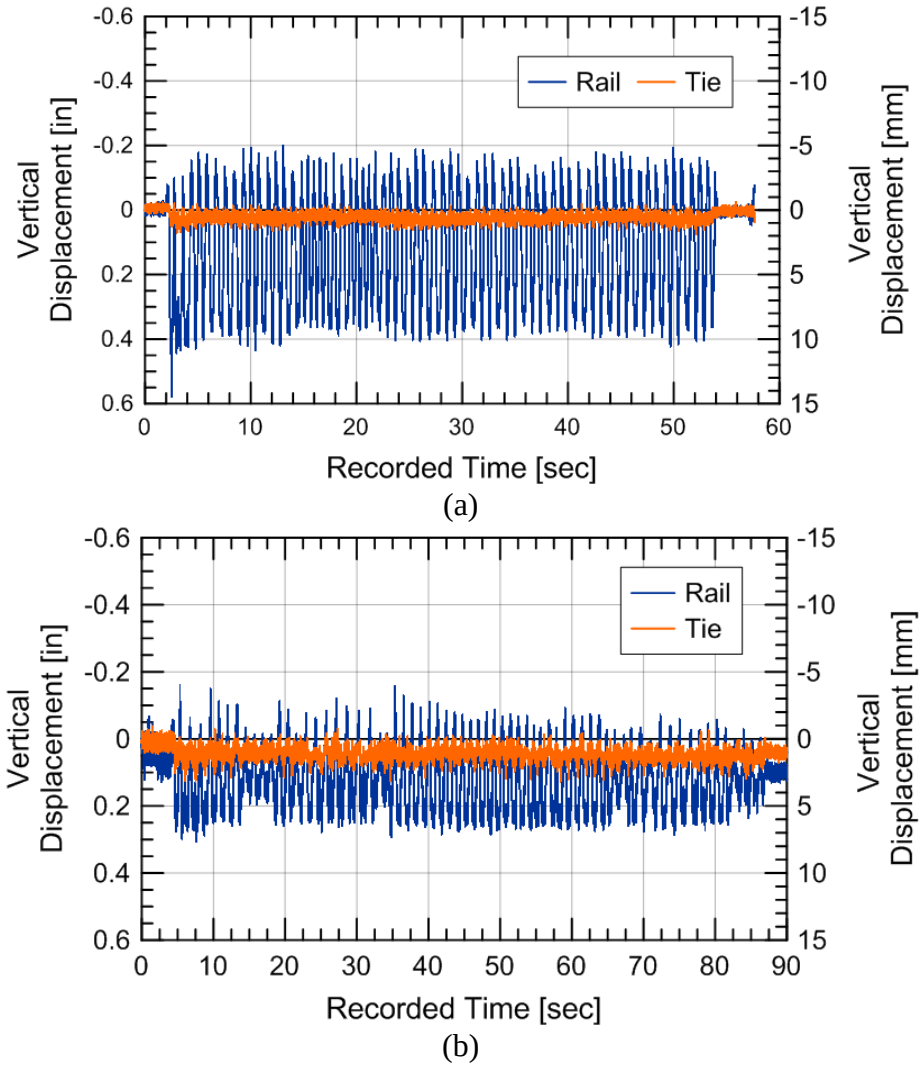

Figure 4.37: Rail and tie displacements at Tie #8 (14 ft.) (a) before tamping on 21 October 2014 (Train #6-1-4) and (b) after pneumatic tamping on 22 October 2014 (Train #6-2-6).

The cumulative rail and tie settlement is estimated to be around 0.55 inches and 0.8 inches, respectively, and no noticeable changes in behavior were observed at Tie #2 (14 ft.) for the remainder of the day.

The results of the analysis suggest:

- After pneumatic tamping, the first train pass immediately compacted the ballast resulting in 0.45 inches (11mm) of rail settlement and 0.7 inches (18 mm) of tie settlement. This occurred because not enough ballast particles were holding up the rail and ties to the specified elevation and therefore immediately "pushed out" during the first train loading.

- The ballast seemed to reach an equilibrium condition after about four trains and resulted in 0.5 inches (13 mm) of rail settlement and 0.8 inches (20 mm) of tie settlement with a 0.3 inch (7 mm) gap between the rail and tie. The transient behavior of the tie was very similar to the pre-tamping conditions.
- Because of the large initial ballast settlements, emphasizing better ballast compaction and density during tamping of high-maintenance regions such as bridge transition zones may reduce this initial settlement resulting in the track geometry holding for longer time periods and hopefully increases tamping cycles for railroad companies.

Analysis #3: Change in displacement in approach

The third analysis investigates the change in displacement at the bridge approach at Site #6. The displacement measurements in Task I only involved a single bridge approach location so this analysis measures the behavior of six ties in the approach region. The testing was performed on 10 June 2015 and involved Tie #5 (9 ft.), Tie #6 (11 ft.), Tie #8 (14 ft.), Tie #9 (16 ft.), Tie #11 (18 ft.) and Tie #12 (20 ft.). The camera locations can be referenced in Figure 4.32(c). The two cameras furthest from the approach were placed at that location to match with previous instrumentation trips and the nearest camera was placed to get a consistent look at a span of eight ties. Three trains were recorded and can be referenced in Table 4.6.

Figure 4.38 shows the rail and tie displacement time histories of an empty freight train at 47 mph (Train #6-4-2). The results show consistent rail and tie behavior except for the first few heavy locomotive axles. The average peak rail and tie displacements at each location for all three trains is displayed in Figure 4.39. The results show significant variation in track behavior with the track locations closest to the bridge abutment displaying peak rail displacements of about 0.35 inches (9.0 mm) and tie displacements of about 0.02 inches (0.5 mm) while rail and tie displacements of 0.12 inch (3.0 mm) are observed farther away from the bridge abutment. The rapid decrease in rail displacement as the train moves farther from the abutment (0.23 inches (6.0 mm) in 11 ft) translates to a rail slope of roughly 1:500 and can result in increased loading within the transition zone (Nicks, 2009). Additionally, a change in tie behavior is observed 15-ft from the bridge abutment where the track switches from having rail-tie gaps to tie-ballast gaps. This switch implies the upward reaction force when two wheels are surrounding the tie is great enough within 15-ft to partially pull out the tie spikes.

Figure 4.38(g) and (h) present the rail and tie time histories in the frequency domain. The results show the majority of information ranging from 1 to 5 Hz, as anticipated.

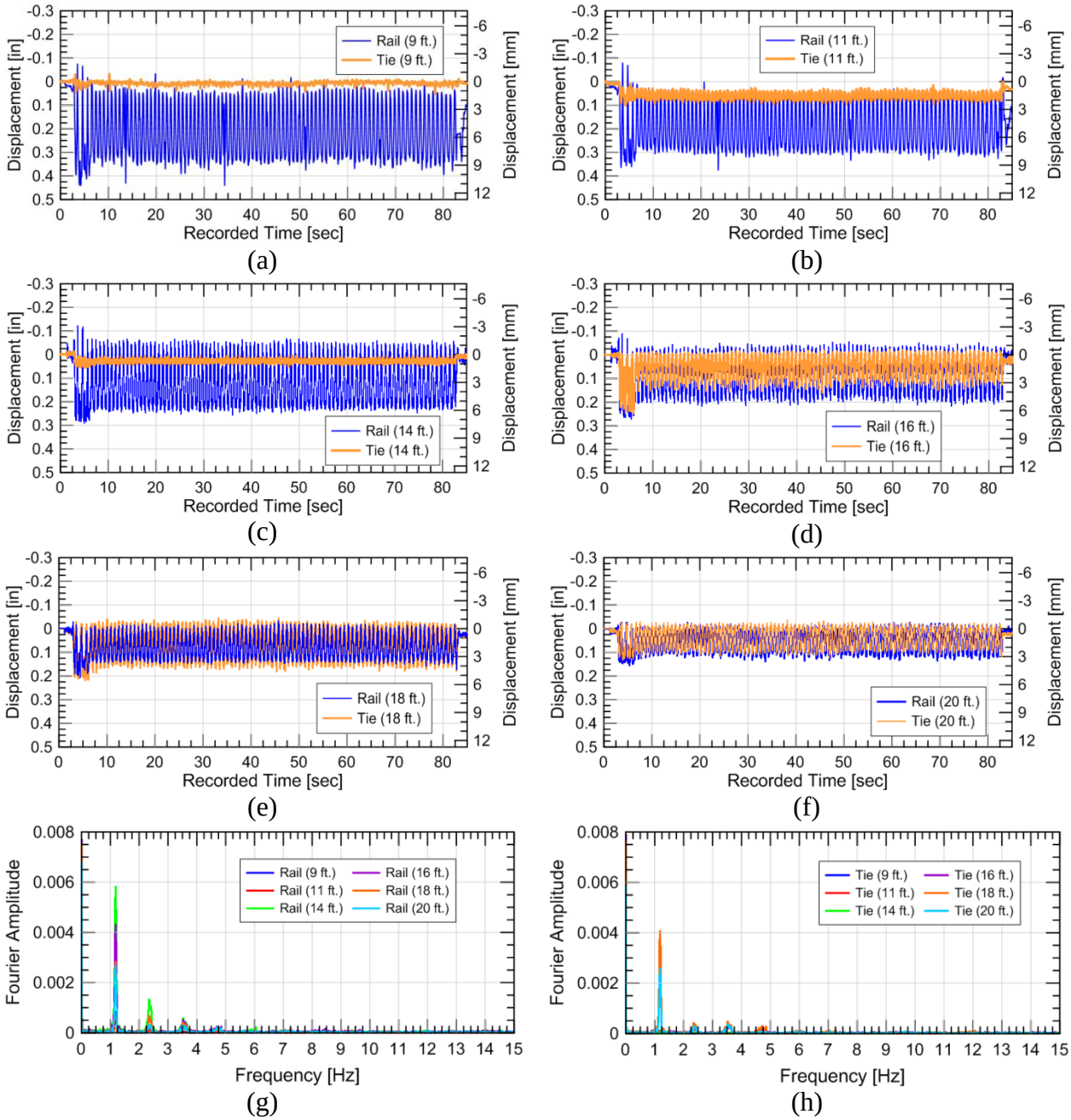

Figure 4.38: **Vertical rail and tie displacement time histories of: (a) Tie #5 (9 ft.), (b) Tie #6 (11 ft.), (c) Tie #8 (14 ft.), (d) Tie #9 (16 ft.), (e) Tie #11 (18 ft.), and (f) Tie #12 (20 ft.) for an empty freight train passing at 76 km/hr (47 mph).**

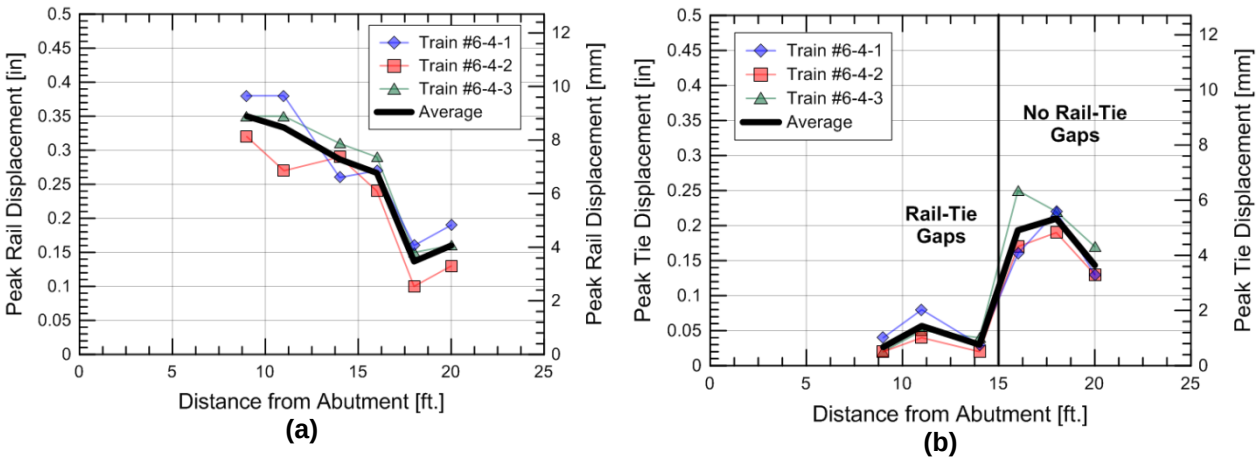

Figure 4.39: Average peak (a) rail and (b) tie displacement with distance at Site #6 on 10 June 2015.

The results show the following:

- A rapid change in rail displacements along the track with the approach experiencing about twice the transient rail displacement than the ties further from the bridge. This suggests the load is being redistributed and possibly concentrated on particular ties.
- The change in behavior at 15-ft with the switch from the majority of displacement occurring from the closure of rail-tie gaps to the majority of displacement occurring from closure of tie-ballast gaps is apparent. This suggests the upward force between wheels is greater enough to pull the spike from the tie within 15-ft but not great enough past 15-ft.

Analysis #4: Change in acceleration in exit

The fourth analysis investigates the change in acceleration as passing trains exit an asphalt crossing. The testing occurred on 10 June 2014 and involved Tie #27 (44 ft.), Tie #29 (48 ft.), Tie #31 (51 ft.), and Tie #33 (55 ft.). The locations can be referenced as Accel #5 through #8 in Figure 4.32(c). The Tie #33 (55 ft.) location was selected because it appeared to be the end of the "dip" and is located 12-ft from the asphalt crossing. Increased loads would be anticipated for exit trains because Tie #33 (55 ft.) is the location in which the exit trains "fall off" from the asphalt crossing. The other three accelerometer locations were placed every other tie away from the crossing to get the response over a span of 11 feet. Additionally, a welded rail joint is located directly next to Tie #33 (55 ft.).

Figure 4.40 presents the response of a northbound (exit off crossing) train consisting of empty hopper cars moving at a velocity of 47 mph (Train #6-4-2). The time histories show high accelerations at Tie #33 (55 ft.) and Tie #31 (51 ft.), which are 12-ft and 16-ft from the asphalt

crossing, respectively. The peak accelerations vary but the response appears to be about 150g at both locations and are attributed to impacts within the superstructure, possibly the influence of the welded rail joint or wheel/fastener impact. This impact is observed at Tie 29 (48 ft.), 19-ft from crossing, but to a much lesser degree at 25g. Tie #27 (44 ft.), 23-ft from crossing, displays little acceleration response of about 5g.

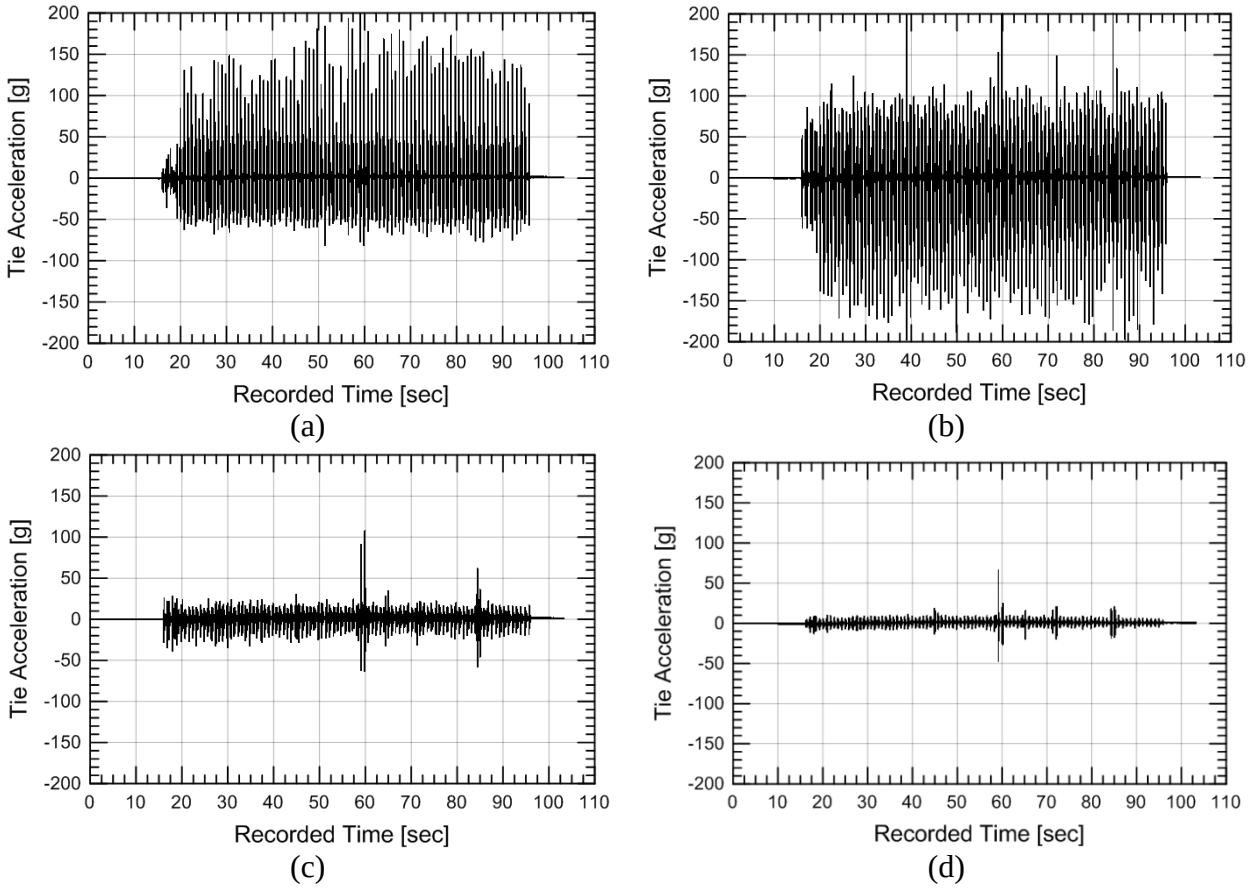

Figure 4.40: Tie acceleration responses from (a) Tie #33 (55 ft.), (b) Tie #31 (51 ft.), (c) Tie #29 (48 ft.), and (d) Tie #27 (44 ft.) on 10 June 2015.

Figure 4.41 shows the average peak acceleration for all three trains recorded on 10 June 2014. Train #6-4-1 is a southbound train (entering crossing) while Trains #6-4-3 and #6-4-3 are northbound (exiting crossing). While all trains show a large differences in response from Tie #27 (44 ft.) and Tie #33 (55 ft.), the difference is greater for the exiting trains.

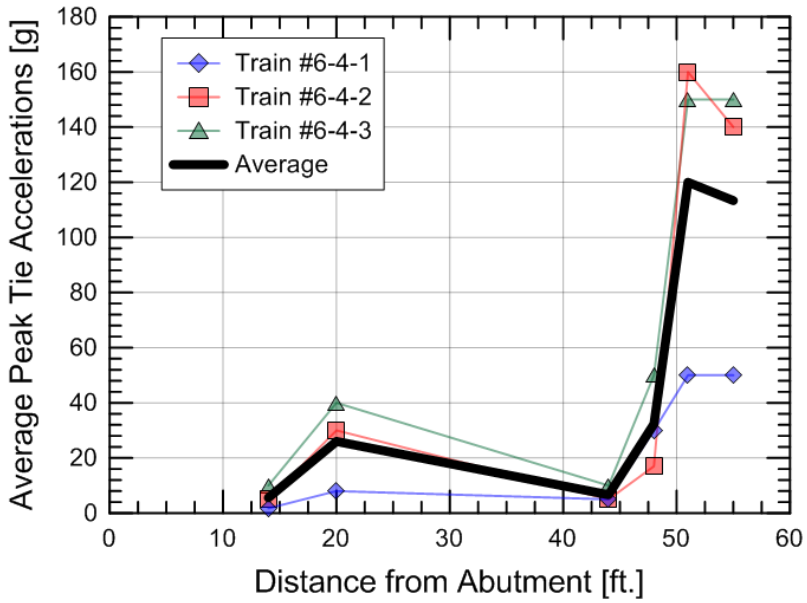

Figure 4.41: Average peak tie accelerations with distance at Site #6 on 10 June 2015.

A difference in the loading environment is expected from this large variation in tie acceleration. Possible explanations could be an impact that occurs after the wheel passes the welded rail joint or from the train "falling off" the crossing and then bouncing back. This would suggest that Ties #33 (55 ft.) and #31 (51 ft.) experience greater loads while Tie #27 (44 ft.) experiences less because of the wheel load oscillations. Combinations of both explanations is also a possibility.

A summary of results from Site #6 are the following:

- The instrumented location is a double transition zone with a history of track geometry problems.
- Variations in peak tie acceleration along the track and time suggest uneven support and load distribution that changes with time.
- The influence of train velocity on tie acceleration was calculated to be 0.12g/mph with no impact and 0.41g/mph with impact. No relation was observed for train weight, type, or direction, however, the author believes the averaging cancels the influence and more information could potentially show an influence.
- On the first train pass after tamping, 0.8 to 0.9 inches (20 to 23 mm) of substructure settlement was observed at an instrumented tie. The tie reverted back to its pre-tamping transient behavior seven trains after tamping.
- A rapid change in rail displacements along the track with the approach experiencing about twice the transient rail displacement than the ties further from the bridge. This suggests the load is being redistributed and possibly concentrated on particular ties.

- A rapid change in tie accelerations at an exit transition was observed with a reduction from about 120g to 5g in the span of four ties. This suggests uneven distribution of loads at exit transition locations.

4.4.7 Site #7

The seventh instrumented site provides an example of a transition zone recently remediated with UTPs. The objectives of the site analysis are to: (7a) compare the various displacement measurements, (7b) investigate the displacement and acceleration behavior along the track, and (7c) investigate the contributions of under-tie pads on approach behavior.

On 31 August 2014, twenty-nine (29) UTPs were installed in the Upland Street southern Track #2 bridge approach along the Amtrak Northeast Corridor near Chester, Pennsylvania. This is the opposite end of the bridge and one track over from Site #5 and the Upland Street site in Task I.

The track superstructure consists of welded rail joints, 136-RE rail, concrete ties at 24-in spacings, and spring clip fasteners. The first 29 concrete ties have UTPs attached to the underbody. The substructure is unknown but clean ballast was installed during the remediation. An HMA layer roughly 12 to 14 inches below the bottom of the installed UTP-fitted concrete ties was discovered when the loader excavated the ballast section in preparation for installing the UTP track panel on 31 August 2014. This HMA layer was installed sometime in the 1990's. The bridge is an short-span open deck timber bridges.

The anticipated benefits of UTPs are the reduction of ballast degradation and possibly densification. The UTP serves as a resilient layer at the tie-ballast interface that provides a cushion between the tie and ballast and dampens track and tie vibrations. The resiliency of the UTP provides a "cushion" for the ballast and can increase the contact area between the UTP and ballast particles. Studies investigating the contact area between concrete ties without UTPs and ballast show contact areas of only 20% (McHenry, 2013), which indicates high particle contact stresses. By increasing the contact area between the UTP and ballast, the ballast particle contact stresses are reduced along with Type II and Type III ballast degradation because these degradation mechanisms result from high stresses within individual ballast particles. An additional benefit of UTPs is they reduce tie degradation, which can result in greater tie-ballast gaps, i.e., additional track movement, and reduced tie performance.

The installation of UTPs in transition zones is a fairly recent development in the U.S. however existing studies in Europe suggest they result in reduced tie and ballast degradation (Schnedier et al., 2011). Class 1 railroads in the United States are beginning to install UTP in transition zones for both concrete and wood ties to reduce ballast and tie degradation.

On 12 August 2015, two instrumentation teams, one from University of Illinois at Urbana-Champaign (UIUC) and the other from Amtrak, installed multiple instruments to evaluate the transient behavior of the southern Track #2 approach of the Upland Street bridge about one year after UTP installation. The instrumentation layout is shown in Figure 4.42(a). The UIUC team measured tie displacement at Ties #4, #5, #20, and #21 at distances 8, 10, 40, and 42 ft., respectively, from the bridge abutment. The Amtrak team measured tie displacements at Ties #10 (6.1 meters/20 feet) and #11 (6.7 meters/22 feet) with an in-house device called a "Bending Beam". The Bending Beam is shown in Figure 4.42(c) and measures the displacement of the moment arm using calibrated strain gauges to +/-10 mm.

Both the UIUC and Amtrak teams also installed accelerometers to measure tie accelerations and calculate tie displacements using double-integration techniques. The UIUC team measured tie accelerations at Ties #1, #4, #8, #14, #20, #28, #31, and #40 at distances 0.6, 2.4, 4.9, 8.5, 12.2, 17.0, 18.9, and 25.0 meters (2, 8, 16, 28, 40, 56, 62, and 82 ft.), respectively, from the bridge abutment using piezo-electric accelerometers. The Amtrak team measured tie accelerations only at Tie #10 at a distance of 6.1 meters (20 ft.) from the bridge abutment also using piezo-electric accelerometers.

All three instruments, video cameras, Bending Beams, and double-integrated accelerometers, have their unique advantages and disadvantages. The video cameras and accelerometers are discussed in previous sections. The Bending Beams directly measure tie displacement at a sampling rate of 10,000 Hz but the Bending Beam is supported on a stake that is placed in the crib. As a result, vertical crib displacement can result in a lower measured displacement than the video cameras or accelerometer measurements.

The train presented is an Acela high-speed passenger train traveling north along Track #2 entering the Upland Street Bridge with a velocity of 110 mph at 12:39 PM on 12 August 2015. Slight variations were observed for different trains but the overall trends are similar so the results of only the 12:39 PM train are presented herein due to space constraints.

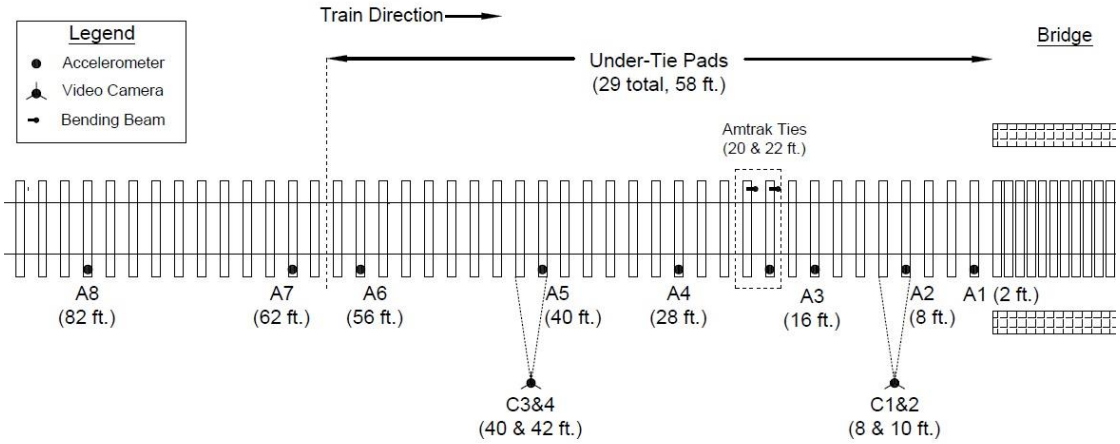

(a)

(b)

(c)

(d)

Figure 4.42: **Upland Avenue northern Track #2 approach with UTPS: (a) diagram showing instrumentation layout, (b) overview photograph of transition with orange targets for video cameras, (c) Bending Beam with reference stake (see arrow), and (d) tie accelerometer.**

Site #7 performed three analyses that are discussed below:

(7a) Compare the various displacement measurements,
(7b) Investigate the displacement and acceleration behavior along the track,
(7c) Investigate the contributions of under-tie pads on approach behavior.

The first analysis, (7a) comparison of various displacement measurements, is to compare the various methods and validate the double-integration estimates at this site. The UIUC video camera and accelerometer results from Tie #4 (8 ft.) are compared in Figure 4.43(a) and (b), respectively. The video camera was filtered using an 8th order low-pass Butterworth filter with a cutoff at 12 Hz. The thick black line represents the filtered response and the thin red line represents the unfiltered response. A low frequency cutoff was necessary due to the camera vibration and rotation not eliminated by the driven stake because the camera was placed on a steep slope close to Track #1. The accelerometers were filtered using a 3rd order bandpass Butterworth filter with cutoffs at 2 Hz and 30 Hz. The high-pass cutoff (2 Hz) was necessary to eliminate drift from the double-integration process because of additional instrumentation noise. This means that the peak-to-peak displacement magnitudes will be valid but the shape of the response may not be properly reconstructed. The comparison of the video camera and accelerometer displacements show the magnitudes from the filtered video camera response (4.5 mm/0.18 in) are in agreement with the double-integration displacement (4.1 mm/0.16 in).

The Bending Beam and accelerometer results at Tie #10 (20 ft.) are compared in Figure 4.43(c) and (d), respectively. The Bending Beam was filtered using a 5th-order low-pass Butterworth filter with a cutoff at 30 Hz while the UIUC accelerometer was filtered in the same manner as described earlier. The comparison shows a smaller displacement measured by the Bending Beam (0.85 mm/0.03 in) than the accelerometer (1.4 mm/0.06 in). A potential explanation for the difference is vertical displacement of the reference stake within the crib that is not accounted for with the Bending Beam measurements.

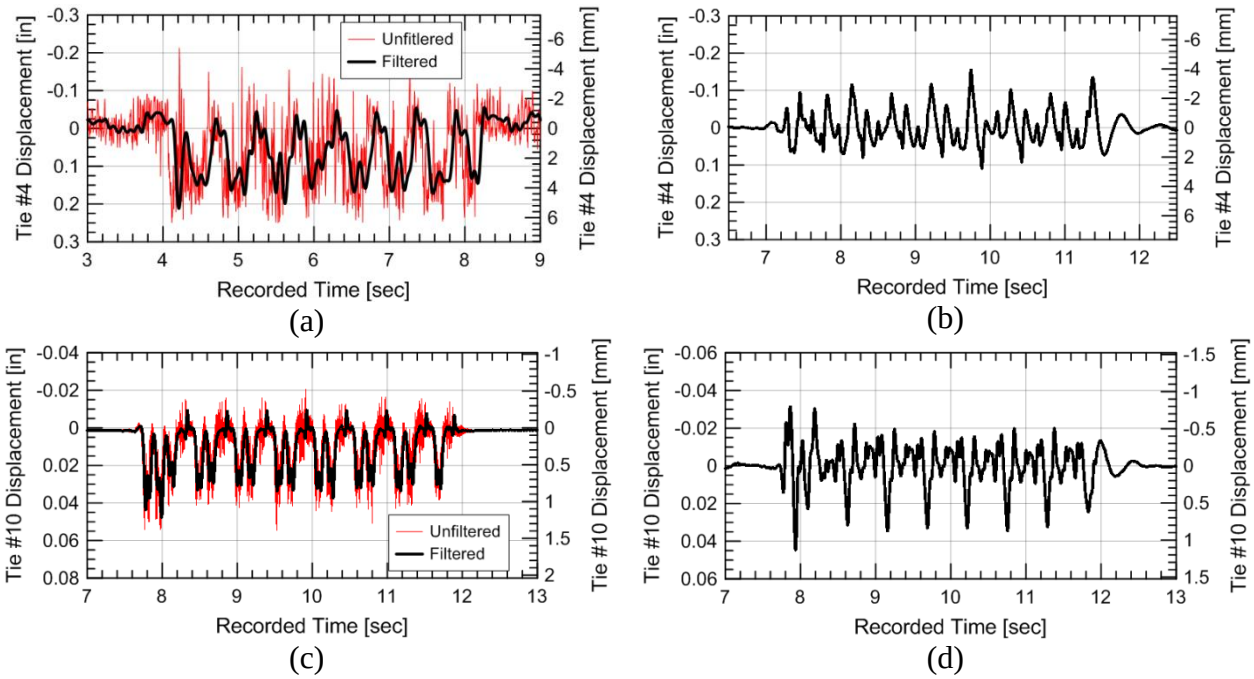

Figure 4.43: Comparison of Tie #4 (8 ft.) response from UIUC: (a) video camera and (b) accelerometer and comparison with response of Tie #10 (20 ft.) from Amtrak: (c) Bending Beam and (d) accelerometer.

The second analysis, (7b) investigate displacement and acceleration behavior along the track, looks how the peak displacement and acceleration values change with distance from the abutment to evaluate changes in behavior along the transition zone. Figure 4.44(a) compares the displacements from all available instruments and the displacement magnitudes show general agreement except for the lowest magnitude being from the Bending Beam displacement, which is probably due to vertical displacement of the reference crib ballast (see Figure 4.42c). In general, the results suggest large transient displacements near the bridge approach that decrease to a local minimum at about Tie #10 (20 ft.) and then slightly increase until the open track is reached.

Figure 4.44(b) shows the average peak tie accelerations with distance. The general response agrees with the tie displacements, in which large accelerations are observed near the bridge abutment and the accelerations decrease until about Tie #10 (6.1 m) and then they increase again until the open track is reached. This increase in displacements with distance could be attributed to the "landing zone" for trains that ran southbound on Track #2 instead of the predominant direction of northbound. No significant difference is observed at the transition between ties with UTPs (Ties #1 through #29) and ties without UTPs (Tie #30+) but this is

anticipated because all of the instrumented ties in the open track are well supported so the benefits of UTPs are not being manifested.

The displacement and acceleration results suggest that the first six to seven ties are unsupported with differing tie-ballast gaps as shown in Figure 4.44(c). This is in agreement with the impact observed at Tie #1 (2 ft.) in the tie acceleration response that was not observed at any other tie. The unsupported ties were also observed visually during train passage.

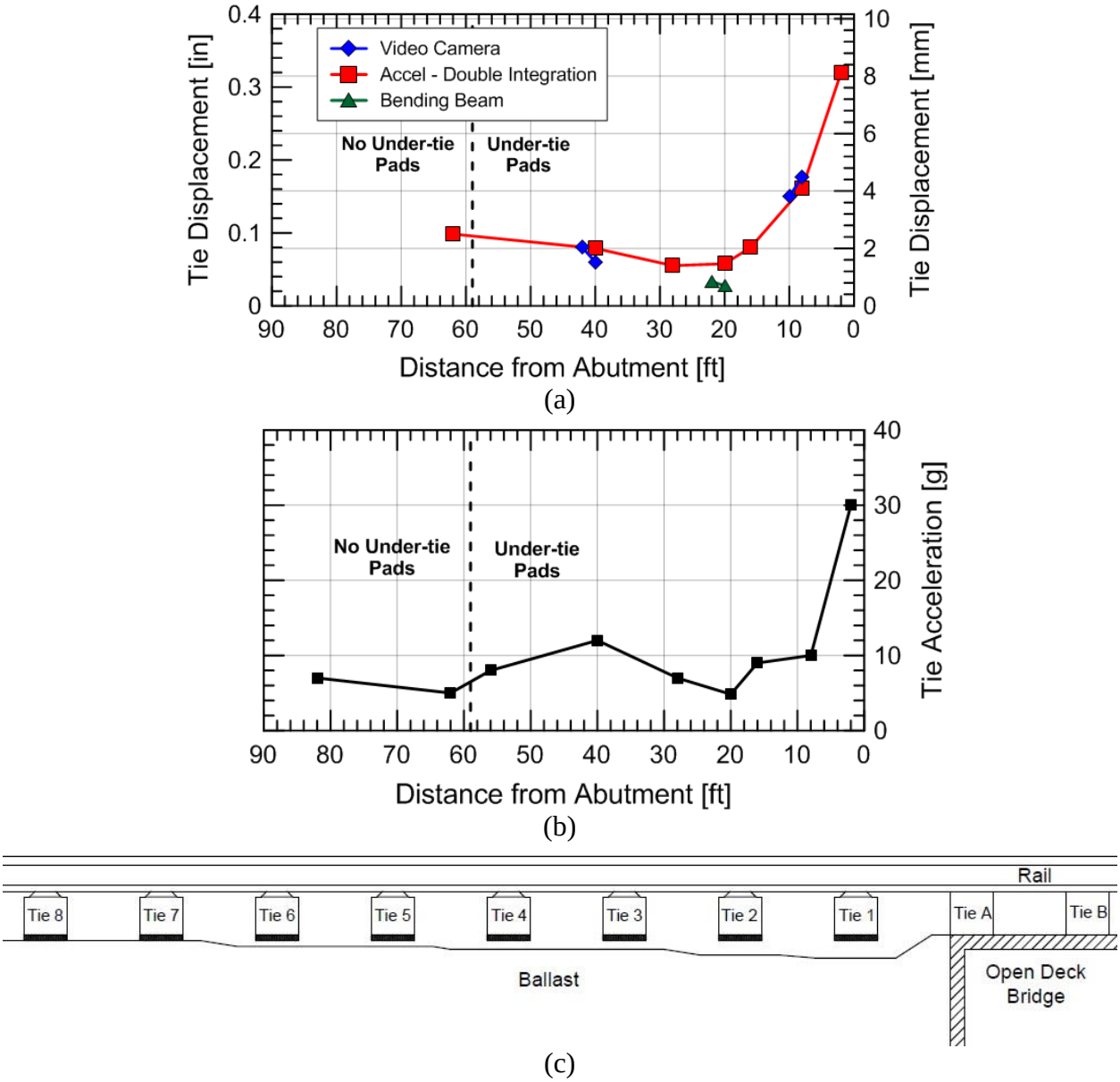

Figure 4.44: **Diagrams of: (a) peak displacement and (b) peak acceleration with distance from the abutment and (c) schematic of track support along the transition zone, which shows Ties #1 through #6 unsupported.**

Track geometry measurements recorded monthly for this approach suggest little change in track geometry has occurred between the installation of the UTPs and the day of testing on 12 August 2015, i.e., after 346 days. It is not clear whether the six to seven unsupported ties near the abutment have existed since UTP installation, i.e., due to inadequate ballast compaction near the bridge abutment, or whether ballast settlement has slowly been accumulating over the 346 days due to increased vehicle loading at the abutment, poor drainage, ballast degradation, and/or tie damage. Regardless, no track geometry problems have developed at the southern Track #2 transition since UTP installation about one year earlier as opposed to 14 mm/yr of settlement measured at the northern Track #3 transition prior to remediation. Unfortunately, direct comparisons with previous analyses at surrounding sites cannot be made due to the use of different instrumentation.

If track geometry continues to hold, UTPs may show to be an effective remedial measure for reducing differential movement at railroad transition zones. It is hoped future monitoring will confirm this initial observation.

A summary of results from Site #7 are the following:

- The installation of UTPs and new ballast at a bridge approach that was experiencing reoccurring track geometry problems appears to have, at least temporarily, held track geometry. The exact contribution of the UTP is unclear but the increased contact area and reduction in ballast particle stress should reduce ballast degradation.
- Both displacement and accelerometers show higher magnitudes at the bridge end and then decreasing values as the open track is reached. This captures the existence of unsupported ties and tie-ballast impacts in the approach.
- The exact contribution of the UTP on bridge approach or open track behavior is unclear from the measurements but the increased contact area and reduction in ballast particle stress should reduce ballast degradation. Future measurements should give a more complete picture.

4.4.8 Site #8

The eighth instrumented site provides a example of the behavior of multiple recently remediated transition zones. The objectives of the site analysis are to: (8a) compare the displacement behavior along the track at four transition zone locations, (8b) compare the displacement behavior at a transition zone remediated with HMA with time, and (8c) compare the acceleration behavior along the track for a transition zone remediated with Geoweb and HMA.

Site #8 consists of four bridge transition zones that accommodates freight traffic with train velocities of about 25 mph, a combined annual traffic of about 30 MGT, and was constructed with transition designs that have resulted in minimal track geometry maintenance since being placed in service in 2015 (~1 years of service from instrumentation date). The track superstructure consists of welded rail joints, 136-RE rail, timber ties at 24-in spacings, spring clip fastening system. The substructure consists of a 12-in ballast layer, either a 6-in geocell or HMA underlayment, an existing subgrade. The track is considered Class II for operations (maximum train velocity of 25 mph).

The original single mainline track bridge The track structure includes an open deck bridge (see Figure 4.45a) and an existing grout filled subgrade on the southern approach of the existing bridge, which was installed at an unknown date. The existing track experienced reoccurring track geometry defects associated with track profile, cross level, and warp defects at the approaches.

In 2015, the bridge was scheduled to be upgraded to a ballasted bridge deck along with the construction of a second ballasted deck bridge directly adjacent to the original, thus creating a double mainline with only 15 MGT per line. The scheduled upgrade of two approaches and the creation of two more provided the railroad company with an opportunity to assess the effectiveness of these various solution combinations, e.g., Geoweb and/or HMA. If the Geoweb application at this location is considered successful and feasible, Geoweb could be installed at a higher MGT and FRA Class Track and eventually be incorporated into Engineering Standards at this railroad. Two photographs of the new bridge is shown in Figure 4.45(b) and (c).

To balance transient displacements between the bridge and approach and reduce the need for maintenance, the design measure are similar to those constructed at Site #1 through #3. The ballasted bridge deck allows some track movement on the bridge, which helps balance the transient and permanent displacements between the bridge and approach. Ballasted bridge decks have reduced maintenance but generally need to be used with stabilization measures in the approach to fully mitigate differential movement at the approach. Concrete curbs of various lengths (typically 7 to 9-ft) provide confinement to the ballast and subgrade at and near the bridge abutment, which creates as a confined transitional zone between the bridge and approach. Increased confinement strengthens the ballast and results in reduced ballast settlement. The last stabilization technique, a geoweb/HMA underlayment, is installed under the ballast to increases

ballast confinement, better distribute the applied load to the subgrade, and provide a barrier/separation layer between the ballast and subballast to reduce subgrade migration into the ballast and water reaching the subgrade.

To compare the response of the Geoweb and HMA underlayment, Geoweb was installed in two approaches while HMA underlayment was installed in one approach. The remaining approach consists of the existing grout slurry. The approach name and locations of the various solutions are listed below and an overview of the four sites is shown in Figure 4.45(d).

(a)

(b)

(c)

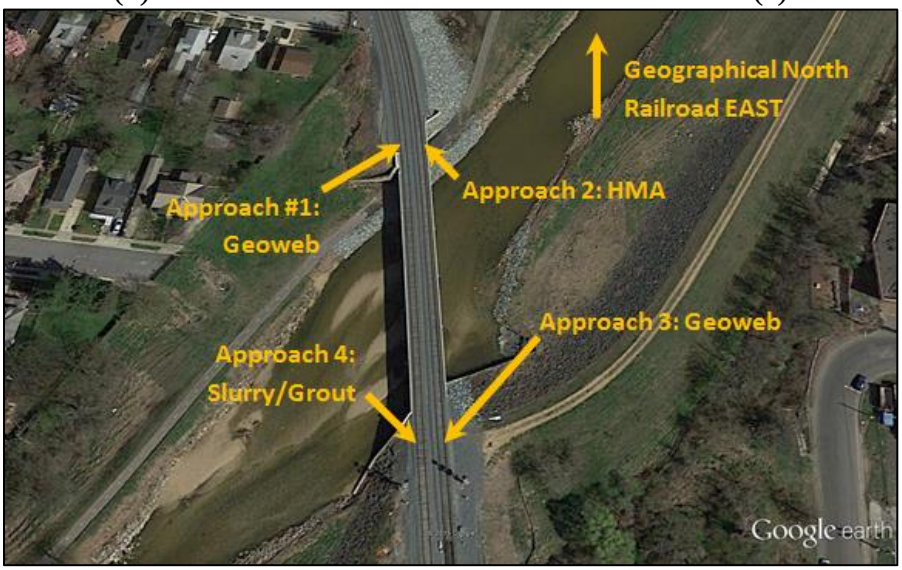

(d)

Figure 4.45: Photographs of (a) new bridge, (b) new bridge looking south, (c) new bridge looking north, and (d) overview of the four approaches for Site #1.

Three days of non-invasive monitoring was performed to assess all four bridge approaches on: 16 November 2015, 18 April 2016, and 19 July 2016. This monitoring was performed to compare the various approach remedial measures and monitor changes over time. Of particular interest is the transient track displacements and tie accelerations from passing trains because these metrics provide insight into track stiffness, support, and service life.

The four approaches were instrumented to varying levels as shown in Figure 4.46. At Approach #1 (Geoweb), all eight accelerometers and two high-speed video cameras were installed. The accelerometers were placed at varying locations 10 to 80 feet from the bridge abutment with the goal of determining if track behavior changed from the approach to open track. The two video cameras were located about 10 and 50 feet from the bridge abutment to compare differences in track behavior between the approach (10 ft) and open track (50 ft).

At Approach #2 (HMA), three high-speed video cameras and eight accelerometers were used to capture the approach response. The video cameras were placed about 14, 23, and 53 feet (4.3, 7.0, and 16 meters) from the bridge abutment and the accelerometers were placed at various distances on the bridge, approach, and open track (Figure 4.46b). The accelerometers were only used on the 18 April 2016 trip but video cameras were used on all three trips to evaluate changes in displacement over time.

At Approach #3 (Geoweb) and Approach #4 (Grout), only high-speed video cameras were used. Five ties were recorded in Approach #3 (Geoweb) on 19 July 2016 while six ties were recorded in Approach #4 (Grout) on 18 April 2016.

The recorded trains varied in type, weight, and length but all had velocities ranging from 15 to 25 mph. To reduce the influence of train type and weight, the locomotives are emphasized in the results as they will have the most consistent weight. Train direction is not observed to influence the displacements or acceleration results.

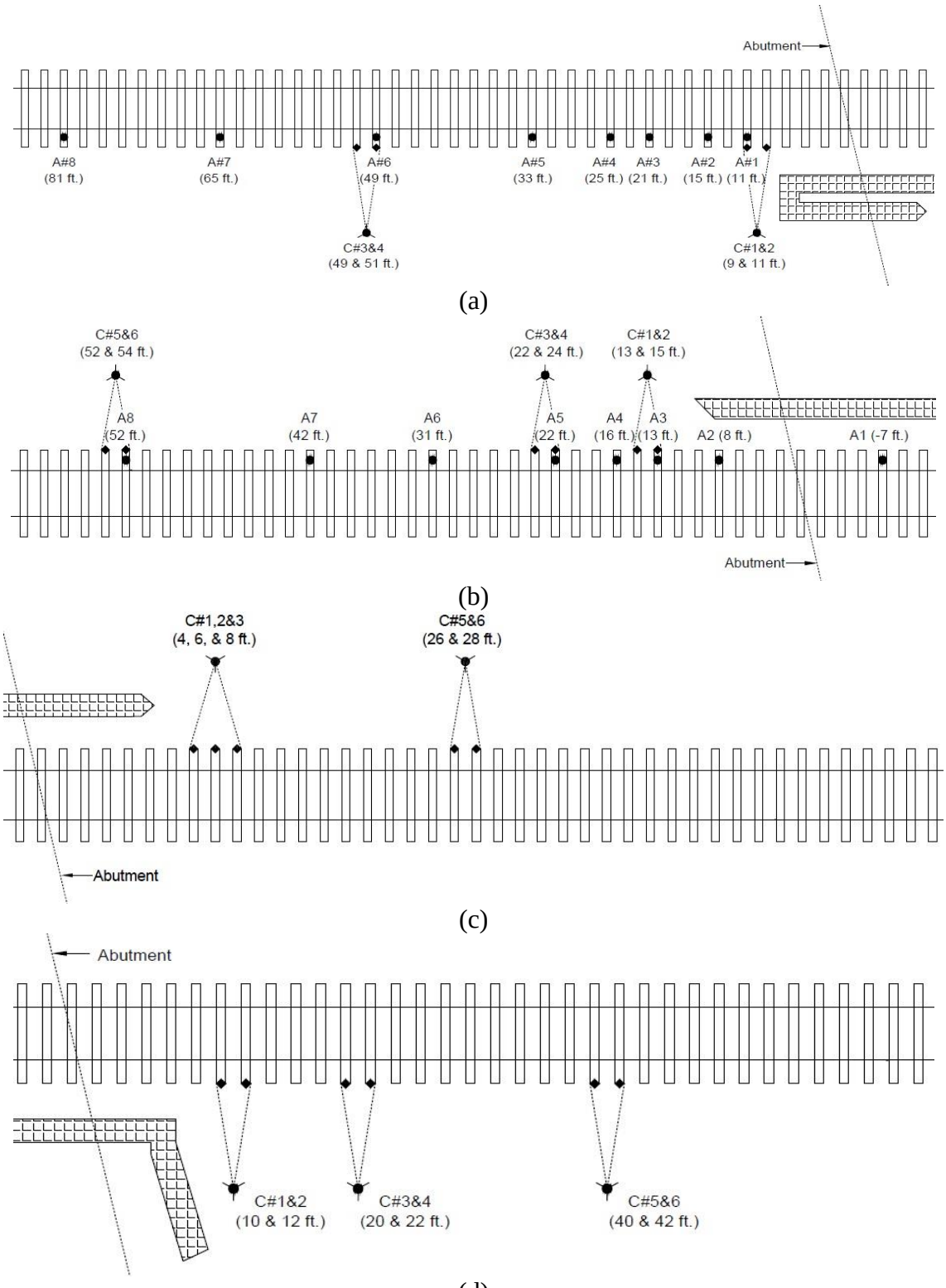

Figure 4.46: Instrumentation layouts at: (a) Approach #1 (Geoweb) on 16 November 2015, (b) Approach #2 (HMA) on 18 April 2016, Approach #3 (Geoweb) on 19 July 2016, and (d) Approach #4 (Pre-existing Grout) on 18 April 2016.

Site #8 performed three analyses that are discussed below:

(8a) compare the displacement behavior along the track at four transition zone locations,
(8b) compare the displacement behavior at Approach #2 (HMA) with time, and
(8c) compare the acceleration behavior along the track for Approach #1 (Geoweb) and Approach #2 (HMA).

To compare the performance of these four bridge approaches, the peak tie displacements are compared to assess the effectiveness of the Geoweb, HMA, and pre-existing subgrade grout remedial measures. The subgrade grout is used as the "control" approach. To avoid differences in peak displacement from varying train weights, the peak displacement magnitudes from the leading locomotives are used because the locomotives applied similar loads.

A comparison of peak transient locomotive tie displacements is displayed in Figure 4.47(a). The results show consistent peak locomotive transient tie displacements of about 3 to 4 mm (0.1 to 0.15 inches) at Approach #1 (Geoweb), which suggests consistent track behavior along the track. Approach #2 (HMA) shows larger transient tie displacements (10 mm or 0.4 inches) near the edge of the concrete curbs but these displacements quickly reduce to only 1 mm (0.04 inches) in the open track. This suggests the track at the edge of the curb is not well supported. Approach #3 (Geoweb) displayed similar behavior as Approach #2 (HMA) with large displacements (11 mm) at the edge of the curbs and then a stiff open track. The cause of the increased transient displacements for the HMA approach, e.g. ballast, subballast, and/or subgrade, is not known but could be from inadequate compaction of the ballast/subballast or increased loading. Approach #4 (Grout) showed about 4 mm (0.15 inches) of transient tie displacement near the curb and remained near constant in the open track.

Figure 4.47(b) shows the change in peak locomotive transient tie displacement over time in Approach #2 (HMA). The results show a gradual increase in tie displacement with time. It is likely that the poorly supported ties at 13-ft and 15-ft from the abutment are causing the train load to be passed to ties further from the abutment, which progressively spreads poor tie support conditions away from the abutment. This can gradually increase the loads on these ties and increase ballast settlement further from the abutment. Subgrade settlement could be a second explanation as both Approach #2 (HMA) and Approach #3 (Geoweb) were installed on new track while Approach #1 (Geoweb) and Approach #4 (Grout) were installed on an existing line.

The accelerations measured at Approach #1 (Geoweb) are displayed in Figure 4.48. The results show the average peak tie accelerations for all eight locations along with peak tie accelerations from Approach #2 (HMA). The results show all of the monitored ties exhibit tie accelerations below 5g, which indicates a smooth load transfer to the ballast and little slack or transient movement in the track, i.e., good tie support. Isolated peak accelerations represent wheel irregularities or wheel/rail movement and are not considered representative of track structure performance. The greatest tie accelerations were observed at Accel #1 (11 ft.) at Approach #1 (Geoweb) and Accel #3 (13 ft.) at Approach #2 (HMA). While observed at similar distances from the abutment, the causes of the higher accelerations appear to be different. The higher acceleration at Approach #1 (Geoweb) is likely caused by the accelerometer being placed at a tie location that is moving independently from the rest of the tie, i.e., a tie splinter or split. This tie defect or split will produce local vibrations that increase the tie acceleration at that particular location on the tie. An unsupported tie is the attributed cause to the higher acceleration in Accel #3 (13 ft.) in Approach #2 (HMA).

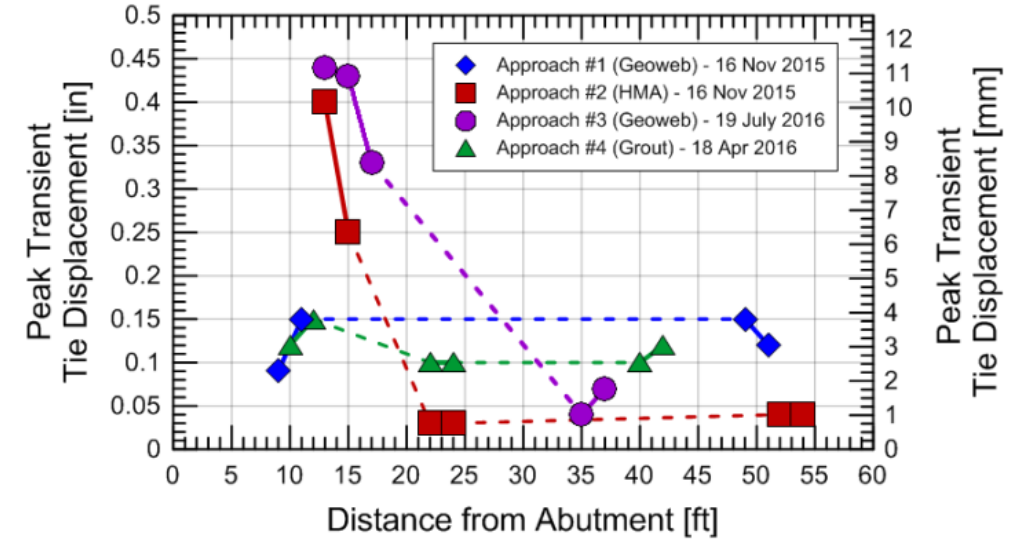

(a)

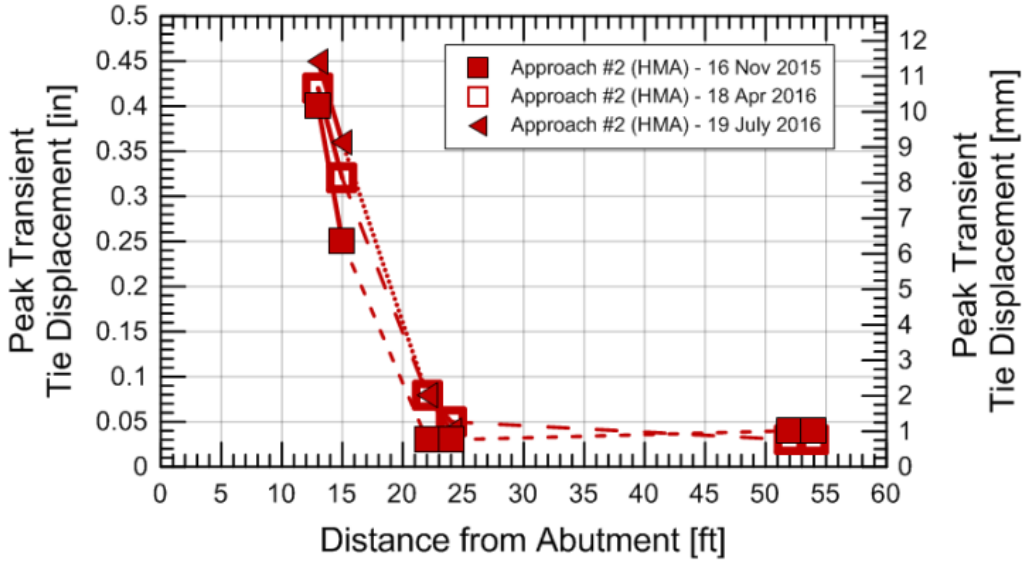

(b)

Figure 4.47: **Transient tie displacement from: (a) Tie #1 (13 ft.) and (b) Tie #6 (54 ft.) in Approach #2 (HMA) from a loaded freight train on 16 November 2015, (c) peak locomotive transient tie displacements for all four approaches, and (d) peak locomotive transient tie displacements at Approach #2 over time.**

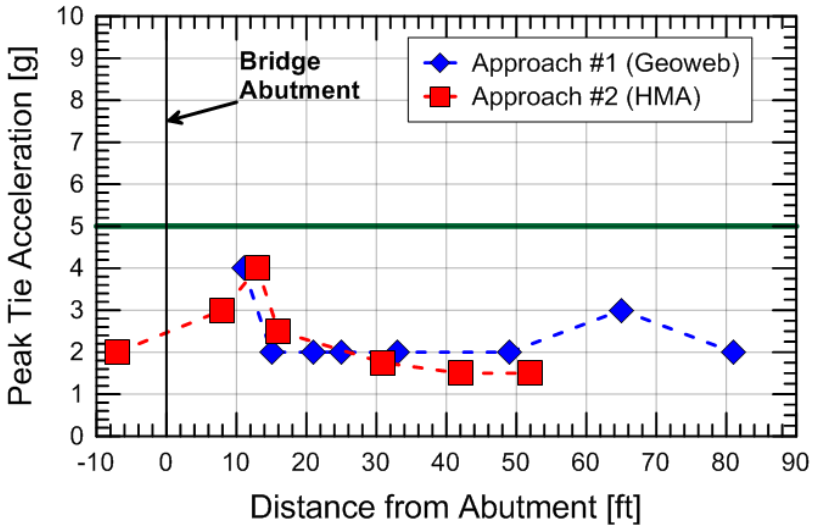

Figure 4.48: Average peak tie accelerations for Approach #1 (Geoweb) and Approach #2 (HMA).

Based on current measurements, all measured approaches have accomplished the design objective of a strong roadbed that allows smooth load transfer from the track to the subgrade. The primary difference between the approaches is the poorly supported ties near the end of the concrete curb on Approach #2 (HMA) and Approach #3 (Geoweb), which is not displayed on Approach #1 (Geoweb) and Approach #4 (Grout). This may be attributed to inadequate compaction of the ballast, reduction in confinement at the end of the curb, or subgrade settlement because Approach #2 and #3 are located on a new line while Approaches #1 and #4 are located on an existing line with a subgrade that had already experienced train and environmental loadings. At this point, it is unclear whether the increased transient displacements near the curb at Approaches #2 and #3 will stabilize or if the transient displacements will cause increased loading and spread ballast degradation to a longer length of track. Site #3 showed similar behavior with larger transient track displacements near the bridge abutment but this track has maintained good geometry over 17 years with an annual load of 70 MGT.

A summary of Site #8 is listed below:

- Ballasted-deck bridges, wing walls, and underlayment of Geoweb and HMA were installed to limit approach settlements and balance displacements.
- Substructure settlement was observed at both ends of a newly installed line while no substructure settlement was observed at both ends of an existing line. This suggests the influence of the subgrade.

- Hanging ties were observed at both ends of the newly installed bridge, however, it is not clear whether track geometry problems will develop as a result.

4.5 Summary and Future Work

The second task involves instrumenting eight transition zone locations with a non-invasive instrumentation setup that measures tie displacement and acceleration. The stated objectives of Task II are the following:

(1) develop non-invasive monitoring system to evaluate the tie-ballast interface,
(2) use track instrumentation to gain evidence of increased loads in transition zones, and
(3) compare the performance of various transition designs.

4.5.1 Summary of Results

The first objective of Task II involved developing a non-invasive monitoring system to evaluate the tie-ballast interface. Chapter 4.2 introduces the instrumentation and the results are presented on Chapter 4.4. A summary is listed below:

- Accelerometers to measure tie accelerations were successfully used at eight site locations and high-speed video cameras to measure rail and tie displacement were successfully used at three site locations. The setup and analysis methods will continually be improved and show potential as a viable instrumentation setup.
- For sites with minimal track geometry problems, tie accelerations remain below 5g to 10g and do not show signs of impacts. More data would be required before conclusive thresholds can be proposed, but a clear difference in behavior between track with minimal track geometry problems and sites with reoccurring track geometry problems suggest tie acceleration can be used as an indicator of track performance.
- Tie displacements are useful for determining the change of displacement along the track and can identify regions of unsupported ties.
- Tie accelerations provide complementary information to tie displacements and can measure impacts, vibrations, and movements that affect the tie. Analyzing tie acceleration records are more complex that displacements and interpretation expertise is required, but it allows for a full diagnosis of track behavior and the potential loading environment.
- Train velocity appears to increase tie acceleration by about 0.1g/mph to 0.15g/mph in track with poor track support and is the most consistent influential factor. Train load, type, and direction are believed to have an influence in certain situations but more data is required before conclusions can be made.

The second objective of Task II involved investigating potential increased loads in track transition zones. The sites used for this analysis are presented in Chapters 4.4.5 and 4.4.6. A summary is listed below:

- Comparing with LVDT measurements at Site #5, a peak in tie acceleration was measured at the instant a concrete tie is believed to have impacted the ballast. The force value is not known, but this suggests the potential for impacts at unsupported ties.
- Analyzing the tie acceleration at multiple locations at Site #6, show much variation with distance and time. This suggests uneven support and load distribution that changes with time.

The third objective of Task II involved comparing the effectiveness of transition designs. All visited sites and their results are presented in Chapter 4.4. A summary is listed below:

- Four sites with minimal track geometry problems had the following transition designs: ballasted-deck bridges, concrete wing walls, HMA or geoweb underlayment, and a compacted subgrade or fill. The purpose of these designs is to balance the transient and permanent displacement between the approach and bridge.
- Under-tie pads (UTPs) appear to have helped reduce the degradation of track geometry at a site that has had historical track geometry problems.
- Superstructure fixes such as increased tie lengths did not appear to mitigate problems. Their benefits are unclear from this study.

4.5.2 Future Work

The non-invasive instrumentation setup developed for Chapter 4 was capable of providing information about track behavior. Continual upgrades of instruments and analysis techniques will improve the setup and its ability to monitor track performance. Suggestions for future work include:

- The incorporation of pressure plates and WILD data, i.e. fixed location measuring dynamic wheel loads, in the analysis. Despite the difficulties of installing pressure plates, this will allow for a better understanding of the relation between tie acceleration and ballast pressure.
- Long-term or continual monitoring of a single location. The multiple site visits at Site #6 and Site #8 provided information on not only the behavior of track at a single time-frame, but how it changes over time. This would be especially helpful for newly installed transition zones and would answer many questions of the depth at which the majority of

settlement occurs, how magnitude of settlement, and whether it is temporary or is expected to continue over time.

CHAPTER 5

TASK III: NUMERICAL MODELING

5.1 Introduction

The third task involves numerically simulating open track and transition zone locations based on the geometry and field data collected in Task I. The simulations involve both static and dynamic analyses and the dynamic analyses incorporate the train truck, rails, ties, ballast, and subgrade.

The objectives of Task III are to:

(1) develop and calibrate both static and dynamic numerical models to determine the Young's Modulus values within the substructure,
(2) use numerical model to identify evidence of increase loads from unsupported ties in the open track and transition zone, and
(3) simulate the progressive settlement of a railway bridge transition zone.

The main impetus for the parametric analyses (Objective 2) is to thoroughly investigate the conditions that can potentially increase wheel and tie loads in transition zones. This can lead to a better conceptual understanding of how the wheel load gets distributed throughout the track system and the conditions that can lead to increased loads. This information can be used to better determined which metrics and track locations should be measured for future field instrumentation setups. The progressive settlement analysis aims to evaluate tie loading and settlement behavior of a transition zone with time instead of assuming a ballast surface profile at a single time-frame. It is suspected that the assumed ballast surface profiles in the parametric analyses will not be representative of physical conditions so the progressive analyses is anticipated to give more representative results.

Chapter 5.2 first introduces the software used for the numerical simulations. The methodology and results from the static inverse analysis is presented in Chapter 5.3. Chapter 5.4 involves the introduction and calibration of an open track model while Chapter 5.5 uses the model to investigate increased loads in the open track. Chapter 5.6 introduces a transition zone model and runs various simulations to investigate increased loads. Chapter 5.7 presents a progressive settlement analysis of a railroad transition zone. A summary of results is presented in Chapter 5.8.

5.2 Software Introduction

Railroad track is a highly complex structure whose analysis involves the interaction between train wheels, rail, fastening systems, ties, ballast, and subgrade. Historically, modeling the track system usually involved either the superstructure, e.g. rail, fastening systems, and ties, or substructure, which includes the ballast and subgrade. To add further complexity, ballast consists of discrete particles of rock that interact in a non-linear manner that cannot be directly replicated by commonly used continuum models beyond highly specific laboratory tests (Salim and Indraratna, 2004; Indraratna et al., 2012). As numerical methods continue to advance, coupling discrete element techniques to model the ballast behavior with continuum methods to model the trains, track superstructure, and subgrade will be desirable. However, these techniques are not advanced enough at this time to be beneficial for this study.

Therefore, two continuum software packages are used to simulate track behavior. The first software package, FLAC3D, is only used for static analyses to back-calculate material properties of the substructure. The second software package, LS-DYNA, is used for dynamic analyses to investigate load distribution and simulate a progressive settlement analyses of a railroad bridge transition zone.

5.2.1 FLAC2D and FLAC3D

FLAC3D v.5.0 (Itasca 2012) is a three-dimensional finite difference method (FDM) software package that specializes in geotechnical continuum problems. It is distributed by the Itasca Consulting Group in Minneapolis, Minnesota. and FLAC stands for Fast Lagrangian Analysis of Continuum. This package is capable of simulating static, dynamic, and hydro-mechanical behavior. The FISH (FLAC-ish) coding language component of FLAC3D allows the user to control almost all aspects of the analysis, including user-defined material models and complex geometries. Other researchers have used FLAC3D to investigate the effect of high-speed trains on transition zones, e.g., Smith et al. (2006) and (2007); Lobo-Guerrero and Vallejo (2006). One limitation of FLAC3D is the difficulty of modeling the superstructure, i.e., rails and ties, because of the increase in execution time when these components are included

In this project, FLAC3D is used for the static inverse analysis to estimate material stiffness or modulus values of the five substructure layers using field measured vertical displacements and wheel loads introduced in Chapter 3. FLAC3D was selected for this analysis

because the FISH coding language allows for complete automation of the static inverse analysis of material stiffness and calibration of the model. This automation is not possible with other track software packages, such as LS-DYNA, GEOTRACK, PLAXIS, etc., because user's cannot introduce code to these packages to automate the inverse analysis, which necessitates time consuming manual iteration.

5.2.2 LS-DYNA

LS-DYNA is a three-dimensional finite element method (FEM) program distributed by Livermore Software Technology Corporation (LSTC) that specializes in non-linear transient dynamic finite element analysis. LS-DYNA stands for the Livermore Software DYNA program, which originated from the 3D finite element program DYNA3D. LS-DYNA is capable of modeling the entire track behavior along with the inclusion of train cars and wheel systems. Other researchers have used LS-DYNA to investigate the effect of freight trains of track systems, e.g., Nicks (2009) and Lundqvist and Dahlberg (2005).

LS-DYNA is used herein to perform dynamic analyses that simulate the entire track structure, train bogey or cart, rail, tie, ballast, and subgrade, and the coupled interaction. Because LS-DYNA is widely used in mechanical engineering applications, e.g. car crash simulations and metal stamping, it is well suited for complex geometries, moving vehicles, and dynamic contact forces.

5.3 Static Inverse Analysis of Field Modulus (FLAC3D)

FLAC3D is used to perform the static inverse analysis that estimates the modulus values of ballast, subballast, and subgrade from the measured field vertical displacements at the Amtrak instrumentation sites. This analysis has two main objectives: (1) estimate Young's Modulus values from the measured field data in Chapter 3 to improve analysis of field behavior, and (2) develop a sound static inverse analysis or modulus back-calculation methodology that can be implemented by other researchers in the future.

For comparison and modeling purposes, Young's Modulus is a more beneficial substructure layer parameter than mobilized stiffness (k_{mob}) because it is independent of layer depth and values can be compared against those determined from laboratory seismic wave

testing. The values can also be used as inputs for numerical models in the future that cannot be calibrated with field data.

Secondly, no agreed methodology for static inverse analyses exist in railroad track analyses so another objective is to illustrate the important factors affecting analysis results and how they influence final output values. The two main factors are non-linearity at the tie-ballast interface from tie-ballast gaps ($\delta_{P=0}$) and non-linear seating displacement (δ_{seat}).

FLAC3D was selected to back-calculate the layer moduli of the monitored railway transitions because the built in FISH (FLAC-ish) coding language allows complete automation of the static inverse analysis. This allowed a single code to perform all analyses without the need for manual iterations.

This section presents the following: (1) methodology of the static inverse analysis and important factors to consider, (2) comparison of various numerical software packages, (3) presentation and discussion of results, and (4) discussion of factors affecting the static inverse analysis.

5.3.1 Methodology

This section presents the methodology of the static inverse analysis using FLAC3D. This model is simpler than the LS-DYNA model used in subsequent analyses but it provides a good estimate of modulus for substructure layers that are advantageous when analyzing multiple sites. Therefore, assumptions such as static loads, symmetry about the rail and instrumented tie centerline, linearly elastic material models, and initial load distributions, e.g., 35%/22.5%/10%, are considered sufficient.

The static inverse analysis with FLAC3D involves a completely automated iterative scheme consisting of the following steps:

1. Creating a five-layer model representing the track and subsurface geometry.
2. Inputting measured wheel loads from measured data
3. Inputting initial estimate of modulus for all five layers
4. Executing the model and comparing outputted transient vertical displacements with measured transient vertical displacements
5. Select new modulus value for all five layers to develop better agreement between calculated and measured transient vertical displacements

6. Iterate until numerical and measured transient vertical displacements compare within an acceptable tolerance (0.01 mm).

One beneficial feature of instrumenting the selected Amtrak NEC sites is the similar subsurface geometry for all six sites. Each site consists of a five-layer system with no vertical or horizontal curves in the track. Therefore, symmetry along the rail and instrumented tie centerline is assumed. Because of these similarities, only layer heights and element densities (number of elements per linear foot) are required as geometric inputs for the FISH code. The geometry and finite difference mesh for Upland (60 ft.) is shown in Figure 5.1 as an example but similar models were created for all of the other instrumented sites.

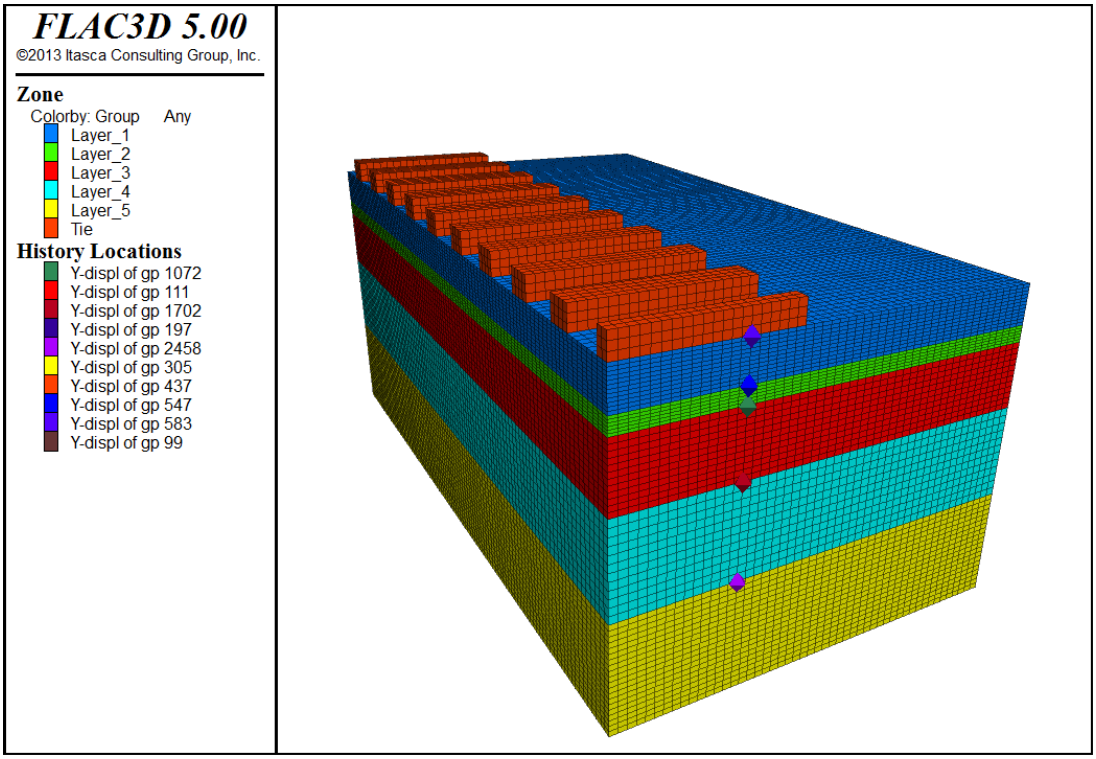

Figure 5.1: FLAC3D mesh for Upland (60 ft.) with LVDT locations shown with small diamonds.

The methodology for selecting input parameters of peak wheel load and measured transient displacement (Steps 2 and 4) are described in Chapter 3.6.5. From the field data, a mathematical relationship between wheel load and transient LVDT vertical displacement was developed to represent the behavior of each substructure layer as a function of applied load. This

method was chosen because the scatter of data and non-linear behavior of the soils can cause maximum values to not be representative of the overall layer behavior.

Due to the linear elastic mathematical representation of the substructure behavior at the Amtrak NEC sites, an arbitrary peak wheel load was assumed to facilitate comparison of the various analyses. As described in Chapter 3.6.5, 100 kN was selected because it is close to the average peak wheel load and is an easy value to work with and to compare with. To determine the transient displacements, the Equations 5.1 and 5.2 are used:

$$\delta_{LVDT\#1} = \frac{P}{k_{mob}} \tag{5.1}$$

$$\delta_{LVDT\#2-5} = \overline{\delta_{P=0}} + \frac{P}{k_{mob}} \tag{5.2}$$

where P is the wheel load (100 kN), k_{mob} is the mobilized LVDT stiffness of the particular layer, and $\overline{\delta_{P=0}}$ is the "apparent gap" of LVDTs #2 – 5.

One important factor that must be addressed during the analysis is non-linearity within the track system. As presented in Chapter 3.6, this non-linearity is often the result of tie-ballast gaps and the displacement required to mobilize frictional resistance in the substructure. However, the numerical model assumes ballast is linear elastic material so the bi-linear model cannot be used without leading to non-represented results. To address this issue, the displacement created from closing the tie-ballast gap ($\delta_{P=0}$) is omitted from LVDT#1 because it does not actually represent the displacement of the ballast. Figure 5.2 shows how this process eliminates the influence of the tie-ballast gap from the analysis to estimate k_{mob}. By only using k_{mob} in the ballast layer, the non-linear influence is eliminated and ballast layer will represent the mobilized ballast response and not tie-ballast gap closure.

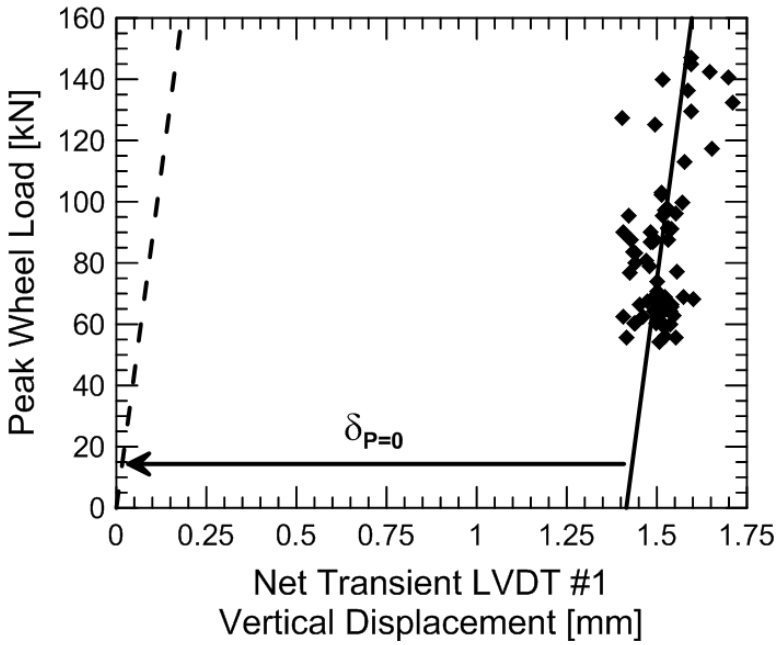

Figure 5.2: LVDT #1 force-displacement behavior of Upland (15 ft.) showing best fit line with and without tie-ballast gap included.

Initial modulus values are inputted into the FISH code and the model is executed until equilibrium is reached. The FISH code then outputs the relative displacement between each LVDT, which are compared to the measured vertical displacements. The difference between the numerical and field displacements of each LVDT is calculated and checked to determine if they are below a specified tolerance (0.01 mm). If not, new modulus values for all five layers are calculated and the process repeated until the difference between the numerical and field transient displacements for all five layers are below the specified tolerance (0.01 mm).

The equation to estimate the new modulus values is:

$$E_{new} = E_{old} * \left(\frac{\delta_{num} - \delta_{field}}{\delta_{field}} \right) \tag{5.3}$$

where E_{new} is the new or updated modulus value, E_{old} is the previous modulus value, δ_{num} is the numerical displacement measured by FLAC3D, and δ_{field} is the field displacement calculated using the methodology in Chapter 6.5. Each inverse analysis requires about 20 minutes to perform due to the automated nature of the analysis in FLAC3D.

A second factor that must be addressed is the load distribution amongst the ties. In this analysis, the distribution of 35%/22.5%/10% is assumed and this is within the range expected of well-supported ties. For unsupported ties, this value will differ and this is discussed in Chapter 5.5.

5.3.2 Comparison with Other Software and Testing Methods

To ensure reliable results, the FLAC3D static inverse analysis modulus values are compared with results from other software and testing techniques. Using the same process as described above, the modulus values are back-calculated using the track software packages GEOTRACK and LS-DYNA. Also, surface wave testing performed during another FRA project (Stark et al., 2016) provides a range of modulus values for ballast and subgrade materials and used for comparison with the inverse analyses to ensure reasonable values are derived.

An example inverse analysis is described in this paragraph to illustrate the process. The example analysis consists of the data recorded from Upland (60 ft.) on 29 January 2013. Upland (60 ft.) was chosen because it displayed the best tie support and track behavior. This means the assumed initial load distribution of 35%/22.5%/10% likely applies and the influence of the gap is smaller than compared to the other NEC sites. The subsurface profile is shown in Figure 5.3. Table 5.1 presents the layer heights and net transient vertical displacements and cumulative transient vertical displacements for each layer.

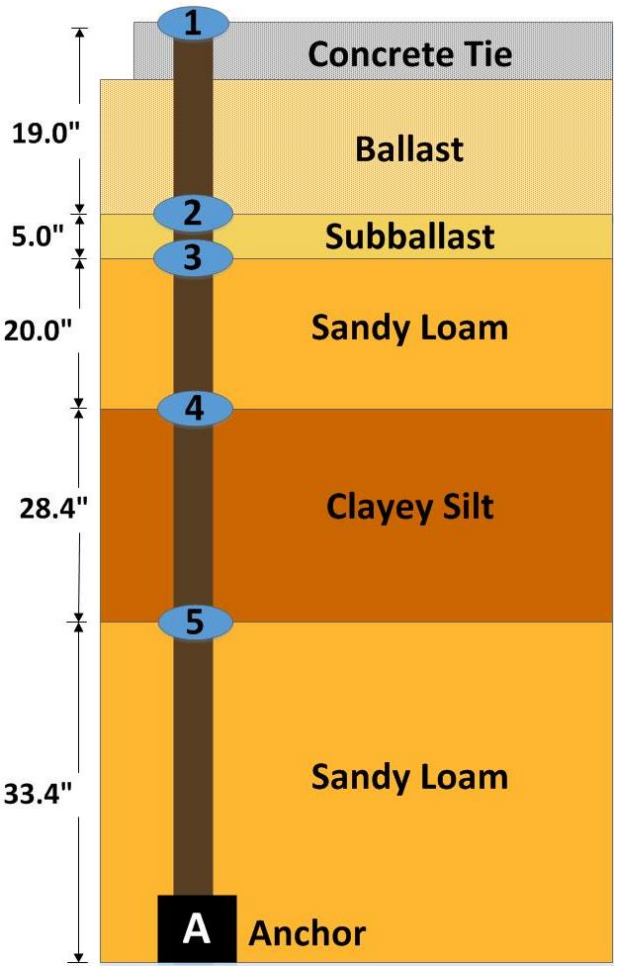

Figure 5.3: **Subsurface profile for MDD location 60 feet north of the Upland Street Bridge (Upland (60 ft).**

Table 5.1: **Substructure values for Upland (60 ft.) on 29 January 2013**

Layer Number	MDD Depth [m]	Layer Thickness [m]	Net Layer Transient Vertical Displacement [mm]	Cumulative Layer Transient Vertical Displacement [mm]
1 - Ballast	0.305	0.305	0.114	1.078
2 - Subballast	0.432	0.127	0.099	0.964
3 – Sandy Loam	0.940	0.508	0.366	0.865
4 – Clayey Silt	1.661	0.721	0.336	0.499
5 – Sandy Loam	2.510	0.849	0.163	0.163

A plan view of the GEOTRACK model and the LS-DYNA mesh used for this analysis are shown in Figures 5.4 and 5.5, respectively. The FLAC3D mesh is shown in Figure 5.1. In GEOTRACK and LS-DYNA, a standard track gauge of 4 feet 8.5 inches and a 136 RE rail are used.

Because GEOTRACK, FLAC3D, and LS-DYNA are all three-dimensional software packages, the actual depth and location of the LVDTs in the MDD string were used in the model. The LVDT depths are shown in Table 5.1 and the MDD is about 3 ft. (0.919 meters) from the center of the tie or 1 ft. and 4 inches (0.381 meters) from the edge of the tie. This location corresponds to the region under Segment #2 in a GEOTRACK analysis (see Figure 5.4). The closest elements and nodes to this location were used to obtain results from FLAC3D and LS-DYNA for comparison with the GEOTRACK results. For example, the Upland (60 ft.) locations of the LVDTs in the MDD string in the FLAC3D mesh are shown in Figure 5.1. In all three software models symmetry is assumed along both the track and Tie 1 centerline to reduce computational complexity.

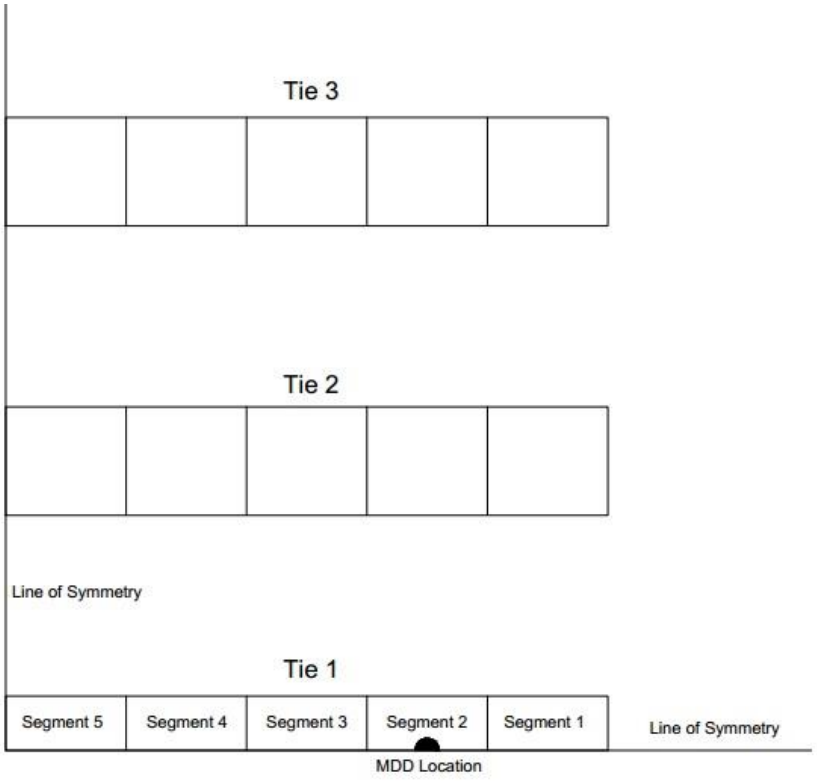

Figure 5.4: Plan view of track model used in GEOTRACK simulation.

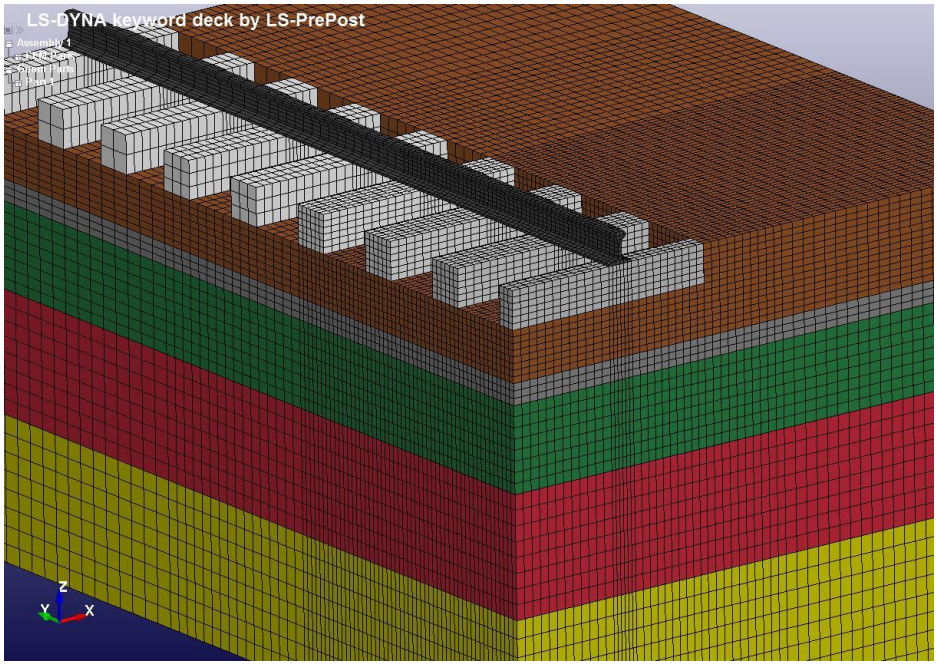

Figure 5.5: LS-DYNA Model for Upland (60 ft.) showing rail and portion of concrete tie.

After completing the iteration process, the final modulus values for all five layers at Upland (60 ft.) on 29 January 2013 are shown in Table 5.2. While there is some variation, the values are relatively close to each other. Differences are likely due to small variations in how the load is distributed amongst the ties.

Table 5.2: Comparison of inverse analysis modulus values for Upland (60 ft.) on 29 January, 2013 at 10:21 A.M.

Layer Number	GEOTRACK [MPa]	FLAC3D [MPa]	LS-DYNA [MPa]
1 - Ballast	171	202	201
2 - Subballast	238	210	278
3 – Sandy Loam	30	30	22
4 – Clayey Silt	32	34	27
5 – Sandy Loam	60	56	47

A second technique to verify the static inverse analysis modulus results is to compare the values in Table 5.2 against other methods for estimating modulus, such as seismic surface wave testing. The ballast modulus from seismic surface wave testing is displayed in Table 5.3 and ranges from 138 to 380 MPa depending on the condition of the ballast. Therefore, the ballast

modulus value of 202 MPa from FLAC3D is in agreement with seismic testing results for ballast that is fouled to clean and slightly wet.

Table 5.3: Range of ballast modulus values obtained from seismic surface wave testing

		Clean ballast	Dry fouled ballast	Wet fouled ballast
Modulus	**[MPa]**	220 – 260	345 – 380	138 - 172

5.3.3 Results

This section presents the results of the static inverse analysis for all six instrumented sites along the Amtrak NEC in Chester, Pennsylvania. Data for this analysis was obtained during four different site visits.

The soil profiles used for these analyses are shown in Chapter 3.2.1 (Figures 3.2 to 3.4) and the transient LVDT vertical displacements are calculated using the methodology and results presented in Chapter 6.5. The modulus values for each layer from the static inverse analyses are shown in Tables A.1 through A.7 in Appendix A.. The results show a wide range of ballast modulus values from LVDTs #1 and #2 while moduli are similar for LVDTs #3 through #5.

The modulus values for each layer are compared to investigate the variation in modulus across the six instrumentation test sites. For example, all of the modulus values for LVDT#1 are compared for the six sites because LVDT#1 is representative of the ballast layer at each of the six sites. LVDT#2 is representative of the subballast layer while LVDTs #3 through #5 yield the modulus of the subgrade layers.

Figure 5.6 compares the modulus values of LVDT#1 (ballast) for all six instrumentation sites for the four different months when data was collected. The red lines show the range in ballast moduli calculated from seismic surface wave testing (140 MPa to 380 MPa) from another FRA project. The numerical values are also displayed in Table A.1 in Appendix A.

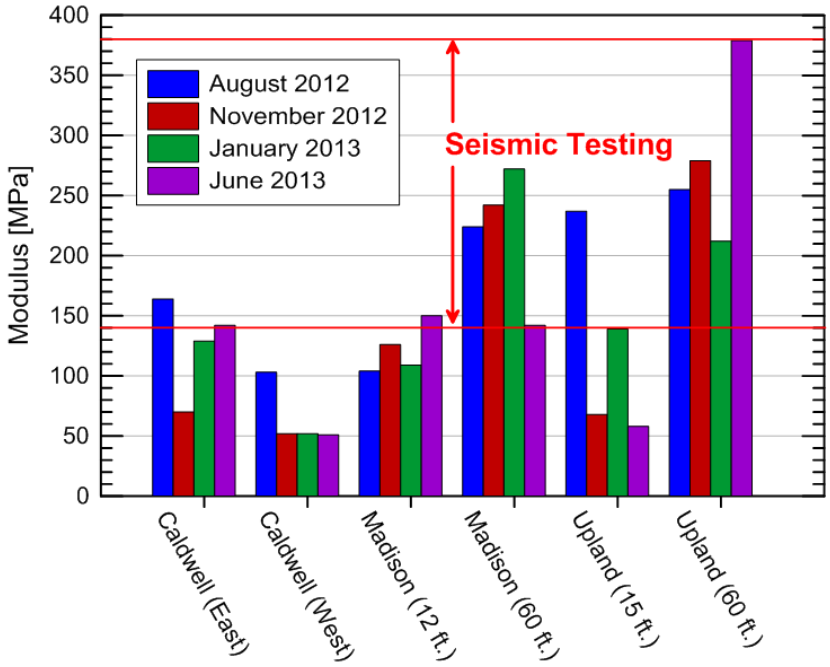

Figure 5.6: **LVDT #1 (ballast) modulus values from static inverse analysis with FLAC3D compared against seismic testing results.**

The results show the majority of ballast moduli fall within the range of values calculated from seismic surface wave testing. Madison (60 ft.) and Upland (60 ft.) report ballast modulus values that are in the best agreement with the seismic testing results. These sites likely contain clean or slightly fouled ballast because they are outside the transition zone. Caldwell (East) and Madison (12 ft.) yielded ballast modulus values along the lower bound of wet highly fouled ballast moduli from the seismic testing. Therefore, it is likely that these two sites are highly fouled and wetted, which was confirmed by field observations. The lower modulus values calculated at Caldwell (East) and Upland (15 ft.) also may be due to very high levels of fouling or load distributions differing from the assumed 35%/22.5%/10% distribution.

The results also show ballast modulus values can vary significantly by month with Upland (15 ft.) showing the largest variation. Because Upland (15 ft.) displays the most unsupported behavior, it is likely the load distribution changes from month to month as the tie reaction does in a similar pattern for Upland (15 ft.).

Figure 5.7 compares calculated modulus values for the subballast, i.e., LVDT#2, for all six instrumented sites for the four months of collected data. The subballast layer (LVDT#2) also exhibits a large variation in modulus with values ranging from 45 MPa to 297 MPa. However,

the large variability is between different sites not at the same site. This may reflect the importance of different material type in the subballast layer on the measured transient vertical displacements and thus the modulus values calculated using the FLAC3D inverse analysis. For example, "hardpan" may be stiffer than fouled ballast with wet plastic silty clay or silty sand. While there are exceptions, the subballast modulus values are relatively consistent with time for a particular site, which may indicate those sites are experiencing better drainage than sites that show variability with time. Some of the instrumentation sites, e.g., Upland (15 ft.), may not be quickly draining precipitation from the subballast and/or underlying layers as evidenced by water seeping through the masonry retaining walls well after a precipitation event. Otherwise a particular site should be expected to yield consistent modulus values because the approach fill material has been in-place for a significant amount of time at the NEC instrumentation sites.

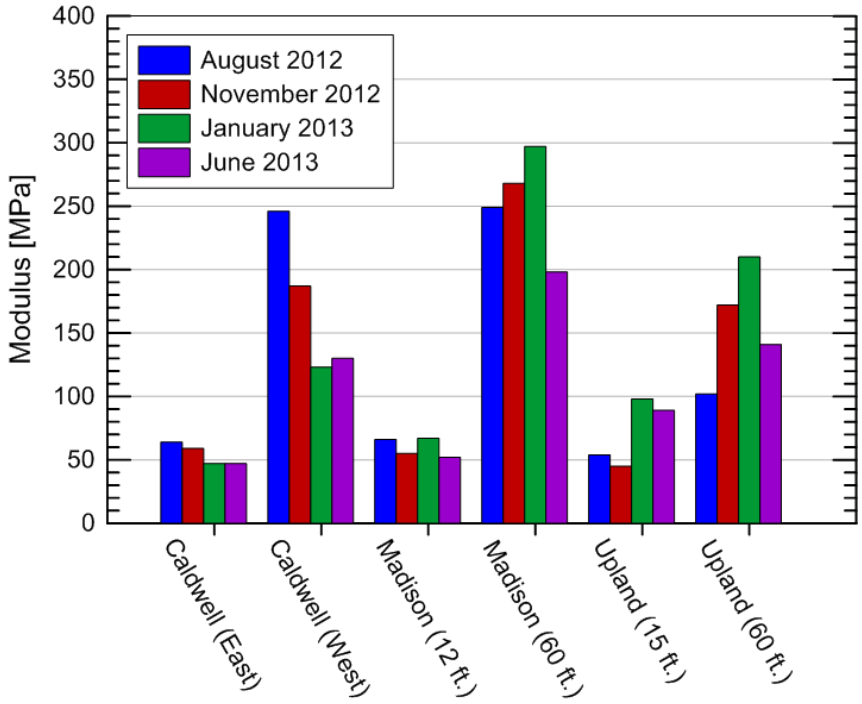

Figure 5.7: LVDT #2 (subballast) modulus values from static inverse analysis with FLAC3D .

Figures 5.8 through 5.10 show the calculated modulus values of the subgrade layers (LVDTs #3, #4, and #5) for all six instrumented sites for the four months of collected data. The red lines show the range in subgrade moduli calculated from seismic surface wave testing (20 MPa to 100 MPa).

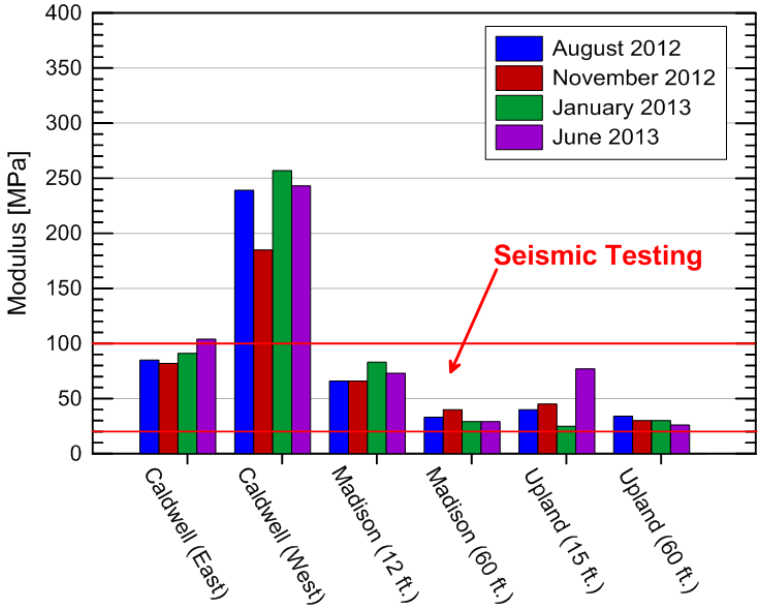

Figure 5.8: **LVDT #3 (subgrade) modulus values from static inverse analysis with FLAC3D compared against seismic testing results.**

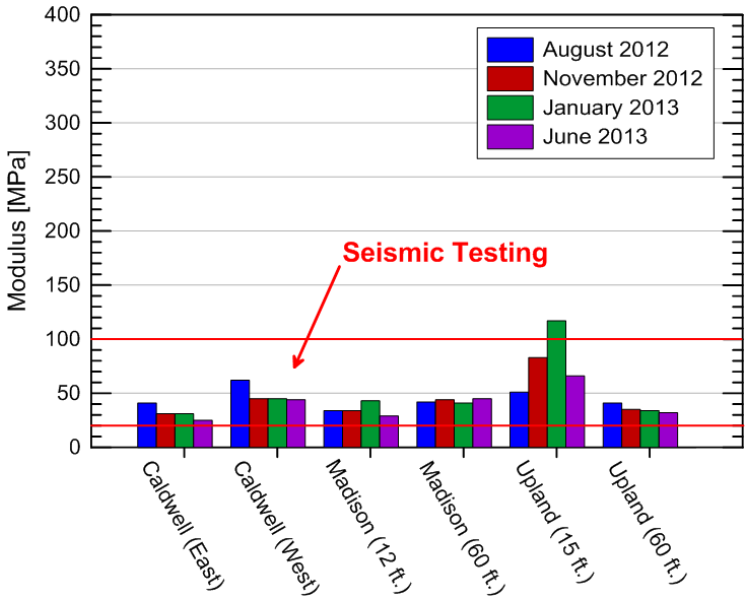

Figure 5.9: **LVDT #4 (subgrade) modulus values from static inverse analysis with FLAC3D compared against seismic testing results.**

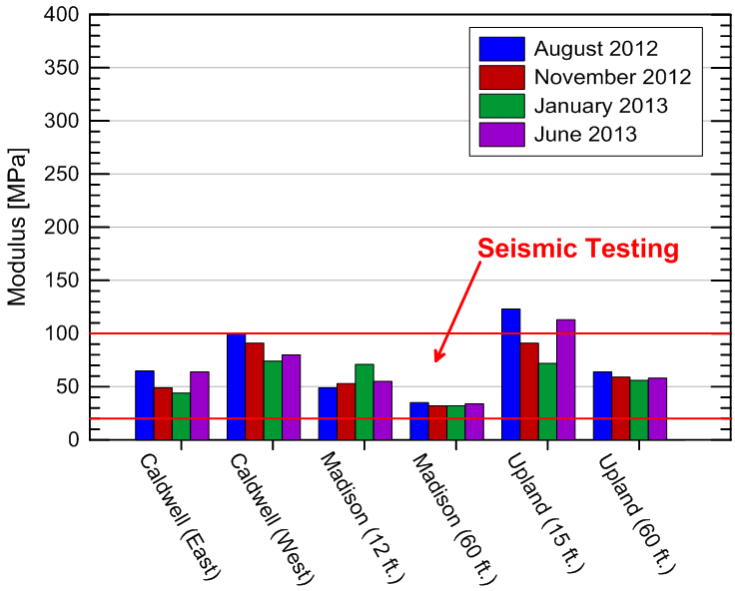

Figure 5.10: LVDT #5 (subgrade) modulus values from static inverse analysis with FLAC3D compared against seismic testing results.

Besides Caldwell (West), all subgrade layers fall within the expected range of 20 to 100 MPa from the seismic surface wave testing of subgrade soils. The Caldwell (West) site may be different because of the material makeup of the soil.

5.3.4 Summary of Static Inverse Analysis

In summary, FLAC3D was used to estimate the in-situ modulus of the five substructure layers at each instrumentation site using static methods. The analysis addressed the influence of the tie-ballast gap to ensure a representative ballast modulus value. The values agree with common laboratory and seismic testing values.

5.4 Dynamic Model Calibration

The section introduces the dynamic finite element model that is used for the remainder of Chapter 5. The numerical software package LS-DYNA was used because it can simulate complex geometries, moving vehicles, and contact surfaces.

This subchapter will (1) introduce the open track model that simulates Upland (60 ft.) in Chapter 3, (2) validate model with a single wheel, (3) validate model with two wheels, and (4) calibrate the model with field data from Upland (60 ft.). The calibrated model will be used for

open track parametric analyses in the next section (Chapter 5.5) and the transition zone analyses in Chapter 5.6 and Chapter 5.7.

5.4.1 Numerical Model

The finite element mesh for the Upland (60 ft.) site (Site #1) is shown in Figure 5.11 and consists of a moving wheels, 136-RE rail, 34 concrete ties, and a substructure that consists of five layers that represents the Upland (60 ft.) instrumented site in Figure 5.3. All elements are modeled as linear-elastic and a line of symmetry is assumed at the track centerline to limit model size and reduce execution time. Of the 34 ties incorporated in the model, only Ties 16 through 24 are of interest in the analysis and the instrumented tie at Upland (60 ft.) is located at Tie 19 for calibration purposes.

The wheels are modeled as a semi-thin-walled cylinder (see Figure 5.12) that moves along the rail at a velocity of 110 mph, which is the operating speed of the Amtrak high-speed trains at the Upland Avenue Bridge. The density of the wheel is such that it applies a static wheel load of 100 kN for the parametric analyses. The rail geometry is modeled after continuous 136-RE rail with the density, Young's Modulus, and Poisson's Ratio representing the steel in a 136-RE rail, which are 7.85 g/cm^3, 200 GPa, and 0.28, respectively. The concrete ties have a spacing of 0.6 m (2 feet), a width of 0.23 m (0.75 feet), and density, Young's Modulus, and Poisson's Ratio matching the values of concrete, which are 2.97 g/cm^3, 21 GPa, and 0.15 respectively. Besides the symmetric boundary condition at the track centerline, the remaining boundaries are pinned and have non-reflective boundary conditions. The non-reflective boundary conditions absorb pressure and shear waves, preventing the pressure waves from reflecting back into the model. The boundary distances were selected to balance computation time and minimize boundary effects. Analyses used to determine the boundary length showed similar results for the selected distance and distances 6 m (20 ft.) greater (<5%) therefore the boundaries are considered sufficient to prevent boundary effects from influencing the model.

A moving wheel was selected over modeling the secondary suspension system with a rolling cart in the Upland (60 ft.) model because analyses with the rolling cart or bogie produced similar results but with ten times longer computational time because of the lack of symmetry and the springs and dashpots required to model the secondary suspension system. However, the full rolling cart is used for modeling the Upland Avenue Bridge transition (Site #2 below) because of

the increased dynamic wheel loads expected in the transition zone from coupling of the front and back axles so a secondary suspension system and coupled wheels are required.

Incorporating differential settlement and track discontinuities is a major focus of this study but to simplify track modeling, the only track defects assumed are tie-ballast gaps, where the bottom of the tie and top of the ballast are separate entities and modeled as contact surfaces. The tie-ballast gap is produced by reducing the vertical element size of ballast elements underneath the tie to replicate ballast settlement. An example is shown in Figure 5.13. The gap height is also assumed to be constant under a single tie. While this paper focuses on the tie-ballast gap, the mechanism of load redistribution can occur from any gap or defect within the track system, i.e. rail-fastener gap, fastener-tie gap, or from sudden changes in substructure modulus (Dahlberg, 2010). In addition, unsupported or poorly supported ties will likely have varying gap heights and ballast stiffness along a tie, which can influence load distribution within a single tie.

The three model outputs from the finite element mesh in Figure 5.11 are wheel-rail contact force, tie-ballast contact forces, and Layer 1 through 5 transient vertical displacements. The wheel-rail and tie-ballast contact forces are calculated using master-slave penalty methods. This method checks for penetration of slave surfaces, i.e. top of rail surface, through the master surface, i.e. bottom of wheel surface, and applies a proportional force to resist the penetration. These forces are defined as wheel-rail and tie-ballast contact forces.

For normalization purposes, the percentage of wheel load carried by the tie is calculated by dividing the tie reaction by the wheel load (load above crib). Assuming all track components are in intimate contact, this value typically ranges from 30 to 50% (AREMA, 2016). This is defined as the normalized tie load as shown in Equation 5.4:

$$Normalized\ Tie\ Load = \frac{Tie\ Reaction}{Wheel\ Load} \tag{5.4}$$

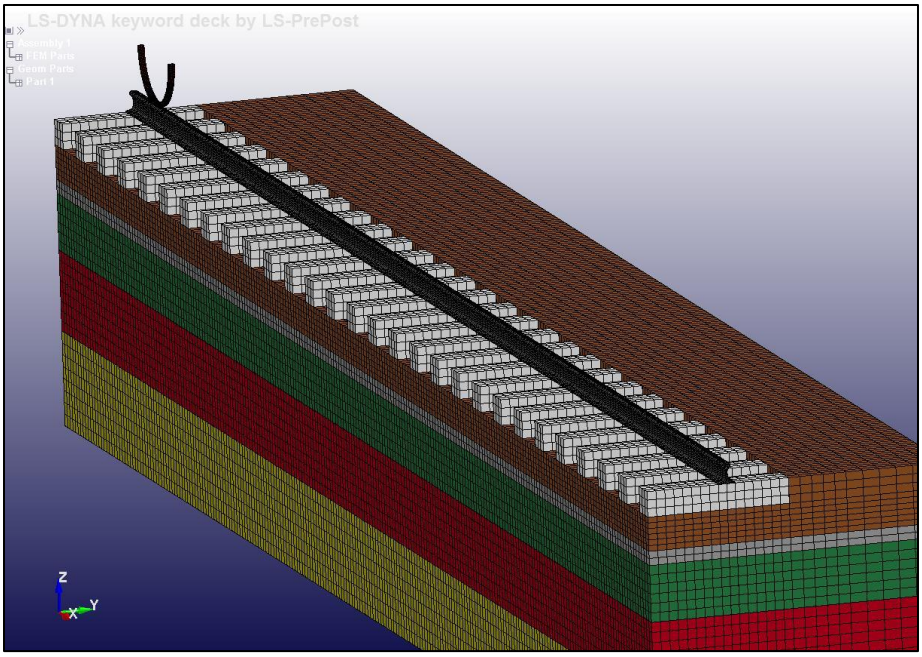

Figure 5.11: LS-DYNA model showing the open track with a sliding wheel.

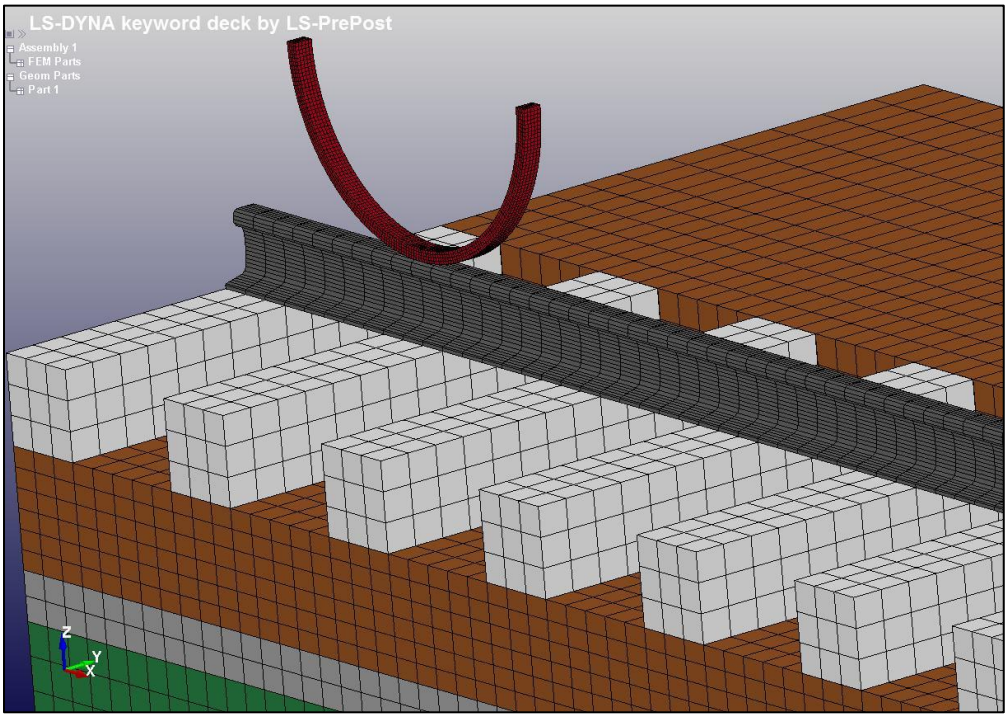

Figure 5.12: LS-DYNA model of wheel.

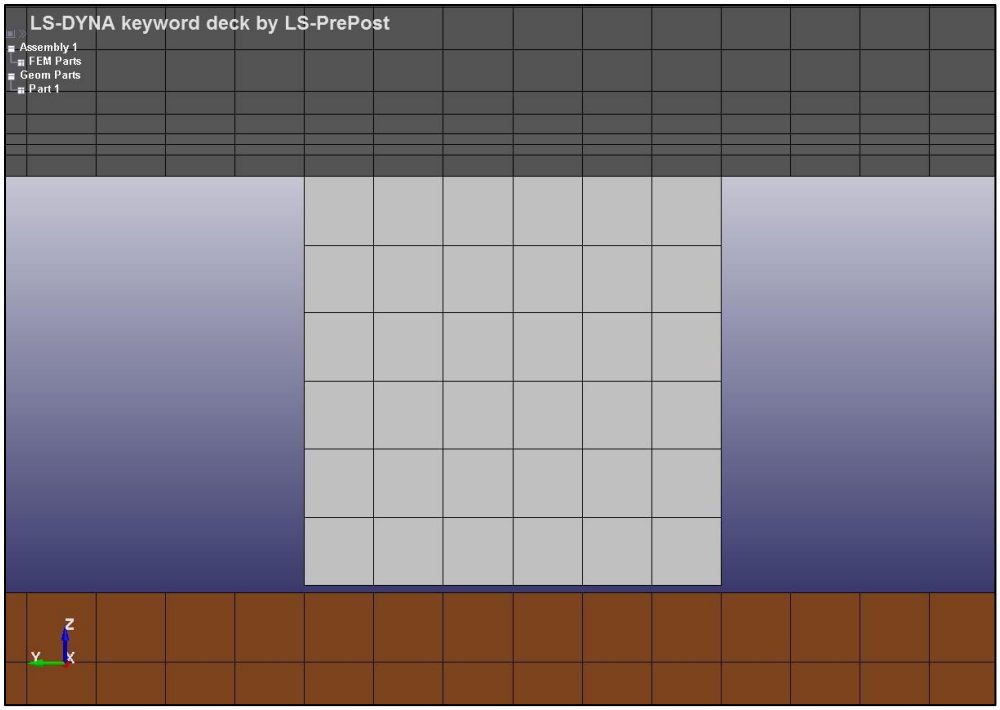

Figure 5.13: Tie-Ballast Gap in LS-DYNA.

5.4.2 Single Wheel

For verification purposes, the model first simulates the response of single wheel with no substructure settlement or tie-ballast gaps. This would be representing the situation in which the response is homogeneous along the track and the track response in linear elastic (Chapter 2.3.1).

For comparison with subsequent analyses that have tie-ballast gaps, the first analysis assumes intimate contact between all of the ties and ballast. This means the tie-ballast gap of the instrumented tie (Tie 19) and the surrounding ties are all set to 0.0 mm. This is commonly observed in railway track and is the assumption used in many existing track models, e.g., GEOTRACK, KENTRACK, etc. (Chang et al., 1980; Rose et al., 2014), so the results can be compared with previous analytical, experimental, field, and numerical results which show the underlying tie receives between 30 and 50% of the applied wheel load with intimate contact (Hay, 1982; Chang et al., 1980; Nicks, 2009; AREMA, 2016).

For the ideal situation of intimate contact between the ties and ballast, the wheel-rail contact force should remain close to the static wheel load throughout the analysis and the maximum tie-ballast contact forces of Ties 15 through 23 should roughly equal 40% of the wheel load, i.e. normalized tie loads of 40%. The time histories of the wheel-rail and tie-ballast contact

forces are shown in Figure 5.14. During the first 0.2 seconds of the analysis, the wheel-rail contact force of the stationary wheel matches the static wheel load, which confirms application of gravity. As the wheel begins moving at 0.2 seconds, high frequency loads are produced. These frequencies also exist physically and the model naturally damps them as the physical rail and tie do in the field. For plotting and comparison purposes, the wheel-rail contact force history is filtered using a 20 Hz filter, which eliminates frequencies above 20 Hz. The filtered and unfiltered responses are plotted in Figure 5.14. The calculated tie-ballast contact forces of ties extending four ties in front (Tie 15) and behind (Tie 24) of the instrumented tie (Tie 19) are also displayed. Filtered tie-ballast contact forces are not necessary because the rail and ties filter out a majority of the high frequency response observed in the wheel-rail contact force.

Once filtered, the wheel-rail contact force shows the wheel load remains close to the static value throughout the analysis. All measured ties show tie-ballast contact forces reaching peaks of about 40% of the wheel load, which is in agreement with previous studies (Chang, 1980; AREMA, 2016). This indicates good load distribution is occurring between ties within the model because all ties are in intimate contact with the ballast. Small differences in maximum tie-ballast contact force do exist and these are attributed to small oscillations in the wheel-rail contact force shown in Figure 5.14.

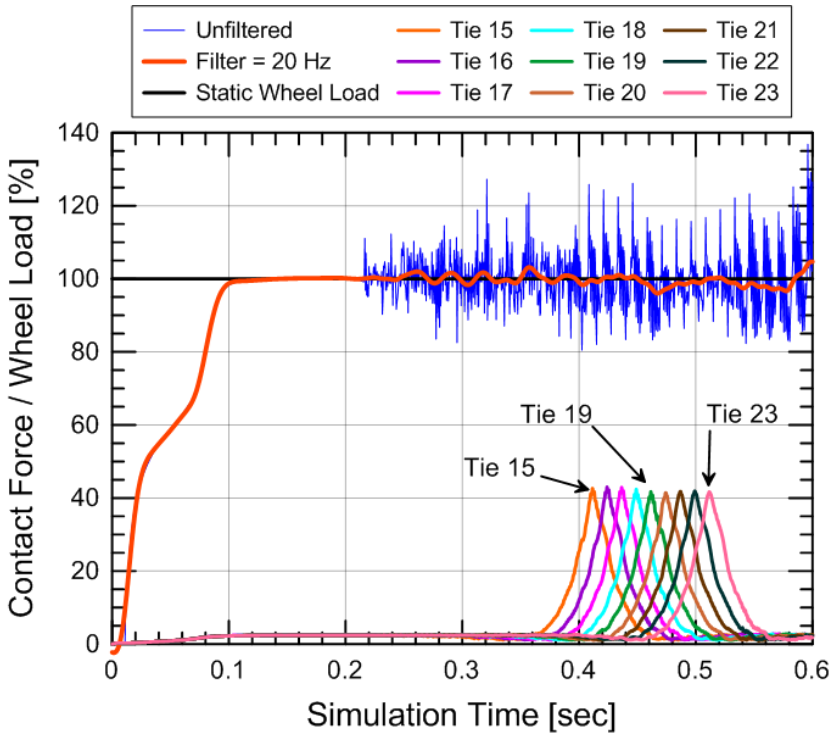

Figure 5.14: Wheel-rail and tie contact force time history. Unfiltered, 20 Hz filtered, and static load are shown.

Figure 5.15 shows the distribution of wheel load amongst the surrounding four ties at the exact timeframe when the wheel is directly over Tie 19 (0.461 seconds). The results show about 40% of the wheel load being applied to Tie 19, 22.5% of the wheel load being applied to Ties 18 and 20, and about 10% of the wheel load being applied to ties 17 and 21. The remaining 5% is taken by ties further away from Tie 19. This leads to the general load distribution of about 40%, 20%, and 10% between adjacent ties.

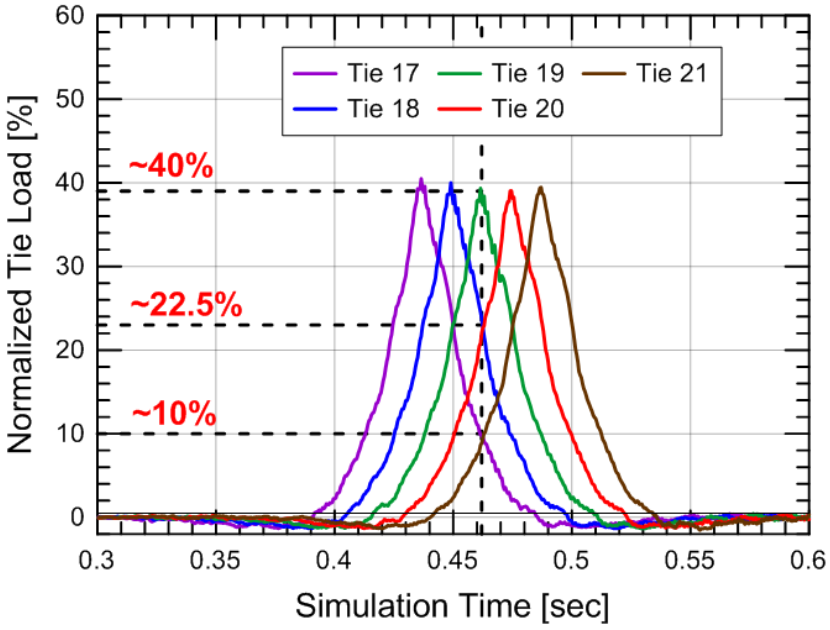

Figure 5.15: Load distribution at a single timeframe.

5.4.3 Two Wheels

The simulation of a single moving wheel across the rail in the previous section incorporates all components required for modeling wheel-rail-tie-ballast interaction except the presence of multiple wheels in the field. Simulating multiple wheels is important not only to accurately the loading applied by a passing train but also to accurately calibrate the model because the field measurements used in the calibration reflect the presence of multiple wheels. This section applies a full train bogey, i.e., two wheel sets to illustrate the influence of two wheels on the model response. In the analysis, a single axle of an Acela power car is modeled.

Figure 5.16 presents the dimensions of an Acela power car including wheel spacing on each bogey. The center-to-center wheel spacing for a single axle is 9-ft and 4-in and these wheel distances will be simulated in the LS-DYNA analysis and is displayed in Figure 5.17.

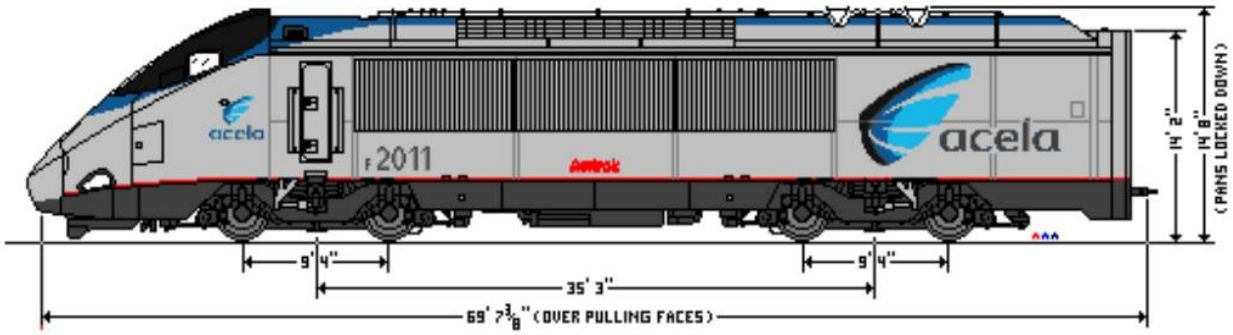

Figure 5.16: Diagram and dimensions of Amtrak Power Car (National Railroad Passenger Corporation, 2005).

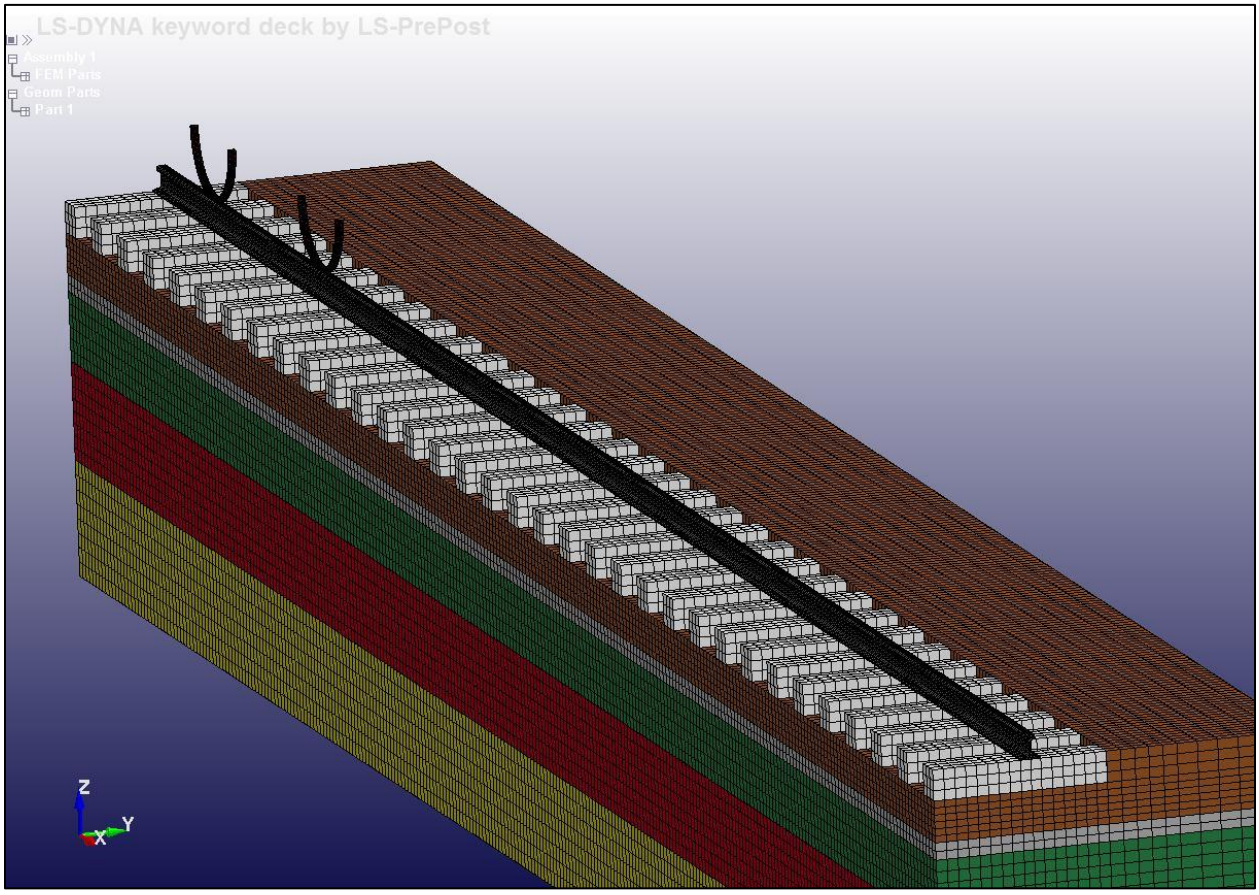

Figure 5.17: LS-DYNA model of Upland (60 ft.) with two wheels.

To verify the model, the initial situation assumes all ties are in intimate contact with the ballast. The two wheel-rail contact forces should remain around the static wheel load throughout the analysis and the peak tie-ballast contact forces should be approximately equal for the both wheels because of intimate tie contact. For the two-wheel analysis, both filtered (20 Hz) wheel-

rail contact force time histories are shown in Figure 5.18 and the normalized tie load time history for Ties 15 through 23 are shown in Figure 5.19.

The results show similar behavior to the response with a single wheel. Therefore, the numerical model behaves as expected under ideal conditions.

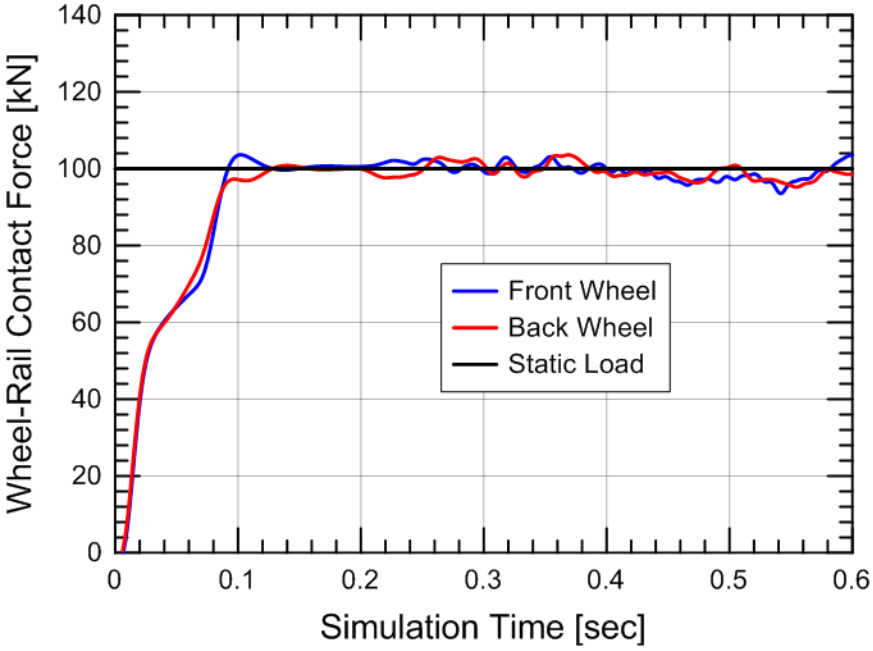

Figure 5.18: Filtered (20 Hz) wheel-rail contact force time history for wheels 1 and 2.

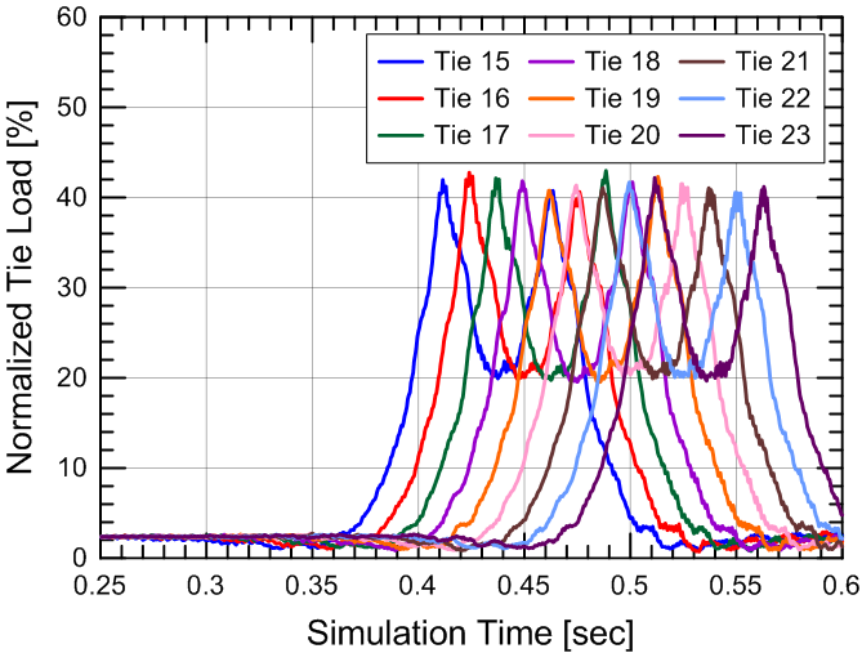

Figure 5.19: Normalized tie load time history for Ties 11 through 19 assuming two wheels.

5.4.4 Field Calibrated Model at Upland (60 ft.)

With the dynamic model developed and validated for ideal conditions, the model will be calibrated to represent the substructure behavior at Upland (60 ft.). This calibration could also be similar to a dynamic inverse analysis as opposed to the static inverse analysis in Chapter 5.3.

This section presents the following: (1) discussion comparing the static and dynamic analyses, (2) review of field measurements used for calibration, (3) calibration assuming equal tie-ballast gaps, and (4) calibration assuming unequal tie-ballast gaps.

5.4.4.1 Static v. Dynamic Analysis

This section summarizes and explains the differences between the static inverse analysis performed with FLAC3D and the field calibrated dynamic analysis performed with LS-DYNA: Key factors are listed below:

1. Computational time: The FLAC3D static inverse analysis takes about 20 minutes for each particular site to estimate modulus values for the ballast, subballast, and the various subgrade layers. The LS-DYNA field calibrated dynamic model, with manual iterations of modulus, requires 3 to 6 days for each site.

2. Scope and Outputs: Both analyses yield layer modulus values however the FLAC3D static inverse analysis only replicates peak transient displacement values while the LS-DYNA field calibrated dynamic model replicates the entire vertical displacement time histories of the tie reaction and measured LVDT displacements.

3. Load Distribution: The FLAC3D static inverse analysis does not directly calculate the distribution of the wheel load to underlying and surrounding ties but requires it to be initially assumed, e.g., 35%/22%/10%, and manually inputted. LS-DYNA calculates the actual load distribution including the influence of tie-ballast gaps and wheel-rail-tie-ballast interactions and the effects on the modulus values.

4. Non-linear Subgrade Response: The FLAC3D and LS-DYNA analyses use different methods to account for the measured non-linear LVDT behavior in the subballast and subgrade layers. The peak wheel load versus peak transient LVDT #2 vertical displacement response at Upland (60 ft.) is shown as an example in Figure 5.20. Significant non-linear behavior is observed and the assumed mathematical models used to estimate the field behavior for FLAC3D and LS-DYNA are shown.

For the FLAC3D static inverse analysis, only peak transient displacements are required therefore an “apparent gap” can be used to account for the non-linear force-displacement

response. For example if a peak wheel load of 100 kN is assumed, the field data in Figure 5.21 shows about 0.1 mm of transient LVDT #2 vertical displacement with an "apparent gap" of about 0.06 mm. Therefore, the numerical FLAC3D analysis varies the Young's Modulus of Layer 2 until 0.04 mm of vertical displacement is obtained (0.1 mm to 0.06 mm). Because both the material model in FLAC3D and the field response are assumed to be linear, the advantage of this method is the FLAC3D model can replicate peak LVDT displacements throughout the entire measured range (60 to 160 kN). This better replicates the mobilized state of the subballast and subgrade under train loading and implies the estimated FLAC3D modulus is a "tangent modulus".

Conversely, LS-DYNA models the entire force-displacement relationship and not just peak transient vertical displacement so an "apparent gap" cannot be used. This means the force-displacement response pass through the origin (apparent gap = 0.0 mm) because the time history includes an unloaded condition (wheel load and displacement = 0), loaded condition (peak wheel load and peak displacement), along with the load-displacement response in-between. This implies the estimated LS-DYNA modulus is a "secant modulus" and is required to calibrate an entire time history displacement relationship.

In summary, while the calibrated LS-DYNA and FLAC3D models both predict 0.1 mm in LVDT #2 for an assumed wheel load of 100 kN, the estimated modulus values will be different because of the different analyses. While the non-linear behavior in the shown example if Figure 5.20 is significant, almost all field measured LVDT responses display small non-linear responses (apparent gap $\approx$ 0.0 mm) so the estimated "tangent modulus" from FLAC3D and "secant modulus" from LS-DYNA are similar. Only LVDT #2 at Upland (60 ft) experiences significant non-linear behavior so the fully non-linear elastic material models in LS-DYNA are required at this time and FLAC3D can be used to estimate moduli.

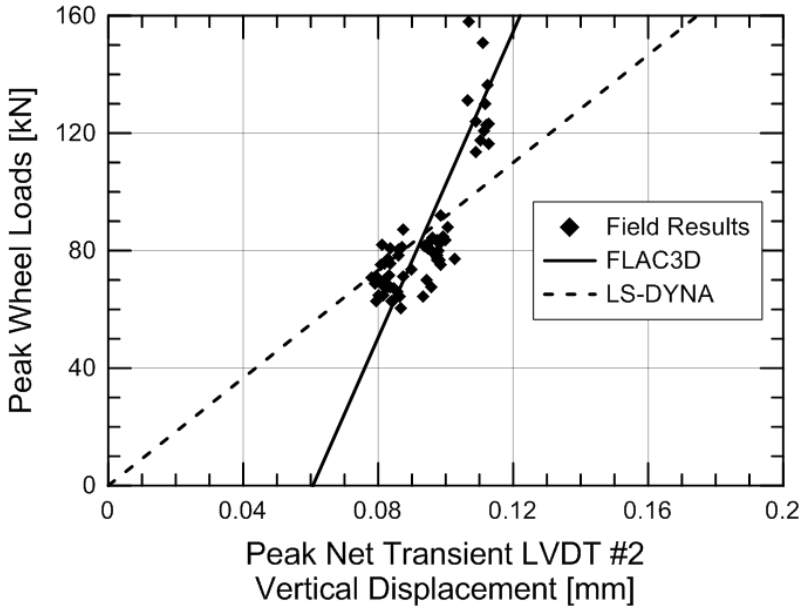

Figure 5.20: Different interpretations of LVDT #2 behavior at Upland (60 ft.) recorded on 29 January 2013 at 10:21 AM from FLAC3D and LS-DYNA.

5.4.4.2 Field Measurements at Upland (60 ft.)

As with the static inverse analysis example in Chapter 5.3, the data recorded at Upland (60 ft.) on 29 January 2012 is used for LS-DYNA calibration. The model replicates the first axle of a single Amtrak power car as two sliding wheels at the wheel spacing shown in Figure 5.16.

The data used for calibration is displayed in Figure 5.21 and shows wheel load, tie reaction, and LVDT displacement time histories of a passing Acela wheelset at the Upland (60 ft.) site. The two measured peak wheel loads are 124 and 123 kN and the corresponding peak tie reactions are 74 and 69 kN. Using Equation (2), the peak normalized tie loads are 59% and 56%. This implies good tie support at this particular location because the normalized tie load is greater than 40%. The time histories show all five LVDTs responded at roughly the same time as the tie reaction measurement, i.e., about 3.96 seconds, which indicates the tie is well supported. The peak vertical displacements are different for each LVDT with maximum transient vertical displacements in LVDTs #1, #3, and #4 of 0.4 to 0.5 mm. LVDT #2, the smallest layer thickness, shows only 0.1 mm of transient vertical displacement while LVDT #5, the deepest layer, shows only 0.2 mm of transient vertical displacement. The cumulative transient vertical displacement of all five LVDTs is about 1.5 mm and this small amount of track movement is also indicative of a well supported tie and thus track.

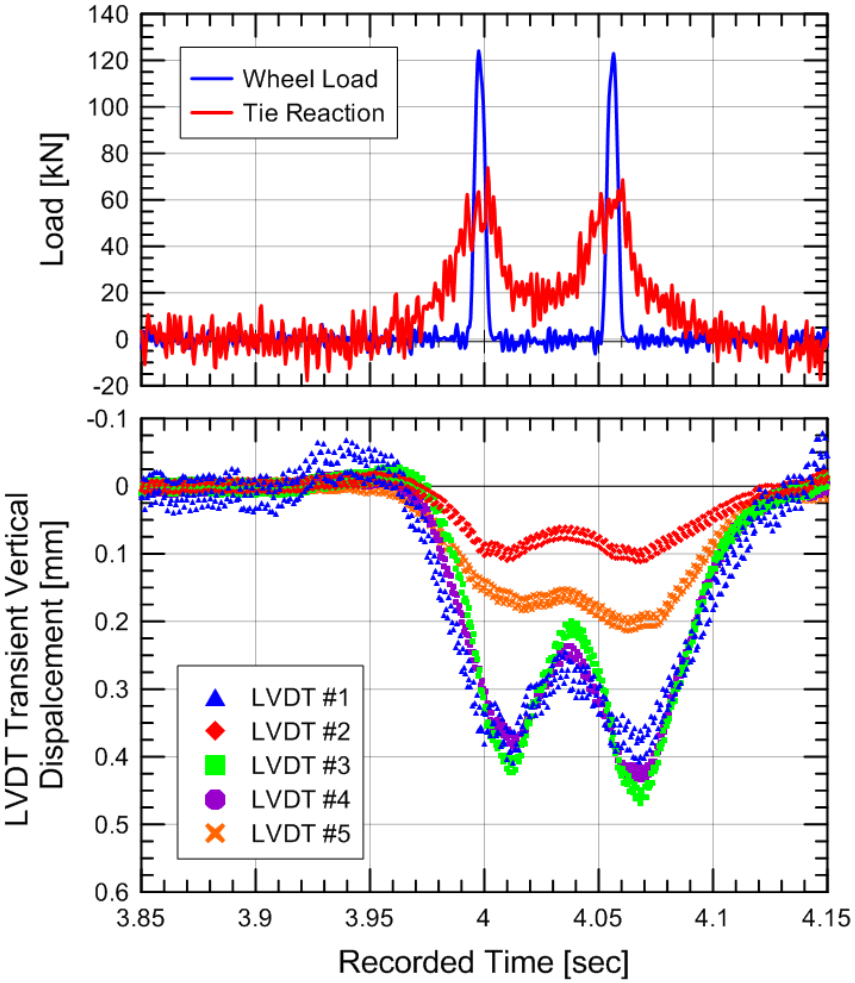

Figure 5.21: Measured wheel load, tie reaction, and transient LVDT displacements at Upland (60 ft.) recorded on 29 January 2013 at 10:21 AM.

5.4.4.3 Methodology

The inputs required for the model include: (1) wheel loading, (2) tie-ballast gap under the instrumented tie (Tie 19), (3) modulus values of the five substructure layers, and (4) tie-ballast gaps of the adjacent ties (Ties 18 and 20). Field measurements are used to determine the (1) wheel loading and (2) tie-ballast gap of the instrumented tie (Tie 19). The two measured peak wheel loads used for calibration are 124 and 123 kN (see Figure 5.21), which yielded an average peak wheel load of 124 kN for these simulations. The density of the wheels in the finite element mesh was set so the static wheel-rail contact force produced an average peak wheel load of 124 kN. The tie-ballast gap of the instrumented tie (Tie 19) was determined to be about 0.25 mm as shown in Figure 3.37.

The remaining two model input parameters, (3) modulus of the five substructure layers (3) and (4) tie-ballast gap of the surrounding ties cannot be determined through the available field measurements. For the first analysis, the tie-ballast gap of the surrounding ties are assumed to be equal to the instrumented tie at 0.25 mm and for the second analysis, they two surrounding tie are assumed to be independent of the instrumented tie.

This inverse analysis was performed by iterating substructure modulus values and tie-ballast gaps of the adjacent ties until the results of the numerical model matched the field measured tie reaction and transient vertical displacements.

Two output parameters are used to verify the calibrated model: (a) tie-ballast contact force and (b) relative layer displacements. The numerical tie-ballast contact force is compared to the field measured tie reaction introduced in the previous section. Both parameters represent the tie load but do so in different manners. Tie-ballast contact force is a direct measurement of tie load while tie reaction force is an indirect measurement that is determined through field measured rail bending. Because tie reaction essentially compares the magnitude of rail bending over the crib with the amount of rail bending over the tie, it may underestimate load transfer if a group of ties are poorly supported because the rail will experience significant bending but can still transfer tie load. This means tie reaction is only considered representative of tie load in well supported conditions, which is reasonable for the Upland (60 ft) site. The relative layer displacement comparison is explained in the previous section.

5.4.4.4 Equal Tie-Ballast Gaps

The first dynamic inverse analysis assumes the tie-ballast gaps of the surrounding ties are equal to the instrumented tie. A diagram is shown in Figure 5.22. This means the only unknown are the Young's Modulus values of the five substructure layers.

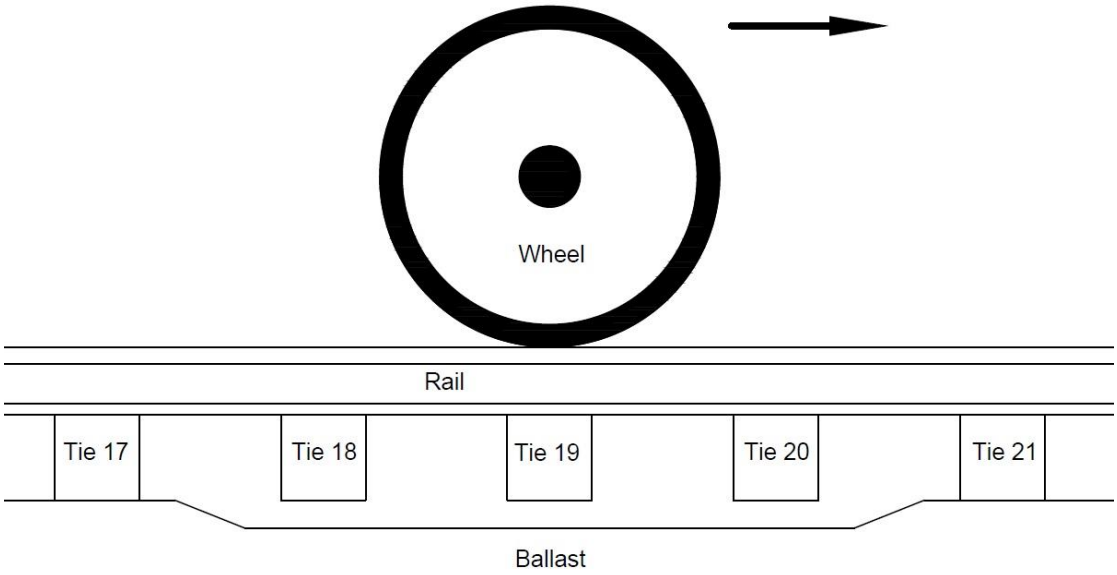

Figure 5.22: Wheel-Rail-Tie-Ballast Model showing equal tie-ballast gaps at Ties 18, 19, and 20.

With these assumed tie-ballast gaps, the layer moduli are estimated using an inverse analysis and presented in Table 5.4: The results of the tie loading and LVDT displacements are displayed in Figure 5.23.

For Figure 5.23(a), the blue line represents the numerical tie-ballast contact force for Tie 19 while the thinner red line represents the field measured tie reaction. Figure 5.23 shows good agreement between the measured and calculated tie-ballast contact force. The measured tie reactions reach about 60 kN while the numerical results show a peak about 40 kN. It is possible that the surrounding ties have tie-ballast gaps greater than 0.25 mm at Upland (60 ft) so more load is redistributed to the instrumented tie than with equal tie-ballast gaps. In this particular LS-DYNA model, Ties 18, 19, and 20 have the same tie-ballast gap of 0.25 mm so the load is distributed fairly evenly. The effect of tie-ballast gaps of different heights are discussed in greater detail in Chapter 5.5.

From Figures 5.23 the following observations are made:

- The calculated and measured peak vertical displacements at each LVDT are in good agreement. This implies the modulus values and initial assumptions of load distribution are representative of field conditions.

- The timing and magnitude of the calculated vertical displacements match field behavior. This suggests that the wheel spacing and velocity are representative of the passing Acela train
- The LS-DYNA results indicate the rail unloads at a quicker rate than field measurements. The slower unloading from the field measurements is likely due to the influence of the next train axle, which is simulated in subsequent analyses with multiple wheels.
- The numerically replicated uplift of LVDT #1 is greater than the measured values. This is likely due to a lack of side friction along the tie resisting movement from ballast in the crib and shoulders.

One of the main deviations between the calibrated model3 and field measurements is the measured tie reactions show higher peak wheel loads than the LS-DYNA tie-ballast contact forces. This is probably due to unequal tie-ballast gap heights between adjacent instead of the same gap of 0.25 mm.

Table 5.4: LS-DYNA estimate modulus values at Upland (60 ft.) for January 2013 assuming equal tie ballast gaps for Ties 18, 19, and 20

Layer 1 [MPa]	Layer 2 [MPa]	Layer 3 [MPa]	Layer 4 [MPa]	Layer 5 [MPa]
264	28	28	39	60

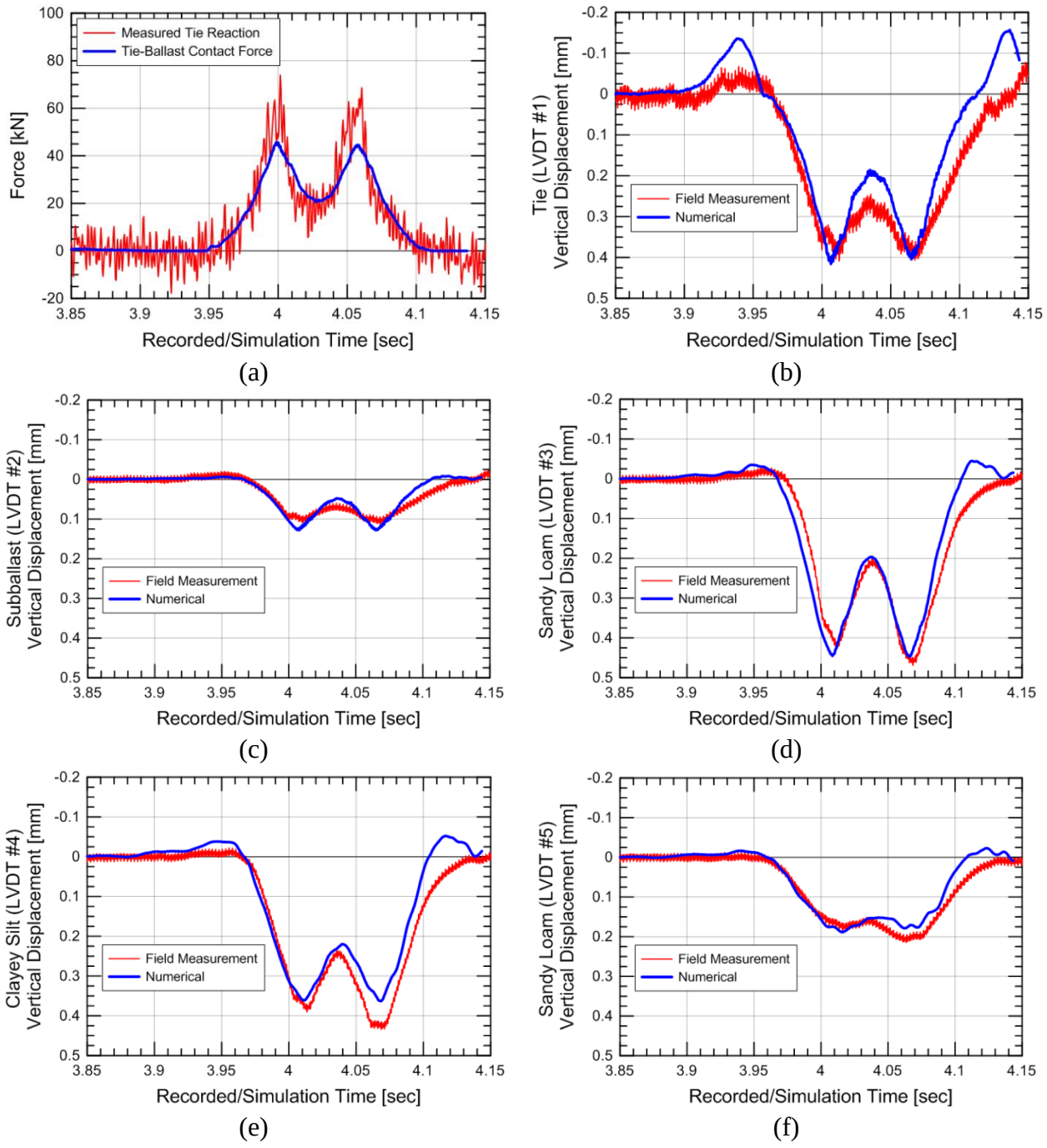

Figure 5.23: **Comparison between field measured and numerical (a) tie reaction and transient displacements at (b) LVDT #1, (c) LVDT #2, (d) LVDT #3, (e) LVDT #4, and (f) LVDT #5 at Upland (60 ft.) for data recorded on 29 January 2013 at 10:21 AM assuming equal tie-ballast gaps.**

5.4.4.5 Unequal Tie-Ballast Gaps

The second dynamic inverse analysis does not assume the tie-ballast gaps of the instrumented and surrounding ties are equal and can be independent of each other. A diagram is shown in Figure 5.24.

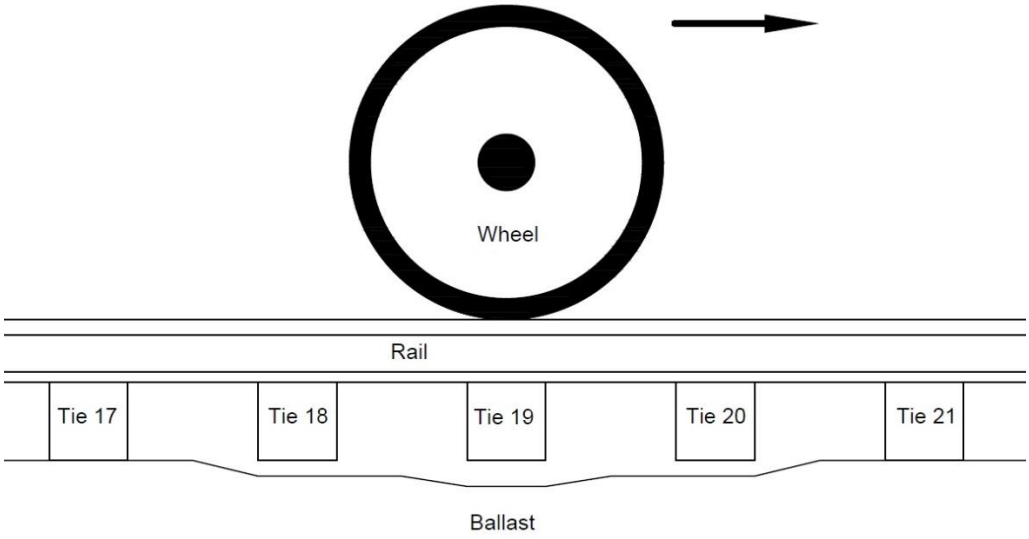

Figure 5.24: Wheel-Rail-Tie-Ballast Model showing unequal tie-ballast gaps at Tie 18, 19, and 20.

Due to the sensitivity of load distribution to different modulus values, a tie-ballast gap height of 0.55 mm is used for Ties 18 and 20 while a gap of 0.25 mm is used for Tie 19 because of field measurements.

The updated tie-ballast gap heights affect the load distribution and the transient displacements under the tie. Therefore, new layer modulus values were estimated using an LS-DYNA inverse dynamic analysis and are shown in Table 5.5. These modulus values are compared to the estimated modulus values from the FLAC3D static inverse analysis in Chapter 5.3 and LS-DYNA analysis in the previous section assuming equal gap heights. The results in Table 5.5 show the estimated modulus values can be significantly different for the three different analyses.

Table 5.5: Comparison of back-calculated modulus values from FLAC3D (Chapter 5.3), LS-DYNA assuming equal tie-ballast gaps (Chapter 5.4.4.4), and LS-DYNA assuming unequal tie-ballast gaps at Upland (60 ft.) for January 2013

Analysis	Layer 1 [MPa]	Layer 2 [MPa]	Layer 3 [MPa]	Layer 4 [MPa]	Layer 5 [MPa]
FLAC3D	201	278	22	27	47
LS-DYNA – Equal Gaps	131	37	29	36	62
LS-DYNA – Unequal Gaps	207	67	33	32	59

For Layer 1, e.g. ballast, the difference in modulus values (201, 131, and 207 MPa) are attributed to the various load distributions of each analysis. If the assumed tie-ballast gaps redistribute the load in a manner that causes the instrumented tie to experience less load (<35%), the stress of the underlying ballast decreases and a stiffer modulus is required to replicate the field measured peak LVDT #1 displacement. For the LS-DYNA analysis with equal tie-ballast gap heights, the load is shed away from the instrumented tie (<35%) resulting in a softer estimated modulus. For the LS-DYNA analysis with unequal gap heights, the load redistributes towards the instrumented tie (>35%), resulting in a stiffer estimated modulus.

For Layer 2, e.g. subballast, the largest moduli difference between the three analyses is observed. The main reason for this difference is how the FLAC3D and LS-DYNA analyses interpret non-linear force-displacement behavior (Figure 5.20). FLAC3D includes an "apparent gap" which results in the estimation of a stiffer subballast "tangent" modulus. LS-DYNA does not include an "apparent gap" so the estimated "secant" modulus will be lower. Also, load distribution can influence the estimated subballast modulus as observed by comparing Layer 2 for both LS-DYNA analyses.

For Layers 3 through 5, only small differences are observed between the estimated modulus values. This is caused by the field measured force-displacement behavior being nearly linear for LVDTs #3 through 5 (apparent gap ≈ 0.0 mm) and the influence of load redistribution decreasing as the layer depth increases. For example, if the load redistributes away from the instrumented tie, LVDT #5 will be more likely to experience the load than LVDT #1 because vertical stress spreads horizontally with depth (2:1 ratio).

Figure 5.20 compares the LS-DYNA model with field measurements and the following observations can be made from these analyses:

- The peak tie-ballast contact force equals the peak tie reaction but the measured tie reaction time history shows quicker rebound or unloading than the LS-DYNA results.
- The LS-DYNA layer displacements are in good agreement with the field LVDT displacements. The main differences are similar to those in Chapter 5.4.4.4, i.e., numerical unloading is quicker and the rebound in Layer 1 is greater than the field results.

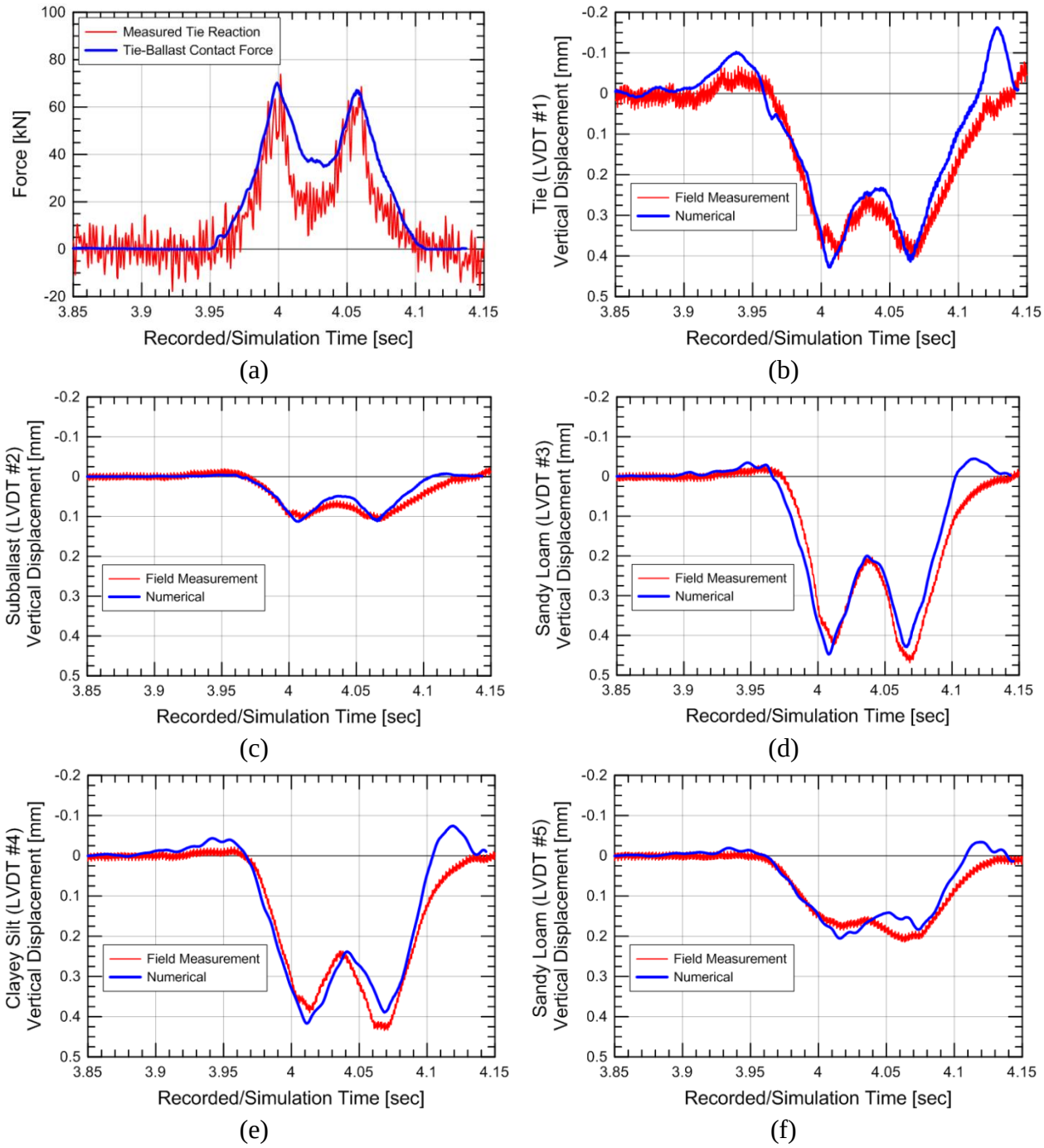

Figure 5.25: **Comparison between field measured and numerical (a) tie reaction and transient displacements at (b) LVDT #1, (c) LVDT #2, (d) LVDT #3, (e) LVDT #4, and (f) LVDT #5 at Upland (60 ft.) for data recorded on 29 January 2013 at 10:21 AM assuming unequal tie-ballast gaps.**

This calibrated model will be used for the basis of the sliding models in Chapter 5.5 and the bridge approach models in Chapters 5.6 and 5.7. A calibrated numerical model was not developed for the bridge approach, i.e. Upland (15 ft.), because insufficient enough information is available to accurately replicate the track geometry. For example, the settlement and tie-ballast gap heights of every tie in the transition zone are not known and are required to model the load redistribution around the instrumented tie. Various tie-ballast gap heights were assumed in the analyses presented in Chapter 5.5 to investigate the range of transition behavior.

5.4.5 Summary

This section summarizes the main findings and conclusions from these analyses:

- In situation of intimate contact, 40% of the wheel load gets distributed to the underlying tie.
- Varying the Young's Modulus value of each substructure layer and the tie-ballast gap height of the adjacent ties gives a numerical model that well represents the measured track behavior at an open track location.

5.5 Open Track Parametric Analysis

The previous section calibrated the numerical model to match field measurements at the Upland (60 ft.) open track site. With a confident model, parametric analyses will be performed to investigate the effect of unsupported ties on the distribution of wheel load throughout the track system. This is one of the unanswered questions from the field instrumentation in Chapter 3 as load redistribution is believed to be a potential factor increasing loads at bridge approaches.

The parametric analysis consists of four different analyses, including the following situation:

(1)	Tie-ballast gap at Tie 19 only	(0 mm to 1 mm)
(2)	Tie-ballast gaps at Ties 18 and 20	(0 mm to 1 mm)
(3)	Equal tie-ballast gaps at Ties 18 to 20	(0 mm to 4 mm)
(4)	Unequal tie-ballast gaps at Ties 18 to 20	(0 mm to 1 mm)

All four analyses use only a single wheel to simplify results and use the layer modulus values determined from the dynamic inverse analysis.

5.5.1 Single Tie Ballast Gap (Instrumented Tie)

The first parametric analysis simulates the effect of an isolated poorly supported tie and assumes a gap only under the instrumented tie (Tie 19) while all of the other ties remain in intimate contact with the ballast (Figure 5.26). The gap at Tie 19 varies from 0.0 mm to 1.0 mm in 0.25 mm intervals.

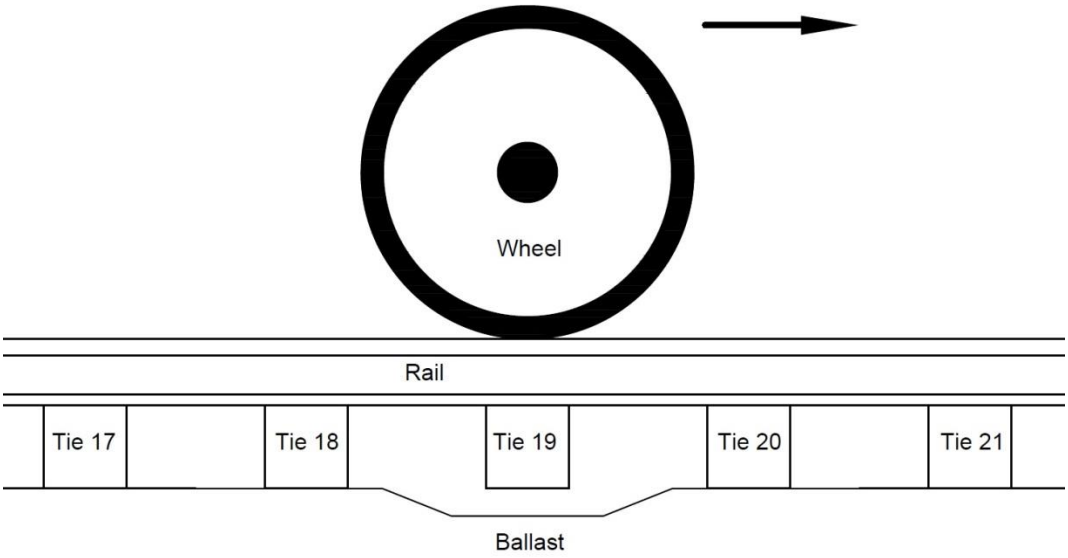

Figure 5.26: Wheel-rail-tie-ballast model showing tie-ballast gap at Tie 19.

Figures 5.27 through 5.29 compare the tie-ballast contact force time histories as normalized tie loads for Ties 19, 18, and 20, respectively for tie-ballast gap heights of: 0.0 mm, 0.25 mm, 0.5 mm, 0.75 mm, and 1.00 mm. While only the maximum normalized tie loads are shown in later analyses, the full time histories are shown in these figures to emphasize changes in behavior due to a moving wheel.

Figure 5.27 shows increasing the tie-ballast gap significantly decreases the maximum normalized tie load for Tie 19. The gap produces more bending in the rail which redistributes the load away from unsupported Tie 19 to the Ties 18 and 20 which increases the load on Ties 18 and 20.

Figure 5.28 shows an increase in maximum normalized tie load and change in behavior of Tie 18 with increasing gap height at Tie 20. The maximum normalized tie load increases because when the wheel is above Tie 18, Tie 19 does not receive any load and the load remains on Tie 18. As the wheel moves to Tie 19, the load continues to remain on Tie 18, increasing the

duration of load on that tie. The response of Tie 20 (see Figure 5.29) is similar to Tie 18 (see Figure 5.28), but with greater normalized tie loads and an increase in force prior to maximum loading instead of after the wheel.

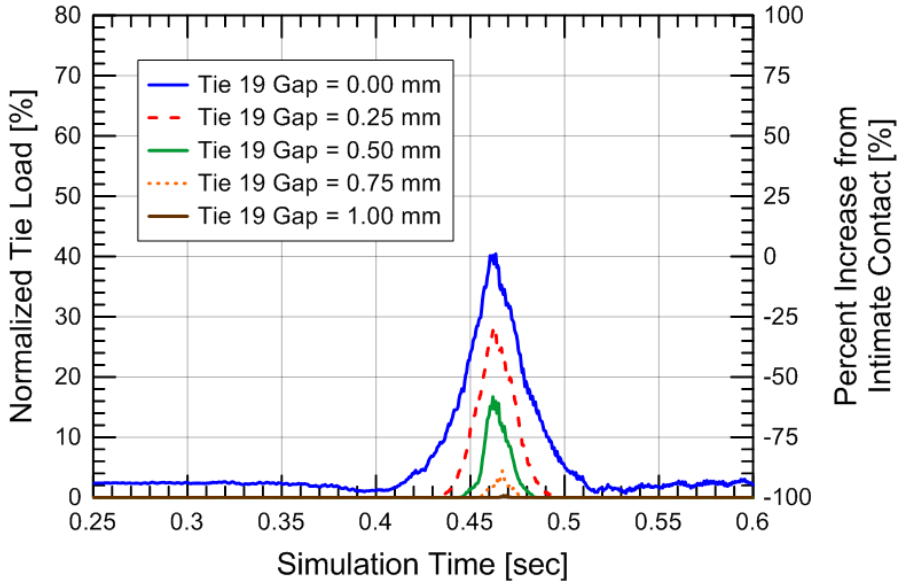

Figure 5.27: Normalized tie load time histories for Tie 19 with various Tie 19 gap heights.

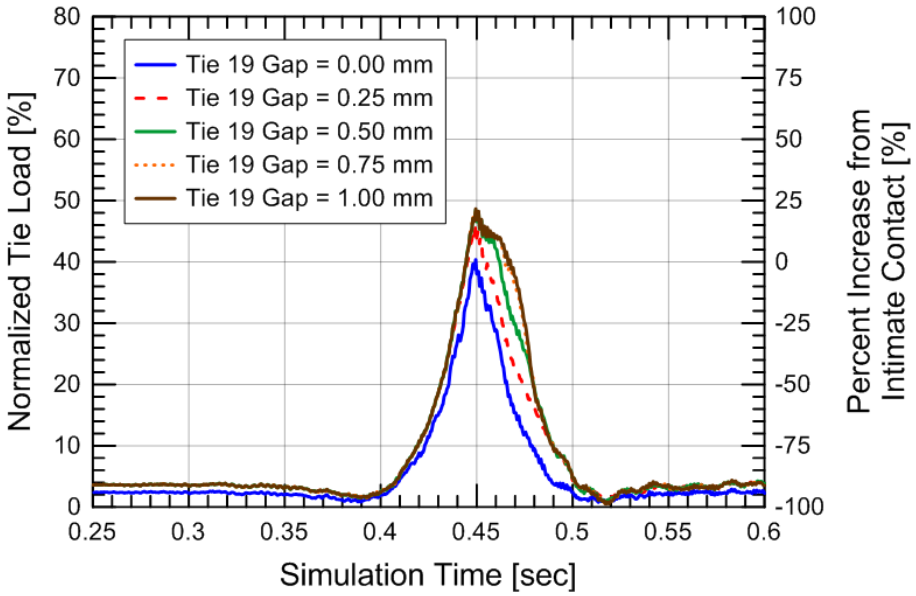

Figure 5.28: Normalized tie load time histories for Tie 18 with various Tie 19 gap heights.

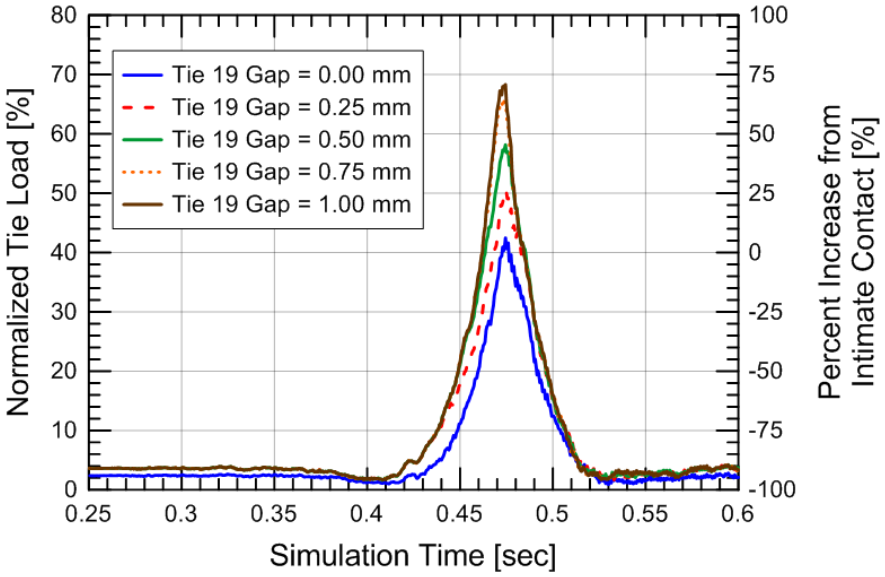

Figure 5.29: Normalized tie load time histories for Tie 20 with various Tie 19 gap heights.

The maximum normalized tie load experienced by Ties 18, 19, and 20 along with their percent increase from intimate contact (normalized tie load = 40%) are shown in Figure 5.30. Referencing Figure 5.15 where the tie-ballast gap at Tie 19 is 0.0 mm, the maximum normalized tie load experienced by Ties 18, 19, and 20 are all about 40% as expected. However as the tie-ballast gap at Tie 19 increases, the additional rail bending required for Tie 19 to establish contact with underlying ballast causes the rail to shed some of the load away from Tie 19 to better supported Ties 18 and 20. At a gap height of 1.0 mm, Tie 19 ceases to contact the ballast during loading (maximum normalized tie load = 0.0%) and Ties 18 and 20 reach their maximum normalized tie loads of 49% and 68%, respectively. This is an increase of 23% and 70% from the assumed 40% at intimate contact. Tie 20 experiences a greater increase than Tie 18 because Tie 20 is located after the unsupported tie (Tie 19) and will have amplified effects from the moving wheel being forced to accelerate upwards after the greater vertical rail displacement above Tie 19. This is the primary difference between the results of this analysis and the previous analysis. The effect on Tie 17 and 21 are minimal (<2% difference) and therefore not displayed.

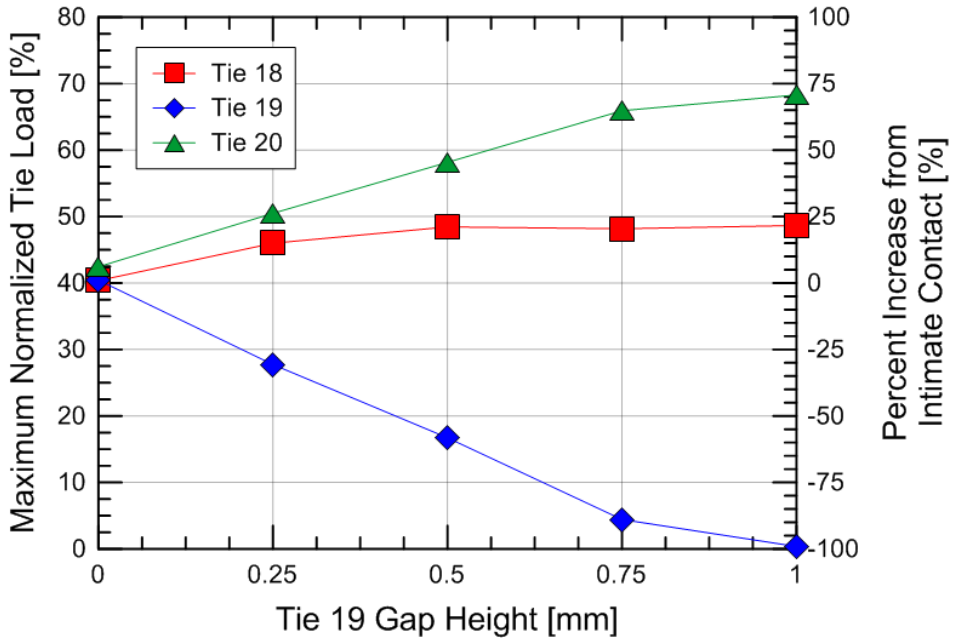

Figure 5.30: Maximum normalized tie load (maximum tie-ballast contact force / wheel load) for Tie 18, 19, and 20 with varying Tie 19 gap heights.

Varying the stiffness of any track component, e.g. stiffening or softening the track response, will vary the results presented in Figure 5.30 but the general trend is expected to hold. A stiffer track will have higher tie loads assuming intimate contact (>40%) but will fully distribute the load at lower tie-ballast gap heights (<1.0 mm) while a softer track will have lower tie loads assuming intimate contact (<40%) but will fully distribute the load at higher tie-ballast gaps (>1.0 mm). This suggests that softer track is preferable when focusing on the load redistribution mechanism.

If the 1.0 mm gap under Tie 19 occurs due to local ballast fouling or poor compaction under Tie 19, it would be physically expected that the ballast under Ties 18 and 20 would settle to a greater rate than Ties 17, 19, and 21 because of the increased load. This would eventually decrease load redistribution as the tie loading becomes more evenly distributed amongst the ties and potentially result in the "stabilization" of the region. This is illustrated in Figure 5.30 by decreasing the "relative" gap height of Tie 19.

5.5.2 Two Tie Ballast Gaps (Adjacent Ties)

In contrast to the previous analysis, the second parametric analysis increases the tie-ballast gap at the adjacent ties (Ties 18 and 20) while the instrumented tie (Tie 19) remains in intimate contact

(Figure 5.31). The gaps at Ties 18 and 20 vary from 0.0 mm to 1.0 mm at 0.25 mm intervals. This results in the opposite situation as the prior analysis in which load was shed away from Tie 19. In this analysis the load sheds away from the adjacent unsupported ties (Ties 18 and 20) and to Tie 19, which increases the load on Tie 19. Because two ties are unsupported instead of one, the maximum normalized tie load at Tie 19 increases from 40% to 74%, an increase of 85% (Figure 5.32).

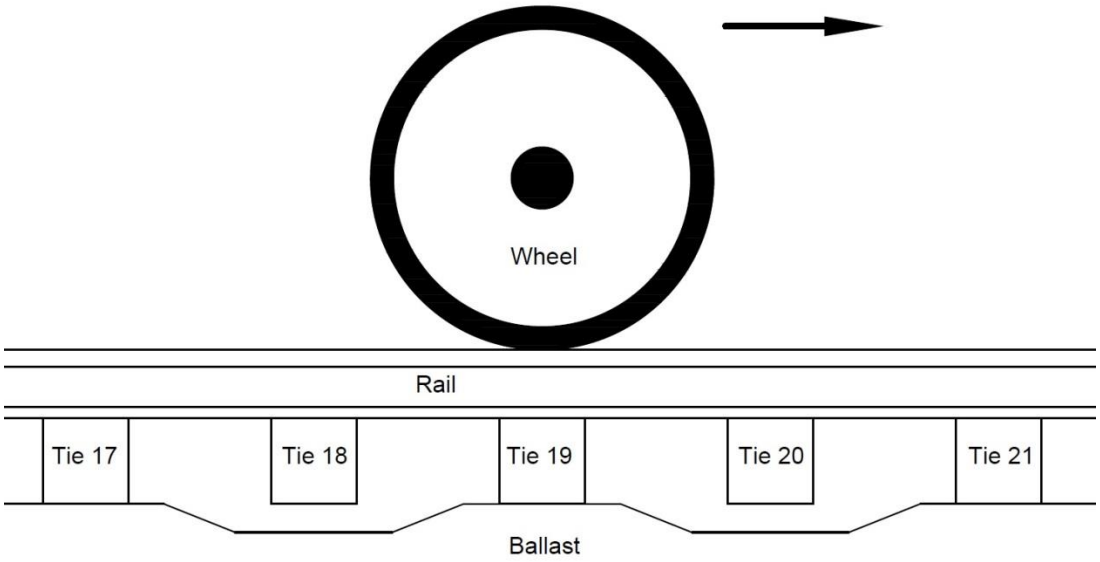

Figure 5.31: Wheel-rail-tie-ballast model showing equal tie-ballast gaps at Tie 18, 19, and 20.

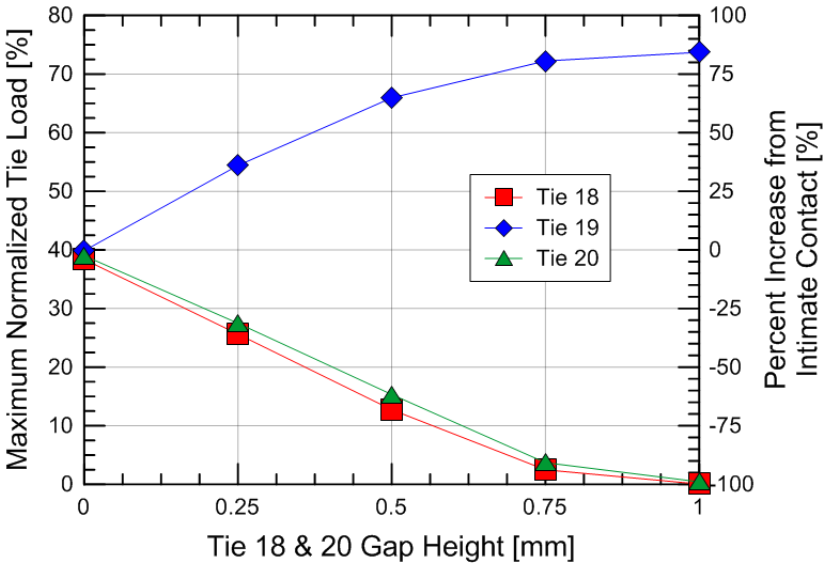

Figure 5.32: Maximum normalized tie load (maximum tie-ballast contact force/wheel load) for Ties 18, 19, 20, and 21 with varying gap heights but Tie 18 = 19 = 20 gap heights.

5.5.3 Three Tie Ballast Gaps (Instrumented and Adjacent Ties)

Unsupported tie behavior are often observed over a group of ties instead of a single tie so the third parametric analysis extends the previous two analyses and investigates the applied loads on supported ties following a group of unsupported ties. This would be representative of a site with localized fouling and the resulting tie-ballast gaps. For this analysis, equal tie-ballast gaps exist at the instrumented tie (Tie 19) and adjacent ties (Ties 18 and 20) and the gap varies from 0.0 mm to 4.0 mm because that is the gap height at which Tie 19 ceases contact with the ballast during loading to model the full range of gap situations (Figure 5.33).

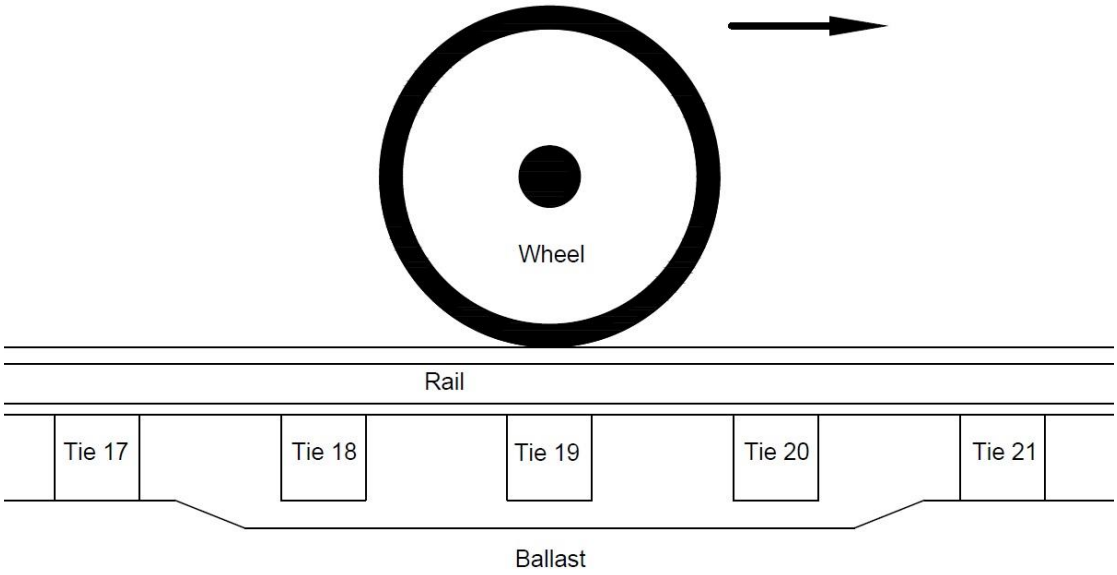

Figure 5.33: Wheel-rail-tie-ballast model showing equal tie-ballast gaps at Tie 18, 19, and 20.

The changes in maximum tie-ballast contact force for Ties 18, 19, 20, and 21 along with their percent increase from intimate contact are illustrated in Figure 5.34. Figure 5.34 shows decreasing maximum normalized tie loads at Ties 18, 19, and 20 while significantly increasing at Tie 21 (~160% at 4.0 mm). The maximum normalized tie load at Tie 19 increases slightly for gap heights of 1.0 to 1.5 mm and then transitions to a completely unsupported condition at a gap of 4.0 mm. Tie 19 experiences larger maximum normalized tie loads than Ties 18 and 20 because it is located between the surrounding supported ties (Ties 17 and 21) so more rail displacement occurs at that location. This allows Tie 19 to establish ballast contact earlier than the adjacent ties (Tie 18 and 20).

The large normalized tie loads experienced by Tie 21 (~160% at 4.0 mm) indicate load redistribution from a group of poorly supported ties can result in large increases in applied load to the next supported tie. This increased load may damage the tie or produce a tie-ballast gap at Tie 21 because of increased settlement. If this occurs, it would be expected that the load would shift to Tie 22 and that tie may develop a tie-ballast gap and be damaged. This "progressive loss of tie support" and/or "progressive tie failure" mechanism can spread the damage of a single or small group of poorly supported ties to a larger track section. This field condition would likely be a group of unsupported ties, e.g. Ties 18 through 20, with a gradual increase in tie support

until a completely supported tie is reached. For example, if Ties 18 through 20 have a gap of 2.0 mm, Tie 21 may have a gap of 1.5 mm, Tie 22 of 1.0 mm, Tie 23 of 0.5 mm, and Tie 24 being completely supported. This configuration would result in a temporarily stable situation impeding the spread of damage until additional substructure settlement occurs. However, track geometry maintenance may still be required. This also suggests that failure of track superstructure components, e.g. rail, fastening systems, and ties, may be due to substructure settlement and problems so understanding substructure behavior is important.

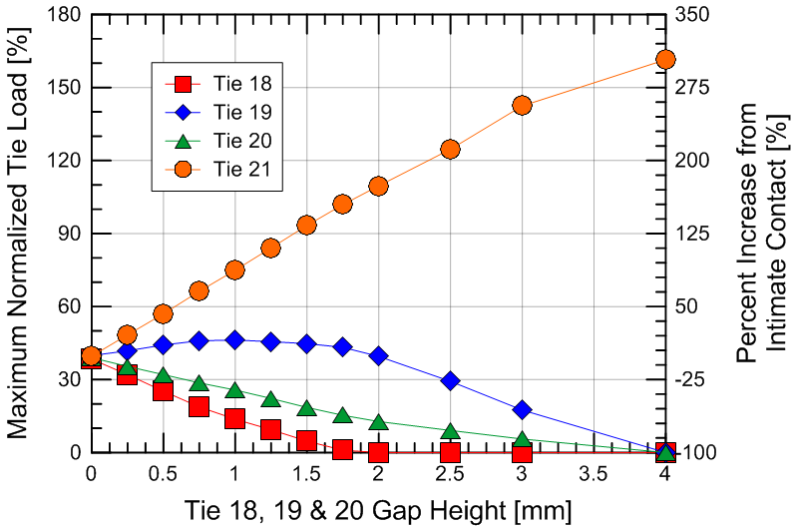

Figure 5.34: Maximum normalized tie load (maximum tie-ballast contact force/wheel load) for Ties 18, 19, 20, and 21 with varying gap heights but Tie 18 = 19 = 20 gap heights.

5.5.4 Varying Tie Ballast Gaps (Instrumented and Adjacent Ties)

The final parametric analysis for a single wheel emphasizes how varying tie-ballast gap heights can significantly alter load redistribution. This is of great importance because tie-ballast gap heights vary in field conditions (Lundqvist and Dahlberg, 2005; Varandas et al, 2011) and measuring the tie-ballast gap height at only a single tie does not provide sufficient information to determine the magnitude of load redistribution.

For this analysis, tie-ballast gaps at Ties 18, 19, and 20 are varied with equal gaps under Ties 18 and 20. This situation is displayed in Figure 5.35. The difference in gap heights from Tie 19 and Ties 18 and 20 illustrates the sensitivity of gaps under adjacent ties to the load redistribution.

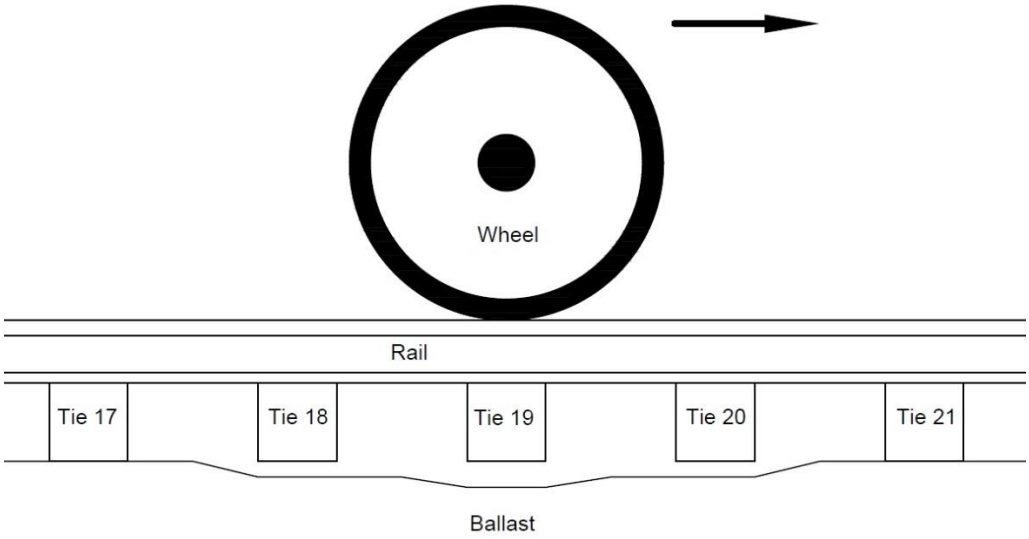

Figure 5.35: Wheel-rail-tie-ballast model showing unequal tie-ballast gaps at Tie 18, 19, and 20.

Figure 5.36 shows the maximum normalized tie load and percent increase from intimate contact results only for the instrumented tie (Tie 19). A wide variation of normalized tie loads is observed (0% to 75%) depending on the gap heights of the instrumented (Tie 19) and adjacent ties (Ties 18 and 20). As expected, the maximum normalized tie loads decrease with increasing tie-ballast gap magnitudes at Tie 19 because the load is shifting towards better supported ties. However, the maximum normalized tie load at Tie 19 increases with increasing tie-ballast gaps at Ties 18 and 20 because those ties are experiencing less load due to decreasing tie support. To demonstrate the sensitivity of load redistribution from tie-ballast gaps of adjacent ties, a 0.75 mm tie-ballast gap at Tie 19 is presented as an example. Depending on the tie-ballast gaps of adjacent ties (Ties 18 and 20), the maximum normalized tie load experienced by Tie 19 ranges from 3 to 55%. This represents a 93% decrease to 38% increase in tie load from the assumption of 40% when all ties are in intimate contact. These two possibilities would significantly change the back-calculated modulus values obtained using FLAC3D in Chapter 5.3.

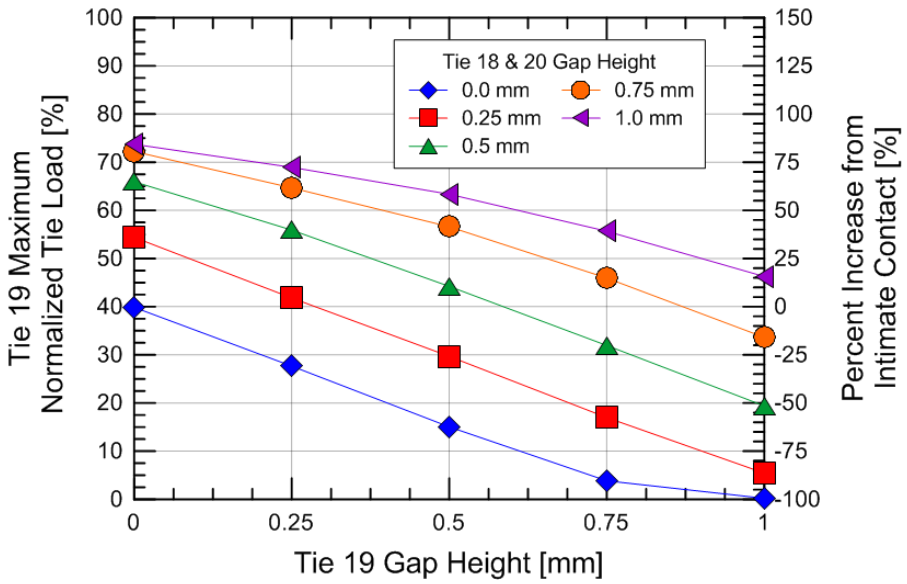

Figure 5.36: Maximum normalized tie load (maximum tie-ballast contact force / wheel load) for Tie 19 with varying Tie 18, 19, and 20 gap heights.

5.5.5 Summary

This section summarizes the main findings and conclusions from these analyses:

- The existence of tie-ballast gaps causes the applied wheel loads to redistribute to surrounding ties with good tie support. Increasing gap heights require greater rail bending to establish contact between the tie and ballast, which sheds the load through the rail to surrounding supported ties.
- A moving wheel causes the load redistribution to favor ties in the direction of movement. The temporary increase in total vertical displacement of the rail from the tie-ballast gap causes an amplification of load at the next supported tie as the wheel must displacement upwards due to supported conditions of that tie. This increase in applied load to the next supported tie promotes “progressive loss of tie support” and “progressive tie failure” by overloading the adjacent or nearby supported tie due to an unsupported or poorly supported tie.
- The tie-ballast gaps of surrounding ties significantly affect load redistribution. This emphasizes the importance of instrumenting a group of ties (at least 5 is recommended) and not a single tie in future studies to model the different tie-ballast gaps along a section of track. Without knowing the tie-ballast gaps for a group of ties, the actual load redistribution cannot be determined, which is needed to accurately predict future performance of this track with and without remedial measures.
- Including multiple wheels in the analysis does not significantly affect the calculated tie-ballast contact force or transient vertical displacement.

5.6 Transition Zone Parametric Analysis

Chapter 5.5 used an open track model to investigate the effects of unsupported ties on the distribution of load throughout the track system. This section expands on that previous work by investigating the effects of a full train truck or rolling cart passing over the bridge abutment at the Upland Avenue site interacts and/or amplifies the applied loads to the ballast when tie-ballast gaps are present.

5.6.1 Numerical Model

The second site involves a bridge transition zone instead of open track to gain insight into increased dynamic loads in transition zones (see Figure 5.37). The bridge structure is modeled after the Upland Street Bridge in Chester, PA and includes a masonry wall, an open deck bridge with timber ties on the bridge, and W-beams underneath the bridge. The stiffness of the bridge is greater than the approach track which is expected to produce impact loads when the front wheels of the cart pass onto the bridge abutment.

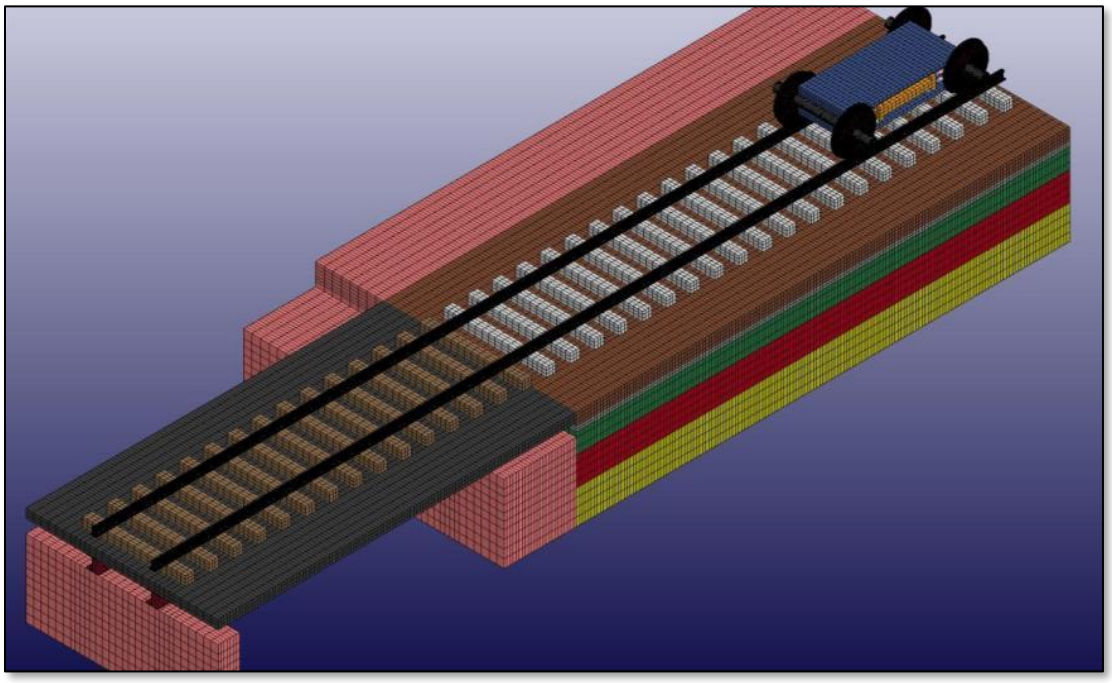

Figure 5.37: LS-DYNA finite element mesh showing Upland Street Bridge approach track site with a rolling cart.

To assist modeling the Upland Avenue Bridge, photos taken from site visits are used. At Upland (15 ft.), the instrumentation site is located seven ties north of the bridge on Track #3, i.e., southbound direction. The photograph in Figure 5.38 is looking north and shows the large masonry wall constructed to elevate the railway at Upland Avenue. The Upland (15 ft) instrumentation site is located just above Mike Tomas' white truck on Track #3, which is one track in from the north-south trending masonry wall. AMTRAK provided the dimensions of the 1902 masonry abutment wall at the Upland Avenue Bridge which is assumed the same geometry for the north-south trending masonry wall (Figure 5.39). The abutment wall is 15' 10" high with an exposed height of 13' 6". The top and base widths of this wall are 5' 8" and 8' 9", respectively.

Figure 5.38: Photograph of masonry walls at Upland Avenue below the Upland (15 ft.) instrumentation location looking north with Mike Tomas' truck adjacent to wall with MDD location on Track #3 above the white truck.

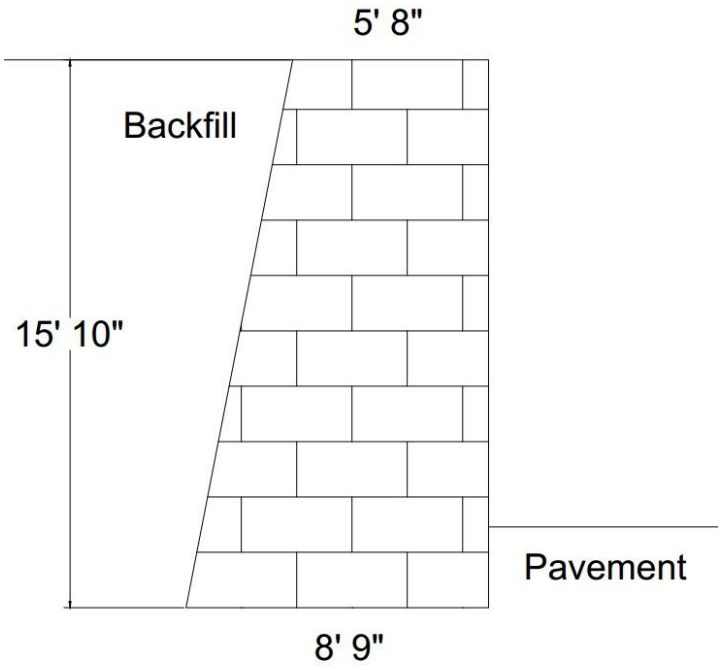

Figure 5.39: Diagram of masonry walls at Upland Avenue below the Upland (15 ft.) instrumentation location. Diagram is courtesy of Steve Chrismer of Amtrak.

Instead of sliding wheels, this site models a cart to simulate the secondary suspension system of a high-speed passenger train. It consists of four wheels with the axles spaced 2.8 m (9.33 ft.) apart to replicate the first bogie of a single Amtrak Acela power car. The cart mass is located at the cart center with a density such that each wheel applies a static wheel load of 100 kN. The axles and cart mass are connected with four sets of vertical and horizontal springs and vertical dampers. The values of the vertical and horizontal springs are 7.3e5 N/m and 2.2e9 N/m and damper values are set to 7.3e6 N*s/m. The velocity of the cart is 110 mph to replicate the operating speed of Amtrak's high speed trains along the Northeast Corridor (NEC).

The substructure layer thicknesses and moduli at the bridge approach site are the same as the open track site. While the same instrumentation as Upland (60 ft.) was also installed 15-ft from the Upland Street Bridge abutment, the available data is not extensive enough to calibrate the bridge approach model because the tie reaction data was not considered representative of the tie loading, ballast settlements, and tie-ballast gaps of the entire transition zone, e.g. first seven to ten ties, as required. In other words, only one tie is instrumented and the highly variable conditions in the transition zone cannot be extrapolated from only one tie. Therefore, the

substructure layers and moduli calibrated from Upland (60 ft.) are used in Upland (15 ft.) model because they are separated by only 45-ft.

5.6.2 No Settlement

Similar to the open track model in Chapter 5.4, the initial simulation assumes no substructure settlement in the approach. This would be isolating the effect of differential stiffness and is imperative for understand more complicated situations when tie-ballast gaps are included. This situation would be representative of newly laid track after immediately after tamping prior to any ballast settlement in the approach track. Previous analyses from the literature can be referenced in Chapter 2.4.3.

The simulation of a bridge approach is more complicated than open track because transition zone loading is affected not only by tie-ballast gaps within the entire approach, e.g. seven to ten ties from the bridge abutment, but also increased dynamic wheel loads resulting from the abrupt change in axle elevation/track stiffness as the front axle contacts the bridge abutment (Nicks, 2009). In the bridge approach model (Figure 5.37), the ties of interest are the seven closest ties to the bridge abutment within the transition zone. These are labeled as Ties 1 through 7 and shown in Figure 5.40. The ties on the bridge are labeled as Tie A, B, etc. to prevent confusion.

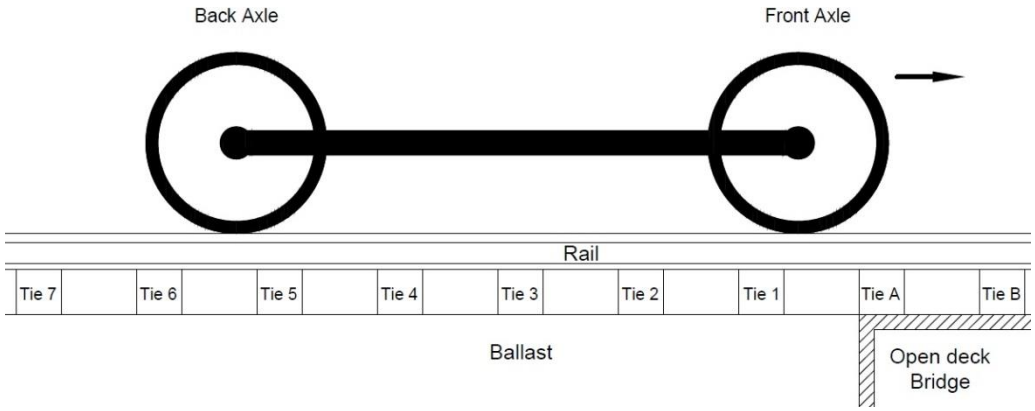

Figure 5.40: Wheel-rail-tie-ballast model showing no tie-ballast gaps.

Figure 5.41(a) and (b) display the four wheel-rail contact forces with time and distance, respectively, in which the front wheel pass the bridge abutment at a simulation time of about 0.68 seconds and the back wheels passing the bridge abutment at a simulation time of about 0.74

seconds. Figure 5.41(a) shows the front wheels experience increased dynamic loads at about 0.68 seconds, the time when the front wheels pass the bridge approach, with the back wheels experiencing an increase in wheel-rail contact force immediately afterwards. The increase in front wheel load is due to the reaction force required to accelerate the wheels and axle upward as the cart travels from the softer approach track (lower wheel elevation) to the stiffer bridge track (higher wheel elevation). The increase in back wheel load is a coupling reaction from upward acceleration of the front axle causing the cart to tilt and consequentially increase the wheel-rail force of the back axle. In this particular analysis, the back wheels then experience a load increase of about 20% in the transition zone, which is similar to previous analyses by Nicks (2009). Because of the 9.33-ft distance between the front and back cart axles, the increased dynamic wheel load occurs about 10-ft or 5 ties away from the bridge abutment, as shown in Figure 5.41(b).

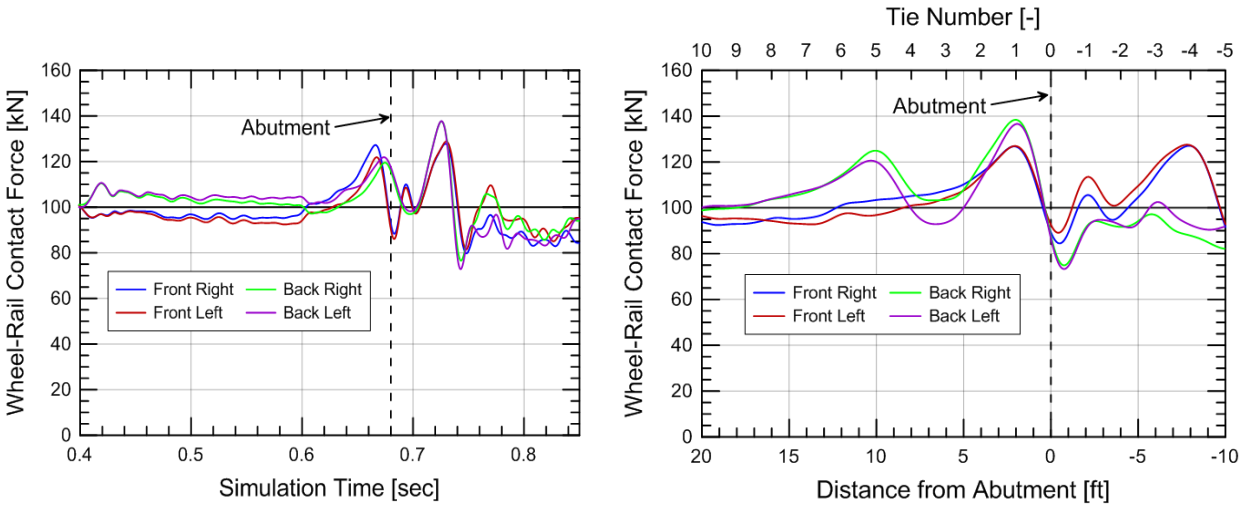

(a) (b)

Figure 5.41: Wheel-Rail Contact Forces with (a) time and (b) distance.

Figure 5.42 shows the normalized tie loads and percent increase in tie load solely from the cart passing the abutment. Prior to the front wheels passing the bridge abutment, the tie-ballast contact force measured is about 80 kN which equates to a normalized tie load of about 40% as expected and discussed in prior sections. Because the increased dynamic load of the back wheel occurs about 10-ft or 5 ties from the bridge abutment when the front wheel hits the abutment, Ties 5 and 6 experience load increases of 20% and 7.5%, respectively (tie-ballast contact force of 97 and 87 kN).

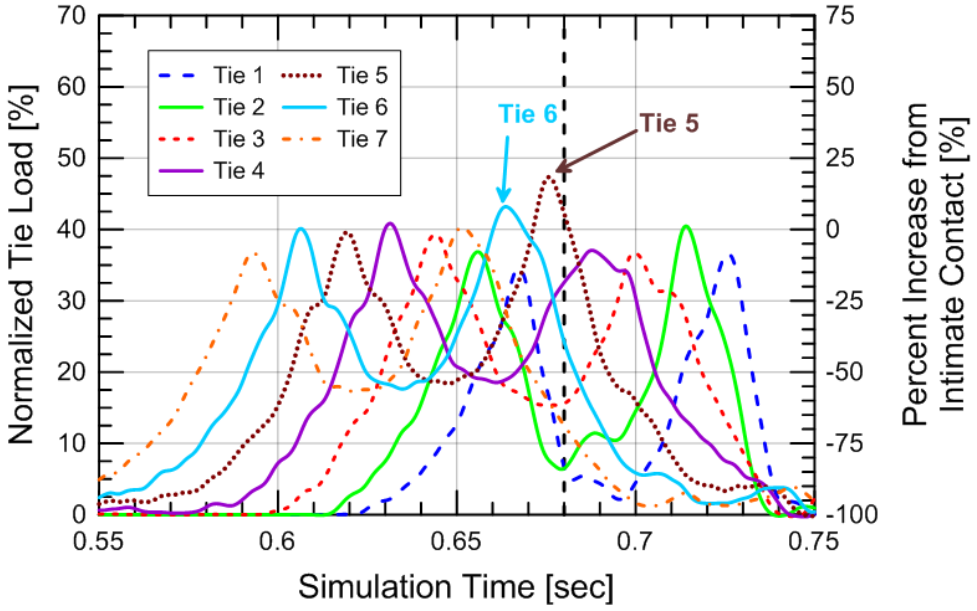

Figure 5.42: Time histories for Ties 1 through 7 in terms of Normalized Tie Loads.

This increase in dynamic wheel and tie load is expected to be dependent on the stiffness and damping of the secondary suspension system along with the differential stiffness between the approach and bridge. If the approach was stiffened or the bridge was allowed more movement by adding a ballasted bridge deck, rubber pads, and/or ballast mats, this dynamic load would decrease so these are possible remedial measures.

5.6.3 Parametric Analysis

Most transition zones experience substructure settlement with repeated loading and can produce unsupported ties in the approach. Examples can be referenced in Chapters 3 and 4. It is anticipated that this differential settlement can increase loads within the approach. To investigate this, a parametric analysis is performed to analyze how loads can increase and concentrate in the approach region.

The primary topics to be addressed in this section are: (1) the increased loading from differential settlement between the bridge deck and transition zone, and (2) the increased loading from differential settlement within the transition zone. To investigate these two topics, this section presents four different bridge approach analyses to illustrate how varying ballast settlement in the transition zone affects the dynamic loading environment.

The analyses are as follows:

- Even Ballast Settlement (0 mm to 16 mm)
- Gradual Increase in Ballast Settlement (0 mm to 2 mm)
- Uneven Ballast Settlement (0 mm to 2 mm)
- Field Measurements – Varandas et al. (2011)

5.6.3.1 Analysis #1: Even Ballast Settlement

Repeated train loadings will eventually cause the ballast to settle over time (Selig and Waters, 1994). The first analysis assumes homogeneous substructure settlement in the transition zone to illustrate the increased dynamic load from differential settlement between the bridge deck and transition zone. A schematic is displayed in Figure 5.43 and shows the rail hanging from the bridge deck with the ties closest to the bridge abutment developing tie-ballast gaps.

Previous analyses in the literature show the increased loads from simulating even ballast settlement in the approach. With 2.0 mm of settlement, Wang et al. (2015) predicted a 75% increase in wheel loads and 57% increase in ballast pressure. This model intends to investigate the increased load at multiple ballast settlement intervals to show how increased tie loads are related to ballast settlement.

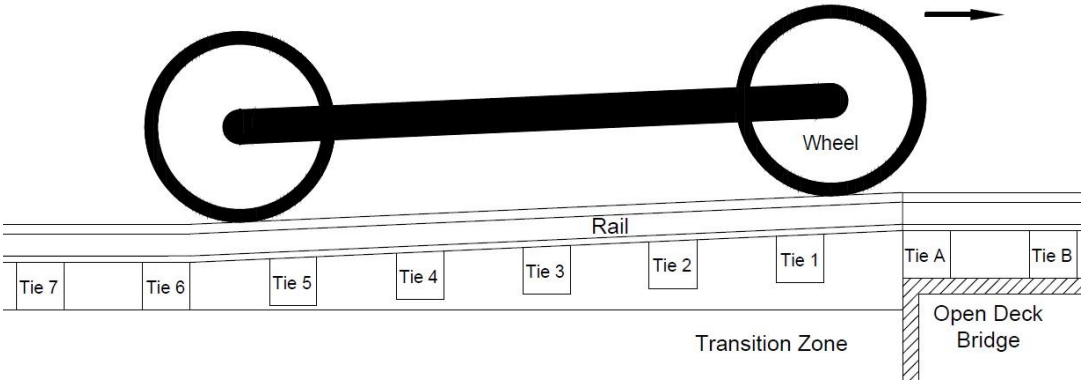

Figure 5.43: Wheel-rail-tie-ballast model showing even substructure settlement.

Settlement magnitudes up to 16 mm were simulated and Figure 5.44 shows the normalized tie load time histories assuming substructure settlements of 8.0 mm. The results show significantly greater tie loads at Ties 5 and 6 with maximum normalized tie load values of 78%

and 60%. Similar to the initial analysis with no ballast settlement, these maximum values occur as the front wheel passes the bridge abutment.

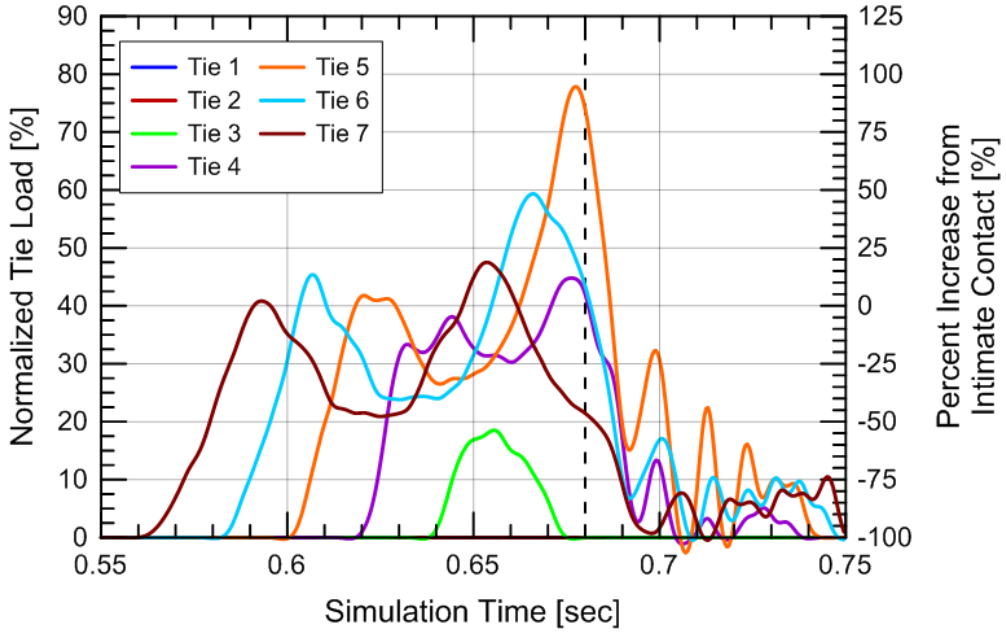

Figure 5.44: Normalized tie loads of Ties 1 through 7 assuming substructure settlements of 8.0 mm.

To illustrate how the maximum normalized tie loads increase with increasing substructure settlement, the maximum normalized tie load values of the seven ties closest to the bridge abutment are displayed in Figure 5.45. At ballast settlement values of 0.0 mm and 8.0 mm, the maximum normalized tie loads can be verified with the time histories in Figures 5.42 and 5.44. Figure 5.45 illustrates that homogenous substructure settlements result in load amplifications primarily at Ties 5 and 6 with maximum normalized tie loads of about 100% at Tie 5 (10 ft). This is nearly a 120% increase in load if the tie and underlying ballast were designed for 40% of the static wheel load. If the cutoff for problematic tie loads is a 50% increase from static values (Plotkin and Davis, 2008), i.e. a normalized tie load of 60%, the models predicts this will occur at ballast settlements of 4.0 mm.

A comparison with the model from Wang et al. (2015) shows similar increases with a 40% increase in tie load as opposed to a 57% increase in ballast pressure at ballast settlements of 2.0 mm. The values compared are different but the increases are within the same range and are considered reasonable.

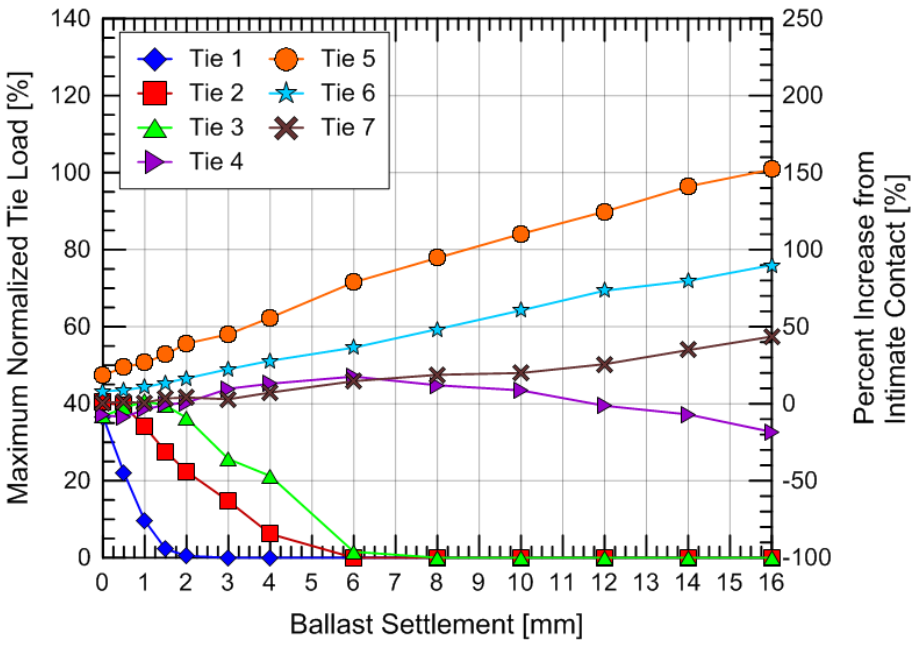

Figure 5.45: Normalized tie loads of back wheel for substructure settlement ranging from 0.0 to 16.0 mm.

This verifies past analyses (Wang et al. 2015; Paixão et al. 2014) that differential settlement is a larger contributor to increased dynamic loads than differential stiffness because of the greater change in wheel elevation and suggests that transition zone design should focus on arresting the substructure settlement in the transition zone before attempting to smooth the transient stiffness between the open track, transition zone, and bridge. This strategy of reducing substructure settlement is more difficult to implement because the ballast will inevitably settle but can be helped by increasing ballast confinement using wing walls, increasing ballast density after tamping, improving load distribution under a single tie with under-tie pads, and improving ballast gradation and drainage.

5.6.3.2 Analysis #2: Gradual Increase in Ballast Settlement

The second bridge approach analysis involves a situation in which the ballast settlement, and therefore tie-ballast gaps, incrementally increase as the bridge abutment is reached. This is illustrated in Figure 5.46 with the ballast settlement under Ties 1 and 2 set to a value of "4x", the ballast settlement under Ties 3 and 4 set to a value of "2x", and the ballast settlement under Ties 5 and 6 set to a value of "x". The settlement magnitude "x" is varied from 0 to 2 mm. This means the gap height of Tie 1 equals 8 mm when Tie 5 is set to 2 mm.

This simulation attempts to replicate behavior observed in Site #6, Site #7, and Site #8 in Task II (Chapters 4.4.6 through 4.4.8). The purpose is not to perfectly replicate conditions but to gain a general understanding of how load is distributed in this scenario. This scenario could occur from greater ballast or subgrade settlements near the approach from various reasons, including: inadequate subgrade compaction near abutment, inadequate ballast compaction or loose ballast from tamping, and degraded or wet fouled ballast

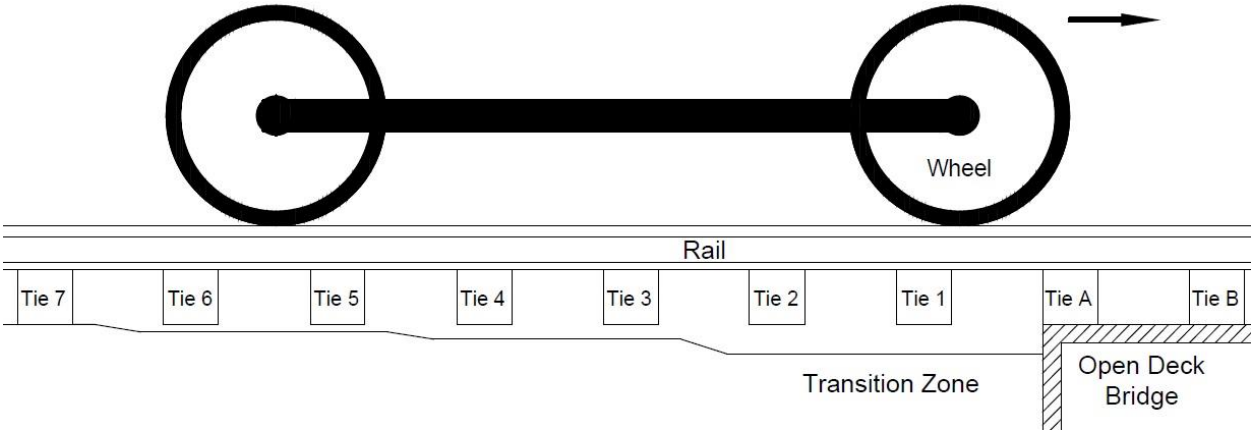

Figure 5.46: Wheel-rail-tie-ballast model showing a gradual increase in substructure settlement.

Figure 5.47 displays the change in maximum normalized tie loads from the back wheels due to variation of ballast settlement "x". For ballast settlement "x" of zero, all ties experience maximum wheel loads of about 30 to 50% (see Figure 5.42). As the ballast settlement increases, the maximum normalized tie load experienced by Ties 5 and 7 increase as well. At a ballast settlement "x" value of 2.0 mm, the maximum normalized tie load of Tie 5 approaches 120%, an increase of 146% from intimate contact assuming a normalized tie load of 40%.

All other ties experience a decrease in maximum normalized tie load with increasing ballast settlement as the load is being distributed away from these ties. This behavior agrees with the open track behavior in Chapter 5.5 because the load is still being redistributed from poorly supported ties to more well supported ties. For example, the good tie support at Tie 7 causes the rail to act like a simply supported beam with pinned connections at the bridge deck, i.e. Tie A, and Tie 7. When loaded, the rail displacement will be greater at Tie 5 than Tie 6 therefore Tie 5 will experience a greater load. This same concept explains why Tie 3 experiences greater load than 4.

The results show loading is sensitive to local differential ballast settlement of 1.0 mm. This difference would be anticipated in physical conditions so increased loading is probable. The increase in load at Ties 5 and 7 explain how the presence of tie-ballast gaps initially located in the first 10 or feet of the transition zone region can result in tie-ballast gaps spreading outwards from subsequent train passes.

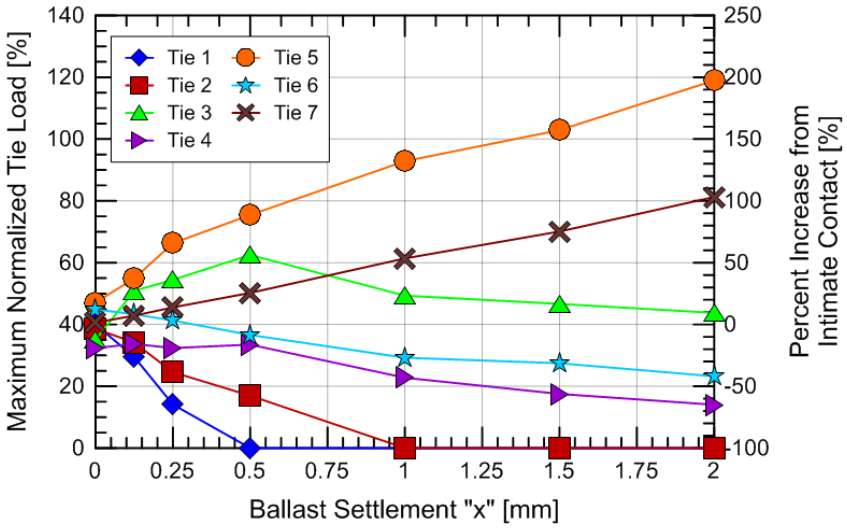

Figure 5.47: Normalized tie loads of back wheel for Tie 1 through 7 for a situation in which the substructure settlement gradually increases.

5.6.3.3 Analysis #3: Uneven Ballast Settlement

The third bridge approach analysis involves a situation in which a single tie (Tie 3) is in intimate contact with the ballast while the ballast under the remaining ties have settled at value "x" (see Figure 5.48). This situation has been observed at Site #5 in Task II (Chapter 4.4.5) and appears because the substructure settlement in the bridge approach will not be homogenous, meaning the substructure will settle more in certain locations than others. This may be due to increased loads, uneven ballast compaction, rail joints, fouling, or drainage concerns.

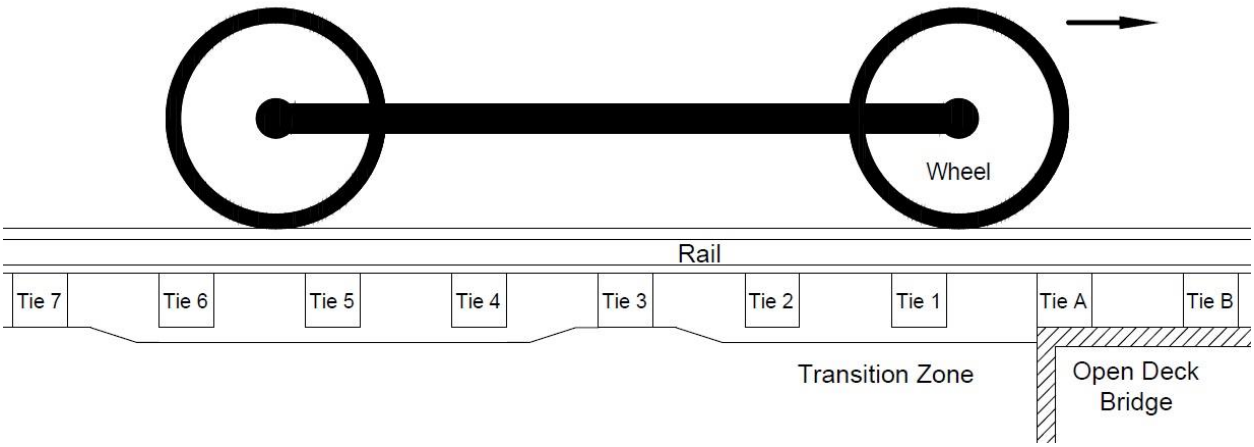

Figure 5.48: Wheel-rail-tie-ballast model showing a uneven substructure settlement.

Figure 5.49 displays the change in maximum normalized tie load due to the variation of ballast settlement "x". As the ballast settlement increases, the maximum normalized tie load experienced by Tie 3 significantly increases. At a ballast settlement value "x" of 2.0 mm, the maximum normalized tie load of Tie 3 surpasses 122%. This represents an increase in tie-ballast load of about 205% from intimate contact in which the normalized tie load is assumed to 40%. Additionally, Tie 7 shows a slight increase in tie load while Ties 1, 2, 4, 5, and 6 show decreases in tie load. This is due to the redistribution of wheel load away from poorly supported ties to the supported ties.

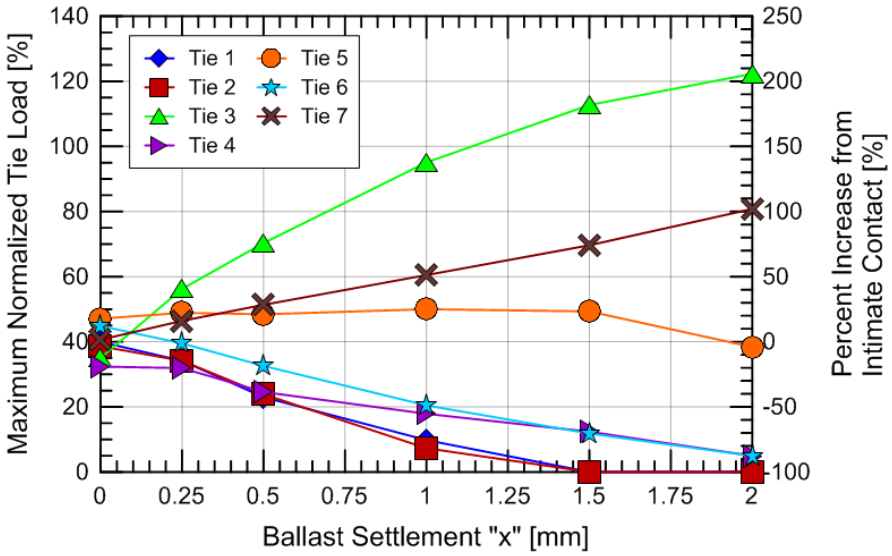

Figure 5.49: Normalized tie loads of back wheel for Tie 1 through 7 for a situation uneven substructure settlement.

This analysis reinforces the sensitivity of load distribution in transition zones. Small differences in local settlement can result in highly concentrated loads in the approach.

5.6.3.4 Analysis #4: Field Measurements

Ballast in transition zones will likely settle at different rates at different locations because of variations in loading, ballast density, and ballast gradation due to particle breakdown and fouling. This produces spatially varying ballast surface profiles and therefore varying tie-ballast gap heights. Multiple field investigations in the literature (see Chapter 2.4.2) and in Task I and II show this trend. To investigate how the ballast surface profile affects wheel load distribution, multiple simulations were conducted with varying ballast surface profiles based on physical field measurements.

Analysis #4 compares the results of Analysis #0, i.e. no ballast settlement or tie-ballast gaps, with two simulations roughly based on transition zone measurements in The Netherlands by Varandas et al. (2011). This field data is used because it maps the tie-ballast gaps over the entire transition zone and better represents field behavior than the three previous analyses described above.

A visual illustration of the transition zone and the ballast settlements under each tie are presented in Figure 5.50 and the maximum normalized tie load values are displayed in a bar chart in Figure 5.51. Figure 5.50 shows the greatest ballast settlement occurring under Ties 2 and 3 with a gradual decrease in ballast settlement outwards from the bridge structure. This condition will still produces a "dip" in the rail at about Tie 4 or 5 because of rail bending.

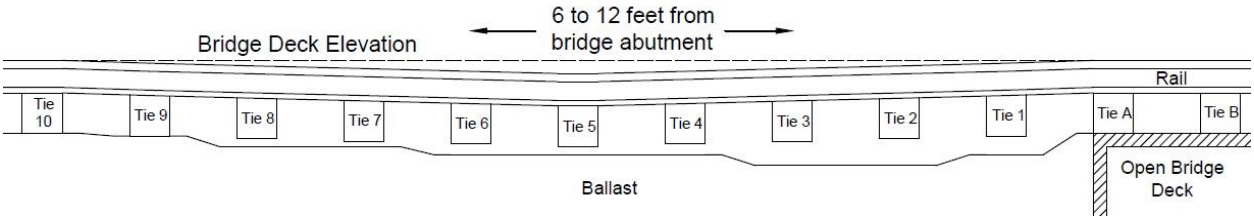

Figure 5.50: Wheel-rail-tie-ballast model showing a ballast surface profile based of field measurements from Varandas et al. (2011).

Three simulations are compared in Figure 5.49. Simulation #1, i.e. Analysis #0, is the control simulation in which no ballast settlement is assumed in the bridge approach (Figure 5.40). Simulation #2 includes ballast settlement and is based off the results from Varandas et al.

(2011). This case assumes ballast settlement occurs in the transition zone but no ballast settlement occurs in the open track, i.e. Tie 10. Simulation #3 is similar to Simulation #2 but with and additional 4 mm of ballast settlement added under all ties. The objective of including Simulation #3 is to investigate the combined effects of differential settlement within the transition zone (Analysis #4, Simulation #2) and differential settlement between the bridge deck and transition zone (Analysis #1). The ballast settlement values can be referenced in Figure 5.51.

The maximum normalized tie load results in Figure 5.51 shows that spatially varying but relatively smooth ballast profiles can still produce significant load redistribution and concentrated tie loads with maximum normalized tie loads ranging from 60 to 90%. Additionally, uniformly increasing ballast settlement in the transition zone results in further increased tie loads and is evident by comparing Simulation #2 and Simulation #3. This agrees with the results of Analysis #1 that differential settlement between the transition zone and bridge deck increases dynamic loads in the transition zone.

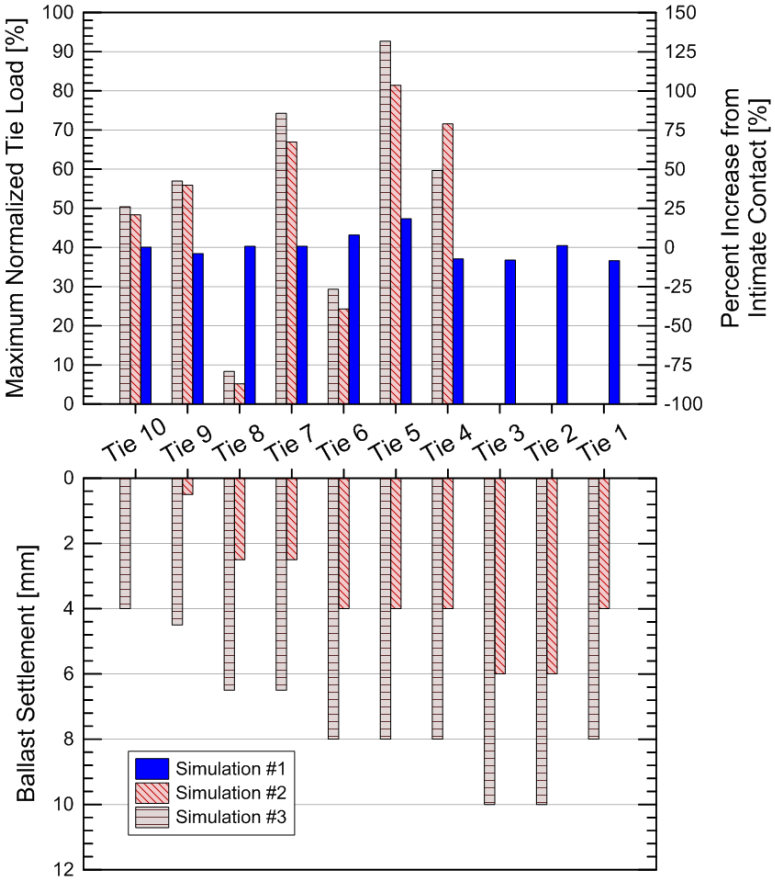

Figure 5.51: Maximum normalized tie load resulting from the respective ballast settlement under Ties 1 through 10 for three different simulations.

In physical track, it would be expected that the ballast under ties that experienced increased tie loads will also experience significantly greater degradation and settlement. Both the ballast surface profile and loading environment would then be expected to shift and concentrate on other ties in the transition zone. This is addressed in Chapter 5.7.

5.6.4 Summary

A numerical model was developed for LS-DYNA analyses that simulates a train truck entering an open deck bridge and is based off the track geometry at Amtrak's Upland Street Bridge in Chester, PA. The objective of the model is to investigate how differential settlement between the bridge deck and transition zone and tie-ballast gaps increase and concentrate dynamic tie loads in the transition zone. The main findings are summarized below:

- Differential stiffness between the bridge deck and transition zone resulted in about a 20% increase in the dynamic back wheel load. This increased wheel load was distributed to the ties 10 and 12 feet from the bridge deck (Ties 5 and 6), resulting in 20% and 7.5% increases in tie load, respectively, at these ties.
- Evenly increasing the ballast settlement in the transition zone produced tie-ballast gaps and increased tie loads by over 100%. This implies the effect of differential settlement between the bridge deck and transition zone has a much greater effect than differential stiffness between the bridge deck and transition zone. This is an important finding because historically the primary root cause associated with transition differential movement was typically stiffness difference.
- Unevenly increasing the ballast settlement in the transition zone also produced tie-ballast gaps and concentrated the wheel load on the most well supported ties. Increases in tie load of over 100% were observed for the most well supported ties. This suggests that differential settlement within the transition zone can be just as detrimental as differential settlement between the bridge deck and transition zone.
- The ballast settlement under each tie as reported by Varandas et al. (2011) was simulated to attempt to analyze the tie loads in physical track. The results of this analysis show increased tie loads of about 50 to over 100%. This suggests that some ties in transitions zones may be experiencing double the tie load than originally anticipated.

5.7 Progressive Settlement Analysis

The final section in Chapter 5 simulates the progressive settlement of a railroad bridge transition zone. The benefit of a progressive settlement over single time-frame analyses (Chapter 5.6) is the

behavior can be tracked with repeated loading and ballast profiles will not be assumed and therefore are believed to be more realistic.

The purpose of this analysis is to: (1) investigate the impact of increased loading in bridge approaches and (2) attempt to numerically explain measured field behavior. Exact matches are not anticipated because the ballast settlement behavior, track substructure conditions, and track superstructure conditions are not homogeneous or known but a conceptual understanding of track behavior can be gained.

5.7.1 Settlement Model

The first step of developing a progressive settlement analysis is to select an appropriate settlement model to represent settlement with repeated loading. To calculate ballast settlement within each iteration step, the empirical settlement model proposed by Sato (1997) and modified by Dahlberg (2001) was used. This model is well suited for differential loading environments, such as transition zones, because the calculated ballast settlement (y) is only a function of the load applied at the tie-ballast interface (P), a primary output of the numerical model. The original empirical settlement model by Sato (1997) was developed from laboratory ballast testing data which is preferred over continuum plasticity laws (Indraratna et al. 2012) built-in to existing numerical software because of greater control of the empirical model and the ability to produce settlement in discrete increments instead of every wheel pass. The notable exception would be the use of discrete element modeling (DEM) but these methods are still in its infancy and the computation power to couple DEM ballast behavior with continuum track components and dynamic loads is beyond current capabilities (Tutumluer et al., 2013; Chen et al., 2015). The empirical settlement relation from Dahlberg (2001) is plotted in Figure 5.52 and displayed in Equation 5.5:

$$y = 5.87E^{-9} * (P - 25)^4 \quad (5.5)$$

where y is the ballast settlement in mm after 10,000 load cycles and P is the tie-ballast contact force in kN. Figure 5.52 also shows a linear settlement model for comparison and will be discussed in subsequent sections.

A simple settlement model that is only a function of tie load is considered suitable for the initial analyses because the goal of the numerical simulation is to conceptually investigate changes in loading environment from the progressive settlement of a transition zone and not replicating or predicting field behavior. Physically, ballast settlement is a complex process that involves particle rearrangement, lateral movement, and degradation and is dependent on numerous factors, including ballast density, gradation, moisture content, rock type, angularity, hardness, confinement, rotation of principal stresses, loading material (concrete v. timber), and impact (Indraratna et al. 2012b). These factors can later be incorporated into the settlement model as required but the effects of ballast density are not expected to affect the general trends. The main assumptions included in the proposed settlement model are:

- The model assumes ballast settlement will not occur at tie loads less than 25 kN and a fourth-power relationship exists between ballast settlement (y) and tie-ballast contact force (P). This makes the model sensitive to higher loads than a linear relationship between ballast settlement and tie-ballast contact force.
- The settlement model does not account for ballast density, gradation, moisture content, rock type, angularity, hardness, confinement, rotation of principal stresses, etc., which has been shown to influence settlement magnitudes. This means the model assumes a homogeneous ballast condition and will not represent: (1) spatially varying ballast conditions, (2) high-magnitude ballast settlement often observed directly after tamping, and (3) decrease in ballast settlement with increasing ballast density. These factors and the implications on model results are discussed in subsequent sections.
- A typical iteration applies 20,000 loading cycles, which is considered to be equivalent to about 0.4 MGT (million gross tons). This value assumes 180 kN (40 kip) axle loads or 90 kN (20 kips) wheel loads and is a reasonable assumption for high-speed passenger trains.
- The model assumes track settlement only occurs in the ballast layer and ballast settlement is homogeneous under the tie.

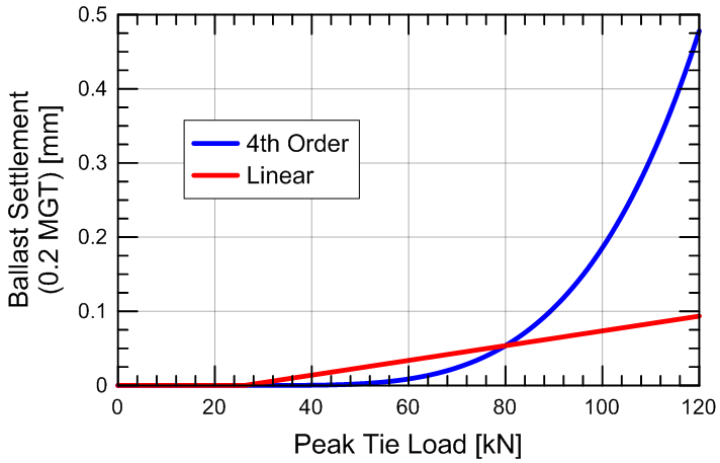

Figure 5.52: Relation between peak tie load and ballast settlement from 10,000 load cycles for a 4th order and linear settlement model.

5.7.2 Iterative Procedure

An iterative procedure is adopted to simulate the settlement of a bridge transition zone because settlement is not built into the numerical model and is expected to change with time. This means the geometry of the mesh is updated prior to every iteration. The four steps of the iteration procedure are described below:

1. A dynamic numerical simulation of the cart passing over the transition zone is completed with the model outputting the wheel loads, tie loads, tie displacement, and ballast displacements.
2. The peak tie loads from both the front and back axle of the cart are determined for Ties 1 through 10.
3. The ballast settlement under Ties 1 through 10 is calculated using the modified Dahlberg (2001) settlement model described above for both the front and back axles independently. The settlement values from each axle are then summed. The settlement of Ties 11 and greater are assumed to be equal to Tie 10 and represent open track.
4. The calculated settlements from Step 3 are added to the existing cumulative settlements under each tie and are incorporated into the numerical model geometry for the next iteration.

An important parameter in the iterative procedure is the representative MGT value of each iteration step, i.e. 0.4 MGT or 20,000 wheel passes. This is conceptually similar to a "time-step" and can significantly affect the simulation results because the transition zone loading environment is sensitive to local differential ballast settlements. This means large iteration steps can produce increased loads that could be avoided if using smaller iteration steps.

To show this, the maximum normalized tie load of a tie within a transition zone (Tie 6 in Figure 5.53) is determined using iteration steps of 0.2, 0.4, and 0.8 MGT. For 0.2 and 0.4 MGT iterative steps, the results are identical and the tie loading seems to be at a stable "equilibrium state". However, the tie loads significantly deviate if assuming iteration steps of 0.8 MGT. This behavior indicates the progressive analysis has come out of "equilibrium" and entered a state in which the load fluctuates between adjacent ties every iteration. In this case, the load path at 4 MGT distributes load onto Tie 6 and away from adjacent Ties 5 and 7. This produces large settlement of the ballast underneath Tie 6. During the next iteration, the load path then shifts away from Tie 6 and onto adjacent Ties 5 and 7, resulting in large settlements under those ties. The process will continue indefinitely unless smaller iteration steps are used to allow the progressive analysis to re-enter a state of "equilibrium". The response from the large iteration steps (0.8 MGT) is not considered representative of physical track because settlement occurs under each single wheel so iterative steps of 0.8 MGT (20,000 load passes) are used.

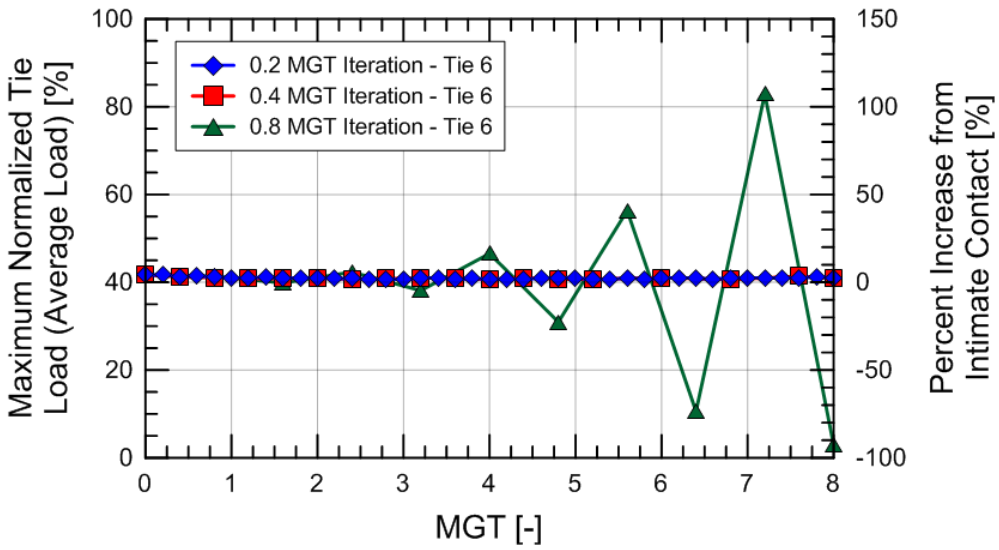

Figure 5.53: Comparison of maximum normalized Tie 6 load (front and back wheel average) with iterations steps of 0.2, 0.4, and 0.8 MGT.

5.7.3 Progressive Settlement Analysis

The results of the progressive analysis suggest transition zones can experience three distinct stages of behavior. Stage 1 is called the "Initial Stage" or "Pre-Equilibrium Stage" and represents the newly constructed track condition in which no substructure settlement has occurred.

Assuming homogenously dense ballast, this stage isolates the effect of differential stiffness between the bridge and approach and represents loading within 0.0 to 0.4 MGT. Stage 2 is called the "Equilibrium Stage" and represents the track response within 0.4 to 28 MGT in this particular analysis but this range will vary significantly or not even appear in physical track. Stage 3 is called the "Post-Equilibrium Stage" and represents the hypothetical track response at iterations greater than 28 MGT in this particular model. Each stage and its unique characteristics are explained in the subsequent sections.

5.7.3.1 Stage 1: First Iteration (0.0 MGT)

The first simulation of the cart passing over the bridge approach assumes newly laid and compacted ballast so no ballast settlement or tie-ballast gaps are present (see Figure 5.40). This simulation is presented in Chapter 5.6.2 and results show a 20% increase in the dynamic back wheel load from static conditions (120 kN) occurs about 10 feet from the bridge abutment. This increased back wheel load is distributed primarily to Ties 5 (10 ft.) and 6 (12 ft.), which show increases of 20% and 7.5%, respectively (normalized tie loads of 47% and 43%) from the assumption of intimate tie-ballast contact (normalized tie load = 40%).

While a normalized tie load of 40% would produce a ballast settlement of 0.11 mm at 0.4 MGT (see Figure 5.52), the increased load at Tie 5 from the coupling of the front and back axles produces 0.18 mm of ballast settlement, almost doubling the "standard settlement". This local differential settlement within the approach is a response to differential stiffness between the bridge and approach.

5.7.3.2 Stage 2: Second Iteration (0.4 MGT)

The ballast settlement from the initial run is incorporated in the numerical model for the second iteration analysis by decreasing vertical grid sizes of the ballast elements underneath each tie in the transition. The differential settlement within the transition zone is expected to change the wheel load distribution amongst the underlying ties and cause the load to shift from ties with the greatest ballast settlement to adjacent ties with lesser amounts of ballast settlement. This load redistribution mechanism is illustrated in Figure 5.54(a) with the second iteration analysis showing a reduction in load at Ties 5 and 6 and in increase in load at Ties 3, 4, and 7. For example, the normalized tie load at Tie 5 from the back wheel decreases from 47% (20%

increase from intimate contact) to 44% (12% increase from intimate contact) and a similar reduction is observed for the front wheel. While this decrease in tie load may not seem significant, the non-linear tie load/ballast settlement relationship reduces the ballast settlement under Tie 5 from 0.18 mm between 0.0 to 0.4 MGT to 0.13 mm between 0.4 to 0.8 MGT (Figure 5.54(b)). This results in Tie 5 and 6 still experiencing the greatest dynamic loads and settlement but to a lesser degree than the Stage 1 analysis (0.0 MGT).

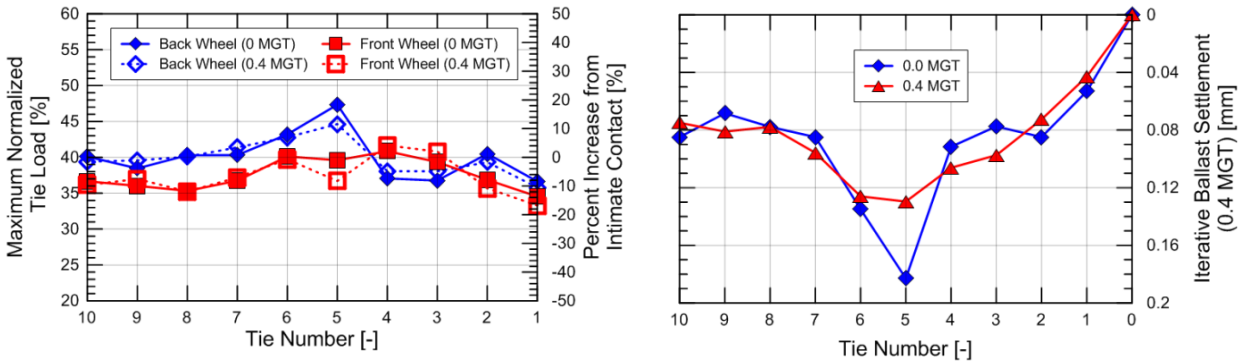

(a) (b)

Figure 5.54: (a) Maximum normalized tie loads and resulting (b) iterative ballast settlement from train passes at 0 and 0.4 MGT.

This suggests the ballast will attempt to settle in a manner that reduces tie loads within the transition zone and allow the transition zone to enter a stage of "equilibrium" in which tie loads are minimized. Therefore, any track experiencing increased loads from differential stiffness, i.e. pre-equilibrium, will subsequently experience differential ballast settlement that results in a better wheel load distribution amongst transition zone ties, i.e. equilibrium.

5.7.3.3 Stage 2: Settlement

To investigate the long-term settlement behavior of the transition zone, the cumulative ballast settlement profile, tie-ballast gaps, and transient displacements are recorded with increasing MGT. The track profile at 28 MGT with proportional but exaggerated settlements is displayed in Figure 5.55(a) and illustrates how the rail hangs from the bridge deck and the development of tie-ballast gaps within the approach. The analysis discontinued at 28 MGT because (1) the progressive analysis was continually requiring smaller iterative steps to remain in "equilibrium" and (2) the assumption of Ties 11+ having identical loading and settlement as Tie 10 did not hold

as the load shifts farther away from the bridge abutment with increasing settlement and load redistribution.

Figure 5.55(b) shows increasing cumulative ballast settlement with increasing MGT and the gradual shifting of maximum cumulative ballast settlement from under Tie 5 (10 ft.) to Tie 7 (14 ft.) during the duration of the analysis. This trend would be expected to continue as the load shifts farther from the bridge abutment. The maximum cumulative settlement at 28 MGT is 9.4 mm at Tie 7 (14 ft.) and the settlement at Tie 10 is 8.9 mm, both of which are close but slightly greater than the 7.6 mm for a normalized tie load of around 40%. Due to the differential settlement between the bridge deck and the transition zone, tie-ballast gaps develop in the transition zone and are shown in Figure 5.55(b). Initially, the tie-ballast gaps appear only under Ties 1 and 2 but gradually expand outwards and increase in magnitude as bridge and open track rail elevations continue to deviate.

The transient displacement from the cart passing over the transition zone is displayed in Figure 5.55(d). This shows a deviation between the settlement and transient displacement profiles where the transition zone (Ties 1 through 8) experience significantly greater displacements than the open track (Tie 10). This behavior agrees with the measured results at multiple transition zone locations (See Chapter 2.4.2, Chapter 3, and Chapter 4). The varying transient displacement in the transition zone is primarily explained by tie-ballast gap magnitudes because the ballast stiffness is assumed to be homogenous and loading is relatively similar across the transition zone (Figure 5.55b). This mirrors the transient behavior of Upland Avenue in Chapter 3.

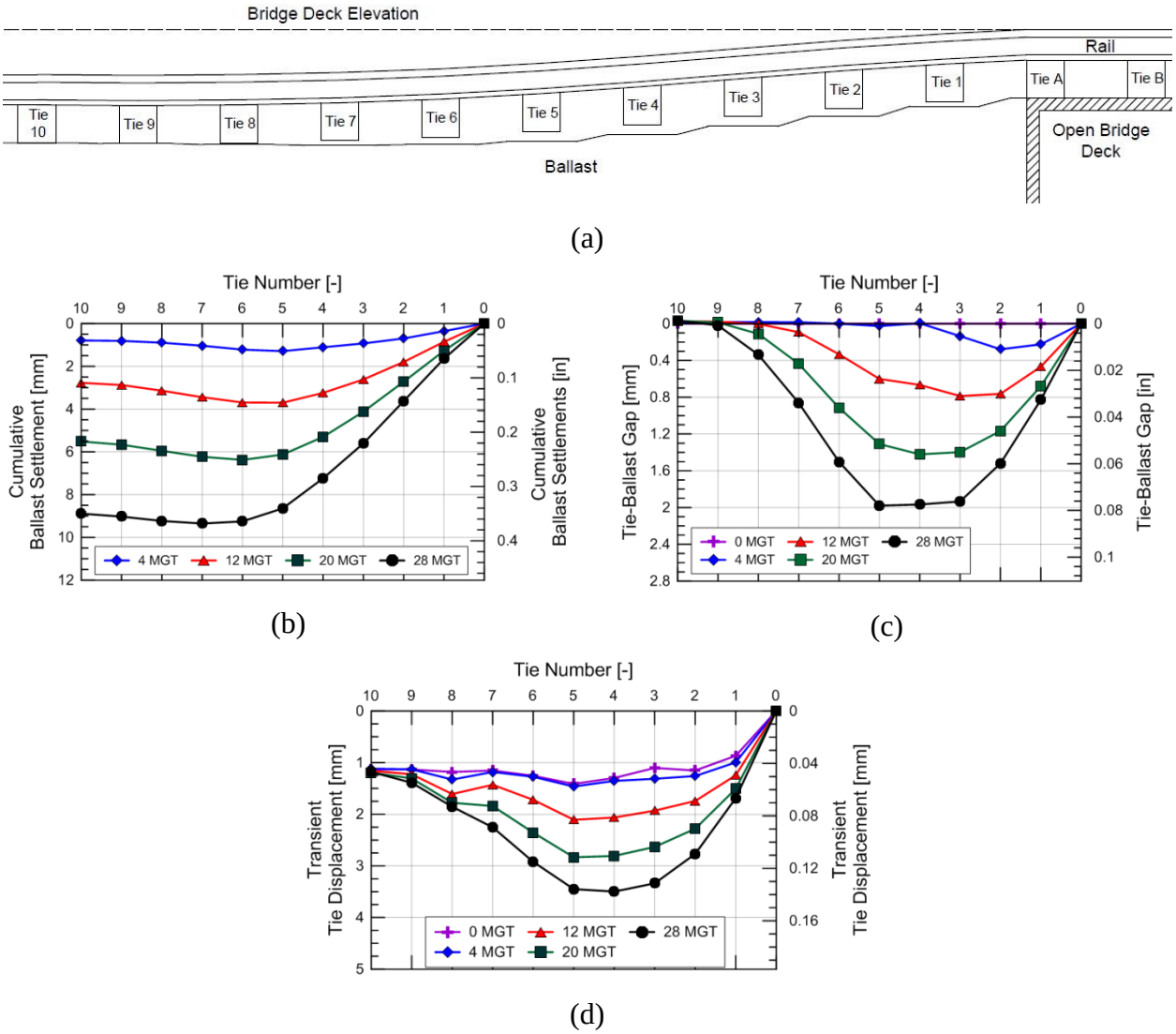

Figure 5.55.: (a) ballast settlement profile at 28.0 MGT and cumulative (b) ballast settlement, (c) tie-ballast gaps, and (d) transient displacement with increasing MGT.

The development of a tie-ballast gap has implications on track behavior because track system discontinuities allow for more movement and impacts between track components, and thus component degradation. For example, the freely moving tie will establish contact with the ballast during train loading and can result in increased tie wear and ballast degradation due to grinding and impact between the tie and ballast. This behavior is covered in Chapter 2.2.4 and Chapter 4.4.5.

5.7.3.4 Stage 2: Loading

The progressive settlement described above and shown in Figure 5.55 is related to the applied tie loads and ballast settlements at each iteration. The changes in wheel loads, tie loads, and iterative ballast settlements with MGT is displayed in Figure 5.56. The results show the peak wheel loads increase from about 120 kN during the first iteration (0.0 MGT) to about 140 kN at 28 MGT. This increased wheel load is typically located over Tie 5 (10 ft.) and is caused by the coupling of the front and back axles as the cart passes from the lower elevated transition zone to the higher elevated bridge deck. The increase in wheel load from 20% to 40% is attributed to the effect of ballast settlement. However, it is lower than predicted from models in which ballast settlement is uniform throughout the transition zone because of the "dip" in rail elevation around Tie 5 that results from uneven ballast settlement.

Figure 5.56(b) displays the normalized back wheel tie loads. A gradual increase in load is observed in Ties 6 through 10 while a gradual decrease in load is observed in Ties 1 through 4. The load experienced by Tie 5 remains essentially constant throughout the analysis excluding the initial run at 0.0 MGT. This load redistribution represents a shift of loading away from the bridge abutment as the ballast near the bridge settles resulting in unsupported ties. More local load redistribution is apparent by comparing Ties 2 and 3 in Figure 5.56(b). Tie 2 (open red squares) experiences a decrease in normalized tie load from about 40% at 0.0 MGT to 24% at 23 MGT. However at 23 MGT, the load experienced by Tie 2 gradually begins to increase while a reduction is observed at Tie 3 (filled green triangles). The sensitivity of load distribution from local differential settlement produces this shift in load and this behavior is expected in most physical track locations. The tie loads from the front wheel remain relatively constant throughout the analysis so they are not displayed.

The iterative ballast settlements (assuming 0.4 MGT intervals or 20,000 loads) is displayed in Figure 5.56(c) and reinforces the significant settlement observed at Tie 5 during the first iteration (0.0 MGT) as the transition zone attempts to reach a state of equilibrium. As MGT continues to increase, the results show a shift in iterative settlement from Tie 5 to Ties 8 through 10 as the load is distributed away from the bridge abutment, agreeing with Figure 5.55(b). It is expected the load and iterative settlement will continue to shift away from the bridge abutment if the analysis continues with loads greater than 28 MGT.

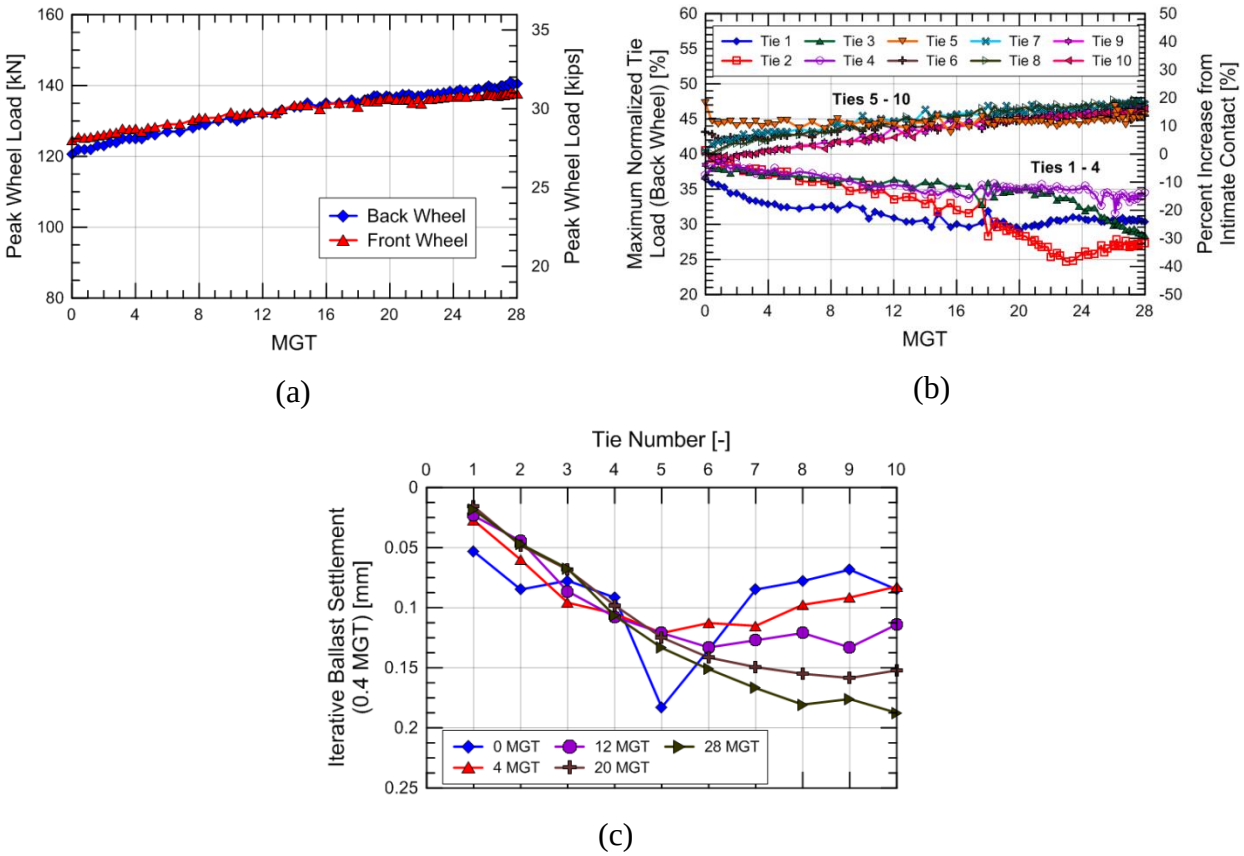

Figure 5.56: Change in (a) peak wheel loads, (b) tie loads from back wheel, and (c) iterative ballast settlements with increasing MGT.

5.7.3.5 Post-Equilibrium

As illustrated in previous sections, selecting an appropriate iterative settlement or "time-step" is important because large settlement increments can cause the progressive analysis to leave a state of equilibrium. This lack of equilibrium results in the increase and fluctuation of tie loads but can be avoided by reducing the time-step, so is considered a numerical artifact. However, the question of what time-step appropriately represents track settlement must be addressed if the analysis is allowed to continue. The typical time-step assumes 0.4 MGT, 20,000 load passes, and a "standard iterative settlement" of 0.11 mm. The smallest time-step used in the analysis assumes 0.1 MGT, 5,000 load passes, and a "standard settlement" of 0.045 mm (45 micrometers).

If the progressive analysis is allowed to continue, the required iteration or time-step to maintain analysis equilibrium and the associated "standard iterative settlement" will continue to decrease. This implies the "boundary condition" of the rigid bridge deck eventually results in a situation in which the track cannot evenly redistribute tie loads and maintain equilibrium because

the differential settlement between the bridge deck and approach is too large. This moves the transition zone into a Stage 3 where a lack of equilibrium produces increased and fluctuating tie loads in the approach.

Because the ballast in the numerical model is assumed to be an idealized continuum material and the settlements occur in discrete intervals at each iteration, the MGT at which the model reaches the "Post-Equilibrium Stage" is dependent on the time-step or how low of a time-step is allowed. However, physical ballast is a granular material with multiple settlement mechanisms, including particle rearrangement, lateral movement, and particle degradation and ballast experiences a wide range of gradations, fouling, rock type, and drainage conditions, all of which affect settlement. This means ballast settlement physically occurs in discrete increments and this increment depends on the settlement mechanism and ballast condition. The range of physical settlement increments and therefore an appropriate range of time-steps are not known at this time so this stage cannot be accurately replicated in a numerical model without field verification. However, the model indicates that physical track will eventually reach a post-equilibrium stage and produce increased dynamic loads but the exact behavior is not known. Ideally, transition zones should not reach this stage via design or remedial measures.

5.7.3.6 Discussion

The results of the progressive settlement analysis provide insight to transition zone performance. As expected, the near rigid bridge deck represents a restricting condition that produces differential settlement between the bridge and approach, resulting in the gradual shifting of tie loads away from the bridge deck. Tie-ballast gaps develop near the entrance bridge abutment in reaction to the differential elevation between the rigid bridge and settling approach.

Comparisons between the results at 28 MGT and field observations show general agreement in behavior but the simulation does not replicate the field measured differential settlement between the transition zone and open track. For example, the difference between ballast settlement in the transition zone and open track in the numerical model (9.35 mm v. 8.89 mm) is less than some field measurements (14 mm v. 1 mm). This suggests the numerical model is not simulating the increased load environment in the transition zone and/or the ballast will settle at greater rates than the predicted settlement relation in Figure 5.52. This will be addressed in detail below.

The results additionally show three stages within the transition zone resurfacing lifespan. The first stage called the initial stage or "pre-equilibrium" stage and generally represents track immediately after tamping with no settlement, i.e. smooth unloaded rail elevations between the bridge and approach. While the constant rail elevation is an ideal condition, the track itself is out of equilibrium because the differential stiffness between the bridge and approach produces an increased load from the coupling of the front and back axles. The track must then react to this increased loading from the differential stiffness between the bridge and approach with local differential settlement within the approach. The local differential settlement better distributes the wheel load amongst the underlying ties and allows the transition zone to reach an equilibrium state in which the normalized tie loads remain close to 40%.

While not simulated, a loose ballast matrix immediately after tamping will result in large initial settlements as the ballast compacts into a more dense state. This post-tamping loose ballast state would also be considered a part of the "pre-equilibrium" stage because the ballast will attempt to reach a density and gradation configuration that is in balance with the external loading. This immediate compaction can result in significant settlement and also significant local differential settlement if the ballast density is spatially varying from tie to tie. If the varying ballast density is great enough, the transition will likely immediately go to the post-equilibrium stage and never reach equilibrium. For transition zones experiencing recurring track geometry problems, this is a likely scenario.

The second stage or equilibrium stage represents ideal transition zone behavior in which the wheel load is well distributed amongst the underlying ties. This occurs when the ballast reaches its unique density and when the local differential settlement within the approach balances the effects from the differential stiffness between the bridge and approach.

The third hypothetical stage is called the post-equilibrium stage and represents a condition in which the transition zone cannot remain in a state of equilibrium and results in increased tie loads from uneven load distribution amongst the ties. In the progressive analysis, this stage could be entered from large iteration steps or from the eventual restricting condition of the bridge deck. However, a transition zone may also enter this stage from loose or varying post-tamping ballast densities, reduced-performance ballast in the approach, varying rates of ballast degradation, or any factor that could prevent the track from remaining in a state of equilibrium.

5.7.4 Additional Analyses

The base progressive analysis simulates the progressive settlement of a transition zone under ideal conditions in which the ballast is represented as a homogenous material with identical settlement behavior along the track. This is unlikely to physically occur as ballast will (1) be tamped at various densities due to inevitable tamping imperfections, (2) experience varying confining pressures and moisture contents, and (3) eventually degrade from ballast breakdown and fatigue, tie-ballast contact, and tamping. This produces a condition in which the ballast is spatially and temporally varying and the ballast will not behave in the manner represented by the settlement model.

The subsequent analyses challenge some assumption of the base progressive analysis and explore unideal conditions to better represent conditions in physical track. The analyses are listed below:

1. The first additional analysis compares the behavior of the assumed 4^{th} order and a linear tie load-settlement model because the relation between tie load and cyclic settlement is still not well understood and could affect model results.
2. The second analysis simulates the progressive settlement assuming iterative steps of 0.8 MGT. The purpose of this analysis is produce an upper bound to better understand the influence of the iteration step and transition zone behavior if loads are expecting to fluctuate back and forth between ties during the progressive settlement.
3. The third analysis assumes a correlation between ballast degradation and tie-ballast gaps to investigate the effect of heterogeneous ballast conditions. Increased ballast settlement from tie-ballast gaps was chosen because it could be mathematically represented and involves less arbitrary and abrupt changes in settlement relations than attempting to represent ballast fouling, varying confining pressures, moisture, or other factors expected in physical track.
4. The fourth analysis is a sensitivity analysis that randomly varies the settlement under each tie at 16 and 28 MGT to represent heterogeneous ballast conditions. The purpose of this analysis is to determine the effect of randomized heterogeneity in track and its effect on increased loads.

5.7.4.1 Analysis 1: Linear Load-Settlement Relationship

The first additional analysis assumes a linear tie load-ballast settlement relationship to check the sensitivity of the tie load-ballast settlement relationship. The relationship in displayed in Figure 5.52 and assumes identical settlement at tie loads of 25 and 80 kN. This linear relation should put more emphasis on lower tie loads (<70 kN) and make the settlement less sensitive to higher loads (>90 kN). The linear ballast settlement equation is displayed in Equation 5.6:

$$y = 9.95E^{-4} * P - 0.0258 \quad (5.6)$$

The analysis assuming the linear settlement relationship above was completed for 8 MGT and showed similar overall behavior as the 4th order relation. Similar to the 4th order analysis, the linear analysis produces a ballast surface profile that attempts to reduce tie loads and greater settlement is experienced under Ties 5 and 6 (Figure 5.57a). The main differences result from the linear relationship being less sensitive to changes in tie load so greater loads but less cumulative settlement is experienced at Ties 4 through 6 while significantly less loads but greater settlement are experienced at Ties 1 through 3 (Figures 5.57a and c). The greater settlement at Ties 1 through 3 also results in larger tie-ballast gap heights (Figure 5.57b).

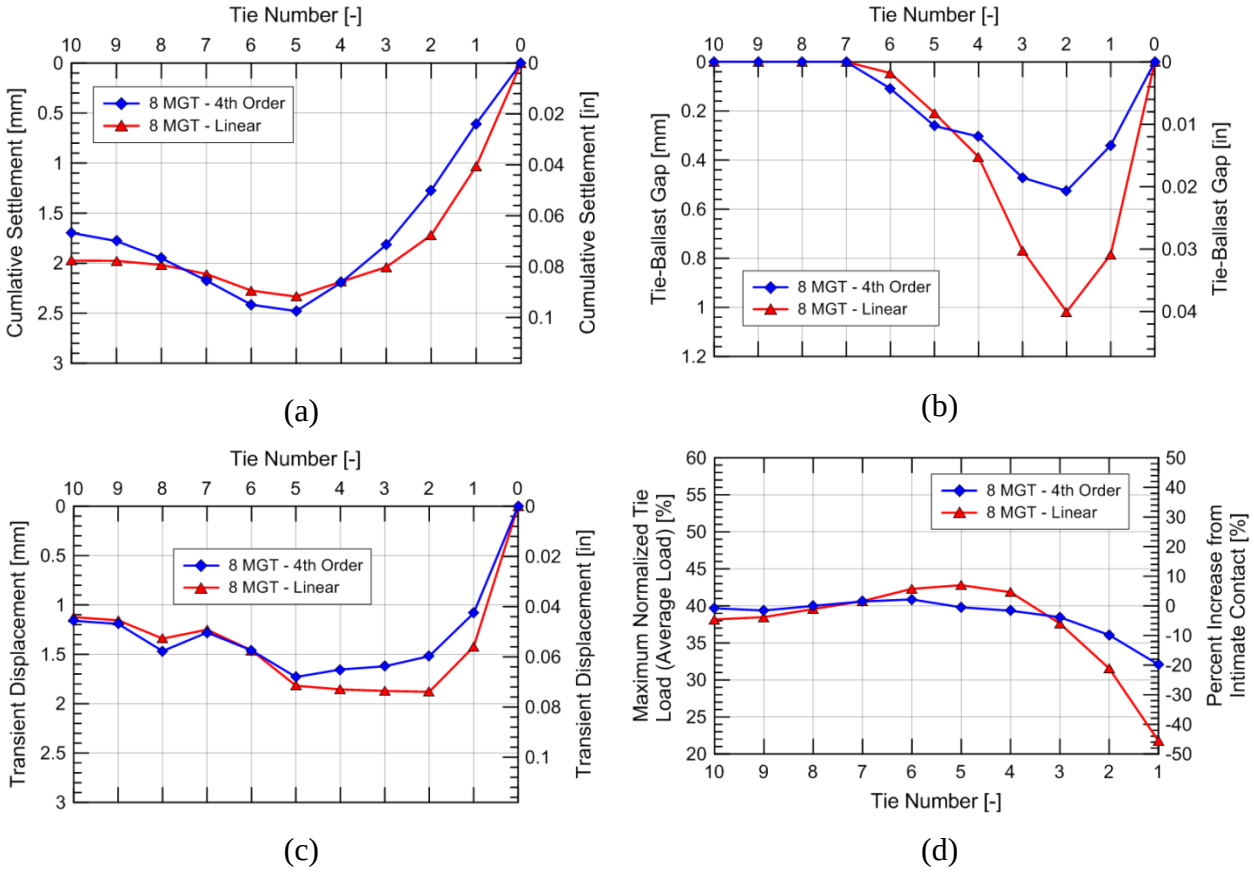

Figure 5.57: Comparison between 4th order and linear relationship for (a) cumulative ballast settlement, (b) tie-ballast gaps, (c) transient displacements and (d) normalized tie loads.

The similar response between the 4th order and linear settlement relations implies that the findings from the study are not dependent on the order of the settlement model. Therefore, the 4th order equation will be used for the remainder of the study.

5.7.4.2 Analysis 2: 0.8 MGT Ballast Iteration Step

The second additional analysis investigates the effects of using iterative steps of 0.8 MGT. The analysis objective is to emphasize the importance of the iteration step in the progressive analysis and secondly to conceptually gain insight into potential behavior of track in the hypothetical post-equilibrium stage. It is not expected that the behavior at iterative steps of 0.8 MGT will physically occur, but the analysis provides a conceptual upper bound on post-equilibrium track behavior.

A diagram of the unloaded track profile at 8.0 MGT is displayed in Figure 5.58 along with a comparison between 0.4 MGT and 0.8 MGT analyses of cumulative ballast settlement and transient tie displacement profiles. The results show significantly greater displacement in the approach as opposed to the 0.4 MGT analysis. The greater settlement is a result of greater loads in the approach (Figure 5.58d) from uneven distribution of wheel loads to the ties. As observed, the tie loading can increase up to 50 to 100%. By comparing the response of Tie 5 and 6 at each iteration in Figure 5.58(e), the tie load clearly fluctuates back and forth between ties at each iteration. This occurs because the high tie load causes the ballast to overcompensate and experience large settlements, which then shifts the load to adjacent ties in subsequent analyses. The assumption of a non-linear tie load-settlement relation means the track region that experiences this load fluctuation will also experience greater settlement.

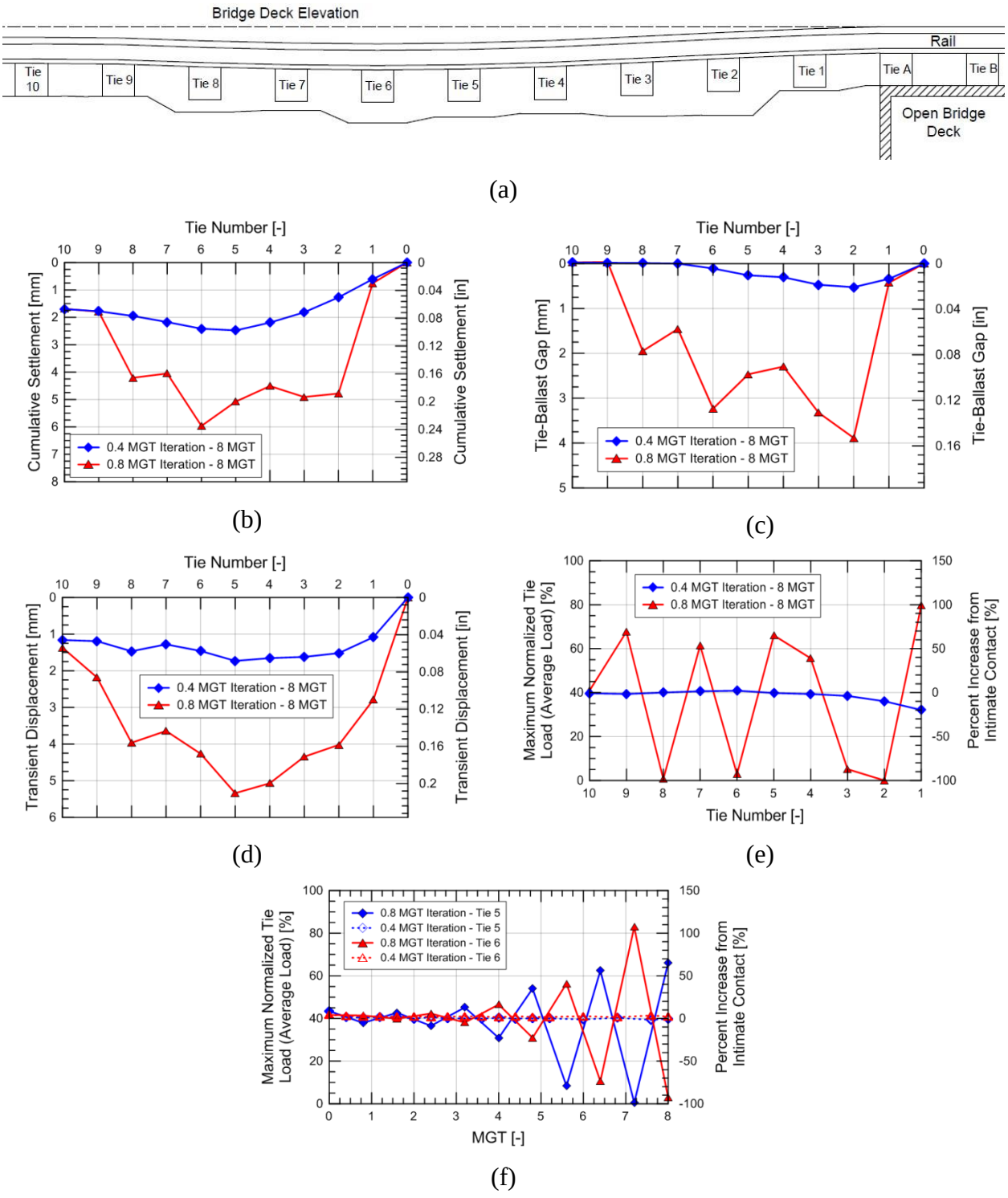

Figure 5.58: **(a) ballast settlement profile at 8.0 MGT and comparison between 0.4 and 0.8 MGT iterative steps with (b) cumulative ballast settlement, (c) tie-ballast gaps, (d) transient tie displacement, (e) tie loading, and (f) Tie 6 loading.**

As mentioned, this analysis is designed to represent an upper bound of track behavior when the approach is in a post-equilibrium state. Physically, except in extreme circumstances, the shifting of load between ties is expected to be more gradual and result in lower increased tie loads than predicted by this analysis. However, larger tie loads can initiate ballast degradation, which can then lead to greater settlements over time in regions where load fluctuation may occur.

5.7.4.3 Analysis 3: Tie-Ballast Gap

The third analysis incorporates the effect of tie-ballast gaps into ballast settlement to simulate the effect of ballast degradation in transition zone settlement. The modification of the settlement relation is based on laboratory testing by Selig and Waters (1994), which shows about triple the ballast settlement with a gap of 1 to 4 mm assuming no fouling. This will be incorporated by modifying the ballast settlement model as shown in Equations 5.7 through 5.9:

$$y = [5.87E^{-9} * (P-25)^4] \qquad (\delta_{gap} < 0.25\ mm) \qquad (5.7)$$

$$y = [5.87E^{-9} * (P-25)^4] * (2 * \delta_{gap} + 0.5) \qquad (0.25\ mm \geq \delta_{gap} > 0.5\ mm) \qquad (5.8)$$

$$y = [5.87E^{-9} * (P-25)^4] * (\delta_{gap} + 1) \qquad (\delta_{gap} \geq 0.5\ mm) \qquad (5.9)$$

where δ_{gap} is the tie-ballast gap height. The analysis assumes that a gap of 0.25 mm or greater must be present before the effect on ballast settlement begins and greater tie-ballast gaps will result in greater settlement.

A diagram of the unloaded track profile at 16.0 MGT is displayed in Figure 5.59 along with comparisons between the basic and modified settlement relation analyses of cumulative ballast settlement and transient tie displacement profiles. Similar to the previous analysis, the results show significantly greater displacement in the approach as opposed to the basic settlement relation analysis. The greater settlement is a result of the development of tie-ballast gaps in the approach and subsequently increased ballast degradation and therefore settlement in that region. The loading in Figure 5.59(d) is not shown to significantly increase except for Ties 8 through 10 as load gets shifted away from ties in the approach to ties in the open track. This also

reinforces the idea that increased loads are not mandatory for accelerated settlement at bridge approaches.

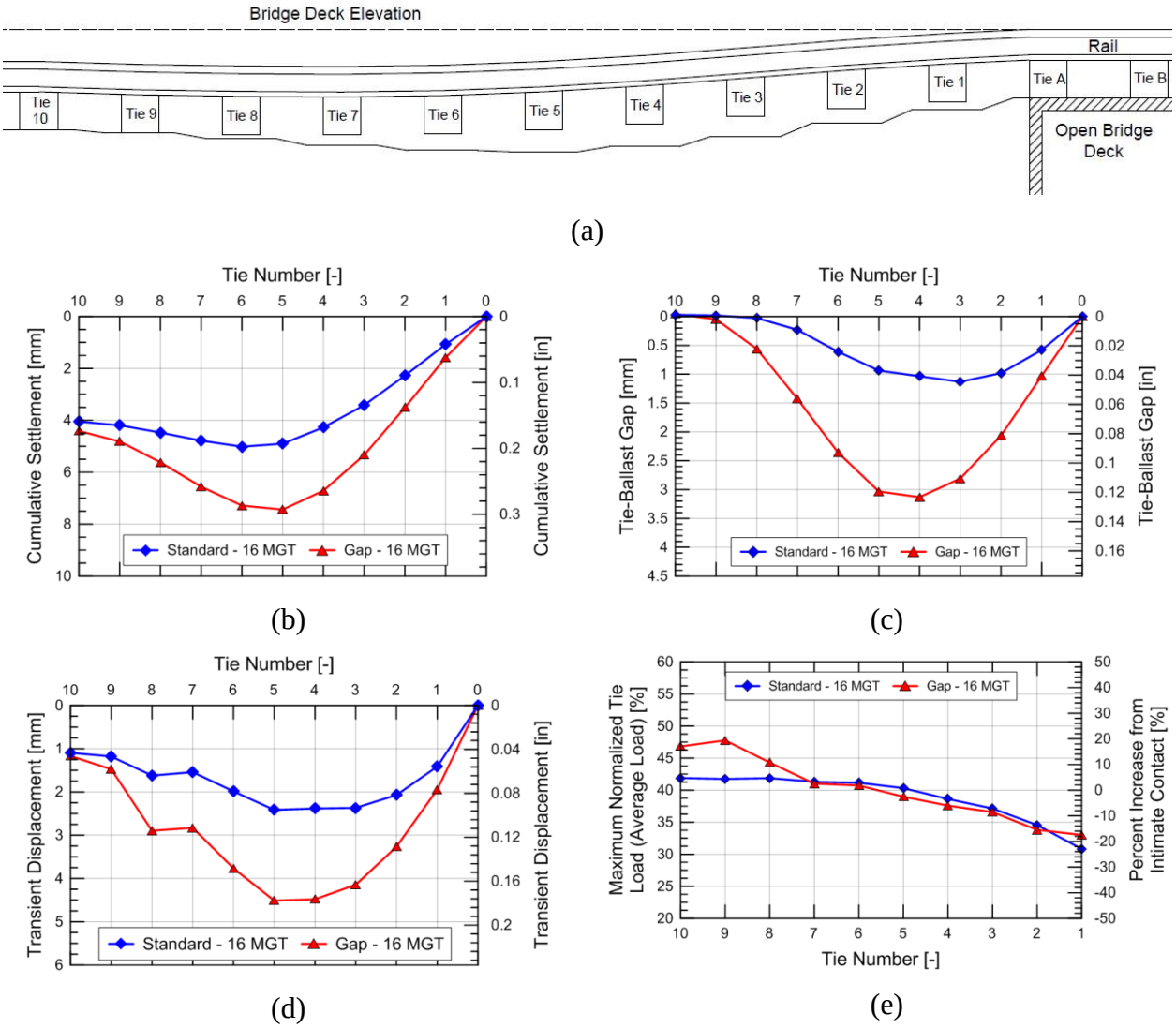

Figure 5.59: (a) ballast settlement profile at 16.0 MGT and comparison between basic and modified settlement relations with (b) cumulative settlement, (c) tie-ballast gaps, (d) transient displacement, and (e) tie loading.

Similar behavior is expected for other types of reduced-performance ballast conditions such as fouling, inadequate drainage, and ballast degradation from tamping. If these factors are combined with the load redistribution from a post-equilibrium transition zone, meaning both increased loading and ballast settlement rates from degradation, settlement rates 14 times greater

in the approach than open track are not unrealistic. This may better explain the differential movement at transition zones.

5.7.4.4 Analysis 4: Sensitivity Analysis

The fourth analysis involves a sensitivity analysis to investigate the effects of heterogeneous ballast in bridge approaches. This analysis attempts to represent ballast that randomly varies in density, gradation, fouling, moisture, or any other factor along the track that can lead to uneven settlements. This variation would not be known so an analysis that accounts for random variations is considered best suited for this particular analysis. To accomplish this, the ballast settlement is randomly varied under each tie within ranges of +/- 0.125 mm, 0.25 mm, and 0.5 mm at 16 and 28 MGT. For each situation (16 and 28 MGT), five analyses are conducted for a total of 30 analyses. As improved and more detailed settlement measurements from physical monitored track are collected, more insight into a correct "random variation" value is anticipated.

An example of the randomly varying cumulative ballast profiles is displayed in Figure 5.60(a). The graph shows a random variation of +/- 0.5 mm at 28 MGT. As expected, the profiles show slight variations in settlement at each tie from the original simulation displayed in the previous section. The loading in Figure 5.60(b), however, displays a wide range of tie loads with percent increased tie load from intimate contact exceeding 80%. This shows that slight settlement variations from the "equilibrium" state can significantly increase loads within the bridge approach and may be a potential explanation for the increased loading and settlement environment.

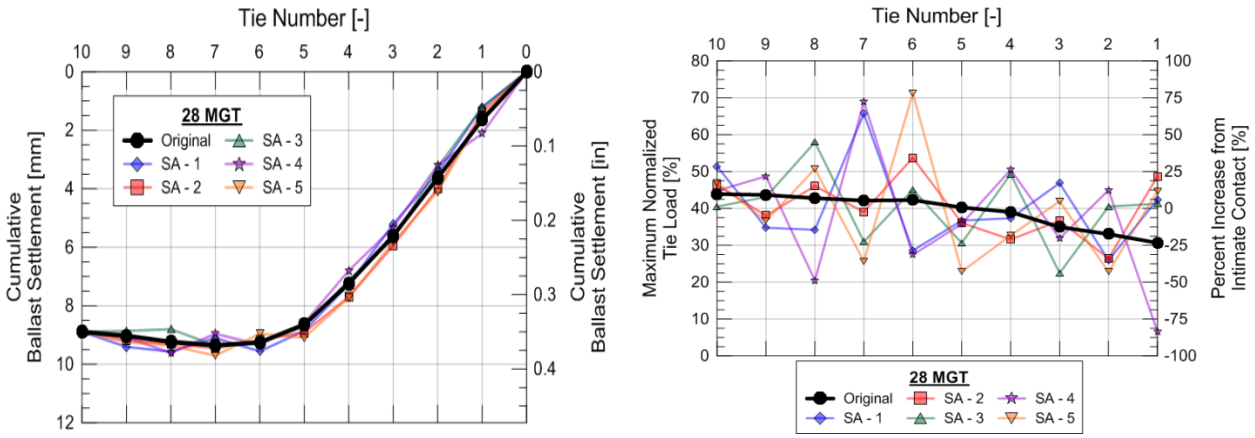

(a) (b)

Figure 5.60: (a) Ballast surface profile and (b) normalized tie loads for sensitivity analysis (SA) with ±0.5 mm variation at 28 MGT.

Figure 5.61 displays the maximum and average normalized tie loads and percent increase deviations from intimate contact for all the analyses. The maximum line displays the maximum and minimum normalized tie loads from all ten ties for all five analyses for each sensitivity analysis. The average line takes the average normalized tie load for all ties for all five analyses that are above 40% (percent increase from intimate contact) and that are below 40% (percent decrease from intimate contact). The results show that the maximum and average loads increase with increasing random settlement deviation. The results also did not show any meaningful difference between 16 and 28 MGT. This means the more random variation in settlement within a transition zone will lead to increased dynamic loads from load concentration.

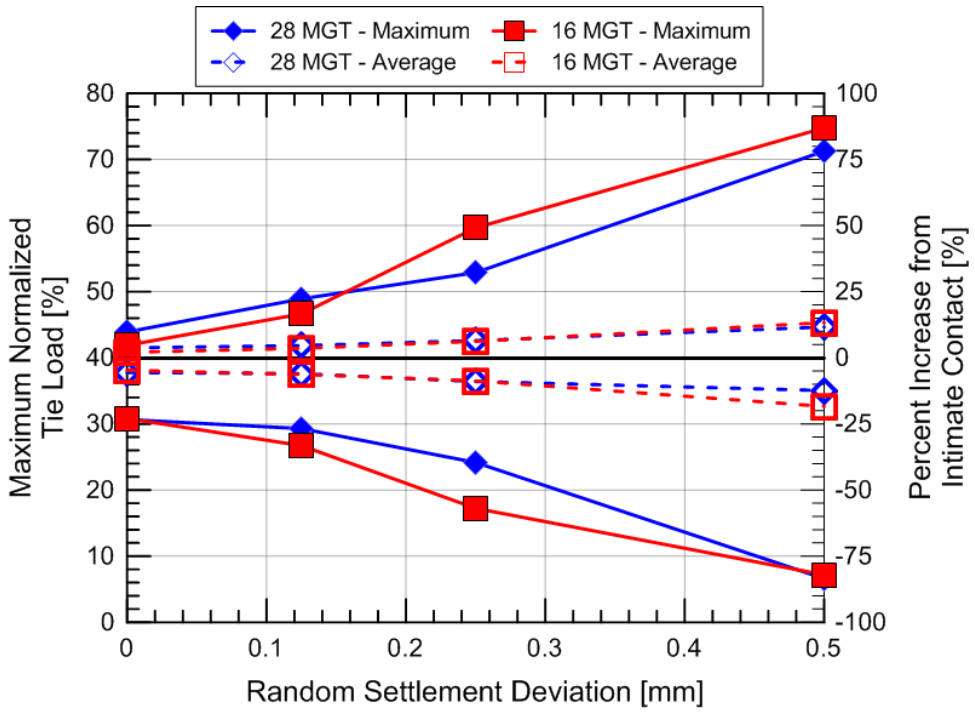

Figure 5.61: Maximum and average tie load deviations from sensitivity analysis.

Comparing the results of Analysis #2 and Analysis #3 suggests that increased settlement in the approach can logically be explained from (1) reduced-performance ballast conditions, e.g. tie-ballast gaps, degradation, fouling, and (2) increased loads from ballast heterogeneity. However, the magnitude of each factor cannot be determined without detailed field investigations

5.7.5 Summary

This section simulates the progressive settlement of railway bridge transition zone with the use of an empirical settlement model. Main findings include:

- Transition zone settlement occurs in three distinct stages: pre-equilibrium, equilibrium, and post-equilibrium. Increased loading and local differential settlement within the approach track occur in the pre- and post-equilibrium stages.
- Ballast settlement in the approach attempts to create a ballast profile that reduces increased tie loads and evenly distributes the wheel load amongst underlying ties. This was true for both 4th-order and linear tie load-settlement models.
- Assuming homogeneous ballast properties and settlement rates, minimal differential settlement is observed between the approach and open track.

- Differential settlement between the approach and open track can be replicated by introducing heterogeneous ballast conditions or conditions that cause the distribution of wheel load to shift between ties over time.

5.8 Summary and Future Work

The third task involves numerically simulating open track and transition zone locations based on the geometry and field data collected in Task I. The simulations involve both static and dynamic analyses and the dynamic analyses incorporate the train truck, rails, ties, ballast, and subgrade.

The stated objectives of Task III were to:

(1) develop and calibrate both static and dynamic numerical models to determine the Young's Modulus values within the substructure,
(2) use numerical model to identify evidence of increase loads from unsupported ties in the open track and transition zone, and
(3) simulate the progressive settlement of a railway bridge transition zone.

5.8.1 Summary of Results

The first objective involved calibrating both static and dynamic numerical model to determine Young's Modulus values within the substructure. The static inverse analysis was completed in Chapter 5.3 and the dynamic inverse analysis was completed in Chapter 5.4. A summary is listed below:

- Both the static and dynamic inverse analyses produced similar Young's Modulus values that are in rough agreement with seismic testing and laboratory testing.
- Both analyses account for non-linearity in the track system. The non-linearity can either be physical discontinuities, i.e. tie-ballast gaps, or non-linear load-displacement material response. The static analysis isolates and subtracts all non-linear aspects to produce a tangent modulus while the dynamic analysis incorporates discontinuities directly but all material behavior is assumed to be defined from a secant modulus. However, tie-ballast gaps are considered the largest non-linear contributor and both analyses address it and produce similar results.
- The static inverse analysis (FLAC3D) is beneficial when only the Young's Modulus values are desired and when time is limited because analyses can be completed in less than a half hour. The dynamic inverse analysis is beneficial for more detailed looked into track conditions, i.e. stresses, loads, etc., and producing model that can be used for dynamic analyses.

The second objective involved investigating potential increased loads from unsupported ties in both the open track and transition zone. The open track analyses were conducted in Chapter 5.5 and the transition zone analyses were conducted in Chapter 5.6. A summary is listed below:

- Increased loads were produced in both the open track and transition zone from unsupported ties. In the open track, load shifts away from the unsupported tie onto surrounding ties and increased tie loads over 50% were simulated, depending on the condition. In the transition zone, a similar mechanism would concentrate load on the most well supported ties and increased loads over 100% were simulated, depending on the condition.
- The distribution of load is very sensitive and a 1 mm ballast settlement difference between ties can lead to over 50% increase of load in the open track and 100% increase of load in the transition zone. An attempt to replicate transition zone field measurements resulted in a 100% increase in load a single tie so increased loads are suspected in transition zones.
- Increased loads in the transition zone appear to be initiated from either (1) differential settlement between the bridge and approach or (2) differential settlement within the approach. The increased load from differential stiffness was not considered influential. This implies that settlement must first occur before initiating increased loads in transition zones.

The third objective involved simulating the progressive settlement of a railway bridge transition zone. The analysis was conducted in Chapter 5.7. A summary is listed below:

- Analyses assuming homogeneous ballast conditions produced tie-ballast gaps and greater transient displacements in the approach, but did not replicate greater permanent displacements in the approach or increased tie loading.
- Analyses producing greater permanent displacements in the approach required heterogeneous ballast conditions, e.g. influence of tie-ballast gap or discrete ballast settlement increments. Increased tie loading was not necessary if the ballast settlement rates are heterogeneous, e.g. influence of tie-ballast gaps or fouling, but increased tie loading was produced from uneven ballast surface profile because of load redistribution.
- Results indicate transition zones experience three distinct stages. Stage 1 is defined as the “initial stage” or “pre-equilibrium stage” and experiences increased tie loading and differential settlement from differential stiffness or low ballast density of after tamping. Essentially, the pre-equilibrium phase involves the transition zone attempting to produce a ballast surface profile that reduces tie loads and brings the transition zone in balance with the internal ballast properties, external geometry and loading conditions. Stage 2 is defined as the “equilibrium stage” and represents a state of balance between the ballast, ballast surface profile, and external conditions. The ballast is suspected to be in a dense

state with little additional settlement from densification and the ballast surface profile will reduce tie loading. Stage 3 is defined as the "post-equilibrium stage" and results from reduced-performance ballast conditions or increased tie loading from impact or differential settlement between or within the approach.

5.8.2 Future Work

Much of the work presented in Chapter 5 involved investigating various theoretical conditions that can produce increased tie loading and a progressive analysis that results in greater permanent displacements in the approach than open track. Those conditions can roughly be summarized as local differential settlement between ties or between the approach and fixed structure. This uneven settlement in the approach is anticipated to results from heterogeneous ballast behavior, such as varying reduced-performance ballast conditions and the influence of tie-ballast gaps. However, these heterogeneous ballast conditions are rarely investigated so little knowledge is known of their potential impact.

Therefore, while the conditions producing increased loads are defined in this thesis, the conditions that represent physical track are not fully known. While more complex numerical models that incorporate rail and tie stresses, rail joints, multiple train trucks, non-linear transient and permanent ballast behavior would be beneficial, a complementary push into investigating site ballast conditions, measuring tie-ballast gap and their impact on ballast settlement, and measuring the tie displacement and the tie-ballast gap height at all approach ties over time would be desired. This information would better direct future numerical model analyses from theoretical conditions to more physically realistic conditions that will be more informative for diagnosing the causes of accelerated settlement at bridge approaches.

CHAPTER 6

TASK IV: ROOT CAUSES AND RECOMMENDATIONS

6.1 Introduction

The previous three Tasks involved the collection and analysis of field data and numerical simulations of track behavior. Despite the complexities of transition zone settlement, the goals of Task IV are to develop a unified theory explaining transition zone settlement and recommendations on how to prevent and remediate the differential movement.

The primary objectives of Task IV are the following:

(1) develop chain of events and list root causes explaining the deterioration of transition zones,
(2) develop strategies for reducing transition zone settlement, and
(3) recommend transition zone design, remedial, and resurfacing measures.

Chapter 6.2 explains the chain of events, Chapter 6.3 lists the root causes, Chapter 6.4 develops strategies for reducing transition zone settlement, Chapter 6.5 recommends design and remedial measures and Chapter 6.6 focuses on resurfacing measures.

6.2 Chain of Events

This section describes the anticipated chain of events that explains the transition zone deterioration observed from literature review in Chapter 2, field measurements in Chapter 3 and 4, and numerical simulations in Chapter 5. These observations suggest transition zone performance can be categorized into three stages:

(1) Compaction Stage,
(2) Equilibrium Stage, and
(3) Post-Equilibrium Stage.

A description of each stage is presented in the subsequent subsections.

6.2.1 Compaction Stage

The compaction stage is defined as the time-frame in which a transition zone experiences rapid settlement from substructure compaction. Additionally, potential differential settlement may occur from increased loads from differential stiffness between the bridge and approach. The term compaction stage is adopted from the "compaction stage" describing initial ballast and track settlement (Chapters 2.2.2 and 2.3.3) because the greatest settlement contributor is anticipated to be from ballast or subgrade compaction. The end of the compaction stage would be defined as when (1) the initial substructure compaction after tamping or track placement has ceased and (2) when the effects of differential stiffness are minimized from differential ballast settlements.

Initially, the state of track should have a constant rail elevation between the open track, transition zone, and bridge. This represents the state immediately after track placement or tamping and is illustrated in Figure 6.1.

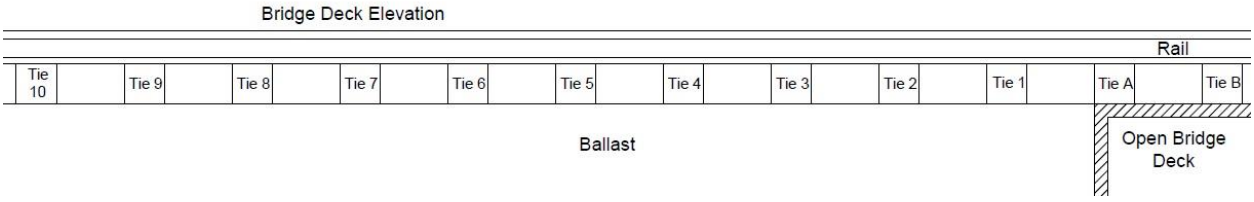

Figure 6.1: Schematic of anticipated rail and ballast profiles during "Stage 1".

However, review of the previous chapters suggests the initial transition zone state is unbalanced and three mechanisms will potentially come into play:

- Rapid ballast settlement after tamping from ballast densification
- Gradual subgrade compaction
- Increased loads from differential stiffness

The first mechanism is anticipated to be the greatest settlement contributor at the majority of transition zone locations. The initial settlement of ballast in triaxial testing is widely acknowledged (see Chapter 2.2.2) and is believed to occur from particle arrangement as the ballast densifies and breakage of ballast corners and angularities, i.e. Type II Damage. Previous field studies have observed this behavior (Figure 2.22 in Chapter 2.3.3) and investigations of track behavior after tamping in Task II have also verified this behavior (Figure 4.36 in Chapter 4.4.6). The influence of this mechanism is highly dependent on the quality of resurfacing with an

initial settlement range of less than 1 mm to over 20 mm. This mechanism will occur throughout the entire track but may be more influential in transition zones due to the difficulty of tamping near fixed structures and the existence of tie-ballast gaps, which will force a looser ballast state to maintain the initial geometry.

Figure 6.2 shows a potential track diagram after the first train pass. Even open track settlement is assumed with slightly greater settlement in the approach from tamping difficulties. It is also possible that the settlements are highly variable due to the presence of existing tie-ballast gaps, heterogeneous ballast conditions, and heterogeneous densities from tamping irregularities.

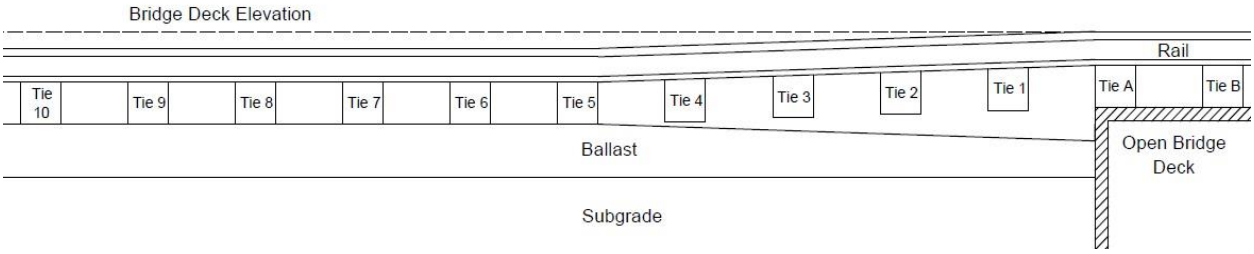

Figure 6.2: Conceptual diagram of a transition zone after first train pass.

The second mechanism is anticipated at site locations in which the subgrade is not compacted to resist the heavy stresses from repeated train loading. Reasons for this could range from neglect to difficulties compacting near a fixed structure. Task II presents evidence of this mechanism in Chapter 4.4.8, in which remediated track locations at existing sites did not experience noticeable permanent settlement while site constructed on new track did. It is suspected that the existing sites already experienced compaction while the new sites are currently going through the process. Therefore, this mechanism is considered problematic for newly constructed site locations. This mechanism will also occur throughout the entire track but may be more influential at transition zones because the difficulty compacting near a fixed structure or if a fill material is used.

Figure 6.3 displays the potential track diagram after the subgrade has begun and compact and settle. As with the Figure 6.2, the difficulty of compacting near the abutment could produce greater settlements within that region.

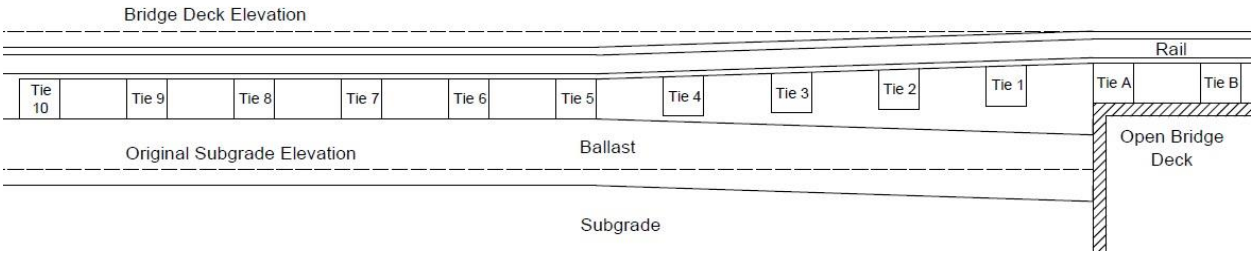

Figure 6.3: Conceptual diagram of a transition zone showing subgrade settlement with time.

The third mechanism is anticipated at track locations with a rapid change in differential stiffness. While numerical studies show the increased load from this mechanism will be localized and not considered detrimental, it still exists and may still play a role especially if the previous two mechanisms are reduced and accounted for. Numerical studies in Chapter 5.7 suggest the local increased load will produce a local increase in ballast settlement (see Figure 6.4). This local differential settlement, however, is anticipated to counteract the differential stiffness and result in a more even distributed of wheel loads to the ties (see Figure 5.52 in Chapter 5.7.3.2). The mechanism is expected to occur only within the transition zone.

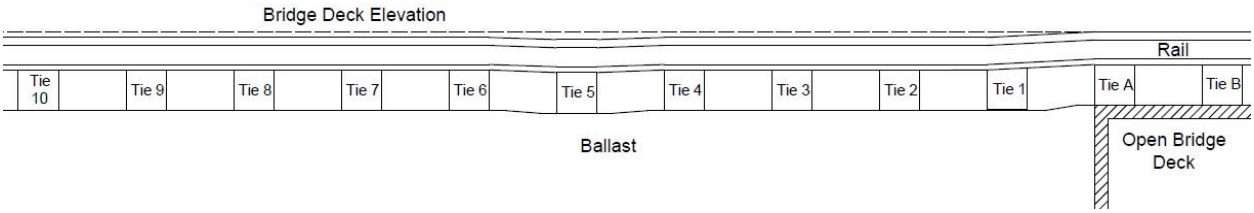

Figure 6.4: Conceptual diagram of greater settlement under Tie 5 due to increased loads from stiffness differentials between the bridge and approach.

All three mechanisms are anticipated to contribute simultaneously but the magnitude and duration can vary significantly depending on the quality of resurfacing, quality of fill and compaction, and the magnitude of stiffness differential. This makes diagnosing the contributing factor difficult from general observation but possible if track behavior is monitored over time beginning immediately after tamping.

6.2.2 Equilibrium Stage

The equilibrium stage is defined as the time-frame in which a transition zone experiences minimal variation in transient behavior with time, even distribution of tie loads, and minimal or gradual settlement within the ballast layer. The term equilibrium stage is proposed because it suggests little variation in transient behavior is anticipated in the immediate future and track geometry will be maintained for a period of time. However, both scenarios in which the transition zone maintains performance indefinitely or eventually deteriorates into the post-equilibrium stage are possible. This is displayed in Figure 6.5 in which Figure 6.5(a) remains in equilibrium stage while Figure 6.5(b) goes into the post-equilibrium stage.

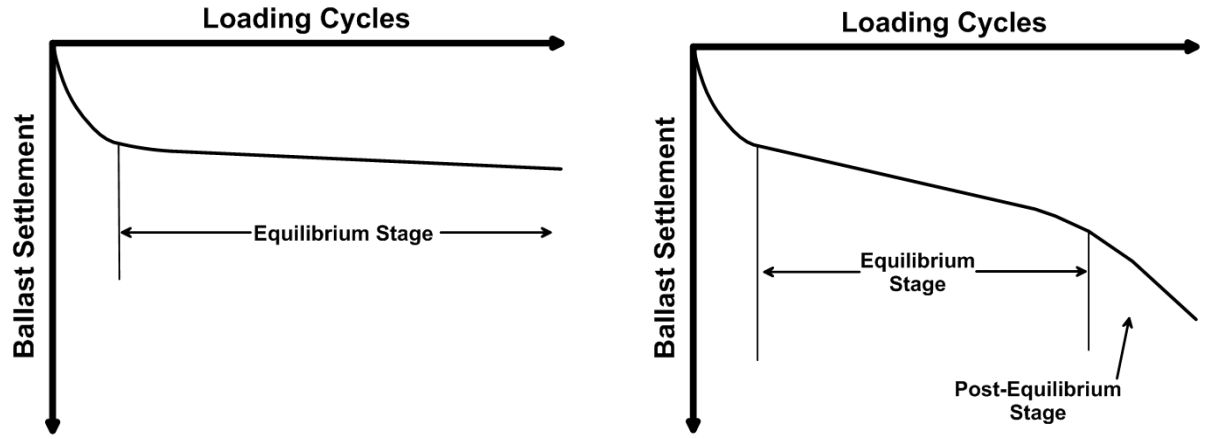

(a) (b)

Figure 6.5: Conceptual illustrations of transition zone (a) remaining in equilibrium stage and (b) transitioning from equilibrium stage to post-equilibrium stage.

6.2.3 Post-Equilibrium Stage

The post-equilibrium stage is defined as the time-frame in which a transition zone experiences accelerated settlements from increased dynamic loads or reduced-performance ballast. Transition zones in this stage typically require frequent maintenance or full renewal of track.

As introduced in Chapter 2.4.3, multiple mechanisms can produce increased loads within the approach. Numerical analyses and field instrumentation suggest that increased loads can occur from differential settlement between the bridge and approach (Chapter 5.6.3), differential settlement within the approach (Chapter 5.6.3), or impacts from the tie contacting the ballast (Chapter 4.4.5). This refers to the loading mechanisms of “rapid change in axle elevation”, load concentration, and tie-ballast impacts, respectively, from Chapter 2.4.3.2. The magnitude and

distribution of increased loading varies significantly depending on the ballast surface profile and track geometry, but all three factors are initiated by ballast settlement within the approach.

Multiple factors producing increased ballast settlement could be incorporated within the reduced-performance ballast condition. Laboratory tests of clean ballast, as referenced in Chapter 2.2.2, suggest low ballast confinement can accelerate ballast settlements, especially when coupled with high-frequency or high-magnitude loading. Wet, fouled ballast, reference Chapter 2.2.3, is an alternative potential explanation with studies showing ten times the rates of settlement than clean ballast even with identical loading. The rate of settlement appears to increase with degree of fouling, plasticity of fouling material, and fouling moisture. Additionally, tie-ballast gaps has shown to increase the ballast settlement rate by up to ten times from laboratory testing. While the reasoning for the increase is not fully explained or potentially known, it is anticipated to be related to the size of the tie-ballast gap.

Figure 6.6 shows two examples of conceptual tie settlement diagrams in the post-equilibrium stage. Figure 6.6(a) shows a site displaying large settlements in the compaction stage, which immediately brings it the post-equilibrium stage. Multiple types of track behavior possibilities are possible at this point, however, the graph shows the possible track behavior if the load is shifting from tie-to-tie over time. This represents the tie experiencing isolated incidents of settlement when the load is concentrated on that tie. Figure 6.6(b) shows a continuous accelerated settlement similar to the Upland (15 ft.) site in Chapter 3.

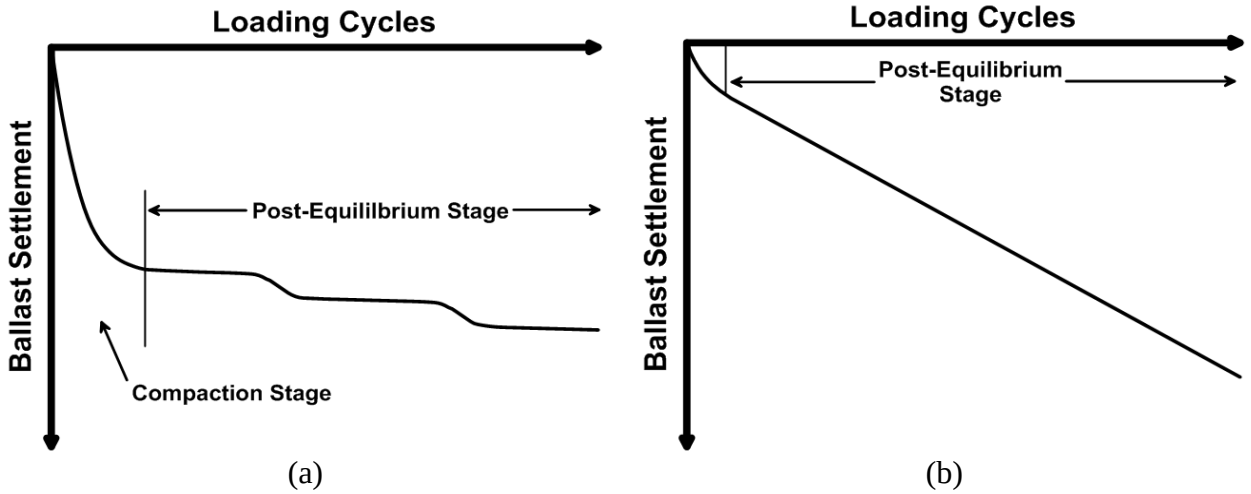

(a) (b)

Figure 6.6: Conceptual illustration of two possible transitions from compaction stage to post-equilibrium stage.

6.2.4 Field Examples

The behavior and causes of transition zone deterioration is site specific so no specific chain of events will explain every transition zone, however, the general pattern has been observed at multiple site locations. Examples of observed transition zone behavior are summarized below.

For example, well-performing transition zones, Site #1 or Site #2 in Task II, will experience minimal substructure settlement in the compaction stage because of the successful design. Therefore, the transition zone will almost immediately proceed and remain in the equilibrium stage as long as the ballast does not deteriorate over time. The anticipated tie settlement behavior is displayed in Figure 6.5(a).

A second example would be a site with fairly well-compacted ballast and subgrade but enough settlement occurred in either the ballast or subgrade layer to produce unsupported ties in the approach. Site #3 or potentially Site #8 in Task II, if conditions stabilize, would be examples of this behavior. While tie-ballast gaps exist, the site would be considered in the equilibrium stage because transient displacements appear to be stable over time, no evidence of increased loads were observed, and track geometry appears to be holding (17 years at Site #3).

A third example would be a site with a well-compacted ballast but an inadequately compacted subgrade. An example would be Site #8 in Task II if the substructure continues to settle. If the fill or natural subgrade is soft, wet plastic clay for example, the settlement of the substructure may proceed for decades and continually require additional ballast to maintain geometry. This site will remain in the compaction stage for the majority of its service life.

A fourth example would be Site #6 in Task II in which the site experienced about 25 mm of ballast settlement immediately after the first train pass due to compaction, rearrangement, and breakage of the ballast. Rail and tie displacement measurements suggest the track returned back to its pre-tamping transient conditions about seven trains after tamping. This suggests a significant compaction stage that immediately jumps to the post-compaction stage. The anticipated behavior is displayed in Figure 6.6(a).

A fifth example would be the Upland Avenue site in Task I in which the site almost immediately proceeds to the post-equilibrium stage after resurfacing. While no data was obtained immediately after tamping, the trend appears to show a constant rate of settlement after resurfacing (~14 mm/yr). This suggests the accelerated ballast settlement is from increased loads and/or reduced-performance ballast conditions. This example is different from the previous

example because the majority of settlement is believed to occur in the compaction stage for the fourth and post-equilibrium stage in the fifth. The anticipated behavior is displayed in Figure 6.6(b).

Other possibilities exist but these five cover the range that was observed within this thesis. More field measurements should be able to give more insight to these examples and more possible chain of events.

6.3 Root Causes

With the chain of events explained, the three root causes introduced in the literature review are proposed:

(1) substructure settlement from densification,
(2) increased loading within the approach, and
(3) increased settlement from reduced-performance materials and conditions.

The three root causes were selected because are they are mechanisms that can put a transition zone into the post-equilibrium stage. By developing strategies to reduce or prevent these three root causes, transition zone performance can be improved.

All three root causes have been introduced within the thesis (see Chapter 2.4.3) but as a general overview, (1) substructure settlement refers to the inevitable settlement of the granular substructure and additionally any compaction immediately after track placement or tamping. This mechanism occurs at every site location and if it is large enough, can initiate the subsequent two mechanisms.

The second mechanism, (2) increased loading within the approach, can refer to wheel-rail impacts from rail joints, rapid change in axle elevation from track locations with differential settlement between the bridge and approach, tie load concentrations from uneven track settlement within an approach, and tie-ballast impacts from the closure of hanging ties. Besides rail joints, all factors that can lead to increased loading require differential settlement between the bridge and approach or within the approach.

The third mechanism, (3) increased settlement from reduced-performance conditions, can refer to loss of confinement, degraded ballast, wet fouled ballast, tie-ballast gaps, broken track components, among others. These factors can be produced from a variety of conditions but are

often the result of increased ballast degradation, potentially from increased loads, tamping, or repeated impact with ties, or blocked drainage. It is suspected that once enough settlement occurs in a transition zone, a negative feedback loop appears in which increased loads degrade the ballast resulting in increased loads and the cycle will continue indefinitely until the ballast is replaced.

6.4 Transition Zone Design/Remediation Strategies

The previous sections present the proposed chain of events and root causes of differential movement at transition zones. This section focuses on design and remedial strategies. The first part of this section presents a unified transition zone design theory that focuses on treating the transition zone as a single system and keeping it in balance. The remaining part of this section identifies problematic regions within the chain of events.

6.4.1 Transition Balance Sheet

All three root causes either involve settlement within the approach or are initiated by differential settlement so an overall strategy that keeps the train axles at a constant elevation during train passage is desirable. To accomplish this, transient and permanent displacements in the approach and bridge must be balanced.

To illustrate the potential sources of detrimental differential transient and permanent displacements between the approach and bridge, a “Transition Balance Sheet” is developed and presented in Figure 6.7. The Balance Sheet lists the many sources of potential transient and permanent displacements in the Approach (A) and Bridge (B) including: (1) rail compression, (2) rail-tie gap, (3) tie pad/plate displacement, (4) tie displacement, (5) tie-ballast gap, (6) ballast displacement, (7) subballast displacement, (8) subgrade displacement, and (9) lateral displacement.

While it is not intended or practical for engineers to physically calculate the potential transient and permanent displacements on the approach or bridge for a variety of reasons, the Transition Balance Sheet will force the engineer to consider all components of the approach and bridge when selecting a design or remediation. For example, even if the ballast is reinforced and the bridge is allowed additional movement, a soft uncompacted subgrade will eventually result in

track geometry problems. Additionally, a soft or stiff subgrade may determine how much movement is desired if remediating a bridge with pads. Therefore, the Balance Sheet is intended as a conceptual tool to emphasize viewing the transition zone as a system instead of individual components. The solutions for achieving balance are introduced in subsequent sections.

Figure 6.8 displays a worst-case scenario of an open-deck bridge in which the approach may experience transient and permanent substructure displacements while the bridge does not. Sites #5 or #6 in Task II are examples. The check marks represent a "potential detrimental displacement" that will be problematic if it is not balanced by the bridge. In this particular case, the "potential detrimental displacement" applies for the entire substructure along with gaps that develop in the track system because of differential permanent substructure displacements.

Approach and Bridge Displacement Component	Potential Transient		Potential Permanent	
	A	B	A	B
Rail compression				
Rail-tie gap				
Tie pad/plate displacement				
Tie displacement				
Tie-ballast gap				
Ballast displacement				
Subballast displacement				
Subgrade displacement				
Lateral displacement				

Figure 6.7: Transition Displacement Balance Sheet to compare Approach (A) and Bridge (B) transient and permanent displacements.

Approach and Bridge Displacement Component	Potential Transient		Potential Permanent	
	A	B	A	B
Rail compression	✓	✓		
Rail-tie gap	✓			
Tie pad/plate displacement	✓	✓		
Tie displacement	✓	✓		
Tie-ballast gap	✓			
Ballast displacement	✓		✓	✓
Subballast displacement	✓		✓	
Subgrade displacement	✓		✓	
Lateral displacement	✓		✓	

Figure 6.8: Transition Displacement Balance Sheet for an open-deck bridge to compare Approach (A) and Bridge (B) transient and permanent.

Site #1, #2, and #8 provide examples of transition zones that are well-designed and have required minimal track geometry maintenance since putting into service. All sites have (1) a ballasted-deck bridge, which allows for more transient and permanent movement on the bridge, (2) confining wing walls to confine and support the ballast while preventing lateral displacements, (3) hot-mixed asphalt or geoweb underlayment to reinforce the ballast, and (4) either an existing subgrade or a pre-compressed fill to limit subgrade displacements. Accounting for these design features in the "Transition Balance Sheet" results in an acceptable balance of the transient and permanent displacements between the approach and bridge. This is displayed in Figure 6.9.

Approach and Bridge Displacement Component	Potential Transient		Potential Permanent	
	A	B	A	B
Rail compression	✓	✓		
Rail-tie gap				
Tie pad/plate displacement	✓	✓		
Tie displacement	✓	✓		
Tie-ballast gap				
Ballast displacement	✓	✓	✓	✓
Subballast displacement				
Subgrade displacement				
Lateral displacement				

Figure 6.9: Transition Balance Sheet to compare Approach (A) and Bridge (B) transient and permanent displacements for Site #1.

6.4.2 Ballast Settlement Reduction Strategies

The root causes introduced in the previous section suggests railroad intervention in at multiple locations within the chain of events may help prevent differential movements at transition zones. This generally means reducing the initial settlement after tamping and preventing accelerated approach settlements from increased loads, tie-ballast gaps, or reduced-performance ballast.

To prevent those factors, the following strategies are recommended:

(1) ensure the ballast and subgrade are as compacted as possible after tamping or being placed in service,
(2) avoid or mitigate the negative influence of tie-ballast gaps, and
(3) avoid or mitigate reduced-performance ballast in the approach.

If these factors can be prevented, field observations suggest the life-span of a transition zone can be extended for decades if not indefinitely. Techniques to accomplish these strategies are listed in the subsequent sections.

6.5 Recommended Design and Remedial Techniques

As introduced in Chapter 2.4.4, multiple transition zone design and remedial techniques have been proposed and separated in four main categories: stiffening of approach superstructure, stiffening of approach substructure, softening of bridge, and mixed solutions. Each technique and category of techniques has their benefits and consequences and a single solution will not be the correct fit for every situation. Therefore, a wide range of techniques are recommended taking into account the effectiveness, cost, and disruption.

The recommendations focus on techniques to improve individual components within the track system. However, it must be emphasized that a single fix may not be sufficient and most successful designs have incorporated multiple solutions.

6.5.1 Bridge Techniques

Softening the track on the bridge is common technique to help balance the displacements between the bridge and approach. Converting bridges from open-deck bridges to ballasted-deck bridges, when used in conjunction with other solutions, has shown to be beneficial. A photograph of ballasted-deck bridge is displayed in Figure 6.10.

Figure 6.10: Photograph of ballasted-deck bridge.

Potential drawbacks from ballasted-deck bridges are the cost and the need to lower the bridge clearance to allow room for the ballast. This makes the upgrade to ballasted-deck bridges in urban areas difficult. Other potential solutions include rail pads or UTPs to soften the track.

Rail pads, UTPs, and ballast mats also can be used in conjunction with ballasted-deck bridges to further soften the track on the bridge. Chapter 2.4.4 presents a study of how the use of UTPs and ballast mats in conjunction with ballasted-deck bridges along with improved drainage in the approach improved track geometry at two test sites. For bridge solutions, attention to the approach is also required to ensure good ballast and subgrade support.

6.5.2 Tie-Ballast Interface

One of the major findings within this study is the influence of tie-ballast gaps on track performance. The strongest correlating factor with ballast settlement was tie-ballast gap height and every track requiring reoccurring maintenance displayed unsupported tie behavior. Unfortunately, the negative effects of tie-ballast gaps are not fully understood but they may potentially redistribute and concentrate loads, increased loads from impacts, and increase ballast degradation and settlement from the continual impact and relative movement. Laboratory studies presented in Chapter 2.2.4 show a potentially large effect but more understanding is necessary. Additionally, the contact area at the tie-ballast interface has been shown to be only 10 to 20% of the available area. This shows the potential for reducing ballast stress and settlement by increasing tie-ballast contact area.

Therefore, a focus on removing or reducing the negative effects of tie-ballast gaps would be beneficial for transition zone performance. One promising technique is the use of UTPs in the approach. A photograph of an UTP attached to a timber tie is displayed in Figure 6.11. While UTPs will soften the track in the approach, it also has the benefits of reducing and better distributing wheel load amongst underlying ties, increasing tie-ballast contact area and improve the distribution of load from the tie to the ballast, improving damping characteristics, and reducing wear on the tie and ballast by acting as a barrier. These benefits are anticipated to reduce ballast degradation and settlement.

UTPs were installed at Site #7 in Task II (Chapter 4.4.7) at a site experiencing historical track geometry problems. After a year of being put in service, minimal change of track geometry was observed. While more installations and service life are required before the benefits of UTPs

can be fully realized, it represents a potentially cheap and effective fix that address the deficiencies of the tie-ballast interface.

Figure 6.11: Photograph of under-tie pad (UTP) on a timber tie.

6.5.3 Ballast

A second major factor in the studies transition zones is ballast settlement. Review of Chapter 2.2 and 2.3 show a wide range of ballast behavior depending on gradation, density, load magnitude, load frequency, confinement, degradation, fouling, and moisture content. This makes understanding of ballast settlement in transition zones difficult without improved knowledge of the in-situ ballast conditions and the effect of the factors listed above.

Therefore, techniques to improve ballast support are desirable. This can range from improving confinement with concrete wing walls (Figure 6.12), providing underlayment support (Figure 6.13) with HMA, geoweb, or geogrid, or even ballast cleaning and replacement. With regards to cleaning and replacement, while it cheap and easy to place a layer of new ballast on a track, once the ballast reaches reduced-performance conditions, the track will likely continue to settle at an accelerated rate indefinitely.

(a) (b)

Figure 6.12: Photographs of concrete wing walls.

(a) (b)

Figure 6.13: Photographs of (a) HMA and (b) geoweb underlayment.

6.5.4 Subgrade

The benefits of subgrade stiffening techniques have not been emphasized in this thesis but still remain important because gradual subgrade settlement will require continual resurfacing and addition of ballast to maintain a smooth geometry for passing trains.

Potential techniques are stiffening the subgrade with grout or cement, geopiers, compacting the fill wet-of-optimum, or using a granular fill with a vegetative soil cover to prevent erosion of the granular fill.

6.6 Recommended Resurfacing Techniques

A potentially underappreciated technique for better maintaining track geometry at transition zones is improving resurfacing techniques. Current methods of resurfacing involve either automated or pneumatic tamping. Automated tamping raises the rail elevation essentially by loosening the ballast underneath the tie. Pneumatic tamping raises the rail elevation by pneumatically pushing new ballast underneath the rail seat (Chapter 2.3.5). Both methods tend to result in rapid track settlement that reverts back to its original elevation and resurfacing is required within a year.

Automated tamping is widely used because of its speed and mechanization and is desirable when resurfacing long stretches of track in short amounts of time with minimal labor. However, a major drawback in the automated tamping procedure is that the ballast is disturbed from its post-compaction equilibrium state and loosened, forcing the ballast to repeat the compaction/post-compaction cycle after each resurfacing event. In addition to the rapid compaction of ballast after tamping, there are multiple additional critiques of the current tamping process. First, current tamping techniques degrade and break down the ballast every resurfacing event, producing degraded ballast that will settle at a quicker rate. This reduces the time between resurfacing events each maintenance cycle. Second, the current techniques will push any degraded and fouled ballast underneath the tie, where it will be the most detrimental to track performance.

While replacement of tamping on a wide-scale it is not anticipated because of its speed and cost-effectiveness, recommendations on how to improve resurfacing techniques at specialized location such as transition zones or special track work (STW), i.e. frogs or switches, are listed below under the categories: pneumatic tamping, stoneblowing, and shims. Many of these solutions are new and not tested but are potentially viable because they address some of the key factors causing ballast settlement immediately after resurfacing.

6.6.1 Pneumatic Tamping

A focus on pneumatically tamping bridges approaches could be beneficial because it allows railroad companies to specifically identify and reinforce problematic areas. Automated tamping is beneficial and cost-effective for large stretches of track while pneumatic tamping may

eventual prove to be more beneficial at specific problematic locations such as transition zones and STW. Three examples of potential improvements are discussed below.

Spot tamping bridge approaches two weeks after resurfacing events could potentially extend the service life of the track between maintenance cycles. The purpose of spot tamping is to identify local regions within the approach that has experienced settlement since resurfacing and to re-tamp those specific areas. This can address the weak spots of the newly tamped approach.

Innovative pneumatic tamping devices that better distributes the ballast underneath the tie without breaking the ballast are available. An example is displayed in Figure 6.14 that compares a typical tamping head and a more innovative design. Photographs of ballast distribution underneath the tie are compared in Figure 6.15. While the authors are unaware of any scientific studies to date, demonstrations show potential in track regions with clean ballast.

(a) (b)

Figure 6.14: Photographs of (a) typical pneumatic tamping head and (b) alternative pneumatic tamping head (courtesy of Robel Company).

(a) (b)

Figure 6.15: Photographs of tie and underlying ballast (a) before and (b) after tamping (courtesy of Robel Company).

An issue that is rarely addressed with the current method of tamping at high-maintenance locations is how new ballast is placed in the crib and squeezes the existing ballast underneath the tie. This implies that the degraded and fouled ballast, which tends to settle at a quicker rate than clean ballast, will be continually reused directly under the tie and result in further ballast degradation. If tamping methods instead pushed the ballast from one side instead of squeezing from both sides, this "ballast rotation" could extend the life and effectiveness of the ballast.

6.6.2 Stoneblowing

Stoneblowing is an alternative resurfacing method that has been developed and implemented in the United Kingdom and parts of Europe. One of the main benefits of stoneblowing is that it leaves the ballast in its post-compaction state and adds additional stone material to fill the tie-ballast gap. The goal of this procedure is to reduce the ballast compaction stage after resurfacing. An additional benefit of stoneblowing is the reduction in ballast degradation with each resurfacing cycle. More information and studies can be referenced in Chapter 2.3.6.

Recently, innovative ideas of combining the benefits of stoneblowing and UTPs by blowing stone mixed with rubber pellets have been tested in the laboratory and has shown to further reduce the breakdown and settlement of the ballast.

6.6.3 Hanging Tie Shims

One potential drawback from stoneblowing is the stones can still degrade, breakdown, and even fall within the voids of the underlying ballast. An alternative to stoneblowing is installing rubber or plastic shims, defined as hanging tie shims (HTS), underneath the tie during resurfacing. This idea has been tested both in the laboratory and in live track. The primary obstacle is getting the shim fully underneath the tie as the underlying angular ballast particles will catch the shim as it slides underneath the tie. Therefore, this technology is considered a work-in-progress.

Two trials have been tested. The first trial involved a laboratory full-scale test track at the RAIL laboratory at the University of Illinois at Urbana-Champaign on 2 September 2014. During testing for an unrelated project, an unsupported tie was observed and provides an opportunity to test the viability of a HTS resurfacing technique. The tie-ballast gap was estimated to be about 1 mm in depth.

A photograph of the full-scale test track is displayed in Figure 6.16(a) and (b) and a diagram of the track layout is presented in Figure 6.16(c). The unsupported tie was located underneath Tie 8-19. Due to the exploratory nature of this experiment, there were restrictions on the ability to move the load frame so only Tie 7-18 could be loaded.

The first trial involved using 0.25-in polyurethane shims as material for the HTS. To install the shims, the rails were jacked and a 10-ft metal rod with string attached to the end was inserted underneath the tie and pulled through. The string, also attached the HTS, allowed the shim to simultaneously be pushed and pulled underneath the tie. Both a single shim and two shims were installed to test the benefits of the shim and load distribution. Photographs of the installation are displayed in Figure 6.17.

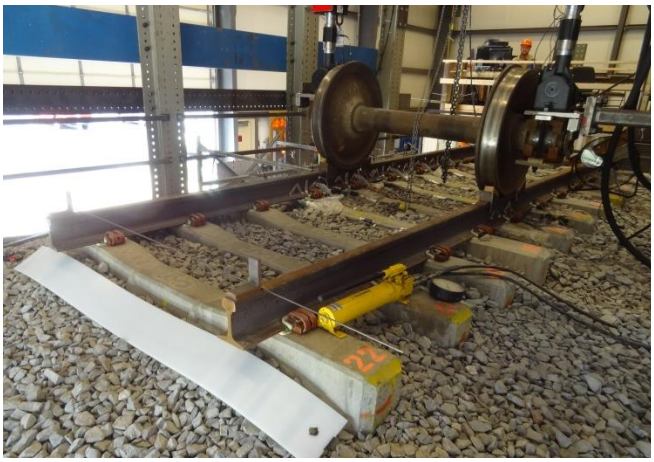

(a)

(b)

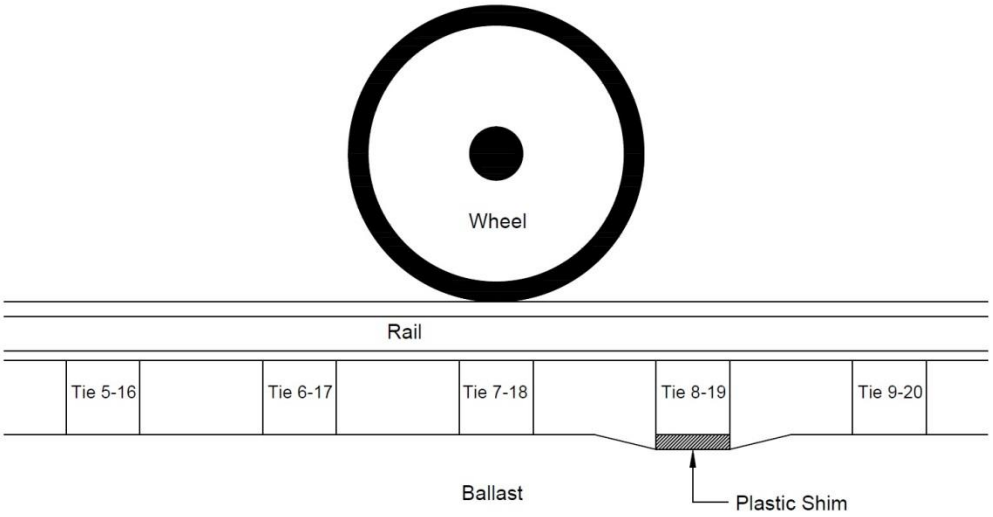

(c)

Figure 6.16: (a,b) Photographs of RAIL lab at UIUC and (c) diagram of testing layout.

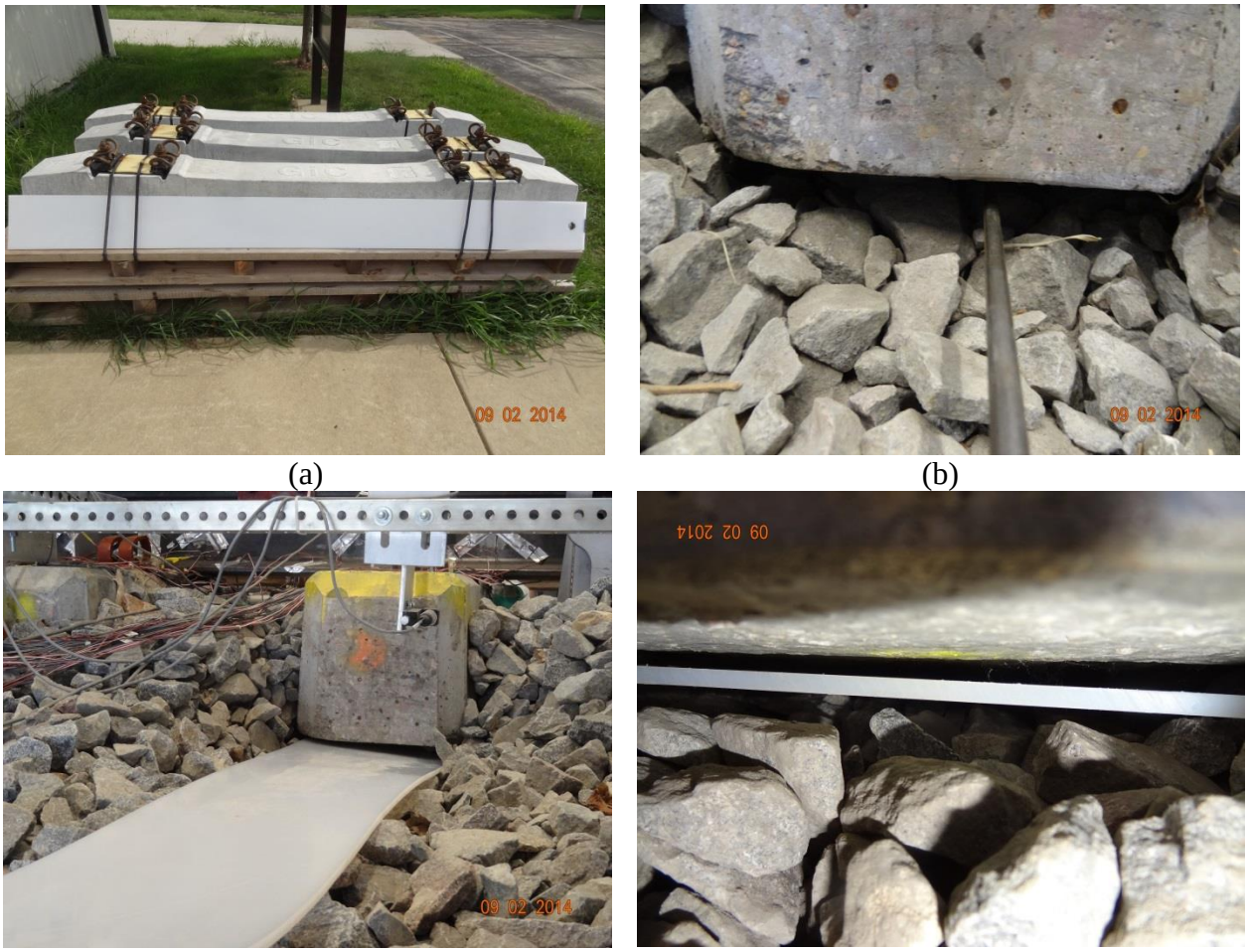

(a) (b)

(c) (d)

Figure 6.17: Photographs of (a) plastic shims, (b) insertion of metal rod underneath tie, (c) insertion of plastic shim under concrete tie, and (d) shim fully inserted underneath tie.

To test the effect of the installed HTS, the test track was loaded in 5-kip increments until a peak load of 40-kips was obtained. The results in Figure 6.18 show the HTS redistributes the wheel load. For example, referencing the originally unsupported Tie 7-18, the original tie-ballast gap is large enough for the entire 40-kip wheel load to be transferred to surrounding ties. As shown in Figure 6.18(b), the peak percent wheel load is 0% for Tie 8-19 and 55% for Tie 7-18. However, after the addition of a single 0.25 inch HTS, the load distribution flips with Tie 8-19 receiving over 50% of the wheel load while Tie 7-18 does not receive any receive any load. The addition of a second shim amplifies this trend.

The purpose of this experiment was to test the viability of HTS installation and the ability of HTS to redistribute load in a railroad track environment. The installation and results show

potential for the use of HTS. Similar to stoneblowing, a major challenge of the HTS installation is determining an appropriate height for the shim.

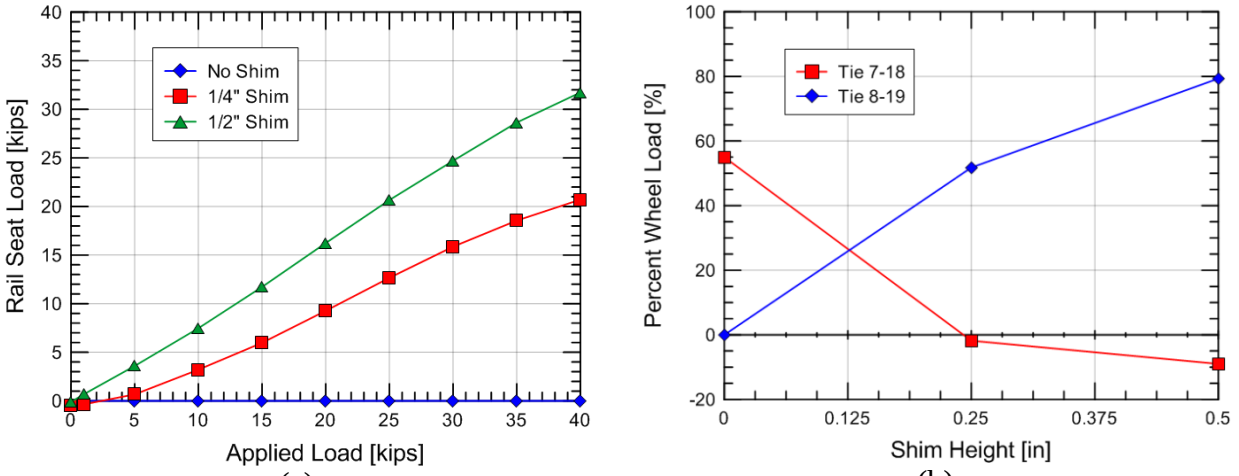

(a) (b)

Figure 6.18: Change in rail seat load for (a) Tie 8-19 with applied load and (b) peak percent wheel load with shim height.

A second iteration involved teaming with Trammco, Inc in the development of a machine that would assist in the installation of a HTS. The details of the installation is proprietary; however, instead of 0.25-in polyurethane shims, 0.25-in rubber shims similar to UTPs were used because the rubber materials is more resilient and has a higher ballast contact area than the polyurethane.

The machine was tested in live track at Site #6 on 11 November 2015 and was ultimately unsuccessful at installing the HTS without removal of the timber ties. The primary issue was angular ballast particles catching the shim and preventing it from being pushed underneath the tie. Improvements to the system are currently underway and further study is required before conclusive evidence on the viability of HTS. A few photographs of the setup are displayed in Figure 6.19.

(a)

(b)

Figure 6.19: Photographs of (a) the HTS installer on track and (b) inserting UTP underneath a timber tie in track.

6.7 Summary and Future Work

The fourth task involves developing a unified theory explaining transition zone settlement and recommendations on how to prevent and remediate the differential movement. The stated objectives of Task IV are:

(1) develop chain of events and list root causes explaining the deterioration of transition zones,
(2) develop strategies for reducing transition zone settlement, and
(3) recommend transition zone design, remedial, and resurfacing measures.

6.7.1 Summary of Results

The first objective of Task IV involved developing a chain of events and list root causes explaining the deterioration of transition zones. The chain of events is addressed in Chapter 6.2 and the list of root causes in Chapter 6.3. A summary is listed below:

- Differential movement at railroad bridge transition zones can be produced from various different mechanisms and each site displays unique behavior and causes of differential movement.
- Root causes of differential movement include: (1) substructure settlement from densification, (2) increased loads in the approach, and (3) increased settlement from reduced-performance materials and conditions.
- Transition zones have been categorized in three primary stages: compaction stage, equilibrium stage, and post-equilibrium stage. Ideally, transition zones should be in the

equilibrium stage and display minimal change in transient behavior with time, even distribution of tie loads, and minimal or gradual ballast settlement.

The second objective of Task IV involved developing strategies for reducing transition zone settlement. This is presented in Chapter 6.4. A summary is listed below:

- A unified strategy for reducing differential movements at transition zones is to ensure balance of the transient and permanent displacements between the approach and bridge and viewing the transition zone as a system instead of individual track components. This can be visualized by using the proposed transition Balance Sheet.
- Specific strategies at reducing substructure settlement in the compaction stage are to increase ballast density after tamping and ensuring proper compaction of the subgrade.
- Techniques to stiffen the subgrade and reduce settlement include: stiffening the subgrade with grout or cement, geopiers, compacting the fill wet-of-optimum, or using a granular fill with a vegetative soil cover to prevent erosion of the granular fill.
- Specific strategies are reducing ballast settlement in the post-equilibrium stage are reducing potential increased load from tie ballast gaps, reducing potential increased ballast degradation from tie-ballast gaps, and preventing and remediating reduce-performance ballast conditions.

The third objective of Task IV involved recommending transition zone design, remedial, and resurfacing measures. The design and remedial techniques are presented in Chapter 6.5 while the resurfacing techniques is covered in Chapter 6.6. A summary is listed below:

- Successful transition zone design and remedial solution tend to incorporate multiple techniques and address the bridge, ballast, and subgrade.
- A promising solution that focuses on the deficiencies of the tie-ballast gap is under-tie pads (UTPs). UTPs reduce and better distribute the wheel load amongst underlying ties, increase tie-ballast contact area and improve the distribution of load from the tie to the ballast, improve damping, and reduce wear on the tie and ballast by acting as a barrier
- Improving resurfacing techniques, i.e. reducing compaction stage of ballast settlement, can be accomplished by changing pneumatic tamping techniques, stoneblowing, or installing hanging tie shims instead of tamping. The goal of all three proposed methods are to keep the compacted ballast in a compacted state and add additional material to compensate for existing settlement.

6.7.2 Future Work

The recommendations provided in Chapter 6 range from successfully tested and implemented ideas to untested conceptual techniques. Suggestions for future work include:

- Implementation and monitoring of more transition zone design and remedial techniques will provide insight into the success of each techniques, the length of time it is successful for, and conditions that it is successful or unsuccessful in.
- Continual upgrades and modifications of resurfacing techniques can lead to a post-resurfacing track with compact ballast that will not experience rapid settlement after the first train pass. This is anticipated to extend the time between future resurfacing events.

CHAPTER 7

SUMMARY AND CONCLUSIONS

7.1 Summary

Differential movements at railroad bridge transition zones is a common problem for the railroad industry and frequent maintenance is often required to maintain an acceptable track geometry for passing trains. This represents an increasing cost and safety concern for railroad companies as freight and passenger lines are expected to be incrementally upgraded to accommodate longer, heavier, and faster trains. For this reason, reliable remediation or resurfacing techniques to mitigate the differential movements are sought after by the railroad industry.

Prior to selecting appropriate remedial techniques, the depth at which the majority of permanent and transient displacement is occurring must be known. Whether it is within the ballast or subgrade is the subject to much debate within the railroad community. To aid determining the problematic depth, this thesis analyzes ten railroad sites to gauge the permanent and transient movement with depth. Eight additional sites with only surface instrumentation were analyzed to expand the number of measured sites.

Multiple root causes of transition zone settlement have been proposed throughout the history of transition zone analysis. These proposed causes often relate to how the rapid change in track structure affects the dynamic track response or focus on the integrity of the substructure. This thesis visits fourteen different bridge approaches to determine the cause of differential movement at each transition zone and how changes in track structure and substructure integrity affect the behavior and settlement. Additionally, three-dimensional dynamic numerical models that simulate the secondary suspension-rail-tie-ballast-subgrade interaction were developed to run parametric analyses on track geometry variables such as ballast settlement that affect the dynamic behavior and loading.

Multiple remediation techniques have been attempted to mitigate the differential movements at railroad bridge transition zones. Multiple locations with various transition designs were investigated the factors that make each technique successful or unsuccessful. Potential improvements in resurfacing techniques are also addressed.

A final factor in this thesis is the development of a non-invasive instrumentation system that can measure important variables of railroad track performance. A system involving high-speed video cameras and accelerometers was developed in this thesis and tested at eight different site locations.

7.2 Conclusions

Based on this study, the following conclusions are drawn concerning the causes of the deterioration of railroad bridge transition zones:

- The root causes of differential movement at railroad bridge transition zones include: (1) inevitable substructure settlements from ballast and subgrade densification as opposed to minimal track settlement on the bridge, (2) increased loading within the bridge approach, and (3) increased settlement within the approach from reduced-performance substructure materials and conditions.
- Increased loading within the approach appears to be initiated by existing differential settlement between the bridge and approach or within the approach. This suggests approach settlement can initiate a negative feedback loop that increasingly deteriorates the transition zone and its components over time.
- Preliminary instrumentation with accelerometers showed evidence of increased loading by measuring increased tie accelerations at the moment of tie-ballast impact and increased tie accelerations at sites displaying reoccurring track geometry problems. Parametric analyses with numerical models showed 100% increases in load from differential movement between the bridge and approach and uneven tie support within the approach.
- Evidence of reduced-performance materials and conditions involved wet, fouled ballast in the approach and the existence of tie-ballast gaps. Previous laboratory tests show both factors can increase ballast settlement by almost 1000%.
- Loose ballast after tamping can result in almost an inch of settlement within the first train pass.

Based on this study, the following conclusions are drawn concerning the stages of the deterioration of railroad bridge transition zones

- Three stages were identified within transition zones: (1) compaction stage, (2) equilibrium stage, and (3) post-equilibrium stage. The compaction stage involves ballast and subgrade compaction after tamping or being placed in service. The equilibrium stage involves minimal change in transient displacement over time, even distribution of tie loads, and gradual or minimal settlement. The post-equilibrium stage involves accelerated

settlement from increased loads and reduce-performance substructure materials and conditions.

- Progressive settlement analyses suggest railroad track will naturally settle in a manner that will reduce loads, assuming ideal conditions. This is anticipated to explain the homogenous behavior at well-performing transition zones. However, increased loads and settlements can occur under heterogeneous conditions, which explain the post-equilibrium stage in which heterogeneous tie support and ballast conditions are observed.

Based on this study, the following conclusions are drawn concerning remedial and resurfacing techniques at railroad bridge transition zones

- Analysis of fourteen different bridge approaches suggest the majority of settlement occurs in the ballast layer for existing lines with possible subgrade settlement in new lines that have not experienced train loading. The majority of transient displacement involves the closure of tie-ballast gaps or other gaps within the track structure. This suggests transition zone should be viewed as a system. To aid this, a Balance Sheet has been proposed which lists all components of a railroad bridge transition zone.
- Suggestions to balance the approach and bridge displacements include: (1) increasing bridge displacement with ballasted-deck bridges, rail pads, tie pads, and ballast mats, (2) increasing ballast support with concrete wing walls and HMA, geoweb, or geogrid underlayment, and (3) increasing subgrade compaction with hydrocompressed fills, grout, geopiers, and other techniques.
- Key factors in mitigating transition zone settlement include: (1) ensure the ballast is compacted after tamping, (2) ensure the subgrade is compacted prior to track construction, (3) avoid or mitigate the negative influence of tie-ballast gaps, and (4) avoid or mitigate the influence of reduced-performance ballast in the approach.
- A strategy to ensure ballast compaction after tamping is to improve resurfacing methods at transition zones. This can include improvements of pneumatic tamping techniques, stoneblowing, or the insertion of shims underneath the tie. Many of these methods are still in development but have potential if proven viable.
- Suggestions to improve subgrade support include stiffening the subgrade with grout or cement, geopiers, compacting the fill wet-of-optimum, or using a granular fill with a vegetative soil cover to prevent erosion of the granular fill.
- A recommendation to mitigate the negative influence of tie-ballast gaps is using under-tie pads (UTPs). These better distribute the wheel amongst underlying ties, increasing ballast contact and improve the distribution of tie load to the ballast, improve damping, and reduce wear of the tie and ballast.
- Replacing fouled ballast and ensuring drainage is also a key factor in avoiding reduced-performance conditions.

7.3 Recommendations for Future Research

The present study makes the following recommendations for future research:

- A key aspect of the study that is not well covered is the influence of tie-ballast gaps on ballast settlement. This study relied on a single laboratory test and additional tests that better describe the influence of tie-ballast gap height, loading frequency, tie material, and ballast conditions would be helpful.
- Improved surveying and field investigations that sample and test the ballast at various track locations would be beneficial to help determine the influence of reduced-performance ballast conditions.
- Due to the complexity of transition zone behavior, instrumenting multiple transition zone and at least a single open track location is recommended to describe the entire length of the transition zone. This allows for better understanding of problematic locations and how unsupported conditions can change with distance and time.
- Use multiple instruments to measure wheel load, rail and tie displacement, tie acceleration, and tie-ballast pressure. This will help better relate the variables and better understand the various loading mechanisms and their influence on ballast loading.

REFERENCES

American Railway Engineering and Maintenance-of-Way Association (2016). AREMA Manual for Railway Engineering, Landover, Maryland, 2012.

Anderson WF and Fair P. (2008). Behavior of Railway Ballast under Monotonic and Cyclic Loading. *Journal of Geotechnical and Geoenviornmental Engineering.* 134(3): 316-327

Anderson JS and Rose JG. (2008). In-Situ Test Measurement Techniques Within Railway Track Structures. *Proceedings of the 2008 Joint Rail Conference.* April, 2008, Wilmington DE.

Banimahd M, Woodward PK, Kennedy J, and Medero GM. (2011). Behavior of train-track interaction in stiffness transitions. *In: Proceedings of the institution of civil engineers-transport*. Vol. 165. Is. 3. Pp. 205 – 214.

Bilow D and Li D. (2005). Concrete Slab Track Test on the High Tonnage Loop at the Transportation Technology Center. *In Proceedings of the 2005 AREMA Annual Conference*

Cantrell DD and Bourgonje TL. (2014). Transition from Bridge End to Bridge and Bridge to Bridge End. *American Railway Engineering and Maintenance-of-Way Association annual Conference*. Chicago, Illinois. Sept, 2014.

Chang CS, Adegoke CW and Selig ET. (1980). GEOTRACK Model for Railroad Track Performance. *Journal of the Geotechnical Engineering Division,* Vol 106, No. 11, November 1980, pp. 1201 – 1218.

Chen C, Indraratna B, McDowell G, and Rujikiatkamjorn C. (2015). Discrete element modelling of lateral displacement of a granular assembly under cyclic loading. *Computers and Geotechnics*. Vol. 69. Pp. 474-484.

Coehlo B, Hölscher P, Priest J, Powrie W, and Barends F. (2011). An assessment of transition zone performance. *Proceedings of the Institution of Mechanical Engineers, Part F: Journal of Rail and Rapid Transit.* Vol 225*, pp. 129-139*

Dahlberg T. (2001). Some railroad settlement models – a critical review. *Proceedings of the Institution of Mechanical Engineers, Part F: Journal of Rail and Rapid Transit.* Vol. 215, pp. 289-300

Davis D, Anaya R, Chrismer S, and Smith L. (2007) Development of a Differential Settlement Model for Design and Maintenance of Track Transitions. *Technology Digest*. Transportation Technology Center, Inc. TD-07-002.

DeBeer M, Horak E, and Visser A. (1989). The Multidepth Deflectometer (MDD) System for Determining the Effective Elastic Moduli of Pavement Layers. *In Nondestructive Testing*

of Pavements and Backcalculation of Moduli, ASTM STP 1026, A. J. Bush-III and G. Baladi, eds., American Society for Testing and Materials, Philadelphia, PA, pp. 70–89.

Douglas SC. (2013). Ballast Quality and Breakdown during Tamping. *Proceedings of 2013 American Railway Engineering and Maintenance-of-Way Association Conference*. Indianapolis, IN.

Ebrahimi A, Tinjum JM, and Edil TB. (2011). Large-Scale, Cyclic Traiaxial Testing of Railway Ballast. *American Railway Engineering and Maintenance-of-Way Association Annual Conference.* Orlando, FL. 2010.

Fair P. (2004). The geotechnical behaviour of ballast materials for railway track maintenance. PhD Thesis, University of Sheffield. Sheffield, UK.

Fröhling RD, Tomas M, Ebersöhn W. (1997). Low Frequency Dynamic Vehicle/Track Interaction: Instrumentation and Measurement. Proceedings of the *6th International Heavy Haul Railway Conference*, Cape Town, South Africa.

Frohling RD. (1998). Low-Frequency Dynamic Vehicle/Track Interaction: Modelling and Simulation. *Vehicle System Dynamics: International Journal of Vehicle Mechanics and Mobility,* 29:S1, pp. 30-46. 1998.

Gao Z, Wolf HE, Dersch MS, Qian Y, and Edwards JR. (2016). Field Measurements and Proposed Analysis of Concrete Crosstie Bending Movements. *American Railway Engineering and Maintenance-of-Way Association annual Conference*. Orlando, Florida. , August, 2016.

Hay WW. (1982). *Railroad Engineering.* New York: John Wiley and Sons.

Han X and Selig ET. (1997). Effects of Fouling on Ballast Settlement. *In Proceedings of 6th International Heavy Haul Railway Conference*. Cape Town, South Africa, April 6-10, 1997.

Harrison HD, Selig ET, Dean FE, and Stewart HE. (1984). Correlation of Concrete Tie Performance in Revenue Service and at the Facility for Accelerated Service Testing. *Research Report for Federal Rail Administration*. FRA/ORD-84/02.1. 1984

Huang H, Dombrow W, and Tutumluer E. (2009). Laboratory characteristics of fouled railroad ballast behavior. *Transportation Research Record: Journal of the Transportation Research Board,* Transportation Research Board of the National Academies, pp 93-101.

Hunt HEM. (1997). Settlement of railway track near bridge abutments. *Proc. Instn Civ Enginrs, Transp,* Vol 123, February, 1997, pp 68-73.

Hyslip J, Li D and McDaniel C. (2009). Railway Bridge Transition Case Study. *In Proceedings, 8th International Conference on Bearing Capacity of Roads, Railways and Airfields*, Champaign, Illinois, Vol. II.

Indraratna B, Ionescu D, and Christie HD. (1998). Shear Behavior of Railway Ballast based on Large-Scale Triaxial Tests. *Journal of Geotechnical and Geoenviornmental Engineering*, Vol 124, No 5, pp 439-449

Indraratna B, Thakur PK, and Vinod JS. (2010). Experimental and Numerical Study of Railway Ballast Behavior under Cyclic Loading. *International Journal of Geomechanics*. Vol 10, No 4, pp 136-144

Indraratna B, Nimbalkar S, Christie D, Rujikiatkamjorn C, and Vinod J. (2010). Field Assessment of the Performance of a Ballasted Rail Track with and without Geosynthetics. *Journal of Geotechnical and Geoenviornmental Engineering*, Vol 136, No 7, pp 907-917.

Indraratna B, Salim W, and Rujikiatkamjorn C. (2012). *Advanced Rail Geotechnology – Ballasted Track.* CRC Press/Balkema, Leiden, The Netherlands.

Indraratna B, Thakur PK, Vinod JS, and Salim W. (2012). Semiemperical Cyclic Densification Model for Ballast Incorporating Particle Breakage. *International Journal of Geomechanics.* Vol 12, No 3, pp 260-271.

Itasca (2012). FLAC3D Manuals, V.5.0

Kaewunruen S and Remennikov AM. (2007). Investigation of free vibrations of voided concrete sleepers in railway track system. *Proc. IMechE. Part F: J. Rail Rapid Transp.* Vol. 221. Pp. 495-507.

Kerr AD and Shenton HW. (1986). Railroad Track Analyses and Determination of Parameters. *Journal of Engineering Mechanics*, ASCE, Vol. 112, No. 11, 1986, pp 1117 – 1134.

Kerr AD, and Moorany BE. (1993). Track transition problems and remedies. *Bulletin 742*, American Railway Engineering Association, Landover, MD.

Kerr AD and Bathurst LAA. (2001). Method for Upgrading the Performance at Track Transitions for High-Speed Service. *DOT/FRA/ORD-02-05*, September 2001.

Kerr AD. (2003). *Fundamentals of Railway Track Engineering*. Simmons-Boardman Books, Inc.

Lackenby J, Indraratna B, McDowell G, and Christie D. (2007). Effect of confining pressure on ballast degradation and deformation under cyclic triaxial loading. *Geotechnique*. Vol 57. No 6, pp 527-536

Lamas-Lopez F, Alves-Fernandes V, Cui YJ, D'Aguiar SC, Calon N, Canou J, Dupla J, Tang AM, and Robinet A. (2014). Assessment of the Double Integration Method using Accelerometers Data for Conventional Railway Platforms. *Proc: 9th International Conference on Engineering Computational Technology.* Stirlingshire, Scotland. Pp. 1 – 18. 2014.

Le Pen L, Watson G, Powrie W, Yeo G, Weston P, and Roberts C. (2014). The behavior of railway level crossings: Insights through field monitoring. *Transportation Geotechnics*. Vol. 1. 2014. Pp. 201-213.

Li D and Selig ET. (1998a). Method for railroad track foundation design I: Development. *Journal of Geotechnical and Geoenviornmental Engineering*, ASCE, April, 1998. Vol. 124. pp. 316–322.

Li D and Selig ET. (1998b). Method for railroad track foundation design II: Applications. *Journal of Geotechnical and Geoenviornmental Engineering*, ASCE, April, 1998. Vol. 124. pp. 323–329.

Li D and Davis D. (2005). Transition of Railway Bridge Approaches. *Journal of Geotechnical and Geoenviornmental Engineering*, ASCE, November, 2005. 131(11): pp. 1392–1398.

Li D, Otter D, and Carr G. (2010). Railway bridge approaches under heavy axle load traffic: problems, causes, and remedies. *Proceedings of the Institution of Mechanical Engineers, Part F: Journal of Rail and Rapid Transit*. Vol. 224, pp. 383 – 390

Li D and Maal L. (2015). Heavy Axle Load Revenue Service Bridge Approach Problems and Remedies. *Proceedings of the 2015 Joint Rail Conference.* March 23-26, 2015, San Jose, California.

Lobo-Guerrero, S., Vallejo, L.E. (2006), "Discrete Element Method Analysis of Railtrack Ballast Degradation during Cyclic Loading". *Granular Matter*. Vol 8. Pp. 195 - 204

Lu S, Arnold R, Farritor S, Fateh M, and Carr G. (2008). On the Relationship between Load and Deflection on Railroad Track Structures. *Proceedings of the AREMA 2008 Annual Conference*, Salt Lake City, UT, September, 2008.

Lundqvist A and Dahlberg T. (2005). Load Impact on Railway Track due to Unsupported Sleepers. *Proceedings of the Institution of Mechanical Engineers, Part F: Journal of Rail and Rapid Transit*. 2005. Vol. 219, pp. 67 – 77

Markine VL, Wang H, and Shevtsov IY. (2014). Experimental Analysis of the Dynamic Behaviour of Railway Track in Transition Zones. *Proceedings of the 9th International Conference on Engineering Computational Technology*, P. Ivanyi and B.H.V. Topping (Editors), Stirlingshire, Scotland.

McHenry M. (2013). “Pressure Measurement at the Ballast-Tie Interface of Railroad Track using Matrix Based Tactile Surface Sensors”. M.S. Thesis, University of Kentucky, Lexington, KY, 2013.

McMichael PL. (1991). The economics of stoneblowing for the maintenance of way. Proceedings of the *1991 International Heavy Haul Railway Conference*, June 1991, Vancouver, B.C., Canada.

Mesri G and Vardhanabhuti B. (2009). Compression of granular material. *Canadian Geotech J*. Vol 46: 369-392

Mishra D, Tutumluer E, Stark TD, Hyslip JP, Chrismer SM, and Tomas M. (2012). Investigation of differential movement at railroad bridge approaches through geotechnical instrumentation. *J Zhejiang Univ-SciA (Appl Phys & Eng)* 12(11), 2012, 814-824

Mishra D, Kazmee H, Tutumluer E, Pforr J, Read D, and Gehringer E. (2013). Characterization of Railroad Ballast Behavior Under Repeated Loading. *Transportation Research Record: Journal of the Transportation Research Board*, No 2374, Transportation Research Board of the National Academies, Washington D.C.

Murray CA, Take WA, and Hoult NA. (2015). Measurement of vertical and longitudinal rail displacements using digital image correlation. *Can. Geotech. J.* 52:141-155. 2015

Nazarian S. (2012). Shave Wave Velocity Profiling with Surface Wave Methods. In *Proceedings of GeoCongress 2012, State-of-the-Art Lecture Volume*, pp. 221-240

Nicks J. (2009). “The Bump at the End of the Railway Bridge”. PhD Thesis, Texas A&M University, College Station, TX, 2009.

Nimbalkar S and Indraratna B. (2016). Improved Performance of Ballast Rail Track Using Geosynthetics and Rubber Shockmat. *Journal of Geotechnical and Geoenviornmental Engineering*, Vol 142, No 8, pp 1-13.

Paixão A, Fortunato E, and Calçada R. (2014). Transition zones to railway bridges: Track measurements and numerical modeling. *Engineering Structures*. Vol. 80, pp. 435-443

Paixão A, Fortunato E, and Calçada R. (2015). Design and construction of backfills for railway track transition zones. *Proceedings of the Institution of Mechanical Engineers, Part F: Journal of Rail and Rapid Transit*. Vol. 229(1), pp. 58 – 70

Patel N and Jordan N. (1996). Ballasted track transitions. *In Proceedings of the 1996 Rapid Transit Conference of the American Public Transit Association*. June 2-6, 1996. Atlanta, GA, pp 116-126.

Pinto N, Ribeiro CA, Gabriel J, and Calçada R. (2015). Dynamic monitoring of railway track displacement using an optical system. *Proc. IMechE. Part F: J. Rail Rapid Transp.* 2015. Vol. 229(3) Pp. 280-290.

Plotkin D and Davis D. (2008). Bridge Approaches and Track Stiffness. DOT/FRA/ORD-08-01, February 2008.

Priest JA, Powrie W, Yang L, Grabe PJ, and Clayton CRI. (2010). Measurements of transient ground movements below a ballasted railway line. *Géotechnique*. 2010. Vol. 60. No. 9. Pp. 667-677

Qian Y, Tutumluer E, Hashash YMA, and Ghaboussi J. (2014). Effects of Ballast Degradation on Permanent Deformation Behavior from Large-Scale Triaxial Tests. *Proceedings of the 2014 Joint Rail Conference*. April 2 – 4. Colorado Springs, CO, USA.

Read D and Li D (2006). Design of Track Transitions. *Research Results Digest 79*, Transit Cooperative Research Program, Transportation Research Board, National Academies, October 2006, 37 p.

Remennikov AM and Kaewunruen S. (2006). Experimental Investigation on Dynamic Railway Sleeper/Ballast Interaction. *Experimental Mechanics.* 2006. 46: 57-66

Remennikov AM and Kaewunruen S. (2008). A review of loading conditions for railway track structures due to train and track vertical influence. *Structural Control and Health Monitoring*. Vol 15. pp207-234.

Rose J and Lees H. (2008). Long-Term Assessment of Asphalt Trackbed Component Materials' Properties and Performance. *Proceedings of the American Railway Engineering and Maintenance-of-Way Association 2008 Annual Conference*, Salt Lake City, UT, September, 2008. 28 pages

Rose JG. (2013). Selected in-track applications and performances of hot-mixed asphalt trackbeds. *Proceedings of the 2013 Joint Rail Conference.* April 15-18, 2013, Knoxville, Tennessee.

Salim W and Indraratna B. (2004). A new elastoplastic constitutive model for coarse granular aggregates incorporating particle breakage. *Canadian Geotechnical Journal,* Vol 41, pp 657-671.

Sasaoka C and Davis D. (2005). "Implementing Track Transition Solutions for Heavy Axle Load Service". *In Proceedings, AREMA 2005 Annual Conference*, Chicago, IL. 2005.

Sato Y. (1997). Optimization of track maintenance work on ballasted track. *In proceedings of the World Congress on Railway Research (WCRR '97*), Florence, Italy, 16-19 November 1997, Vol. B, pp. 405-411.

Schnedier, P, Bolmsvik R, and Nielsen JCO. (2011). In situ performance of a ballasted railway track with under sleeper pads. *Proceedings of the Institution of Mechanical Engineers, Part F: Journal of Rail and Rapid Transit*. 2011. Vol. 225, pp. 299 – 309

Selig ET, DelloRussoV, and Laine KJ. (1992). Sources and Causes of Ballast Fouling. *Report No. R-805.* Association of American Railroads. Technical Center, Chicago, 1992.

Selig ET and Waters JM. (1994). Track Geotechnology and Substructure Management. London: Thomas Telford.

Silva FCM, Logistica MRS, Paiva CEL, and Aguiar PR. (2007). Evaluation of Track / Ballast Behavior under Increased Axle Load: Measuring Deflection on Track. *IHHA Specialist Technical Session (STS).* Kiruna, Sweden. 2007.

Smith, M.E., P.-E. Bengtsson, G.Holm. (2006). Three-dimensional analyses of transition zones at railway bridges. *Sixth European Conference on Numerical Methods in Geotechnical Engineering*, NUMGEO6, Graz, Austria, pp. 237-242.

Smith, M.E., P-E. Bengtsoon, G. Holm (2007). Three-dimensional numerical analyses of a full-scale instrumented railway embankment. *Geotechnical Engineering in Urban Enviornments. Proceedings of: 14th European Conference on Soil Mechancis and Geotechnical Engineering*. Madrid, Spann. September 24-27, 2007. Pp. 413-148

Sol-Sánchez M, Moreno-Navarro F and Rubio-Gámez MC. (2016a). Analysis of ballast tamping and stone-blowing process on railway track behavior: the influence of using USPs. *Geotechnique*. Vol 66. No 6, pp 481-489.

Sol-Sánchez M, Pirozzolo L, Moreno-Navarro F, and Rubio-Gámez MC. (2016b). Reducing railway maintenance: the effectiveness of combining the stoneblowing technique with rubber elements from waste tires. *Proceedings of Transportation Research Board 95th Annual Conference*. Washington D.C.

Stark TD, Wilk ST, Thompson HB, Sussmann TR, Baker M, and Ho CL. (2016). Evaluating fouled ballast using seismic surface waves. *Proceedings of the 2016 Joint Rail Conference.* April 12-15, 2016, Columbia, South Carolina.

Sun QD, Indraratna B, and Nimbalkar S. (2016). Deformation and Degradation Mechanisms of Railway Ballast under High Frequency Cyclic Loading. *Journal of Geotechnical and Geoenviornmental Engineering*. Vol 142, No 1.

Sussmann T and Selig E. (1998). Evaluation of Increased Axle Loading on Northeast Corridor Track Substructure. Test Report for Amtrak (National Railroad Passenger Corporation), Ernest T. Selig Inc., Hadley, MA.

Sussmann T and Selig E. (2000). Resilient Modulus Backcalculation Techniques for Track. *Performance Confirmation of Constructed Geotechnical Facilities:* pp. 401-411.

Sussmann TR, Ebersöhn W, and Selig ET. (2001). Fundamental Nonlinear Track Load-Deflection Behavior for Condition Evaluation. *Transportation Research Record: Journal of the Transportation Research Board*, Transportation Research Board of the National Academies, 1742, 61-67

Sussmann TR, Ruel M, and Chrismer SM. (2012).Source of Ballast Fouling and Influence Considerations for Condition Assessment Criteria. *Transportation Research Record: Journal of the Transportation Research Board*, Transportation Research Board of the National Academies, No. 2289. Washington, D.C., 2012. Pp. 87-94.

Sussmann TR, Thompson HB, Stark TD, Wilk ST, and Ho CL. (2015). Use of Seismic Surface Wave Testing to Assess Track Substructure Conditions. *Proceedings of Railway Engineering-2015 Conference*, June 30th – July 1st. Edinburgh, Scotland.

Taherinezhad J, Sofi M, Mendis PA, and Ngo T. A Review of Behavior of Prestressed Concrete Sleepers. *Special Issue: Electronic Journal of Structural Engineering*. 13(1). 2013

Talbot, AN. (1919). *Stresses in Railroad Track*. The Second Progress Report of the ASCE-AREA Special Committee on Stresses in Railroad Track, Reprinted, 1980. Published by the American Railway Engineering Association (AREA).

Tennakoon N, Indraratna B, Rujikiatkamjorn C, Nimbalkar S, and Neville T. (2012). The Role of Ballast-Fouling Characteristics on the Drainage Capacity of Rail Substructure. *Geotechnical Testing Journal*, Vol. 35, No. 4.

Thakur PK, Vinod JS, and Indraratna B. (2013). Effect of confining pressure and frequency on the deformation of ballast. *Geotechnique*. Vol 63, No 9, pp 786-790.

Track Safety Standards. (2014). Part 213, Subpart A to F, Class of Track 1 – 5. Office of Safety, FRA, U.S. Department of Transportation.

Tutumluer E, Stark TD, Mishra D, Hyslip J, Tomas M, and Chrismer S. (2012). "Investigation and Mitigation of Differential Movement at Railway Transitions for US High Speed Passenger Rail and Joint Passenger/Freight Corridors". *Proceedings of the ASME 2012 Joint Rail Conference (JRC2012),* April 17-19, 2012. Philadelphia, Pennsylvania, USA.

Tutumluer E, Qian Y, Hashash YMA, Ghaboussi J, and Davis DD. (2013). Discrete element modelling of ballasted track deformation behaviour. *International Journal of Rail Transportation*. Vol. 1, Nos. 1-2. Pp. 57-73.

Van Dyk BJ, Edwards JR, Dersch MS, Ruppert CJ, and Barkan CPL. (2016). Evaluation of dynamic and impact wheel load factors and their application in design processes. *Proceedings of the Institution of Mechanical Engineers, Part F: Journal of Rail and Rapid Transit*. 2016. Vol. 0, pp. 1 – 11

Varandas JN, Hölscher P, and Silva MAC. (2011). Dynamic Behaviour of Railway Track on Transition Zones. *Computer and Structures*, 89, pp. 1468-1479

Wang H, Markine VL, Shevtsov IY, and Dollevoet R. (2015). Analysis of the Dynamic Behavior of a Railway Track in Transition Zones with Differential Settlement. *Proceedings of the 2015 Joint Rail Conference.* March 23-26, 2015, San Jose, California.

Woodward PK, Kacimi A, Laghrouch O, Medero G, and Banimahd M. (2002). Application of polyurethane geocomposites to help maintain track geometry for ballasted high-speed railway tracks. *Zhejiang Univ-SciA (Appl Phys & Eng)* 12(11), 2012, 1-12.

APPENDIX A

Appendix A assembles the Young's Modulus values calculated from the static inverse analysis in Chapter 5.3. Table A.1 lists the ballast Young Modulus values while Tables A.2 through

Table A.1: Comparison of ballast moduli from static inverse analysis using FLAC3D for all MDD Instrumented Sites

	Caldwell Avenue		Madison Avenue		Upland Avenue	
	East [MPa]	West [MPa]	12 ft. [MPa]	60 ft. [MPa]	15 ft. [MPa]	60 ft. [MPa]
August 2012	164	103	104	224	237	255
November 2012	70	52	126	242	67	279
January 2013	132	51	110	271	200	202
June 2013	141	51	150	142	59	379

Table A.2: Inverse analysis of modulus with time at Caldwell (East) using FLAC3D

LVDT	August 2012 [MPa]	November 2012 [MPa]	January 2013 [MPa]	June 2013 [MPa]
1	164	70	132	141
2	64	59	47	47
3	85	82	91	104
4	41	31	31	25
5	65	49	44	64

Table A.3: Inverse analysis of modulus with time at Caldwell (West) using FLAC3D

LVDT	August 2012 [MPa]	November 2012 [MPa]	January 2013 [MPa]	June 2013 [MPa]
1	103	52	51	51
2	246	187	123	130
3	239	185	257	243
4	62	45	45	44
5	100	91	74	80

Table A.4: Inverse analysis of modulus with time at Madison (12 ft.) using FLAC3D

LVDT	August 2012 [MPa]	November 2012 [MPa]	January 2013 [MPa]	June 2013 [MPa]
1	104	126	110	150
2	66	55	67	52
3	66	66	83	73
4	34	34	43	29
5	49	53	71	55

Table A.5: Inverse analysis of modulus with time at Madison (60 ft.) using FLAC3D

LVDT	August 2012 [MPa]	November 2012 [MPa]	January 2013 [MPa]	June 2013 [MPa]
1	224	242	271	142
2	249	268	297	198
3	33	40	29	29
4	42	44	41	45
5	35	32	32	34

Table A.6: Inverse analysis of modulus with time at Upland (15 ft.) using FLAC3D

LVDT	August 2012 [MPa]	November 2012 [MPa]	January 2013 [MPa]	June 2013 [MPa]
1	237	67	200	59
2	54	45	98	89
3	40	45	25	77
4	51	83	117	66
5	123	91	72	113

Table A.7: Inverse analysis of modulus with time at Upland (60 ft.) using FLAC3D

LVDT	August 2012 [MPa]	November 2012 [MPa]	January 2013 [MPa]	June 2013 [MPa]
1	255	279	202	379
2	102	172	210	141
3	34	30	30	26
4	41	35	34	32
5	64	59	56	58